Ricerca di Sistema elettrico

Raccolta delle principali attività di diffusione

G. Puglisi

RACCOLTA DELLE PRINCIPALI ATTIVITÀ DI DIFFUSIONE

G. Puglisi (ENEA)

Settembre 2018

Indice

1   Introduzione

Il rapporto descrive le attività messe in atto per la comunicazione e diffusione dei risultati prodotti dal progetto D1 "tecnologie per costruire gli edifici del futuro" relativo all'Accordo di Programma MiSE-ENEA, piano annuale di realizzazione 2017.

Tali attività sono state suddivise, per ciascuna linea in cui è diviso il progetto, in:

▪ pubblicazioni su riviste specializzate o su atti di convegni,

▪ presentazioni a convegni.

Nei paragrafi successivi si riportano rispettivamente l'elenco delle pubblicazioni, gli articoli integrali e le pe presentazioni ai convegni.

2   ELENCO PUBBLICAZIONI

Di seguito sono riportate le pubblicazioni suddivise per linee.

Linea A
- "Green and low-cost hydrophobic coating based on ZnO NPs and stearic acid", Carmela Tania Prontera, Giuliano Sico, Maria Montanino, Maria Grazia Maglione, Paolo Tassini, Alessandro Pezzella, Carla Minarini, Paola Manini Ischia Advanced School of Organic Chemistry (IASOC 2018), Napoli, September 22-25 2018.
- "From Melanins to OLED Devices: Designing Electroluminescent Materials Inspired to Human Pigments", P. Manini, C. T. Prontera, V. Criscuolo, A. Pezzella, O. Crescenzi, M. Pavone, M. d'Ischia, M. G. Maglione, P. Tassini, C. Minarini CIMTEC 2018: 8th Forum on New Materials, Perugia, June 10-14 2018.
- "New insights into the Electronic-Ionic conduction modelfor eumelanin thin films", Carmela T. Prontera, Paola Manini, Alessandro Pezzella, Valeria Criscuolo, Clara Santato, Ri Xu, Marco Rolandi, Roberto Di Capua, Gabriella De Luca, BioEl2019 International Winterschool on Bioelectronics, Kirchberg in Tirol, Austria, March 11-16 2018.
- Canale , M. Dell'Isola , G. Ficco , B. Di Pietra, A. Frattolillo: Estimating the impact of heat accounting on Italian residential energy consumption in different scenarios. Energy & Buildings 168 (2018) 385–398
- M. R. Mancini, D. Mirabile Gattia, F. Girardi, L. Petrucci, Study on improved cements with Graphene Oxide, ISMANAM2018,2-6 luglio 2018, Roma, Italia
- M.R. Mancini, R. Mancini, D. Mirabile Gattia, F. Girardi, L. Petrucci, C. Russo, Use of Graphene oxide for the preparation of reinforced cement-based composites, Nanoinnovation2018 11-14 settembre 2018, Roma, Italia

Linea B
- Di Somma, M., Graditi, G., Mongibello, L., Bertini, I., Puglisi, G., 2018. Trade-Off Solutions between Economy and CO_2 Emissions for the Daily Operation of a Distributed Energy System: A Real Case Study in Italy. EEEIC / I&CPS Europe 2018.
- Caliano, M., Bianco, N., Graditi, G., Mongibello, L., 2018. Experimental and numerical study on a lab–scale latent heat storage prototype for cooling applications. 36a Conferenza UIT, Catania, Italia, 25-27 Giugno 2018.

- Di Somma, M., Yan, B., Bianco, N., Mongibello, L., Naso, V, 2017. Multi-objective design optimization of distributed energy systems through cost and exergy assessments. Applied Energy, 204, pp. 1299-1316.
- Mongibello, L., Bianco, N., Caliano, M., Graditi, G., 2018. Numerical simulation of an aluminum container including a phase change material for cooling energy storage. Appl. Syst. Innov., 1, 34.
- B. Di Pietra, M. Borasio, M. Caldera, G. Puglisi, F. Zanghirella, S. Caruso, "Teleriscaldamento attivo e solar district heating: la situazione in Europa e in Italia", Aicarr Journal n50, maggio 2018
- N. Nicotra, M. Caldera, P. Leone, F. Zanghirella, Model-based analysis of thermal energy storage for multiple temperature level heat supply, Applied Thermal Engineering, vol. 141, pp. 288-297.

Linea C
- Carlo Alberto Campiotti, Germina Giagnacovo, Luca Nencini, Alessandro Campiotti, Green Coverings for improving Energy efficiency of Buildings, Proceedings Supplement of " Quality-Access to Success" Journal Vol 19, S1, 2018 Indexed Wos, Scopus, Ebsco (ISSN1582-2559)
- Carlo Alberto Campiotti, Germina Giagnacovo, Luca Nencini, Matteo Scoccianti, Luciano Consorti, Carlo Bibbiani, Le coltri vegetali nel settore residenziale, Ambiente e Innovazione, DOI 10.12910/EAI 2018-039
- C. Bibbiani, A. Campiotti, G. Giagnacovo, L. Incrocci, A. Pardossi A. Latini, E. Schettini, Green roofs and green façades for improving sustainability of towns, Acta Hortic. 1215. ISHS 2018. DOI 10.17660/ActaHortic.2018.1215.61.
- C. Bibbiani, F. Fantozzi, C. Gargari, C.A. Campiotti, L. Incrocci and A. Pardossi, Supporting producers in designing more efficient and low-impact green roofs through the Life Cycle Analysis: environmental and energy performance, Acta Hortic. 1215. ISHS 2018. DOI 10.17660/ActaHortic.2018.1215.61.
- R. Di Bonito, D. Biagiotti, G. Giagnacovo, C. Viola and C.A Campiotti, Sustainable and energy saving urban horticulture on rooftop gardens in Mediterranean climatic conditions, Acta Hortic. 1215. ISHS 2018. DOI 10.17660/ActaHortic.2018.1215.61.
- E. Schettini, C.A. Campiotti, G. Scarascia Mugnozza, I. Blanco and G. Vox, Green walls for building microclimate control, Acta Hortic. 1215. ISHS 2018. DOI 10.17660/ActaHortic.2018.1215.61.

Linea D
- M.Botticelli, G.Comodi, A.Monteriù, A. Pallante, S.Pizzuti, Day-ahead multi-objective energy optimization of a smart building in a dynamic pricing scenario, 10th international conference on Improving Energy Efficiency in Commercial Buildings and Smart Communities (IEECB&SC'18), 21-22 March 2018, Frankfurt, Germany
- Moretti E., Zinzi M., Merli F., Buratti C., Optical, thermal, and energy performance of advanced polycarbonate systems with granular aerogel, (2018) Energy and Buildings, 166, pp. 407-417
- Luigi Giovannini, Fabio Favoino, Valentina Serra, Michele Zinzi , Thermo-chromic glazing in buildings: a novel methomagfafafasfafafafdological framework for a multi-objective performance evaluation, 10th International Conference on Applied Energy (ICAE2018), 22-25 August 2018, Hong Kong,China

linea E
- Matteo Caldera, Giovanni Puglisi, Fabio Zanghirella, Paola Ungaro, Giuliano Cammarata, "Numerical modelling of the thermal energy demand in Italian households statistical data", International Journal of Heat and Technology, vol. 36, n°2, June 2018, pp 381-390
- Alessandro Federici, Chiara Martini e Paola Ungaro. "Efficienza energetica: combustibile nascosto dell'economia e fonte di risparmio per le famiglie italiane", Energia, Ambiente e Innovazione 1/2018, DOI 10.12910/EAI2018-017.

- Alessandro Federici, Domenico Prisinzano, Amalia Martelli, Chiara Martini, Roberto Moneta, "Fiscal deduction in Italy for energy efficiency in residential buildings: Some insights", Economics and Policy of Energy and Environment 1-2/2017 pp. 15-29.
- Alessandro Federici, "Main Energy Efficiency measures in Italy", presentazione per il 42° meeting del Working Party on Energy Efficiency dell'International Energy Agency dell'11 settembre 2018

3 Articoli e presentazioni a convegni.

Green and low-cost hydrophobic coating based on ZnO NPs and stearic acid

Carmela Tania Prontera,[a] Giuliano Sico,[b] Maria Montanino,[b] Maria Grazia Maglione,[b] Paolo Tassini,[b] Alessandro Pezzella,[a] Carla Minarini,[b] Paola Manini[a]

(a) Department of Chemical Sciences, University of Naples "Federico II" via Cintia no. 4, 80126 Napoli, Italy.
(b) Laboratory of Nanomaterials and Devices, ENEA C. R. Portici, Piazzale E. Fermi, 80055 Portici (NA), Italy
carmelatania.prontera@unina.it

ZnO nanostructures and Hydrophobicity

After the discovery of superhydrophobic surfaces in Nature (e.g. lotus leaf), many artificial superhydrophobic coatings have been fabricated by mimicking Nature. The most of the studies carried out in this sense have been focused on:

1) the creation of a certain micro/nano-roughness structures promoting the entrapment of the air in the space between the rough and weakening the water-surface interaction;
2) the surface absorption/chemical functionalization with hydrophobic compounds masking the original surface wettability.

ZnO nanostructures like **nanowire**, **nanowall**, **nanorods**, **nanoflowers** are reported in literature as biocompatible hydrophobic materials. Also the chemical modifications with low surface energy molecules is able to further improve the hydrophobic character of ZnO nanostructures.
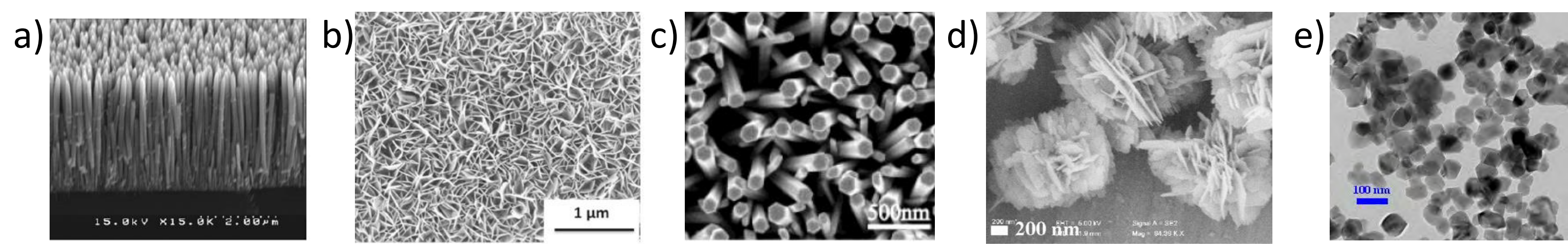
ZnO Nanostructures: a) nanowires; b) nanowalls; c) nanorods; d) nanoflowers; e) nanoparticles.

Nanoparticles Functionalization and Thin Film Deposition

1-step process

Ethanol
= ZnO NPs
COOH = Stearic acid

Functionalized ZnO NPs

Gravure printing/ Airbrushing

PEN substrate

Printed 1-step/Airbrushed 1-step

2-steps process

Gravure printing/ Airbrushing

PEN substrate
Printed ZnO/Airbrushed ZnO

Gravure printing/ Airbrushing
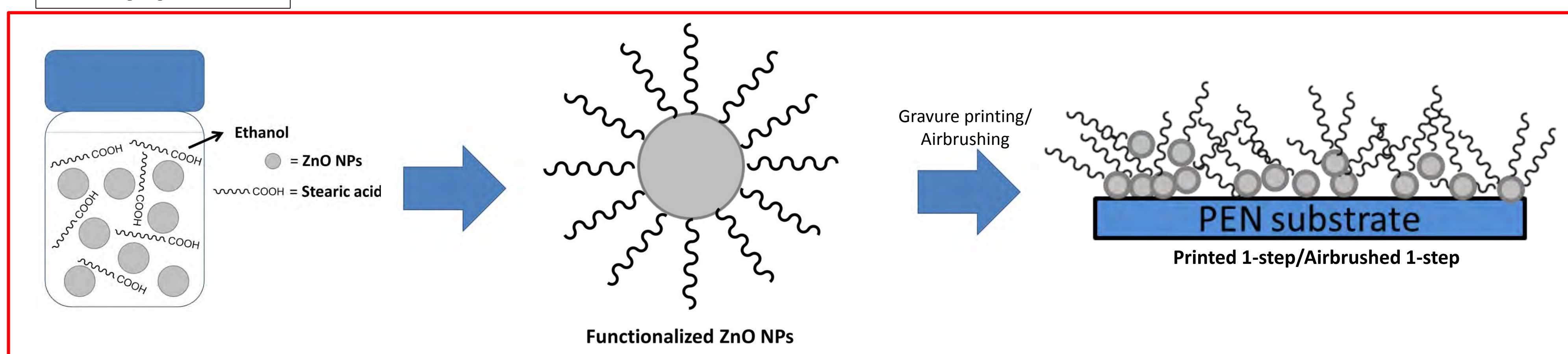
PEN substrate
Printed 2-steps/Airbrushed 2-steps
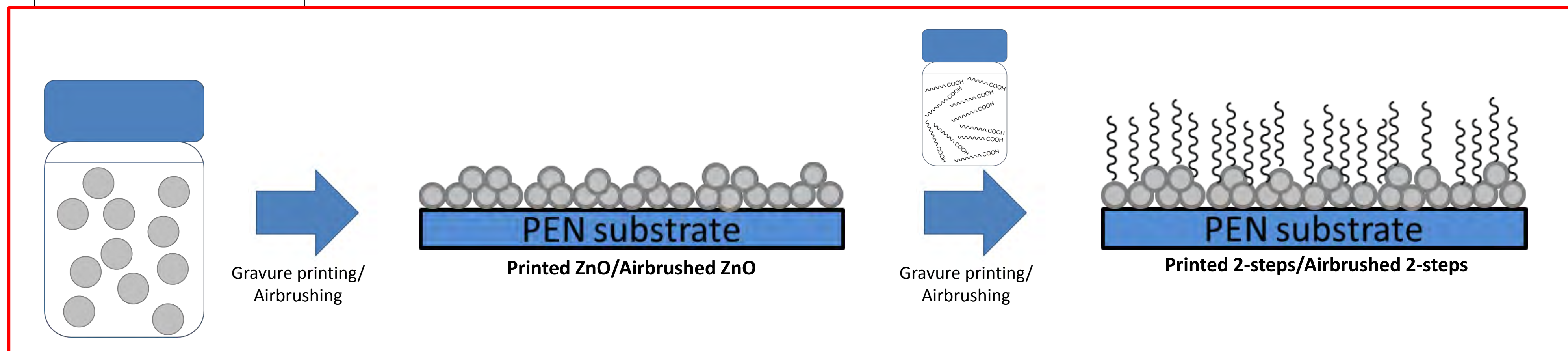
Here we report on the development of easy and low cost procedures for the preparation of hydrophobic coatings based on ZnO nanoparticles functionalized with stearic acid.
Airbrushing and Gravure Printing deposition techniques are exploited as high throughput and industrial scalable technologies.

Two different approaches were pursued.

- **1-step deposition process**. ZnO nanoparticles are functionalized with stearic acid and the composite material is deposited on PEN substrate by airbrushing and gravure printing.

- **2-steps deposition process**. First ZnO nanoparticles are deposited on PEN substrate by printing or airbrushing, then stearic acid is deposited on ZnO nanoparticles and a thermal treatment is carrier out to trigger the in situ ZnO nanoparticles functionalization.

Chemical and Morphological Characterization

a) FTIR Spectra — legend: ZnO, 1 step, 2 steps

b) UV-Vis Spectra — legend: Printed ZnO, Airbrushed ZnO, Printed 2-steps, Airbrushed 2-steps, Printed 1-step, Airbrushed 1-step

c)
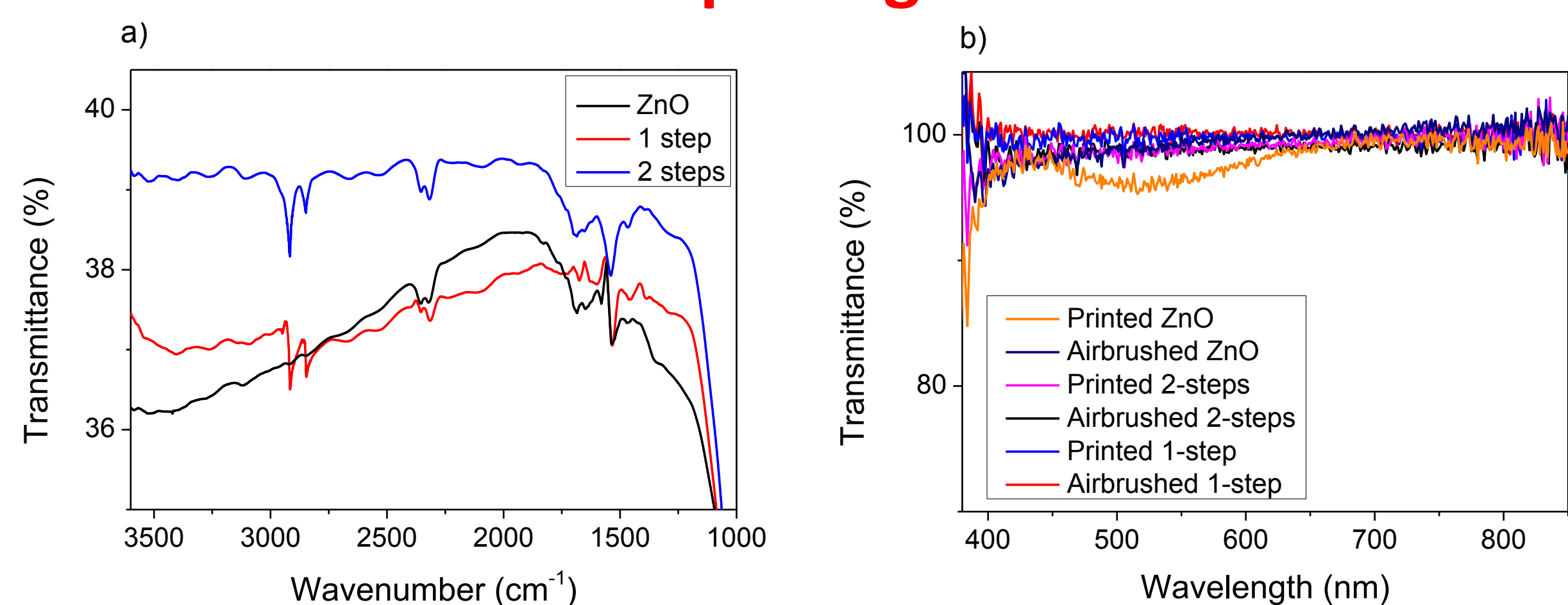
	Sq (nm)	Water Contact Angle (°)	
Printed ZnO	10	26	
Airbushed ZnO	8	100	
Printed (2-steps)	70	115	
Airbrushed (2-steps)	10	102	
Printed (1-step)	13	99	
Airbrushed (1-step)	14	95	

a) FTIR Spectra; b) UV-Vis Spectra; c) Morphological and contact angle characterization

Water Vapour barrier determination

Electrical calcium test

gas volume   glass lid   adhesive
electrode   calcium   electrode
barrier substrate

$$Ca + 2H_2O \rightarrow Ca(OH)_2 + H_2$$

Conductive   Insulating

$J_{ss} = dy/dx$

Increasing lag time
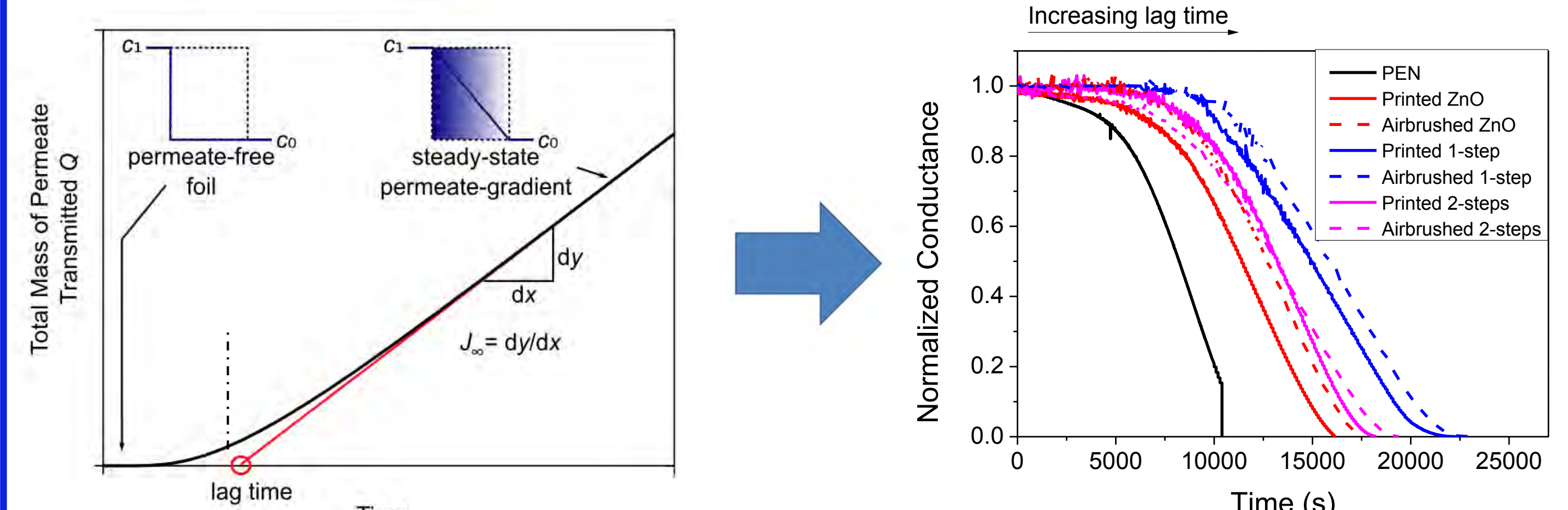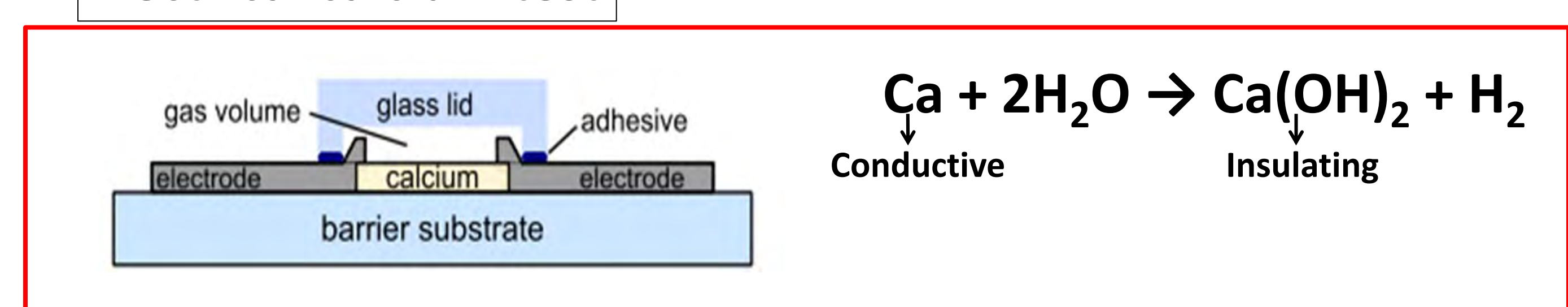
	PEN	Print. ZnO	Airbr. ZnO	Print. 1-step	Airbr. 1-step	Print. 2-steps	Airbr. 2-steps
WVTR g/m²/day @ 38°C, 90% RH	1.58	1.18	1.24	0.89	0.96	1.27	1.02
Lag time (h)	1.51	2.13	2.33	2.63	2.98	2.47	2.26

Conclusions

- Hydrophobic and transparent coatings based on ZnO nanoparticles functionalized with stearic acid were obtained with easy and low cost approaches;
- the electrical calcium test was used to determine the water vapor barrier of the substrates with the hydrophobic coating and as indirect measurement of the film uniformity;
- the improvement of the barrier properties consists in an improvement of the lag time since the hydrophobicity is able to slow down the adsorption phase of the permeation process;
- the best results were achieved with the one-step deposition procedure.

References:
[1] P. Kar et al. Applied Surface Science 2010, 256, 4995–4999.
[2] S. Sutha et al. Bull. Mater. Sci. 2017, 40, 505-511.
[3] X. Feng et al. J. Am. Chem. Soc. 2004, 126, 62-63.
[4] Y. Wang et al. Superlattices and Microstructures 2012, 51, 128-134.
[5] S. Schubert et al. Rev Sci Instrum 2011, 82, 094101.

From melanins to OLED devices: designing electroluminescent materials inspired to human pigments

Paola Manini,

Carmela Tania Prontera, Valeria Criscuolo, Alessandro Pezzella, Orlando Crescenzi, Michele Pavone, Marco d'Ischia

Dept. Chemical Sciences,
Univ. Napoli Federico II, Napoli, I-80126, Italy

Maria Grazia Maglione, Paolo Tassini, Carla Minarini

Lab. Nanomaterials and Devices,
ENEA C. R. Portici, Portici (Napoli), I-80055, Italy

Melanins, a two centuries long story

1840. BERZELIUS INTRODUCES FOR THE FIRST TIME THE TERM "MELANINS" FROM THE ANCIENT GREEK "MELANOS" TO INDICATE THE HUMAN DARK PIGMENT EXTRACTED FROM EYE MEMBRANES.

THE MELANIN KINGDOM

Nitrogenous Containing Melanins

Nitrogen-Free Melanins

Eumelanins
Black to dark brown, insoluble

Pheomelanins
Red-yellow, alkali -soluble

Allomelanins
Dark-brown, insoluble

Man

Mammals

Birds

Cephalopods

L-Tyrosine

5-S-Cysteinyldopa

5,6-Dihydroxyindole

Dopamine

Catechols

Homogentisic acid
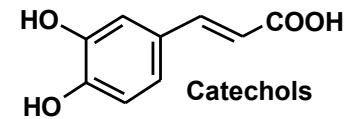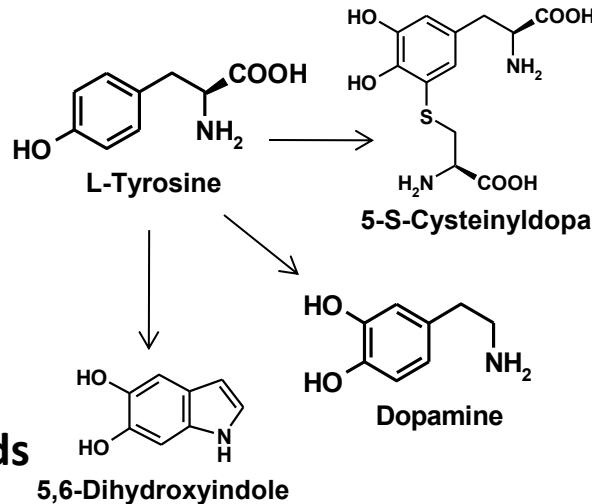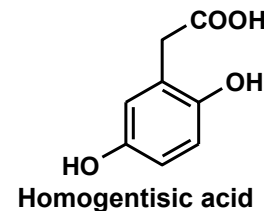
1,8-Dihydroxynaphthalene

Plants

Bacteria
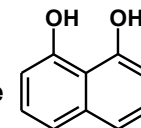
Fungi

Melanins: beyond pigmentation

Pigment Cell Melanoma Res. **21**; 192–199   ORIGINAL ARTICLE

The radioprotective properties of fungal melanin are a function of its chemical composition, stable radical presence and spatial arrangement

Ekaterina Dadachova[1]*, Ruth A. Bryan[1], Robertha C. Howell[1], Andrew D. Schweitzer[1], Philip Aisen[2], Joshua D. Nosanchuk[3,4] and Arturo Casadevall[4,3]
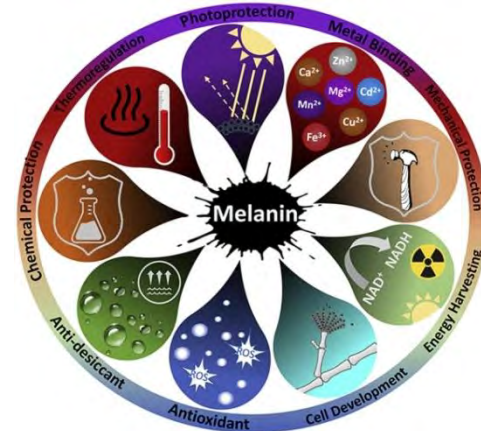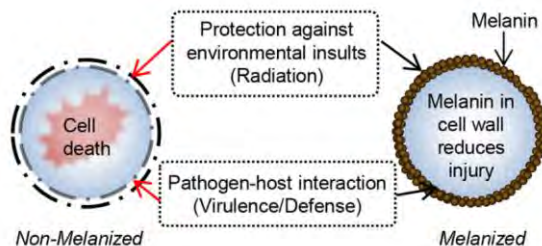
Chem. Rev. 2014, 114, 5057–5115   Review

pubs.acs.org/CR

Polydopamine and Its Derivative Materials: Synthesis and Promising Applications in Energy, Environmental, and Biomedical Fields

Yanlan Liu,[†,‡] Kelong Ai,[†] and Lehui Lu*[†]

Mater. Horiz., 2015, 2, 212

Stem cell-compatible eumelanin biointerface fabricated by chemically controlled solid state polymerization†

Alessandro Pezzella,*[a] Mario Barra,[b] Anna Musto,[cd] Angelica Navarra,[cd] Michela Alfè,[e] Paola Manini,[a] Silvia Parisi,[cd] Antonio Cassinese,[b] Valeria Criscuolo[a] and Marco d'Ischia[a]
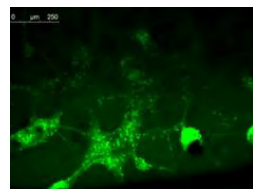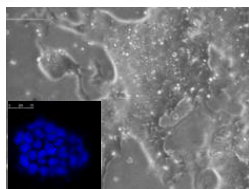
Eumelanin-coated plate before seeding

Undifferentiated embryonic stem cells grown for 2 days

Embryonic stem cells differentiated into neurons

ACS APPLIED MATERIALS & INTERFACES   Review

Cite This: ACS Appl. Mater. Interfaces 2018, 10, 7523–7540   www.acsami.org

Polydopamine Surface Chemistry: A Decade of Discovery

Ji Hyun Ryu,[†] Phillip B. Messersmith,*[‡,§] and Haeshin Lee*[‖,⊥]

MELANINS IN ORGANIC ELECTRONICS

Conducting Polymers

Science Vol. 183, 1974

JOHN MCGINNESS
PETER CORRY, PETER PROCTOR

Amorphous Semiconductor Switching in Melanins

Abstract. *Melanins produced synthetically and isolated from biological systems act as an amorphous semiconductor threshold switch. Switching occurs reversibly at potential gradients two to three orders of magnitude lower than reported for inorganic thin films, and comparable to gradients existing in some biological systems. Of a number of other biological materials tested, only cytochrome c acted similarly, but at the high potential gradients reported for thin film amorphous semiconductors.*

Nobel Prize in Chemistry in 2000 to Alan Heeger, Alan McDiarmid and Hideki Shirikawa

Alan G. MacDiarmid
Professor at the University of Pennsylvania, Philadelphia, USA

Hideki Shirakawa
Professor Emeritus, University of Tsukuba, Japan

Alan J. Heeger
Professor in the University of California at Santa Barbara, USA

CHEMISTRY OF MATERIALS Chem. Mater. 2015, 27, 436–442 Article pubs.acs.org/cm

Protonic and Electronic Transport in Hydrated Thin Films of the Pigment Eumelanin

Journal of Materials Chemistry C
Materials for optical, magnetic and electronic devices

Journal of Materials Chemistry B ROYAL SOCIETY OF CHEMISTRY

PAPER 2015, 3, 5070 View Article Online

Supplementing π-systems: eumelanin and graphene-like integration towards highly conductive materials for the mammalian cell culture bio-interface†
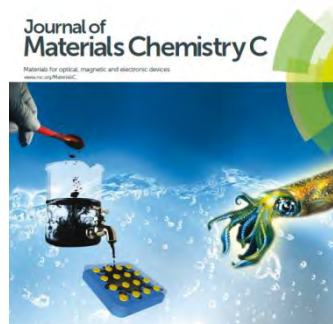
A water-soluble eumelanin polymer with typical polyelectrolyte behaviour by triethyleneglycol N-functionalization† **2015, 3, 2810**

Journal of Materials Chemistry B RSC Publishing

PAPER 2013, 1, 3843 View Article Online

Irreversible evolution of eumelanin redox states detected by an organic electrochemical transistor: en route to bioelectronics and biosensing

RSC Advances

PAPER 2015, 5, 56704 View Article Online

Boosting, probing and switching-off visible light-induced photocurrents in eumelanin-porous silicon hybrids

Eumelanin–PEDOT:PSS Complementing En Route to Mammalian-Pigment-Based Electrodes: Design and Fabrication of an ITO-Free Organic Light-Emitting Device **2017, 3, 1600342**

ADVANCED ELECTRONIC MATERIALS
www.advelectronicmat.de

BLACK-INSPIRED COLOURS
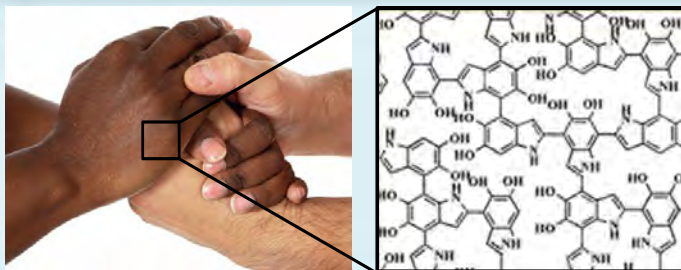
1. Selection of the melanin pigment
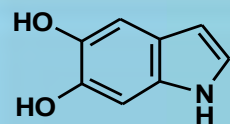
5,6-Dihydroxyindole
(DHI)

2. Identification of the monomer precursor

3. Chemical manipulation affording electroluminescent heterocyclic platforms
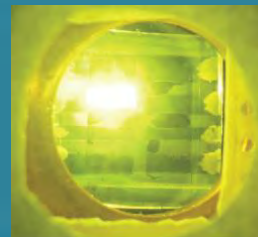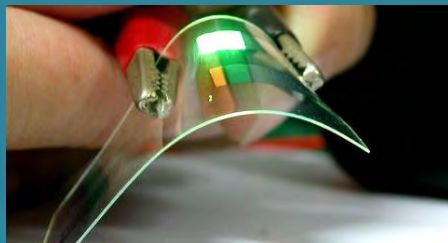
4. Device fabrication

5. Colour in OLEDs

THE OLED TECHNOLOGY

1879 Incandescent Lamp

1926 Fluorescent Lamp

1933 Halogen Lamp
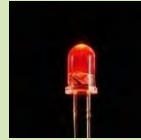
1962 First LED

1987 First OLED

The Solid State Lighting Era

ADVANTAGES
- Compatibility with different substrates
- Light, flat, flexible and large area devices
- Use of low-cost roll-to-roll and printing technologies
- Wide color tunability

Structure of an Organic Light Emitting Diode (OLED)

Cathode
EIL
HBL
EL
HIL
Anode
Substrate
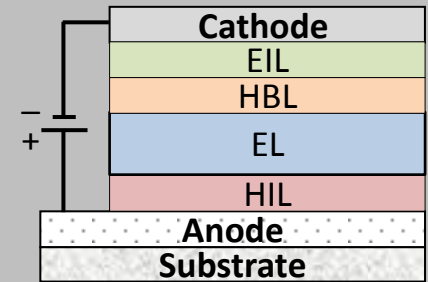
Lumiblade OLED Philips lighting

The Swarm - Audi
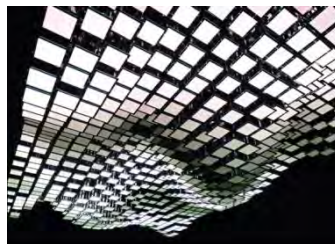
WHITEvoid living sculpture Philips

Blushing Dress Philips

OLED TV - Samsung

Pulse oximetry sensor Covidien

Flexible plastic substrate
Red OLED
Green OLED
OPD

RESEARCH ON OLEDs : MAIN GOALS

Efficient electroluminescent materials

Types of emitting materials

Fluorescene material Internal quantum efficiency ~25%

Phosphorescence material Internal quantum efficiency ~100%

Thermally activated delayed fluorescence material Internal quantum efficiency ~100%

Design of new device functioning
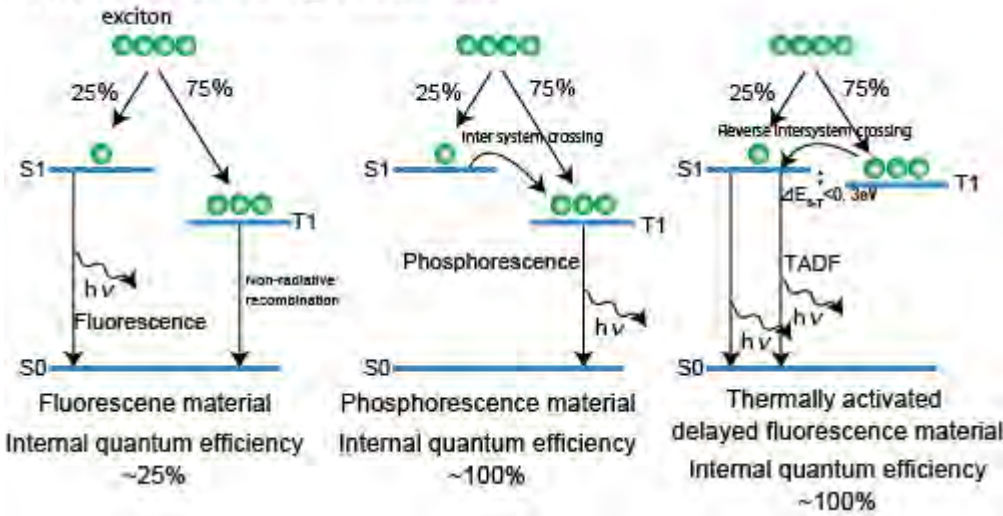
Transparent OLED

Active Matrix OLED (AMOLED)
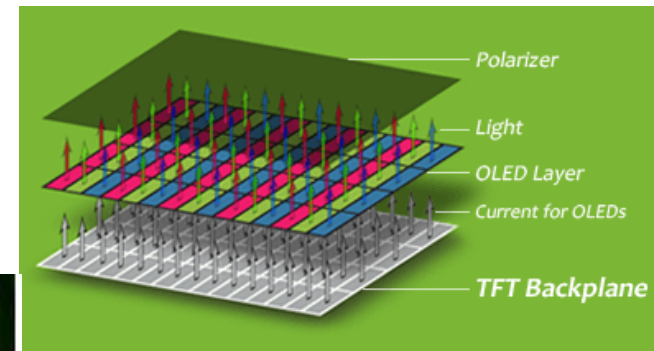
Design of new shapes of the device
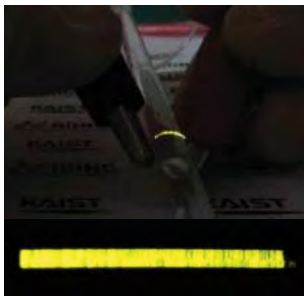
Fiber-coated OLED **Fiber-encapsulated OLED** **Nanopatterned OLED**
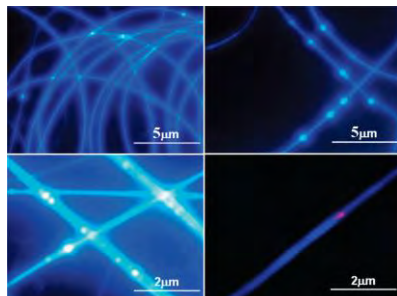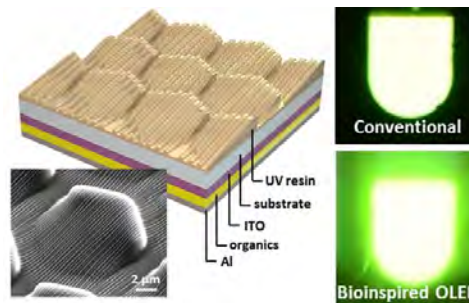
The Oxidative Reactivity of 5,6-Dihydroxyindole Under Acidic Conditions

2,7'-dimer

Tetramer

EUMELANINS

5,6-Dihydroxyindole (DHI)

Neutral pH

Acid pH

2,3'-dimer

Symmetrical

Asymmetrical

TRIAZATRUXENES

J. Org. Chem. **1998**, *63*, 7002

MELANIN – INSPIRED TRIAZATRUXENES

R = -CH$_3$, 5,6-Dimethoxyindole
R = -Bn, 5,6-Dibenzyloxyindole

R' = n-C$_{11}$H$_{23}$
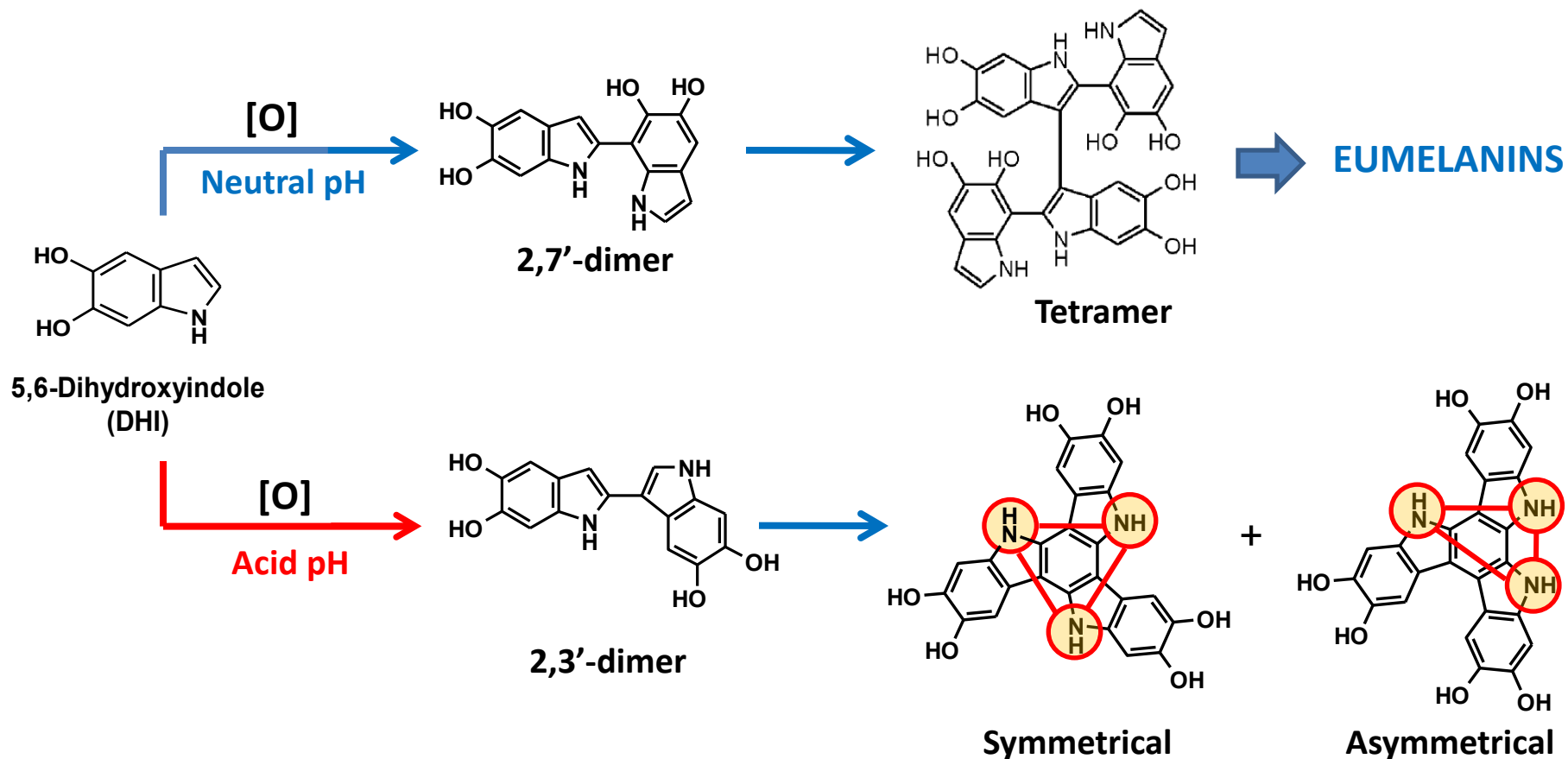
J. Org. Chem. **1998**, *63*, 7002
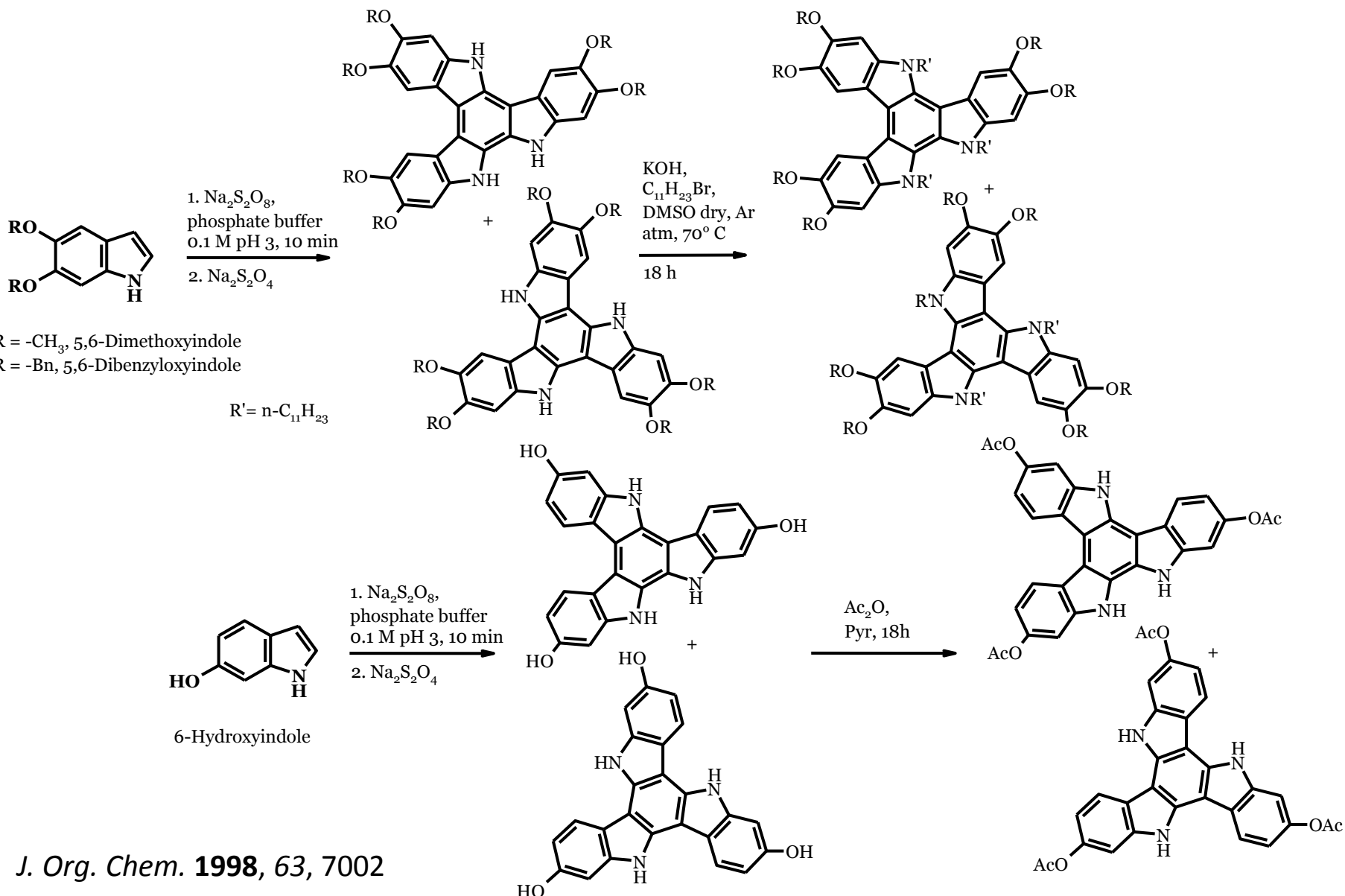
TRIAZATRUXENES: PROPERTIES AND APPLICATIONS
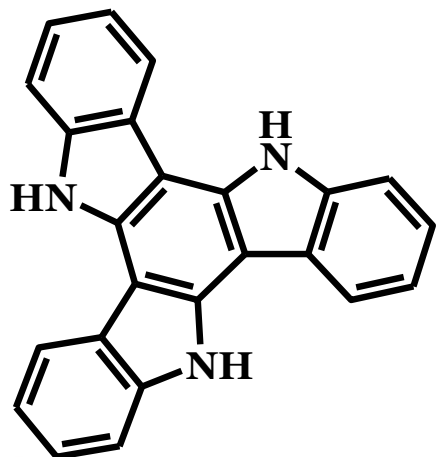
- Good charge mobility
- Reversible redox process
- Amorphous thin films
- Supramolecular aggregates thanks to π-stacking interactions

Solar cells

Journal of Materials Chemistry C

REVIEW

View Article Online
View Journal | View Issue

CrossMark

Triazatruxene-based materials for organic electronics and optoelectronics

Cite this: *J. Mater. Chem. C*, 2016, 4, 10574

Xiang-Chun Li,[a] Chun-Yu Wang,[a] Wen-Yong Lai[*ab] and Wei Huang[ab]
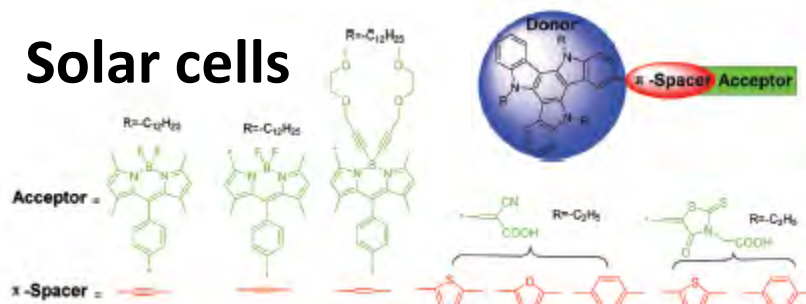
Liquid crystals
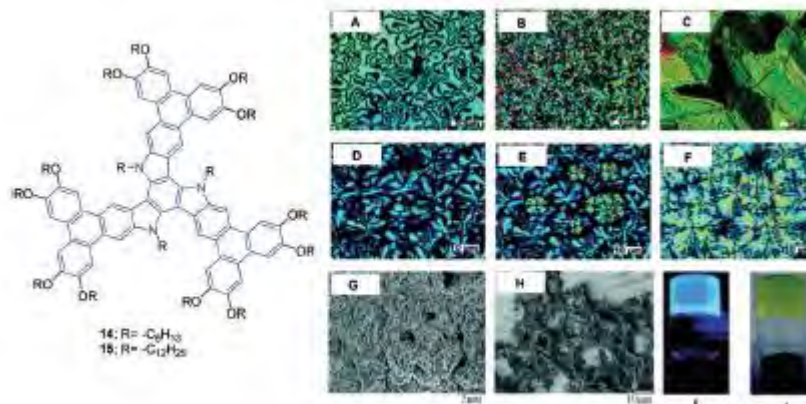
Hole transporting materials
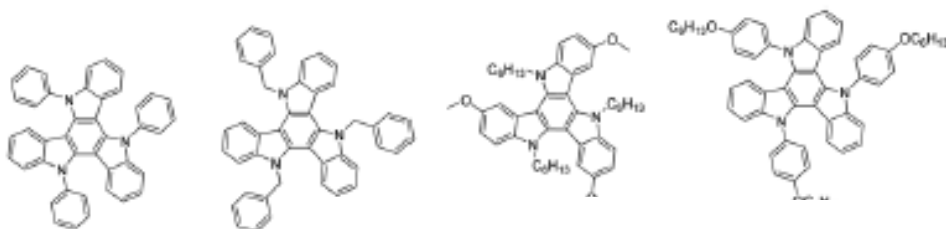
14: R= -C$_6$H$_{13}$
15: R= -C$_{12}$H$_{25}$

Photo-Physical properties of Symmetrical and Asymmetrical Triazatruxenes

Absorption and fluorescence in DMSO

Sym **Asym**

Legend:
- 1a_Abs
- 1a_PL
- 2a_Abs
- 2a_PL
- 1b_Abs
- 1b_PL
- 2b_Abs
- 2b_PL
- 1c_Abs
- 1c_PL
- 2c_Abs
- 2c_PL
- 1d_Abs
- 1d_PL
- 2d_Abs
- 2d_PL

Absorption and fluorescence as thin films

Sym **Asym**

Legend:
- 1a_Abs
- 1a_PL
- 2a_Abs
- 2a_PL
- 1b_Abs
- 1b_PL
- 2b_Abs
- 2b_PL
- 1d_Abs
- 1d_PL
- 2d_Abs
- 2d_PL
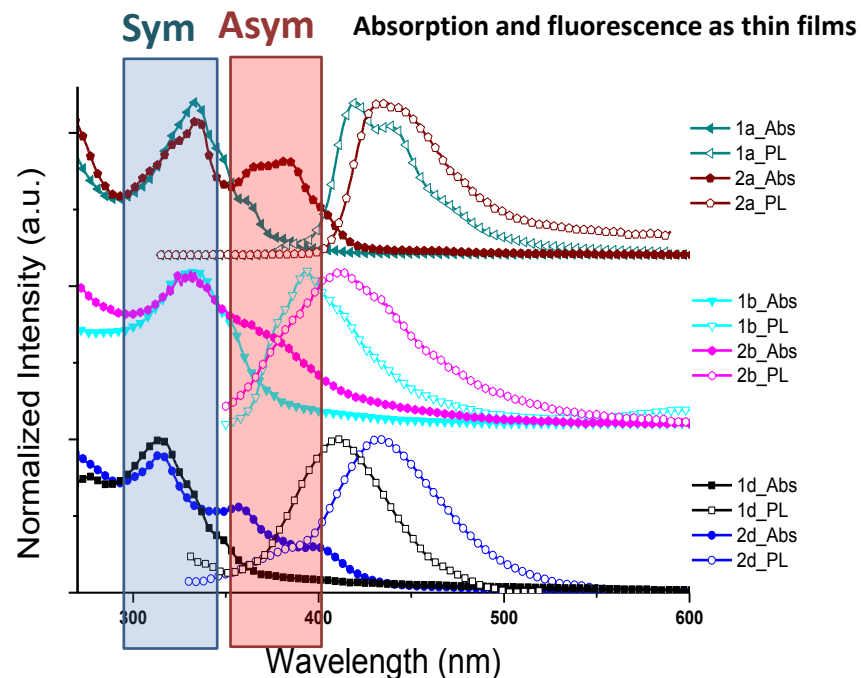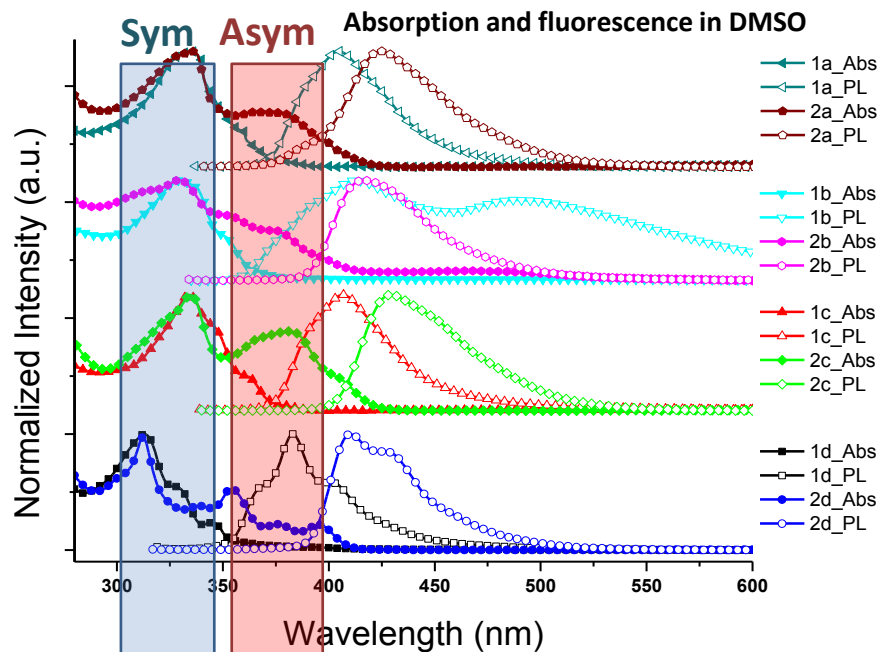
- Asymmetrical series show more complex absorption profiles
- Absorption and emission maxima of asymmetrical isomers are shifted at higher wavelenghts
- Lower E_g^{opt} for the asymmetrical series
- Asymmetrical isomers showed higher fluorescence quantum yields

Series	Φ (%) *	
	Sym	**Asym**
a diMeO	19	28
b diBnO/NH	-	20
c diBnO/NC11	2	41
d 6-OH	12	39

*referred to quinine sulphate in 0.5 M H_2SO_4 ($\Phi = 0.546$)

ELECTRONIC PROPERTIES OF SYMMETRICAL AND ASYMMETRICAL TRIAZATRUXENES

Symmetrical

HOMO-LUMO gap 4.37 eV
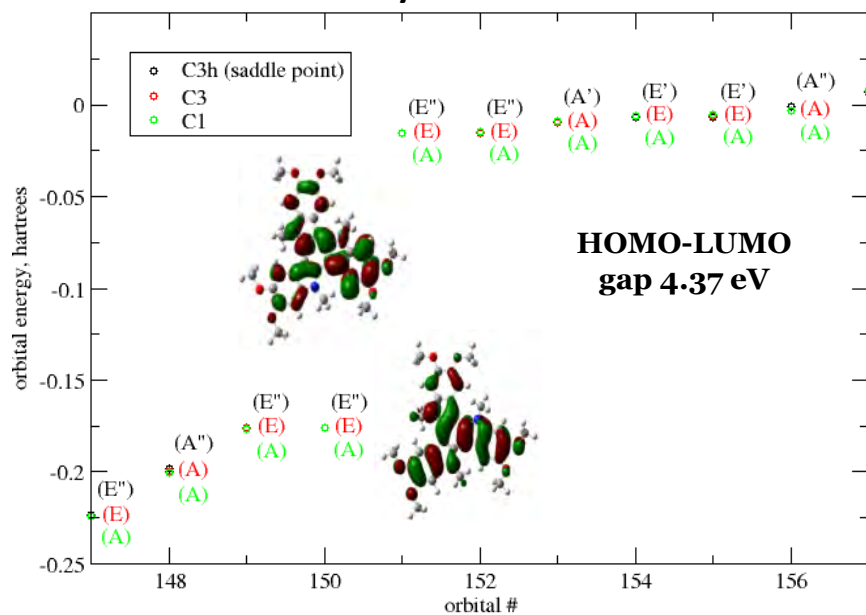
Asymmetrical

HOMO-LUMO gap 3.98 eV

TD DFT calculation showed for asymmetrical triazatruxenes a lower HOMO-LUMO gap

Thin Film Morphology and Self-Assembly Behaviour in Solution

AFM

Asym

Asym

Sym

Sym

^{1}H NMR tritration

c=1.3 mM; c=3 mM; c=10 mM
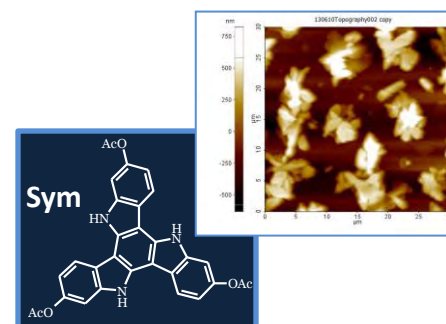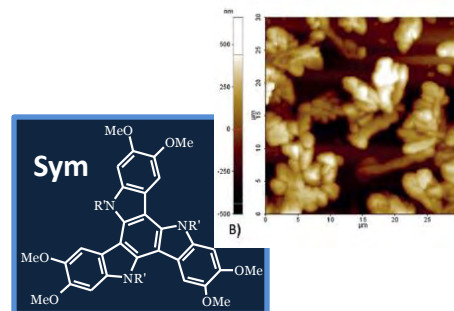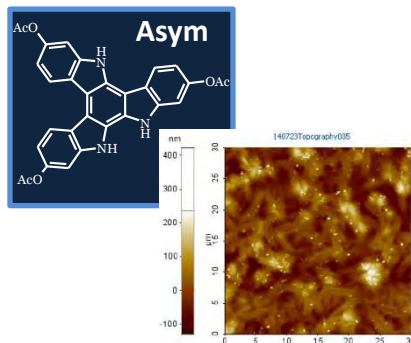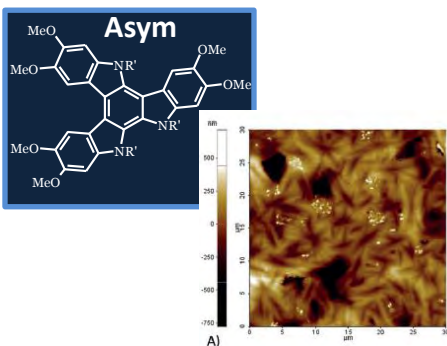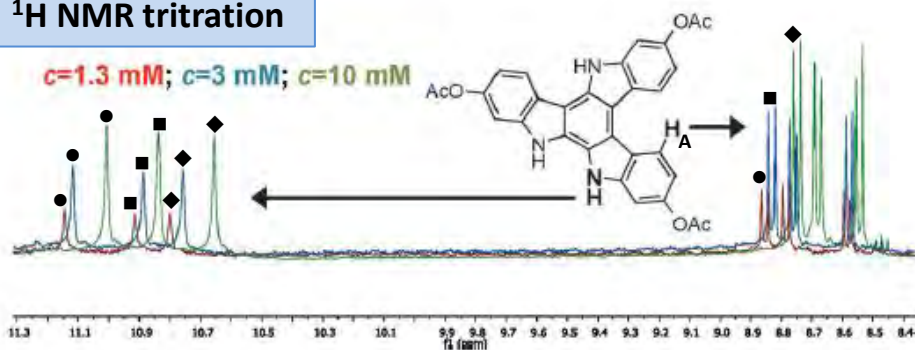
The lack of symmetry in the TAT backbone drives more efficient aggregating interactions

-NH

$\Delta\delta$ = 14.1%

$\Delta\delta$ = 22.0%

$\Delta\delta$ = 28.9%

δ (ppm)

c (mM)

H$_A$

$\Delta\delta$ = 11.0%

$\Delta\delta$ = 10.9%

$\Delta\delta$ = 4.0%

δ (ppm)

c (mM)
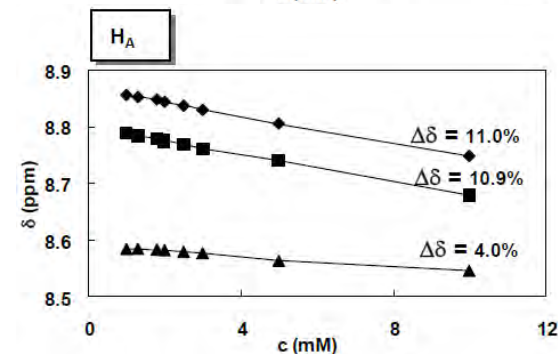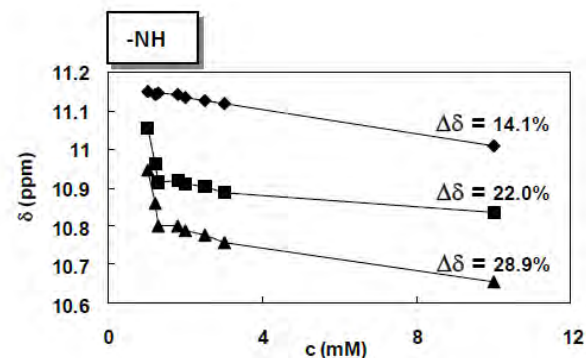
OLED DEVICES WITH ASYMMETRICAL TRIAZATRUXENES

Device configuration

THICKNESSES OF LAYERS

Calcium 20 nm
Aluminum 80 nm
Alq$_3$ 10 nm
BCP 9 nm
ATAT-PVK (5% w/w) 20 nm
PEDOT:PSS 40 nm
ITO 200 nm

R = n-C$_{11}$H$_{23}$

Electroluminescence spectra

- 2a 10% in PVK
- 2a 5% in PVK
- 2a 2% in PVK
- PVK

ATAT
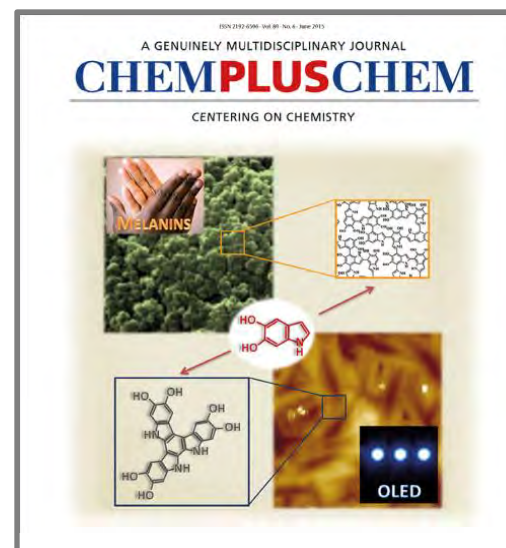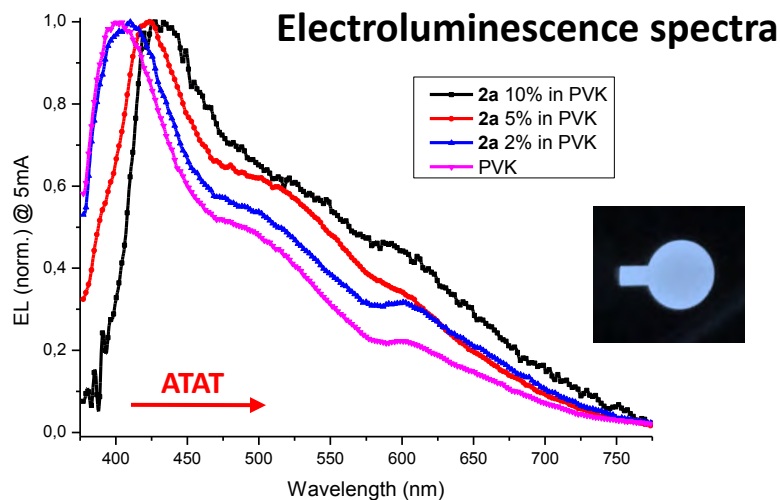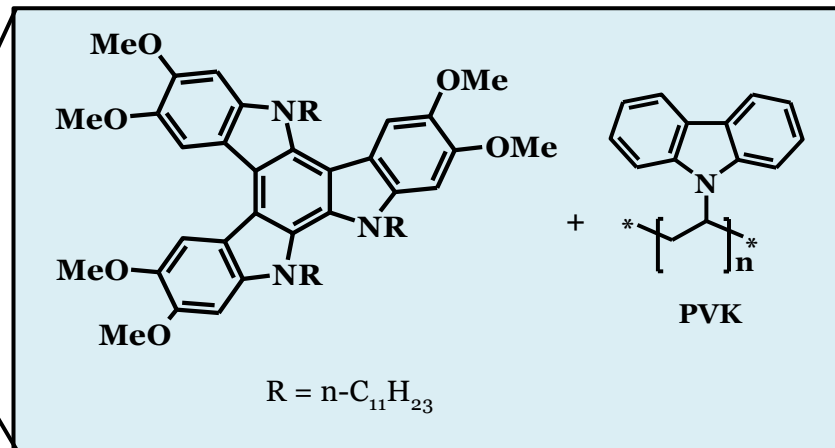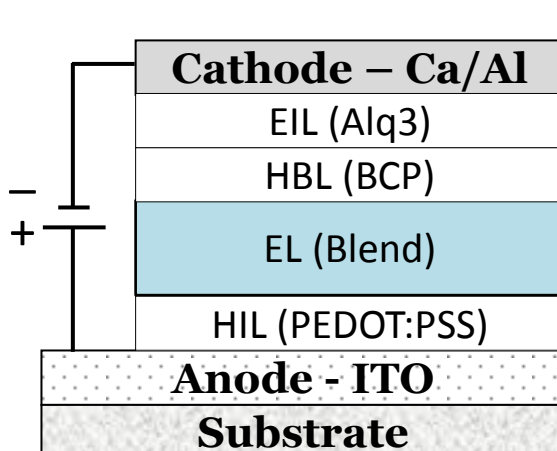
ChemPlusChem **2015**, *80*, 919

TRANSITION METAL COMPLEXES IN OPTOELECTRONIC DEVICES

Chem Soc Rev

Chemical Society Reviews
www.rsc.org/chemsocrev

ISSN 0306-0012
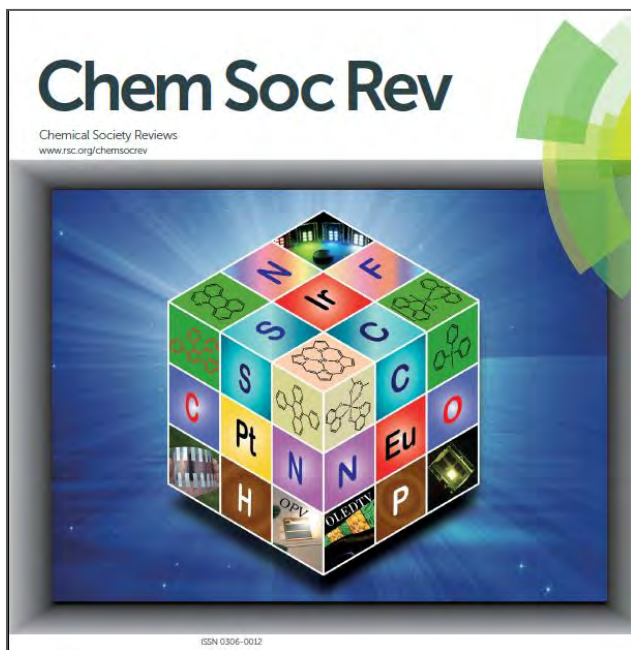
Recent progress in metal–organic complexes for optoelectronic applications

Hui Xu,*[ab] Runfeng Chen,[bc] Qiang Sun,[b] Wenyong Lai,[c] Qianqian Su,[b] Wei Huang*[cd] and Xiaogang Liu*[be]

Volume 43 | Number 10 | 21 May 2014 | Pages 3207–3812
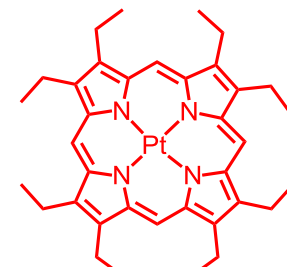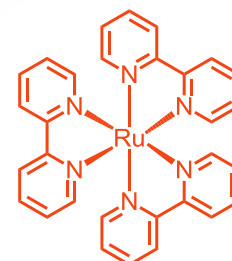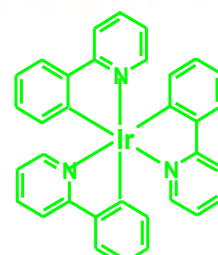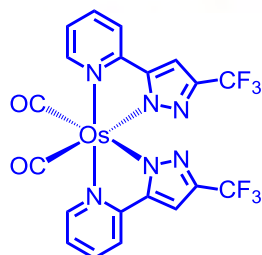
Dye-sensitised solar cells (DSSCs)
Ecole Polytechnique Federal de Lausanne
SwissTech Convention Center
Daniel Schlaepfer e Catherine Bolle

Organic Light Emitting Diodes (OLEDs)
Flying Ribbon I
Aldo Cibic - Blackbody

MAIN PROPERTIES OF IRIDIUM COMPLEXES OF RELEVANCE FOR OPTOELECTRONICS

- Electronic layout enabling spin orbit coupling
- Phosphorescent emissions associated with high Φ_{ph} and short τ_T
- Tunable photo-physical properties
- Stable and accessible redox states

Melanin – inspired iridium(III) complexes

M = Ir,   X = C
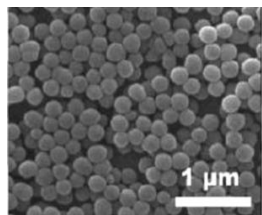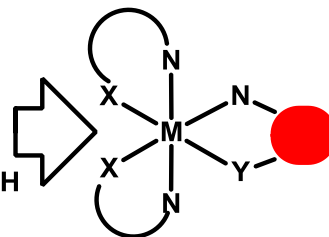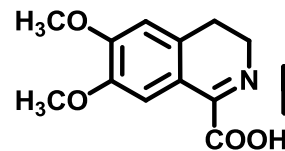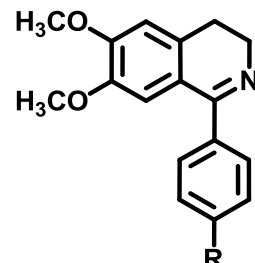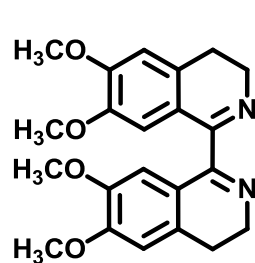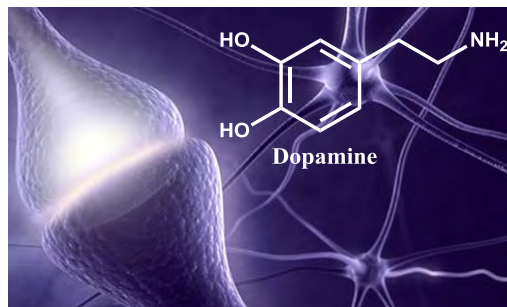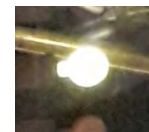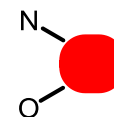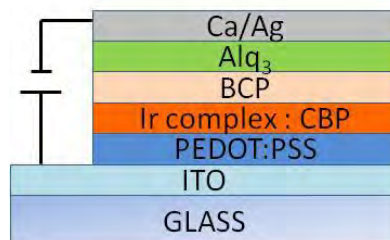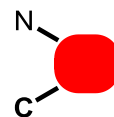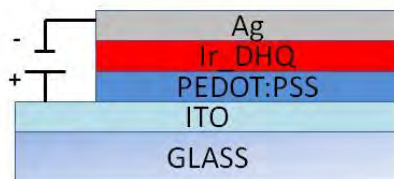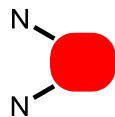
Dopamine– inspired (3,4-dihydro)isoquinoline ligands
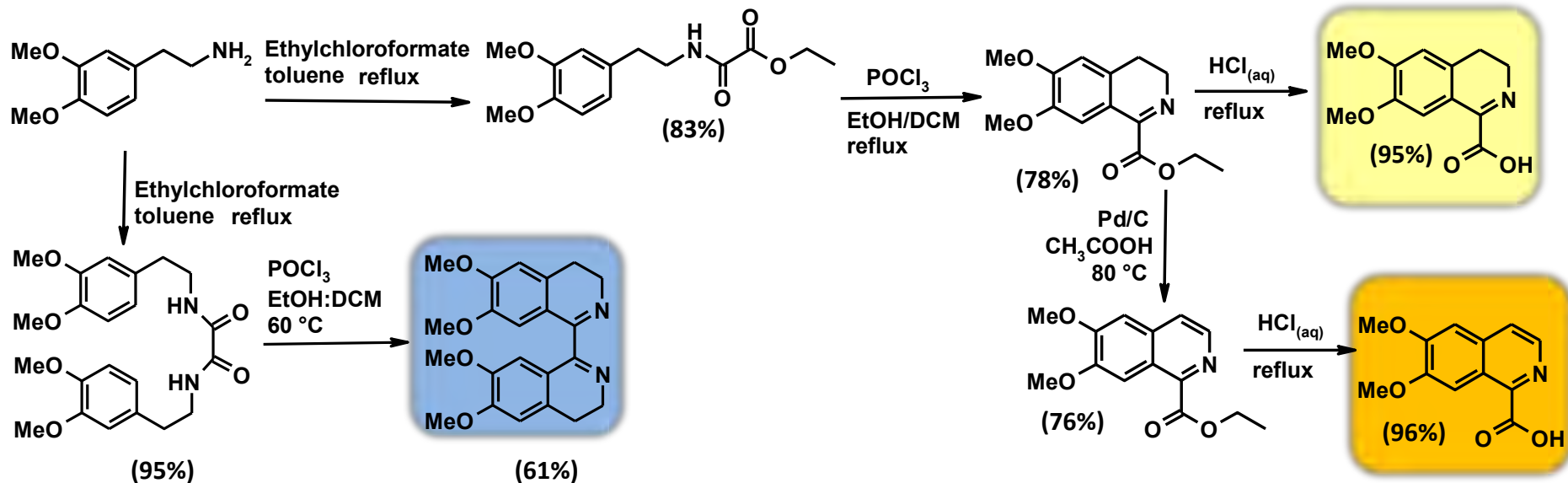
Synthesis of iridium complexes with C^N ligands

R = H   Ir_PHQ_1   (16%)
R = F   Ir_FPHQ_1   (59%)
R = OMe   Ir_OMePHQ_1 (16%)
R = CN   Ir_CNPHQ_1   (22%)

R = H   Ir_PHQ_2   (14%)
R = F   Ir_FPHQ_2   (21%)
R = OMe   Ir_OMePHQ_2 (11%)
R = CN   Ir_CNPHQ_2   (15%)

R = H   Ir_PHQ_3   (5%)
R = F   Ir_FPHQ_3   (6%)
R = OMe   Ir_OMePHQ_3 (6%)
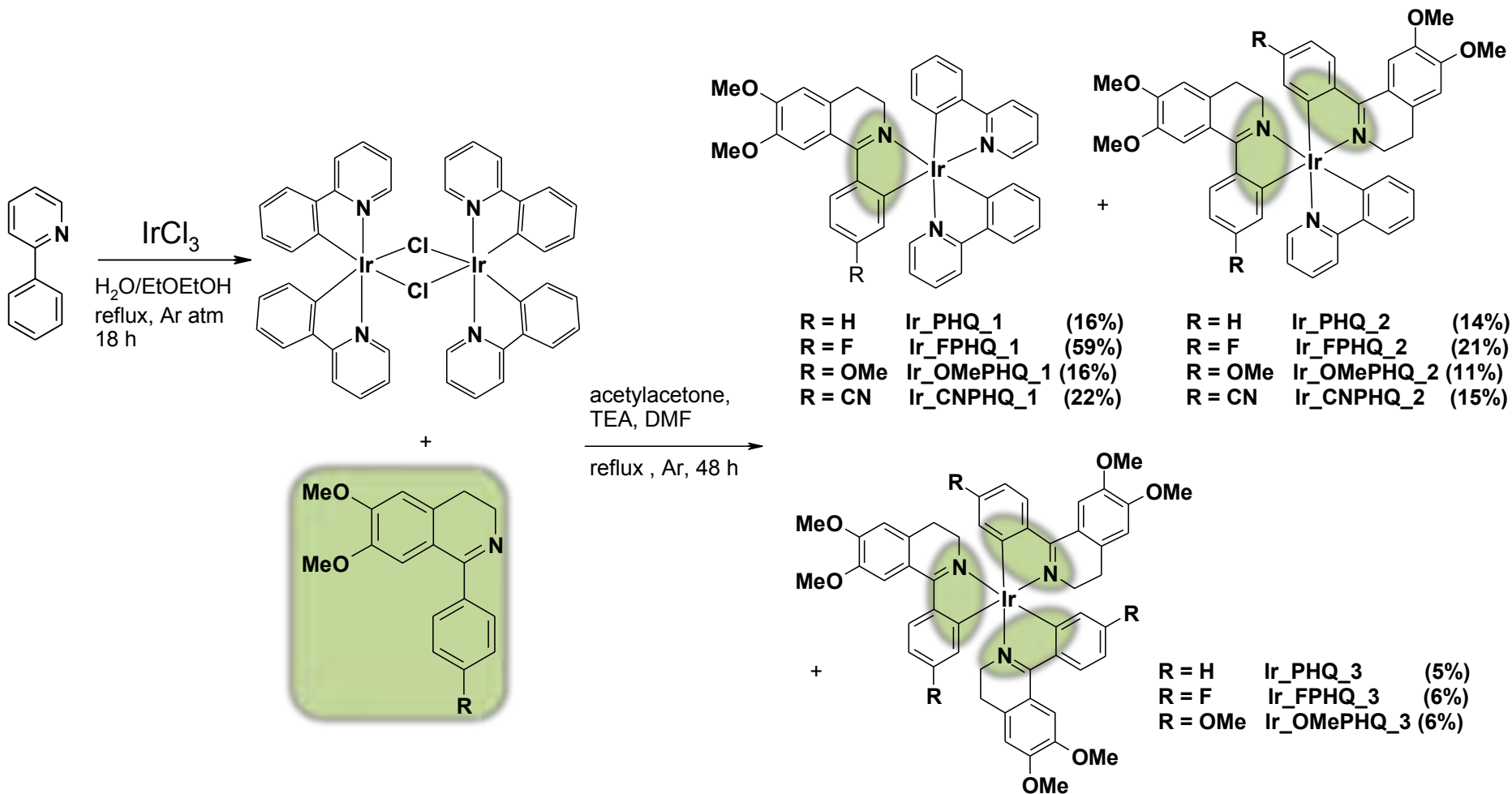
Photo-Physical properties of the Iridium complexes : the ligand effect

Ir(ppy)₂PhQ

Irppy(PhQ)₂

Ir(PhQ)₃
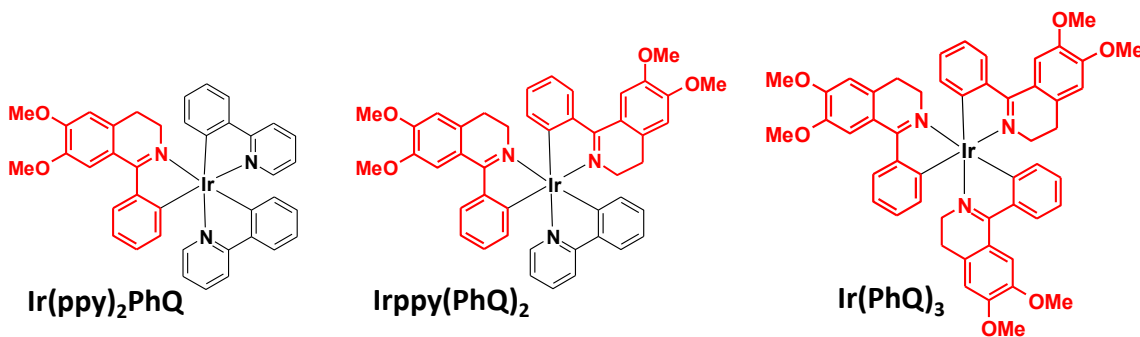
Emission spectra registered in dilute DCM solutions

Absorption spectra registered in dilute DCM solutions
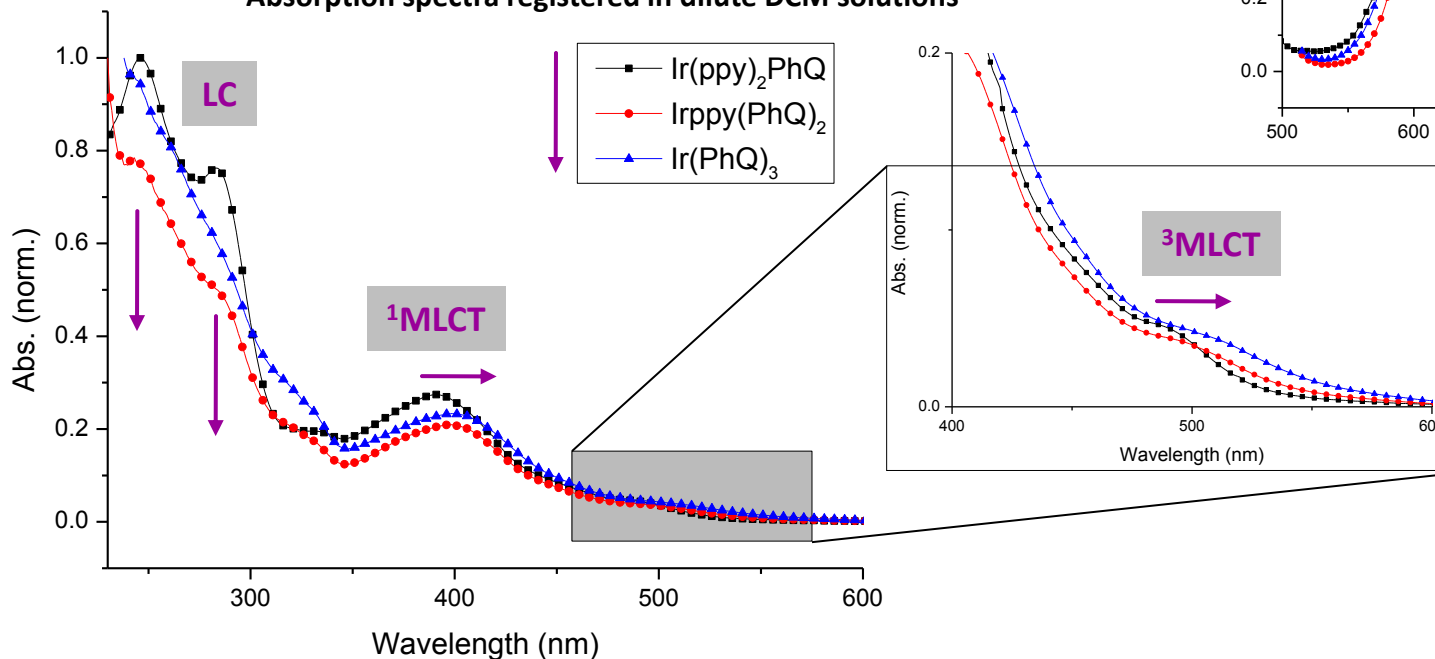
LC

¹MLCT

³MLCT

PHOTO-PHYSICAL PROPERTIES OF THE IRIDIUM COMPLEXES : THE SUBSTITUENT EFFECT

Absorption spectra registered in dilute DCM solutions
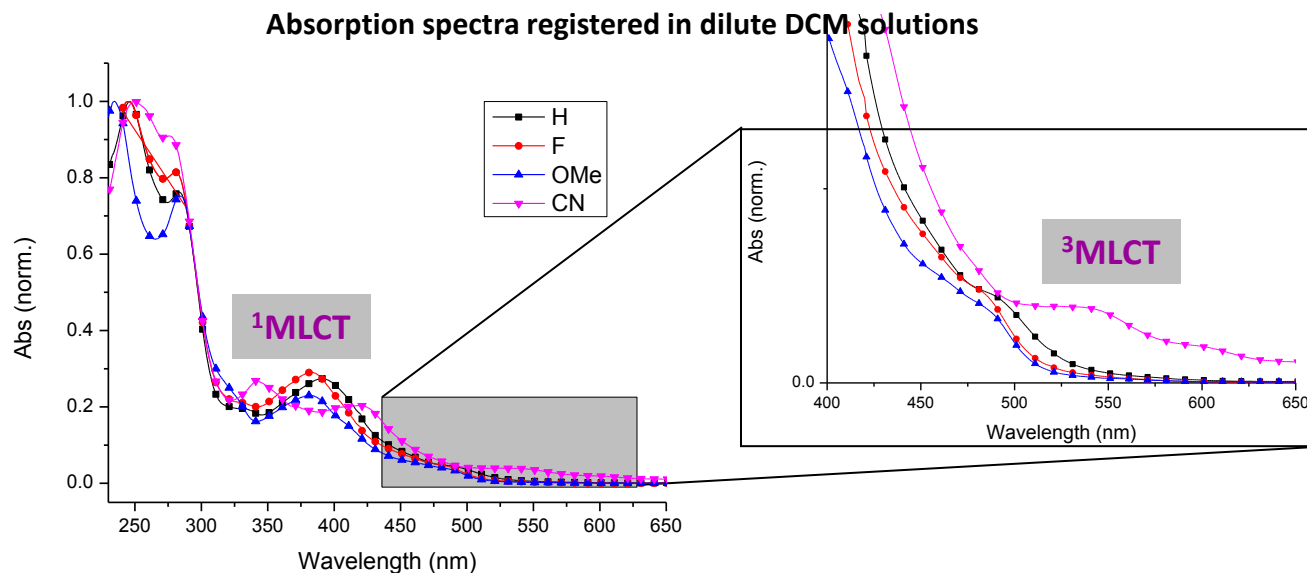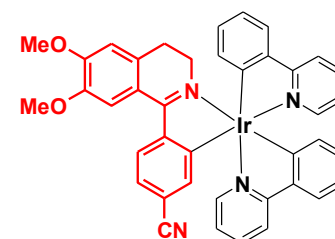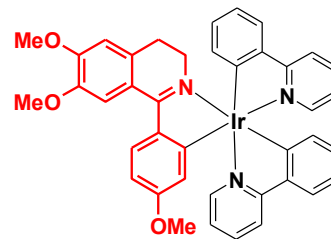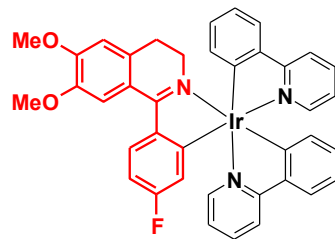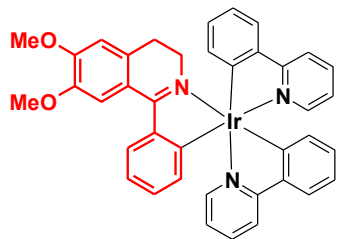
PHOTO-PHYSICAL PROPERTIES OF THE IRIDIUM COMPLEXES : THE SUBSTITUENT EFFECT
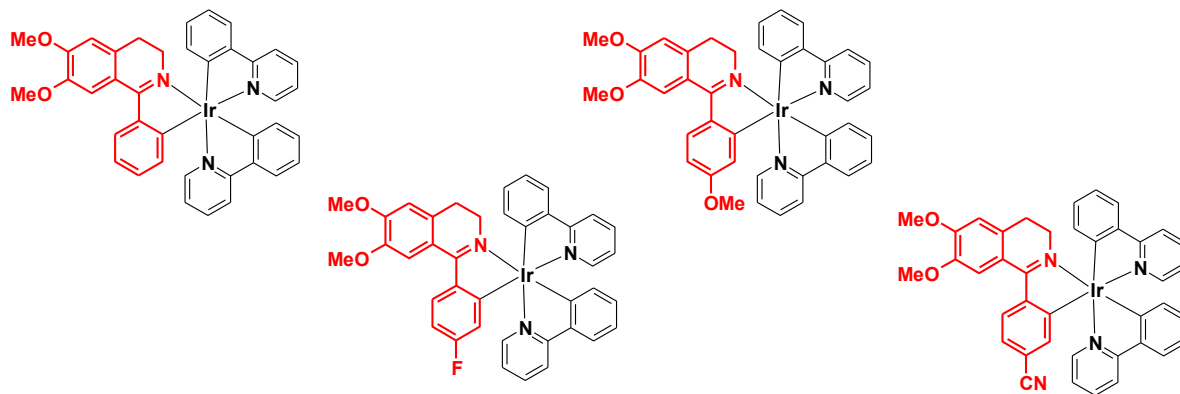
Emission spectra registered in dilute DCM solutions
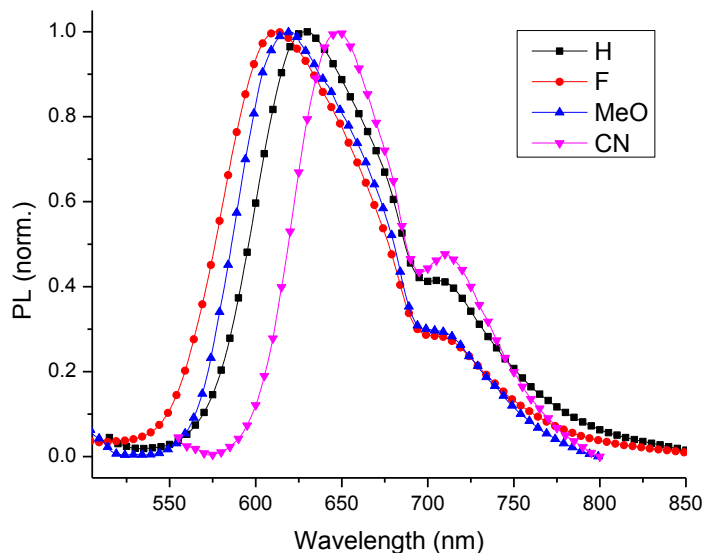
Compound	Φ (λ_em, nm)	Φ (λ_em, nm) no O₂
Ir(ppy)₂PHQ	0.41%	0.30%
Irppy(PHQ)₂	0.14%	0.26%
Ir(PHQ)₃	0.18%	0.23%
Ir(ppy)₂FPHQ	0.24%	0.70%
Irppy(FPHQ)₂	0.15%	0.40%
Ir(FPHQ)₃	0.19%	0.22%
Ir(ppy)₂MeOPHQ	0.21%	0.61%
Irppy(MeOPHQ)₂	0.15%	0.23%
Ir(MeOPHQ)₃	0.13%	0.19%
Ir(ppy)₂CNPHQ	0.11%	0.14%
Irppy(CNPHQ)₂	0.14%	0.15%

Φ determined relatively to fluorescein
(Φ = 0.9 in 0.1 M solution of NaOH)

PHOTO-PHYSICAL PROPERTIES OF THE IRIDIUM COMPLEXES : THE SUBSTITUENT EFFECT

Ir(ppy)$_2$PhQ — E_g^{opt} (eV) vs Hammett constant σ — $R^2 = 0.961$

Irppy(PhQ)$_2$ — E_g^{opt} (eV) vs Hammett constant σ — $R^2 = 0.968$

Ir(ppy)$_2$PhQ — Emission energy (eV) vs Hammett constant σ — $R^2 = 0.985$

Irppy(PhQ)$_2$ — Emission energy (eV) vs Hammett constant σ — $R^2 = 0.949$
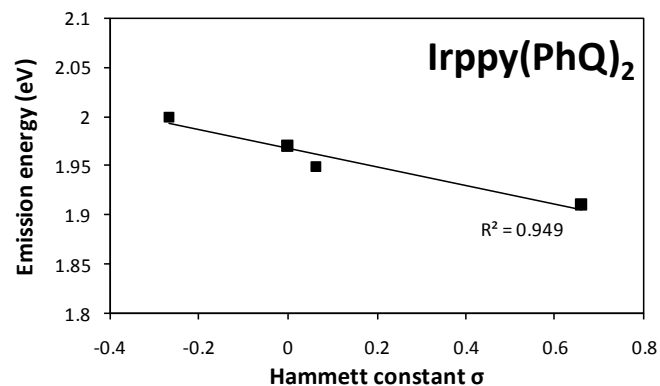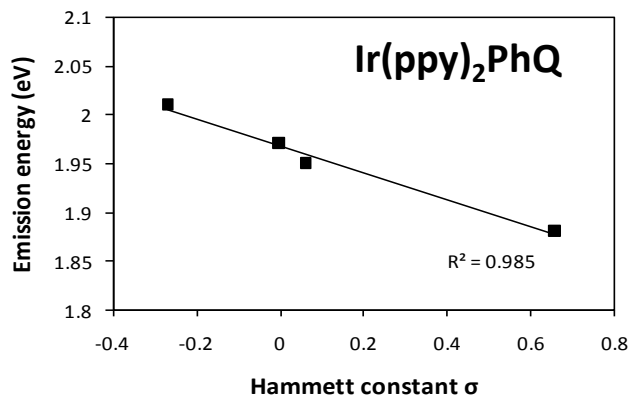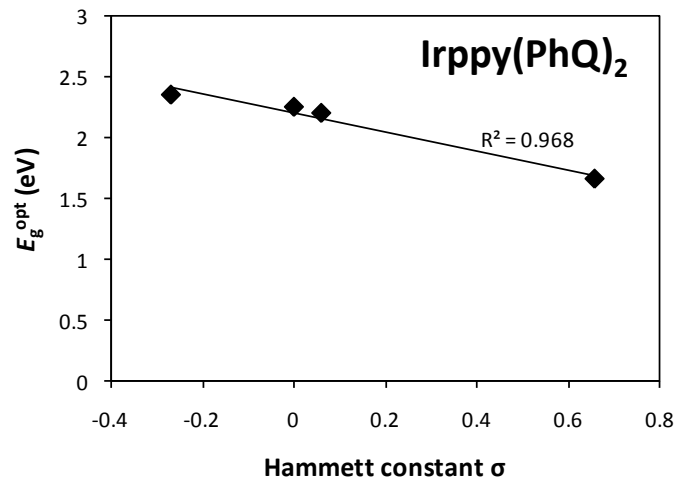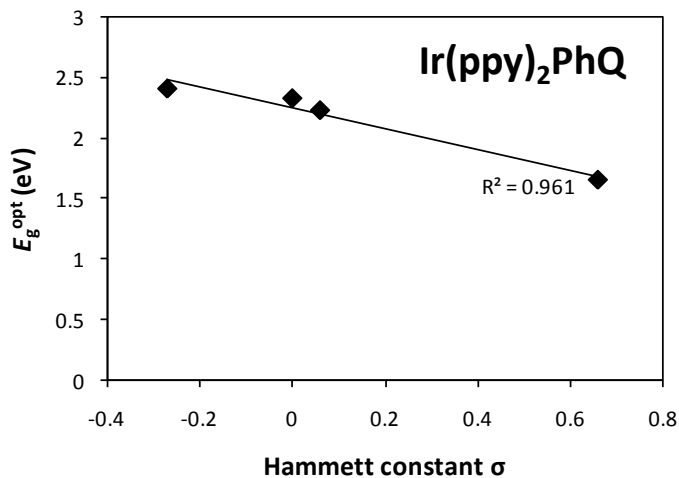
Electron releasing groups σ < 0

Electron withdrawing groups σ > 0

FABRICATION OF OLED DEVICES
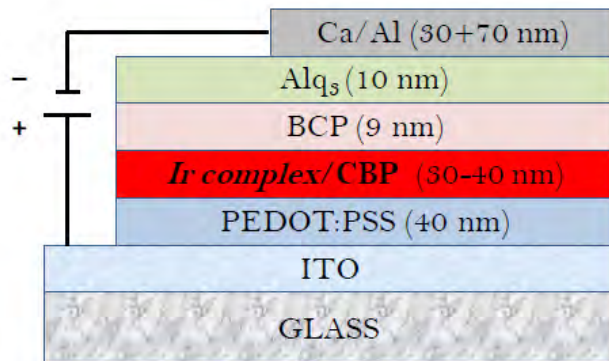
Structure of the OLED device

Ca/Al (30+70 nm)
Alq₃ (10 nm)
BCP (9 nm)
Ir complex/CBP (30-40 nm)
PEDOT:PSS (40 nm)
ITO
GLASS

•**Blends of the iridium complex (2, 6 or 12 %) in CBP**
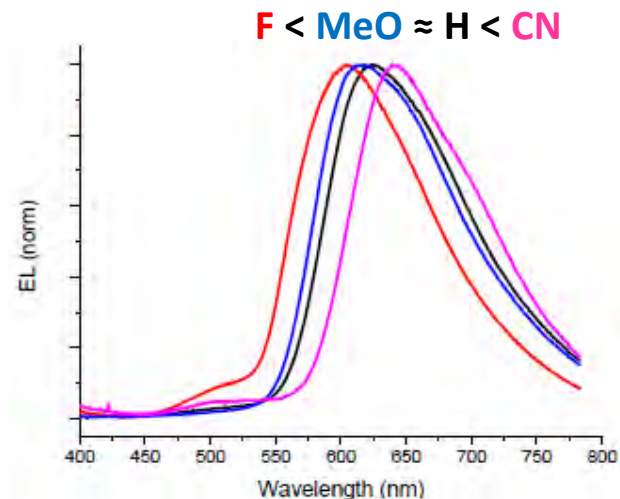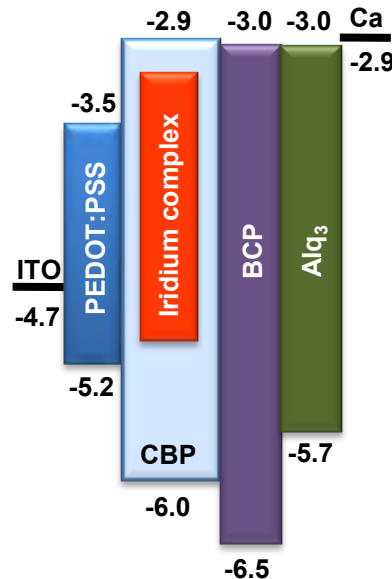
- Best performances with 2% Ir complex.
- Highest luminances: **1092 cd/m²** with Irppy(FPHQ)$_2$ and **2474 cd/m²** with Ir(ppy)$_2$MeOPHQ.
- Substituent effect on the emission maximum is F→OMe→H→CN (from 580 with F to 640 with CN).

F < MeO ≈ H < CN

$Ir(ppy)_x(PhQ)_y$

IrFPHQ devices | IrOMePHQ devices | IrPHQ devices | IrCNPHQ devices

y : 1 → 3

$Ir(ppy)_2(X)PhQ$

Synthesis of iridium complexes with N^N ligands

1. DCM/MeOH, reflux, 45min
2. NH4PF6

PF6−

Ir_DHQ
(65%)
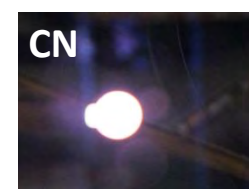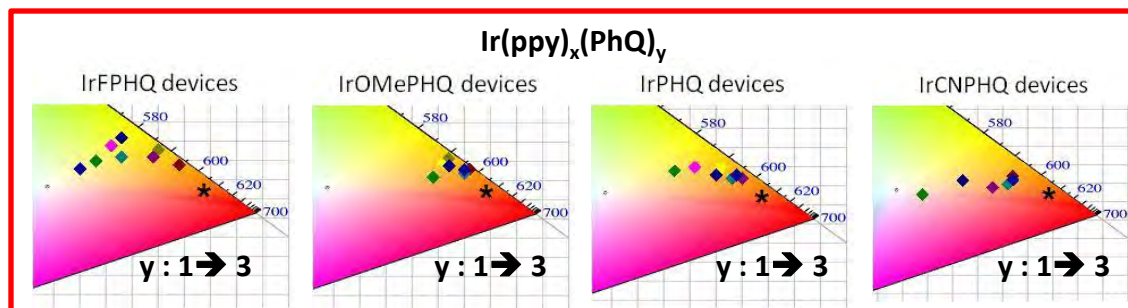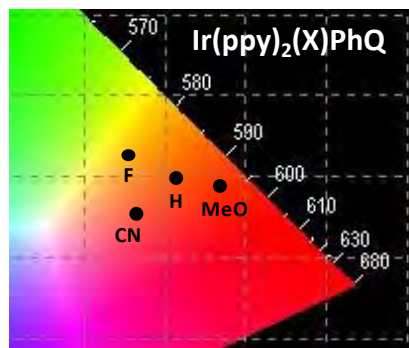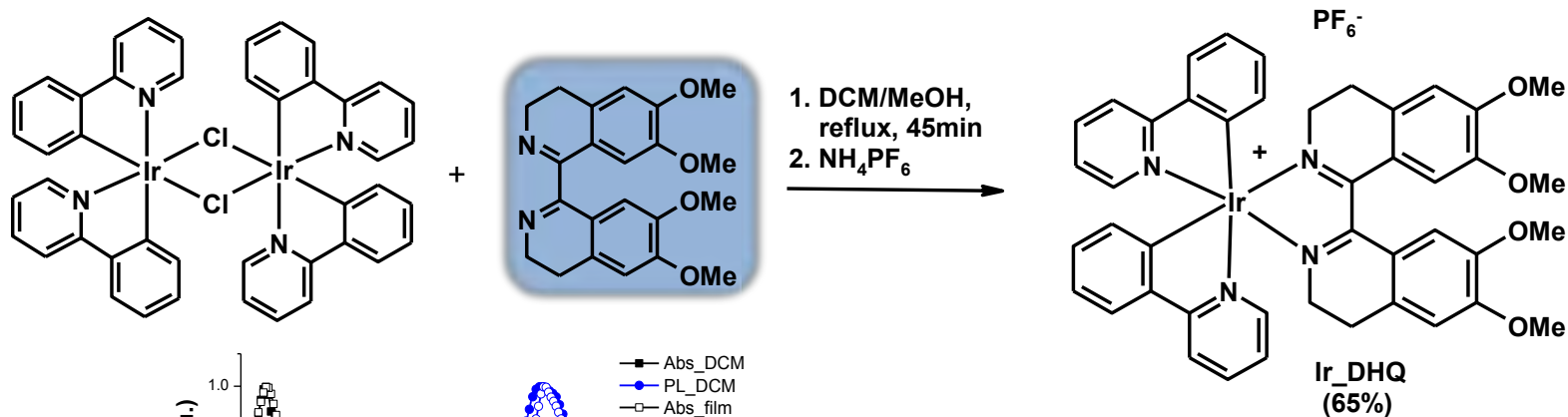
Unusual *cis* arrangement of the ppy units
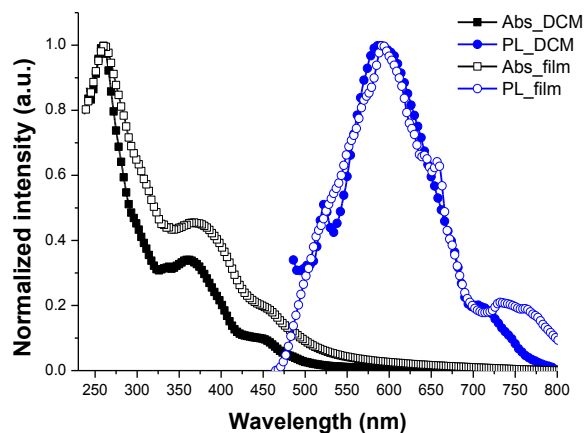
Experimental PL spectrum (442nm pump)
Peak1 (E3)
Peak2 (E2)

1H NMR

Pump @ 442 nm

T = 9K

SYNTHESIS OF IRIDIUM COMPLEXES WITH N^N LIGANDS

PF_6^-

Ir_DHQ

OMe
OMe
OMe
OMe

IONIC LIQUID (IL)

Dimethylimidazolium dimethylphosphate (DMIDMP)
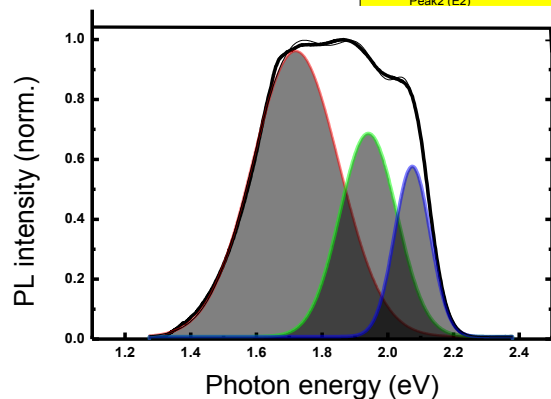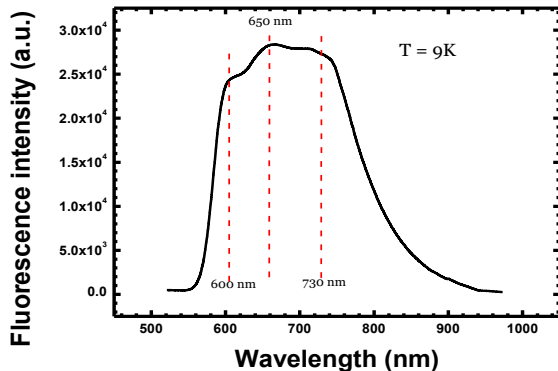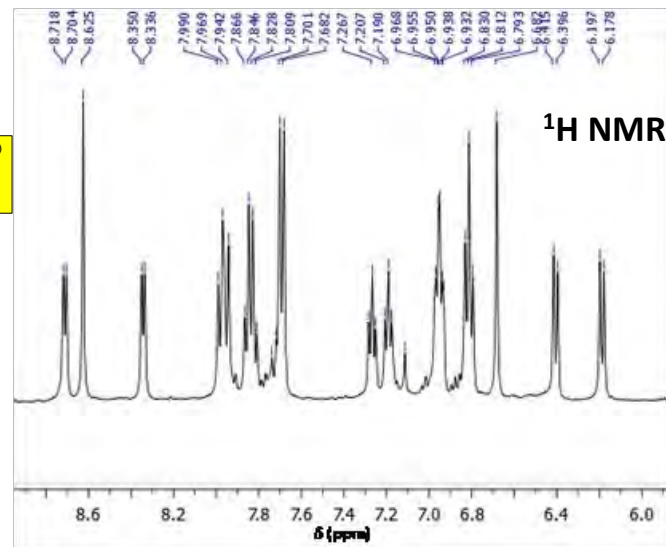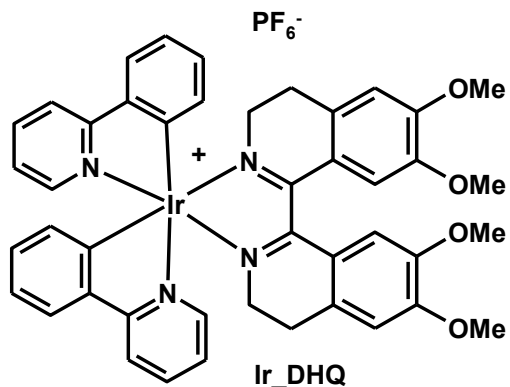
Device #	Configuration	L_{max}^a (cd/m^2)	Efficacy$_{max}^a$ (cd/A)	Power efficiency$_{max}^a$ (lm/W)	t_{on}^b (min)	EL^c λ_{max} (nm)	CIE (x,y)
1	ITO/PEDOT:PSS/cis-**1** (50nm)/Ca/Al	2.9	2.0×10^{-3}	8.3×10^{-4}	19	660	(0.63, 0.36)
2	ITO/PEDOT:PSS/cis-**1** (100nm)/Ca/Al	1.9	2.7×10^{-3}	9.1×10^{-4}	30	668	(0.60, 0.38)
3	ITO/PEDOT:PSS/cis-**1** (50nm)/Ag	13.1	6.5×10^{-3}	3.0×10^{-3}	10	657	(0.61, 0.38)
4	ITO/PEDOT:PSS/cis-**1** (100nm)/Ag	62.9	2.3×10^{-2}	5.2×10^{-3}	40	662	(0.63, 0.37)
5	ITO/PEDOT:PSS/cis-**1** : DMI-DMP (2:1)^d/Ca/Al	5.5	1.1×10^{-2}	4.9×10^{-3}	7	653	(0.62, 0.37)
6	ITO/PEDOT:PSS/cis-**1** : DMI-DMP (1:2)^d/Ag	20.1	1.7×10^{-2}	2.2×10^{-3}	19	633	(0.56, 0.43)
7	ITO/PEDOT:PSS/cis-**1** : DMI-DMP (2:1)^d/Ag	162.2	11.0×10^{-2}	5.7×10^{-2}	30	645	(0.61, 0.39)
8	ITO/PEDOT:PSS/cis-**1** : DMI-DMP (4:1)^d/Ag	70.3	2.7×10^{-2}	5.1×10^{-3}	43	677	(0.63, 0.37)
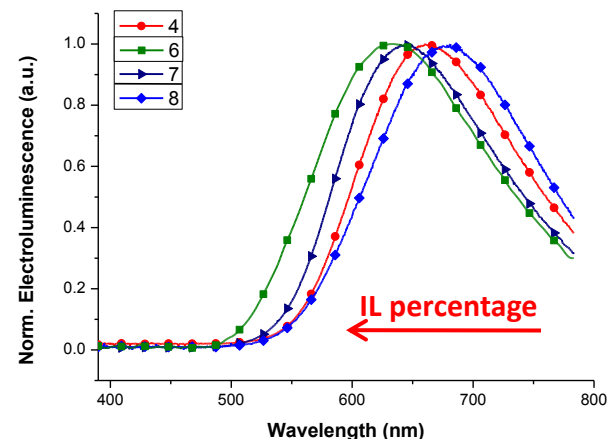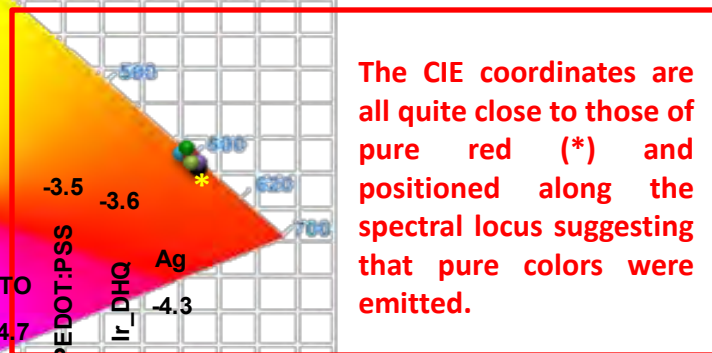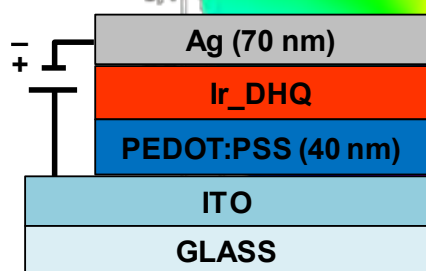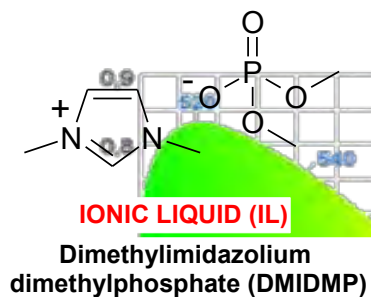
Ag (70 nm)
Ir_DHQ
PEDOT:PSS (40 nm)
ITO
GLASS

-3.5   -3.6

ITO   PEDOT:PSS   Ir_DHQ   Ag   -4.3

-4.7

-5.2   -5.3

The CIE coordinates are all quite close to those of pure red (*) and positioned along the spectral locus suggesting that pure colors were emitted.

IL percentage

Norm. Electroluminescence (a.u.)

Wavelength (nm)

Legend: 4, 6, 7, 8

Synthesis of iridium complexes with N^O ligands

Ir(ppy)₂DHIq (77%)

Ir(ppy)₂Iq (80%)

SYNTHESIS OF IRIDIUM COMPLEXES WITH N^O LIGANDS

Ir(ppy)₂DHIq

Ir(ppy)₂Iq
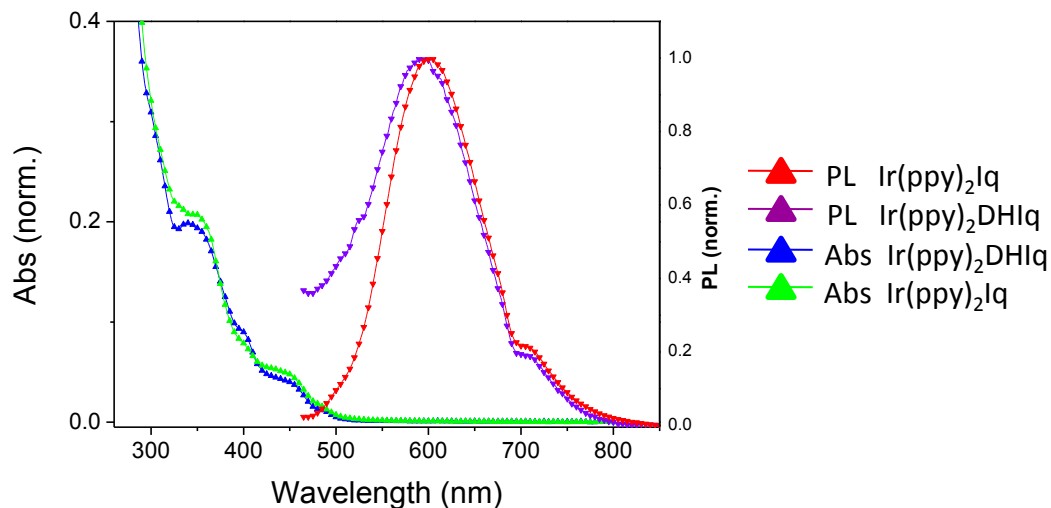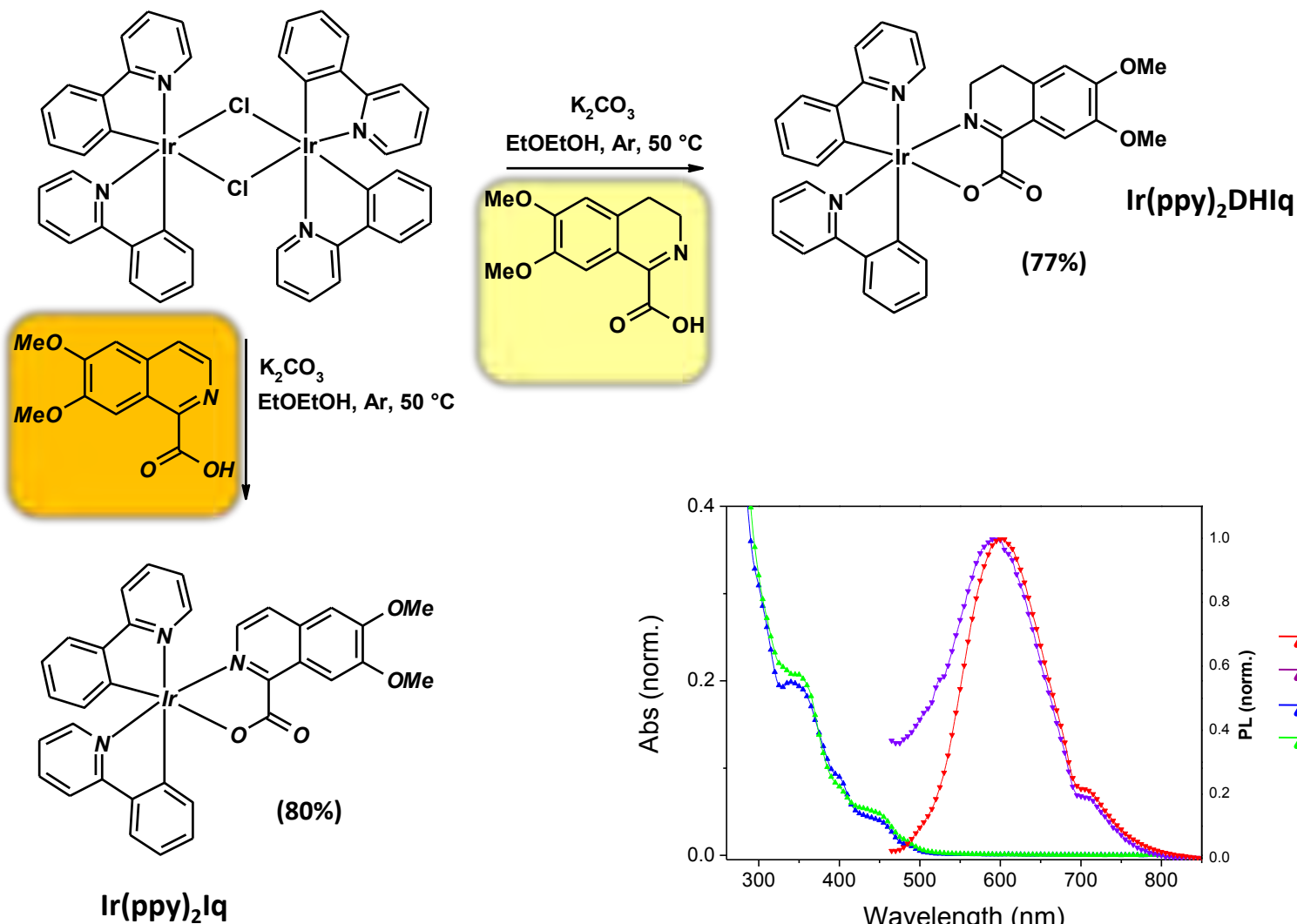
Configuration of the OLED device

Ca/Ag
Alq₃
BCP
Ir complex : CBP
PEDOT:PSS
ITO

CIE plot

Device Ir 6%	Luminance Max (cd/m²)	Efficiency Max (cd/A)	λ_{max} EL (nm)	Device Ir 12%	Luminance Max (cd/m²)	Efficiency Max (cd/A)	λ_{max} EL (nm)
Ir(ppy)₂Iq	2403@8.4 V	1.75@7.8 V	565	Ir CQ	7161@9.3 V	3.6@8.2 V	576
Ir(ppy)₂DHIq	3031@11.3 V	1.09@8.4 V	548	IrCHQ	996@9.5 V	0.45@8.5 V	567

UniNA Team

Dept. Chemical Sciences
Dr Valeria Criscuolo
Dr Carmela Tania Prontera
Dr Ludovico Migliaccio
Dr Alessandro Pezzella
Prof. Michele Pavone
Prof. Orlando Crescenzi
Prof. Marco d'Ischia

Dept. Physics
Dr Mario Barra
Dr Stefano Lettieri
Prof Antonio Cassinese
Prof. Pasqualino Maddalena

ENEA Team

Lab. Nanomaterials and devices
Dr Maria Grazia Maglione
Dr Paolo Tassini
Dr Carla Minarini

FINANCIAL SUPPORT

Ministero dello Sviluppo Economico

MINISTERO DELL'ISTRUZIONE, DELL'UNIVERSITÀ E DELLA RICERCA

Asymmetric Triazatruxene (ATAT)
R = -(CH₂)₁₀CH₃
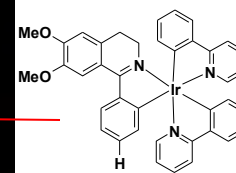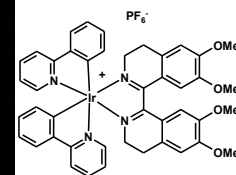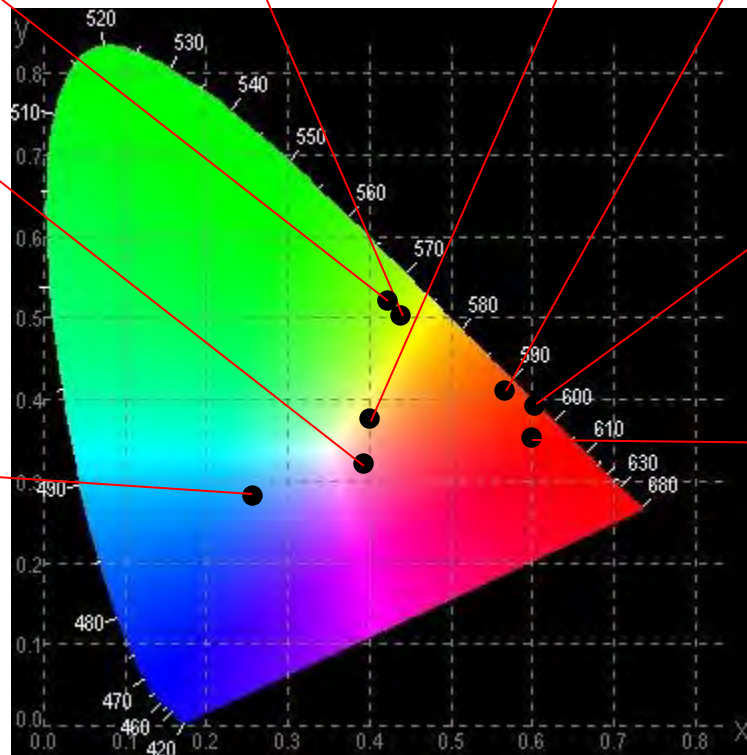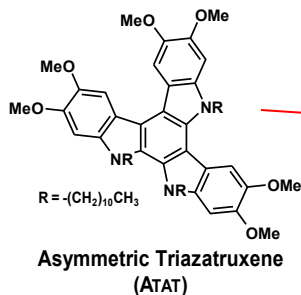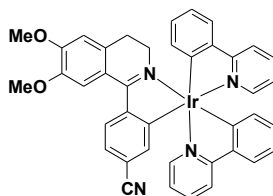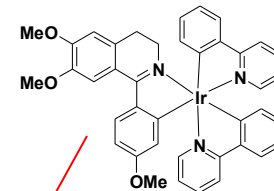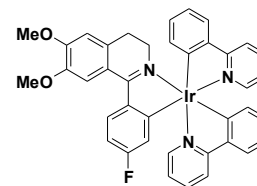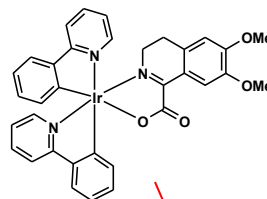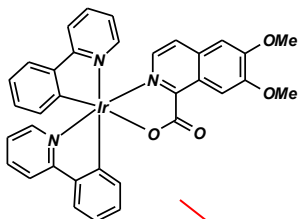
Complesso Universitario Monte Sant'Angelo

14th International Conference on Modern Materials and Technologies (CIMTEC 2018) - 8th Forum on New Materials

Perugia, June 10 – 14, 2018
paola.manini@unina.it

New insights into the Electronic-Ionic conduction model for eumelanin thin films

Carmela T. Prontera,[a] Paola Manini,[a] Alessandro Pezzella,[a] Valeria Criscuolo,[a] Clara Santato,[b] Ri Xu,[b] Marco Rolandi,[c] Roberto Di Capua,[d] Gabriella De Luca[d]

[a] Dept. of Chemical Sciences, University of Naples "Federico II", Via Cintia 4, I-80126 Naples, Italy
[b] Département de Génie Physique, École Polytechnique de Montréal, C.P. 6079, Succ. Centre ville, Montréal, Québec, Canada H3C 3A7
[c] Dept. of Electrical Engineering, University of California, 1156 High Street, Santa Cruz, CA (USA).
[d] Dept. of Physics, University of Naples "Federico II", Via Cintia 4, I-80126 Naples, Italy

carmelatania.prontera@unina.it

UNIVERSITY OF CALIFORNIA SANTA CRUZ

POLYTECHNIQUE MONTRÉAL LE GÉNIE EN PREMIÈRE CLASSE

EUMELANINS

Black insoluble animal biopolymers derived from tyrosine via 5,6-dihydroxyindole intermediates

Occurrence:
human and mammalian skin, eyes and substantia nigra, bird feathers, cephalopod ink

Biological Functions:
photoprotection, metal and drug binding, antioxidant

Eumelanin biosynthesis

L-Tyrosine → 5,6-Dihydroxyindole (DHI) + 5,6-Dihydroxyindole-2-carboxylic acid (DHICA) → Eumelanins
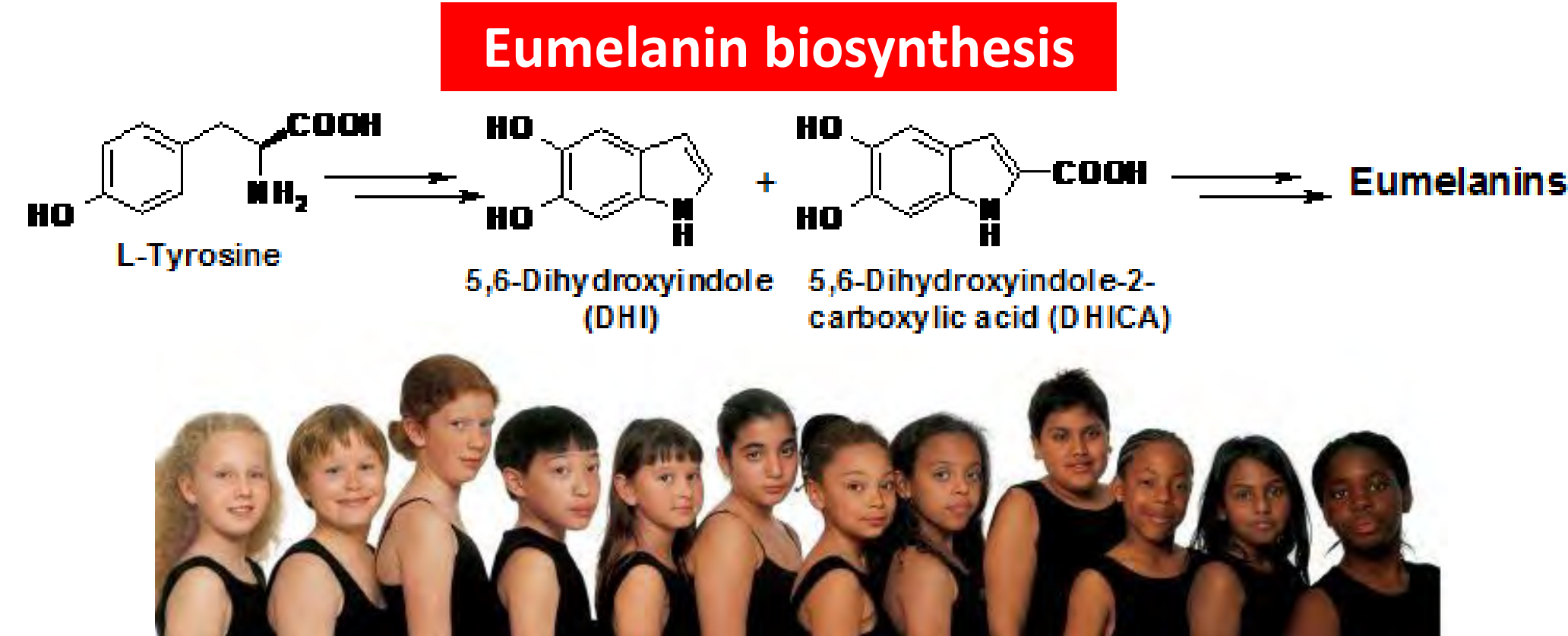
Physico-chemical properties

a) Broadband absorption in the UV-visible spectrum;
b) Nearly quantitative non radiative conversion of absorbed photon energy;
c) **Water-dependent hybrid ionic–electronic conductor behaviour;**
d) Metal ion-binding properties;
e) Redox behavior;
f) Persistent epr signal;
f) Peculiar onion-like supramolecular organization consisting of stacked planar structures.

WATER-DEPENDENT HYBRID IONIC-ELECTRONIC CONDUCTOR BEHAVIOUR: STATE OF THE ART

H_2Q ... Q ... $+ 2H_2O \rightleftharpoons 2H_3O^+ + 2$ ... SQ^-
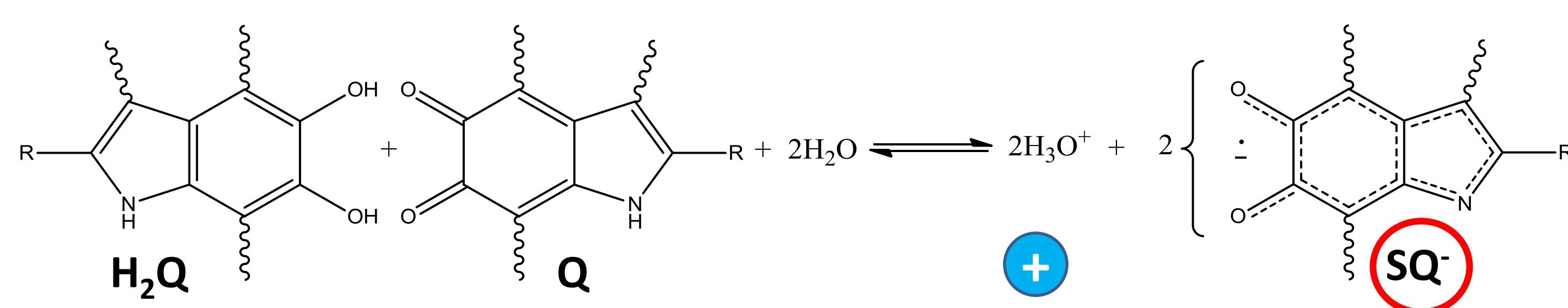
WATER CAN INDUCE A CHEMICAL SELF-DOPING BY DRIVING THE PRODUCTION OF EXTRINSIC FREE RADICALS AND HYDRONIUM IONS

Free radicals (electrons) ← Water Absorption → Hydronium ions (protons)

Electronic Conduction ... *Protonic Conduction*

• dissociated proton ⊙ unpaired electron of SQ

Thanks to the high adhesion features of eumelanin films allowing hydration dehydration cycles, it was possible to demonstrate the reversibility of the effect of water in enhancing the electrical conductivity of eumelanin thin films

H_2O

Mostert et al. PNAS, vol. 109 , no. 23, 8943–8947 (2012)
Santato et al. Chem. Mater. 27, 436–442 (2015)

Pezzella et al. Mater. Horiz. 2, 212-220 (2015)
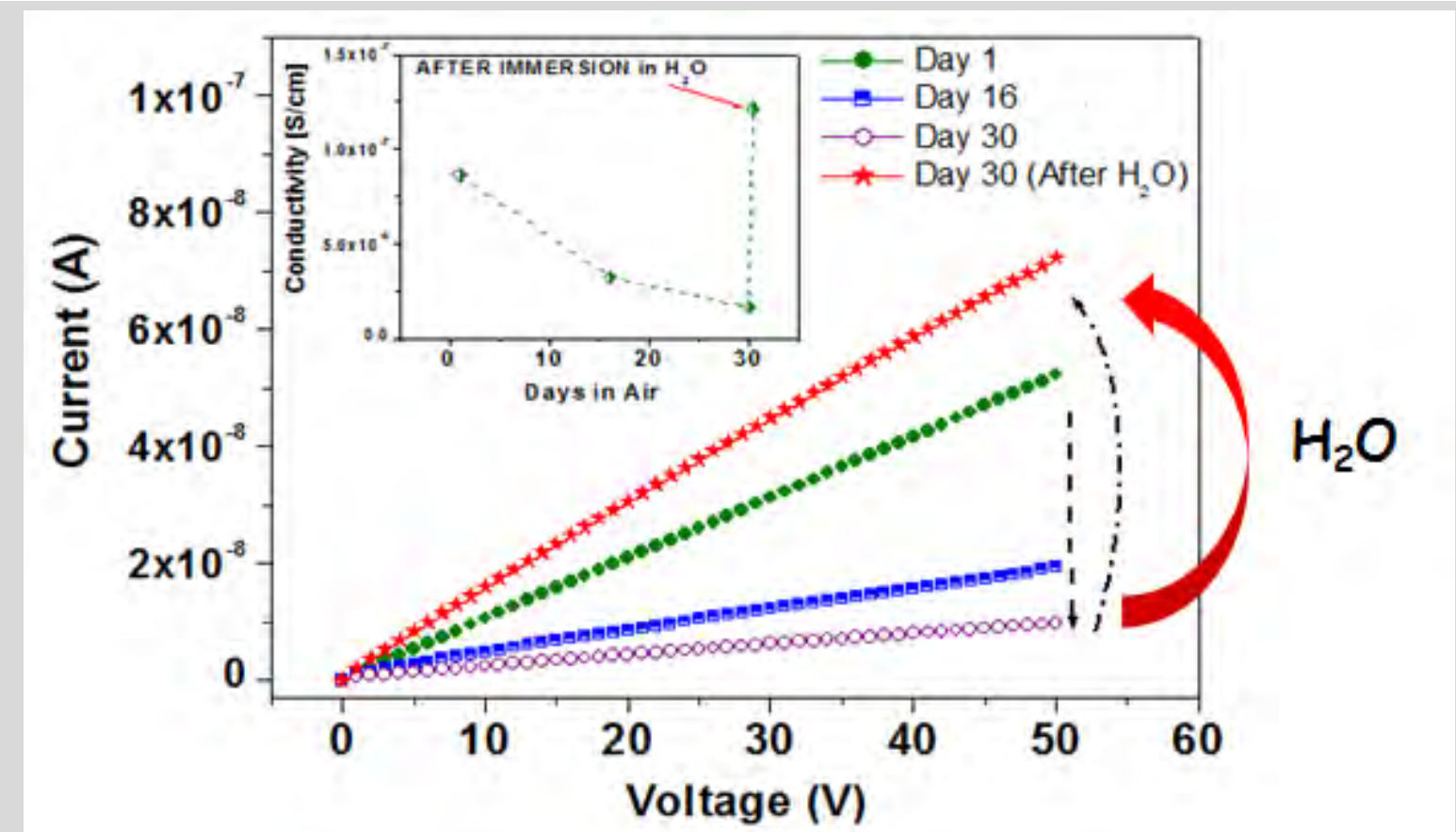
EUMELANIN-BASED DEVICE PREPARATION

DHI and/or DHICA deposition → Spin coating → DHI/DHICA film → **AISSP** NH₃ (air) exposure polymerization → EUMELANIN
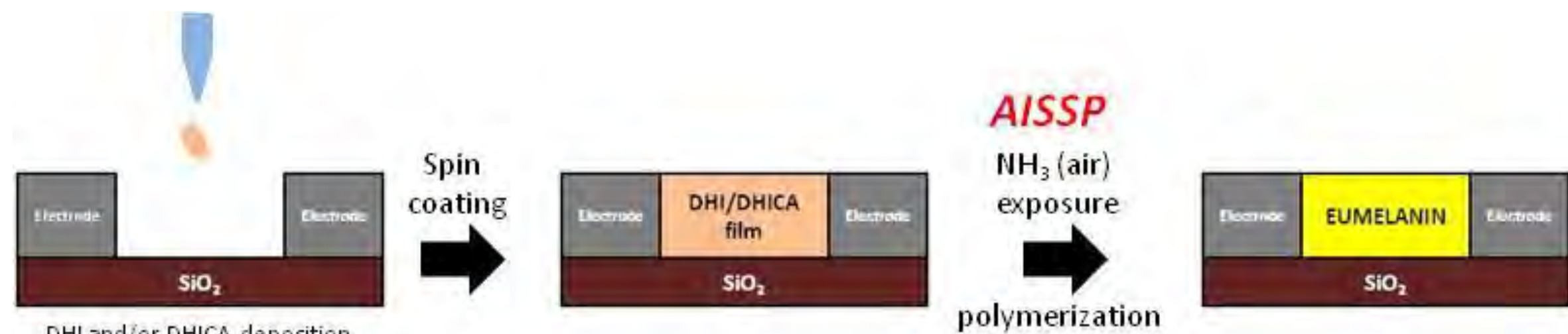
Eumelanin thin films were deposited between the electrodes via the ammonia-induced solid state polymerization (AISSP) processing technique: DHI and DHICA are soluble in several organic solvent and gives quite homogeneous thin films on different kind of substrate by spin coating processing. Given the high reactivity of the monomers, by exposing the thin film to a mild oxidizing atmosphere it is possible to observe the rapid conversion into the dark melanic polymer.

ELECTRONIC CONDUCTION
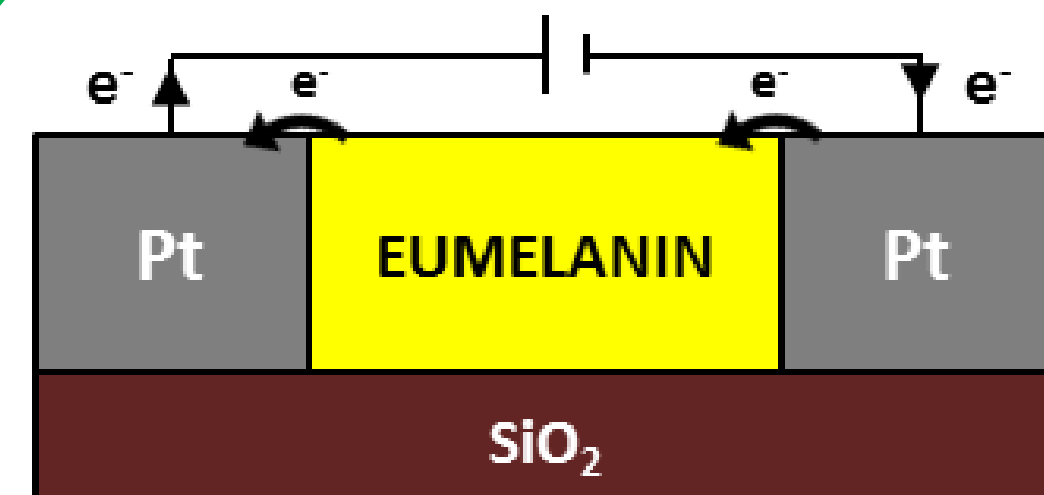
The water-dependence of eumelanin conductivity was investigated by *I-V* measurements by using a device set-up with two Pt electrodes in a planar configuration.

Measurements were carried out by varying the following parameters:
■ DHICA content   ■ relative humidity (RH)   ■ hydratation time

a) hydratation time = 5h
Legend: 90RH, 80RH, 65RH, 26RH
σ (S*cm^{-1}) vs % DHICA

b) hydratation time = 15h
Legend: 90RH, 80RH, 70RH, 30RH
σ (S*cm^{-1}) vs % DHICA
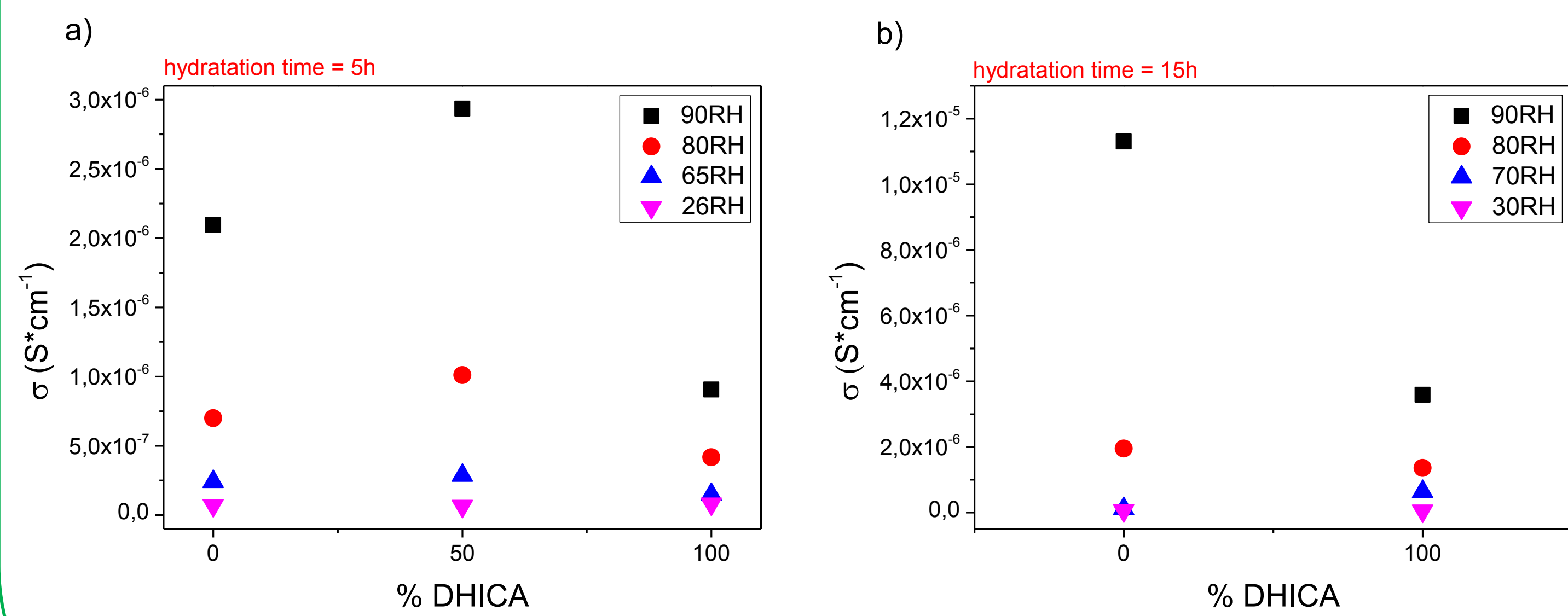
Electrical conductivity calculated from I-V measurements at 0.6 V, sweeping rate = 0.5 mV/s, W = 4 mm, t = 70 nm, l = 10 μm.

PROTON CONDUCTION

$PdH \leftrightarrow Pd + H^+ + e^-$
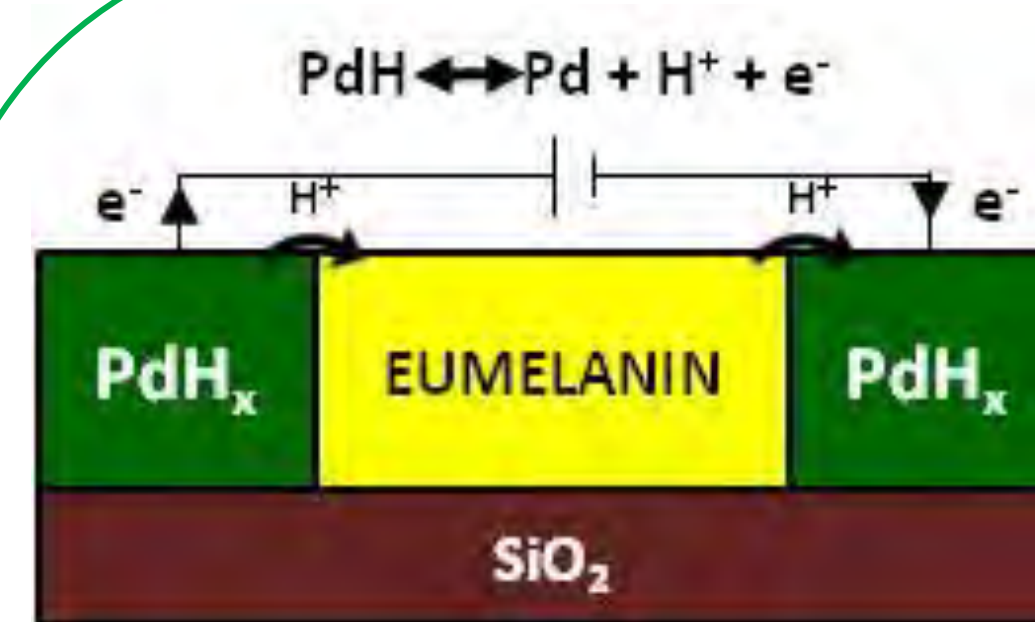
Proton conduction was investigated by *I-V* and *I-t* measurements with Pd electrodes in a planar two-electrode configuration.
Under a hydrogen atmosphere, Pd forms palladium hydride (PdH_x) and the electrodres act as protodes.

Measurements were carried out by varying:
■ DHICA content   ■ relative humidity (RH)   ■ gaseous hydrogen content

a) Legend: 50RH 0H₂, 50RH 5H₂, 90RH 0H₂, 90RH 5H₂
σ (S*cm^{-1}) vs % DHICA

b) Legend: 50RH 0H₂, 50RH 5H₂, 90RH 0H₂, 90RH 5H₂
σ (S*cm^{-1}) vs % DHICA
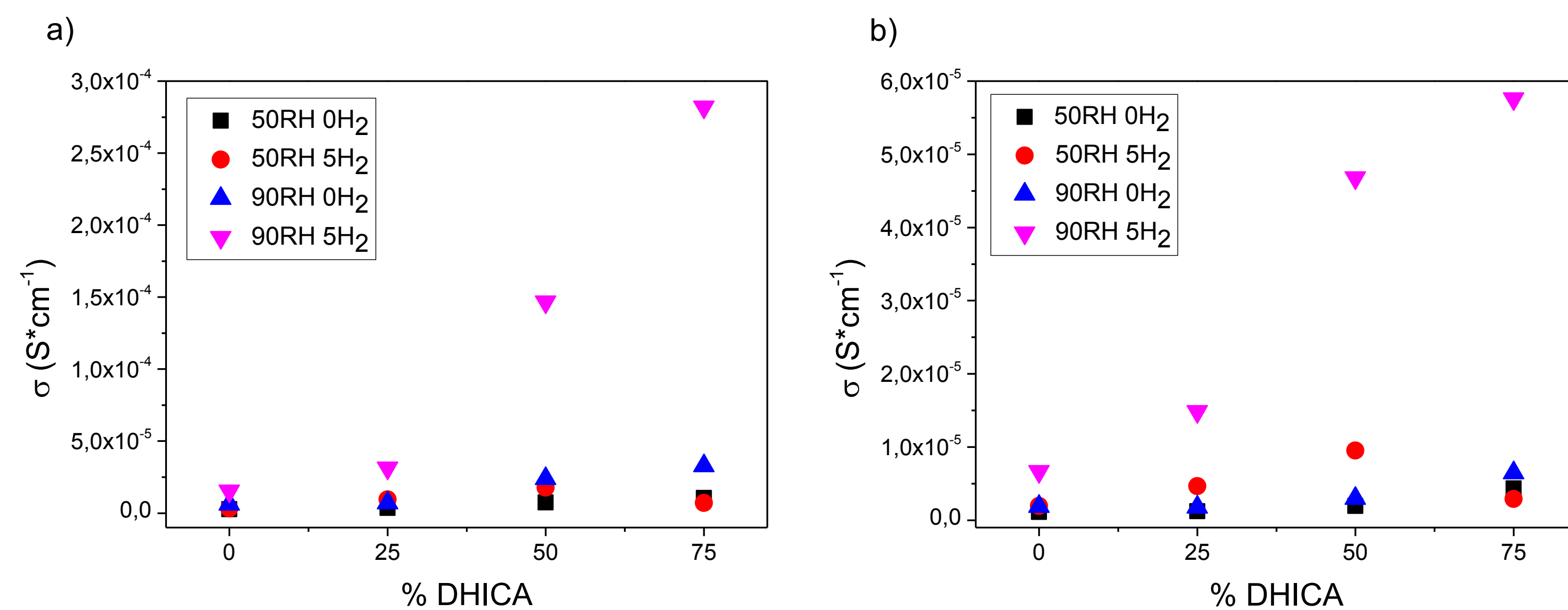
Electronic/proton conductivity calculated from I-V measurements at 1 V, sweeping rate = 50 mV/s, W = 0.5 mm, t = 100 nm, l = 10 μm, hydratation time ≈ 1h

Electronic/proton conductivity calculated from I-t measurements at 1 V and 200 s, sweeping rate = 50 mV/s, W = 0.5 mm, t = 100 nm, l = 10 μm, hydratation time ≈ 1h

CONCLUSIONS

➢ Higher degree of hydration enhance the overall conductivity of eumelanin films;
➢ The hydratation time strongly affect the electrical conductivity, with long hydratation times increasing the conductivity;
➢ The presence of gaseous hydrogen gives a further enhancement of the conductivity in high hydration states suggesting that proton conduction within the film is involved in charge transport;
➢ The growing percentage of DHICA leads to an enhancement of the electrical conductivity, in particular proton transport (Panel 5), at the highest humidity values reaching a maximum value of 3×10^{-4} Scm^{-1}, suggesting that the presence of carboxylic groups can effectively help the proton hopping throughout the eumelanin backbone.
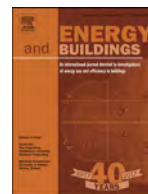
Estimating the impact of heat accounting on Italian residential energy consumption in different scenarios

L. Canale[a], M. Dell'Isola[a,*], G. Ficco[a], B. Di Pietra[b], A. Frattolillo[c]

[a] Department of Civil and Mechanical Engineering (DICEM), University of Cassino and Southern Lazio, Via G. Di Biasio 43, 03043 Cassino, Italy
[b] ENEA, Technical Unit for Energy Efficiency, Via Principe di Granatelli 24., 90139 Palermo, Italy
[c] DICAAR, Department of Civil and Environmental Engineering and Architecture, University of Cagliari, via Marengo 2, 09123 Cagliari, Italy

ABSTRACT

Directive 2012/27/EU has set the obligation for buildings supplied by central heating sources, or by district heating/cooling networks, to install individual heat metering and accounting systems. In Italy, almost 5 million dwellings are potentially subject to this obligation. To estimate the related potential benefit the knowledge of the energy saving achievable from the installation of such systems is needed. Unfortunately, in literature a wide range of variability of this benefit has been found and studies regarding Italian buildings are still lacking. The present study is aimed to estimate the impact of this EU policy in terms of potential energy saving in Italy. To this end, the authors first performed an experimental campaign on about 3000 dwellings located in major Italian cities, to assess the potential benefit obtainable. A model to estimate the energy consumption for space heating in the residential building stock has then been developed considering the building typologies and their main technical characteristics. An average benefit of about 11% has been found, leading to an estimated energy saving at national level ranging from 0.3% to 1.9% of whole energy consumption for space heating, depending on the effectiveness of applicable economic incentives and legal obligation scenarios.

© 2018 Elsevier B.V. All rights reserved.

1. Introduction

As well known, the Energy Efficiency Directive (EED) [1] established that energy consumers should be given easy and free access to consumption data through individual metering, allowing a better awareness about their energy use. To this aim, European Union (EU) has set the obligation for apartment and multi-apartment buildings supplied by a common central heating source or by a district heating/cooling network, to install sub-metering systems to allow a fair heat cost allocation, as long as the installation of such systems is technically feasible and cost-efficient.

With respect to the above-mentioned obligation, Member States adopted different approaches at the policy level [2]. In Germany and Austria, for example, individual metering for space heating is compulsory for almost the majority of the buildings supplied by a common central heating source. Sweden and Finland exempt nearly all the buildings potentially subject to the obligation, since the effectiveness of such measure at their actual climatic and operating conditions has not yet been demonstrated [3–5]. Despite it is explicitly required that installation of sub-metering systems

is mandatory only if technically feasible and cost-efficient, specific indications at the policy level are still lacking in actual regulation, especially from an economic point of view (e.g. neither a reference energy saving nor standard costs have been set). As a consequence, a wide discretion is left to technicians in exempting or obliging the installation of heat accounting systems in a given building. Furthermore, it is not specified if the economic feasibility analysis has to be performed considering the building primary energy calculated at standard rating conditions (i.e. Asset Rating, AR) rather than the actual primary energy consumed during the use of a building over a fixed time period (i.e. Operational Rating, OR).

Heat accounting systems mainly belong to two different categories [2,6,7]: direct (i.e. heat meters) and indirect (e.g. Heat Cost Allocators, HCA). EED has set the installation of direct heat meters as a priority. Unfortunately, due to the heating plant configuration (e.g. vertical mains in old buildings), technical (e.g. when flow and return pipes are not easily accessible) and architectural (e.g. in historical buildings) constraints, the installation of direct heat meters is often technically unfeasible in existing buildings [6]. On the other hand, indirect systems (e.g. HCA), are almost always technically feasible in older heating plants. Empirica GmbH [7] provides useful information about some of these issues in a guideline developed under a specific EU contract.

* Corresponding author.
 E-mail address: dellisola@unicas.it (M. Dell'Isola).

Nomenclature

EP_H	Primary energy for space heating [kWh m^{-2} year $^{-1}$]
$EP_{H,min}$	Minimum value of primary energy for obliged buildings making efficient the installation of Heat Accounting and Thermoregulation systems [kWh m^{-2} year^{-1}]
HDD	Heating Degree Day [°C d]
h	Inter-storey height [m]
U	Thermal transmittance [W m^{-2} K^{-1}]
η	System efficiency [–]

Subscripts

d	distribution
f	floor
gen	generation
r	roof
wall	walls
win	windows

Abbreviations and acronyms

AEEGSI	Italian Regulatory Authority for Electricity Gas and Water
AiCARR	Italian Association for Air Conditioning, Heating and Cooling
AR	Asset Rating
BTM	Building Typology Matrix
CA	Construction Age
CHS	Centralized Heating Systems
EED	Energy Efficiency Directive
ENEA	Agency for New Technologies, Energy and Sustainable Economic Development
ESCO	Energy Service Company
EU	European Union
HAT	Heat Accounting and Thermoregulation
HCA	Heat Cost Allocators
ISTAT	Italian National Institute of Statistics
NEBs	National Energy Balances
OR	Operational Rating
PBT	Payback Time
REBs	Regional Energy Balances
TRV	Thermostatic Radiator Valve

Italy transposed article 9 of EED without any substantial changes through Legislative Decree n. 102/2014 and subsequent modifications and integrations [8], setting the obligation to install individual heat metering systems by June 30th 2017. Due to the characteristic of the Italian building stock and to the fact that heating plants with vertical mains configuration are the most widespread in Italy, it is believed that in almost all existing buildings subject to the EED obligation indirect heat accounting systems will be installed. Moreover, in Italy when indirect system are used, the obligation to install heat accounting systems is combined also with the installation of thermostatic valves on each radiator [8]. Therefore, in the following the installation of indirect Heat Accounting and Thermoregulation systems (HAT) is analysed.

The "General Survey of Population and Housing" [9] performed by ISTAT highlighted that about 18.75% of Italian dwellings is supplied by a common central heating source. This means that almost 5 million dwellings are potentially obliged to install HAT systems [10,11]. This would result in a potential capital flow of about 4–5 billion €, in the case that every dwelling supplied by a central heating system would fulfil the legislative obligation. Hence, the definition of the related installation costs represents a crucial is-

sue in the analysis of the impact of this policy measure. The average cost of HAT systems ranges between 600 and 1200 €/dwelling, depending on several aspects, such as the type of HCA (i.e. single sensor, two-sensors) and TRV (mechanical, electronic), the number of dwellings in the building and on the type of heating plant available. These costs include also the design of the heat allocation system, the installation of data gathering devices, the adjustment of the heating plant itself and the related masonry works [2,7,12–14]. As regards payback time (PBT), Celenza et al. [2] show PBT for HAT systems variable between 3 and 16 years when the building energy need ranges from 300 to 100 kWh m^{-2} year^{-1}. In their analysis an expected benefit of 25% (i.e. the average benefit estimated for Central-European countries) and the absence of fiscal incentives have been assumed. At policy level, in Italy the installation of HAT systems is promoted to 50% of costs, if performed individually as a "building automation" system, and to 65% of costs if performed in combination with partial or integral substitution of the heating system [15]. Furthermore, when landlords are unable to access the fiscal benefit, this latter may be also transferred to an Energy Service Company (ESCO). In order to determine the effectiveness of this policy, it is thus necessary to carefully assess the actual energy saving achievable from the installation of indirect HAT systems. However, the amount of the energy saving is expected to be highly dependent on: *i)* the type and the set-up of the thermoregulation system [16], *ii)* the actual operating conditions of the heating system [17], *iii)* the balancing of the heating system [16]; *iv)* the type of feedback and the users' awareness [18,19].

However, there is still a considerable resistance to the installation of HAT systems due to the significant issues in the transition between old and new heat cost charging criteria and to the uncertainty about the metrological reliability of HAT systems [20,21]. Moreover, thanks also to the quite low investment costs related, the installation of HAT systems certainly represents an effective strategy to reduce the energy consumption of the existing buildings, being particularly suitable in historical or protected as cultural heritage ones [6,22]. Nevertheless, many issues are delaying the spread of HAT systems in Italy. In fact, data from the heating systems register of the Lombardia Region [23] show that more than 50% of the obliged buildings has not yet installed heat accounting systems, despite it was mandatory since 2014 and subsequently postponed. On the other hand, in Central-European countries the installation rate of heat accounting systems is certainly higher, since they are historically more widespread [24]. As regards the heating system regulation in Italy, in Lombardia Region [23] about 60% of heating systems is regulated by individual dwelling thermostats with on/off or proportional control, while in about 18% regulation is absent. These figures may be reasonably applied to whole Italy.

Potential energy saving related to the spread of individual metering for space heating in the Italian building stock has not yet been determined, also because the scientific literature on the effects of the installation of HAT systems in Mediterranean climates is still lacking. In other EU Member States, mainly located in North-Central Europe, the potential energy saving has been estimated by Felsmann et al. [25] in a range of about 8–40% and, sometimes, opposing outcomes emerge [4]. In the scientific literature, only few studies are based on the actual measurement of the energy saving and have been carried out after the experimental observation of the buildings before and after the installation of HAT systems. Among these, Cholewa and Siuta-Olcha [26] analysed in a multifamily building located in Poland for over 17 heating seasons, the energy consumption of 40 dwellings all equipped with Thermostatic Radiator Valves (TRV) and only half of which equipped with Heat Cost Allocators (HCA). The experimental data highlighted higher energy savings in the dwellings equipped with both TRV and HCA compared to the ones with only TRV (18.8%

one year after the installation and a further 7.8% two years after the installation). Paulsen and Gullev [27] also observed a reduction of heat consumption up to 30% due to the transition to individual metering, analysing the energy consumption of representative dwellings during the period 1991–2005. However, to the authors' best knowledge, no long-term experimental campaign for an empirical assessment of the benefit expected from the installation of HAT systems was performed in Italy. Thus, it is nearly unfeasible to estimate with a good confidence their actual effects on a national scale.

In order to estimate the impact of an energy policy, the complex issue to investigate energy consumption of large-scale building stocks should be considered. The scientific literature concerning the methodologies for assessing the energy performance of building stocks is quite rich, because of the related importance in identifying effective policy strategies for incentivising refurbishment actions. In this sense, two main approaches have been widely used to model the energy demand on an urban scale [28–30]: the top-down, mainly based on historical data analysis, and the bottom-up. The latter, relying on physical features of the buildings (such as geometry, thermal transmittance, equipment and appliances etc.), is able to determine the total energy demand of a residential building stock with higher accuracy showing also flexibility to model possible scenario's changes. However, when these methodologies are applied to the Italian residential building stock, the lack of data about the energy performance of buildings (such as thermal transmittance, systems efficiencies etc.) makes it difficult to determine its actual energy need. Anyway, efforts have been made mainly on regional level, [31,32]. Ballarini et al. [33] applied the building typology method defined within the TABULA project for Piemonte region to the entire Italian residential building stock by means of a quasi-steady approach, in order to assess the effectiveness of different retrofitting actions.

Nevertheless, the development of a model to predict energy consumption in residential sector and the knowledge of a statistical benefit related to the installation of HAT systems should be useful at the policy level to assess the effectiveness of incentive measures and, on the practical hand, to help technicians in analysing the economic feasibility of such systems. With the necessary adjustments, the results of the present research should also be extended to other EU countries adequately considering the specific aspects which make the Italian building stock different from the European ones such as: *i)* the major influence of solar heat gains; *ii)* the lower consumption for space heating associated with Mediterranean climatic conditions; *iii)* the significant differences between the energy performance of existing buildings (especially those built in the post-war period and those in the last twenty years); *iv)* the current heat cost charging criteria normally based on floor area or installed power rather than on individual consumption.

In this scenario, this work is aimed to assess the potential of Italian policies about individual heat metering in the residential sector. To this end, an experimental campaign has been performed on a sample of about 3000 dwellings in 50 buildings located in the Italian regions mainly concerned by the obligation to install HAT systems. The mean energy saving resulting from the experimental campaign has been extended to the whole Italian residential building stock, through the development of a bottom-up model able to predict the mean energy consumption for residential space heating. The model has been validated and calibrated comparing the calculated energy need for space heating with energy data from the Regional Energy Balances (REBs) and National Energy Balances (NEBs). An economic feasibility constraint was applied under three different incentive scenarios in force in the Italian fiscal policy to achieve the estimation of the real reduction of energy consumption at national level. In fact, depending on incentives, the eco-
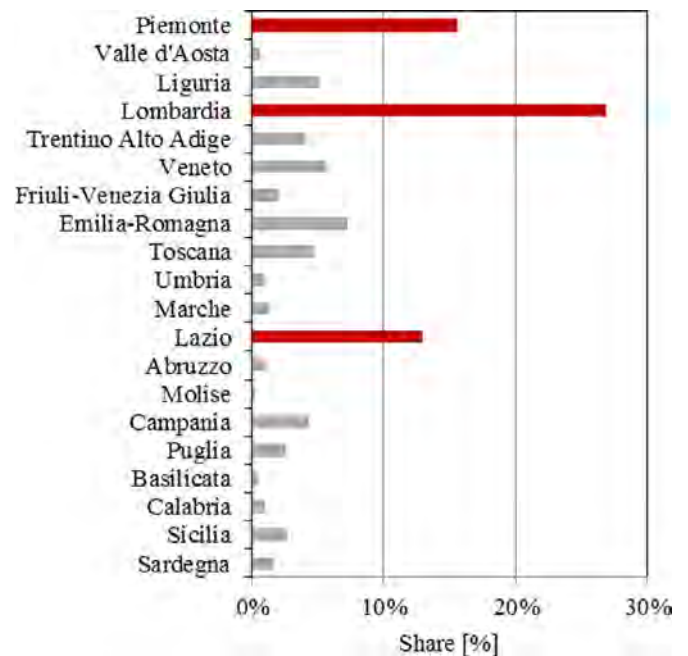
Fig. 1. Regional share of dwellings supplied by CHS (source: ISTAT).

nomic feasibility analysis applied to the Italian building stock will determine different spread of HAT installations and, consequently, different reduction rates of annual energy consumption.

2. Methods

In the following, an experimental approach on a limited sample of representative buildings aimed to estimate the energy saving after the installation of HAT systems is first presented. Subsequently, a methodology to estimate the energy consumption for space heating in the national building stock is proposed and the available scenarios related to incentive policies and to obligation approaches are discussed.

2.1. Experimental campaign to estimate the mean Italian energy saving

A sample of 3047 dwellings in 50 buildings has been investigated in the experimental campaign presented in this paper. The authors selected the sample with respect to size, construction age and climatic conditions representative of the Italian building stock potentially subject to the obligation to install HAT systems.

The investigated buildings are located in three representative regions (i.e. Piemonte, Lombardia and Lazio) summing about 55% of dwellings potentially subject to the obligation to install HAT systems in Italy (see Fig. 1 and Table 1). Moreover, the buildings belong to the more widespread Italian climatic zones E (i.e. with a number of HDD – Heating Degree Days – between 1401 and 2100 °C d) and D (i.e. with a number of HDD between 2101 and 3000 °C d). In fact, about 50% and 20% of Italian cities belong to D and E climatic zones, respectively.

In Table 2 the main characteristics of the investigated buildings are reported. The investigated buildings were all built between 1900 and 1990 and they are supplied by natural gas Centralized Heating Systems (CHS) whose energy consumption for space heating was measured through diaphragm gas meters [34]. Hot water production in each dwelling was provided through autonomous systems and, therefore, heat accounting for this purpose was not required. With regard to the heating plant, the heating fluid distribution is performed through vertical mains and heating bodies are

Table 1
Italian dwellings classified by heating plant (source: ISTAT).

Heating plant	Absolute values	Percentage values
Centralized	4 871 072	18.75%
Individual	15 717 341	60.51%
Single devices supplying the whole dwelling	2 137 636	8.23%
Single devices supplying only part of the dwelling	3 246 891	12.50%
TOTAL	25 972 940	100.00%

Table 2
Characteristics of the investigated buildings sample.

Buildings	Age	U-value [Wm^{-2} K^{-1}]			
		Wall	Roof	Floor	Windows
4	Ante 1930	1.10÷1.40 Solid bricks masonry (50/60 cm)	2.00÷2.50 Vault with bricks and steel beams	2.00÷2.50 Vault with bricks and steel beams	4.90 Single glass, wood frame
16	Between 1950 and 1970	1.10÷1.20 Hollow wall brick masonry (30/40 cm)	1.40÷1.70 Reinforced brick concrete slab	1.40÷1.70 Reinforced brick-concrete slab	4.90 Single glass, wood frame
30	Between 1971 and 1990	0.75÷0.90 Hollow wall brick masonry (30/40 cm), low insulation	1.00÷1.20 Reinforced brick-concrete slab, low insulation	1.00÷1.20 Reinforced brick-concrete slab, low insulation	3.70 Double glass air filled, metal frame, no thermal break

represented by cast iron radiators. Low insulated pipes mainly run into the external walls. Before the installation of HAT systems, all dwellings were regulated by individual dwelling thermostats with on/off control system.

In all the investigated dwellings HCA, TRV and balancing valves have been installed and the whole building energy consumption was recorded for at least two heating seasons (the ones before and after the installation of HAT systems). In addition, for few buildings the energy consumption data available also for the heating season two years after the installation of HAT systems have been analysed in order to assess the benefit over time. For each heating season, the external temperature data were analysed in order to normalize energy consumption to the climatic conditions, through the division of energy consumption by the actual HDD calculated according to EN ISO 15927-6 [35]. Thirteen buildings of the sample have undertaken a major retrofit intervention, replacing the existing boiler with a high efficiency one together with the HAT systems installation. Although the present analysis regards the effects of the installation of HAT systems, also the reduction in energy consumption of these buildings has been analysed, in order to allow a further understanding about the possible benefits achievable by the combined effect of different retrofitting actions.

2.2. Estimating the Italian residential energy consumption for space heating and the related energy savings

To estimate the Italian energy consumption for space heating, a calculation method based on the classification of the building stock in building typologies [36–38] has been developed. The modelling scheme followed five subsequent phases, as shown in Fig. 2.

In *phase 1,* data from the latest "General Survey of Population and Housing" of ISTAT have been analysed and a first classification of the national building typologies has been performed. To this aim, the building category (single/two/multi-family buildings) and Construction Age (CA) have been considered. This required a preliminary analysis of the Italian building stock, in which peculiar national and regional features have been identified with regard to buildings' geometry (i.e. number of floors, net floor area, inter-storey height etc.) and to the available heating systems sources (i.e. centralized or autonomous).

Phase 2 concerned the characterization of the different building typologies by assigning a given shape, heating system efficiency and first attempt thermal transmittances retrievable from the existing scientific literature [33,38]. To this aim, the authors developed a Building Typology Matrix (BTM) of the residential building stock for each Italian climatic zone. This has been tailored to each Italian region through the main geometrical peculiarities of each regional building stock, derived from both Italian and European statistical databases.

In *phase 3* the estimation of regional energy consumption for space heating has been performed in AR conditions, deriving then the corresponding one in OR conditions through suitable reduction coefficients available in the scientific literature [40,41]. Data on actual energy consumption of each region have been obtained from the available European databases and from REBs (provided by ENEA).

In *phase 4* a check has been made in order to verify the deviation between the primary energy need estimated through the developed model and corresponding data from REBs. Subsequently, a tuning of the thermal transmittances has been performed to achieve a correspondence between the estimated and the actual primary energy within ±2%.

In *phase 5* the potential energy saving corresponding to applicable incentives and legal obligation constraints at national level and related to HAT systems installation have been estimated for suitable scenarios, also performing an economic feasibility assessment on the above defined national building typologies.

In detail, the ISTAT clusters Italian dwellings in 6 categories and 9 CA (between 1918 and 2006). An overview of the data analysis performed is given in Table 3 and Fig. 3. Data include also single-family buildings (clearly not obliged to install HAT systems) since they contribute to the national energy consumption for space heating. For the sake of simplicity, three CAs have been considered.

The same classification has been applied to the BTM, which consists of 54 rows (9 CA and 6 dimensional categories). Geometrical and thermo-physical properties have been assigned to each row as a function either of the CA or of the building dimensional category as follows:

(i) inter-storey height (h), variable as a function of the CA; in absence of national statistical data of the residential buildings, values in [39] have been considered although they are
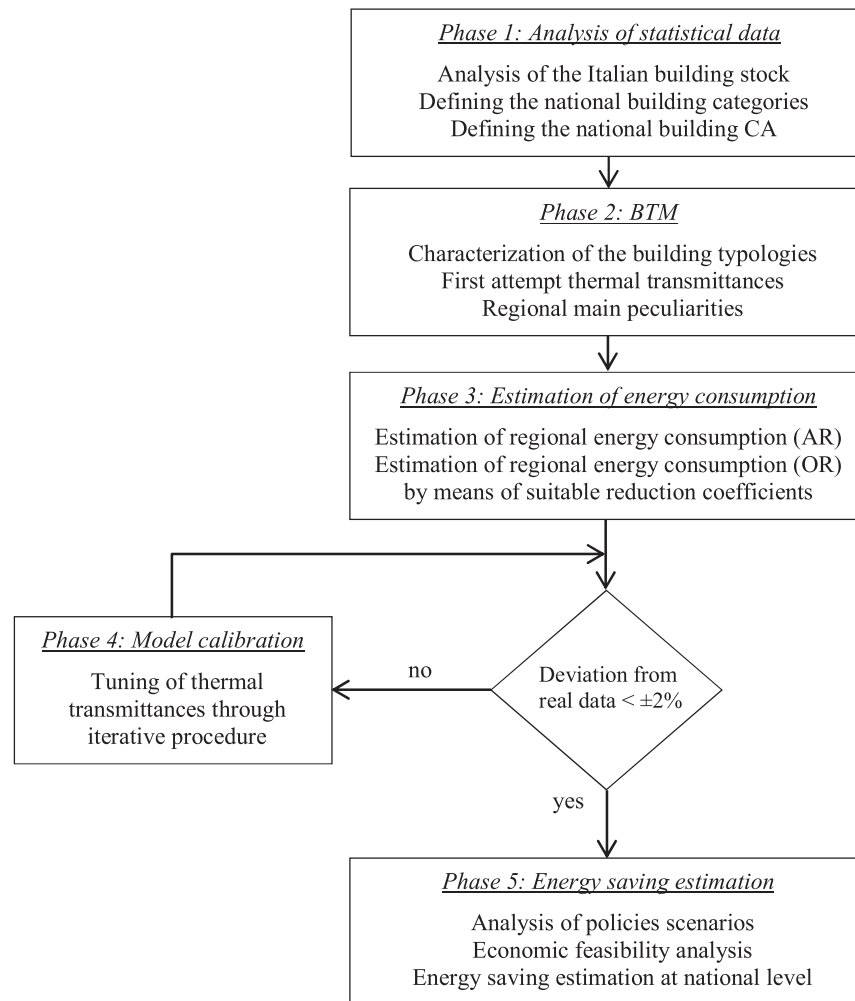
Fig. 2. Flow chart of the developed model.

Table 3
Italian dwellings occupied by residents classified by category and construction age.

Building category	Number of dwellings in the building	Absolute values	Share	Before 1980	Between 1981 and 2000	After 2001	All ages
Single-family	1	4 688 972	19%	14.27%	3.82%	1.39%	19.48%
Two-family	2	3 995 081	17%	12.32%	3.32%	0.96%	16.60%
Multi-family	3–4	3 518 114	15%	44.85%	13.28%	5.79%	63.92%
	5–8	3 443 130	14%				
	9–15	3 044 095	13%				
	>15	5 375 902	22%				
Total		24 065 294	100%	71.44%	20.43%	8.13%	100.00%

related to offices since these are generally located in multi-purpose buildings;

(ii) wall, roof, floor, and window thermal transmittances (U_{wall}, U_r, U_f, U_{win}) variable as a function of the CA and climatic zone [33];

(iii) generation system efficiency, η_{gen}, as a function of the building category and CA [42].

The distribution, emission and thermoregulation systems efficiencies, (η_d, η_e, η_r respectively) have been considered constant and equal to 0.95. Such figure is related to an average efficiency of the entire building stock and not of the investigated buildings sample and it is conceivably related to traditional plants with low thermal inertia and with simple temperature control. The authors assumed the average value of the corresponding efficiencies in UNI 11300-2 [43]. Furthermore, the following features have been considered: i) parallelepiped shape; ii) transparent/opaque surfaces ratio equal to 1/8 (i.e. the Italian legal limit in force).

For each building typology, the following further assumptions have been made: i) 15% increasing factor for thermal bridges (available literature data [44,45] show that the total impact of thermal bridges on the heating energy need ranges between 7% and 28%); ii) no heat exchanges with unheated spaces. It is underlined that the arbitrariness of some of the aforementioned assumptions derives both from the lack of reliable empirical data of the constructive features of the Italian building stock and from the need to have a general model that could represent a heterogeneous building stock. Anyway, all the aforementioned assumptions are expressly declared, and authors will refine them when more detailed data will be available.

Due to the lack of data about the status of the existing Italian building stock, the first-attempt thermal transmittances have been
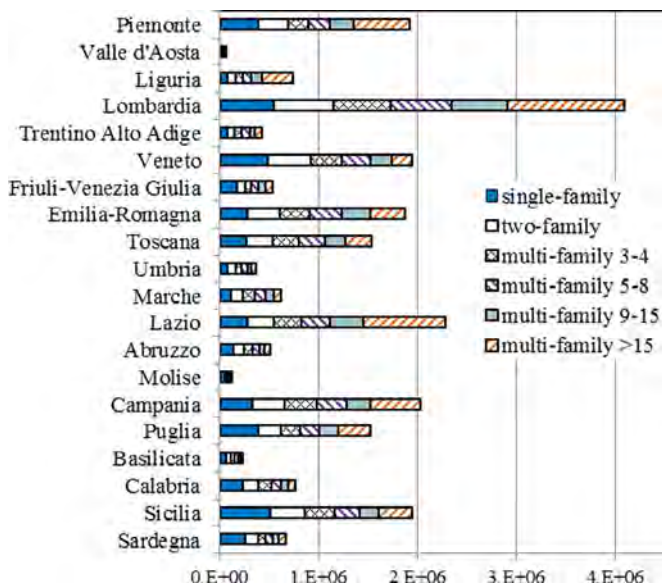
Fig. 3. Number of dwellings per region and per building type.

obtained from data available in literature [33]. A graphic representation of BTM is given in Fig. 4. These data have been calibrated to the different climatic zones and regional areas.

The BTM has been tailored to each Italian region using the following parameters:

– the mean regional floor area [9];
– the mean number of building floors by building size, obtained through a dwellings-weighted average, variable as a function of the building size [9].

Finally, historical data of HDD for each region have been obtained from Eurostat database [46].

The estimation of the building energy need for space heating has been performed according to the standard EN ISO 13790 [47]. Then, the primary energy for space heating $EP_{H,AR}$ at standard rating conditions (i.e. AR) of each building typology has been estimated according to EN 15316 [48]. On the other hand, the estimation of the actual primary energy consumption at the real condition of use of the heating plant must be taken into account. Thus, the estimated primary energy consumption in AR conditions has been multiplied by suitable reduction coefficients to obtain the primary energy consumption of the Italian building stock in OR conditions, $EP_{H,OR}$. The aforementioned coefficients have been estimated by ENEA [40,41] through a sample analysis of about 20 thousand dwellings performed in the Italian territory for each climatic zone and building typology.

With the aim to assess the error associated with the hypotheses introduced, data about actual national and regional energy consumption have been collected from REBs [49] and NEBs [50]. The energy consumption related to the sole space heating of residential buildings in single regions has been obtained from the whole residential consumption data (available from REBs and including air cooling, lighting and household electrical appliances, cooking and hot water production), through the Italian mean share for space heating. In particular, the latter ranges from about 65% to 70% of the whole Italian residential energy consumption, with a mean value of about 68% in the period from 1990 to 2015 [50]. In order to achieve a correspondence between the estimated and the actual primary energy consumption within ±2%, a calibration of the model has been performed by applying corrective coefficients to the first attempt thermal transmittances. This step has been necessary for both reducing the error due to the unavoidable uncertainty

of the basic assumptions (e.g. thermo-physical properties, simplified geometry and shape etc.) and obtaining reasonable regional and national energy saving estimates.

Once obtained a reliable estimate of the residential energy consumption for space heating, different applicable fiscal incentive scenarios [15] have been analysed, since they could determine different spread rates of HAT systems by reducing the related investment costs. In particular these are:

– zero incentives (when landlords have insufficient income to meet the fiscal advantage);
– 50% of total costs incentive (applicable when the sole installation of HAT systems is performed and landlords have sufficient income to meet the fiscal benefit);
– 65% of total costs incentive (when the installation of HAT systems is performed together with the replacement of the boiler and landlords have sufficient income to meet the fiscal benefit).

Finally, an economic feasibility assessment according to the standard EN ISO 15459 [51] was performed on the above described building categories, with the aim to determine the minimum value of primary energy for space heating $EP_{H,min}$ above which buildings should be obliged at the policy level to install HAT systems. In particular, $EP_{H,min}$ has been calculated by iterating the cost-benefit method in Celenza et al. [2] to each building typology, until a net present value equal to zero occurs at the 10th year of the analysis. The energy benefit resulting from the experimental campaign (see Section 3.1) has been considered and the following assumptions have been made [7,9,12,52]:

– dwelling floor area equal to 97 m^2;
– mean rooms number equal to 6;
– investment and operational costs for the Italian market;
– market interest rate of 4.50%;
– energy cost equal to 0.085 €/kWh, derived from the cost of natural gas monthly updated by AEEGSI [53].

The calculated $EP_{H,min}$ has then been applied as limit value of the estimated primary energy in AR and OR conditions of each building type, above which the installation of HAT systems is profitable. The respective scenarios have been simulated to estimate the related potential and the effective energy saving. In fact, while the first option is more easily applicable, since it is independent from how the heating system is used and from the unavoidable climatic variability (which are unlikely a priori predictable), the latter is more accurate in estimating the effective saving obtainable and, therefore, more effective in assessing energy efficiency retrofit interventions.

3. Results and discussions

3.1. Estimation of energy savings consequent to the installation of HAT systems

In Table 4, for the buildings in which the sole installation of HAT systems has been performed, the energy consumption data recorded before and after the installation of HAT systems are reported together with the climatic data. In order to take into account the annual climatic variability, energy consumption data have been divided by the actual HDD, available for each heating season. The last two columns refer, respectively, to the percentage variation in energy consumption recorded one year after the installation of HAT systems and to the further variation observed two years after the installation, when available. Each row in the table represents a single investigated building.

The majority of the investigated buildings showed a reduction of energy consumption for space heating due to the installation of HAT systems. However, the variability of the estimated energy

Table 4

Energy consumptions variation due the sole installation of HAT systems.

Region	Number of dwellings	Previous normalized consumption [kWh °C⁻¹ d⁻¹]	Actual HDD [°C d]	Normalized consumption after 1 year [kWh °C⁻¹ d⁻¹]	Actual HDD [°C d]	Normalized consumption after 2 years [kWh °C⁻¹ d⁻¹]	Actual HDD [°C d]	Var. after 1 year [%]	Var. after 2 years[a] [%]	Mean variation After 1 year [%]	After 2 years[a] [%]
Piemonte	105	280.81	2501	293.01	2297	292.67	2281	4.4%	−0,1%	−5.5%	−2.3%
	48	144.96	2119	146.64	2199	n/a	n/a	1.2%	n/a		
	36	100.52	2119	76.42	2199	n/a	n/a	−24.0%	n/a		
	21	62.88	2119	52.07	2199	n/a	n/a	−17.2%	n/a		
	30	86.42	2297	78.81	2356	77.01	2424	−8.8%	−2,1%		
	40	55.86	2501	64.67	2297	63.29	2424	15.8%	−2,5%		
	24	82.26	2297	70.79	2356	68.26	2424	−13.9%	−3,1%		
	68	221.45	2424	195.82	2501	185.11	2297	−11.6%	−4,3%		
Lazio	58	256.04	1408	217.90	1476	n/a	n/a	−14.9%	n/a	−17.1%	n/a
	36	104.29	1565	83.74	1579	n/a	n/a	−19.7%	n/a		
	21	141.32	1716	116.75	1579	n/a	n/a	−17.4%	n/a		
	54	248.00	1565	202.77	1579	n/a	n/a	−18.2%	n/a		
Lombardia	50	153.73	1899	153.68	1906	n/a	n/a	−0.0%	n/a	−3.4%	n/a
	650	1941.98	1899	1866.57	1906	n/a	n/a	−3.9%	n/a		
	110	331.95	1899	351.21	1906	n/a	n/a	5.8%	n/a		
	45	180.87	1899	143.05	1906	n/a	n/a	−20.9%	n/a		
	240	727.80	1899	740.43	1906	n/a	n/a	1.7%	n/a		
	20	79.78	1899	73.35	1906	n/a	n/a	−8.1%	n/a		
	25	73.77	1899	73.28	1906	n/a	n/a	−0.7%	n/a		
	25	100.22	1899	89.56	1906	n/a	n/a	−10.6%	n/a		
	70	222.30	1899	214.74	1906	n/a	n/a	−3.4%	n/a		
	30	101.48	1899	96.19	1906	n/a	n/a	−5.2%	n/a		
	20	61.10	1899	60.66	1906	n/a	n/a	−0.7%	n/a		
	40	132.43	1899	126.81	1906	n/a	n/a	−4.2%	n/a		
	50	155.53	1899	154.65	1906	n/a	n/a	−0.6%	n/a		
	70	227.79	1899	221.98	1906	n/a	n/a	−2.6%	n/a		
	60	194.67	1899	211.78	1906	n/a	n/a	8.8%	n/a		
	40	112.44	1899	123.57	1906	n/a	n/a	9.9%	n/a		
	40	121.92	1899	120.33	1906	n/a	n/a	−1.3%	n/a		
	60	189.82	1899	187.87	1906	n/a	n/a	−1.0%	n/a		
	40	108.18	1899	108.13	1906	n/a	n/a	−0.0%	n/a		
	90	320.08	1899	299.40	1906	n/a	n/a	−6.5%	n/a		
	90	345.43	1899	310.53	1906	n/a	n/a	−10.1%	n/a		
	40	118.72	1899	112.85	1906	n/a	n/a	−5.0%	n/a		
	40	124.06	1899	117.55	1906	n/a	n/a	−5.3%	n/a		
	15	51.08	1899	49.46	1906	n/a	n/a	−3.2%	n/a		
	70	273.35	1899	220.72	1906	n/a	n/a	−19.3%	n/a		
	Mean annual energy saving									−8.7%	−2.3%

[a] Additional variation referred to the difference between energy consumptions 1 and 2 years after the HAT systems installation.

Basic clustering		Geometrical properties	Building performance parameters	
Size (i)	Age (j)	Interstorey height $h(j)$	Thermal transmittance $U(j)$	System efficiencies
1 Single-family				
2 Two-family				
3 Multi-family 3/4				$\eta_{gen}(i,j)$
4 Multi-family 5/8	CA-1	h_1	$U_{wall1}, U_{r1},$ $(...)$	$\eta_d, \eta_e, \eta_r,$ constant
5 Multi-family 9/15				
6 Multi-family >15				
7 Single-family				
8 Two-family				
9 Multi-family 3/4				$\eta_{gen}(i,j)$
10 Multi-family 5/8	CA-2	h_2	$U_{wall2}, U_{r2},$ $(...)$	$\eta_d, \eta_e, \eta_r,$ constant
11 Multi-family 9/15				
12 Multi-family >15				
.. Single-family				
.. Two-family				
... Multi-family 3/4				
.. Multi-family 5/8	$(...)$	$(...)$	$(...)$	$(...)$
... Multi-family 9/15				
... Multi-family >15				
49 Single-family				
50 Two-family				
51 Multi-family 3/4				$\eta_{gen}(i,j)$
52 Multi-family 5/8	CA-9	h_9	$U_{wall9}, U_{r9},$ $(...)$	$\eta_d, \eta_e, \eta_r,$ constant
53 Multi-family 9/15				
54 Multi-family >15				

Fig. 4. Graphical representation of the BTM for a given climatic zone.
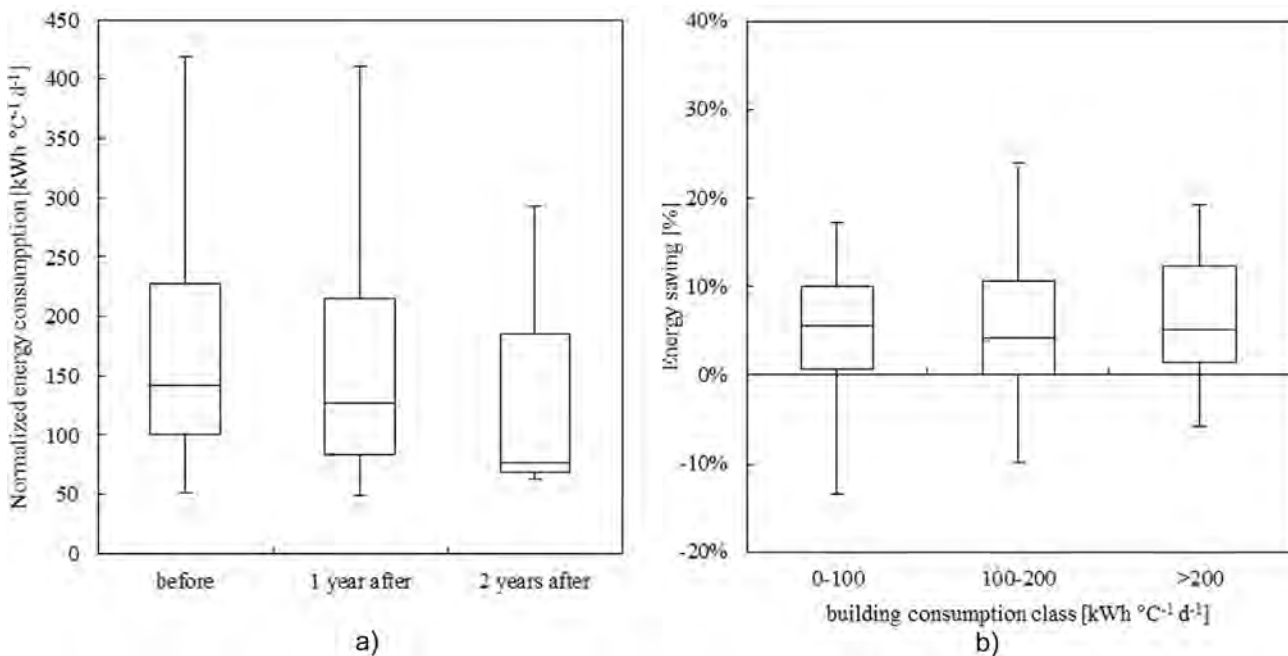
Fig. 5. Analysis of energy consumptions of the investigated buildings before and after the installation of the sole HAT systems in terms of: a) Normalized energy consumption, b) Energy saving.

saving is high. In fact, only 17 buildings have undergone a high energy saving (between 5% and 24%), whereas in 13 buildings this was lower (from 0 to 5%). In 7 buildings an increase of energy consumption even occurred (up to about 15% in the worst case). The results are shown in Fig. 5. In particular, Fig. 5(a) clearly shows an energy consumption reduction over time, while Fig. 5(b) highlights energy savings of higher energy consuming buildings are more reliable than those of lower ones, since data dispersion is lower as buildings' energy consumption increases.

The results also highlight a huge difference between the two investigated climatic zones in terms of mean energy saving achieved after the installation of HAT systems. In fact, for buildings located in Lombardia and Piemonte (prevalent climatic zone E) a lower benefit (about 3.5% and 5.5% respectively) has been estimated. On the other hand, the mean energy saving in Lazio (prevalent climatic zone D) is about 17%. Such relevant figure is probably due to the fact that thermoregulation is more effective where solar heat gains are higher. In the few buildings in which energy consumption data two years after the installation of HAT systems were available, an additional benefit of about 2.3% has been observed. This effect is also described in the current scientific literature [26,54], although in the present experimental campaign a lower value has been found. It is believed that the same may apply to the other investigated buildings.
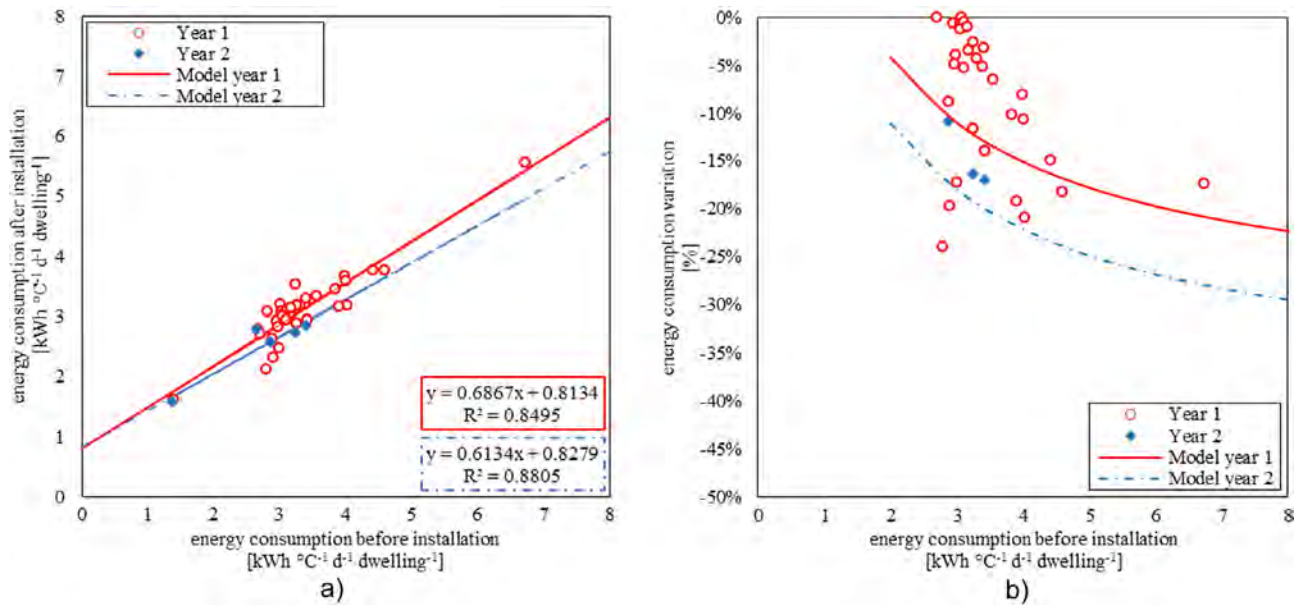
Fig. 6. Regression analysis of investigated buildings in terms of energy consumption before and after the installation of the sole HAT systems in terms of: a) Specific energy consumption, b) Energy saving.

Thus, the authors estimated the Italian mean expected energy saving of about 11%. This figure was obtained by simply averaging the benefit observed in the three investigated regions, equal to 8.7% one year after the installation of HAT systems, and then considering the additional benefit of 2.3% observed two years after (see Table 4). This value has been used to estimate the overall potential of the current policy about individual heat metering for space heating in Italy.

The energy consumption data have been also normalized with respect to the number of dwellings per building, for a "specific dwelling consumption" analysis. Fig. 6(a) shows a linear correlation between the specific energy consumption before and after the installation of HAT systems. In this figure, the bisector line represents the locus of points in which no variation of energy consumption occurs after the installation of HAT systems, while the lower and the upper areas represent, respectively, the decreased and increased energy consumption regions. The figure shows that high energy-consuming buildings gain a greater energy benefit from the installation of HAT systems. In Fig. 6(b), the regression curve between the energy saving and the specific energy consumption per dwelling before the installation is presented. Such curve should then be used to estimate the expected energy benefit, as a function of the specific consumption of the building before the installation of HAT systems. It can be noticed that the expected benefit is negligible for low consumption buildings, whereas for higher ones it is higher and tends to a constant value. Both the curves of the expected benefit one and two years after the installation show the same trend, with a quite constant shift.

The same analysis has been extended to the buildings in which the HAT systems were installed together with the replacement of the old boiler with a high efficiency one (all located in Piemonte, climatic zone E). In this case, a higher energy saving has always been observed, ranging from about 15 to 35% and none of the buildings increased energy consumption. Table 5 shows that the mean annual benefit was about 24.3% one year after the retrofit and that an additional benefit of about 5.7% was recorded two years after. Although there is a mutual influence of different energy retrofits carried out simultaneously, assuming negligible variation of the new boiler efficiency during the first two years, it is possible to attribute the increase of energy saving between the first

and the second year to the sole effect of HAT systems. This result remarks the relevance of the end user awareness to obtain more significant energy savings.

Fig. 7(a) also highlights that energy consumption data two years after the retrofit intervention are more reliable than the ones before. Furthermore, referring to the box plot in Fig. 7(b), it is confirmed that the data dispersion is lower for higher energy consuming buildings.

Fig. 8(a) and (b) show similar trends to those found in buildings in which the installation of the sole HAT systems was performed, although with specific benefits and data dispersion significantly higher, as expected.

3.2. Energy consumption for space heating in Italy

Table 6 presents the results of the validation and calibration of the model described in Section 2.2, showing the differences between the energy consumption data available from REBs and the ones estimated using the developed model. It can be pointed out that the mean deviation between the primary energy consumption for space heating in Italian regions calculated through the model and the corresponding data from REBs is initially within about ±22%. Subsequently, thanks to the calibration of U-values of building stocks of each single region, such deviation decreases to about ±2.0%, which is considered acceptable for the purpose of the present analysis.

Fig. 9(a) shows the $EP_{H,min}$ for obliged buildings making efficient the installation of HAT systems resulting from the economic feasibility analysis, as a function of the number of dwellings in the building and of the three different incentive scenarios. Furthermore, in Fig. 9(b), the simple PBT is reported as a function of the primary energy EP_H (regardless of whether in AR or OR conditions) for a number of dwellings in the building equal to 10. It is important to highlight that for buildings with a number of dwelling higher than 10 the simple PBT resulting from the economic feasibility analysis does not vary significantly.

Finally, in Table 7 the estimated energy saving obtainable through different incentive policies and obligation approaches is reported.

Table 5
Energy consumption in buildings where HAT systems were installed together with boiler replacement.

Number of dwellings	Previous consumption [kWh °C⁻¹ d⁻¹]	HDD [°C d]	Normalized consumption after 1 year [kWh °C⁻¹ d⁻¹]	HDD [°C d]	Normalized consumption after 2 years [kWh °C⁻¹ d⁻¹]	HDD [°C d]	Variation after 1 year [%]	Variation after 2 years* [%]
30	111.80	2297	93.44	2356	81.15	2424	−16.4%	−11.0%
52	211.74	2501	160.59	2297	178.70	2281	−24.2%	8.6%
13	68.12	2297	55.56	2356	45.13	2424	−18.4%	−15.3%
13	62.40	2424	51.52	2101	57.18	2119	−17.4%	9.1%
21	99.70	2297	74.84	2356	66.86	2424	−24.9%	−8.0%
140	403.22	2297	322.36	2356	288.02	2424	−20.1%	−8.5%
20	125.26	2297	95.69	2356	79.15	2424	−23.6%	−13.2%
50	172.83	2356	122.84	2424	100.18	2424	−28.9%	−13.1%
40	170.76	2297	141.10	2356	127.65	2424	−17.4%	−7.9%
18	94.40	2424	61.09	2501	61.47	2297	−35.3%	0.4%
40	180.38	2297	139.91	2356	130.36	2424	−22.4%	−5.3%
18	95.76	2297	62.58	2356	54.05	2424	−34.7%	−8.9%
21	86.27	2297	61.49	2356	62.61	2424	−28.7%	1.3%
Mean variation							−24.3%	−5.6%

* Additional variation between year 1 and year 2.
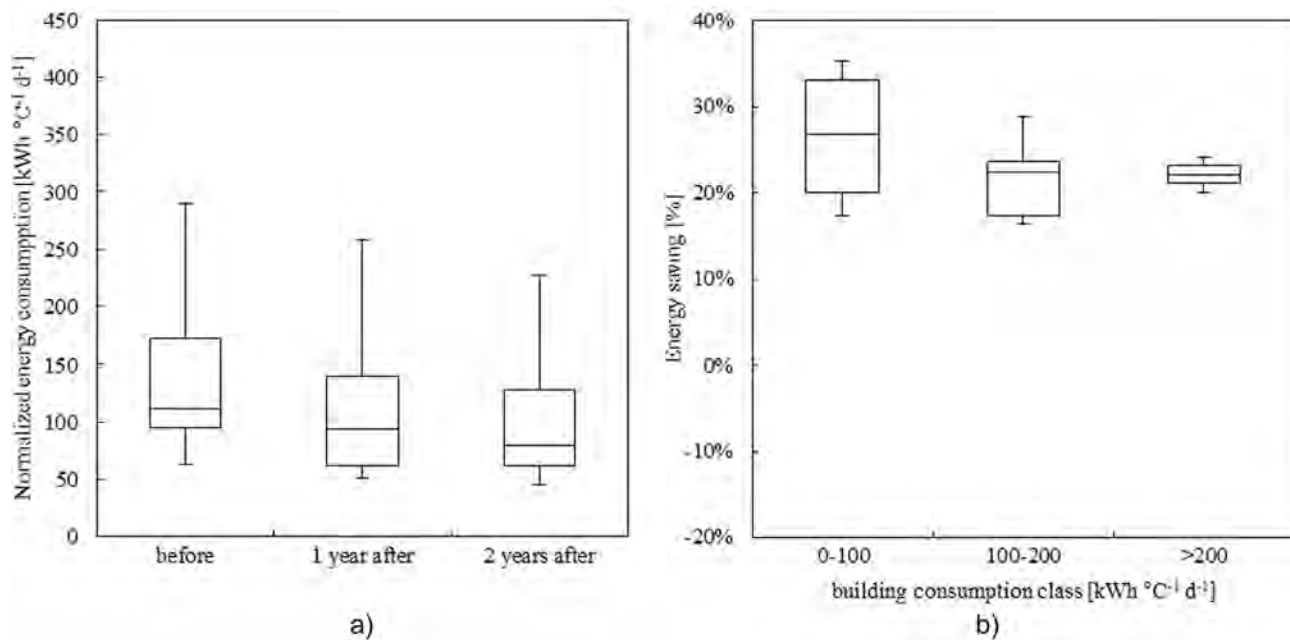
Fig. 7. Analysis of energy consumption of the investigated buildings before and after the installation of the HAT systems performed together with the replacement of the boiler in terms of: a) Normalized energy consumptions, b) Energy saving.

From data in Table 7, it can be pointed out that if all the potentially obliged dwellings in Italy would install HAT systems, this can lead to an overall annual energy saving in residential sector ranging between 0.3% and 1.9%, corresponding to 0.056 and 0.399 Mtoe, respectively. Furthermore:

- nearly all the regions in Southern Italy would be exempted to install HAT systems, since negligible savings occur for both AR and OR approaches regardless of the incentive scenarios; this was expected as a result of the lower energy consumption associated with Mediterranean climate;
- significant energy savings are achievable only in the Central-Northern Italy regions; as for example, in Lombardia Region an energy saving of 75% of the whole national one (i.e. 0.042 out of 0.056 Mtoe) in OR approach without incentives has been estimated; this results from both the climatic conditions and the highest number of buildings potentially subject to the obligation;

- the AR obligation approach shows higher energy saving in respect to the OR one, especially in absence of incentives; in this case, a 0.9% energy saving of the national energy consumption in AR obligation occurs, which corresponds to about 0.3% in OR; as expected, this is due to the lower value of energy consumption estimated in OR which affects the calculated energy saving per year for each building typology;
- the 50% and 65% incentive scenarios present quite similar results at national level (especially for the AR obligation approach).

4. Conclusions

In this paper, the potential of the EU and Italian policy of mandatory installation of individual metering and thermoregulation systems for space heating has been analysed for the residential building stock in Italy. To this aim, the energy consumptions of 3047 dwellings in 50 buildings, located in the major Italian regions (i.e. Piemonte, Lombardia and Lazio) have been investigated before
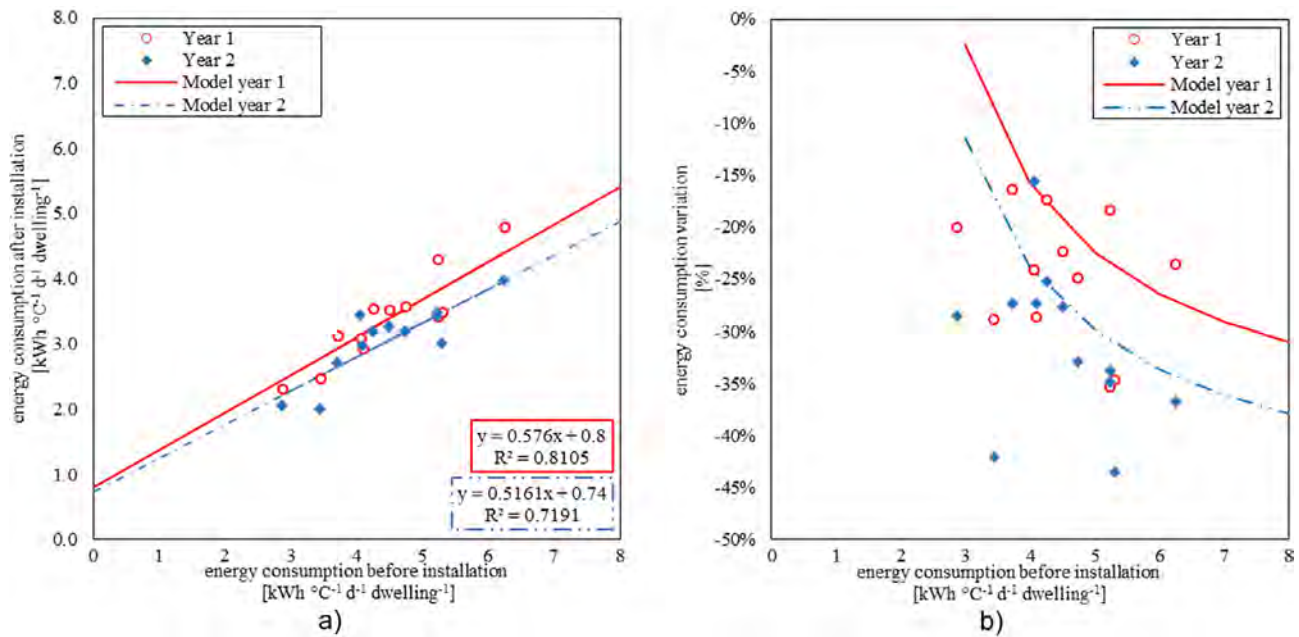
Fig. 8. Regression analysis of investigated buildings in terms of specific energy consumption before the installation of HAT systems performed together with the replacement of the boiler: a) specific energy consumption after the installation, b) energy saving after the installation.

Table 6
Comparison between energy consumption for space heating estimated by the developed model and REBs/NEBs in 2015 [49,50].

Region		REBs [Mtoe]	Data from model validation		Data from model with *U*-values calibration	
			[Mtoe]	Deviation [%]	[Mtoe]	Deviation [%]
North	Piemonte	2.076	2.046	−1.5%	2.081	0.2%
	Valle d'Aosta	0.093	0.074	−19.9%	0.092	−1.2%
	Liguria	0.552	0.571	3.4%	0.549	−0.6%
	Lombardia	4.960	3.842	−22.5%	5.037	1.5%
	Trentino Alto Adige	0.585	0.663	13.3%	0.589	0.7%
	Veneto	1.926	2.319	20.4%	1.926	0.0%
	Friuli-Venezia Giulia	0.461	0.533	15.7%	0.469	1.7%
	Emilia-Romagna	2.114	1.841	−12.9%	2.150	1.7%
Center	Toscana	1.419	1.415	−0.3%	1.415	−0.3%
	Umbria	0.410	0.389	−5.1%	0.412	0.5%
	Marche	0.554	0.572	3.3%	0.551	−0.5%
	Lazio	1.711	1.375	−19.7%	1.686	−1.5%
	Abruzzo	0.397	0.361	−9.3%	0.405	1.9%
South and Islands	Molise	0.118	0.135	14.2%	0.117	−1.3%
	Campania	1.234	1.201	−2.6%	1.234	0.0%
	Puglia	0.834	0.999	19.9%	0.837	0.4%
	Basilicata	0.158	0.174	9.9%	0.156	−1.5%
	Calabria	0.275	0.333	21.0%	0.275	−0.1%
	Sicilia	0.743	0.689	−7.4%	0.744	0.0%
	Sardegna	0.331	0.294	−11.1%	0.326	−1.3%
Italy		20.951	19.825	−5.4%	21.050	−0.5%

and after the installation of HAT systems. The experimental results show that:

– a mean benefit of about 8.7% has been found one year after the installation of HAT systems;
– an additional benefit of about 2.3% has been found two years after the installation of HAT systems, thus a total mean benefit of 11.0% is potentially achievable through the installation of HAT systems;
– the variation of energy consumption after the installation of HAT systems is very wide, due to the building characteristics and to the operative conditions of the heating plant; in any case, authors believe that the effectiveness of such systems is strongly dependent on user's awareness;
– the combined effect of the installation of HAT systems together with the replacement of the boiler always resulted in higher

energy savings and in a further decrease of energy consumption two years after the energy retrofit;
– the percentage energy saving increases as the specific consumption of the building increases and tends to stabilize to a constant value;
– although the energy saving of buildings located in warmer climate is in absolute lower in respect to the colder one, the percentage benefit is higher in presence of relevant solar gains contribution, thanks to the greater effectiveness of the thermoregulation systems.

The authors developed a model to predict the Italian residential energy consumption for space heating, also on a regional scale. The developed model allowed to estimate with a good accuracy the potential energy saving related to the installation of individual heat metering systems, taking into account the economic feasibil-
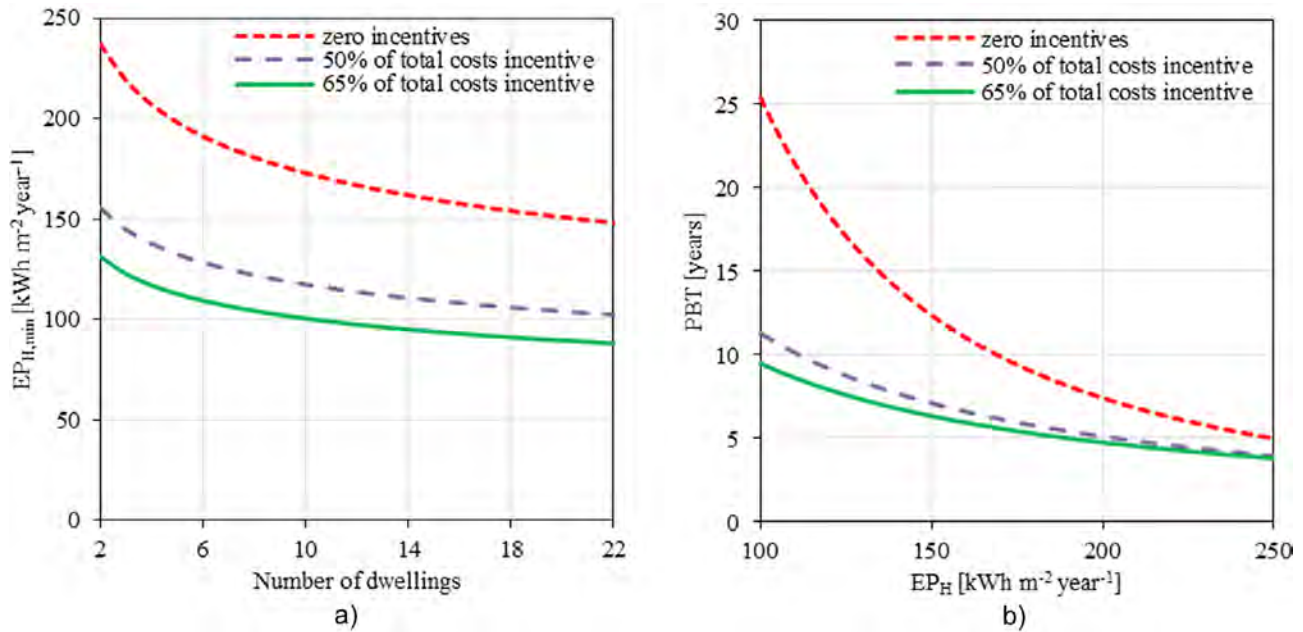
Fig. 9. Results of the economic feasibility analysis making efficient the installation of HAT in different incentive scenarios: a) $EP_{H,min}$ as a function of the number of dwellings; b) PBT as a function of EP_H.

Table 7
Energy savings achievable through different fiscal policies and obligation approach [Mtoe].

Region		Fiscal policy 1 (0% incentives)		Fiscal policy 2 (50% incentives)		Fiscal policy 3 (65% incentives)	
		OR	AR	OR	AR	OR	AR
North	Piemonte	0.000	0.019	0.034	0.056	0.041	0.065
	Valle d'Aosta	0.002	0.003	0.004	0.004	0.004	0.004
	Liguria	0.000	0.004	0.003	0.015	0.006	0.017
	Lombardia	0.042	0.089	0.107	0.141	0.128	0.143
	Trentino Alto Adige	0.011	0.016	0.019	0.023	0.022	0.024
	Veneto	0.000	0.000	0.003	0.014	0.008	0.017
	Friuli-Venezia Giulia	0.000	0.000	0.000	0.002	0.002	0.005
	Emilia-Romagna	0.000	0.030	0.021	0.036	0.027	0.037
Center	Toscana	0.000	0.007	0.005	0.017	0.010	0.018
	Umbria	0.000	0.003	0.002	0.004	0.003	0.004
	Marche	0.000	0.001	0.001	0.004	0.002	0.005
	Lazio	0.000	0.012	0.006	0.037	0.014	0.043
	Abruzzo	0.000	0.000	0.000	0.002	0.000	0.003
South and Islands	Molise	0.000	0.000	0.000	0.001	0.000	0.001
	Campania	0.000	0.000	0.000	0.007	0.000	0.008
	Puglia	0.000	0.000	0.000	0.001	0.000	0.003
	Basilicata	0.000	0.000	0.000	0.001	0.000	0.001
	Calabria	0.000	0.000	0.000	0.000	0.000	0.000
	Sicilia	0.000	0.000	0.000	0.001	0.000	0.001
	Sardegna	0.000	0.000	0.000	0.001	0.000	0.002
Italy (Mtoe)	0.056	0.186	0.204	0.366	0.268	0.399	
Italy (share[a])		0.3%	0.9%	1.0%	1.7%	1.3%	1.9%

[a] Share referred to the total energy consumption for space heating in residential sector of 21.1 Mtoe estimated in 2015.

ity constraint fostered by the European Directive 2012/27/EU, under three incentive scenarios (i.e. 0–50–65% of related costs) and two obligation approaches (i.e. OR and AR). The application of the model to the Italian residential building stock shows that:

- in Italy the installation of HAT systems in the residential building stock can lead to a potential energy saving ranging from 0.056 to 0.399 Mtoe/year (i.e. from 0.3 to 1.9% of the estimated energy consumption for space heating of Italy);
- from a policy perspective, the installation of HAT systems is ineffective in the South Italian regions regardless of existing incentives;
- fiscal incentives applied in Central/North Italy lead to significantly higher energy savings;

- the AR obligation approach leads to higher benefits in respect to the OR one, especially in the no-incentives scenario.

The authors believe the results presented in this paper should be useful for defining national policies to be adopted for the spread and the effective use of individual heat metering and charging systems. In fact, they allow both to better understand the expected effectiveness of the current regulation and to improve the effectiveness of monitoring and incentive actions, which may be addressed to the regions with a higher energy saving potential. In addition, the results obtained can also be used by designers for the assessment of the economic feasibility of the installation of HAT systems.

Acknowledgments

References

[1] European Commission, Directive 2012/27/EU of the European Parliament and of the Council of 25 October 2012 on energy efficiency, amending Directives 2009/125/EC and 2010/30/EU and repealing Directives 2004/8/EC and 2006/32/EC, 2012.

[2] L. Celenza, M. Dell'Isola, G. Ficco, M. Greco, M. Grimaldi, Economic and technical feasibility of metering and sub-metering systems for heat accounting, Int. J. Energy Econ. Policy 6 (3) (2016) 581–587.

[3] P. Koski, Study of Cost Effectiveness of Individual Heat Meters and Heat Cost Allocators in Apartment Buildings in Finland, EED, CA, 2014.

[4] A. Carlsson, C. Engström, B. Jönsson, Individual Metering and Charging in Existing Buildings, Boverket, 2015 (Report 2015:34).

[5] S. Siggelsten, S. Olander, Individual metering and charging of heat and hot water in Swedish housing cooperatives, Energy Policy 61 (2013) 874–880.

[6] L. Celenza, M. Dell'Isola, G. Ficco, B.I. Palella, G. Riccio, Heat accounting in historical buildings, Energy Build. 95 (2015) 47–56.

[7] Empirica GmbH, Guidelines on good practice in cost-effective cost allocation and billing of individual consumption of heating, cooling and domestic hot water in multi-apartment and multi-purpose buildings, Version dated 30th May 2016.

[8] Repubblica Italiana, Decreto Legislativo 4 luglio 2014, n. 102, Gazzetta Ufficiale della Repubblica Italiana (in Italian), 2014.

[9] ISTAT, Censimento Popolazione Abitazioni 2011, ISTAT, Available at: http://dati-censimentopopolazione.istat.it/Index.aspx?lang=it (last accessed 2017/09/19).

[10] European Commission, Evaluation Report Covering the Evaluation of the EU's Regulatory Framework for Electricity Market Design and Consumer Protection in the Fields of Electricity and Gas, Evaluation of the EU Rules on Measures to Safeguard security of Electricity Supply and Infrastructure Investment (Directive 2005/89), Commission Staff Working Document, Brussels, 2016.

[11] L. Castellazzi, Y. Saheb, P. Zangheri, K. Bodis, Individual heat metering – setting the scene, Workshop on Heat Metering, Efficient Heat Cost Allocation and Billing – Challenges and Opportunities, Paris, May 5th and 6th, 2015.

[12] AEEGSI, Documento per la consultazione. Regolazione in materia di obblighi e fornitura e installazione di sistemi di misura nel settore del teleriscaldamento e del teleraffrescamento. (In Italian), Autorità per l'energia elettrica il gas e il sistema idrico, 2016.

[13] AEEGSI, Regolazione dei costi del servizio di suddivisione delle spese per riscaldamento, raffrescamento e acqua igienico sanitaria, tra le diverse unità immobiliari nei condomini e negli edifici polifunzionali. Ricognizione del mercato e orientamenti per la definizione dei costi indicativi di riferimento per i fornitori del servizio. (In Italian), Autorità per l'energia elettrica il gas e il sistema idrico, 2017.

[14] Building Research Establishment Ltd, 2012. District heating – Heat metering Cost Benefit Analysis. Available at(last accessed 2018/01/15) (last accessed 2018/01/15) https://www.gov.uk/government/uploads/system/uploads/attachment_data/file/48389/5462-district-heating-heat-metering-cost-benefit-anal.pdf.

[15] Agenzia delle Entrate, Circolare 18/E del 06/05/2016. Questioni interpretative in materia di IRPEF prospettate dal Coordinamento Nazionale dei Centri di Assistenza Fiscale e da altri soggetti (in Italian), 2016.

[16] T. Cholewa, A. Siuta-Olcha, C.A. Balaras, Actual energy savings from the use of thermostatic radiator valves in residential buildings – Long term field evaluation, Energy Build. 151 (2017) 487–493.

[17] T. Cholewa, A. Siuta-Olcha, M.A. Skwarczynski, Experimental evaluation of three heating systems commonly used in the residential sector, Energy Build. 43 (9) (2011) 2140–2144.

[18] S. Andersen, R.K. Andersen, B.W. Olesen, Influence of heat cost allocation on occupants' control of indoor environment in 56 apartments: Studied with measurements, interviews and questionnaires, Build. Environ. 101 (2016) 1–8.

[19] S. Darby, 2016. The Effectiveness of Feedback on Energy Consumption. Available at:(last accessed: 2018-01-15), Environmental Change Institute, University of Oxford, (last accessed: 2018-01-15), Environmental Change Institute, University of Oxford http://www.eci.ox.ac.uk/research/energy/downloads/smart-metering-report.pdf.

[20] M. Dell'Isola, G. Ficco, F. Arpino, G. Cortellessa, L. Canale, A novel model for the evaluation of heat accounting systemsreliability in residential buildings, Energy Build. 150 (2017) 281–293.

[21] G. Ficco, L. Celenza, M. Dell'Isola, P. Vigo, Experimental comparison of residential heat accounting systems at critical conditions, Energy Build. 130 (2016) 477–487.

[22] V. Monetti, E. Fabrizio, M. Filippi, Impact of low investment strategies for space heating control: application of thermostatic radiators valves to an old residential building, Energy Build. 95 (2015) 202–210.

[23] Infrastrutture Lombarde, Available at: https://www.dati.lombardia.it/d/at9e-gkx8/visualization (last accessed: 2018/01/09).

[24] L. Castellazzi, Analysis of Member States' rules for allocating heating, cooling and hot water costs in multiapartment/ purpose buildings supplied from collective systems, 2017.

[25] C. Felsmann, J. Schmidt, T. Mróz, Effects of Consumption-Based Billing Depending on the Energy Qualities of Buildings in the EU, Technische Universität Dresden, Politechnika Poznańska, 2015.

[26] T. Cholewa, A. Siuta-Olcha, Long term experimental evaluation of the influence of heat cost allocators on energy consumption in a multifamily building, Energy Build. 104 (2015) 122–130.

[27] M. Paulsen, L. Gullev, The installation of meters leads to permanent changes in consumer behaviour, News from DBDH 3/2006, 2006.

[28] M. Kavgic, A. Mavrogianni, D. Mumovic, A. Summerfield, Z. Stevanovic, M. Djurovic-Petrovic, A review of bottom-up building stock models for energy consumption in the residential sector, Build. Environ. 45 (2010) 1683–1697.

[29] M. Brøgger, K. Bjarne Wittchen, Estimating the energy-saving potential in national building stocks – a methodology review, Renewable Sustainable Energy Rev. (2017).

[30] L.G. Swan, V.I. Ugursal, Modeling of end-use energy consumption in the residential sector: a review of modeling techniques, Renewable Sustainable Energy Rev. 13 (8) (2009) 1819–1835.

[31] L. Filogamo, G. Peri, G. Rizzo, A. Giaccone, On the classification of large residential building stocks by sample typologies for energy planning purposes, Appl. Energy (2014) 825–835.

[32] G.V. Fracastoro, M. Serraino, A methodology for assessing the energy performance of large scale building stocks and possible applications, Energy Build. 43 (2011) 844–852.

[33] I. Ballarini, V. Corrado, F. Madonna, S. Paduos, F. Ravasio, Energy refurbishment of the Italian residential building stock: energy and cost analysis through the application of the building typology, Energy Policy 10 (2017) 148–160.

[34] G. Ficco, Metrological performance of diaphragm gas meters in distribution networks, Flow Meas. Instrum. 37 (2014) 65–72.

[35] European Committee for Standardization, EN ISO 15927-6 Hygrothermal performance of buildings – Calculation and presentation of climatic data – Part 6: Accumulated temperature differences (degree-days), 2007.

[36] I. Ballarini, S.P. Corgnati, V. Corrado, Use of reference buildings to assess the energy saving potentials of the residential building stock: the experience of TABULA project, Energy Policy 68 (2014) 273–284.

[37] T. Loga, B. Stein, N. Diefenbach, TABULA building typologies in 20 European countries-making energy-related features of residential building stocks comparable, Energy Build. 132 (2016) 4–12.

[38] E.G. Dascalaki, K. G.Droutsa, A.B. Constantino, S. Kontoyiannidis, Building typologies as a tool for assessing the energy performance of residential buildings – a case study for the Hellenic building stock, Energy Build. 43 (12) (2011) 3400–3409.

[39] F. Margiotta, G. Puglisi, Caratterizzazione Del Parco Edilizio Nazionale Determinazione dell'edificio Tipo Per Uso Ufficio (in Italian), Ministero dello Sviluppo Economico, ENEA, 2009.

[40] G. Puglisi, F. Zanghirella, P. Ungaro, G. Cammarata, A methodology for the generation of energy consumption profiles in the residential sector, Int. J. Heat Technol. 34 (3) (2016) 491–497.

[41] M. Caldera, G. Puglisi, F. Zanghirella, F. Margiotta, P. Ungaro, V. Talucci, G. Cammarata, Proposal of a survey-based methodology for the determination of the energy consumption in the residential sector, Int. J. Heat Technol. 35 (2017) S152–S158.

[42] V. Corrado, I. Ballarini, S.P. Corgnati, Building Typology Brochure – Italy Fascicolo Sulla Tipologia Edilizia Italiana (In Italian), Politecnico di Torino – Dipartimento Energia; Gruppo di Ricerca TEBE, Torino, 2014.

[43] Ente Nazionale Italiano di Unificazione, UNI/TS 11300-2 Prestazioni energetiche degli edifici – Parte 2: Determinazione del fabbisogno di energia primaria e dei rendimenti per la climatizzazione invernale, per la produzione di acqua calda sanitaria, per la ventilazione e per l'illuminazione in edifici non residenziali (in Italian), 2014.

[44] H. Erhorn, H. Erhorn-Kluttig, M. Citterio, M. Cocco, D. van Orshoven, A. Tilmans, P. Schild, P. Bloem, K. Engelund Thomsen, J. Rose, An effective Handling of Thermal Bridges in the EPBD Context. Final Report of the IEE ASIEPI Work on Thermal Bridges., ASsessment and Improvement of the EPBD Impact (ASIEPI), 31st, March 2010.

[45] G. Evola, G. Margani, L. Marietta, Energy and cost evaluation of thermal bridge correction in Mediterranean climate, Energy Build. 43 (9) (2011) 2385–2393.

[46] EUROSTAT, eurostat – Your key to European statistics, Eurostat, Available at: http://ec.europa.eu/eurostat/data/database , (last accessed 2017/09/19).

[47] European Committee for Standardization, EN ISO 13790 Energy performance of buildings – Calculation of energy use for space heating and cooling, 2008.

[48] European Committee for Standardization, EN 15316 (series) Heating systems in buildings – Method for calculation of system energy requirements and system efficiencies, 2007.

[49] ENEA, Osservatorio politiche energetico-ambientali regionali e locali, Italian National Agency for New Technologies, Energy and Sustainable Economic Development, Available at: http://enerweb.casaccia.enea.it/enearegioni/UserFiles/Pianienergetici/pianienergetici.htm , (last accessed 2017/09/19).

[50] ODYSSEE, ODYSSEE-MURE database, Enerdata. Available at: http://odyssee.enerdata.net/database/ (last accessed 2017/09/19).

[51] European Committee for Standardization, EN 15459 Energy performance of buildings – Economic evaluation procedure for energy systems in buildings, 2007.

[52] AiCARR, La fattibilità tecnico-economica dei sistemi di contabilizzazione dei consumi di energia termica. (In Italian), Associazione Italiana Condizionamento dell'Aria, Riscaldamento, Refrigerazione, 2017.

[53] AEEGSI, Andamento del prezzo del gas naturale per un consumatore domestico tipo in regime di tutela, Available at: https://www.autorita.energia.it/it/dati/gp27new.htm# (last accessed: 2017/09/19).

[54] S. Siggelsten, Reallocation of heating costs due to heat transfer between adjacent apartments, Energy Build. 75 (2014) 256–263.

Study on improved cements with Graphene Oxide

Rita Mancini[1], **Daniele Mirabile Gattia*[1]**, Fabio Girardi[2], Lorenzo Petrucci[1]

[1]SSPT-PROMA-MATPRO, ENEA, CR Casaccia Via Anguillarese 301, 00123 Roma
[2]FSN-FISS-CRGR, ENEA, CR Casaccia Via Anguillarese 301, 00123 Roma

*daniele.mirabile@enea.it

Abstract

The preparation of reinforced cements is an important field of research and different approaches are followed, as for example modifying the composition, in order to obtain composites with improved properties. In this work the preparation of Portland Cement with Graphene Oxide is reported. Graphene Oxide (GO) has been produced by using modified Hummers method. Graphene oxide has been mixed with cement in different ways in order to ascertain the suitable method to obtain optimized results. Samples with different concentrations of GO (0.03%, 0.039%, 0.05%, 0.06%) have been prepared. After 28 days the samples have been investigated by different techniques: Thermogravimetric Analysis (TGA), Scanning Electron Microscopy (SEM), X-Ray Diffraction (XRD) and mechanical tests. SEM allowed to study the microstructure and identify the GO inside the cement matrix. The compressive trials were performed by an uniaxial press averaging results from three tests per type of sample. Surprisingly low quantities of GO added to the cement demonstrated to increase significantly the mechanical performances of the base cement. This work reports results which are promising for the development of new cements for particular applications.

Experimental section

GRAPHENE OXIDE SYNTHESIS: GO was synthetized by Modified Hummers' method starting from commercial graphite powders performing chemical oxidation using sulfuric acid (H_2SO_4), potassium permanganate ($KMnO_4$) and hydrogen peroxide (H_2O_2).
The graphene oxide sludge has been washed and then sonicated to ensure the complete exfoliation of the platelets [1,2].
Characterization: TGA/DTA, FTIR, UV-Vis, SEM, Compression test

UV-VIS

XRD

TGA (C)

SEM

FTIR

As produced GO

GO dispersion unstable in basic solutions
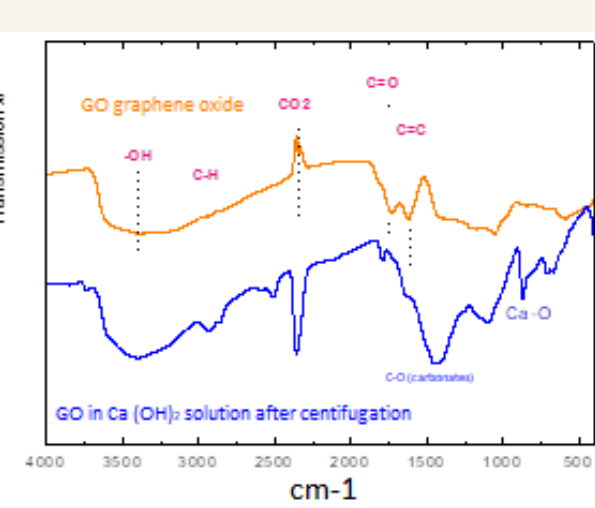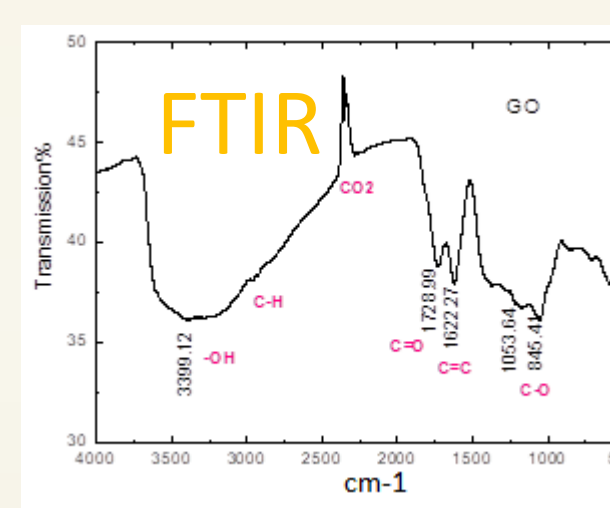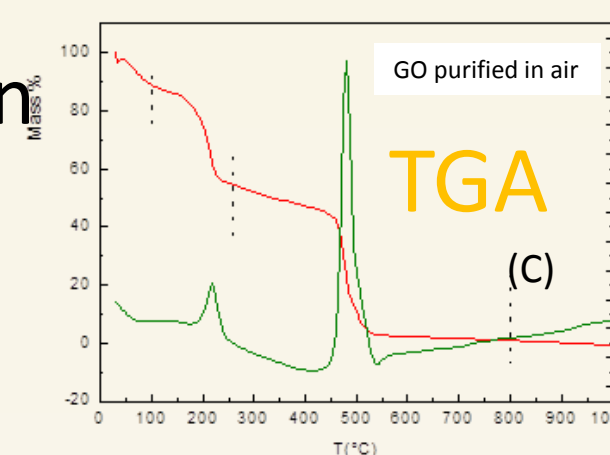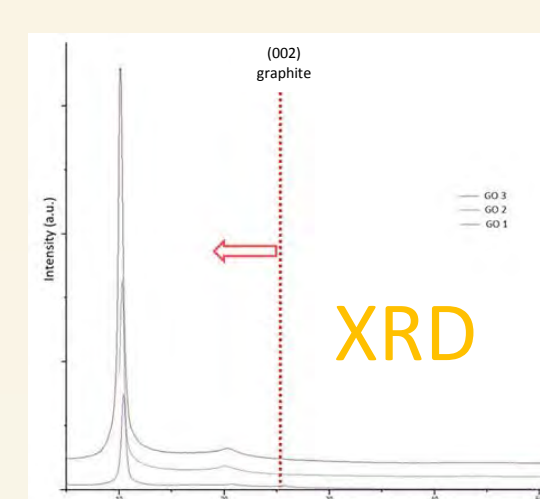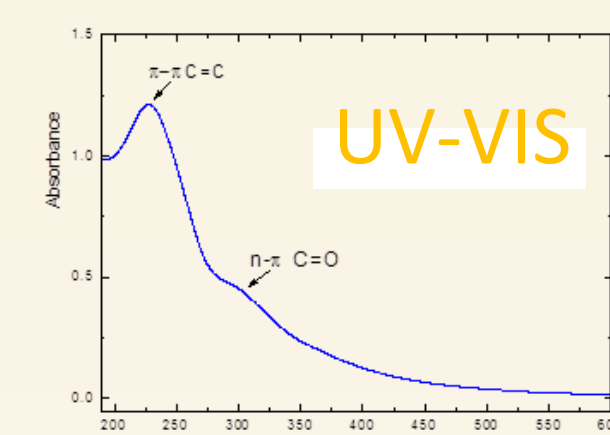
Cement preparation:
1) mixed by adding a suspension of GO in water
2) mixing directly the powders before adding water

Samples with different concentrations of GO (0.03%, 0.039%, 0.05%, 0.06%) have been prepared. Samples have been cured for 28 days in environmental test chamber
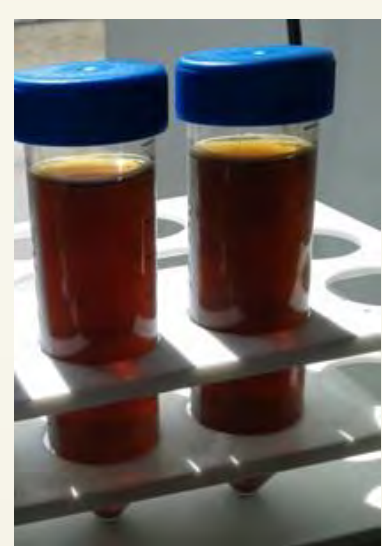
UNI EN 206-1: 2006

20 °C – 95% humidity

Results and discussions

SEM allowed to study the microstructure and identify the GO inside the cement matrix. SEM images revealed, even at low concentrations, how GO is strongly interconnected with the matrix and homogenously dispersed within it. The GO is present in the form of large sheets, even if some sub- and micrometric aggregates were observed. The sheets seems to "contain" the matrix particles as a sort of tie-sheet and partially filling the porosities.
XRD revealed that no substantial modifications in phase composition has been induced by the presence of GO.

The compressive trials were performed by an uniaxial press averaging results from three tests per type of sample. The samples showed a typical hourglass shape after breakage. Low quantities of GO added to the cement demonstrated to increase significantly the mechanical performances of the base cement.
In particular it has been observed that preparing the samples mixing directly the powders an increase in compression strenght of about 40 % has been measured.

The pecurial morphology observed by microscopy observations could be at the a base of best performances of the sample with GO respect to simple cement ones.

SEM

EDS

XRD
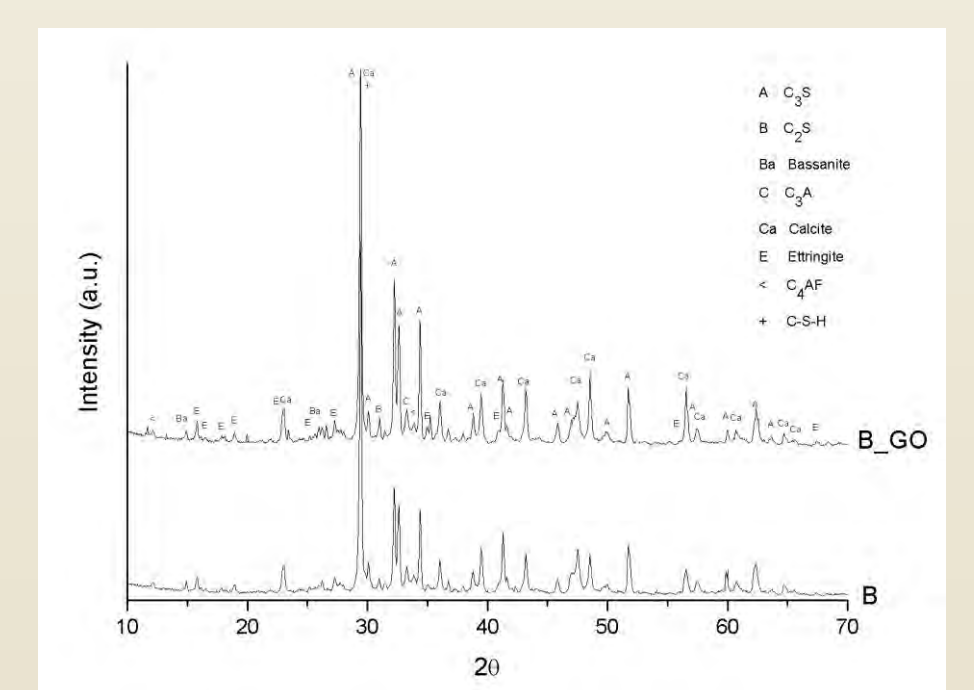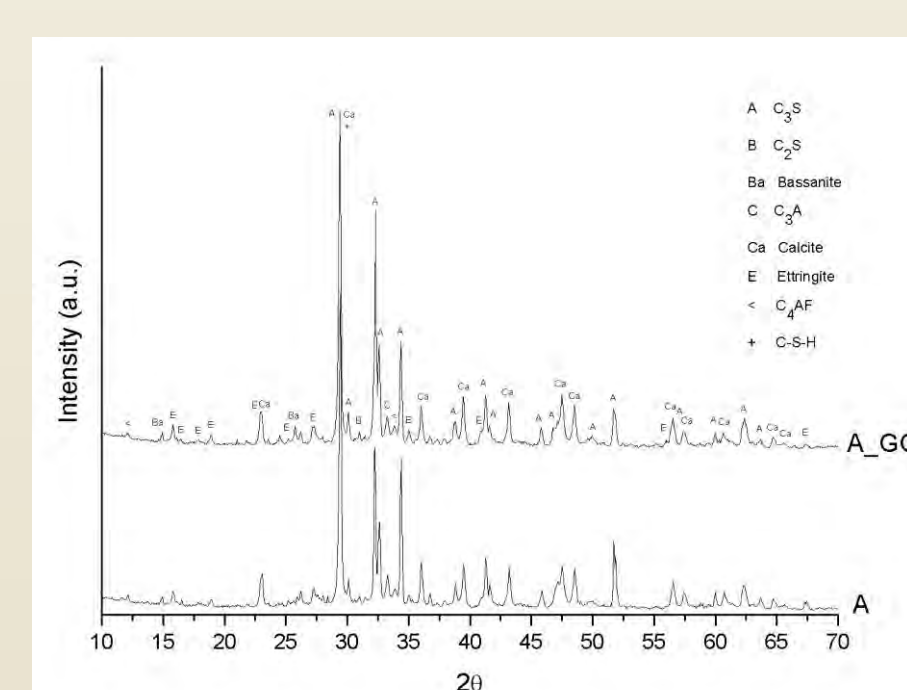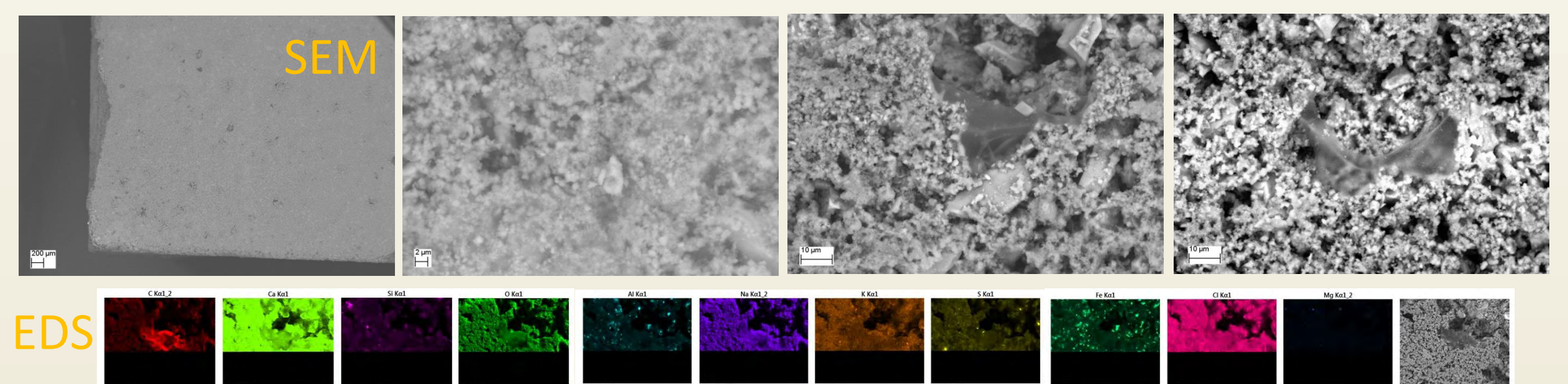
Compression test

Conclusions

In this work GO has been prepared by modified Hummer's method with the aim of preparing GO-reinforced cement. Different samples have been prepared with increasing concentration of GO. It has been observed that small quantities of GO, less than 0.05 wt%, increase largely the compression strength of cement composites prepared. Microstructural observations performed by SEM suggest that GO acts as a binder and aggregating agent which seems to "contain" the matrix particles as a sort of tie-sheet and partially filling the porosities. These observations put some highlights on improved mechanical behavior of GO-reinforced cements.

[1] L. Kou, H. He, C. Gao "Click chemistry approach to functionalize two-dimensional macromolecules of graphene oxide nanosheets" (2010), Nanomicro Lett., 2, 177
[2] T. N. Blanton, D. Majumdar, "X-ray diffraction characterization of polymer intercalated graphite oxide" JCPDS-International Centre for Diffraction Data (2012) ISSN 1097-0002

Use of Graphene oxide for the preparation of reinforced cement-based composites

ENEA

Nano 2018 Innovation
Conference & Exhibition
Rome, 11-14 September

**Maria Rita Mancini[1], Daniele Mirabile Gattia[1], Lorenzo Petrucci[1],
Claudio Russo[2], Fabio Girardi[3]**

[1]SSPT-PROMA-MATPRO-ENEA, [2]SSPT–BIOAG-PROBIO-ENEA, [3]FSN-FISS-CRGR-ENEA,
ENEA: CR Casaccia Via Anguillarese 301, 00123 Roma   rita.mancini@enea.it

Abstract

Important challenges in the building and construction sector in the future will face the preparation of cements with improved mechanical properties. In this direction an attempt is the preparation of composites with suitable additives which interact with cement matrix. In this framework, this work report about the use of Graphene Oxide (GO) as reinforcing agent of Portland Cement. Graphene Oxide is an interesting 2D nanomaterial with important properties and it can be used for different technological applications as nano-scale electronic components, devices based on field emission, sensors, catalysis, composites materials. The GO has been firstly synthesised by a modified Hummers method and successively purified for acid traces removal. The material produced has been largely characterized by (TG-DTA), (XRD), (FTIR), (SEM). The cement-GO composite has been prepared at different concentrations of GO ranging from 0.03% till 0.06%. for the mixing of cement/GO components two routes have been followed: mixing cement with GO solutions (S-L) or dry mixing the two powders (S-S). The samples, with cubic geometry, have been maturated in a temperature and humidity controlled chamber with for 28 days. After complete curing the samples have been investigated by SEM, XRD, TG-DTA and mechanical tests. SEM revealed that GO is present both in the form of large convoluted sheets and of micrometric aggregates in the porosities of cement matrix . The compressive trials were performed by an uniaxial press averaging results from three tests per type of sample. Surprisingly low quantities of GO added to the cement in case of (S-L) mixing route demonstrated to increase significantly the mechanical performances of the base cement. These tests demonstrated an important improvement of GO containing composites mechanical performances respect to initial Portland cement. This work reports results which are promising for the development of new cements for particular applications

GRAPHENE OXIDE SYNTHESIS:

GO was synthetized by Modified Hummers' method starting from commercial graphite powders performing chemical oxidation using sulfuric acid (H_2SO_4), potassium permanganate ($KMnO_4$) and hydrogen peroxide (H_2O_2).
Characterization: TGA/DTA, FTIR, UV-Vis, SEM, Compression test

As produced GO

Experimental section

XRD

UV vis

XRD
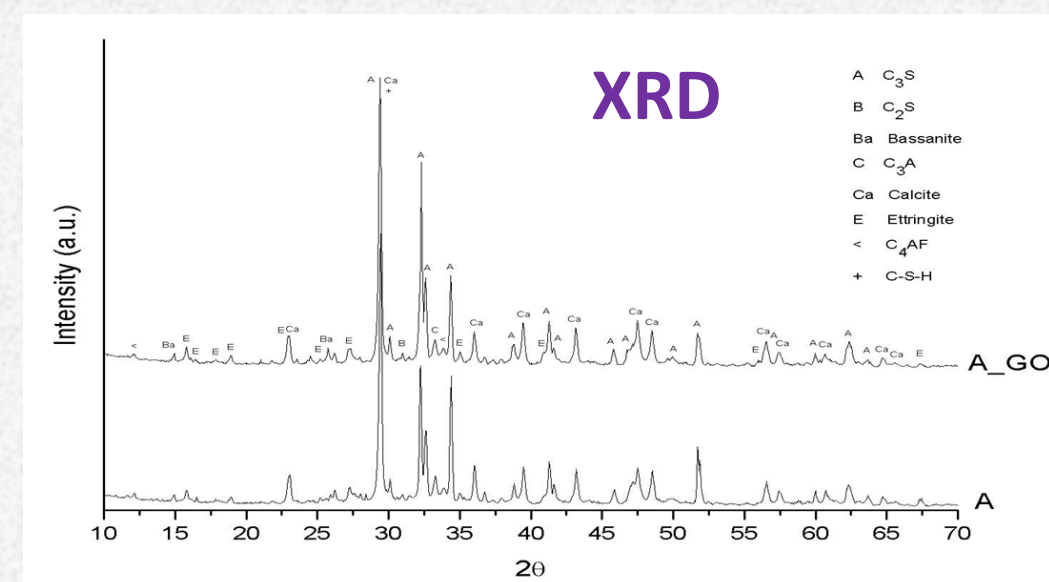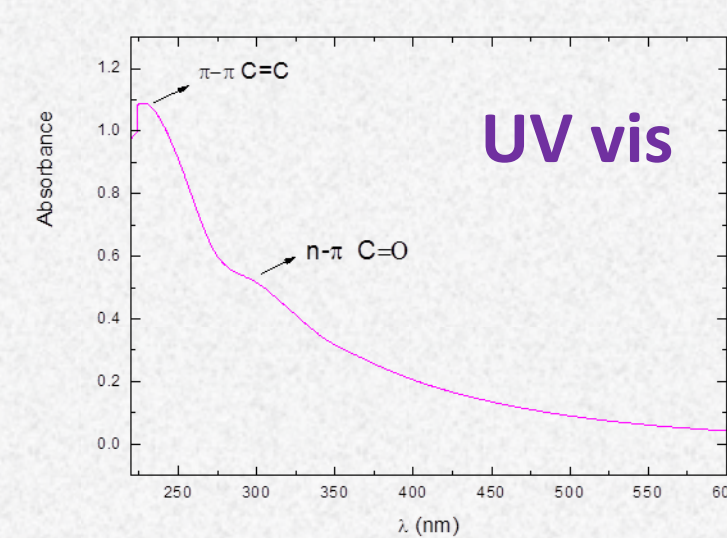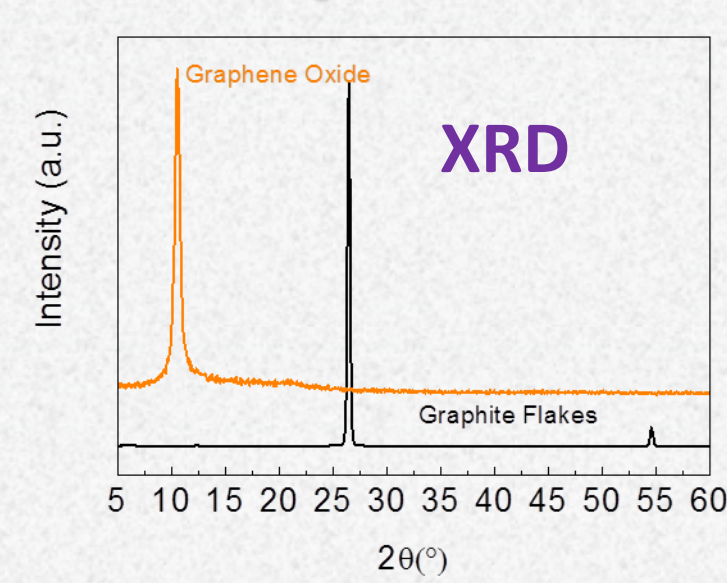
COMPOSITES PREPARATION:

S-L: mixed by adding a suspension of GO in water
   GO wt%: 0.03, 0.039 and 0.055
S-S mixing directly the powders before adding water
   GO wt%= 0.05%
Samples have been cured for 28 days in environmental test chamber

UNI EN 206-1: 2006

20 °C – 95% humidity

Results and discussions

SEM allowed to study the microstructure and identify the GO inside the cement matrix. SEM images revealed, even at low concentrations, how GO is strongly interconnected with the matrix and homogenously dispersed within it. The GO is present in the form of large sheets, even if some sub- and micrometric aggregates were observed. The sheets seems to "contain" the matrix particles as a sort of tie-sheet and partially filling the porosities.

SEM
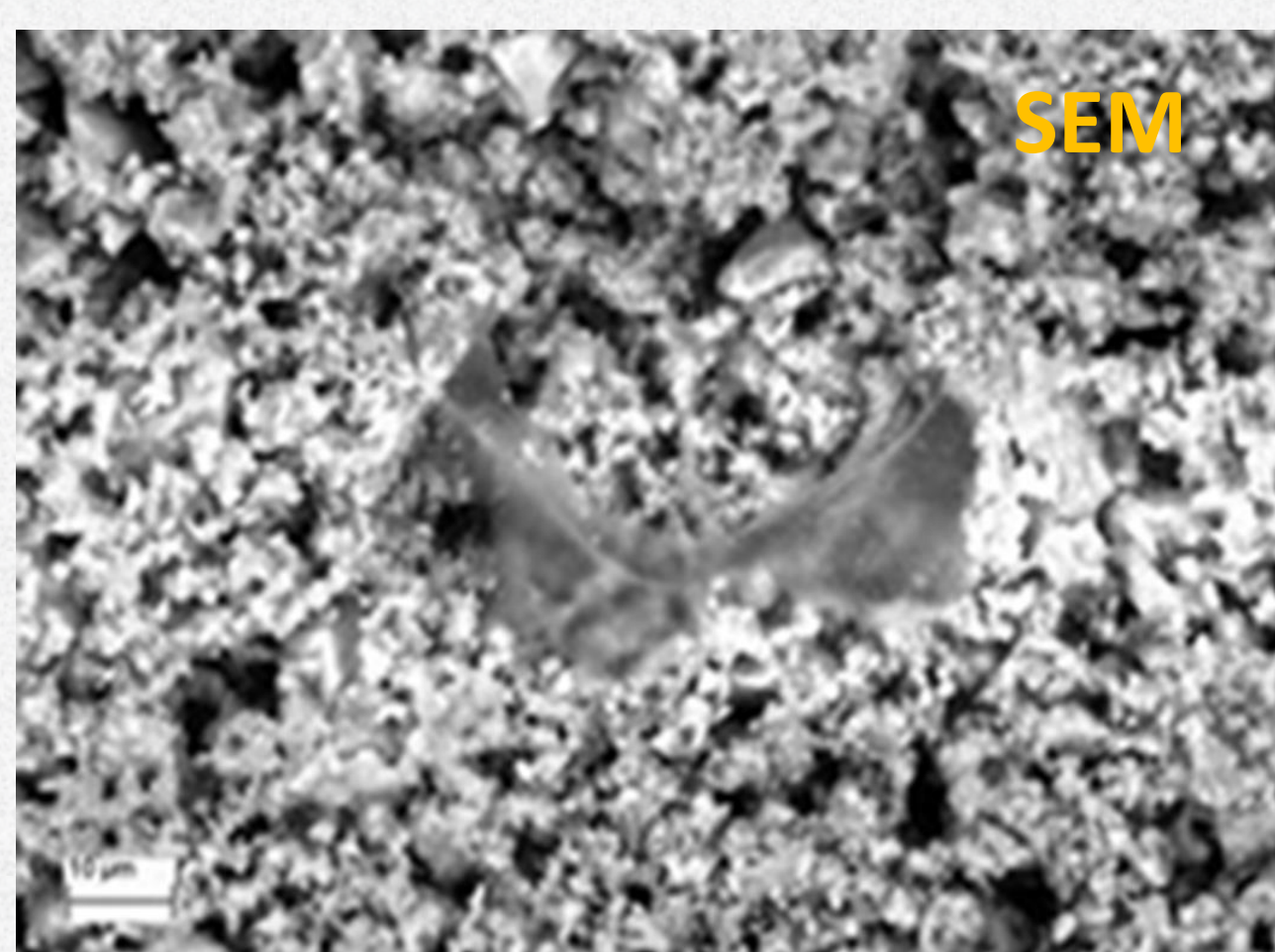
The peculiar morphology observed by microscopy observations could be at the a base of improved performances of the samples with GO respect to simple cement ones.

The compressive trials were performed by an uniaxial press averaging results from three tests per type of sample. The samples showed a typical hourglass shape after breakage.
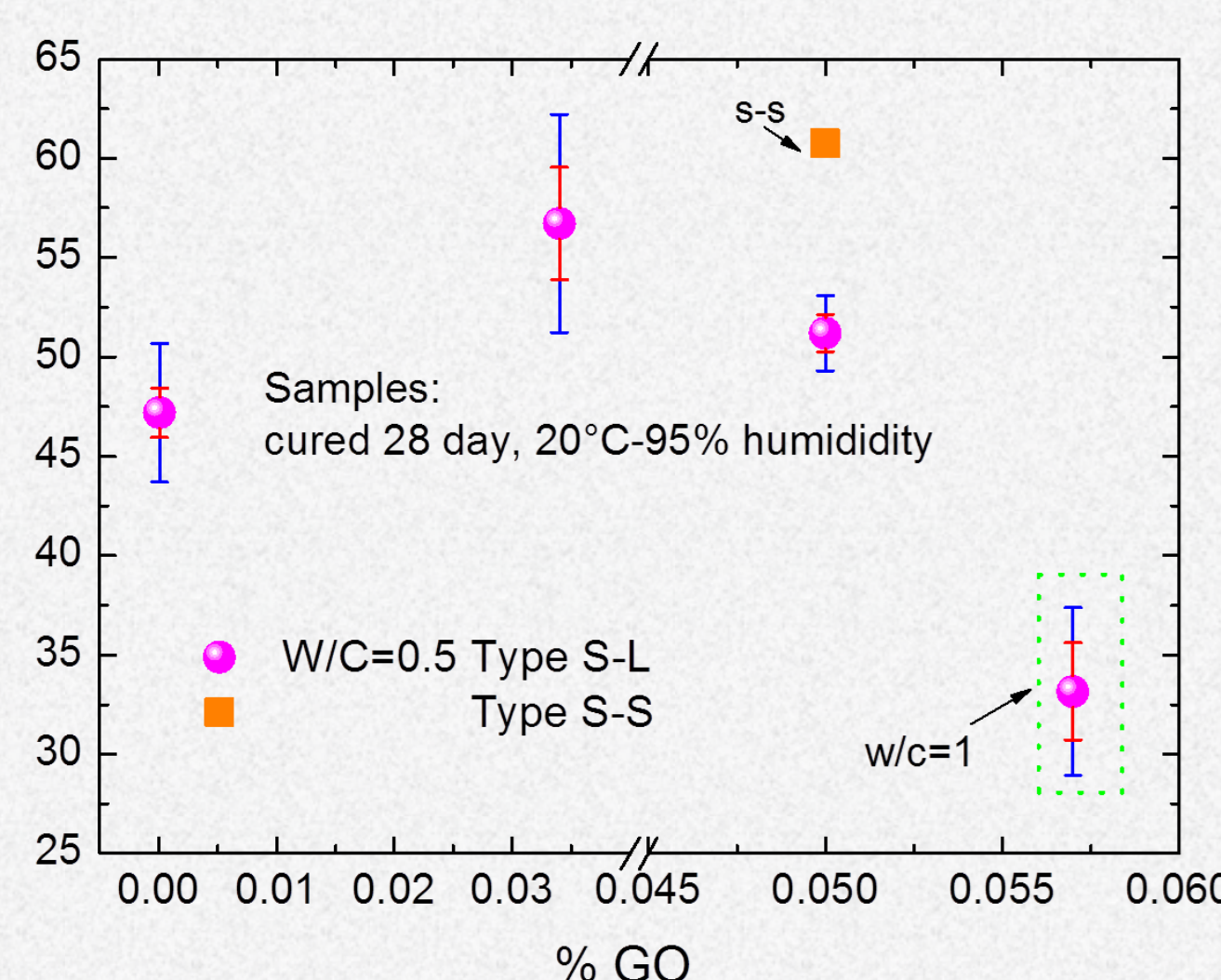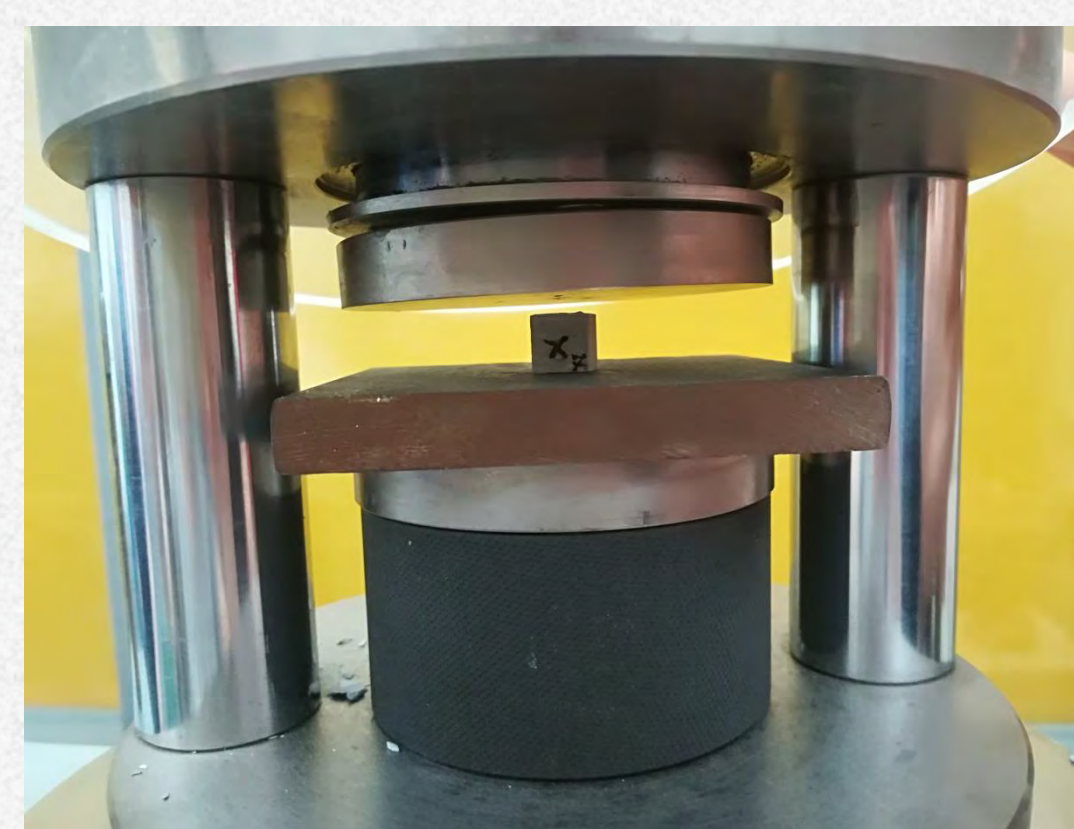
Compressive strength tests with various GO concentrations

Low quantities of GO added to the cement demonstrated to increase significantly the mechanical performances of the base cement. In particular, the sample obtained by S-L route Cement+0.035 wt%GO shows an increase in compression strenght of about 20 % respect to the pure cement, while for the sample S-S Cement+0.05 wt% GO the increment is about 35%.

Conclusions

In this work GO has been prepared by modified Hummer's method with the aim of preparing GO-reinforced cement. Different samples have been prepared with increasing concentration of GO. It has been observed that small quantities of GO, less than 0.05 wt%, increase largely the compression strength of cement composites prepared. Microstructural observations performed by SEM suggest that GO acts as a binder and aggregating agent which seems to "contain" the matrix particles as a sort of tie-sheet and partially filling the porosities. These observations put some highlights on improved mechanical behavior of GO-reinforced cements.

[1] Chen J., Yao B., Li C.,, "Shi G., An improved Hummers method for eco-friendly synthesis of graphene oxide", Carbon 64 (2013), 225
[2] L. Kou, H. He, C. Gao "Click chemistry approach to functionalize two-dimensional macromolecules of graphene oxide nanosheets" (2010), Nanomicro Lett., 2, 177
[3] T. N. Blanton, D. Majumdar, "X-ray diffraction characterization of polymer intercalated graphite oxide" JCPDS-International Centre for Diffraction Data (2012) ISSN 1097-0002

Trade-off solutions between economy and CO_2 emissions for the daily operation of a distributed energy system: a real case study in Italy

Marialaura Di Somma
Giorgio Graditi
Luigi Mongibello
Energy Technologies Department
ENEA
Portici, Naples (Italy)

Ilaria Bertini
Giovanni Puglisi
National Agency for Energy Efficiency
ENEA
Rome (Italy)

Abstract—Thanks to their numerous economic and environmental benefits, Distributed Energy Systems (DES) are considered as a sustainable alternative to traditional energy supply. To maximize the DES operators' profits while also containing emissions, daily operation is crucial. In this paper, the operation problem is addressed for a real DES in Italy by considering economic and environmental aspects. The DES consists of a Combined Heat and Power system, condensing and conventional boilers, and absorption and electric chillers. The end-users are an office building, a theater hall, and a residential building cluster, which is connected to the DES through a district heating network (DHN). A multi-objective linear programming problem is formulated based on the real constrains for devices and DHN with the aim to find the optimal operation strategies of the DES, which maximize the operator's profit and minimize the net CO_2 emissions, while satisfying the users demand. The Pareto frontier is found through the weighted-sum method, by using branch-and-cut. The method is implemented for a winter day of December, by using experimental data for electrical and thermal demand of end-users. The results show that the optimization method is efficient in finding good trade-off solutions between economy and CO_2 emissions. Moreover, the economic/environmental performances of the DES with optimized operation are much better than those found for the current operation strategies. In addition, the effects of the Italian white certificates scheme on the DES performances are also investigated.

Keywords—Distributed energy system; daily operation; multi-objective optimization, white certificates scheme

I. INTRODUCTION

Distributed energy systems (DES) typically consist of small-scale technologies providing electricity and thermal energy close to end-users. Thanks to their numerous economic and environmental benefits, DES are considered a promising option to traditional energy supply. However, to achieve the expected benefits, the daily operation is crucial, and it presents several challenges due to the different energy devices and energy carriers used to satisfy the time-varying user demand [1]-[3]. Therefore, for a specific DES consisting of various devices, the operation should be optimized in order to find the most suitable operation strategies to satisfy the time-varying electrical and thermal

demand of a specific end-user, while respecting the technical constraints of the devices [1]. Several works in the literature focused on the operation optimization of DES through formulating mixed-integer optimization models for scheduling multiple energy devices with the aim to minimize the daily energy cost [4], [5]. However, beyond economy, environmental issues related to CO_2 emissions are also needed to be considered as a crucial aspect for the long-run sustainability of energy supply. In such a context, a multi-objective approach can help to find economic/environmental trade-off solutions for the operation strategies of DES [6], [7].

In this paper, a multi-objective optimization model is developed for a real DES located in Italy, with the aim to find trade-off solutions between economic and environmental aspects for the daily operation. The DES under consideration consists of a Combined Heat and Power (CHP) system, condensing and conventional boilers, and absorption and electric chillers. The end-users are an office building owned by the DES operator, a theater hall, and a cluster of 31 residential buildings with 640 apartments, which is connected to the DES through a district heating network (DHN). A multi-objective linear programming problem (MOLP) is formulated based on the real constrains for the devices and the DHN with the aim to find the optimal operation strategies of the DES which maximize the operator's profit and minimize CO_2 emissions, while satisfying the time-varying electrical and thermal demand of connected end-users. The total daily operator's profit to maximize represents the economic objective, whereas the total daily net CO_2 emissions to minimize represent the environmental objective. The economic objective is implemented as minimizing the minus-profit, and the Pareto frontier is thus found by minimizing a weighted sum of the economic and environmental objectives, by using branch-and-cut. The model is implemented for a winter day of December, by using experimental data for elecrical and thermal demand of end-users. Results show that the optimization method is efficient in finding trade-off solutions between economy and CO_2 emissions. The economic/environmental performances of the DES with

optimized operation are much better than those found for the current operation strategies. In addition, the effects of the Italian white certificates scheme on the DES performances are also investigated.

II. DESCRIPTION OF THE DES IN ITALY

Figure 1 shows the scheme of the existing DES, with all the possible routes of energy flows to meet the users demand. The DES consists of a CHP system with a gas-fired internal combustion engine as prime mover, a condensing boiler, two conventional boilers, a single-stage absorption chiller and an electric chiller. For the office building, the electrical demand can be satisfied by the CHP and the grid power, whereas both the theater hall and the residential building cluster are not electrically served by the DES operator. For both the office building and the theater hall, the heat demand can be satisfied by the CHP and the boilers, whereas the cooling demand can be satisfied by the absorption and electric chillers. As for the residential building cluster, the heat demand can be satisfied by the CHP and the boilers through the DHN. In the summer period, it is not served by the DES operator for domestic hot water and cooling purposes. Moreover, the electricity provided by the CHP can be sold back to the grid. The technical characteristics of the energy devices in the DES are shown in Table I.
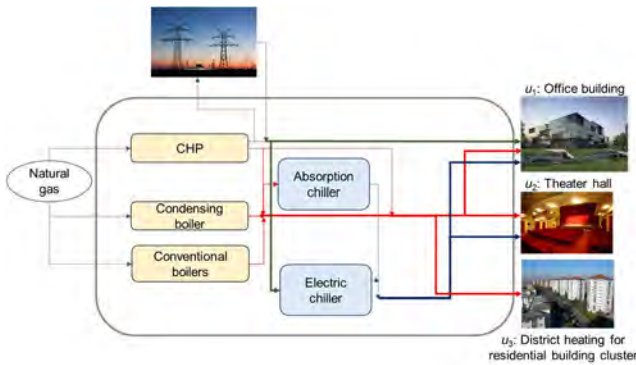
Fig. 1. Scheme of the DES in Italy

TABLE I. TECHNICAL CHARACTERISTICS OF ENERGY DEVICES IN THE DES

Energy device	Size	Efficiency	
		El	Th
CHP *DEUTZ TCG 2020K*	970 kW$_e$	0.386	0.463
Condensing boiler *Viessmann Vitocrossal 300*	895 kW$_{th}$	-	0.93
Conventional boilers (2) *Viessman Vitomax 200*	2600 kW$_{th}$ (2)	-	0.90 (2)
Electric chiller *TRANE RTWB 214*	435 kW$_c$	-	4.4
Single-stage absorption chiller *BROAD BDH20*	195 kW$_c$	-	0.75

The DHN used for the residential building cluster is of meshed/branched direct type and it is connected to the DES through a heat exchange station. Figure 2 shows the layout of the neighborhood under consideration. The blue buildings are connected to the DHN through a direct connection, the green ones are connected inderectly to the DHN through a heat exchanger substation, whereas the red one is the office building owned by the DES operator [8]. The total DHN has been designed for a maximum heat rate equal to 13.10 MW$_{th}$, by taking into account both the thermal losses and

the contemporaneity coefficient. The thermal demands of end-users are known based on experimental measures made available through remote and mobile monitoring systems.

Fig. 2: Layout of the neighborhood under consideration [8]

III. PROBLEM FORMULATION

The problem is to commit and dispatch the energy devices in the DES (see Figure 1) with the aim to maximize the operator's profit while reducing the CO_2 emissions, and it is formulated as a MOLP. In the problem, the binary decision variables are the on/off status of the devices, whereas the continuous decision variables are the energy rates provided by the devices, the electricity taken from the grid and the electricity from CHP sold back to the grid.

A. Objective functions

1) Economic objective: The economic objective is to maximize the total daily operator's profit, *Prof*, which is related to the total revenue for selling the electricity provided by the CHP back to the grid and thermal energy to end-users, and to the total energy cost for buying electricity from the grid and gas for the CHP and boilers:

$$Prof = R^{Sell,grid} + R^{Sell,users} - C^{Energy} \quad (1)$$

which can be equivalently expressed as:

$$Prof = \sum_t \{ E_{CHP,t}^{Sell} \Pi_t^{DA} + \sum_{\substack{u \\ u \neq u_1}} (H_{u,t}^{Dem} \Pi_{heat}^{Dem})$$

$$- [E_t^{Buy} \Pi_t^{Grid} + \sum_i (G_{i,t}^{Buy} \Pi^{Gas})] \} Dt,$$

$$i \in \{CHP, CondBoil, ConvBoil_1, ConvBoil_2\} \quad (2)$$

In (2): $E_{CHP,t}^{Sell}$ is the power sold back to the grid at time t and day-ahead (DA) market price Π_t^{DA}; $H_{u,t}^{Dem}$ is the heat rate demand of user u at time t; Π_{heat}^{Dem} is the price of selling thermal energy to users; E_t^{Buy} is the grid power bought at time t and price Π_t^{Grid}; $G_{i,t}^{Buy}$ is the total amount of gas consumed by the device i, bought at time t and price Π^{Gas}; and Dt is the length of the time interval (1 hour). Note that the thermal energy is sold only to users 2 and 3, since the office building is owned by the DES operator. Moreover, the heat rate demand of users 2 and 3 refer to the total final

demand, which is subtracted by the thermal losses occurring in the heating pipelines assumed equal to 20%.

2) Environmental objective: The environmental objective, is to mimimize the total net daily CO_2 emissions, *Env*, as the emissions related to the electricity taken from the grid and the gas consumed by the CHP and boilers, subtracted by the avoided CO_2 emissions related to the electricity sold back to the grid:

$$Env = CO_2^{Oper} - CO_2^{Avoid} \qquad (3)$$

which can be equivalently expressed as:

$$Env = \sum_t \{E_t^{Buy} CI^{Grid} + \sum_i (G_{i,t}^{Buy} CI^{Gas}) - E_{CHP,t}^{Sell} CI^{Grid}\} Dt,$$
$$i \in \{CHP, CondBoil, ConvBoil_1, ConvBoil_2\} \qquad (4)$$

In (4), CI^{Grid} is the carbon intensity of the power grid to which the system is connected, corresponding to the amount of emissions per unit of generated electrical energy, which depends on the fuel mix of power generation, and CI^{Gas} is the carbon intensity of the natural gas [1].

B. Operation constraints

1) Energy devices: To maintain the problem linearity, in the operation constraints of devices, the efficiencies are assumed constant and not varying with the generation levels of devices [1] - [6].

a) CHP system: The total power, $E_{CHP,t}$, is limited by the minimum, E_{CHP}^{min}, and maximum, E_{CHP}^{max}, rated output, if the device is on (i.e., $x_{CHP,t}$ is equal to 1):

$$E_{CHP}^{min} x_{CHP,t} \le E_{CHP,t} \le E_{CHP}^{max} x_{CHP,t}, \ \forall t \qquad (5)$$

where the total power provided by the CHP is equal to the sum of the power for self-use, $E_{CHP,t}^{Self}$, and the power sold back to the grid, $E_{CHP,t}^{Sell}$:

$$E_{CHP,t} = E_{CHP,t}^{Self} + E_{CHP,t}^{Sell}, \ \forall t \qquad (6)$$

For all devices in the DES, the capacity constraint can be formulated as in (5). The amount of natural gas required by the CHP, $G_{CHP,t}^{Buy}$, is formulated as:

$$G_{CHP,t}^{Buy} = E_{CHP,t} / (\eta_{CHP,e} LHV_{gas}), \ \forall t \qquad (7)$$

where $\eta_{CHP,e}$ is the electrical efficiency and LHV_{gas} is the lower heat value of natural gas. The heat rate recovered by the CHP, $H_{CHP,t}$, is formulated as:

$$H_{CHP,t} = E_{CHP,t} \eta_{CHP,th} / \eta_{CHP,e}, \ \forall t \qquad (8)$$

where $\eta_{CHP,th}$ is the thermal efficiency of the CHP. In the winter period, the thermal energy recovered by the CHP can be used to satisfy the thermal demand of the office building, the theater hall, and the building clusters (through the DHN), whereas, in the summer period, it can be used to power the absorption chiller.

b) Condensing and conventional boilers: The amount of gas required by the condensing boiler, $G_{CondBoil,t}^{Buy}$, to provide the heat rate, $H_{CondBoil,t}$ is formulated as:

$$G_{CondBoil,t}^{Buy} = H_{CondBoil,t} / (\eta_{CondBoil,th} LHV_{gas}), \ \forall t \qquad (9)$$

where $\eta_{CondBoil,th}$ is the thermal efficiency of the condensing boiler. The amount of gas required by the conventional boilers can be formulated as in (9). Similarly to the CHP, also for the boilers, in the winter period the thermal energy provided can be used to satisfy the thermal demand of the three users, whereas, in the summer period, it can be used to power the absorption chiller.

c) Absorption chiller: In the summer period, the cooling rate provided by the absorption chiller, $C_{AChil,t}$ is formulated as:

$$C_{AChil,t} = COP_{AChil} \sum_i H_{i,t}^{Cool},$$
$$i \in \{CHP, CondBoil, ConvBoil_1, ConvBoil_2\}, \forall t \qquad (10)$$

where COP_{AChil} is the coefficient of performance, and $H_{i,t}^{Cool}$ is the heat rate provided for cooling purposes by device *i*.

d) Electric chiller: In the summer period, the power required by the electric chiller, $E_{EChil,t}^{Req}$, to provide the cooling rate, $C_{EChil,t}$ is formulated as:

$$E_{EChil,t}^{Req} = C_{EChil,t} / COP_{EChil}, \ \forall t \qquad (11)$$

where COP_{EChil} is the coefficient of performance.

2) Operation constraints for the DHN: As mentioned earlier, the DHN is used to satisfy the thermal demand of the residential building clusters. In the winter period, the sum of the heat rates provided by the CHP and boilers has to be lower or equal to the maximum heat rate allowable for the DHN, H_{DHN}^{max}:

$$\sum_i H_{i,u,t} \le H_{DHN}^{max}, \ u = u_3,$$
$$i \in \{CHP, CondBoil, ConvBoil_1, ConvBoil_2\}, \forall t \qquad (12)$$

where $H_{i,u,t}$ is the share of the heat rate provided by the device *i* at time *t* for the user 3 (district heating for the residential building cluster). In the summer period, the residential building cluster is not served by the DES operator.

C. Energy balances

1) Electricity balance: In the winter period, the electricity demand of the office building, u_1, has to be satisfied by the CHP and the power grid.

$$E_{u,t}^{Dem} = E_{CHP,u,t}^{Self} + E_{u,t}^{Buy}, u = u_1, \forall t \qquad (13)$$

whereas the users 2 and 3 are not electrically served by the DES operator. In the summer period, the electricity balance can be formulated similarly to (13), by also considering the power required by the electric chiller as a load.

2) Thermal balance: In the winter period, the heat demand of all users can be satisfied by the CHP and boilers:

$$H_{u,t}^{Dem} = \sum_i H_{i,u,t},$$
$$i \in \{CHP, CondBoil, ConvBoil_1, ConvBoil_2\}, \forall u, \forall t \qquad (14)$$

Note that in (14), the heat demand of user 3 refers to the demand at the secondary side of the heat exchanger through which the DHN is connected to the DES, by accounting for the thermal losses in the DHN heating pipelines. In the

summer period, the cooling demand for users 1 and 2 can be satisfied by the absorption and the electric chillers:

$$C_{u,t}^{Dem} = \sum_i C_{i,u,t}, \; i \in \{AChil, EChil\}, u \in \{u_1, u_2\}, \forall t \quad (15)$$

D. Multi-objective optimization method

The optimization problem involves two objective functions, i.e., the daily operator's profit to maximize and the daily net CO_2 emissions to minimize. In order to use the weighted-sum method, which is widely used in the literature as an efficient optimization method providing proper and representative trade-off solutions on the Pareto frontier [7], [9], the economic objective is implemented as minimizing the minus-profit. Therefore, to solve this multi-objective optimization problem, a single objective function is formulated as a weighted sum of the minus-profit, (-Prof), and the net CO_2 emissions, Env to be minimized:

$$FO = c\omega(-Prof) + (1-\omega)Env \quad (16)$$

where the constant c is a scaling factor allowing c(-Prof) and Env have the same order of magnitude. For $\omega=1$ and $\omega=0$, the solutions that minimize the minus-profit (i.e., maximizing the operator's profit), and minimize the net CO_2 emissions, are found, respectively. The economic/environmental trade-off solutions on the Pareto frontier can be found by varying the weight ω in the interval $0 - 1$. The problem formulated above is linear and involves both discrete and continuous variables. Branch-and-cut as a powerful instrument for mixed-integer linear problems is therefore used.

IV. TESTING RESULTS

In the real case study, reference is made to a winter weekday of December.

A. Input data

The hourly load profiles for heat and electricity demand of end-users are based on experimental measures. For the electricity demand, since only monthly consumptions are available, the electrical hourly load profile for the office building is built based on typical hourly load profiles for the end-user under consideration [10]. Based on the Italian BTA6 tariff for industrial use [11], the time of use (TOU) tariff varies in the range 0.074-0.096 €/kWh. The tariff for industrial use is also adopted for the unit price of natural gas assumed as 0.343 €/Nm^3. For both the prices, reference is made to the energy quotas. The DA market price for the period under consideration is built based on [12], and it varies in the range 0.044-0.072 €/kWh. The price for selling thermal energy to end-users is assumed as 0.089 €/kWh. The carbon intensities of the power grid and natural gas are equal to 0.330 kgCO$_2$/kWh and 0.202 kgCO$_2$/kWh (1.927 kgCO$_2$/Nm^3), respectively [1], [13].

B. Current operation strategies of the Italian DES

The current operation strategies of the Italian DES in the winter weekday of December are shown in Fig. 3 for electricity. The CHP is generally on during the hours with higher DA market prices from 7:00 to 23:00, and most of the power is sold back to the grid. The grid power is used to meet the electrical demand of the office building when the grid price of TOU tariff is lower (from 0:00 to 6:00 and 24:00).
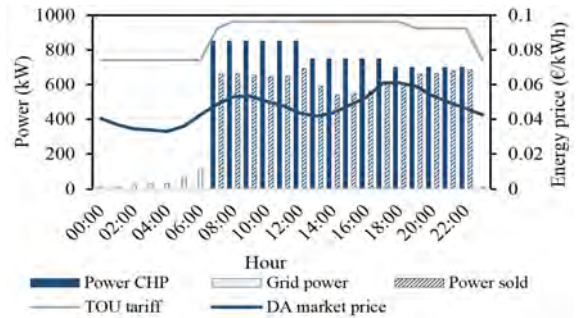
Fig. 3. Current operation strategies of the DES in the winter weekday of December for electricity

As for condensing and conventional boilers, they work during the entire day, by providing 23.77 MWh of thermal energy. The operator's profit and net CO_2 emissions are evaluated based on the input data defined earlier, and they are equal to 352.28 €, and 9087.27 kgCO_2, respectively. The various amounts of costs, revenues and emissions evaluated for the current operation strategies are shown in Table II.

TABLE II. REVENUES/COSTS AND EMISSIONS FOR THE CURRENT DAILY OPERATION STRATEGIES OF THE DES IN THE WINTER WEEKDAY OF DECEMBER

Current daily operation strategies	Revenues (€)		Costs (€)	Emissions (kgCO$_2$)	
	$R^{Sell,grid}$	$R^{Sell,users}$	C^{Energy}	CO_2^{Oper}	CO_2^{Avoid}
	512.59	2054.75	2215.06	12418.66	3331.39

C. Optimization results

1) Pareto frontier: The optimization model is implemented by using IBM ILOG CPLEX Optimization Studio Version 12.6. The problem can be solved in a few minutes with a PC with 2.60 GHz (2 multi-core processors) Intel® Xeon® E5 CPU and 32G RAM. The Pareto frontier is shown in Fig. 4, and it is obtained by varying the weight by 0.1 from 1 to 0.
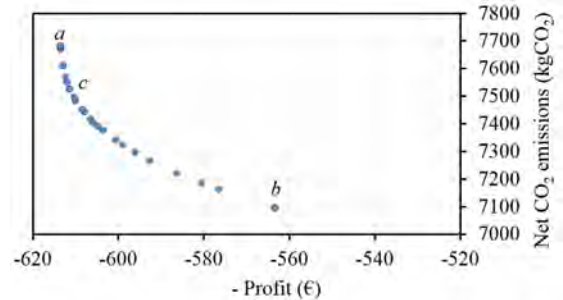
Fig. 4. Pareto frontier

The point *a* is obtained under the economic optimization, and the economic objective function (-Prof) is minimum, thereby corresponding to the maximum operator's profit equal to 613.39 €, whereas the net CO_2 emissions are maximum and equal to 7679.78 kgCO_2. Conversely, the point *b* is obtained under the environmental optimization, and the economic objective function (-Prof) is maximum, thereby corresponding to the minimum operator's profit equal to 563.11 €, whereas the net CO_2 emissions are

minimum and equal to 7093.92 kgCO$_2$. The various amounts of costs, revenues and emissions at the points *a* and *b* on the Pareto frontier are shown in Table III. The point *c* is also chosen to show the economic/environmental performances of the DES for an equal weight of the two objectives. At this point, as compared to the economic optimization, for a profit's reduction of 0.30%, the net CO$_2$ emissions reduce by about 2%.

TABLE III. REVENUES/COSTS AND EMISSIONS AT EXTREME AND TRADE-OFF POINTS ON THE PARETO FRONTIER

Point	Revenues (€)		Costs (€)	Emissions (kgCO$_2$)	
	$R^{Sell,grid}$	$R^{Sell,users}$	C^{Energy}	CO_2^{Oper}	CO_2^{Avoid}
a Eco optimization	560.35	2054.75	2001.71	11236.6	3556.86
b Env optimization	897.85	2054.75	2389.49	13424.9	6330.98
c Eco/Env trade-off	658.17	2054.75	2101.4	11797	4269.4

By comparing the optimization results with those evaluated for the current operation strategies of the DES, it can be noted that a strong increase of the operator's profit and a significant reduction of net CO$_2$ emissions are attained at extreme and trade-off points of the Pareto frontier. The maximum increase of the operator's profit equal to 42.57% is achieved under the economic optimization, whereas the maximum reduction of net CO$_2$ emissions equal to 21.94% is obtained under the environmental optimization.

2) Optimized operation strategies of the DES: Each point on the Pareto frontier corresponds to different operation strategies of the DES. For the illustration purpose, the optimized operation strategies of the DES are shown for points *a* and *b* on the Pareto frontier in Fig. 5 for electricity.
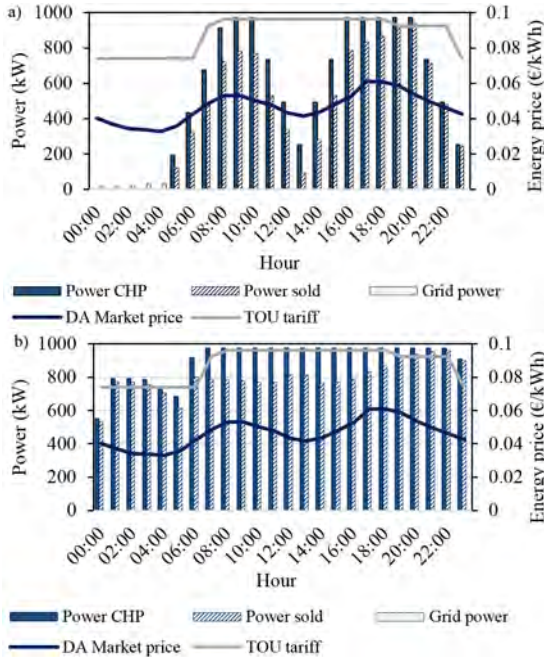
Fig. 5. Optimized operation strategies of the DES for electricity under a) economic optimization and b) environmental optimization

Similarly to what occurs for the current operation strategies of the DES, most of the power provided by the CHP is sold back to the grid under both the economic and environmental optimization. However, the working hours of

the CHP under the economic optimization are lower than those under the environmental optimization. In this latter case, through a larger usage of the CHP, a larger amount of waste heat can be used for thermal demand of all users, thereby reducing the CO$_2$ emissions related to the natural gas consumption in boilers. Under the economic optimization, grid power is used to meet the electrical demand of the office building when the grid price of TOU tariff is lower (from 0:00 to 5:00), whereas the power provided by the CHP is sold back to the grid when the DA market price is higher. This allows to maximize the operator's profit. Under the environmental optimization, the operation strategies of the DES are not sensitive to energy prices. In detail, grid power is never used, and a larger amount of electricity is sold back to the grid, independently from the DA market price. This allows to increase the amount of avoided CO$_2$ emissions, thereby minimizing the net CO$_2$ emissions.

Fig. 6 shows the heat energy balance for points *a* and *b* on the Pareto frontier for the residential building cluster (user#3), which is characterized by the largest heat demand. It can be noted that the thermal energy provided by the CHP for user#3 is much larger under the environmental optimization than under the economic one, consistently with the operation strategies of the DES for electricity shown in Fig. 5. Under the economic optimization, the condensing boiler is preferred to the conventional boilers, due to the higher conversion efficiency. Under the environmental optimization, most of thermal demand of user#3 is covered by the CHP, and conventional boilers are never used. This result highlights the inconvenience of this technology for the environmental objective. The trend of the share of each device in heat energy balance for users #1 and #2 is similar.
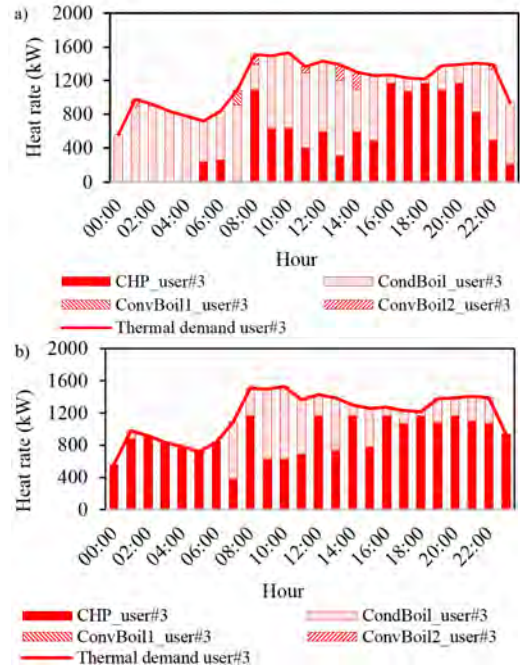
Fig. 6. Heat energy balance for user#3 under a) economic optimization and b) environmental optimization

D. Effects of white certificates scheme on the economic/environmental performances of the DES

In Italy, for CHPs with a size lower or equal to 1 MW_e and a primary energy saving (PES) higher than 0, the incentive scheme is based on white certificates (WC). Since the CHP in the DES respects these requirements, the effects of WC scheme on the economic/environmental performances of the DES are investigated. The WC scheme modeling in the optimization problem is discussed in the Appendix.

By considering the WC scheme for the current operation strategies of the DES for the winter day of December, the operator can gain 1.36 WC, and his profit is thus equal to 488.28 €. The effect of the WC scheme on the optimized operation strategies of the DES is null under the environmental optimization, whereas it is maximum under the economic optimization. In detail, in this latter case, the operator gains 2.19 WC and his profit is equal to 805.39 €, whereas the net CO_2 emissions are equal to 7217.9 $kgCO_2$. Therefore, as compared to the results found under the economic optimization in the case without WC schemes, the operator's profit increases by 23.94%, and the net CO_2 emissions reduce by 6.01%. This strong variation is due the electricity provided by the CHP, which strongly increases, since it leads to large primary energy savings with the corresponding revenues related to WC. This result also explains the small variation for both profit and emissions between the economic and environmental optimizations. In this latter case, the net CO_2 emissions remain equal to 7093.92 $kgCO_2$, whereas the operator's profit is equal to 802.9 €. The increase of the profit as compared with the case without WC scheme is only due to the revenue related to WC, since the operator gains 2.4 WC. These latter are due to the large number of working hours of the CHP under the environmental optimization. Also in the presence of WC scheme, the economic/environmental performances of the DES with optimized operation are much better than those related to the current operation strategies.

V. Conclusions

In this paper, the operation problem is addressed for a real DES located in Italy by considering both economic and environmental aspects. A MOLP is formulated based on the real constrains for devices and DHN with the aim to find the optimal operation strategies of the DES, which maximize the operator's profit and minimize the net CO_2 emissions. The Pareto frontier is found by minimizing a weighted sum of the minus profit and net CO_2 emissions by using branch-and-cut. The method is implemented for a winter day of December, by using experimental data for electricity and thermal demand of end-users. Results show that several trade-off points for economy and CO_2 emissions can be found on the Pareto frontier. Moreover, the economic/environmental performances of the DES with optimized operation are much better than those found for the current operation strategies. The effects of the Italian white certificates scheme on the DES performances are also investigated and results show that this incentive scheme allows to improve both the economic and environmental performances of the DES.

APPENDIX: WC SCHEME MODELING

According to the Italian regulation, each certificate attests the saving of a TOE, and its value is about 100 €. Therefore, WC represent a possible revenue for the DES operator. The economic objective function, *Prof*, is formulated as:

$$Prof = R^{Sell,grid} + R^{Sell,users} + R^{WC} - C^{Energy} \qquad (A1)$$

where R^{WC} is the revenue related to WC, and it is the product of the value of each WC and their number. This latter is formulated as:

$$WC = \sum_t (E_{CHP,t} / \eta_{ref,e} + H_{CHP,t} / \eta_{ref,th} - G^{Buy}_{CHP,t} LHV_{gas}) cK \quad (A2)$$

where: $\eta_{ref,e}$ and $\eta_{ref,th}$ are the Italian reference efficiencies for the separate generation for electricity and heat, respectively; *c* is a constant taking into account the conversion from kWh to TOE, and *K* is a coefficient varying with the size of the CHP unit.

REFERENCES

[1] M. Di Somma, G. Graditi, E. Heydarian-Forushani, M. Shafie-Khah, P. Siano. "Stochastic optimal scheduling of distributed energy resources with renewables considering economic and environmental aspects". Renewable Energy, vol. 116, pp. 272-287, 2018.

[2] M. Di Somma, B. Yan, N. Bianco, P. B. Luh, G. Graditi, L. Mongibello, V. Naso. "Multi-objective operation optimization of a Distributed Energy System for a large-scale utility customer". Applied Thermal Engineering, vol. 101, pp. 752-761, 2016.

[3] B. Yan, P.B. Luh, G. Warner, P. Zhang, "Operation and design optimization of microgrids with renewables". IEEE Transactions on Automation Science and Engineering, vol.14(2), pp. 573-585, 2017.

[4] B. Yan, P.B. Luh, B. Sun, C. Song, C. Dong, Z. Gan, et al., "Energy-efficient management of eco-communities", in: *Proceedings of IEEE CASE*; Madison, USA, 2013. August 17-20.

[5] X. Guan, Z. Xu, Q. Jia, "Energy-efficient buildings facilitated by microgrid", IEEE Trans Smart Grid, vol.1, pp. 466-473, 2011.

[6] H. Ren, W. Zhou, K.I. Nakagami, W. Gao, Q. Wu, "Multi-objective optimization for the operation of distributed energy systems considering economic and environmental aspects", Appl. Energy vol. 87, pp. 3642-3651, 2010.

[7] A. Alarcon-Rodriguez, G. Ault, G. Galloway, "Multi-objective planning of distributed energy resources: a review of the state-of-the-art", Renew. Sustain. Energy Rev. vol.14, pp.1353-1366, 2010.

[8] M. Badami, A. Portoraro, "Analisi di performance e monitoraggi energetici di reti termiche distribuite", Report (in Italian) RdS/PAR2013/056, Politecnico di Torino, 2014.

[9] G. Mavrotas, "Effective implementation of the ε-constraint method in multi-objective mathematical programming problems", Applied mathematics and computation, vol.213, no.2, pp. 455-465, 2009.

[10] U. Ciarniello, G. Orsini, F. Santi. 1.2.2-Indagine sui consumi e sulla diffusione delle apparecchiature nel settore terziario in Italia. Technical Report RSE A5-053452 (In Italian) (2005) Available: http://www.rse-web.it/documenti.page?RSE_manipulatePath=yes&RSE_originalURI=/documenti/documento/313056&country=ita

[11] Servizio elettrico nazionale. Available: https://www.servizioelettriconazionale.it/it-IT/tariffe/altri-usi/bta-6-trioraria

[12] GME, Available: http://www.mercatoelettrico.org/It/

[13] IEA, "CO_2 emissions from fuel combustion-Highlights", 2017. Available: https://www.iea.org/publications/freepublications/publication/CO2EmissionsfromFuelCombustionHighlights2017.pdf .

Experimental and numerical study on a lab–scale latent heat storage prototype for cooling applications

M Caliano[1*], N Bianco[1], G Graditi[2], L Mongibello[2]

[1] Dipartimento di Ingegneria Industriale (DII) – Università di Napoli Federico II, P.le V. Tecchio, 80 – 80125 Napoli, Italy
[2] ENEA – Italian National Agency for New Technologies, Energy and Sustainable Economic Development, Portici Research Center, P.le E.Fermi, 1 - 80055 Portici (NA), Italy

*E-mail: martina.caliano@enea.it

Abstract. Latent thermal energy storage systems using phase change materials (PCMs) represent an effective way of storing thermal energy because of high-energy storage density and the isothermal nature of the storage process. In the current study, the charging and discharging characteristics of a lab-scale latent heat storage (LHTES) prototype for cooling applications are experimentally and numerically studied. Two numerical models are developed to analyze the performance characteristics of the LHTES prototype: a conductive model and a conductive-convective model. Effective heat capacity (EHC) method is implemented to consider the latent heat of the phase change material. The governing equations involved in the models are solved using the finite element based software product, COMSOL Multiphysics, and the initial and the boundary conditions are determined on the basis of the data obtained from the experimental tests. Numerically predicted temperature variations of the models during charging and discharging processes are compared with the experimental data extracted from the lab-scale LHTES prototype, and a good agreement between them is found when the conductive-convective model is used, while high deviation is observed in case of use of the conductive model. Other results are presented in terms of the performance parameters such as charging/discharging time, energy storage charge/discharge rate, and melt fraction.

1. Introduction

Latent thermal energy storage systems (LHTES) using phase change materials (PCMs) are one of the most efficient methods to store thermal energy. The use of PCM provides higher heat storage capacity and more isothermal behavior during charging and discharging processes, compared to sensible heat storage systems [1]. Therefore, many authors have evaluated experimentally and numerically the LHTES systems performance, analyzing different storage configurations and comparing different numerical models [2-8]. Niyas et al. [9] analyzed experimentally two latent thermal energy storage systems based on PCM for medium and high temperature applications. In another work [10], the same authors, studied numerically the performance of a lab-scale LHTES prototype for heat storage applications. Neumann et al. [11] developed a simplified approach for simulating latent thermal energy storage systems based on PCMs consisting of a fin-and-tubes heat exchanger. They compared the results from simulation to the ones of experimental tests carried out on two different storages varying their geometric configuration. Seddegh et al. [12] developed and compared two numerical models for studying a shell-and-tube LHTES system: a conduction model and a conduction-

convection model. They observed that the results obtained with the conduction-convection model agreed with the experimental results.

In the current study, the charging and discharging characteristics of a lab-scale latent heat storage prototype for cooling applications are experimentally and numerically studied. In order to analyze the performance characteristics of the LHTES prototype, two numerical models are developed: a conductive model and a conductive-convective model. Effective heat capacity (EHC) method is implemented to consider the latent heat of the phase change material. The governing equations involved in the models are solved using the finite element based software product, COMSOL Multiphysics, and the initial and the boundary conditions are determined on the basis of the data obtained from the experimental tests. Numerically predicted temperature variations of the models during charging and discharging processes are compared with the experimental data extracted from the lab-scale LHTES prototype. Results of combined conduction-convection model agree well with the experimental data, while in case of conductive model, results show a high deviation between experimental and numerical data. Moreover, results show that, in the current application, the discharging process is a natural convection dominated process, while the charging one is a conduction dominated process.

2. Description of the experiment test

The employed experimental apparatus consists of a LHTES unit, a climatic chamber, five thermocouples, a data acquisition unit, and a computer. The storage unit consists of an aluminium cylindrical container of 250 cm height and radius equal to 6.9 cm filled with 2.40 kg of a biological PCM, which characteristics are shown in Table 1, as given by the producer. T-type thermocouples with an accuracy of ±0.5°C are used to measure the module local temperature at five points located on the same horizontal cross section placed at 9 cm from the container bottom: on the axis, and at four points at a distance of 3.45 cm from the axis arranged to form a cross. Fig. 1 shows the LHTES prototype filled with liquid PCM, and the climatic chamber used to carry out the experimental tests. The temperature data acquisition is conducted by means the of the National Instruments NI 9213 acquisition module, using the NI cRIO 9066 controller. The experimental measurement data are recorded with sample time of 1 second.

(a) LHTES unit with liquid PCM.   (b)   Thermocouples arrangement.   (c)   Climatic chamber.

Fig. 1. Pictures of the LHTES unit and the climatic chamber.

Table 1. Thermo-physical properties of the storage material.

Properties	
Melting point [T_M (°C)]	15
Latent heat [L_h (kJ kg^{-1})]	182
Thermal conductivity (W m^{-1} K^{-1})]	
Solid [k_S]	0.25
Liquid [k_L]	0.15
Density (kg/m^3)	
Solid [ρ_S]	950
Liquid [ρ_L]	860
Specific heat (J kg^{-1} K^{-1})	
Solid [$C_{p,S}$]	2250
Liquid [$C_{p,L}$]	2560

The experimental tests are carried out by varying the air temperature inside the climatic chamber. For the charging process, starting from the uniform temperature condition T_0=23.8°C, at which all the PCM is liquid, one hour temperature ramp is set up to bring the climatic chamber internal temperature to the charging temperature T_c=7°C; then the temperature inside the climatic chamber is kept at T_c until the PCM is completely solidified. For the discharging process, one hour temperature ramp is set up to bring the climatic chamber internal temperature to the discharging temperature T_d=23°C; then the temperature inside the climatic chamber is kept at T_d until the PCM is completely melted.

2.1. Experimental results

Fig. 2 shows the temperature variation of the LHTES system obtained from the experiments. In detail, the variation of the local temperature at the central position and of the average of the temperatures measured with the four lateral thermocouples, for both charging and discharging process are reported. From these results, it can be seen that, during the charging process, the PCM undergoes solidification at a temperature slightly lower than 15°C. Similarly, it can be seen that, during the discharging process, the PCM starts melting at temperature lower than 15°C.

(a)   Charging process.   (b)   Discharging process.
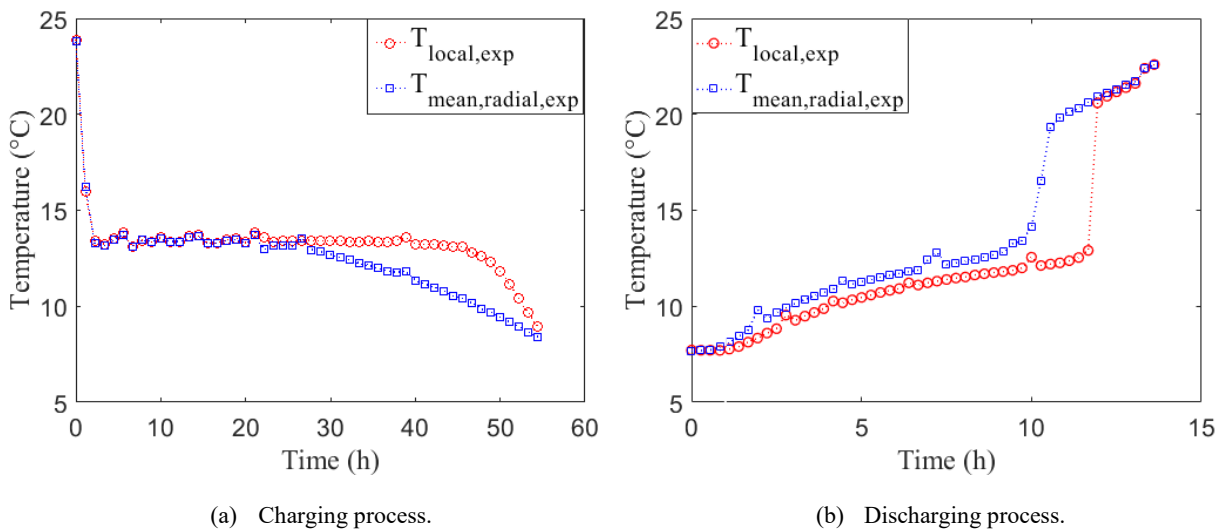
Fig. 2. Experimental results.

3. Numerical modelling

The geometry of the storage prototype and the symmetric boundary conditions of the experimental tests allow to implement 2D axisymmetric numerical models. Therefore, two 2D axisymmetric numerical models are developed for simulating the charging and discharging process of the considered storage unit: a conductive-mechanism-based model, and a conductive-convective-mechanism-based model.

3.1. Conductive model

In order to perform the numerical simulation of the considered storage unit, in case of conductive model, the modelling is carried out through the energy equation (1), valid for both solid and liquid phases, and the following assumptions are considered: (i) PCM is homogenous and isotropic; (ii) phase change during solidification/melting occurs in a temperature range; (iii) negligible convective mechanisms.

(i)   energy equation

$$\rho_{PCM} c_{p,PCM} \frac{\partial T}{\partial t} = \nabla \cdot \left(k_{PCM} \nabla T \right) \tag{1}$$

In eq. (1), ρ_{PCM} is the density of the PCM, T is the temperature, $c_{p,PCM}$ is the heat capacity, and k_{PCM} is the thermal conductivity.

The PCM properties, such as k_{PCM}, ρ_{PCM}, and $c_{p,PCM}$ are considered constant over the entire domain: k_{PCM} is fixed equal to the solid phase thermal conductivity, whereas ρ_{PCM} and $c_{p,PCM}$ equal to the average value between the values of the liquid and solid phase.

To simulate the phase change process, the effective heat capacity method (EHC) is implemented, according to which the material effective heat capacity ($c_{p,PCM}$) depends on the latent heat of fusion (L_h) of the PCM.

$$c_{p,PCM} = c_p + L_h \frac{d\varphi(T)}{dT} \tag{2}$$

In eq. (2), $\varphi(T)$ is a non-dimensional parameter that varies during the phase transition as follows:

$$\varphi(T) = \begin{cases} 0, & T < \left(T_M - \Delta T_M \right); \\ \dfrac{T - T_M + \Delta T_M}{2\Delta T_M}, & \left(T_M - \Delta T_M \right) \leq T \leq \left(T_M + \Delta T_M \right); \\ 1, & T > \left(T_M + \Delta T_M \right) \end{cases} \tag{3}$$

In detail, $\varphi(T)$ is 0 in the solid phase; $\varphi(T)$ is 1 in the liquid phase, and $0 < \varphi(T) < 1$ in the transition zone.

3.2. Conductive-convective model

In case convective mechanisms are considered, the developed thermal model is based on the following assumptions: (i) PCM is homogenous and isotropic; (ii) phase change during solidification/melting occurs in a temperature range; (iii) the volume expansion during phase change is ignored; (iv) liquid PCM is Newtonian and treated with the laminar flow model. The modelling is carried out through the following equations:

(i)   energy equation

$$\rho_{PCM} c_{p,PCM} \left(\frac{\partial T}{\partial t} + \bar{v} \cdot \nabla T \right) = \nabla \cdot \left(k_{PCM} \nabla T \right) \tag{4}$$

(ii)   continuity equation

$$\nabla \cdot \bar{v} = 0 \tag{5}$$

(iii) momentum equation

$$\rho_{PCM} \left(\frac{\partial \bar{v}}{\partial t} + \bar{v} \nabla \cdot \bar{v} \right) = -\nabla p + \mu_{PCM} \nabla^2 \bar{v} + \bar{F}_b \tag{6}$$

where p is the pressure, μ_{PCM} is the dynamic viscosity, and $\bar{v}$ is the velocity vector.

In eq. (6), $\bar{F}_b$ represents the Boussinesq approximation added to the momentum equation for including the buoyancy effects, and it is evaluated according to eq. (7).

$$\bar{F}_b = \rho_{PCM} \bar{g} \beta \left(T - T_M \right) \tag{7}$$

In eq. (7), $\bar{g}$ and β are the gravitational acceleration and the thermal expansion coefficient, respectively.

Also in this case, the PCM properties, such as k_{PCM}, ρ_{PCM}, and $c_{p,PCM}$ are considered constant over the entire domain, and to simulate the phase change process, the effective heat capacity method, presented in section 3.1, is implemented. As concerns the PCM dynamic viscosity μ_{PCM}, it is evaluated according to eq. (8), in order to impose a zero velocity in the solid region of the PCM.

$$\mu_{PCM} = \mu_L (1 + S(T)) \tag{8}$$

$$S(T) = C \frac{\left(1 - \varphi(T) \right)^2}{\varphi(T)^3 + \delta} \tag{9}$$

In eq. (9), C and δ are arbitrary constant: δ is usually equal to 10^{-3}, and C, that defines the velocity variation into the phase transition zone, is usually between 10^3 and 10^7. In this work, a value of 10^5 is used for charging process and 10^3 for discharging process.

3.3. Initial and Boundary condition
Initially (t=0), the temperature is fixed equal to the temperature measured at the start-up of the experimental tests, and, obviously only in the case in which convective mechanisms are included, a no-flow condition is set, i.e. the liquid PCM velocity is given zero over the entire domain. For each t>0, the boundary conditions, for charging and discharging process, are set according to the experimental test, described in section 2. The bottom and top surfaces of the storage unit are considered adiabatic, while the boundary condition relative to the lateral surface is set according to eq. (10):

$$\begin{cases} q_l = h_l \left(T - T_\infty \right), & r = r_{max}, 0 \le l \le l_{max} \\ q_s = h_s \left(T - T_\infty \right), & 0 \le r \le r_{max}, l = l_{max} \end{cases} \tag{10}$$

In eq. (10), q_l is the heat flux relative to the lateral surface of the storage unit, h_l is the heat transfer coefficient relative to the lateral surface of the storage unit, T_∞ is equal to the air temperature inside the

climatic chamber, and r and l are the radius and the height of the storage unit, ranging from zero to a maximum value depending on the storage unit dimension.

The convective heat transfer h_l is set at 27 W/(m²K), evaluated according to the empirical correlation for vertical cylinder subjected to transverse flow under forced convection conditions of ref. [12].

3.4. Numerical treatment and mesh generation

The governing equations are solved with the finite element simulation software COMSOL Multiphysics 5.3a. The non-linearity of the problem is resolved through a segregated approach. The backward differentiation formula is adopted for the time stepping in both charging and discharging, by setting the simulation initial time step to 10^{-4} s and by using a no-fixed maximum time step. Physics-controlled meshes are used, and for both developed model, a grid independence test is conducted. The simulations are performed with a Dell Precision T7610 workstation, equipped with two Intel Xeon E5-2687 w2 processors and a RAM of 64 GB and 1866 MHz clock. Fig. 3 shows the 2D meshed computational domain of the LHTES prototype in case of conductive-convective model. Moreover, the figure shows the points at which the temperature measurements are carried out to conduct the validation, or rather the central point, placed on the container axis, and indicated with TC and the lateral one, indicated with TL.
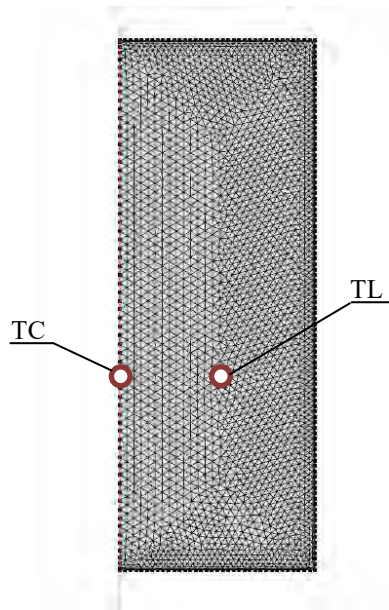
Fig. 3. Meshed computational domain of LHTES prototype
and measurements points.

4. Results

In the following sub-sections, the validation, and various results obtained from the numerical simulations of the lab-scale LHTES prototype during charging and discharging process are presented and discussed.

4.1. Models validation

To validate the developed numerical models for the charging and discharging process, the variation of the local temperature at position TC in the LHTES prototype, from simulations, is compared with the corresponding temperature values obtained from the experiments, while the variation of the local temperature at position TL in the LHTES prototype, from simulations, is compared with the average temperature variation of the PCM obtained from the experiments.

For the charging process, the numerical simulations are carried out by setting the solidification temperature (T_S) at 13°C and a solidification temperature range of 4°C is used, while, for the

discharging process, a melting temperature (T_M) of 15°C and a melting temperature range of 11°C are used.

Fig. 4 and 5 show the comparison between the experimental and numerical values for charging and discharging process, respectively. From these figures, it can be noted that in case of results obtained with the conductive-convective model, there is a close agreement between the experimental and numerical data. Indeed, the maximum deviation is about 1°C during both charging and discharging processes, and also when there is the maximum deviation, the trend of the numerical curves resembles the same as the experimental curves. In case of results obtained with the conductive model, there is a high deviation between experimental and numerical data. In this case, the maximum deviation, that is observed when all the PCM is liquid, because of the absence of the convective mechanisms, is about 9.4°C and 7°C during charging and discharging processes, respectively. Indeed, the trend of the numerical curves do not resemble the same as the experimental curves, and show that, in case of purely conductive model, phase change starts much later.

It is clear that the conductive model is not suitable for describing the heat transfer phenomena for both charging and discharging process. For this reason, only the main results obtained in the case of the use of conductive - convective model are reported in the following.

Fig. 4. Model validation: charging.
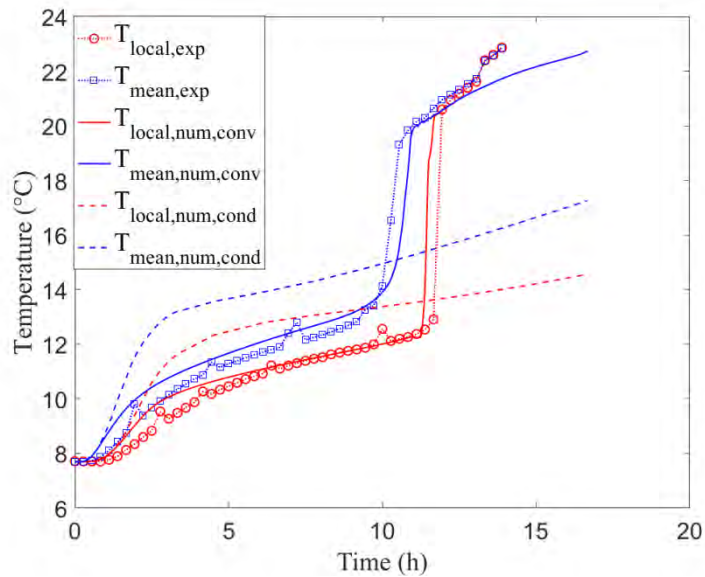
Fig. 5. Model validation: discharging.

4.2. Melt fraction and charging/discharging time

Fig. 5 (a) and (b) show the average melt fraction variation of the LHTES system during the charging and discharging process, respectively, evaluated as the volumetric average melt fraction of all mesh elements of the numerical model. Melt fraction is a key performance parameter which depicts the latent heat storage and discharge characteristics during the charging and discharging process. Moreover, the velocity variation of the melt fraction as function of temperature provides information about the velocity and the effectiveness of the charging and discharging processes.

It can be seen from Fig. 5 (a) and (b) that the average melt fraction of the LHTES system is 1/0 at the start of the charging/discharging processes, at $t = 0$ h, then it starts to decrease/increase. The solidification rate, during the charging process, is initially fast, then it decreases, whereas, due to the

formation of the solid PCM on the prototype walls, that acts reducing the heat transfer rate. During the discharging, the melting rate is relatively fast for all process. The difference between the trends is mainly due to the contribution of natural convection heat transfer that occurs during the discharging process. As it can be seen from Fig. 5 (a) and (b), the charging process is much slower than the discharging one, indeed, the LHTES system is fully charged at about 50h, and discharged at about 15h.

(a) Charging process.   (b) Discharging process.
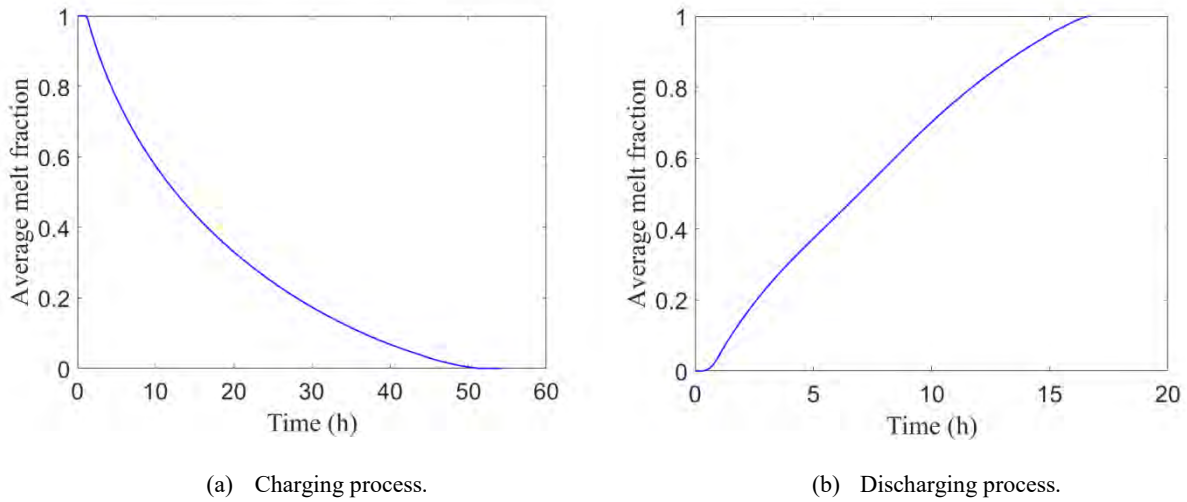
Fig. 6. Average melt fraction variation.

4.3. Cooling thermal energy storage and discharge

Fig. 6 (a) and (b) show the total cooling energy storage rate of the LHTES system during the charging and discharging process, respectively. For convention, the incoming cooling energy is assumed positive, whereas the outcome cooling energy is assumed negative. The total cooling energy stored (E_{stored}) and discharged ($E_{discharged}$) from the PCM, and its sensible ($E_{sens,c}$ and $E_{sens,d}$) and latent ($E_{lat,c}$ and $E_{lat,d}$) contributions, are key parameters for evaluating the thermal performances of the storage unit, and are calculated as the integral of the heat flux across the prototype boundaries.

(a) Charging process.   (b) Discharging process.
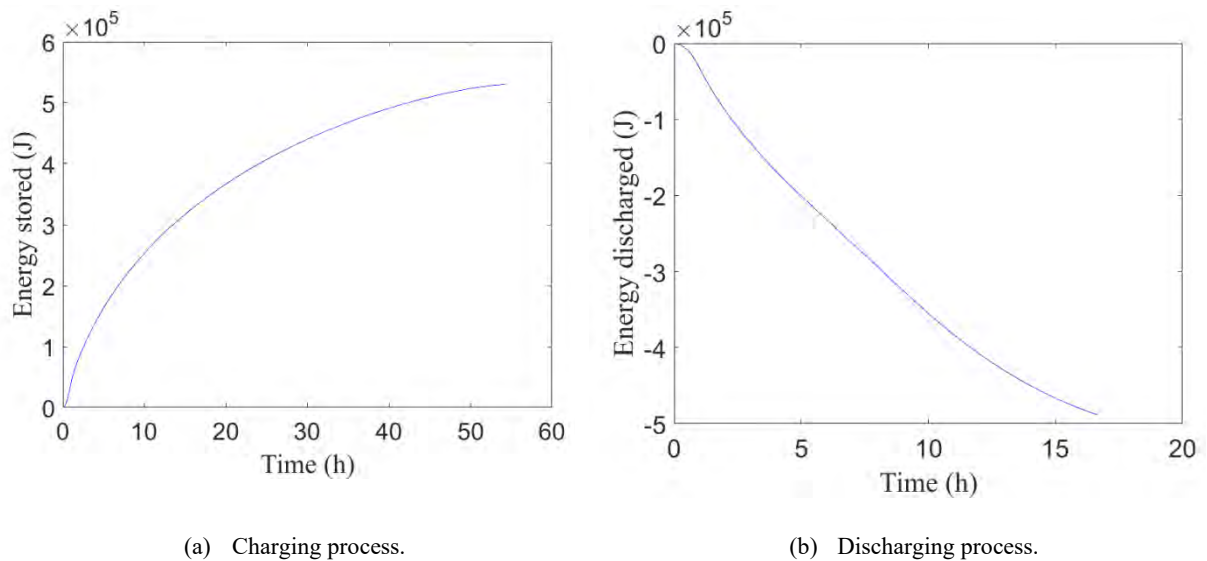
Fig. 7. Cooling energy storage/discharge rate.

Initially cooling energy gets stored/discharged in the form of sensible cooling energy only. Once the PCM reaches near the phase change temperature, cooling energy gets stored/discharged in the form of latent cooling energy. Similarly, after phase change of PCM, cooling energy is stored/discharged in the form of sensible cooling energy. The total cooling energy stored by the PCM is about 530 kJ, while the total cooling energy discharged by the PCM is about -488 kJ. As to the sensible and latent contributions of the total cooling energy stored and discharged by the PCM, they are shown in Table 2.

Table 2. Sensible and latent contributions of cooling energy stored and discharged.

Energy stored (kJ)	
Sensible contribution	93
Latent contribution	437
Energy discharged (kJ)	
Sensible contribution	-51
Latent contribution	-437

5. Conclusions

In this work, the charging and discharging characteristics of a lab-scale latent heat storage prototype for cooling applications are experimentally and numerically studied. Two numerical models are developed to analyse the performance characteristics of the LHTES prototype: a purely conductive model and a conductive-convective model. Performance parameters such as melt fraction, charging/discharging time, and energy storage/discharge rate are evaluated, and the following conclusions are derived:

- Good agreement with the experimental data are found with the conductive-convective model.
- Charging is a conduction dominated process, while discharging is a convection dominated process. For that, charging process is much slower than discharging one.
- The LHTES system takes about 50h to be fully charged, and about 15h to be fully discharged.
- The total amount of energy stored during charging is 530 kJ and during discharging is -488 kJ.

6. Nomenclature

C	Constant in eq. (11)	ρ	Density (kg/m^3)
c_p	Heat capacity (J/kg/K)	*Subscript*	
h	Heat transfer coefficient (W/m^2/K)	c	Charging
k	Thermal conductivity (W/m/K)	cond	Conductive
l	Length of module (m)	conv	Convective
L_h	Latent heat of fusion (kJ/kg)	d	Discharging
r	Radius of module (m)	exp	Experimental
T	Temperature (°C)	L	Liquid
t	time (h)	l	Lateral
TL	Lateral position	lat	Latent
TC	Central position	M	Melting
ΔT	Range of fusion (°C)	num	Numerical
Greek symbols		PCM	Phase change material
δ	Constant in eq. (9)	S	Solid
μ	Dynamic viscosity (Pa·s)	s	Superior
φ	Melt fraction	sens	Sensible

References

[1]   E. Oró, A. de Gracia, A. Castell, M.M. Farid, L.F. Cabeza. Review on phase change materials (PCMs) for cold thermal energy storage applications. Applied Energy 99 (2012) 513–533.

[2]   M.M. Farid, F.A. Hamad, M. Abu-Arabi. Melting and solidification in multidimensional geometry and presence of more than one interface. Energy Conversion and Management 39 (1998) 809–818.

[3]   M. Lacroix. Numerical simulation of a shell-and-tube latent heat thermal energy storage unit. Solar Energy 50 (1993) 357–367.

[4]   K.W. Ng, Z.X. Gong, A.S. Mujumdar. Heat transfer in free convection-dominated melting of a phase change material in a horizontal annulus. International Communications in Heat and Mass Transfer 25 (1998) 631–640.

[5]   P. Lamberg, R. Lehtiniemi, A.M. Henell. Numerical and experimental investigation of melting and freezing processes in phase change material storage. International Journal of Thermal Science 43 (2004) 277–287.

[6]   M. Esapour, M.J. Hosseini, A.A. Ranjbar, Y. Pahamli, R. Bahrampoury. Phase change in multi-tube heat exchangers. Renewable Energy 85 (2016) 1017–1025.

[7]   Y. Zhang, K. Du, J.P. He, L. Yang, Y.J. Li. Impact factors analysis of the enthalpy method and the effective heat capacity method on the transient nonlinear heat transfer in phase change materials (PCMs). Numerical Heat Transfer Part A 65 (2014) 66–83.

[8]   Y. Allouche, S. Varga, C. Bouden, A.C. Oliveira. Validation of a CFD model for the simulation of heat transfer in a tubes-in-tank PCM storage unit. Renewable Energy 89 (2016) 371–379.

[9]   H. Niyas, C.R.C. Rao, P. Muthukumar. Performance investigation of a lab-scale latent heat storage prototype - Experimental results. Solar Energy 155,(2017) 971-984.

[10]   H. Niyas, S. Prasad, P. Muthukumar. Performance investigation of a lab–scale latent heat storage prototype – Numerical results. Energy Conversion and Management 135 (2017) 188–199.

[11]   H. Neumann, V. Palomba, A. Frazzica, D. Seiler, U. Wittstadt, S. Gschwander, G. Restuccia. A simplified approach for modelling latent heat storages: Application and validation on two different fin-and-tubes heat exchangers. Applied Thermal Engineering 125 (2017) 41-52.

[12]   H.D. Baehr, K. Stephan. Heat and Mass Transfer, second edition, 2006. Springer.
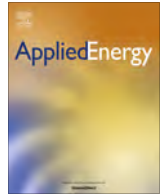
Multi-objective design optimization of distributed energy systems through cost and exergy assessments ☆

M. Di Somma [a,*], B. Yan [b], N. Bianco [c], G. Graditi [a], P.B. Luh [b], L. Mongibello [a], V. Naso [c]

[a] ENEA, Italian National Agency for New Technologies, Energy and Sustainable Economic Development, CR Portici, 80055 Portici, Italy
[b] Department of Electrical and Computer Engineering, University of Connecticut, Storrs, CT 06269, USA
[c] Dipartimento di Ingegneria Industriale (DII), Università degli studi Federico II, P.le Tecchio, Napoli 80125, Italy

HIGHLIGHTS

- Exergy in design optimization of distributed energy systems (DESs).
- Multi-objective design optimization of DESs through cost and exergy assessments.
- Balancing solutions for planners based on economic and sustainability priorities.
- Cost and primary exergy of DESs reduced by 21–36% as compared with conventional systems.
- Exergy analysis for sustainable development of energy supply systems.

ARTICLE INFO

ABSTRACT

In recent years, distributed energy systems (DESs) have been recognized as a promising option for sustainable development of future energy systems, and their application has increased rapidly with supportive policies and financial incentives. With growing concerns on global warming and depletion of fossil fuels, design optimization of DESs through economic assessments for short-run benefits only is not sufficient, while application of exergy principles can improve the efficiency in energy resource use for long-run sustainability of energy supply. The innovation of this paper is to investigate exergy in DES design to attain rational use of energy resources including renewables by considering energy qualities of supply and demand. By using low-temperature sources for low-quality thermal demand, the waste of high-quality energy can be reduced, and the overall exergy efficiency can be increased. The goal of the design optimization problem is to determine types, numbers and sizes of energy devices in DESs to reduce the total annual cost and increase the overall exergy efficiency. Based on a pre-established DES superstructure with multiple energy devices such as combined heat and power and PV, a multi-objective linear problem is formulated. In modeling of energy devices, the novelty is that the entire available size ranges and the variation of their efficiencies, capital and operation and maintenance costs with sizes are considered. The operation of energy devices is modeled based on previous work on DES operation optimization. By minimizing a weighted sum of the total annual cost and primary exergy input, the problem is solved by branch-and-cut. Numerical results show that the Pareto frontier provides good balancing solutions for planners based on economic and sustainability priorities. The total annual cost and primary exergy input of DESs with optimized configurations are reduced by 21–36% as compared with conventional energy supply systems, where grid power is used for the electricity demand, and gas-fired boilers and electric chillers fed by grid power for thermal demand. A sensitivity analysis is also carried out to analyze the influence of energy prices and energy demand variation on the optimized DES configurations.

© 2017 Elsevier Ltd. All rights reserved.

1. Introduction

In recent years, depletion of fossil energy resources and global warming problems have prompted worldwide awareness about sustainability of energy supply. In such context, Distributed Energy Systems (DESs) have been recognized as a promising option for

---

Nomenclature

A	area (m^2)
c	constant in Eq. (34) (kW h/€)
C	cost (€)
C_c	specific capital cost (€/kW) - (€/kW h) - (€/m^2)
$C_{d,hr}$	cooling rate (kW)
COP	coefficient of performance
CRF	capital recovery factor
DR	maximum ramp-down rate (kW)
D_t	length of the time interval (h)
e	minimum part load
$E_{d,hr}$	electricity rate (kW)
ex_{Bio}	specific chemical exergy of biomass (kW h/kg)
ex_{NG}	specific chemical exergy of natural gas (kW h/N m^3)
Ex	exergy (kW h)
$Ex_{d,hr}$	exergy rate (kW)
F_{obj}	objective function
F_q	Carnot factor
G	natural gas volumetric flow rate (N m^3/h)
$H_{d,hr}$	heating rate (kW)
I	total solar irradiance (kW/m^2)
LHV_{Bio}	lower heat value of biomass (kW h/kg)
LHV_{NG}	lower heat value of natural gas (kW h/N m^3)
n_i	total number of energy devices associated with technology i
N	lifetime (years)
OM	O&M cost (€/kW h)
P_{Bio}	biomass price (€/ton)
P_e	electricity price (€/kW h)
P_{NG}	natural gas price (€/N m^3)
r	interest rate
$R_{d,hr}$	energy rate (kW)
S	designed size (kW) – (kW h)
T	temperature (K)
UR	maximum ramp-up rate (kW)
x	binary decision variable

Greek symbols

ε_{gen}	exergy efficiency of electricity generation
ς_{FUEL}	exergy factor of fuel
η	efficiency
φ	storage loss fraction
ψ	overall exergy efficiency
ω	weight in Eq. (34)

Superscript/subscripts

0	reference
Abs	absorption chiller

ASHP	air source heat pump
Bio	biomass
Bioboil	biomass boiler
CHP NGICE	combined heat and power with gas-fired internal combustion engine
CHP NGMTG	combined heat and power with gas-fired micro-turbine
coll	collector
d	day
dem	demand
DHW	domestic hot water
e	electricity
ES	electrical storage
FUEL	fuel
GRID	power grid
hr	hour
i	index of technology
in	input
INV	investment
j	energy carrier
l	range
k_i	energy device associated with technology i
K_i	maximum number of energy devices associated with technology i
max	maximum
min	minimum
NG	natural gas
NGboil	gas-fired boiler
O&M	operation and maintenance
out	output
PV	photovoltaic
req	required
SC	space cooling
SH	space heating
SOLAR	solar
ST	solar thermal
sto	stored
TES	thermal energy storage
th	thermal
TOT	total

Acronyms

CHP	combined heat and power
DES	distributed energy system
MOLP	multi-objective linear programming
O&M	operation and maintenance

sustainable development of future energy systems [1–6]. A DES refers to a multi-input and multi-output energy system, consisting of multiple small-scale technologies, including renewable ones and storage units, providing electric and thermal energy close to end-users [1–8]. Therefore, as compared with conventional energy supply systems, DESs may employ a wide range of technologies, thereby offering the possibility to integrate renewables as well as to recover waste heat from power generation processes for thermal purposes in buildings [2–4]. The application of DESs has increased rapidly in recent years with the supportive government policies and financial incentives [1,3,4,8]. However, to achieve the expected potentials of DESs, it is necessary to determine the system configuration rationally by selecting the appropriate energy devices, and identifying their numbers and sizes, and the corresponding operation strategies, to match energy requirements of a specific end-user [2,9–11]. Design optimization of a DES is therefore essential for future energy planning, and inherently involves multiple and conflicting objectives [12–15]. For instance, the interest of DES developers in achieving a system configuration with lowest costs might conflict with the interest of energy legislations such as the EU ones in increasing sustainability of energy supply, which can be attained by reducing the waste of fossil energy resources and environmental impacts [15,16]. In such a context, a multi-objective approach helps identify balancing solutions to promote participation in the decision-making process and facilitate collective decisions [12].

According to [16], application of exergy principles in building energy supply systems may promote rational use of energy resources, by taking into account the different energy quality levels of energy supply and those of building demand. Electrical and

chemical energy are high-quality energy, whereas low-temperature heat is low-quality energy. In current energy supply systems, energy is commonly supplied as electricity or as fossil energy carriers, whose energy quality is unnecessarily high to meet low-quality thermal demand in buildings, and the First Law of Thermodynamics does not consider the energy quality degradation occurring in such processes. Conversely, based on the Second Law of Thermodynamics, by reducing the supply of high-quality energy for thermal demand in buildings through the usage of low-temperature sources, efficient use of the potential (i.e., quality) of the energy resources is promoted. Since energy resources, and particularly fossil fuels, are limitedly available, better exploiting their potential allows to reduce their waste. In this way, lifetime of fossil fuels can be extended, and the environmental impacts derived from their use can be reduced [16]. In the literature, exergy analysis has been linked to sustainability of energy supply which is essential for the long run, since it clearly identifies the efficiency in energy resource use, by considering their potential; and the importance of including exergy in energy legislations was discussed [16–21]. Exergy was investigated in performance evaluation of single energy supply systems, as cogeneration systems [22–25], renewable energy sources [26,27], various types of heat pumps [28–30], and thermal energy storage [31–33] with the aim to reduce energy quality degradation in designing and managing these systems, thereby improving sustainability of energy supply. DESs provide a great opportunity to demonstrate the effectiveness of exergy analysis in designing more sustainable energy systems since multiple energy resources with different energy quality levels can be used to satisfy user various demand with different quality levels. By using low exergy sources, e.g., solar thermal or waste heat of power generation, for low-quality thermal demand, and high exergy sources for electricity demand, the waste of high-quality energy can be reduced, thereby increasing the overall exergy efficiency of DESs.

In previous work, exergy modeling and optimization were investigated in DES operations through a multi-objective approach [34,35]. Based on fixed DES configurations (types, numbers and sizes of energy devices), optimized operation strategies were established by considering energy costs and exergy efficiency. As for design optimization of DESs, most studies in the literature focused on minimizing the total annual cost (annualized investment costs and annual operating costs of the system) as a crucial objective for DES developers [2,36–42]. Beyond minimizing costs only, design optimization of DESs through multi-objective approach to reduce also environmental impact was analyzed. In [43], a multi-objective linear programming (MOLP) model was established to find the optimal configuration and operation of a DES for an industrial area while reducing the total annual cost and CO_2 emission. The problem was solved by using the compromise programming method. In [44], a MOLP model was developed to optimally design and operate an energy system consisting of buildings equipped with small-size Combined Heat and Power (CHP) plants, with the aim to reduce both annual costs and CO_2 emission. In [45], a general framework was developed to study the application of energy hubs for determining the optimal design and operation of DESs in urban areas according to economic and environmental objectives, and the multi-objective optimization problem was solved by using branch-and-cut. In all the analyzed works, before optimizing the design, "superstructures" were pre-established with energy devices chosen among the most commonly used ones in practical DESs. Moreover, to identify the size of an energy device, several sizes were pre-fixed as possible choices to be selected through binary decision variables [2,36–40,44,45]. However, it is difficult to select the sizes among the almost infinite possible solutions available in the market. Conversely, the size of an energy device was a continuous decision variable within the entire available size range, with efficiencies as well as specific capital and operation and maintenance (O&M) costs assumed constant in the entire size range and their variations with the sizes were not considered [41,42]. The size of an energy device was a continuous decision variable within the entire available size range in [43], with prices and efficiencies approximated as linear functions of the size.

The innovation of this paper is to investigate exergy in DES design optimization through a multi-objective approach to attain rational use of energy resources considering economic and sustainability priorities. A superstructure is pre-established with multiple energy devices, such as CHPs with natural gas-fired internal combustion engines and micro-turbines as prime movers, natural gas and biomass boilers, solar thermal collectors, PV, reversible air-source heat pumps, single-stage absorption chillers, and electrical and thermal energy storage devices. Given user demand includes electricity, domestic hot water, space heating, and space cooling. To take both cost and exergy assessments into account, a MOLP problem is formulated, and the goal is to determine types, numbers and sizes of energy devices in the DES with the corresponding operation strategies on the Pareto frontier, thereby providing different design options for planners based on short- and long-run priorities. In modeling of energy devices, the key novelty is that the entire size ranges available in the market as well as the variations of efficiencies, specific capital and O&M costs with sizes are taken into account, based on a detailed market analysis. These characteristics are usually piecewise linear functions of the device size, which is a continuous decision variable, thereby making the problem nonlinear. To maintain the problem linearity, the key idea is to divide the entire size range of an energy device into several small ranges, so that these characteristics can be assumed constant in each size range. The daily operation of energy devices is modeled based on previous work on operation optimization of DESs [34]. The economic objective is formulated as the total annual cost (total annualized investment cost, total annual O&M and energy cost) to be minimized. The exergetic objective is to maximize the overall exergy efficiency of the DES, defined as the ratio of the total annual exergy required to meet the given energy demand to the total annual primary exergy input to the system. Assuming known the energy demand, the total exergy required to meet the demand is also known. Therefore, the exergetic objective is formulated as the total annual primary exergy input to be minimized. By minimizing a weighted sum of the total annual cost and primary exergy input, the problem is solved by branch-and-cut. The general mathematical formulation established and the optimization method provided could be applicable in real contexts, thereby providing decision support to planners. Given the input data, such as end-user demand, local climate data, energy prices and technical and economic information of the candidate energy devices, the model allows to obtain their optimized combination, and the corresponding operation strategies through cost and exergy assessments. As an illustrative example, the model is implemented for a hypothetic building cluster located in Italy. The optimization is carried out on an hourly basis for four representative season days. Numerical results demonstrate that exergy analysis is a powerful tool for designing more sustainable energy supply systems based on the use of renewables and low-temperature sources for thermal demand in buildings, and that good balancing options for planners are found on the Pareto frontier. Moreover, the total annual cost and primary exergy input of DESs with optimized configurations are significantly reduced, by 21–36% as compared with conventional energy supply systems, where grid power is used for the electricity demand, natural gas boilers for domestic hot water and space heating demand, and electric chillers fed by grid power for space cooling demand. In addition, a sensitivity analysis is carried out to analyze the influence of key parameters such as energy

prices and energy demand variation on the optimized DES configurations and the related economic and exergetic performances.

In the following, Section 2 is on the problem formulation and the optimization method. Numerical testing is presented and discussed in Section 3. Sensitivity analysis is presented in Section 4.

2. Problem formulation and optimization method

The superstructure of the DES under consideration is shown in Fig. 1. The energy devices are chosen among the most commonly used ones in practical DESs.

Electricity demand and electricity required by heat pumps can be satisfied by grid power, by the electricity provided by CHPs with natural gas-fired internal combustion engines and micro-turbines as prime movers, PV, and by the electricity discharged from the electrical storage. It is assumed that all the electricity provided by CHPs and PV is self-consumed, while no extra electricity is sold back to the power grid. Domestic hot water demand can be satisfied by thermal energy provided by CHPs, natural gas and biomass boilers, solar thermal collectors, and by thermal energy discharged from the storage. Space heating demand can be satisfied by thermal energy provided by CHPs, natural gas and biomass boilers, heat pumps, and by thermal energy discharged from the storage. Space cooling demand can be satisfied by thermal energy provided by CHPs, natural gas and biomass boilers through the absorption chillers, heat pumps, and by thermal energy discharged from the storage.

In the following, the decision variables are first introduced in Section 2.1. The economic and exergetic objectives are presented in nd 2.22.3, respectively. The constraints are established in Section 2.4. The optimization method is discussed in Section 2.5.

2.1. Decision variables

In the optimization problem, the decision variables include: existence, numbers, and sizes of energy devices; operation status (on/off) and energy rates provided by energy devices; capacities of electrical and thermal storage devices; electricity and heat rate input and output to/from electrical and thermal storage devices,

respectively; and electricity rate bought from the power grid. Existence and operation status of energy devices are binary. Numbers of energy devices are also determined through binary decision variables to be explained later. All the other decision variables are continuous.

2.2. Economic objective

The economic objective is to minimize the total annual cost of the DES, C_{TOT}, formulated as the sum of the total annualized investment cost, and the total annual O&M and energy costs:

$$C_{TOT} = C_{INV} + C_{O\&M} + C_{FUEL} + C_{GRID}, \quad (1)$$

where C_{INV} is the annualized investment cost of all energy devices in the DES; $C_{O\&M}$ is the total annual O&M cost of all energy devices; C_{FUEL} is the total annual cost of consumed fuels; and C_{GRID} is the annual cost of purchasing electricity from the power grid.

The total annualized investment cost of the energy devices is formulated as:

$$C_{INV} = \sum_i \sum_{k_i}^{K_i} CRF_i(C_{c,i}S_{i,k_i}),$$

$$CRF_i = r(1+r)^{N_i} / \left[(1+r)^{N_i} - 1\right], \quad (2)$$

where CRF_i is the capital recovery factor of technology i; K_i is the maximum number of energy devices associated with technology i, which is assumed to be known; k_i is the energy device associated with technology i; S_{i,k_i} is the designed size of device k_i; $C_{c,i}$ is the specific capital cost; r is the interest rate; and N_i is the lifetime. The size of electrical and thermal energy storage devices represents the capacity expressed in kW h, and the specific capital cost is expressed in €/kW h. The size of the solar thermal collectors is expressed in terms of the total surface of collectors to be installed, and the specific capital cost is expressed in €/m².

The total annual O&M cost of energy devices is formulated as:

$$C_{O\&M} = \sum_i \sum_{k_i}^{K_i} \sum_d \sum_{hr} OM_i R_{i,k_i,d,hr} D_t, \quad (3)$$

<table>
<tr><td colspan="7" align="center">**Supply**</td><td>**Demand**</td></tr>
</table>
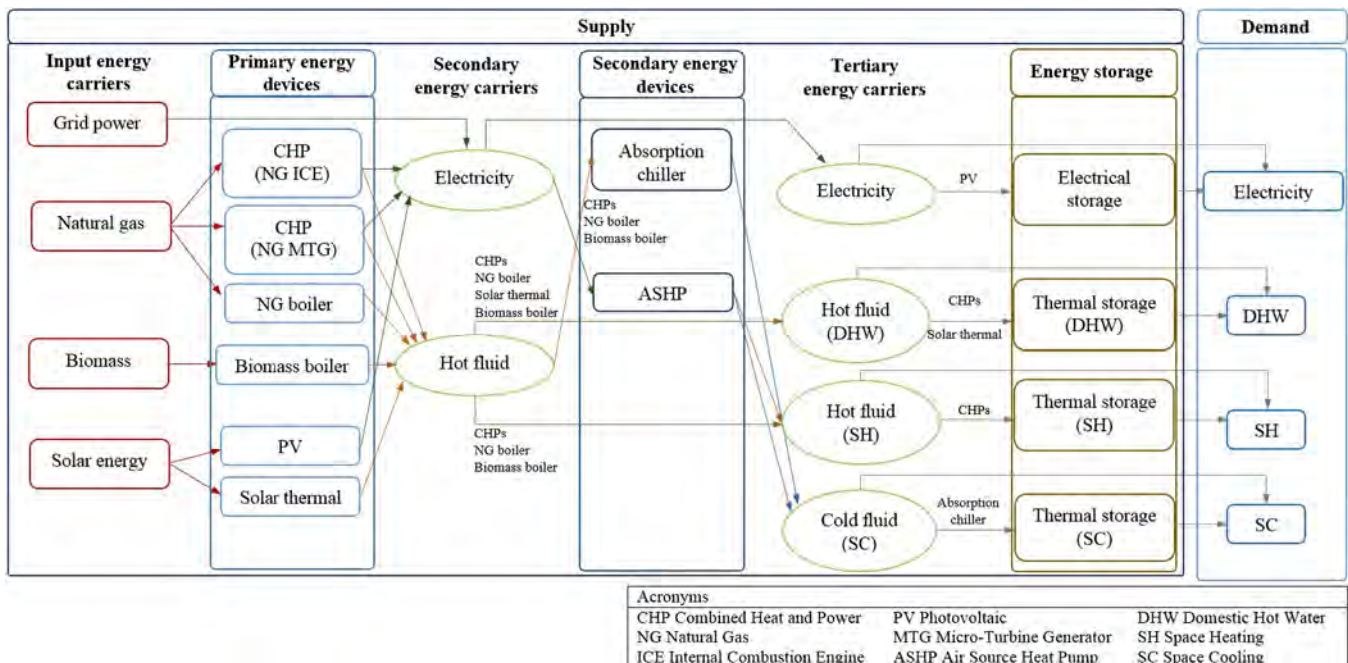
Fig. 1. Superstructure representation of the DES for the design optimization problem.

where OM_i is the O&M cost of the technology i; $R_{i,k_i,d,hr}$ is the energy rate provided by the energy device k_i at hour hr of day d; and D_t is the length of the time interval (1 h). For electrical and thermal storage devices, the O&M costs are based on their capacities.

The total annual cost of the consumed fuels is formulated as:

$$C_{FUEL} = \sum_{i \in \{CHP\,NGICE,\, CHP\,NGMTG,\, NG\,boil\}} \sum_{k_i}^{K_i} \sum_d$$
$$\sum_{hr} P_{NG}\left(R_{i,k_i,d,hr}/(\eta_i LHV_{NG})\right)D_t + \sum_{i \in \{Bioboil\}}$$
$$\sum_{k_i}^{K_i} \sum_d \sum_{hr} P_{Bio}\left(R_{i,k_i,d,hr}/(\eta_i LHV_{Bio})\right)D_t, \tag{4}$$

where η_i is the energy efficiency (thermal or electrical); P_{NG} and P_{Bio} are the price of natural gas and biomass, respectively; and LHV_{NG} and LHV_{Bio} are the lower heat value of natural gas and biomass, respectively.

The annual cost of purchased grid power is formulated as:

$$C_{GRID} = \sum_d \sum_{hr} P_{e,hr} E_{GRID,d,hr} D_t, \tag{5}$$

where $P_{e,hr}$ is the time-of-day unit price of electricity from the power grid, and $E_{GRID,d,hr}$ is the electricity rate taken from the grid.

2.3. Exergetic objective

The exergetic objective is to maximize the overall exergy efficiency of the DES, ψ, defined as the ratio of the total annual exergy output, Ex^{out}, to the total annual primary exergy input, Ex_{in} [34,46,47]:

$$\psi = Ex^{out}/Ex_{in}. \tag{6}$$

The total annual exergy output is the total annual exergy required to meet the given user demand in the whole year, formulated as:

$$Ex^{out} = \sum_{dem} \sum_d \sum_{hr} Ex^{dem}_{d,hr} D_t, \quad dem \in \{e, DHW, SH, SC\}, \tag{7}$$

where $Ex^{dem}_{d,hr}$ is the total exergy rate required to meet the electricity and thermal demand (domestic hot water, and space heating and cooling). In buildings, energy demands are characterized by different energy quality levels. To meet the electricity demand, the highest quality of energy is needed. The exergy rate required to meet the electricity demand, $Ex^e_{d,hr}$, can be evaluated as follows [34,35,48]:

$$Ex^e_{d,hr} = E^e_{d,hr}, \quad \forall d, \forall hr, \tag{8}$$

where $E^e_{d,hr}$ is the electricity demand rate.

As for thermal demand, the energy quality depends on temperature required – the lower the temperature required, the lower the exergy [16,48]. The exergy rate required to meet the demand of domestic hot water can be formulated as:

$$Ex^{DHW}_{d,hr} = H^{DHW}_{d,hr} F^{DHW}_{q,d,hr}, \quad \forall d, \forall hr, \tag{9}$$

where $H^{DHW}_{d,hr}$ is the heat demand rate for domestic hot water, and $F^{DHW}_{q,d,hr}$ is the Carnot factor, formulated as [16,34,35,48]:

$$F^{DHW}_{q,d,hr} = 1 - T_{0,d,hr}/T^{DHW}_{req}, \quad \forall d, \forall hr, \tag{10}$$

which depends on both the temperature required for the domestic hot water, T^{DHW}_{req}, which is assumed to be known based on [49], and the reference temperature, $T_{0,d,hr}$, assumed to be known as the averaged ambient temperature at hour hr of day d [16,34]. The exergy rate required to meet the demand of space heating and cooling can be formulated similarly.

At the supply side, the input energy carriers are grid power, natural gas, biomass, and solar energy. The total annual primary exergy input is formulated as:

$$Ex_{in} = \sum_j \sum_d \sum_{hr} Ex_{j,d,hr} D_t, \quad j \in \{GRID, FUEL, SOLAR\}, \tag{11}$$

where $Ex_{j,d,hr}$ is the exergy rate input to the DES related to the energy carrier j. As well as for the demand side, also the supply side is characterized by different energy quality levels.

Electricity from the power grid is an energy carrier provided by power generation plants, and the exergy input rate to the DES, $Ex_{GRID,d,hr}$, depends on the exergy efficiency of the plants, ε_{gen} [34,35]:

$$Ex_{GRID,d,hr} = E_{GRID,d,hr}/\varepsilon_{gen}, \quad \forall d, \forall hr, \tag{12}$$

The exergy input rates of fuels (natural gas and biomass) depend on their specific chemical exergy:

$$Ex_{FUEL,d,hr} = \sum_{i \in \{CHP\,NGICE,\, CHP\,NGMTG,\, NGboil\}} \sum_{k_i}^{K_i} ex_{NG}(R_{i,k_i,d,hr}/(\eta_i LHV_{NG}))$$
$$+ \sum_{i \in \{Bioboil\}} \sum_{k_i}^{K_i} ex_{Bio}(R_{i,k_i,d,hr}/(\eta_i LHV_{Bio})),$$
$$ex_{FUEL} = \varsigma_{FUEL} LHV_{FUEL},$$
$$FUEL \in \{NG, Bio\}, \forall d, \forall hr, \tag{13}$$

where ex_{FUEL} is the specific chemical exergy of the fuel, and ς_{FUEL} is the exergy factor [50].

As for solar energy, thermal energy output of the solar thermal collectors at the corresponding temperature levels, and electricity output of PV are considered as the primary energy sources [51,52], respectively. The exergy input rate to solar thermal collectors, $Ex_{ST,d,hr}$, is formulated as:

$$Ex_{ST,d,hr} = H_{ST,d,hr}(1 - T_{0,d,hr}/T^{out}_{coll}), \quad \forall d, \forall hr, \tag{14}$$

where $H_{ST,\,d,\,hr}$ is the heat rate provided by solar thermal collectors, and $T_{0,d,hr}$ and T^{out}_{coll} are the reference temperature, assumed as the averaged ambient temperature at hour h of day d [16,34], and the temperature of the heat transfer fluid at the exit of the collector field (assumed constant), respectively.

The exergy input rate to PV, $Ex_{PV,d,hr}$, is formulated as:

$$Ex_{PV,d,hr} = E_{PV,d,hr}, \quad \forall d, \forall hr. \tag{15}$$

where $E_{PV,\,d,\,hr}$ is the electricity rate provided by PV.

Therefore, the exergy rate of solar energy input to the DES is formulated as:

$$Ex_{SOLAR,d,hr} = Ex_{ST,d,hr} + Ex_{PV,d,hr}, \quad \forall d, \forall hr. \tag{16}$$

Since energy demand as well as the temperatures required for the demand of domestic hot water, and space heating and cooling are assumed known, the total exergy required to meet the demand is also known, and the overall exergy efficiency can be increased by reducing the total primary exergy input. Therefore, the exergetic objective is formulated as the total annual primary exergy input to the DES to be minimized as in Eq. (11).

2.4. Constraints

The constraints in the optimization problem include design constraints, energy balances and operation constraints, as discussed below.

2.4.1. Design constraints

The designed size of the energy device k_i has to be within the minimum and maximum sizes of the related technology $S_i^{\min}$ and $S_i^{\max}$ available in the market:

$$S_i^{\min} x_{i,k_i} \leqslant S_{i,k_i} \leqslant S_i^{\max} x_{i,k_i}, \quad k_i \leqslant K_i, \quad n_i = \sum_{k_i}^{K_i} x_{i,k_i}, \quad \forall i, \tag{17}$$

where x_{i,k_i} is a binary decision variable, which is equal to 1 if the device k_i is implemented in the DES configuration; and n_i is the total number of energy devices associated with technology i implemented in the DES configuration. As for solar collector and PV arrays, the total designed area has to be lower than the available one. In the design optimization problem, the entire size range available in the market as well as the variations of efficiencies, specific capital and O&M costs with sizes, are taken into account. These characteristics are usually piecewise linear functions of the size, which is a continuous decision variable, thereby making the problem nonlinear. To avoid this, the key idea is to divide the entire size range of an energy device into several small ranges, so that these characteristics can be assumed constant in each size range. Consider CHP with a natural gas-fired internal combustion engine as an example. The designed size of CHP in range l is limited by its minimum and maximum values $S_{CHP\,NGICE}^{\min,l}$ and $S_{CHP\,NGICE}^{\max,l}$ in this range:

$$S_{CHP\,NGICE}^{\min,l} x_{k_{CHP\,NGICE}}^l \leqslant S_{k_{CHP\,NGICE}}^l \leqslant S_{CHP\,NGICE}^{\max,l} x_{k_{CHP\,NGICE}}^l,$$
$$\sum_l x_{k_{CHP\,NGICE}}^l \leqslant 1, \quad \forall l, k_{CHP\,NGICE} \leqslant K_{CHP\,NGICE}, \tag{18}$$

where $S_{k_{CHP\,NGICE}}^l$ and $x_{k_{CHP\,NGICE}}^l$ are defined similarly as in Eq. (17) in range l. Also the summation of binary decision variables $x_{k_{CHP\,NGICE}}^l$ over l has to be smaller than or equal to 1, ensuring that at most one range can be selected for each energy device associated to each technology.

2.4.2. Energy balances

To satisfy the given user demand, electricity, domestic hot water, and space heating and cooling energy balances are formulated in the following.

For electricity, the sum of the electricity demand and the total electricity required by the reversible air source heat pumps has to be satisfied by the sum of the total electricity provided by CHPs, PV, grid power, and electrical storage:

$$E_{d,hr}^e + \sum_{k_{ASHP}} E_{k_{ASHP},d,hr} = E_{PV,d,hr} + \sum_{k_{CHP\,NGICE}} E_{k_{CHP\,NGICE},d,hr}$$
$$+ \sum_{k_{CHP\,NGMTG}} E_{k_{CHP\,NGMTG},d,hr} + E_{GRID,d,hr}$$
$$+ E_{ES,d,hr}^{e,out} - E_{ES,d,hr}^{e,in}, \quad \forall d, hr, \tag{19}$$

where $E_{ES,d,hr}^{e,out}$ and $E_{ES,d,hr}^{e,in}$ are the electricity rates discharged and charged from/to the storage, respectively, which are both continuous decision variables.

For the domestic hot water demand, the demand has to be satisfied by the total thermal energy provided by CHPs, natural gas and biomass boilers, solar thermal collectors, and thermal storage:

$$H_{d,hr}^{DHW} = \sum_{k_{CHP\,NGICE}} H_{k_{CHP\,NGICE},d,hr}^{DHW} + \sum_{k_{CHP\,NGMTG}} H_{k_{CHP\,NGMTG},d,hr}^{DHW}$$
$$+ \sum_{k_{NGboil}} H_{k_{NGboil},d,hr}^{DHW} + \sum_{k_{Bioboil}} H_{k_{Bioboil},d,hr}^{DHW} + H_{ST,d,hr} + H_{TES,d,hr}^{DHW,out}$$
$$- H_{TES,d,hr}^{DHW,in}, \quad \forall d, hr, \tag{20}$$

where $H_{TES,d,hr}^{DHW,out}$ and $H_{TES,d,hr}^{DHW,in}$ are the heat rates discharged and charged from/to the storage, respectively, which are both continuous decision variables.

The space heating and space cooling energy balances are formulated in a similar way.

2.4.3. Operation constrains

For most of the energy devices included in the DES superstructure, the common constraint is the capacity constraint. The energy rate provided by each energy device is limited by its minimum part load and the capacity, if the device is on. Still considering the CHP with a natural gas-fired internal combustion engine as an example, the electricity rate, $E_{k_{CHP\,NG\,ICE},d,hr}$, is limited by the minimum and maximum rated output $E_{k_{CHP\,NG\,ICE}}^{\min}$ and $E_{k_{CHP\,NG\,ICE}}^{\max}$, if the device is on:

$$E_{k_{CHP\,NG\,ICE}}^{\min} x_{k_{CHP\,NG\,ICE},d,hr} \leqslant E_{k_{CHP\,NG\,ICE},d,hr} \leqslant E_{k_{CHP\,NG\,ICE}}^{\max} x_{k_{CHP\,NG\,ICE},d,hr},$$
$$\forall k_{CHP\,NGICE}, \quad \forall d, hr, \tag{21}$$

where $x_{k_{CHP\,NG\,ICE},d,hr}$ is the on/off status of CHP. The minimum part load and the maximum rated output are obtained based on the design capacity of CHP as follows:

$$E_{k_{CHP\,NGICE}}^{\min} = e_{k_{CHP\,NGICE}} \sum_l S_{k_{CHP\,NGICE}}^l, \quad E_{k_{CHP\,NGICE}}^{\max} = \sum_l S_{k_{CHP\,NGICE}}^l,$$
$$\forall k_{CHP\,NGICE}, \tag{22}$$

where $e_{k_{CHP\,NG\,ICE}}$ is the minimum part load expressed in percentage of the designed size. The product of one continuous and one binary decision variables is linearized in a standard way [53].

In the following, the additional constraints of each energy device are presented.

2.4.3.1. CHP systems. Two types of CHPs are involved in the DES superstructure, i.e., CHPs with gas-fired internal combustion engine and with micro-turbines. They consist of prime movers to meet the electricity load, and heat recovery units providing thermal energy to meet the demand of domestic hot water and space heating, and to meet the demand of space cooling through absorption chillers. Operation constraints for CHPs with gas-fired internal combustion engine as prime mover are presented below.

The ramp rate constraint limits the variations in the power generation between two successive time steps to be within the ramp-down, $DR_{k_{CHP\,NGICE}}$, and ramp-up, $UR_{k_{CHP\,NGICE}}$ [34,54]:

$$DR_{k_{CHP\,NGICE}} \leqslant E_{k_{CHPNGICE},d,hr} - E_{k_{CHPNGICE},d,hr-1} \leqslant UR_{k_{CHPNGICE}},$$
$$\forall k_{CHP\,NG\,ICE}, \quad \forall d, hr, \tag{23}$$

where the ramp-down and the ramp-up and are expressed in percentage of the designed size.

The volumetric flow rate of natural gas, $G_{k_{CHP\,NGICE},d,hr}$, required by the CHP to provide the electricity rate, $E_{k_{CHP\,NG\,ICE},d,hr}$, is formulated as:

$$G_{k_{CHP\,NGICE},d,hr} = E_{k_{CHP\,NGICE},d,hr}/(\eta_{e,k_{CHP\,NGICE}} LHV_{NG}),$$
$$\forall k_{CHP\,NGICE}, \quad \forall d, hr. \tag{24}$$

In the above, $\eta_{e,k_{CHP\,NGICE}}$ is the electrical efficiency of the CHP, formulated as:

$$\eta_{e,k_{CHP\,NGICE}} = \sum_l x_{k_{CHP\,NGICE}}^l \eta_{e,k_{CHP\,NGICE}}^l, \quad \forall k_{CHP\,NGICE}, \tag{25}$$

where $\eta_{e,k_{CHP\,NGICE}}^l$ is the electrical efficiency of the CHP in the range l.

The heat rate recovered from the CHP, $H_{k_{CHP\,NGICE},d,hr}$, is formulated as:

$$H_{k_{CHP\,NGICE},d,hr} = E_{k_{CHP\,NGICE},d,hr}\eta_{th,k_{CHP\,NGICE}}/\eta_{e,k_{CHP\,NGICE}},$$
$$\forall k_{CHP\,NGICE}, \quad \forall d, hr, \tag{26}$$

where $\eta_{th,k_{CHP\,NGICE}}$ is the thermal efficiency of the CHP defined similarly as in Eq. (25).

The heat rate recovered by CHP is subdivided to meet the demand of domestic hot water and space heating, and to meet the demand of space cooling through the absorption chillers:

$$H_{k_{CHP\,NGICE},d,hr} = H^{DHW}_{k_{CHP\,NGICE},d,hr} + H^{SH}_{k_{CHP\,NGICE},d,hr}$$
$$+ H^{SC}_{k_{CHP\,NGICE},d,hr}, \quad \forall k_{CHP\,NGICE}, \quad \forall d, hr. \quad (27)$$

Constraints for CHPs with micro-turbines as prime movers are similar to those formulated above.

2.4.3.2. Boilers. Natural gas and biomass boilers may be involved to meet the demand of domestic hot water, space heating, and to meet the demand of space cooling through absorption chillers. Operation constraints for gas-fired boilers are presented below.

The volumetric flow rate of natural gas, $G_{k_{NGBoil},d,hr}$, required by the gas-fired boiler to provide the heat rate, $H_{k_{NGBoil},d,hr}$, is formulated as:

$$G_{k_{NGBoil},d,hr} = H_{k_{NGBoil},d,hr}/(\eta_{th,k_{NGBoil}} LHV_{NG}), \quad \forall k_{NGBoil}, \quad \forall d, hr, \quad (28)$$

where $\eta_{th,k_{NGBoil}}$ is the thermal efficiency of the boiler defined similarly as in Eq. (25). The heat rate provided by the boiler is subdivided to meet the demand of domestic hot water and space heating, and to meet the demand of space cooling through the absorption chillers:

$$H_{k_{NGBoil},d,hr} = H^{DHW}_{k_{NGBoil},d,hr} + H^{SH}_{k_{NGBoil},d,hr} + H^{SC}_{k_{NGBoil},d,hr},$$
$$\forall k_{NGBoil}, \quad \forall d, hr. \quad (29)$$

Constraints for biomass boilers are similar to those formulated above.

2.4.3.3. Solar energy systems. Solar PV and solar thermal collectors may be involved to meet the electricity load and the domestic hot water demand, respectively.

The electricity rate provided by solar PV, $E_{PV,d,hr}$, is formulated as [36,55]:

$$E_{PV,d,hr} = A_{PV}\eta_{PV}I_{d,hr}, \quad \forall d, hr, \quad (30)$$

where A_{PV} is the total area to be installed, η_{PV} is the electrical efficiency, and $I_{d,hr}$ is the hourly solar irradiance in day d.

The heat rate provided by solar thermal collectors can be expressed in a similar way.

2.4.3.4. Absorption chiller. Absorption chillers may be involved to meet the demand of space cooling, powered by the total thermal energy recovered from CHPs, and provided by natural gas and biomass boilers. The cooling rate provided by the absorption chiller, $C_{k_{Abs},d,hr}$, is expressed as:

$$C_{k_{Abs},d,hr} = \left(\sum_{k_{CHP\,NGICE}} H^{SC}_{k_{CHP\,NGICE},d,hr} + \sum_{k_{CHP\,NGMTG}} H^{SC}_{k_{CHP\,NGMTG},d,hr} + \sum_{k_{NGboil}} H^{SC}_{k_{NGboil},d,hr} \right.$$
$$\left. + \sum_{k_{Bioboil}} H^{SC}_{k_{Bioboil},d,hr} \right) COP_{k_{Abs}}, \quad \forall k_{Abs}, \quad \forall d, hr, \quad (31)$$

where $COP_{k_{Abs}}$ is the coefficient of performance of the absorption chiller defined similarly as in Eq. (25).

2.4.3.5. Reversible air source heat pump. Reversible air source heat pumps may be involved to meet the space heating and cooling demand in heating and cooling mode, respectively. In the heating mode, the electricity rate required by the air source heat pump, $E^{SH}_{k_{ASHP},d,hr}$, to provide the heat rate, $H^{SH}_{k_{ASHP},d,hr}$, is formulated as:

$$E^{SH}_{k_{ASHP},d,hr} = H^{SH}_{k_{ASHP},d,hr}/COP^{SH}_{k_{ASHP}}, \quad \forall k_{ASHP}, \quad \forall d, hr, \quad (32)$$

where $COP^{SH}_{k_{ASHP}}$ is the coefficient of performance of the heat pump in the hating mode defined similarly as in Eq. (25).

Modeling of cooling mode is similar to that of heating described above.

2.4.3.6. Energy storage devices. For the operation of energy storage devices, the amount of energy stored at the beginning of each time interval equals the non-dissipated energy stored at the beginning of the previous time interval (based on the storage loss fraction), plus the net energy flow (energy input rate to the storage minus energy output rate from the storage) [2,34]. For the electrical energy storage, it can be expressed as:

$$E^{e,sto}_{ES,d,hr} = E^{e,sto}_{ES,d,hr-1}(1 - \varphi_{ES}(D_t)) + (E^{e,in}_{ES,d,hr} - E^{e,out}_{ES,d,hr})D_t,$$
$$\forall d, hr, \quad (33)$$

where $\varphi_{ES}(D_t)$ is the loss fraction, which takes into account the dissipated energy during the time interval, D_t.

Modeling of thermal storage systems for domestic hot water, and space heating and cooling is similar to that described above.

2.5. Optimization method

With the exergetic objective function formulated in Eq. (11) and the economic one formulated in Eq. (1), the problem has two objective functions to be minimized. To solve this multi-objective optimization problem, a single objective function is formulated as a weighted sum of the total annual cost, C_{TOT}, and the total annual primary exergy input, Ex_{in}, to be minimized:

$$F_{obj} = c\omega C_{TOT} + (1 - \omega)Ex_{in}, \quad (34)$$

where constant c is a scaling factor, chosen such that $c\,C_{TOT}$ and Ex_{in} have the same order of magnitude. The Pareto frontier is found by varying the weight ω in the interval 0–1. The solution that minimizes the total annual cost can be found when $\omega = 1$, whereas the one that minimizes the total annual primary exergy input (i.e., maximizes the overall exergy efficiency) can be found when $\omega = 0$. The problem formulated above is linear, and involves both discrete and continuous variables. Branch-and-cut, which is powerful for mixed-integer linear problems, is therefore used.

3. Numerical testing

The method developed in Section 2 is implemented by using IBM ILOG CPLEX Optimization Studio Version 12.6. A hypothetic cluster of 30 buildings of residential sector located in Turin (Italy) is chosen as the targeted end-user. The optimization is carried out on an hourly basis for a representative day per season to reduce the variables number and the model complexity [2,41,42].

In the following, the input data are described in Section 3.1. The Pareto frontier is presented in Section 3.2. The optimized DESs configurations obtained under the economic and exergetic optimization as well as under two representative trade-off points on the Pareto frontier are compared in Section 3.3. The operation strategies of the energy devices in the optimized DES configurations under the economic and exergetic optimization are presented in Section 3.4.

3.1. Input data

The required input data include energy demand of the building cluster, solar energy availability, prices and exergy factors of primary energy carriers, and technical and economic information of energy devices as presented in the following.

3.1.1. Energy demand of the building cluster

Each building is assumed to have a surface area of 5000 m², and a shape factor S/V of 0.5 m⁻¹. The hourly energy rate demand for electricity, domestic hot water, space heating, and space cooling of the building cluster for four representative season days are built based on [56–58], as shown in Fig. 2. To compute the annual energy requirements of the building cluster, the year is assumed to include 90 days in the cold season (December – February), 92 days in the cold mid-season (October 15 – November 30, and March 1 – April 15), 91 days in the hot mid-season (April 15 – May 31, and September 1 – October 15), and 92 days in the hot season (June – August). This assumption is based on the climatic characteristics of the zone, and on the period established by the current Italian law when it is possible to turn on the heating systems in the relative climatic zone (from mid-October to mid-April). Table 1 shows the annual energy requirements of the building cluster.

3.1.2. Solar energy availability

Information about solar energy is taken from the meteorological data in Turin [59]. The hourly solar irradiance on a 35° tilted surface for each representative season day is evaluated as the average of the hourly mean values of the solar irradiance in the corresponding hour of all days in the relative season. The average hourly solar irradiance profiles for the four representative season days are shown in Fig. 3. The maximum available area for installation of solar collector and PV arrays is assumed as 5000 m².

3.1.3. Prices and exergy factors of primary energy carriers

Energy prices are chosen according to the Italian market. The unit price of grid power is assumed as 0.15 €/kW h, whereas the unit prices of natural gas and biomass (wood pellet) are assumed as 0.477 €/N m³, and 120 €/ton, respectively. The exergy efficiency of power generation plants is assumed as 0.40, based on the fossil

Table 1
Annual energy requirements of the building cluster (MW h).

Season	Electricity	Domestic hot water	Space heating	Space cooling
Cold	1114	544.3	6227	0
Cold-mid	1139	556.4	3378	0
Hot-mid	1126	550.3	0	0
Hot	1139	556.4	0	3235

fuel energy mix for electricity production and on the average efficiency of fossil fuel-fired electricity production in Italy [60,61]. The exergy factors of natural gas and biomass are assumed as 1.04 and 1.16 [50], respectively. In the evaluation of the Carnot factor for the solar exergy input rate (Eq. (14)), the temperature of the heat transfer fluid at the exit of the collector field is assumed constant and equal to 353.15 K.

3.1.4. Technical and economic information of energy devices

The technical and economic information of energy devices are summarized in Table 2, and they are based on a detailed market analysis [36–38,44,62–69]. For each energy device, Table 2 shows: the minimum and maximum sizes, specific capital costs, O&M costs, efficiencies and lifetime. For CHPs, specific capital costs, O&M costs as well as electrical and thermal efficiencies strongly vary with the sizes. For CHPs with gas-fired internal combustion engine and with micro-turbines, the entire size ranges available in the market are divided into several small ranges, respectively, while the characteristics assumed in each size range are shown in Fig. 4a and b [62,64,68]. Similarly, the capital cost of single-stage absorption chillers is also subject to economies of scale, and the specific capital cost assumed in each size range is shown in Fig. 5 [64,68]. Conversely, O&M costs and efficiencies are assumed constant and equal to the average values in the size range, due to the slight variation of these characteristics with sizes. For
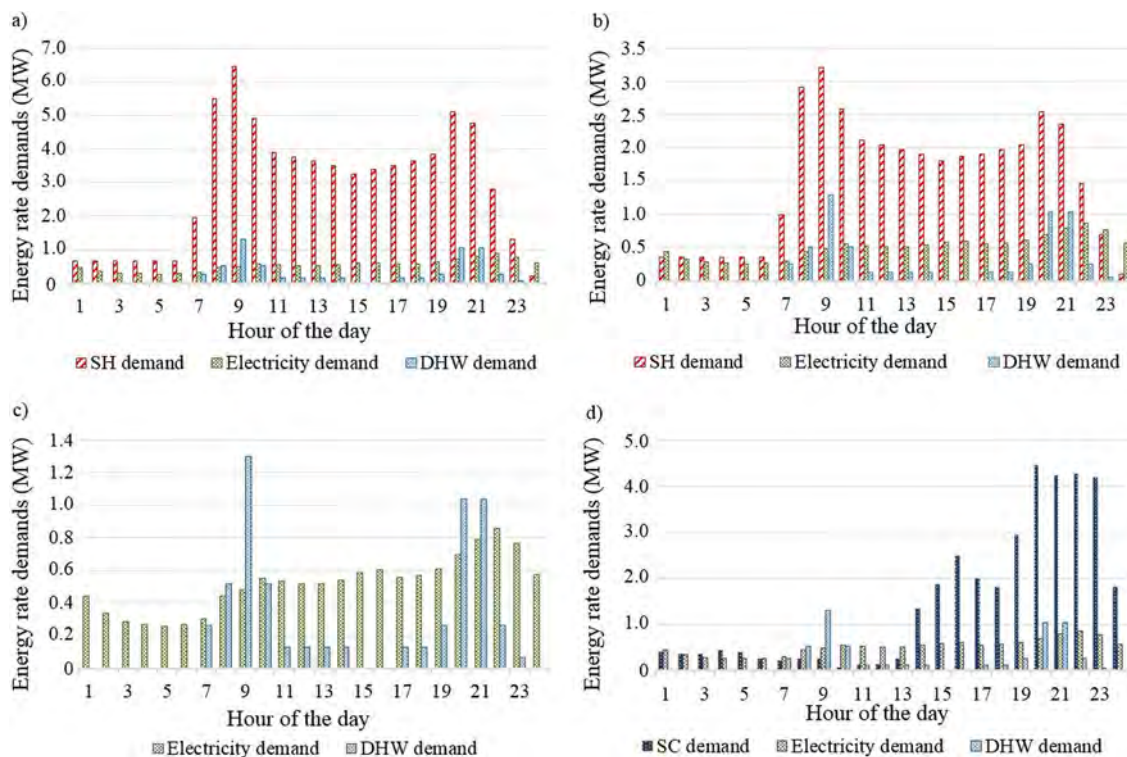
Fig. 2. Hourly mean energy rate demand of the hypothetic building cluster: (a) a representative cold season day; (b) a representative cold mid-season day; (c) a representative hot mid-season day; and (d) a representative hot season day.
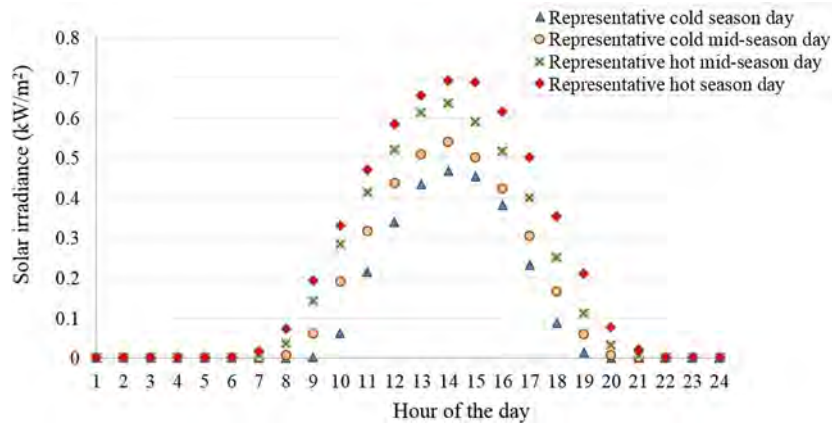
Fig. 3. Average hourly solar irradiance profiles for the four representative season days.

Table 2
Technical and economic information of energy devices.

Energy device	Size range (kW)	Specific capital cost	O&M costs (€/kW h)	Efficiency		Lifetime
				Electrical	Thermal	
CHP NG ICE	20–5000	840–1495 €/kW	0.008–0.023	0.28–0.41	0.40–0.68	20
CHP NG MTG	30–300	1630–2492 €/kW	0.011–0.019	0.26–0.32	0.44–0.52	20
NG boiler	10–2000	100 €/kW	0.0014		0.9	15
Biomass boiler	10–2000	400 €/kW	0.0027		0.85	15
Solar PV	–	2000 €/kW$_p$	0.010		0.14	30
Solar thermal	–	200 €/m^2	0.0057		0.6	15
Air-source heat pump	10–5000	460 €/kW	0.0025		COP^{SH} = 3.5 COP^{SC} = 3.0	20
Absorption chiller	10–5000	230–510 €/kW	0.0020		COP = 0.8	20
Electrical storage	–	350 €/kW h	0.005	φ_{ES} = 0.25		5
Thermal storage	–	20 €/kW h	0.0012		φ_{TES} = 0.05	20
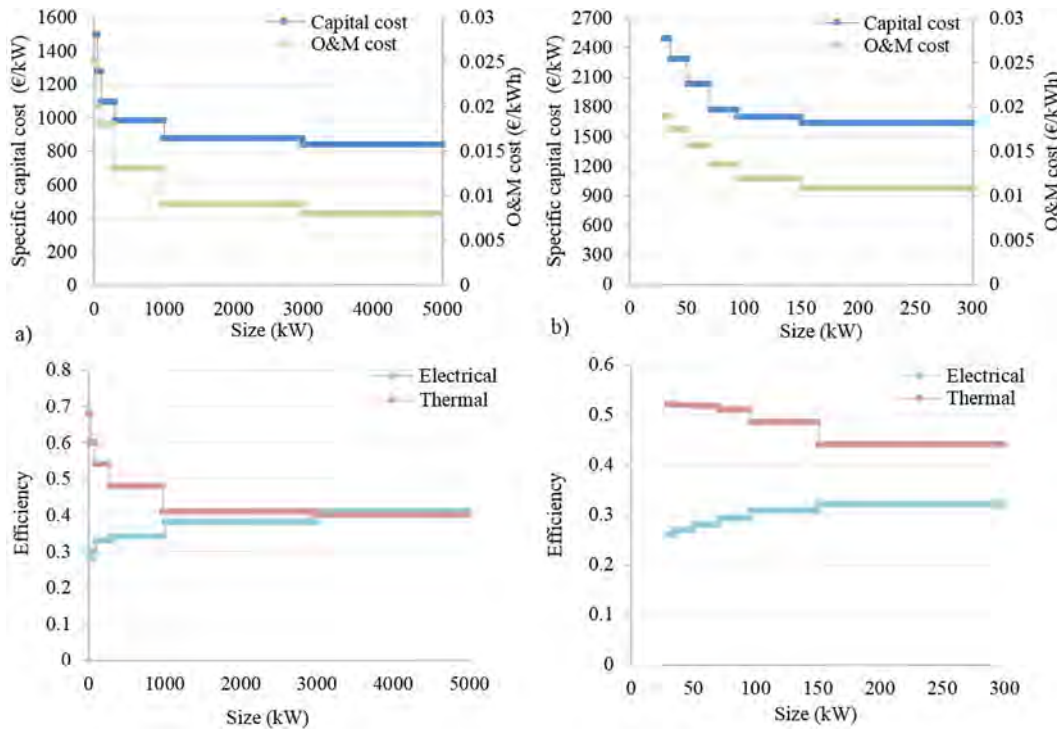
Fig. 4. Specific capitals costs and efficiencies vs. sizes of: (a) CHP with gas-fired internal combustion engine and (b) CHP with gas-fired micro-turbines.
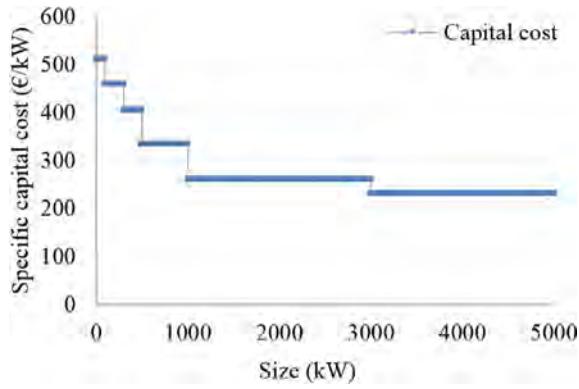
Fig. 5. Specific capital cost vs. size of single-stage absorption chillers.
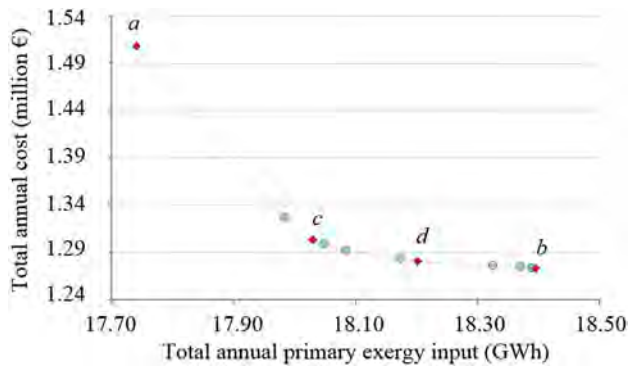
Fig. 6. Pareto frontier.

boilers and air-source heat pumps, the specific capital costs, O&M costs and efficiencies are assumed constant and equal to the average value in the size range considered, due to the slight variation of these characteristics with sizes [63,65–68]. Lead-acid batteries are

assumed as electrical storage devices [38]. Moreover, the maximum number of energy devices associated to each technology is assumed as two. To evaluate the total annualized investment cost, the interest rate is assumed as 5%.

3.2. Pareto frontier

For the numerical testing, there are 50,552 constraints; 19,065 binary decision variables; 4,139 other decision variables; and 121,736 non-zero coefficients. The optimization problem can be solved within few hours with a mixed integer gap lower than 0.15% with a PC with 2.60 GHz (2 multi-core processors) Intel(R) Xeon(R) E5 CPU and 32G RAM. The Pareto frontier is shown in Fig. 6. The point marked with *a* is obtained under the exergetic optimization ($\omega = 0$), where the total annual cost is 1.508 MEuro and the total annual primary exergy input is 17.740 GW h. The point marked with *b* is obtained under the economic optimization ($\omega = 1$), where the total annual cost is 1.273 MEuro and the total annual primary exergy input is 18.394 GW h. The points between these two extreme points are found by subdividing the weight interval into 10 equally-spaced points. Each point on the Pareto frontier corresponds to a different optimized configuration of the DES, thereby providing different design options for planners based on short- and long-run priorities.

3.3. Optimized DES configurations

The optimized configurations of the DESs (numbers, sizes and total installed capacities of energy devices), and the economic and exergetic performances for points *a* and *b* on the Pareto frontier are shown in Table 3. For the illustration purpose, the points marked with *c* and *d* in Fig. 6 are chosen to show the optimized configuration of the DES under a higher weight of 0.8 for the exergetic objective ($\omega = 0.2$), and a higher weight of 0.6 for the economic objective ($\omega = 0.6$), respectively.

Under the exergetic optimization, the total capacity of CHPs with gas-fired internal combustion engine is the largest among

Table 3
Optimized solutions at points *a*, *b*, *c* and *d* on the Pareto Frontier.

Optimized solutions		Point *a*	Point *c*	Point *d*	Point *b*
CHP NG ICE	Number	2	2	2	2
	Sizes (MW$_{el}$)	1.122–1.981	0.372–1.190	0.30–1.095	0.30–1.0
	Total (MW$_{el}$)	3.103	1.562	1.395	1.30
CHP NG MTG	Number	2	0	0	0
	Sizes (MW$_{el}$)	0.095–0.270	–	–	–
	Total (MW$_{el}$)	0.365	–	–	–
NG boiler	Number	0	0	1	2
	Sizes (MW$_{th}$)	–	–	0.538	0.261–0.696
	Total (MW$_{th}$)	–	–	0.538	0.957
Biomass boiler	Number	0	0	0	0
	Sizes (MW$_{th}$)	–	–	–	–
	Total (MW$_{th}$)	–	–	–	–
Solar PV	Size (MW$_{el}$)	0.446	0.452	0.485	0.485
	Area (m^2)	4593	4746	5000	5000
Solar thermal	Size (MW$_{th}$)	0.169	0.106	–	–
	Area (m^2)	407	254	–	–
Air-source heat pump	Number	2	2	2	2
	Sizes (MW$_{th}$)	2.120–3.0	0.721–3.0	0.268–2.925	0.269–2.595
	Total (MW$_{th}$)	5.120	3.721	3.193	2.864
Absorption chiller	Number	2	1	1	1
	Sizes (MW$_{th}$)	0.50–0.968	1.265	1.0	1.0
	Total (MW$_{th}$)	1.468	1.265	1.0	1.0
Electrical storage	Total capacity (MW h$_{el}$)	0	0	0	0
DHW storage	Total capacity (MW h$_{th}$)	1.062	1.670	1.906	2.093
SH storage	Total capacity (MW h$_{th}$)	1.60	1.315	1.585	1.425
SC storage	Total capacity (MW h$_{th}$)	0.182	0.485	1.233	1.976
Total annual cost (million €)		1.508	1.303	1.280	1.273
Total annual primary exergy input (GW h)		17.740	18.030	18.326	18.394

the four configurations, and similarly for CHPs with gas-fired micro-turbine. This highlights the importance of CHPs for the exergetic objective, due to the possibility of waste heat recovery for thermal purposes, thereby promoting efficient use of the energy resource through a better exploitation of its potential. The large-size CHPs with gas-fired internal combustion engine are selected to satisfy the high electricity loads, whereas the small-size CHPs with micro-turbine are selected to satisfy the low electricity loads. As ω increases, only CHPs with internal combustion engines are selected instead of CHPs with micro-turbines, due to their higher total energy efficiency and lower investment and O&M costs. The chosen CHPs are one small and one large in order to cover most of the electricity load until their minimum part loads. However, the total capacity of CHPs with internal combustion engines reduces, reaching the minimum under the economic optimization, mostly due to the high investment cost. Conversely, the total capacity of natural gas boilers reaches the maximum under the economic optimization, due to the low investment and O&M costs, whereas they are not selected under the exergetic optimization and under a higher weight of the exergetic objective (at point *c*). This result clearly indicates that natural gas, as a high-quality energy resource, should not be used for low-quality thermal demand.

Biomass boilers are not selected in any configuration. The absence of biomass boilers under the exergetic optimization clearly shows that exergy analysis is a powerful tool for designing more sustainable energy supply systems, showing that biomass as a high-quality renewable energy resource, should not be used for low quality thermal demand. Biomass could be used instead for meeting high exergy demand such as for electricity generation, with a better exploitation of the potential of the fuel. In DES design optimization, minimization of not only fossil but also renewable exergy input promotes efficient use of all energy resources, while highlighting that even renewable energy sources need to be used efficiently based on their potential. This result agrees with those presented in [34], where in the operation optimization of a DES, biomass boilers were not used under the exergetic optimization, but they were used under the energy cost minimization due to the low price of biomass. Moreover, this result also agrees with those presented in [16], where different energy systems (i.e., gas-fired boiler, biomass boiler, ground-source heat pump, and waste district heat) were compared through exergy analysis to meet thermal demand in buildings. It was shown that exergy input of the biomass boilers is the largest among the four options, since biomass, although renewable, is a high-quality energy resource, thereby resulting to be not convenient to meet low-quality thermal demand. As for DES design optimization, also under the economic optimization, biomass boilers are not selected due to the high investment cost.

As for solar energy systems, the entire available area is occupied in all the optimized configurations. Under the economic optimization, the entire area is occupied by PV arrays, highlighting the convenience of this technology for the economic objective, especially thanks to the current low costs. The size of PV arrays decreases as ω decreases, reaching the minimum under the exergetic optimization, since the available area is also occupied by solar thermal collectors, whose area is equal to 0 under the economic optimization, and reaches the maximum under the exergetic optimization. This result highlights the convenience of solar thermal for the exergetic purpose, due to the low exergy related to the thermal energy output from the collectors, used to meet the low-quality thermal demand.

The total capacities of air-source heat pumps and absorption chillers increase as ω decreases, reaching the maximum under the exergetic optimization, highlighting their convenience for the exergetic purpose, due to the high conversion efficiency and the

possibility of waste heat recovery for space cooling demand, respectively. When ω increases, their total capacities reduce, thereby reducing the total annual cost. Electrical storage (i.e., lead–acid battery) is never selected. The high investment cost makes this technology not competitive. Therefore, it is not selected under the economic optimization. Under the exergetic optimization, electrical storage is not selected mostly due to the high storage loss fraction. As for thermal storage for space cooling demand, the capacity strongly increases as the weight for the economic objective increases, reaching the maximum under the economic optimization. This result clearly shows the economic convenience of the thermal storage for the space cooling demand, whose capacity is strongly related to the sizing of absorption chillers. With larger storage capacity, smaller size of absorption chillers are needed, and the total investment cost reduces.

The capacity of thermal storage for domestic hot water demand is maximum under the economic optimization. The capacity of thermal storage for space heating demand slightly changes with the weight and is maximum under the exergetic optimization. Differently from the thermal storage for space cooling, whose capacity is strongly related to the sizing of absorption chillers, the capacities of thermal storage for domestic hot water and space heating demand mostly depend on the amount of exhaust gas recovered by CHPs, and therefore depend on the operation strategies of multiple energy devices to be discussed later.

The total annual cost and primary exergy input are also investigated for a conventional energy supply system, where grid power is used for the electricity demand, gas-fired boilers for domestic hot water and space heating demand, and electric chillers fed by grid power for space cooling demand. The total annual cost is equal to 1.914 MEuro, and the total annual primary exergy input is equal to 27.641 GW h. Fig. 7 shows the reduction in total annual cost and primary exergy input of the DES configurations at points *a*, *b*, *c* and *d* on the Pareto frontier, as compared with the conventional energy supply system. The maximum reduction in total annual cost, equal to 33.5%, is attained under the economic optimization, whereas the reduction in the total annual primary exergy input is the minimum one, equal to 33.5%. Conversely, the maximum reduction in total annual primary exergy input, equal to 35.8%, is attained under the exergetic optimization, whereas the reduction in total annual cost is the minimum one, equal to 21.2%. Therefore, in all the optimized DES configurations, strong reduction in total annual cost and primary exergy input is attained as compared with the conventional energy supply system.
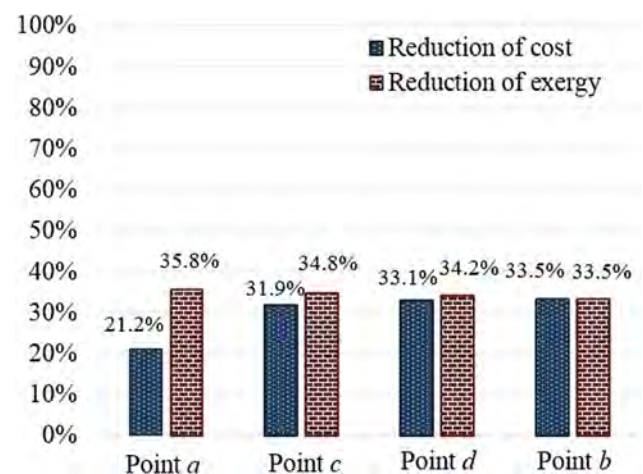
Fig. 7. Reduction in total annual cost and primary exergy input of the optimized DES configurations at points *a*, *b*, *c* and *d* on the Pareto frontier, as compared with the conventional energy supply system.

3.4. Operation strategies of energy devices in the optimized DES configurations under economic and exergetic optimization

For different optimized DES configurations, different operation strategies of energy devices are found. For the illustration purpose, the operation strategies of the energy devices in the optimized DES configurations obtained under the exergetic and economic optimization in the four representative season days are compared in Fig. 8.

Fig. 8a for electricity, shows the total grid power, and the total electricity provided by CHPs and PV to meet the load as the sum of the total demand and the total electricity required by air-source heat pumps in the four representative season days. Under both exergetic and economic optimization, electricity from power grid is generally lower than the electricity provided by CHPs, highlighting that CHP is convenient for both objectives. Moreover, CHPs with micro-turbines are used only under the exergetic optimization, since they are not selected under the economic optimization as presented in the previous subsection, and the electricity provided is smaller than that provided by CHPs with internal combustion engines, coherently with the larger size of the latter CHPs. In the hot mid-season day, the total electricity provided by CHPs is lower than in the other days under both the exergetic and economic optimization, since only electricity and domestic hot water demand need to be satisfied in this day. In this day, under the exergetic optimization, the electricity from power grid is larger than in

the other days, and it is also larger than the total electricity provided by CHPs, due to the contribution of solar thermal to meet the domestic hot water demand, as shown in Fig. 8b. It can be also noted that the electricity provided by PV is slightly larger under the economic optimization than under the exergetic one, coherently with the larger size of PV attained under the economic optimization as discussed in the previous subsection.

Fig. 8b for domestic hot water demand shows the total thermal energy provided by CHPs, gas-fired boilers, solar thermal collectors, as well as the total thermal energy input and output to/from the storage to meet the total demand in the four representative season days. Under the economic optimization, the thermal energy from exhaust gas is larger than under the exergetic one. This is due to the fact that, in absence of solar thermal, a larger amount of exhaust gas is used to meet the demand as compared to the exergetic optimization. Natural gas boilers are only used under the economic optimization, since they are not selected under the exergetic optimization as presented in the previous subsection. As for thermal storage, it is generally more used under the economic optimization than under the exergetic one, due to the larger amount of exhaust gas, which also explains the larger capacity required under the economic optimization.

Fig. 8c for space heating and cooling demand shows the total thermal energy provided by CHPs, gas-fired boilers, air-source heat pumps, absorption chillers as well as the total thermal energy input and output to/from the storage systems to meet the total
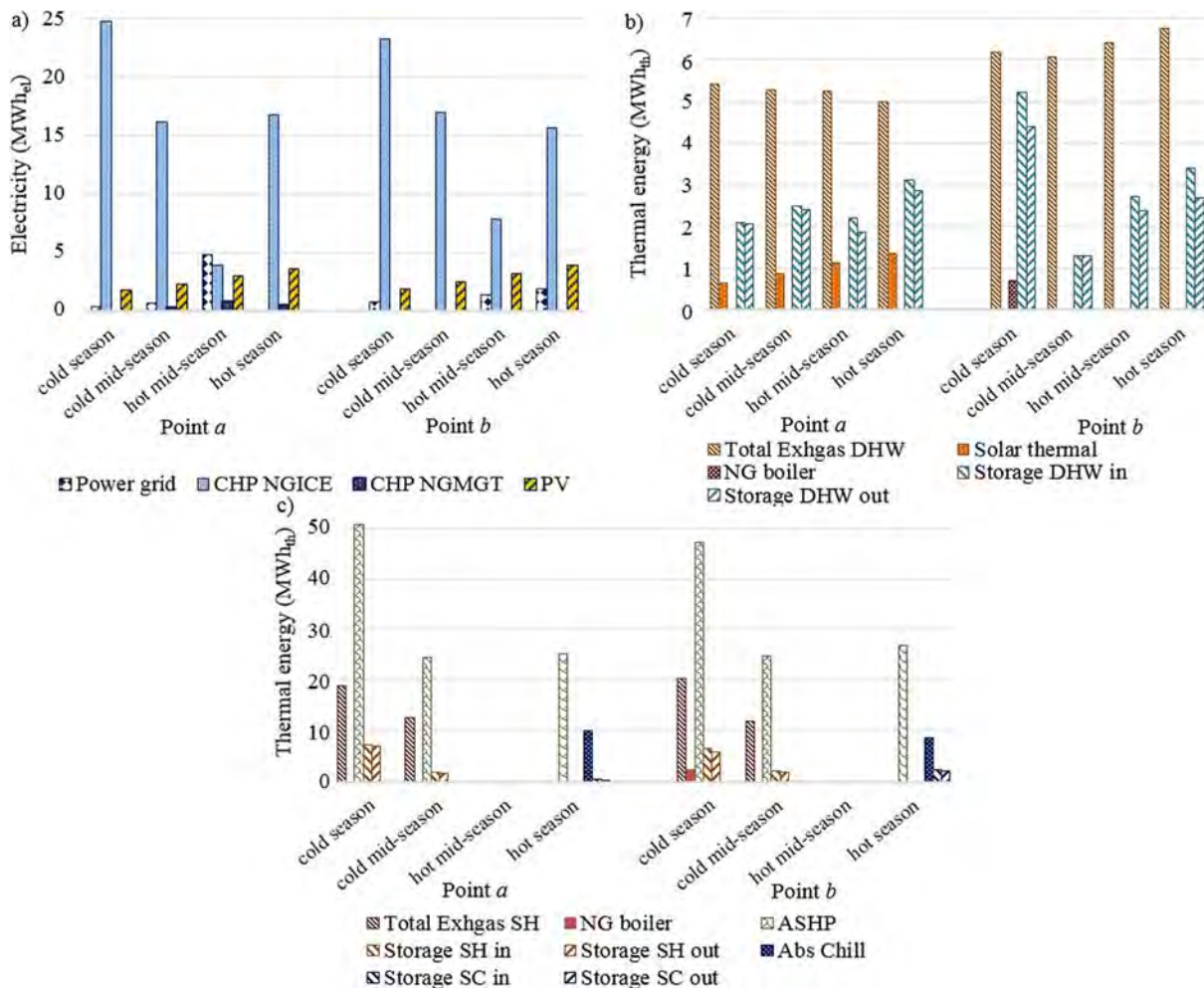
Fig. 8. Operation strategies of optimized DES configurations at points a and b in the four season days for (a) electricity; (b) domestic hot water; and (c) space heating and cooling.

demands in the four representative season days. For space heating, heat pumps are mostly used to meet the demand under both exergetic and economic optimization, highlighting that this technology is convenient for both the objectives. Heat pumps are generally more used under the exergetic optimization than under the economic one. Similarly to the case of domestic hot water demand, natural gas boilers are only used under the economic optimization. As for thermal storage, the slightly larger capacity required under the exergetic optimization than under the economic one is due to the fact that with a larger usage of heat pumps to meet the demand, a larger amount of exhaust gas is dispatched to charge the storage, as compared with what occurs under the economic optimization. For space cooling demand, similar to space heating demand, heat pumps are mostly used to meet the demand under both exergetic and economic optimization. The thermal energy provided by the absorption chillers is larger under the exergetic optimization than under the economic one, coherently with the larger size attained under the exergetic optimization as presented in the previous subsection. As for thermal storage, it is much more used under the economic optimization than under the exergetic one, in accordance to the larger capacity required under the economic optimization.

4. Sensitivity analysis

A sensitivity analysis is carried out to investigate the influence of key parameters such as energy prices and energy demand scale on the optimized DES configurations and the related economic and exergetic performances. In the following, the results of the sensitivity analysis on energy prices and energy demand scale are presented and discussed in s 4.1 and 4.2, respectively.

4.1. Energy price sensitivity

The operation strategies of energy devices strongly depend on energy prices, which in turn affect their combination and sizes in the DES configurations attained by the optimization model. With the increasing consumption of energy resources, energy prices are expected to increase in next years. In the multi-objective optimization problem, the effect of the energy price increase is maximum under the economic optimization, while no effects are under the exergetic optimization. Results of the economic optimization carried out by considering the increase of electricity and natural gas price are presented and discussed in the following. As for biomass, the effect of the price increase is not investigated, since even with the current price, biomass boilers are not selected under the economic optimization.

4.1.1. Electricity price sensitivity under the economic optimization

The results obtained for electricity price increases of 25% until 100% of the current value are compared in Fig. 9. Fig. 9a shows the increase in the total annual cost and primary exergy input as compared with those obtained with the current electricity price. It can be noted that the economic performance are more affected by the electricity price increase than the exergetic ones. However, the effect of electricity price increase on the economic performance is not that significant: when the electricity price is twice of the current one, the increase in the total annual cost is less than 2%. This is due to the fact that, even with the current electricity price, electricity from the power grid is much less than that provided by CHPs as discussed in the previous section.

For the illustration purpose, the total installed capacities of energy devices in the optimized DES configurations obtained with 50% and 100% electricity price increase and those obtained with the current electricity price are compared in Fig. 9b. As the electric-ity price increases, the total installed capacity of CHP with gas-fired internal combustion engine increases, since CHPs become more convenient. Similar to the current electricity price, also with higher electricity prices, CHPs with gas-fired micro-turbine are not chosen, due to the high investment costs. When electricity price increases, the size of PV systems reduces, due to the larger capacity of CHPs used to meet the electricity load. Solar thermal is not selected as occurs with the current electricity price. The total capacity of air-source heat pumps and gas-fired boilers remains almost unchanged. However, the total capacity of heat pumps reaches the maximum when the electricity price is twice of the current one due to their high conversion efficiencies, whereas the contrary occurs for gas-fired boilers. With larger usage of heat pumps, boilers are less used to meet the space heating demand. Biomass boilers are not selected due to the high investment costs. As for absorption chillers, the total capacity reaches the maximum when the electricity price is twice of the current one, mainly due to the larger usage of CHPs and consequent larger amount of exhaust gas used for the space cooling demand. This latter also explains the significant increase of the capacity of storage for the space cooling demand occurring when the electricity price increases.

The effect of electricity price increase on the exergetic performances is negligible. However, the small increase in the total annual primary exergy input occurring for higher electricity prices is due to the reduction in the usage of PV systems and the consequent larger usage of natural gas in CHPs to meet the electricity load. This result highlights the importance of PV systems for the exergetic purpose, since the usage of electricity from PV systems to meet high-quality electricity demand results to be better than burning natural gas.

4.1.2. Natural gas price sensitivity under the economic optimization

For natural gas price increases of 25% until 100% of the current value, the results are compared in Fig. 10. Fig. 10a shows the increase in the total annual cost and primary exergy input as compared with those obtained with the current natural gas price. It can be noted that the natural gas price increase has larger effects on both the economic and exergetic performances than electricity price increase: when the natural gas price is twice of the current one, the increase in the total annual cost and primary exergy input are equal to 22.6% and 33.5%, respectively. With the current price, natural gas is the most used primary energy carrier, since it is used to feed both CHPs and gas-fired boilers, which are much used under the economic optimization, as discussed in the previous section. Therefore, the effect of natural gas increase on the economic and exergetic performances becomes significant.

The total installed capacities of energy devices in the optimized DES configurations obtained with 50% and 100% natural gas price increase and those obtained with the current natural gas price are compared in Fig. 10b. As the natural gas price increases, the total installed capacity of CHP with gas-fired internal combustion engine dramatically reduces, reaching the minimum when the gas price is twice of the current one, whereas CHPs with gas-fired micro-turbine are not selected as occurs with the current natural gas price. The total installed capacity of gas-fired boilers reduces as the gas price increases, even though the reduction of the total capacity is not such significant as that of CHPs. This is because when natural gas price increases, grid power becomes much more convenient than CHPs to meet the electricity load, due to the high investment costs. The increase of natural gas price has a lower impact on the installed capacity of gas-fired boilers. Although the gas price increase, gas-fired boilers have low investment costs, and they are still convenient for the economic objective. When natural gas price increases, biomass boilers become more convenient than gas-fired boilers, and they are selected in the optimized DESs configurations, although their investment
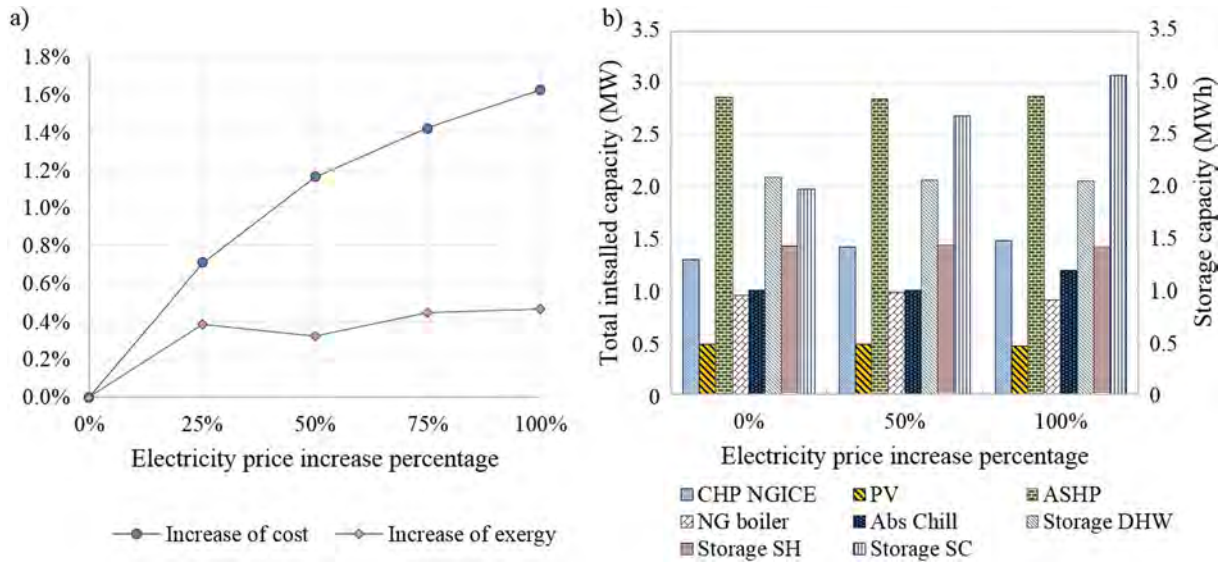
Fig. 9. (a) Economic and exergetic performance of optimized DES configurations under the economic optimization for electricity price increases of 25% until 100% of the current value. (b) Total installed capacity of energy devices for various electricity price increases.
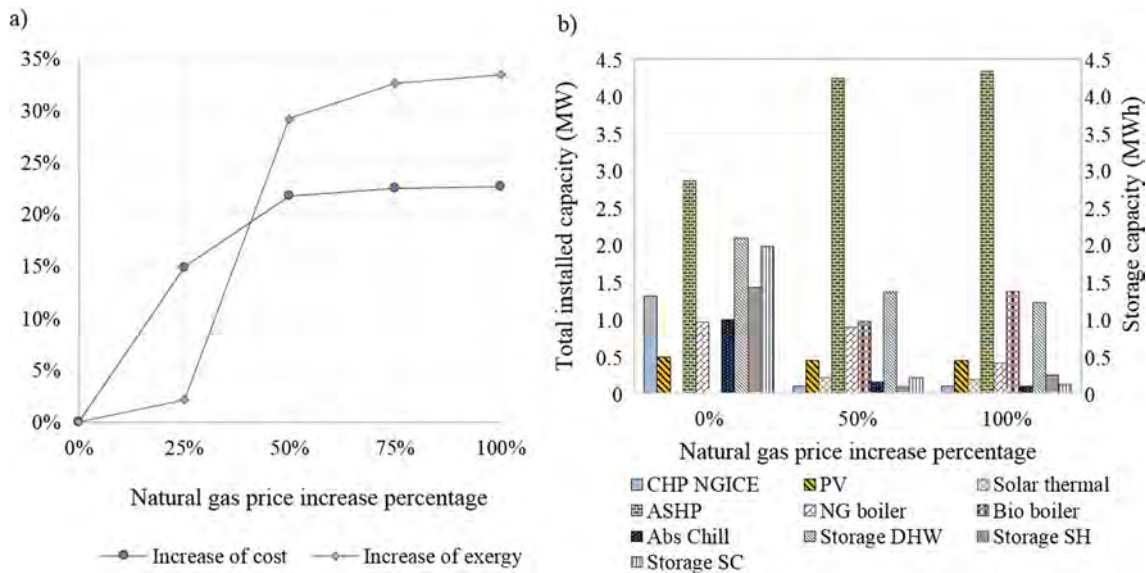
Fig. 10. (a) Economic and exergetic performance of optimized DES configurations under the economic optimization for natural gas price increases of 25% until 100% of the current value. (b) Total installed capacity of energy devices for various natural gas price increases.

costs are higher. For higher natural gas prices, the size of PV systems reduces, since the available area for installation of solar systems is also occupied by solar thermal collectors used to meet the demand of domestic hot water. As for air-source heat pumps, their installed capacity significantly increases when natural gas price increases, due to the strong reduction of exhaust gas from CHPs to meet the demand of space heating and cooling. This latter also explains the significant reduction of the total installed capacity of absorption chillers and of the required capacity of the storage for space cooling demand. The reduction of exhaust gas from CHPs under higher natural gas prices also explains the reduced required capacities of storage for domestic hot water and space heating demands. Similar to the current natural gas price, electrical storage is not selected due to the high investment costs.

The strong reduction in the usage of CHPs is one of the most important factors influencing the strong increase in the total annual primary exergy input occurring for natural gas price

increases higher than 25% of the current value. This result underlines the importance of waste heat recovery from CHPs for the exergetic perspective, since, in absence of exhaust gas, other combustion-based energy devices are used to meet the thermal demand, thereby increasing the waste of high-quality energy. Another important factor influencing the increase in the total annual primary exergy is the usage of biomass boilers used to meet the thermal demand. As discussed earlier, biomass is a high-quality renewable energy resource, and it should not be used to meet low-quality thermal demand.

4.2. Energy demand scale sensitivity

The types, number and sizes of energy devices in the DES configurations strongly depend on energy demand, which is one of the uncertainty factors at the demand side. In the multi-objective optimization problem, the effect of energy demand variation is

observable at all the points of the Pareto frontier. For the illustration purpose, the effect of energy demand variation (both electricity and thermal) is investigated under the economic and exergetic optimization in the following.

4.2.1. Energy demand scale sensitivity under the economic optimization

The results obtained under the economic optimization for energy demand decrease and increase of 25% until 50% of the current one, respectively, are compared in Fig. 11. According to Fig. 11a, both the total annual cost and primary exergy input vary almost linearly with the energy demand variation. For energy demand increase of 50% of the current one, the increase in total annual cost and primary exergy input reaches the maximum, equal to 50.0% and 53.5%, respectively. For energy demand decrease of 50% of the current value, the reduction in total annual cost and primary exergy input reaches the maximum, equal to 48.8% and 50.4%, respectively.

For the illustration purpose, the total installed capacities of energy devices in the optimized DES configurations obtained with 50% energy demand decrease and 50% energy demand increase are compared with those obtained with the current energy demand in Fig. 11b. As the energy demand increases, the total installed capacities of most of the energy devices increase. The size of PV systems remains unchanged, occupying the entire available area. CHPs with gas-fired micro-turbine are not selected in the optimized DES configurations, as occurs with the current energy demand. As for thermal storage, the total capacities increase as the energy demand increases, due to the larger amount of exhaust gas from CHPs dispatched to the storage devices. Similar to the current energy demand, the electrical storage is not selected due to the high investment costs. The increase in the total annual primary exergy input is mostly due to the larger usage of grid power to meet the electricity load, and the larger usage of gas-fired boilers to meet the thermal demand.

As the energy demand decreases, the total installed capacities of most of the energy devices decrease. Differently to the case of energy demand increase, the size of PV systems also decreases, and solar thermal is selected for the demand of domestic hot water. The area occupied by solar energy systems is equal to 3464 m^2, lower than the available one. As for thermal storage,

the total capacities reduce as the energy demand reduces, due to the lower amount of exhaust gas from CHPs dispatched to the storage devices. The decrease in the total annual primary exergy input is mostly due to the lower usage of grid power to meet the electricity load, and the lower usage of gas-fired boilers to meet the thermal demand.

Under the economic optimization, CHPs with gas-fired internal combustion engine, gas-fired boilers and air-source heat pumps are the energy devices which are most influenced by the energy demand variation. When the energy demand is 50% higher than the current one, the total capacities of CHPs, boilers and heat pumps increase by 53.8%, 69.4%, and 55.9%, as compared to those obtained with the current energy demand, respectively. Conversely, when the energy demand is 50% lower than the current one, their total capacities decrease by 53.8%, 58.9%, and 54.7%, respectively. The variation of energy demand has also noticeable effects on the capacities of storage for domestic hot water and space cooling demand. When the energy demand is 50% higher than the current one, the capacities of storage for domestic hot water and space cooling increase by 56.7% and 86.7%, respectively, whereas for energy demand decrease of 50% than the current one, they reduce by 65.4% and 19.3%, respectively.

4.2.2. Energy demand scale sensitivity under the exergetic optimization

The results obtained under the exergetic optimization for energy demand decrease and increase of 25% until 50% of the current one, respectively, are compared in Fig. 12. Fig. 12a shows the reduction/increase in the total annual cost and primary exergy input as compared with those obtained with the current energy demand. Similar to what occurs under the economic optimization, both the total annual cost and primary exergy input vary almost linearly with the energy demand variation. For energy demand increase of 50% of the current one, the increase in total annual cost and primary exergy input reaches the maximum, equal to 42.5% and 51.2%, respectively. For energy demand decrease of 50% of the current value, the reduction in total annual cost and primary exergy input reaches the maximum, equal to 43.0% and 51.7%, respectively.

The total installed capacities of energy devices in the optimized DES configurations obtained with 50% energy demand decrease
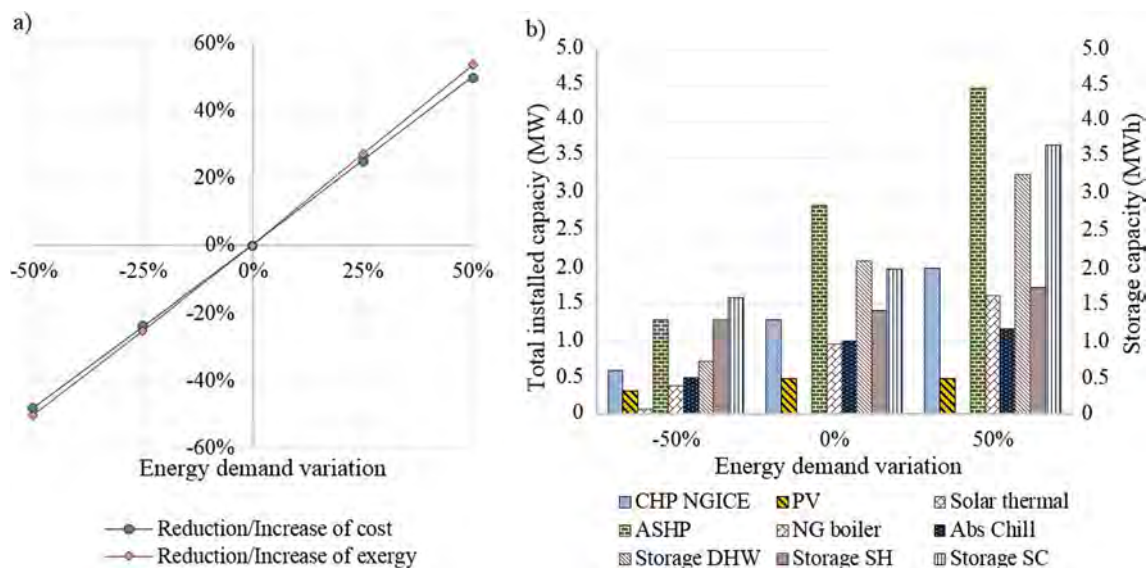
Fig. 11. (a) Economic and exergetic performance of optimized DES configurations under the economic optimization for energy demand decrease and increase of 25% until 50% of the current one, respectively. (b) Total installed capacity of energy devices for various energy demand decreases/increases.
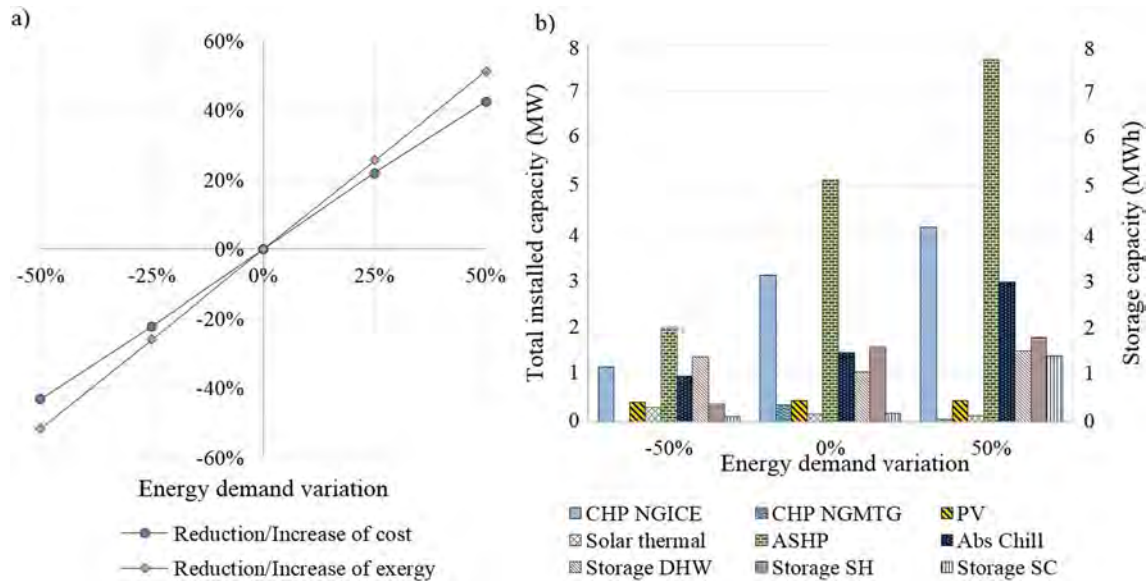
Fig. 12. (a) Economic and exergetic performance of optimized DES configurations under the exergetic optimization for energy demand decrease and increase of 25% until 50% of the current one, respectively. (b) Total installed capacity of energy devices for various energy demand decreases/increases.

and 50% energy demand increase are compared with those obtained with the current energy demand in Fig. 12b. As the energy demand increases, the total installed capacities of most of the energy devices increase. The opposite occurs for CHPs with gas-fired micro-turbine. The choice of only one CHP with gas-fired micro-turbine of 53 kW is related to the sizes of CHPs with gas-fired internal combustion engines, which are equal to 1.152 MW and 2.978 MW, instead of 1.122 MW and 1.981 MW attained with the current energy demand. Although the total capacity increases by 33.1% as compared to that obtained with the current energy demand, the size of the smaller CHP only increases by 2.7%. Therefore, these two CHPs, with the increase of electricity demand and the electricity required by heat pumps, can satisfy most of the total electricity load until their minimum part loads. The size of solar thermal also reduces as the energy demand increases, due the increase of the PV size, which occupy a larger area. As for thermal storage, the total capacities increase as the energy demand increases, due to the larger amount of exhaust gas from CHPs dispatched to the storage devices. The increase in the total annual cost is mostly due to larger investment costs related to the larger sizes of CHPs, air-source heat pumps and absorption chillers.

As the energy demand decreases, the total installed capacities of most of the energy devices decrease. For energy demand decrease of 50% than the current one, CHPs with gas-fired micro-turbine are not selected. This is related to the sizes of CHPs with gas-fired internal combustion engines, which are equal to 0.227 MW and 0.937 MW. The size of the smaller CHP decreases by 79.8% as compared to the smaller one in the current case. Therefore, the two CHPs can satisfy most of the total electricity load until their minimum part loads. Differently from the case of energy demand increase, the size of PV systems decreases, whereas the size of solar thermal increases. However, in all the optimized DES configurations, the entire available area for solar energy systems is occupied. As the energy demand decreases, the total capacities of storage for space heating and cooling reduce, due to the lower amount of exhaust gas from CHPs dispatched to the storage devices. As for thermal storage for domestic hot water, the total capacity increases, due to the larger amount of thermal energy from solar thermal dispatched to the storage. The reduction in the total

annual cost is mostly due to lower investment costs related to the lower sizes of CHPs, air-source heat pumps and absorption chillers.

Under the exergetic optimization, CHPs with gas-fired internal combustion engine and with micro-turbine, air-source heat pumps, and absorption chillers are the energy devices which are most influenced by the energy demand variation. When the energy demand is 50% higher than the current one, the total capacities of CHPs with gas-fired internal combustion engine, heat pumps, and absorption chillers increase by 33.1%, 50.0%, and 100.0%, as compared to the those attained with the current energy demand, respectively. The total capacity of CHPs with micro-turbine reduces by 85.5%. Conversely, when the energy demand is 50% lower than the current one, their total capacities decrease by 62.5%, 60.7%, and 34.3%, respectively, and CHPs with micro-turbine are not selected. The variation of energy demand has also noticeable effects on the size of solar thermal, which reduces by 21.6% for energy demand increase of 50%, and increases by 82.1% for energy demand decrease of 50%. Remarkable effects of energy demand variation can be also noted on the capacities of storage for space heating and cooling demand.

5. Conclusions

In this paper, exergy is investigated in design optimization of distributed energy systems (DESs) for sustainable development of energy supply systems through multi-objective approach for not neglecting the crucial economic factor. Based on a pre-established DES superstructure with multiple energy devices such as combined heat and power and PV, a multi-objective linear programming problem is formulated to determine types, numbers and sizes of energy devices in the DES with the corresponding operation strategies in order to reduce the total annual cost and increase the overall exergy efficiency. In modeling of energy devices, the entire size ranges available in the market as well as the variations of efficiencies, specific capital and operation and maintenance costs with sizes are taken into account. The Pareto frontier is found by minimizing a weighted sum of the total annual cost and primary exergy input. The problem is solved by branch-and-cut. The

models and methods provided can be applied in real contexts. Given the needed input data, the model allows to obtain the optimized combination of the candidate energy devices and the corresponding operation strategies through cost and exergy assessments, thereby providing decision support to planners.

Numerical results demonstrate that exergy analysis is a powerful tool for designing more sustainable energy supply systems based on the use of renewables and low-temperature sources for thermal demand in buildings, and on a better exploitation of the high potential of fossil fuels. Moreover, the Pareto frontier provides good balancing solutions for planners based on economic and sustainability priorities. It is found that, through proper design optimization, DESs can offer a good investment opportunity when compared with conventional energy supply systems, through rational use of energy resources. The total annual cost and primary exergy input of DESs with optimized configurations are significantly reduced as compared with a conventional energy supply system, where grid power is used for the electricity demand, gas-fired boilers for domestic hot water and space heating demand, and electric chillers fed by grid power for space cooling demand. As compared with the conventional case, the maximum reduction in the total annual cost and primary exergy input are equal to 33.5% and 35.8%, respectively. Also in the other points of the Pareto frontier, a strong reduction in total annual cost and primary exergy input is attained. In addition, a sensitivity analysis is carried out to analyze the influence of key parameters, such as energy prices and energy demand variation on the optimized DES configurations and the related economic and exergetic performances. It is found that natural gas price increase has larger effects than the electricity price increase on the optimized DES configurations and economic and exergetic performances, whereas the effects of energy demand variation are noticeable under both the economic and the exergetic optimization. The results found in this work clearly indicate that, among the candidate energy devices, combined heat and power systems with gas-fired internal combustion engine are the best options for both reduction of cost and primary exergy input, whereas solar energy systems are important for the exergetic purpose.

Although there are no exergy requirements as a methodology or an indicator yet in current energy legislations, results underline that exergy assessments may allow to meet the main goal of energy legislations in improving sustainability of energy supply. Minimization of not only fossil but also renewable exergy input promotes an efficient energy resource use through the reduction of the waste of high-quality energy, by avoiding burning processes and substituting them by low-temperature sources for thermal demand in buildings.

References

[1] Kari A, Arto S. Distributed energy generation and sustainable development. Renew Sustain Energy Rev 2006;10:539–58.
[2] Ren H, Gao W. A MILP model for integrated plan and evaluation of distributed energy systems. Appl Energy 2010;87(3):1001–14.
[3] Akorede MF, Hizam H, Poresmaeil E. Distributed energy resources and benefits to the environment. Renew Sustain Energy Rev 2010;14:724–34.
[4] Pepermans G, Driesen J, Haesoldoncklx D, Belmans R, D'haeseleer W. Distributed generation: definition, benefits and issues. Energy Policy 2005;33:787–98.
[5] Söderman J, Pettersson F. Structural and operational optimisation of distributed energy systems. Appl Therm Eng 2006;26:1400–8.
[6] Bayod-Rujula AA. Future development of the electricity systems with distributed generation. Energy 2009;34(3):377–83.
[7] Huang J, Jiang C, Xu R. A review on distributed energy resources and microgrid. Renew Sustain Energy Rev 2008;12(9):2472–83.
[8] Han J, Ouyang L, Xu Y, Zeng R, Kang S, Zhang G. Current status of distributed energy system in China. Renew Sustain Energy Rev 2016;55:288–97.
[9] Chinese D, Meneghetti A. Optimisation models for decision support in the development of biomass-based industrial district-heating networks in Italy. Appl Energy 2005;82(3):228–54.
[10] Manfren M, Caputo P, Costa G. Paradigm shift in urban energy systems through distributed generation: methods and models. Appl Energy 2011;88(4):1032–48.
[11] Ruan Y, Liu Q, Zhou W, Firestone R, Gao W, Watanabe T. Optimal option of distributed generation technologies for various commercial buildings. Appl Energy 2009;86(9):1641–53.
[12] Ren H, Zhou W, Nakagami KI, Gao W, Wu Q. Multi-objective optimization for the operation of distributed energy systems considering economic and environmental aspects. Appl Energy 2010;87(12):3642–51.
[13] Pohekar SD, Ramachandran M. Application of multi-criteria decision making to sustainable energy planning—a review. Renew Sustain Energy Rev 2004;8(4):365–81.
[14] Wang JJ, Jing YY, Zhang CF, Zhao JH. Review on multi-criteria decision analysis aid in sustainable energy decision-making. Renew Sustain Energy Rev 2009;13(9):2263–78.
[15] Alarcon-Rodriguez A, Ault G, Galloway G. Multi-objective planning of distributed energy resources: a review of the state-of-the-art. Renew Sustain Energy Rev 2010;14:1353–66.
[16] ECBCS – Annex 49 – Low Exergy Systems for High Performance Buildings and Communities, homepage. Available <http://www.ecbcs.org/annexes/annex49.htm>.
[17] Dincer I, Rosen MA. Energy, environment and sustainable development. Appl Energy 1999;64(1):427–40.
[18] Dincer I, Rosen MA. Exergy-energy, environment and sustainable development. 1st ed. Oxford, UK: Elsevier Publication; 2007.
[19] Dincer I, Rosen MA. Exergy: energy, environment and sustainable development. Newnes; 2012.
[20] Wall G, Gong M. On exergy and sustainable development—part 1: conditions and concepts. Exergy Int J 2001;1(3):128–45.
[21] Rosen MA, Dincer I, Kanoglu M. Role of exergy in increasing efficiency and sustainability and reducing environmental impact. Energy Policy 2008;36(1):128–37.
[22] Bilgen E. Exergetic and engineering analyses of gas turbine based cogeneration systems. Energy 2000;25(12):1215–29.
[23] Gonçalves P, Angrisani G, Rosselli C, Gaspar AR, Da Silva MG. Comparative energy and exergy performance assessments of a microcogeneration unit in different electricity mix scenarios. Energy Convers Manage 2013;73:195–206.
[24] Feidt M, Costea M. Energy and exergy analysis and optimization of combined heat and power systems. Comparison of various systems. Energies 2012;5:3701–22.
[25] Barelli L, Bidini G, Gallorini F, Ottaviano A. An energetic–exergetic analysis of a residential CHP system based on PEM fuel cell. Appl Energy 2011;88(12):4334–42.
[26] Hepbasli A. A key review on exergetic analysis and assessment of renewable energy resources for a sustainable future. Renew Sustain Energy Rev 2008;12(3):593–661.
[27] Kalogirou SA, Karellas S, Badescu V, Braimakis K. Exergy analysis on solar thermal systems: a better understanding of their sustainability. Renewable Energy 2016;85:1328–33.
[28] Hepbasli A, Akdemir O. Energy and exergy analysis of a ground source (geothermal) heat pump system. Energy Convers Manage 2004;45(5):737–53.
[29] Tsaros TL, Gaggioli RA, Domanski PA. Exergy analysis of heat pumps. ASHRAE Trans 1987;93(2):1781–93.
[30] Crawford RR. An experimental laboratory investigation of second law analysis of a vapor-compression heat pump. ASHRAE Trans 1988;94(2):1491–504.
[31] Bjurström H, Carlsson B. An exergy analysis of sensible and latent heat storage. J Heat Recov Syst 1985;5(3):233–50.
[32] Dincer I. On thermal energy storage systems and applications in buildings. Energy Build 2002;34(4):377–88.
[33] Koca A, Oztop HF, Koyun T, Varol Y. Energy and exergy analysis of a latent heat storage system with phase change material for a solar collector. Renewable Energy 2008;33(4):567–74.
[34] Di Somma M, Yan B, Bianco N, Luh PB, Graditi G, Mongibello L, et al. Operation optimization of a distributed energy system considering energy costs and exergy efficiency. Energy Convers Manage 2015;103:739–51.
[35] Yan B, Di Somma M, Bianco N, Luh PB, Graditi G, Mongibello L, et al. Exergy-based operation optimization of a distributed energy system through the energy-supply chain. Appl Therm Eng 2016;101:741–51.
[36] Mehleri ED, Sarimveis H, Markatos NC, Papageorgiou LG. A mathematical programming approach for optimal design of distributed energy systems at the neighbourhood level. Energy 2012;44:396–1104.
[37] Mehleri ED, Sarimveis H, Markatos NC, Papageorgiou LG. Optimal design and operation of distributed energy systems: application to Greek residential sector. Renewable Energy 2013;51:331–42.
[38] Hawkes AD, Leach MA. Modelling high level system design and unit commitment for a microgrid. Appl Energy 2009;86(7):253–1265.
[39] Omu A, Choudhary R, Boies A. Distributed energy resource system optimisation using mixed integer linear programming. Energy Policy 2013;61:249–66.
[40] Wouters C, Fraga ES, James AM, Polykarpou EM. Mixed-integer optimisation based approach for design and operation of distributed energy systems. In: Power engineering conference (AUPEC), 2014 Australasian Universities IEEE. p. 1–6.
[41] Zhou Z, Zhang J, Liu P, Li Z, Georgiadis MC, Pistikopoulos EN. A two-stage stochastic programming model for the optimal design of distributed energy systems. Appl Energy 2013;103:135–44.

[42] Zhou Z, Liu P, Li Z, Ni W. An engineering approach to the optimal design of distributed energy systems in China. Appl Therm Eng 2013;53:387–96.

[43] Buoro D, Casisi M, De Nardi A, Pinamonti P, Reini M. Multicriteria optimization of a distributed energy supply system for an industrial area. Energy 2013;58:128–37.

[44] Bracco S, Dentici G, Siri S. Economic and environmental optimization model for the design and the operation of a combined heat and power distributed generation system in an urban area. Energy 2013;55:1014–24.

[45] Maroufmashat A, Sattari S, Roshandel R, Fowler M, Elkamel A. Multi-objective optimization for design and operation of distributed energy systems through the multi-energy hub network approach. Ind Eng Chem Res 2016;55 (33):8950–66.

[46] Ramirez-Elizondo LM, Paap GC, Ammerlaan R, Negenborn RR, Toonssen R. On the energy, exergy and cost optimization of multi-energy-carrier power systems. Int J Exergy 2013;13:364–85.

[47] Krause T, Kienzle F, Art S, Andersson G. Maximizing exergy efficiency in multicarrier energy systems. In: Proceedings of IEEE power and energy society general meeting; Minneapolis, USA; 2010 June 25–29.

[48] Lu H, Alanne K, Martinac I. Energy quality management for building clusters and districts (BCDs) though multi-objective optimization. Energy Convers Manage 2014;79:525–33.

[49] ANSI/ASHRAE Standard 55. Thermal environmental conditions for human occupancy; 2013. <http://www.techstreet.com/products/1868610>.

[50] Kotas YJ. The exergy method for thermal plant analysis. reprint ed. Malabar, FL: Krieger; 1995.

[51] Torìo H, Angelotti A, Schmidt D. Exergy analysis of renewable energy-based climatisation systems for buildings: a critical view. Energy Build 2009;41:248–71.

[52] Torìo H, Schmidt D. Framework for analysis of solar energy systems in the built environment from an exergy perspective. Renew Energy 2010;35:2689–97.

[53] Available online: <http://www.ibm.com/developerworks/forums/thread.jspa?threadID=368044>.

[54] Aiying R, Risto L. An effective heuristic for combined heat-and-power production planning with power ramp constraints. Appl Energy 2007;84:307–25.

[55] Weber C, Shah N. Optimisation based design of a district energy system for an eco-town in the United Kingdom. Energy 2011;36(2):1292–308.

[56] Mongibello L, Bianco N, Caliano M, Graditi G. Influence of heat dumping on the operation of residential micro-CHP systems. Appl Energy 2015;160:206–20.

[57] Barbieri ES, Melino F, Morini M. Influence of the thermal energy storage on the profitability of micro CHP systems for residential building applications. Appl Energy 2012;97:714–22.

[58] Bianchi M, De Pascale A, Spina PR. Guidelines for residential micro-CHP systems design. Appl Energy 2012;97:673–85.

[59] ASHRAE International Weather files for Energy Calculations (IWEC weather files). Users manual and CD-ROM, American Society of Heating, Refrigerating and Air-Conditioning Engineers, Atlanta, GA, USA; 2001.

[60] Deloitte. European Energy Market reform – Country Profile: Italy. Available online: <https://www2.deloitte.com/content/dam/Deloitte/global/Documents/Energy-and-Resources/gx-er-market-reform-italy.pdf>.

[61] Trudeau N, Francoeur M. Energy Efficiency indicators for Public Electricity Production from fossil fuels. OECD/IEA; 2008.

[62] Darrow K, Tidball R, Wang J, Hampson A. Catalog of CHP technologies; 2015. Available: <https://www.epa.gov/sites/production/files/2015-07/documents/catalog_of_chp_technologies.pdf>.

[63] Technology Data for Energy Plants. Energinet.dk; 2012. Available: <https://www.energinet.dk/SiteCollectionDocuments/Danske%20dokumenter/Forskning/Technology_data_for_energy_plants.pdf>.

[64] Goldstein L, Hedman B, Knowles D, Freedman SI, Woods R, Schweizer T. Gas-fired distributed energy resource technology characterizations. National Renewable Energy Laboratory; 2003, NREL/TP-620-34783. Available: <http://www.nrel.gov/docs/fy04osti/34783.pdf> <http://www.nrel.gov/docs/fy04osti/34783.pdf>.

[65] Technology Roadmap: Energy-efficient Buildings: Heating and Cooling Equipment. OECD/IEA; 2011. Available: <https://www.iea.org/publications/freepublications/publication/buildings_roadmap.pdf>.

[66] Research on cost and performance of heating and cooling technologies. Final Report. Department of Energy and Climate Change; 2013. Available: <https://www.gov.uk/government/uploads/system/uploads/attachment_data/file/204275/Research_on_the_costs_and_performance_of_heating_and_cooling_technologies__Sweett_Group_.pdf>.

[67] Heat Pumps: Technology Brief. IEA-ETSAP and IRENA; 2013. Available: <https://www.irena.org/DocumentDownloads/Publications/IRENA-ETSAP%20Tech%20Brief%20E12%20Heat%20Pumps.pdf>.

[68] Combined Heat and Power: Policy Analysis and 2011 – 2030 Market Assessment. ICF International, Inc; 2012. Available: <http://www.energy.ca.gov/2012publications/CEC-200-2012-002/CEC-200-2012-002.pdf>.

[69] Thermal Energy Storage: Technology Brief. IEA-ETSAP and IRENA; 2013. Available: <https://www.irena.org/DocumentDownloads/Publications/IRENA-ETSAP%20Tech%20Brief%20E17%20Thermal%20Energy%20Storage.pdf>.

Numerical Simulation of an Aluminum Container including a Phase Change Material for Cooling Energy Storage

Luigi Mongibello [1,*], Nicola Bianco [2], Martina Caliano [2] and Giorgio Graditi [1]

[1]   ENEA—Italian National Agency for New Technologies, Energy and Sustainable Economic Development, Portici Research Center, P.le E.Fermi, 1-80055 Portici (NA), Italy; giorgio.graditi@enea.it

[2]   Dipartimento di Ingegneria Industriale (DII)—Università di Napoli Federico II, P.le V. Tecchio, 80-80125 Napoli, Italy; nicola.bianco@unina.it (N.B.); martina.caliano@enea.it (M.C.)

*   Correspondence: luigi.mongibello@enea.it; Tel.: +39-081-772-3584

check for updates

Abstract: Thermal energy storage systems can be determinant for an effective use of solar energy, as they allow to decouple the thermal energy production by the solar source from thermal loads, and thus allowing solar energy to be exploited also during nighttime and cloudy periods. The current study deals with the modelling and simulation of a cooling thermal energy storage unit consisting of an aluminum container partially filled with a phase change material (PCM). Two unsteady models are implemented and discussed, namely a conduction-based model and a conduction-convection-based one. The equations systems relative to both the models are solved by means of the Comsol Multiphysics finite element solver, and results are presented in terms of temporal variation of temperature in different points inside the PCM, of the volume average liquid fraction, and of the cooling energy stored and released through the aluminum container external surface during the charge and discharge, respectively. Moreover, the numerical results obtained by the implementation of the above different models are compared with experimental ones obtained with a climatic chamber. The comparison between numerical and experimental results indicate that, for the considered cooling energy storage unit, free convection plays a crucial role in the heat transfer inside the liquid PCM and cannot be neglected.

Keywords: cooling energy storage; phase change material (PCM); numerical simulation; experimental validation

1. Introduction

A properly designed thermal energy storage system can improve the exploitation and profitability of many renewable and conventional energy sources. For instance, in solar thermal systems, thermal storage can allow to overcome the mismatch between supply and demand. In conventional natural gas-fueled cogeneration systems, thermal storage can be used to produce electricity when it is more economically convenient, namely for self-consumption or when the selling price is high, without wasting thermal energy, which is instead accumulated for a later use. As concerns the storage materials, water is the most used, mainly because water has a high specific heat, is not toxic, and has practically no cost. However, in the last years phase change materials (PCMs) used as thermal energy storage materials have attracted great attention, essentially because, in general, they are characterized by high thermal energy storage densities, and permit to store thermal energy in a narrow temperature range.

Many works have addressed the use of PCMs for storing thermal energy from the solar source for various applications, ranging from solar water heating to solar cooling by absorption or adsorption

refrigeration systems [1–6]. Charvát et al. [7] analyzed the use of a paraffin-based PCM as thermal energy storage material in a solar air-based thermal system. Kabeel at al. [8] investigated the effects of the presence of a paraffin wax in the bottom plate of a solar still for water desalination. Allouhi et al. [9] performed numerical simulations to characterize the melting and solidification processes of a PCM integrated in a solar collector. Zhao et al. [10] developed a control strategy and implemented different models to simulate different operation modes of a solar heating system, including a PCM-based storage tank, over the entire heating season. Moreover, many applications of PCMs have considered cold thermal energy storage [11]. Aljehani et al. [12] simulated a phase change composite consisting of a paraffin wax and expanded graphite for cold thermal energy storage in air conditioning applications. They also performed an experimental validation of numerical results. Bejarano et al. [13] modeled and simulated a novel cold energy storage system based on PCMs. Cheng and Zhai [14] modeled and simulated a cold thermal energy storage system consisting of a packed bed with multiple PCMs. In this work, an experimental validation of numerical results is also reported.

Various models have been developed for the numerical simulation of PCM-based thermal energy storage systems, most of which have been reported in reviews [15–17]. Farid et al. [18] successfully applied the effective heat capacity (EHC) method for simulating 2D heat transfer with phase change. Lacroix [19] developed a model to simulate a shell-and-tube thermal energy storage unit with the PCM on the shell side. Ng et al. [20] employed the finite element method to simulate the convection-dominated melting of a PCM in a cylindrical-horizontal annulus. Lamberg et al. [21] implemented both the effective heat capacity method and the enthalpy method to simulate the melting and solidification processes of a PCM. They also compared the numerical results, which were obtained using the FEMLAB solver, with experimental ones. Esapuor et al. [22] implemented the enthalpy method to perform 3D simulations of a PCM in multi-tube heat exchanger units. Allouche et al. [23] developed and validated a computational fluid-dynamic (CFD) model for the numerical simulation of a PCM slurry in a horizontal tank. Niyas et al. [24] developed a numerical tool to simulate a lab-scale PCM-based shell-and-tube thermal energy storage system by employing the EHC method. Neumann et al. [25] proposed and validated a simplified modelling approach for the numerical simulation of PCM-based fin-and-tube heat exchangers. Li et al. [26] proposed a numerical model to simulate the heat transfer inside an open-cell metallic foam filled PCM.

The current study focuses on the simulation of an aluminum container partially filled with a phase change material. A conduction-based model and a conduction-convection-based one are implemented for the purpose, and numerical results are compared with experimental ones obtained with a climatic chamber. The main contribution of this manuscript is that it presents an experimental validation of two different modelling approaches implemented to simulate the cooling energy charge and discharge of a real PCM-based cooling energy storage unit.

The description of the experimental apparatus and experimental results are presented in Section 2. The balance equations systems relative to both the models are detailed in Section 3. The numerical results and the comparison with experimental ones are discussed in Section 4, and the main conclusions are reported in Section 5.

2. Experimental Apparatus and Results

Figure 1 shows the aluminum cylindrical container used in the experimental test. Its height is 25.0 cm and internal radius is 6.9 cm. Furthermore, it is partially filled with 2.4 kg of a commercial bio-based phase change material, whose characteristics are shown in Table 1.

Temperature measurements inside the phase change material are all done on the same horizontal section, at a distance of 9 cm from the container bottom, by five T-type thermocouples of class 1. One measuring point is located on the container axis, while the other four points are located at a distance of 3.45 cm from the axis. These are arranged to form a cross as shown in Figure 1b. Temperature data acquisition is done with a sample time of 1 s, by means the of the National Instruments NI 9213

module, using the NI cRIO 9066 controller. Figure 2 shows the climatic chamber used to realize the experimental test.
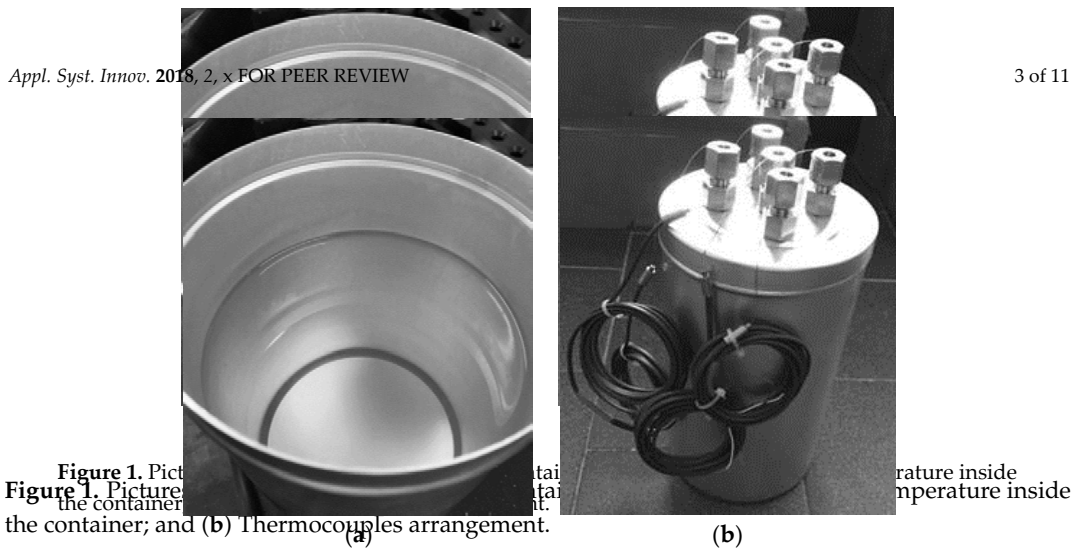
Figure 1. Pictures of the cylindrical aluminum container: (**a**) Liquid PCM at room temperature inside the container; and (**b**) Thermocouples arrangement.

Table 1. Thermo-physical characteristics the PCM.

Property	Value
Melting point (°C)	15
Latent heat (kJ kg^{-1})	182
Thermal conductivity (W m^{-1} K^{-1})	
Solid	0.25
Liquid	0.15
Density (kg m^{-3})	
Solid	950
Liquid	860
Specific heat (J kg^{-1} K^{-1})	
Solid	2250
Liquid	2560

Figure 2. Picture of the climatic chamber used for the experimental test.

The container is put in the climatic chamber on a 2-cm thick rigid sheet of polyurethane foam for the thermal insulation of the container bottom side, with all the PCM in the liquid state, and at a uniform temperature equal to 23.8 °C (room temperature). Then, the experimental test steps are applied sequentially:

uniform temperature equal to 23.8 °C (room temperature). Then, the following four steps are applied sequentially:

1. one-hour temperature ramp is applied to bring the internal temperature of the climatic chamber to the cooling energy charge temperature Tc = 7 °C;

2. the climatic chamber internal temperature is kept at Tc for 72 h;

3. one-hour temperature ramp is applied to bring the internal temperature of the climatic chamber to the cooling energy discharge temperature Td = 23 °C;

4. the temperature inside the climatic chamber is kept at Td until all the measured temperatures inside the PCM are well above the phase change temperature (15 °C).

As it can be argued, the main contributions to the cooling energy charge and discharge are represented by steps 2 and 4, respectively. Nonetheless, in the numerical simulation of the PCM thermal behavior, steps 1 and 3 are also simulated.

Experimental Results

2.1. Experimental Results

Figures 3 and 4 show the temporal profile of the temperature relative to the measuring point on the container axis, which is indicated with T_A, and the temporal profile of the average of the temperatures relative to the mid-radius measuring points, which is indicated with $T_{MR,average}$, during the cooling energy charge and discharge, respectively.

Figure 3. Temperature temporal profiles during PCM cooling energy charge (steps 1 and 2).

Figure 4. Temperature temporal profiles during PCM cooling energy discharge (steps 3 and 4).

It can be noticed that, as expected, the charge phase is much slower than the discharge one. This is due to the formation of solid PCM on the internal wall of the aluminum container during the cooling energy charge, which acts as a thermal insulation layer for the heat transfer between the liquid PCM and the external cooled air (internal environment of the climatic chamber). Conversely, during the discharge phase the convective mechanisms inside of the liquid PCM, which forms on the internal walls of the container, accelerate the heat transfer inside the liquid PCM and solid PCM. Moreover, the Figure 3 shows that once the solid-liquid heat transfer is slightly lower than 15 °C, namely the one given by the PCM manufacturer reported in Table 1.

discharge phase, the convective mechanisms inside the liquid PCM, which forms on the internal wall of the container, accelerate the heat transfer towards the internal solid PCM. Moreover, Figure 3 shows that the effective solidification temperature is slightly lower than 15 °C, namely the one given by the PCM manufacturer reported in Table 1.

3. Simulation Models

The axial symmetry of the PCM container and of the boundary conditions permits to implement 2D axisymmetric models, and thus to obtain a relatively low computational cost of numerical simulations. Therefore, two unsteady 2D axisymmetric numerical models are developed for simulating the cooling energy charge and discharge of the phase change material: a conduction-based model and a conduction–convection-based model.

3.1. Conduction-Based Model

This model is based on the following main assumptions: (i) the phase change material is homogenous and isotropic; (ii) the thermo-physical properties of the phase change material are considered to be constant and equal to the average values between the liquid and solid phases; (iii) the volume expansion/reduction during phase change is ignored; (vi) phase change during solidification/melting occurs in a temperature range; (v) negligible convective mechanisms. The energy balance equation is given by:

$$\rho_{PCM}\, c'_{p,PCM}\frac{\partial T}{\partial t} = k_{PCM}\nabla^2 T \tag{1}$$

where T is the temperature, t is the time variable, ρ_{PCM} is the density of the PCM, and k_{PCM} is the PCM thermal conductivity.

The phase change is simulated by means of the effective heat capacity method (EHC). According to EHC, the material effective heat capacity $c'_{p,PCM}$ is expressed as a function of the latent heat of fusion of the PCM L_h as follows:

$$c'_{p,PCM} = c_{p,PCM} + L_h\frac{d\varphi(T)}{dT} \tag{2}$$

where $c_{p,PCM}$ is the average PCM specific heat, and $\varphi(T)$ is a non-dimensional parameter, which is 0 in the solid phase, 1 in the liquid phase and between 0 and 1 in the transition zone. The latter can be expressed as:

$$\varphi(T) = \begin{cases} 0, & T < (T_M - \Delta T_M) \\ \frac{T - T_M + \Delta T_M}{2\Delta T_M}, & (T_M - \Delta T_M) \leq T \leq (T_M + \Delta T_M) \\ 1, & T > (T_M + \Delta T_M) \end{cases} \tag{3}$$

where T_M is the melting temperature, and ΔT_M is half the temperature phase change range that goes from $(T_M - \Delta T_M)$ to $(T_M + \Delta T_M)$.

3.2. Conduction-Convection-Based Model

In this case, two further assumptions are made as concerns the modelling of the liquid PCM flow, namely that liquid PCM is Newtonian and the flow is laminar. The continuity, momentum and energy balance equations are written as follows:

$$\nabla \cdot \overline{v} = 0 \tag{4}$$

$$\rho_{PCM}\left(\frac{\partial \overline{v}}{\partial t} + (\overline{v}\cdot\nabla)\overline{v}\right) = -\nabla p + \mu'_{PCM}\nabla^2\overline{v} + \overline{F} \tag{5}$$

$$\rho_{PCM}\, c'_{p,PCM}\frac{\partial T}{\partial t} + \rho_{PCM}c_{p,PCM}\overline{v}\cdot\nabla T = k_{PCM}\nabla^2 T \tag{6}$$

where p is the pressure, μ'_{PCM} is the modified dynamic viscosity, and $\overline{v}$ is the velocity vector.

In Equation (5), $\overline{F}$ represents the Boussinesq approximation, which is added to the momentum equation for including the buoyancy effects, and it is evaluated according to Equation (7):

$$\overline{F_b} = \rho_{PCM}\overline{g}\beta(T - T_M) \tag{7}$$

where $\overline{g}$ and β are the gravitational acceleration and the isobaric thermal expansion coefficient, respectively.

The effective heat capacity $c'_{p,PCM}$ is calculated as previously described in Section 3.1, while the modified dynamic viscosity μ'_{PCM} is evaluated according to Equation (8), in order to force zero velocity in the solid PCM.

$$\mu'_{PCM} = \mu_{PCM}(1 + S(T)) \tag{8}$$

where μ_{PCM} is the dynamic viscosity of liquid PCM. The variable S is given by:

$$S(T) = C\frac{(1 - \varphi(T))^2}{(\varphi(T))^3 + \delta} \tag{9}$$

In Equation (9), the constant δ, typically fixed to 10^{-3}, serves to prevent null denominator, while the constant C affects the PCM flow into the phase transition zone, and it is usually between 10^3 and 10^{10}. Table 2 reports the values of the parameters T_M, ΔT_M and C used in this work. This combination of values, which were chosen among different tested ones, is the one presenting the best match between experimental and numerical results.

Table 2. Values of T_M, ΔT_M and C employed in the numerical simulations.

Parameter	Charge	Discharge
T_M (°C)	12.5	15
ΔT_M (°C)	1	5.5
C	$10^{3.7}$	$10^{3.8}$

3.3. Initial and Boundary Conditions

The simulations of cooling energy charge and discharge of the PCM are performed separately. With reference to the experimental test described in Section 2, as regards the implementation of the conduction-based model, the PCM initial temperature for the charge simulation is fixed equal to the temperature measured at the start-up experimental test, while, for the discharge simulation, the PCM initial temperature is fixed equal to the measured temperature at the start-up of step 3. The boundary conditions are set according to the experimental test. In particular, the bottom and top surfaces of the cylindrical computational domain relative to the PCM are considered to be adiabatic, while the boundary condition relative to the lateral surface is set according to Equation (10):

$$q_l = h_l(T - T_\infty), \quad r = r_{max}, 0 \le z \le z_{max} \tag{10}$$

where q_l is the heat flux relative to the lateral surface, h_l is the heat transfer coefficient relative to the lateral surface, T_∞ is equal to the air temperature inside the climatic chamber, and r and z are the radial and axial coordinates, respectively. The convective heat transfer coefficient h_l is fixed to 30.2 W/(m² K) in the cooling energy charge, and to 29.1 W/(m² K) in the discharge. These values of h_l were calculated by means of a correlation for cylinders subjected to transverse external forced flow [27], and were obtained using a measured average air velocity inside the climatic chamber of 3.3 m/s.

The above conditions are also applied for the implementation of the conduction–convection-based model. In this case, the initial velocity is set to zero in both charge and discharge, while a no-slip wall boundary condition is applied to all the external surfaces of the computational domain delimiting the phase change material.

3.4. Numerical Solver

For both the implemented models, the governing equations are solved with the finite element simulation software COMSOL Multiphysics 5.3a. The non-linearities are resolved through a segregated approach. The backward differentiation formula is adopted for the time stepping, with the initial time step fixed to 10^{-4} s and no-fixed maximum time step. Since the PCM volume variations during phase changes are not simulated for both the models, the the 2D computational domain, evaluated by means of the PCM weight and average density, remains fixed. It consists of a rectangle with a height of 17.73 cm and a width of 6.90 cm. Physics-controlled meshes are used, and for both developed model grid independence of results is assured. The simulations are performed with a Dell Precision T7610 workstation, equipped with two Intel Xeon E5-2687 w2 processors and a RAM of 64 GB and 1866-MHz clock.

4. Results

Figure 5 shows a comparison between the temporal variation of experimental temperatures inside the PCM, relative to the measuring points indicated in Section 2, and the corresponding numerical temperatures during the cooling energy charge. It can be seen that there is a good agreement between the numerical temperatures relative to the conduction–convection-based model and the experimental temperatures, while the temperature profiles resulting from the implementation of the conduction-based model fail to match the experimental ones during the first and last parts of the charging process. This is essentially because the conduction-based model does not permit to simulate the mixing of liquid PCM inside the aluminum container in the initial part of the cooling energy charge. Thus, the resulting temperature profiles present a slower decrease. Of course, this behavior at the initial part of the charge influences the entire charge process simulated by the conduction-based model. Indeed, in the last part of charge, the simulated temperature $T_{A,cond}$ presents a sensible deviation from the corresponding experimental temperature.

Figure 6 shows the comparison between the temporal variation of experimental and numerical temperatures inside the PCM relative to the cooling energy discharge. It can be seen that, in the initial part of discharge, the simulated temperatures relative to both the implemented models are are in good agreement with the experimental ones. This is because conduction heat transfer is the dominant heat transfer mechanism in the first part of discharge, when great part of the PCM is in the solid state, and the melted PCM is limited in a narrow layer close to the container internal wall. Heat transfer by free convection inside the PCM becomes higher as the melted layer thickness increases. Indeed, Figure 6 shows that, in the last part of discharge, the temperature profiles relative to the conduction-based model are very far from the experimental ones, differently from the ones relative to the conduction-convection-based model which present a better behavior in the last part of discharge.

From the above, it can be stated that the conduction-based model is not suitable for the present application. For this reason, only the main results obtained with conduction-convection-based model are reported and discussed in the following.
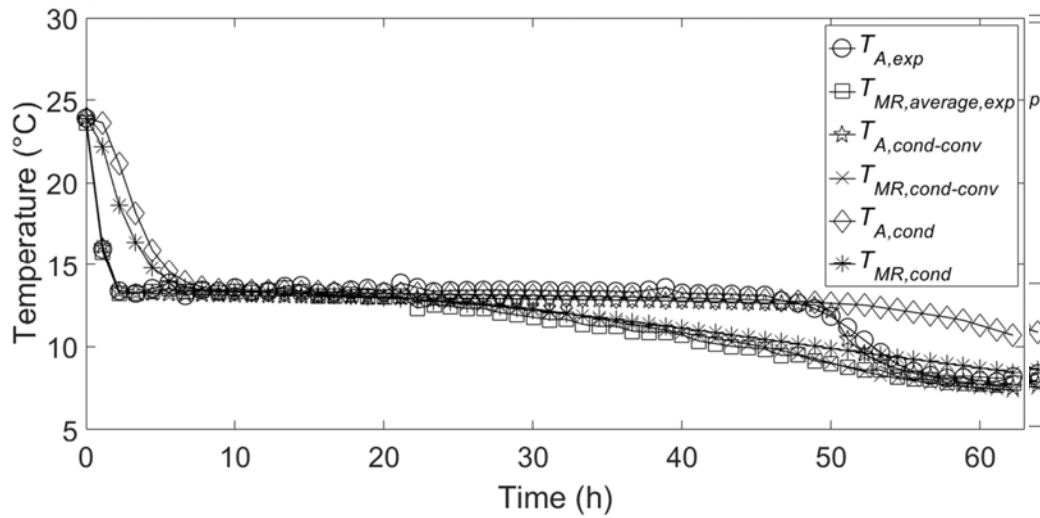
Figure 5. Temporal variation of experimental and numerical temperatures during cooling energy charge.
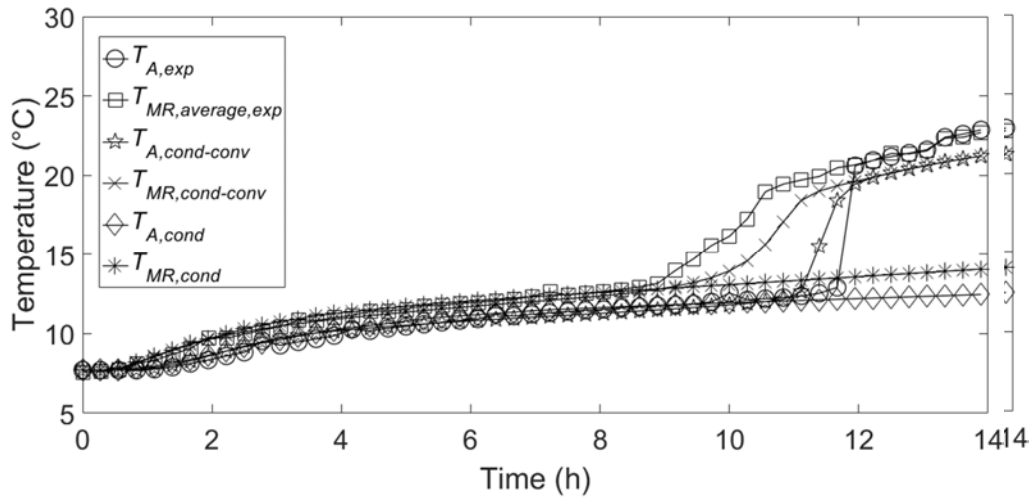
Figure 6. Temporal variation of experimental and numerical temperatures during cooling energy discharge.

Figures 5,6 shows the temporal variation of the average liquid fraction of PCM volume during cooling energy charge and discharge, respectively, obtained by the conduction-convection-based model. Figure 7a clearly shows that the PCM solidification rate is relatively high in the first part of the charge, before it slows down as the thickness of the solid layer at the container wall increases. Indeed, from the beginning of step 9, PCM volume-average liquid fraction reaches 0.5 after 23 hours, whereas the complete solidification of PCM is reached after about 63 hours. Conversely, Figure 7b shows that, during the cooling energy discharge, the melting rate is initially relatively low, before it becomes higher as the melted fraction increases, or in other words, as heat transfer by free convection inside the PCM becomes higher. In Figure 7b it can be noted that the PCM is not completely melted at the end of the discharge simulation. This last result is not in contrast with the experimental observations, since actually the PCM was not completely melted at the end of the experimental test. However, the real liquid fraction at the end of the experimental test was not measured, and probably it was higher than the simulated one obtained with the conduction-convection-based model, since the model underestimates the temperatures at the end of the discharge process, as it is be seen in Figure 6.

Similar considerations as those made for Figure 7a,b can be made for Figure 8a,b, which report the temporal variation of total cooling energy stored by the PCM during cooling energy charge and released during discharge, respectively.

Finally, Table 3 reports the sensible and latent contributions of the total cooling energy stored and discharged at the end of charge and discharge, respectively.
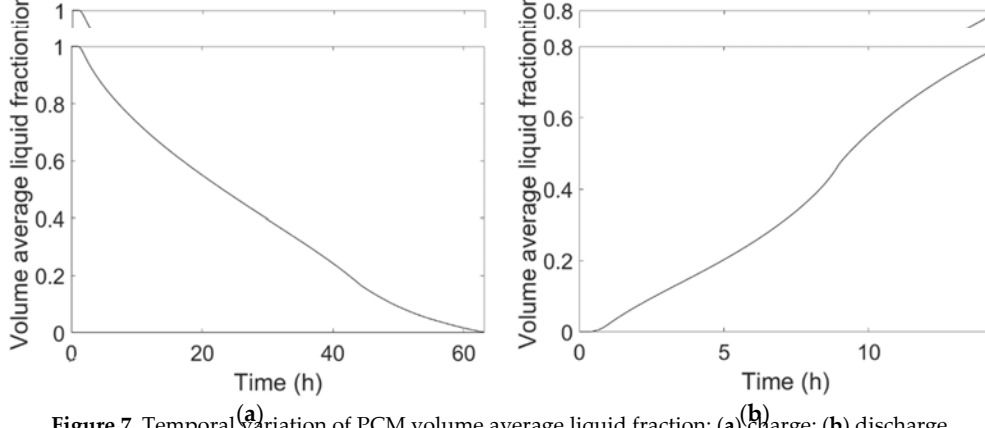
Figure 7. Temporal variation of PCM volume average liquid fraction: (**a**) charge; (**b**) discharge.
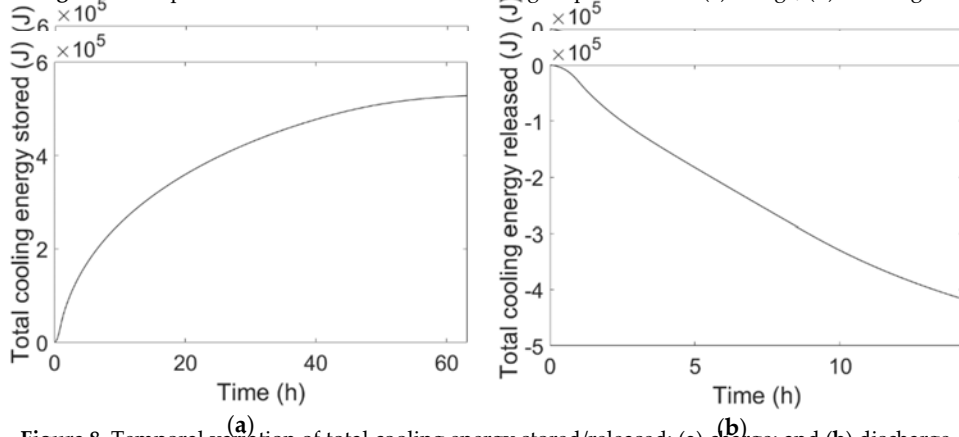
Figure 8. Temporal variation of total cooling energy stored/released: (**a**) charge; and (**b**) discharge.

Table 3. Sensible and latent contributions of total cooling energy stored and discharged.

Parameter	Value
Cooling energy stored (kJ)	92
Sensible contribution	436
Latent contribution	
Cooling energy released (kJ)	−72
Sensible contribution	−344
Latent contribution	

5. Conclusions

In the present work, two different unsteady models are implemented in order to simulate the cooling energy charge and discharge of a cooling thermal energy storage unit consisting of an aluminum container partially filled with a phase change material: a conduction-based model and a conduction-convection-based one. The numerical results obtained by the implementation of the above

different models are compared with experimental ones obtained with a climatic chamber. The main conclusions of the present work, argued by comparing the numerical and experimental results, are:

- The conduction-based model is not appropriate for the considered cooling energy storage application since free convection plays a crucial role in the heat transfer inside the liquid PCM, and thus cannot be neglected;
- The numerical results obtained by the implementation of the conduction–convection-based model are in good accordance with experimental ones;
- The conduction–convection-based model underestimates the temperatures inside the PCM at the end of the cooling energy discharge phase.

References

1. Khan, M.M.A.; Saidur, R.; Al-Sulaiman, F.A. A review for phase change materials (PCMs) in solar absorption refrigeration systems. *Renew. Sustain. Energy Rev.* **2017**, *76*, 105–137. [CrossRef]
2. Kapsalis, V.; Karamanis, D. Solar thermal energy storage and heat pumps with phase change materials. *Appl. Therm. Eng.* **2016**, *99*, 1112–1224. [CrossRef]
3. Wang, Z.; Qiu, F.; Yang, W.; Zhao, X. Applications of solar water heating system with phase change material. *Renew. Sustain. Energy Rev.* **2015**, *52*, 645–652. [CrossRef]
4. Zhou, Z.; Zhang, Z.; Zuo, J.; Huang, K.; Zhang, L. Phase change materials for solar thermal energy storage in residential buildings in cold climate. *Renew. Sustain. Energy Rev.* **2015**, *48*, 692–703. [CrossRef]
5. Pandey, A.K.; Hossain, M.S.; Tyagi, V.V.; Rahim, N.A.; Selvaraj, J.A.L.; Sari, A. Novel approaches and recent developments on potential applications of phase change materials in solar energy. *Renew. Sustain. Energy Rev.* **2018**, *82*, 281–323. [CrossRef]
6. Khan, M.M.A.; Ibrahim, N.I.; Mahbubul, I.M.; Ali, H.M.; Saidur, R.; Al-Sulaiman, F.A. Evaluation of solar collector designs with integrated latent heat thermal energy storage: A review. *Sol. Energy* **2018**, *166*, 334–350. [CrossRef]
7. Charvát, P.; Klimeš, L.; Ostry, M. Numerical and experimental investigation of a PCM-based thermal storage unit for solar air systems. *Energy Build.* **2014**, *68*, 488–497. [CrossRef]
8. Kabeel, A.E.; Elkelawy, M.; Din, H.A.E.; Alghrubah, A. Investigation of exergy and yield of a passive solar water desalination system with a parabolic concentrator incorporated with latent heat storage medium. *Energy Convers. Manag.* **2017**, *145*, 10–19. [CrossRef]
9. Allouhi, A.; Ait Msaad, A.; Benzakour Amine, M.; Saidur, R.; Mahdaoui, M.; Kousksou, T.; Pandey, A.K.; Jamil, A.; Moujibi, N.; Benbassou, A. Optimization of melting and solidification processes of PCM: Application to integrated collector storage solar water heaters (ICSSWH). *Sol. Energy* **2018**, *171*, 562–570. [CrossRef]
10. Zhao, J.; Ji, Y.; Yuan, Y.; Zhang, Z.; Lu, J. Seven Operation Modes and Simulation Models of Solar Heating System with PCM Storage Tank. *Energies* **2017**, *10*, 2128. [CrossRef]
11. Oró, E.; de Gracia, A.; Castell, A.; Farid, M.M.; Cabeza, L.F. Review on phase change materials (PCMs) for cold thermal energy storage applications. *Appl. Energy* **2012**, *99*, 513–533. [CrossRef]
12. Aljehani, A.; Razack, S.A.K.; Nitsche, L.; Al-Hallaj, S. Design and optimization of a hybrid air conditioning system with thermal energy storage using phase change composite. *Energy Convers. Manag.* **2018**, *169*, 404–418. [CrossRef]
13. Bejarano, G.; Suffo, J.J.; Vargas, M.; Ortega, M.G. Novel scheme for a PCM-based cold energy storage system. Design, modelling, and simulation. *Appl. Therm. Eng.* **2018**, *132*, 256–274. [CrossRef]

14. Cheng, X.; Zhai, X.; Wang, R. Thermal performance analysis and optimization of a cascaded packed bed cool thermal energy storage unit using multiple phase change materials. *Appl. Energy* **2018**, *215*, 566–576. [CrossRef]

15. Dutil, Y.; Rousse, D.R.; Salah, N.B.; Lassue, S.; Zalewski, L. A review on phase-change materials: Mathematical modeling and simulations. *Renew. Sustain. Energy Rev.* **2011**, *15*, 112–130. [CrossRef]

16. De Gracia, A.; Cabeza, L.F. Numerical simulation of a PCM packed bed system: A review. *Renew. Sustain. Energy Rev.* **2017**, *69*, 1055–1063. [CrossRef]

17. Al-abidi, A.A.; Mat, S.B.; Sopian, K.; Sulaiman, M.Y.; Mohammed, A.T. CFD applications for latent heat thermal energy storage: A review. *Renew. Sustain. Energy Rev.* **2013**, *20*, 353–363. [CrossRef]

18. Farid, M.M.; Hamad, F.A.; Abu-Arabi, M. Melting and solidification in multidimensional geometry and presence of more than one interface. *Energy Convers. Manag.* **1998**, *39*, 809–818.

19. Lacroix, M. Numerical simulation of a shell-and-tube latent heat thermal energy storage unit. *Sol. Energy* **1993**, *50*, 357–367. [CrossRef]

20. Ng, K.W.; Gong, Z.X.; Mujumdar, A.S. Heat transfer in free convection-dominated melting of a phase change material in a horizontal annulus. *Int. Commun. Heat Mass Transf.* **1998**, *25*, 631–640. [CrossRef]

21. Lamberg, P.; Lehtiniemi, R.; Henell, A.M. Numerical and experimental investigation of melting and freezing processes in phase change material storage. *Int. J. Therm. Sci.* **2004**, *43*, 277–287. [CrossRef]

22. Esapour, M.; Hosseini, M.J.; Ranjbar, A.A.; Pahamli, Y.; Bahrampoury, R. Phase change in multi-tube heat exchangers. *Renew. Energy* **2016**, *85*, 1017–1025. [CrossRef]

23. Allouche, Y.; Varga, S.; Bouden, C.; Oliveira, A.C. Validation of a CFD model for the simulation of heat transfer in a tubes-in-tank PCM storage unit. *Renew. Energy* **2016**, *89*, 371–379. [CrossRef]

24. Niyas, H.; Prasad, S.; Muthukumar, P. Performance investigation of a lab–scale latent heat storage prototype—Numerical results. *Energy Convers. Manag.* **2017**, *135*, 188–199. [CrossRef]

25. Neumann, H.; Palomba, V.; Frazzica, A.; Seiler, D.; Wittstadt, U.; Gschwander, S.; Restuccia, G. A simplified approach for modelling latent heat storages: Application and validation on two different fin-and-tubes heat exchangers. *Appl. Therm. Eng.* **2017**, *125*, 41–52. [CrossRef]

26. Li, W.Q.; Qu, Z.G.; He, Y.L.; Tao, W.Q. Experimental and numerical studies on melting phase change heat transfer in open-cell metallic foams filled with paraffin. *Appl. Therm. Eng.* **2012**, *37*, 1–9. [CrossRef]

27. Baehr, H.D.; Stephan, K. *Heat and Mass Transfer*, 2nd ed.; Springer: Berlin/Heidelberg, Germany, 2006.
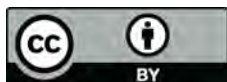
TRADE-OFF SOLUTIONS BETWEEN ECONOMY AND CO_2 EMISSIONS FOR THE DAILY OPERATION OF A DISTRIBUTED ENERGY SYSTEM: A REAL CASE STUDY IN ITALY

MARIALAURA DI SOMMA [1], ILARIA BERTINI [2], GIORGIO GRADITI [1], LUIGI MONGIBELLO [1], GIOVANNI PUGLISI [2]

[1]: Energy Technologies Department, ENEA, Portici, Naples (Italy), [2]: Energy Efficiency Department, ENEA, Rome (Italy)

Introduction

Distributed energy systems (DES) typically consist of small-scale technologies providing **electricity and thermal energy close to end-users**. Thanks to their numerous **economic and environmental benefits**, DES are considered a **promising option to traditional energy supply**.

To achieve the expected economic and environmental benefits, the **daily operation** is **crucial**, and it presents **several challenges** due to the different energy devices and energy carriers used to satisfy the time-varying user demand.

In this work, **a multi-objective optimization model** is developed for a **real DES located in Italy**, with the aim to find **trade-off solutions** between **economic and environmental aspects** for the daily operation.

Description of the Italian DES

Energy devices in the DES

Energy device	Size	Efficiency	
		El	Th
CHP (NG ICE)	970 kW$_e$	0.386	0.463
Condensing boiler	895 kW$_{th}$	-	0.93
Conventional boilers (2)	2600 kW$_{th}$ (2)	-	0.90 (2)
Electric chiller	435 kW$_c$	-	4.4
Single-stage absorption chiller	195 kW$_c$	-	0.75
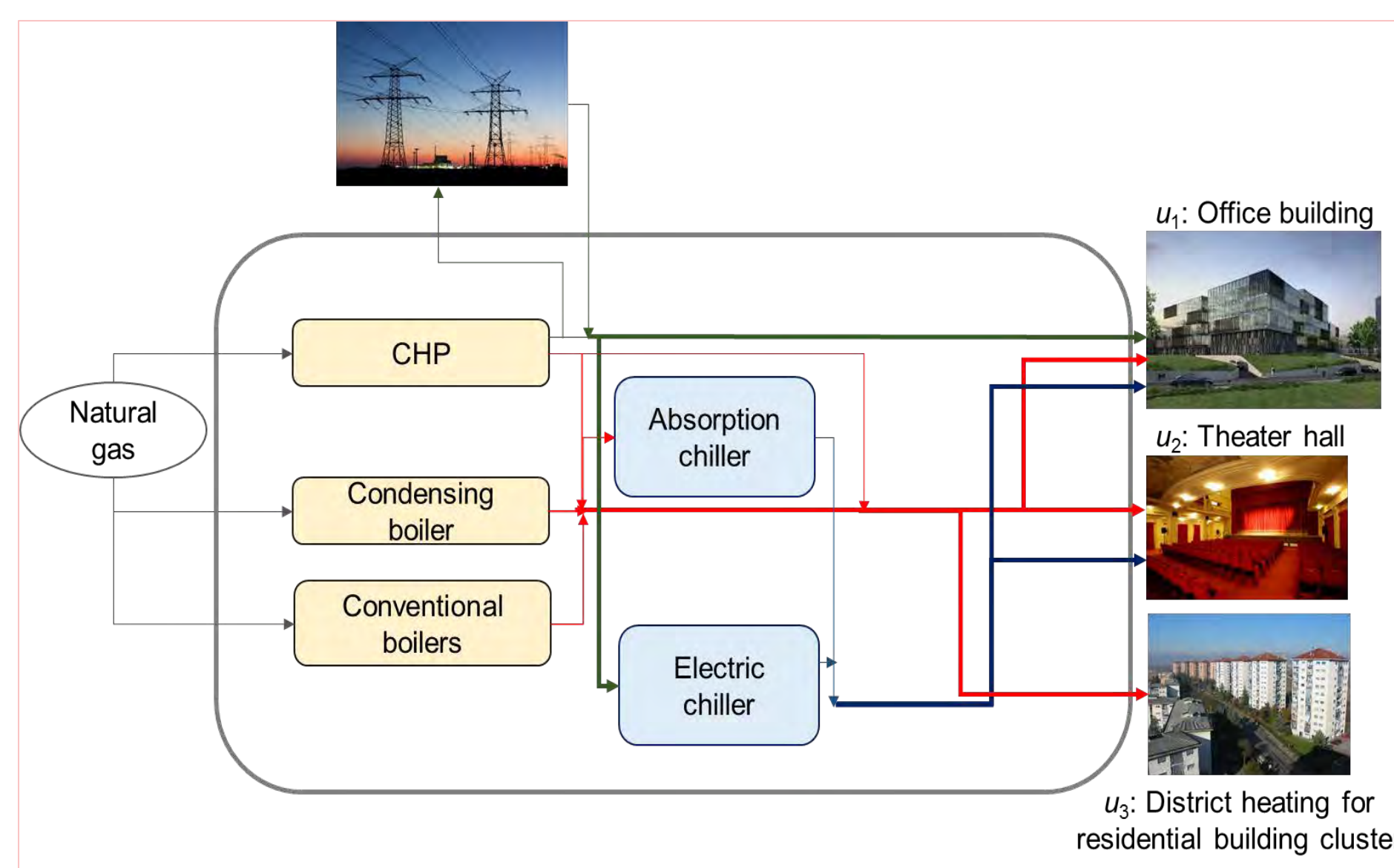
Figure 1: Scheme of the DES in Italy

End-users

Office building owned by the DES operator

Theater hall

Cluster of 31 residential buildings with 640 apartments, which is **connected to the DES through a district heating network** (DHN)

Problem Formulation & Solution Methodology

A **multi-objective linear programming** (MOLP) **problem** is formulated **based on the real constrains for the devices and the DHN** with the aim to find the **optimal operation strategies** of the DES which **maximize the operator's profit and minimize CO_2 emissions**, while satisfying the time-varying electrical and thermal demand of connected end-users.

Objective functions

Economic objective: maximize the total daily operator's profit:

$$Prof = R^{Sell,grid} + R^{Sell,users} - C^{Energy}$$

Environmental objective: minimize the total daily net CO_2 emissions:

$$Env = CO_2^{Oper} - CO_2^{Avoid}$$

Problem constraints

Operation constraints
- Energy devices (capacity constraint)
- DHN (capacity constraint)

Energy balances
- Electricity
- Thermal (heat and cooling)

Solution Methodology

A **single objective function** is formulated **as a weighted sum of the minus-profit and the net CO_2 emissions** to be minimized:

$$FO = c\omega(-Prof) + (1-\omega)Env$$

The problem is solved by using **branch-and-cut**

Effects of White Certificates scheme on the DES performances

The CHP in the DES respects the requirements to accede **the Italian WC incentive scheme**

For the **current operation strategies**, the operator can gain **1.36 WC**, and his **profit** is equal to **488.28 €**

Under the **economic optimization**, the operator gains **2.19 WC** and his **profit** is equal to **805.39 €**, whereas the **net CO_2 emissions** are equal to **7217.9 kgCO$_2$**.

Under the **environmental optimization**, the operator gains **2.4 WC** and his **profit** is equal to **802.9 €** whereas the **net CO_2 emissions** are equal to **7093.92 kgCO$_2$**.

Testing Results

Reference is made to a **winter weekday of December**
Hourly profiles for heat and electricity demand of end-users are based on **experimental data**

Current operation strategies

Revenues (€)		Costs (€)	Emissions (kgCO$_2$)	
$R^{sell,grid}$	$R^{sell,users}$	C^{Energy}	CO_2^{Oper}	CO_2^{Avoid}
512.59	2054.75	2215.06	12418.66	3331.39

$Prof = 352.28$ €
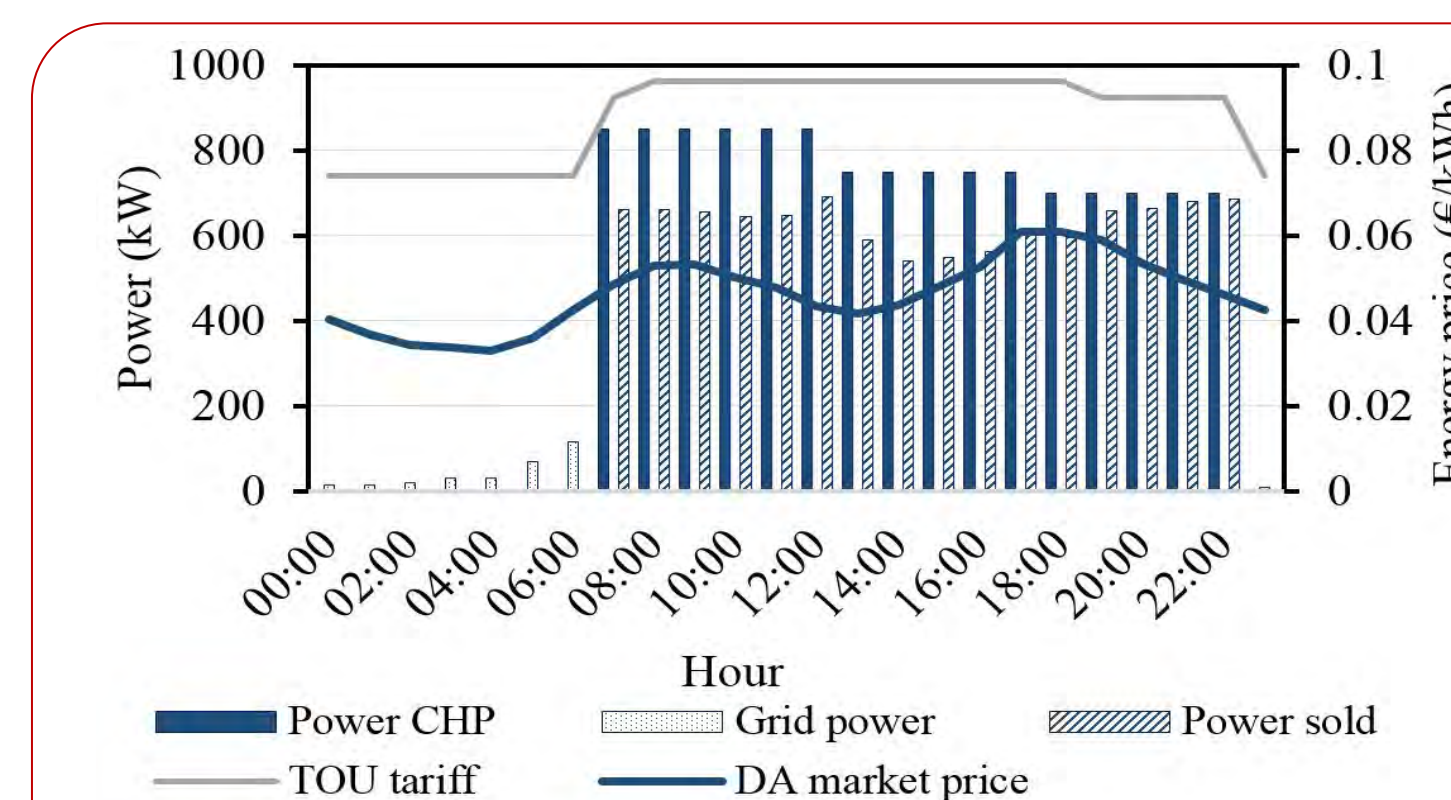
$Env = 9087.27$ kg$_{CO2}$

Figure 2: Current operation strategies of the DES

Optimization Results
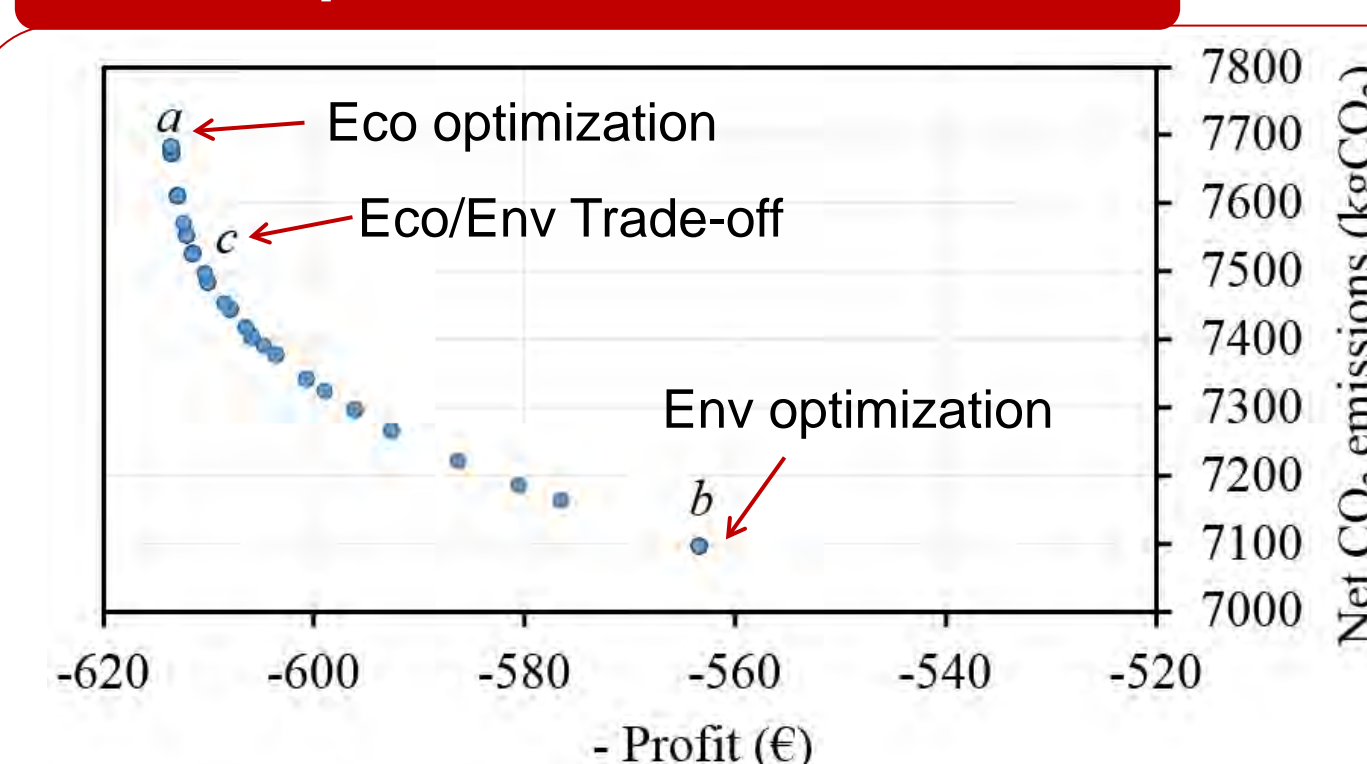
Figure 3: Pareto frontier

Point a: $Prof = 613.39$ € $Env = 7679.78$ kg$_{CO2}$

Point b: $Prof = 563.11$ € $Env = 7093.92$ kg$_{CO2}$

Point c: $Prof = 611.52$ € $Env = 7527.6$ kg$_{CO2}$

At **all points of the Pareto frontier**, a **strong increase of the operator's profit** and a **significant reduction of net CO_2 emissions** are attained as compared with the current case (non-optimized operation strategies).
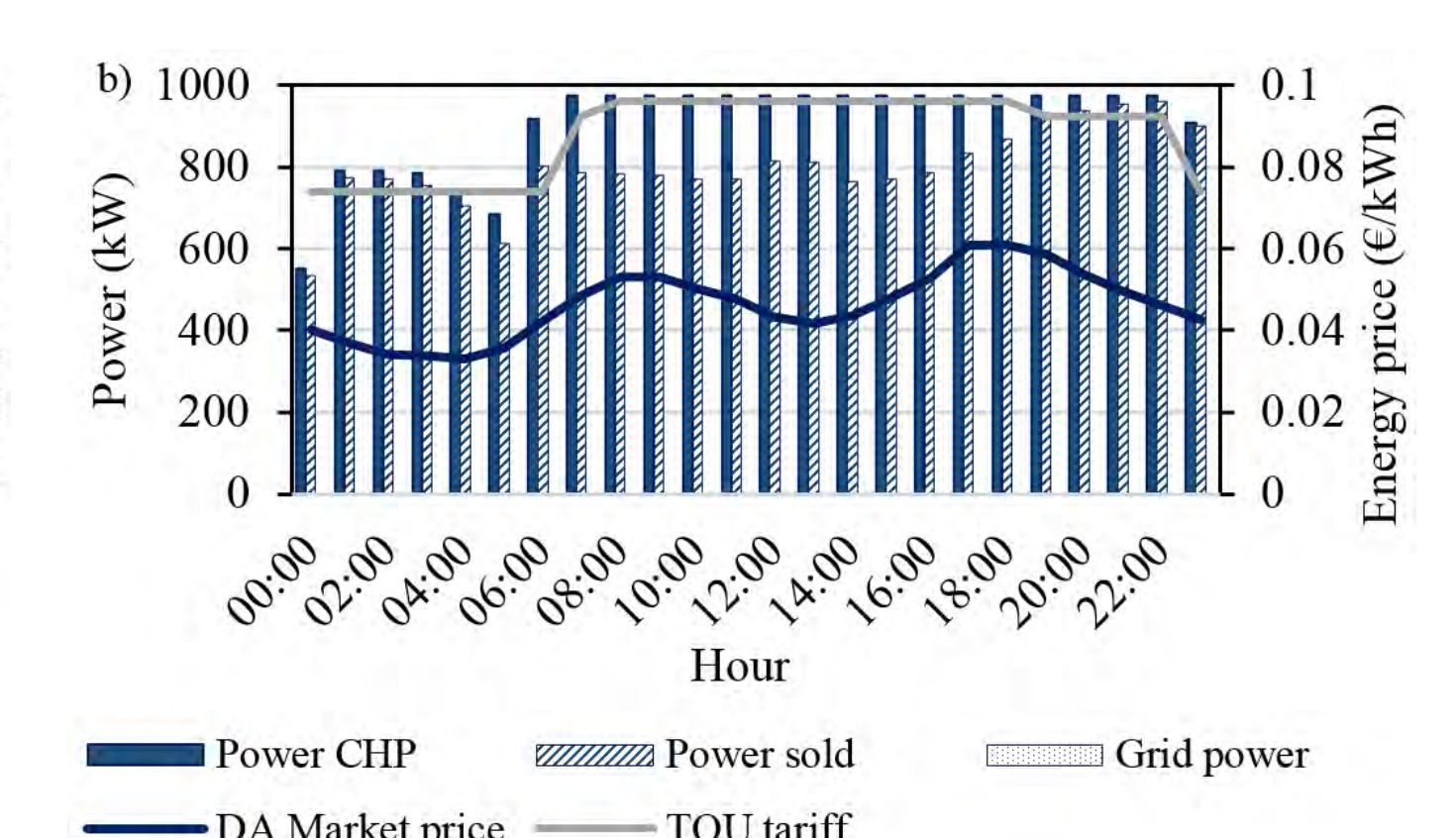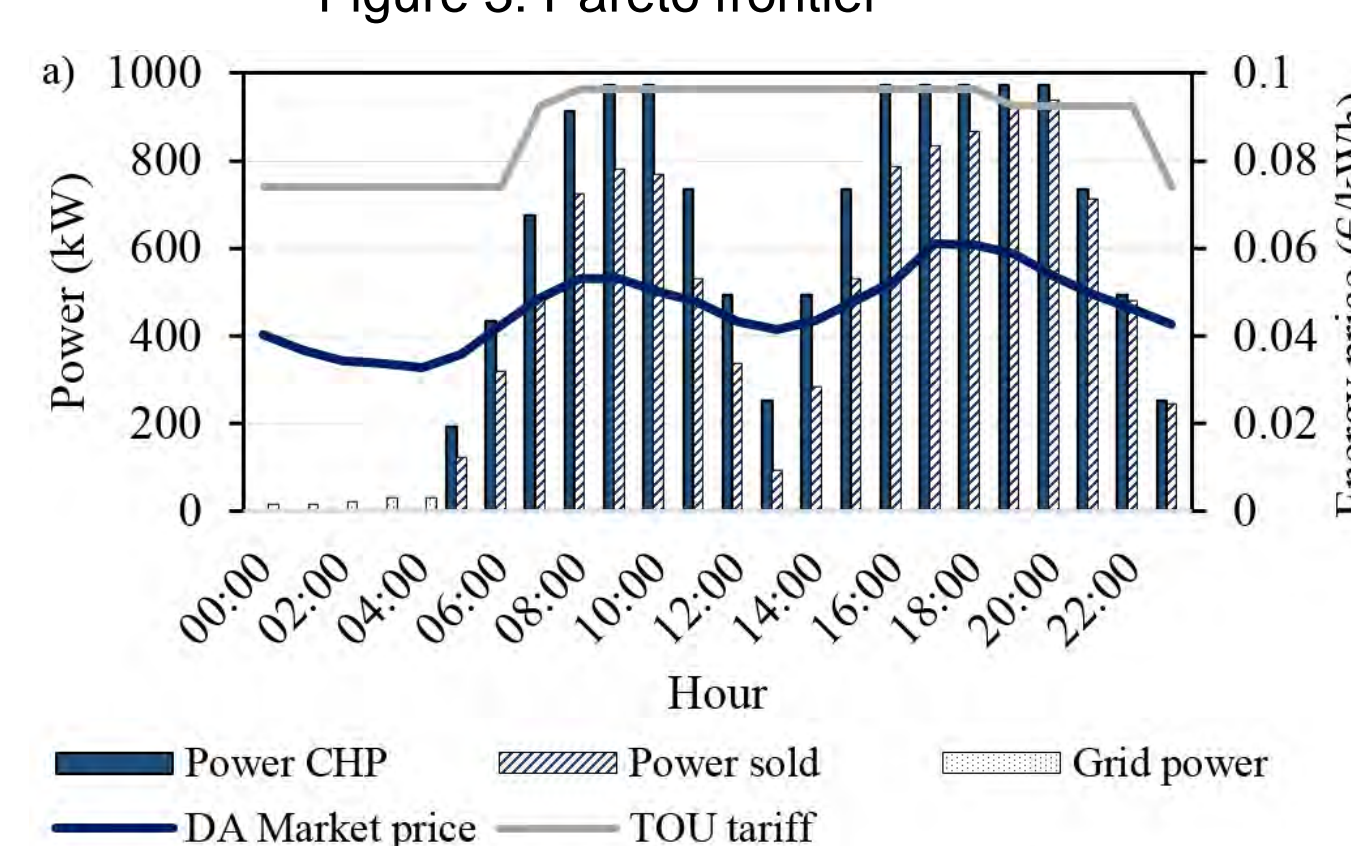
Fig. 4. Optimized operation strategies of the DES for electricity under a) *eco optimization* and b) *env optimization*

Under the **economic optimization**:
- The power from CHP is sold back to the grid when the day-ahead market price is higher
- The grid power is used when the grid price of TOU tariff is lower

Under the **environmental optimization**:
- The working hours of the CHP are larger.
- A larger amount of waste heat can be used for thermal demand of all users, thereby reducing the emissions related to the gas consumption in boilers

Conclusions & key findings

- In this work, the **operation problem** is addressed for a **real DES located in Italy** through a **multi-objective approach**.
- A **MOLP** problem is formulated with the aim to find the **optimal operation strategies** of the DES, which maximize the **operator's profit** and minimize the **net CO_2 emissions**.
- Testing results show that **several trade-off points for economy and CO_2 emissions** can be found on the **Pareto frontier**.
- The **economic/environmental performances of the DES** with optimized operation are **much better** than those found for the **current operation strategies**.
- The **Italian WC incentive scheme** allows to **improve both the economic and environmental performances** of the DES.

Teleriscaldamento attivo e solar district heating: la situazione in Europa e in Italia

A che punto siamo sulle reti di teleriscaldamento attivo? Un'analisi su aspetti tecnici e regolatori, considerando il rapporto tra l'utility e il prosumer

di B. Di Pietra, M. Borasio, M. Caldera, G. Puglisi, F. Zanghirella, S. Caruso*

UN SIGNIFICATIVO CONTRIBUTO al raggiungimento degli obiettivi fissati dalle politiche energetiche e ambientali potrebbe arrivare dalla riduzione della quota di combustibili fossili largamente utilizzati nelle centrali termiche collegate alle reti di teleriscaldamento, promuovendo l'integrazione con fonti rinnovabili, con benefici anche in termini di migliore utilizzazione e di maggiore resa annuale degli impianti FER. Secondo i dati AIRU (AIRU, 2017), gli impianti FER allacciati a reti di TLR in Italia hanno registrato una notevole crescita: bioenergie, 623 MW_t, geotermia, 135 MW_t, pompe di calore, 47 MW_t, recupero di calore da processi industriali, 41 MW_t, e recentemente anche solare termico, 1 MW_t a Varese.

Nonostante la modesta potenza installata, il solare termico, ST, è tra le fonti di energia più promettenti per l'integrazione nelle reti TLR esistenti, i Solar District Heating, SDH. Un impianto solare termico può essere collegato alla rete secondo due differenti modalità, centralizzata e distribuita (Battisti, 2013): negli impianti centralizzati il campo solare è connesso direttamente alla centrale di produzione e spesso è di proprietà della utility che gestisce la rete; un impianto distribuito invece alimenta la rete di teleriscaldamento senza essere direttamente collegato alla centrale termica e spesso la rete è utilizzata anche come accumulo di calore dove poter immettere l'energia termica prodotta in eccesso durante i periodi di basso carico.

In particolare la rete di TLR può essere definita attiva se ad essa sono collegate utenze dotate di impianti di produzione di energia termica in grado di scambiare energia con la rete in modo bidirezionale tramite apposite sottostazioni (dalla rete all'utenza o dall'utenza alla rete). Qui di seguito si intende fare il punto della situazione sulle reti di teleriscaldamento attivo attualmente operanti nel contesto europeo, con particolare riferimento al SDH, prendendo in considerazione aspetti tecnici e regolatori. Lo studio si inserisce nell'ambito delle attività di Ricerca di Sistema Elettrico previste nell'Accordo di Programma ENEA – MiSE.

Aspetti tecnici

Le reti di teleriscaldamento attivo distribuite comportano una modifica della funzione dell'utente da semplice consumatore a prosumer, in grado sia di prelevare che di fornire energia termica alla rete a seconda delle proprie esigenze e della produzione del proprio impianto (Brange et al., 2016). Le reti di TLR attivo possono portare diversi vantaggi al gestore e agli utenti prosumer:

- aumento delle ore/anno di funzionamento degli impianti FER;
- produzione e distribuzione di energia in punti della rete diversi da quelli in cui vi è l'effettivo consumo;
- migliore gestione dell'energia termica in eccesso prodotta dall'impianto FER;
- aumento dell'efficienza e della produzione annua;
- aumento della quota rinnovabile distribuita con il teleriscaldamento;
- eventuale miglioramento della classe energetica degli edifici allacciati.

In linea teorica, la connessione alla rete di TLR degli impianti ST può essere effettuata secondo quattro schemi:

- R/M, prelievo dal ramo di ritorno e immissione nel ramo di mandata;
- M/M, prelievo dal ramo di mandata e immissione nel ramo di mandata;
- R/R, prelievo dal ramo di ritorno e immissione nel ramo di ritorno;
- M/R, prelievo dal ramo di mandata e immissione nel ramo di ritorno;

il confronto tra questi schemi è indicato in Tabella 1, dalla quale si ricava che le configurazioni più diffuse e vantaggiose risultano essere R/M e

R/R. La prima non modifica direttamente la temperatura di ritorno nella rete, aspetto rilevante per l'utility, e garantisce elevati rendimenti del ST; tuttavia, questa soluzione richiede una pompa a portata variabile per reimmettere il fluido termovettore nel ramo di mandata e può inoltre determinare sbilanciamenti idraulici, soprattutto in piccole reti esistenti. La seconda configurazione consente di massimizzare il rendimento e la resa dell'impianto ST, grazie alle minori temperature di funzionamento dei collettori solari, e comporta i minori costi di gestione, tuttavia l'aumento della temperatura sul ramo di ritorno può essere svantaggiosa sia per l'utility sia per gli utenti, che possono risentire delle immissioni di energia termica a monte del proprio collegamento.

La fattibilità economica dello scambio sul posto, net-metering, termico richiede una attenta valutazione dei layout di connessione degli impianti distribuiti alla rete. Inoltre, è necessario considerare l'eventuale convenienza energetica ed economica per l'utente e in particolare i consumi elettrici legati al sistema di pompaggio della sottostazione.

Il teleriscaldamento attivo in Europa

Le prime applicazioni di teleriscaldamento attivo abbinate alle energie rinnovabili sono state realizzate nei Paesi del nord Europa a partire dagli anni '80. Attualmente vi sono più di 200 impianti SDH allacciati alle reti di teleriscaldamento in 11 Stati europei: Danimarca, Svezia, Austria, Germania, Finlandia, Norvegia, Francia, Olanda, Italia, Svizzera e Polonia. La maggior parte di queste realizzazioni sono di tipo centralizzato, tuttavia un numero crescente di impianti ST è collegato alla rete in modalità net-metering; molte informazioni sono disponibili sul sito web www.solar-district-heating.eu.

Nei Paesi in cui sono presenti le principali esperienze di TLR attivo, ovvero Svezia, Austria, Germania e Danimarca, esistono circa 42 impianti ST integrati negli edifici e connessi alla rete. In alcune realtà, tra cui Malmo e Graz, l'energia termica prodotta dagli impianti ST non viene inviata direttamente alla rete principale, bensì a una rete secondaria di bassa pressione che la distribuisce su scala locale e che è collegata alla rete principale tramite scambiatori di calore. Tali reti secondarie agevolano l'allacciamento degli utenti, in quanto possono lavorare a pressioni e temperature minori.

La prima esperienza di teleriscaldamento attivo risale al 1994 presso una scuola pubblica di Skive, in Danimarca (Scafer et al., 2014). Nonostante il ruolo pionieristico nell'ambito del net-metering termico, negli ultimi anni in Danimarca sono stati privilegiati impianti ST centralizzati di grandi dimensioni; per via di queste scelte, attualmente si contano solamente quattro impianti ST collegati alla rete TLR in configurazione di scambio sul posto, aventi dimensioni coincidenti con la superficie delle coperture o delle facciate degli edifici.

La Svezia può contare su uno dei più avanzati sistemi di teleriscaldamento in Europa e su una elevata diffusione di rinnovabili (Werner, 2017). Secondo i dati dell'Associazione per il teleriscaldamento svedese vi sono 30 impianti ST distribuiti connessi alle reti TLR. Nella maggior parte dei casi, gli impianti solari hanno superficie di captazione inferiore a 1000 m² e le reti TLR sono prive di accumulo stagionale. Il quartiere Bo01 di Malmo, riportato in Figura 1, è un esempio di riqualificazione urbana avente l'obiettivo di creare un'area residenziale in grado di coprire il fabbisogno termico ed elettrico utilizzando esclusivamente fonti rinnovabili. Nella rete di Malmo Bo01 i nove impianti ST distribuiti integrati in copertura agli edifici sono di proprietà dell'utility che li gestisce, la E.ON Svezia.

In Austria quasi tutti gli impianti di TLR attivo si trovano nella città di Graz, mentre in Germania si contano tre impianti di TLR attivo, di cui due a Pirna e uno ad Amburgo.

Aspetti economici e regolatori

In Svezia la diffusione del teleriscaldamento attivo ha indotto i gestori delle reti a redigere appositi contratti di scambio sul posto, nei quali vengono stabilite regole tecniche ed economiche stipulate con i prosumer (Werner, 2017). Nella maggior parte dei casi il proprietario dell'impianto solare termico è il singolo utente o un consorzio costituito dai proprietari degli edifici su cui sono installati i collettori solari. Tali soggetti si fanno carico dell'investimento necessario per l'allacciamento alla rete (sottostazione inclusa). I principali termini contrattuali riguardano la tipologia di allacciamento della sottostazione alla rete, i limiti di temperatura e pressione per l'immissione in rete, il periodo di funzionamento in scambio sul posto, la periodicità e la responsabilità della manutenzione, le tariffe dell'energia termica acquistata e ceduta, la periodicità della misura e dei pagamenti, la durata del contratto e l'eventuale diritto dell'utility di trasferire il contratto a una società terza. Ad esempio, nel caso dell'impianto di Gardesten a Goteborg sono applicati prezzi di cessione variabili con la stagionalità, maggiori nel periodo invernale, intermedi nelle mezze stagioni, minori nei mesi estivi, mentre a Molkom l'utente può cedere l'energia termica in eccesso a un prezzo pari al 50% del prezzo di acquisto, che nel 2016 era intorno a 70 €/MWh [1]. Per quanto riguarda l'impianto di

🇬🇧

ACTIVE DISTRICT HEATING AND SOLAR DISTRICT HEATING: AN OVERVIEW IN EUROPE AND ITALY

The reduction of the fossil fuels largely used in central heating plants feeding district heating networks can make a significant contribution to the achievement of the goals set by the energy and environmental policies. A possible option may be to promote the integration of renewable energy sources into the existing district heating networks, which may also lead to an improved yield of RES systems if compared to a stand-alone configuration. Despite its marginal diffusion, solar district heating (SDH) may play an important role for improving the efficiency of existing district heating systems. This study aims at reviewing the situation of active district heating systems currently operative in Europe, with a special focus on SDH, basing on technical and regulatory aspects between the utility and the prosumer. The analysis of the European experiences shows that different approaches have been adopted with interesting results, above all when the network has been designed for an active operation and on site exchange. As regards the Italian context, it shows a good potential also thanks to the Legislative decree 102/2014 that has introduced national rules and has set the basis for the development of efficient district heating networks.

Keywords: **active district heating, prosumer, solar district heating**

Figura 1 – Quartiere di Bo01, Malmo Foto: K. Lee

Vaxjo, la produzione dell'impianto ST connesso alla rete in modalità di scambio sul posto, pari a 138 MWh/anno, risulterebbe del 33% superiore alla produzione in configurazione a isola, stimata in 104 MWh/anno (Di Pietra et al, 2014). Il costo totale di questo impianto, pari a 178 mila euro, è stato coperto per il 24% dagli incentivi statali.

In Austria le reti di teleriscaldamento attivo sono generalmente di proprietà delle ESCO, che si fanno carico della realizzazione degli impianti collocati sulle coperture di edifici privati e pubblici, come nel caso UPC-Arena di Graz, della gestione e manutenzione degli impianti, della misura e della vendita dell'energia termica al gestore della rete di TLR e agli utenti allacciati alla rete. Dal canto loro, i proprietari degli edifici godono di tariffe vantaggiose rispetto al prezzo di acquisto di energia termica dalla rete, proporzionali alla quantità di energia termica prodotta dall'impianto solare installato sulla loro proprietà.

La peculiarità della situazione tedesca consiste nella possibilità per gli utenti di "conservare" l'energia termica prodotta in eccesso durante la stagione estiva immettendola nella rete, per poi prelevarla successivamente in caso di bisogno, per cui la rete svolge la funzione di accumulo termico; è previsto un costo per lo stoccaggio. Ad esempio, nella città di Amburgo, la utility E.ON Hanse Warme gestisce il TLR nel distretto est della città e permette l'allacciamento a impianti solari con superficie maggiore di 100 m²; l'energia termica in eccesso può essere immagazzinata per un massimo di otto mesi in appositi serbatoi stagionali interrati oltre a utilizzare la rete stessa come accumulo.

La situazione in Italia

Nonostante siano trascorsi più di vent'anni dalla prima realizzazione di TLR attivo in Danimarca, il teleriscaldamento attivo è ancora assente in Italia. Il quadro nazionale è caratterizzato dalla presenza di reti TLR principalmente nelle regioni centro-settentrionali, con un numero limitato di operatori e una integrazione verticale tra le varie attività.

Al fine di individuare i possibili ostacoli tecnico-gestionali alla diffusione del SDH, è stato sottoposto un questionario ad alcuni operatori delle reti di TLR urbano, i cui risultati sono riportati in (Di Pietra et al., 2014). Dalle risposte è emerso che

allo stato attuale l'applicazione del teleriscaldamento attivo tramite net-metering termico in reti esistenti è ostacolata dalla variabilità delle condizioni di lavoro e dal rischio percepito dai gestori che il recupero termico immesso dai prosumer possa "inquinare" il flusso termico di ritorno in centrale, riducendo l'efficienza dei cogeneratori. In tale contesto, la soluzione preferibile sarebbe una gestione diretta degli impianti ST in configurazione centralizzata.

Tra le condizioni di lavoro delle reti esistenti, la possibilità di connettere un impianto ST dipende dalle temperature di esercizio. Nelle reti ad alta temperatura di mandata, T > 110 °C, la connessione di impianti ST potrebbe essere limitata al preriscaldamento sul ritorno, fattore considerato poco vantaggioso dai gestori della rete. Al contrario, una rete gestita a temperatura medio-bassa, T < 85 °C, consentirebbe la connessione di impianti ST sul ramo di mandata. In base al censimento AIRU, circa il 21% delle reti in esercizio presenterebbe una temperatura di mandata inferiore a 85 °C e, almeno sulla base di questo parametro, potrebbe essere compatibile con l'allacciamento di impianti ST.

A livello regolatorio, per molto tempo in Italia il quadro è stato frammentato. Recentemente, il D.Lgs. 102/2014 (Parlamento Italiano, 2014) ha introdotto una regolamentazione a livello nazionale. In particolare, il decreto attribuisce ad ARERA specifiche funzioni di regolazione e controllo, oltre al compito di individuare le condizioni di riferimento per la connessione alle reti, al fine di favorire l'integrazione di nuove unità di generazione dell'energia termica e il recupero del calore disponibile in ambito locale. Si tratta di un compito chiave per lo sviluppo del settore nel prossimo futuro, che pone le basi legislative favorevoli all'integrazione del solare termico, soprattutto nell'ottica delle reti di teleriscaldamento e teleraffrescamento efficienti, definite come quelle reti che usano, in

alternativa, almeno:
a) il 50% di energia derivante da fonti rinnovabili;
b) il 50% di calore di scarto;
c) il 75% di calore cogenerato;
d) il 50% di una combinazione delle precedenti.

Conclusioni

Lo studio ha evidenziato come nei vari Paesi europei siano state adottate soluzioni gestionali e regolatorie differenti che tuttavia hanno portato a risultati interessanti, soprattutto qualora la rete sia stata progettata sin dall'inizio per essere compatibile con l'allacciamento di utenze in modalità di scambio termico bidirezionale.

Un impianto con net-metering termico può essere in grado di garantire, soprattutto in presenza di incentivi statali, un costo dell'energia termica prodotta confrontabile con il prezzo di acquisto dalla rete.

Il settore del TLR in Italia presenta ancora margini di sviluppo. In tale contesto, il D.Lgs. 102/2014 ha introdotto una regolamentazione a livello nazionale che influenzerà lo sviluppo del settore nel prossimo futuro, soprattutto nell'ottica delle reti di teleriscaldamento e teleraffrescamento efficienti. ■

* *Biagio Di Pietra, Matteo Caldera, Giovanni Puglisi e Fabio Zanghirella,* ENEA, Unità Tecnica Efficienza Energetica *Marcello Borasio e Sebastiano Caruso,* Politecnico di Torino

BIBLIOGRAFIA
• AIRU. 2017. Annuario 2017. Il riscaldamento urbano. Milano: Associazione Italiana Riscaldamento Urbano (AIRU), dicembre 2017.
• Riccardo Battisti, 2013. Impianti solari termici per reti di teleriscaldamento, Dario Flaccovio Editore, Luglio 2013
• Brange L., Englund J., Lauenburg P. 2016. Prosumers in district heating networks – a Swedish case study, Applied Energy, 164, 492-500.
• Lennermo G., Lauenburg P. 2016. Feed-in from distributed solar thermal plants in district heating systems. Proceedings of 4th International Solar District Heating Conference, 21-22 September, Denmark.
• Schafer K., Schlegel B.F., Pauschinger T. 2014. Decentralized feed-in of solar heat into district heating net-works – a technical analysis of realized plants. Proceedings of 2nd Internationsl SDH Conference, 3-4 June, Germany.
• Werner S. 2017. District heating and cooling in Sweden. Energy, 126, 419-429.
• Di Pietra B., Pannicelli A., Puglisi G., Zanghirella F., "Sviluppo dei modelli per l'analisi energetica del servizio di scambio sul posto termico applicato alle reti di teleriscaldamento in presenza di impianti solari distribuiti", Report Rds/PAR2013/054, ENEA, 2014.
• Parlamento Italiano. 2014. Attuazione della direttiva 2012/27/UE sull'efficienza energetica, che modifica le direttive 2009/125/CE e 2010/30/UE e abroga le direttive 2004/8/CE e 2006/32/CE. D.Lgs. 4 luglio 2014, n.102. GU Serie Generale n.165 del 18.07.2014.

WEBGRAFIA
[1] Swedish District Heating Association, [online], http://www.svenskfjarrvarme.se/In-English/District-Heating-in-Sweden/ (in svedese)

Green roofs and green façades for improving sustainability of towns

C. Bibbiani[1,a], A. Campiotti[2], G. Giagnacovo[2], L. Incrocci[3], A. Pardossi[3], A. Latini[2], E. Schettini[4] and G. Vox[4]

[1]Dept. of Veterinary Science, University of Pisa, Italy; [2]ENEA - Italian National Agency for New Technologies, Energy and Sustainable Economic Development, Rome, Italy; [3]Dept. of Agriculture, Food and Environment, University of Pisa, Italy; [4]Dept. of Agricultural and Environmental Science, University of Bari, Italy.

Abstract

Nowadays, buildings in Europe account for a consumption of 40% of total energy use and about 65% of total electricity consumption. According to the European Directive on the energy performance of buildings (EPBD Directive), solutions such as green roofs and green walls can help to reduce energy consumptions and the greenhouse gases emissions by buildings. The installation of plant systems covering some surfaces of the building allows to reach an improvement of the building's energy efficiency mainly by reducing the energy demand for cooling in warm periods. The green layers used for buildings contribute to improve thermal insulation, since they reduce the direct solar radiation while the evaporative cooling contributes to create a better local microclimate. This paper provides the first data collected by a green wall prototype in progress at ENEA Casaccia Centre to investigate the effects of this natural green solution on the energy efficiency of buildings. The project was funded by the Programme Research of Electrical System, and is being carried out in cooperation with the Universities of Pisa, Bari and Viterbo.

Keywords: energy efficiency, green roof, green walls, GRW, green infrastructures, urban ecology

INTRODUCTION

Within the 20-20-20 by 2020 strategy the EU agreed on a threefold set of targets addressing greenhouse gas (GHG) emissions, renewable energies (RES) and energy efficiency (EE). Since buildings are responsible for 40% of energy consumption and 36% of CO_2 emissions in the EU Directive Energy Performance of Buildings (European Commission, 2010) one of the ways to improve energy efficiency in the buildings sector is to promote plant systems like green roof (GRF) and green wall (GRW), mainly in commercial and civil buildings. The use of vegetation contributes to ameliorate the negative thermal effects of conventional building since plants of GRW absorb most solar radiation (evapotranspiration, photosynthesis, etc.) releasing water vapour which increases the air humidity and decreases the air temperature. GRWs are also in tune with the Directive on the energy performance of buildings which outlines that GI (green infrastructures) solutions such as green roofs and walls can help reduce GHG emissions on urban areas, and improve the appearance of the cities (European Commission, 2013). In addition, the Covenant of Mayors of European Commission outlined to develop innovative technologies to combat the urban heat island effect (UHI, an elevation of temperature due to the high concentration of heat absorbed and re-irradiated by rooftops and pavements) through green roofs and walls or networks of green spaces as ventilation areas.

GREEN ROOF AND GREEN WALLS

Today, establishing vegetation on rooftops and walls of buildings attracts more and more attention in many cities of the world. Green roofs and walls systems offer a number of benefits, e.g., minimize contaminants from rainwater, reduce potential damages from storm-

water, and contribute to improve environmental quality of urban areas. If widely adopted in the cities, GRW can also reduce the UHI effect and hence greenhouse gas (GHG) emissions, thus contributing significantly to both the sustainability and aesthetical environment of cities (Santamouris, 2014; Schettini et al., 2016).

The selection of native plant species with suitable characteristics as low water demand, speed of growing, disease and pest resistance, transmissivity and reflectivity power, represents another important area of research (Trepanier et al., 2009). Therefore, a number of regulations were established to define standards and guidelines for designing and constructing buildings incorporating of GRF systems (Perini, 2013). Furthermore, this plant technology today is also regarded as an important solution for improving energy efficiency of buildings by reducing energy demand of HVAC systems especially in summer periods (Kumar and Kaushik, 2005). In order to evaluate the capacity of plant species on the variation of cooling load demand in buildings, some authors (Ariaudo et al., 2009; Campiotti et al., 2013; Vox et al., 2017) took into account the density of the plant leaves, defined as "green factor" by the following equation:

$$K_g = (T_s - T_{gw})/(T_s - T_{air}) = 1 - \tau_g \cdot h_e/h_e^*$$

where, τ_g = solar transmission coefficient of the green layer; h_e, h_e^* = surface heat transfer coefficient without and with the green layer; T_{gw} = external surface temperature of the green wall; T_s = external surface temperature of the bare wall; T_{air} = external air temperature.

The K_g factor varies between 0 and 1, the former when no temperature decrease is obtained by the green wall, the latter when T_{gw} is equal to T_{air}. The coefficients τ_g and h_e^* come from test values and therefore the K_g factor can be easily calculated by the reported equation. Many possibilities exist for constructing GRWs, depending on the characteristics of both buildings and local climate. Whenever possible it is advisable to leave a small gap between the wall of the building and the supporting structure in order to maximize the effects of summer cooling and winter insulation (chimney effect). However, for reasons of eco-sustainability, the plant systems should use only raining and/or recycled water distributed by hydroponics closed-loop systems, provided with a biofiltration system to allow to capture, reuse and treat nutrient solutions and water.

Although data on GRWs are available from a number of areas (mainly Germany, France and Italy in Europe, North America and many countries in Asia), most of them are not transferable to specific climatic conditions of other countries. Thus, ENEA has started a project action at the Centre ENEA, located north of Rome (latitude: 42°02'36"N, longitude: 12°18'28"E) (Figure 1). The objective of this project was to start collecting data to define materials, energetic parameters, plant species, and information on construction, maintenance and costs of GRW. The plant grow system is fed by a nutrient solution which is re-circulated from a manifold, and then collected in a gutter where it is filtered and re-circulated to the plants.

Figure 1. Green wall prototype installed at the ENEA Casaccia Centre.

A set of different plant species were grown on the wall, i.e., *Hedera elix, Lonicera holprolifici, Partenocissus quinquefolia, Trachelosperum jasminoides*. The experimental data were collected by means of a data logger (CR10X, Campbell, Logan, UT, USA).

The data were measured at a frequency of 60 s, averaged every 15 min and stored in the data logger, by a pyranometer (CMP6-L, Campbell, Logan, UT, USA) for the solar radiation, and by Rotronic-Hygroclip-S3 sensors for the external air temperature. The temperature of the external plaster surfaces exposed to the solar radiation was measured using thermistors (Tecno.El S.r.l., Rome, Italy).

From the first data, it is strongly evident how the green covering reduces the incidence of solar radiation and the temperature of the building's walls. This is more evident during the warmer periods as shown in Figures 2 and 3.
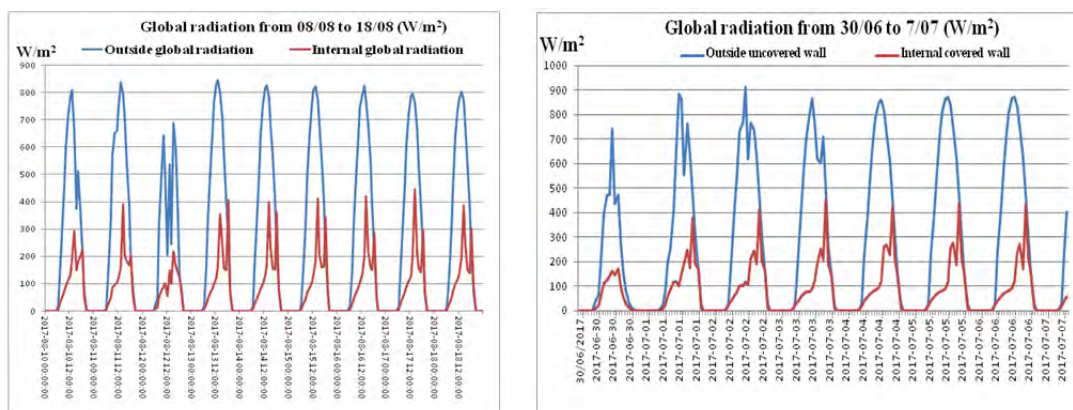
Figure 2. Variation of solar radiation on the wall.
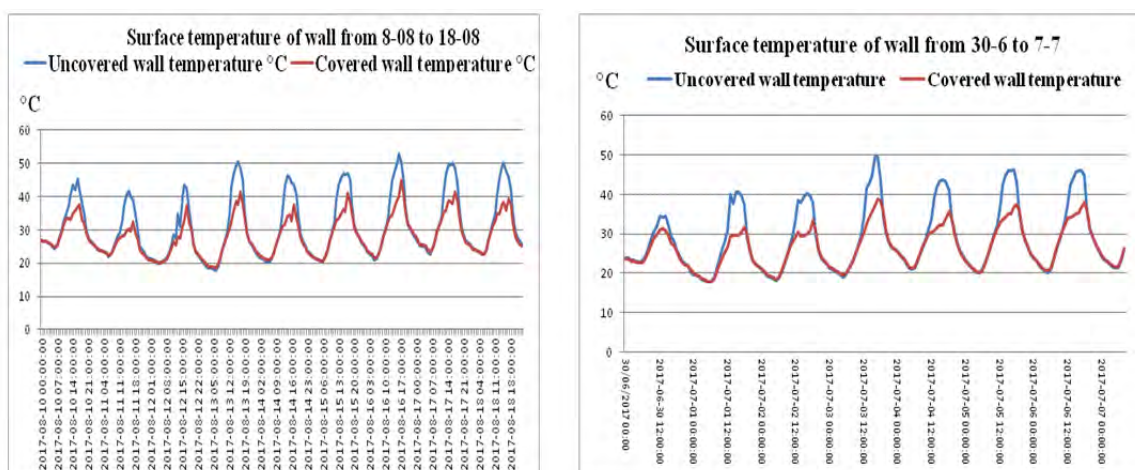
Figure 3. Variation of wall temperature.

RESULTS AND DISCUSSION

The first data collected on the ENEA prototype of a green wall showed a strong reduction of the solar radiation values on the wall shaded with the plants which led to a lower external temperature of the wall in comparison with the wall not covered with the plant system. However, there is still a lack of quantifiable data to definitely account the benefits that the plant system can really provide to the energy efficiency of the test-building.

However, the GRW application represents an entirely new market opportunity for a number of companies, with benefits for the entire economy of cities. On the other hand, this natural solution can identify and encourage synergies between adapting buildings to climate change and mitigating their GHG emissions, recognizing potential for multiple benefits. Governments should encourage GRW systems, especially in densely populated urban areas in order to cut solar heat gain thus reducing the building energy-use in summer, also with benefit for the heat island effect in metropolitan cities. A widespread use of the different

typologies of GRWs can become a part of the actions response to the objectives of both the Kyoto Protocol and the European Energy Efficiency Directive. Furthermore, new building constructions should include systems which use the grey-water coming from the building itself, in order to save the building's potable water use. Features should also include photovoltaic systems to produce the energy needed autonomously.

CONCLUSIONS

Further work at ENEA will focus on the study of energy efficiency performances of both the roof and the walls of buildings provided with vegetated surfaces, in order to allow collection of data to fully explore the mechanisms underlying the energy efficiency potential of plant systems, and to develop a technical guide with the blue lines for the sustainable application of GRWs in cities.

Literature cited

Ariaudo, F., Fracastoro, G.V., and Corgnati, S. (2009). Cooling load reduction by green walls: results from an experimental campaign. Paper presented at: 4th International Building Physics Conference (Istanbul, Turkey).

Campiotti, C.A., Schettini, E., Alonzo, G., Viola, C., Bibbiani, C., Scarascia Mugnozza, G., Blanco, I., and Vox, G. (2013). Building green coverings for a sustainable use of energy. J. Agric. Eng. 44 (S2), 253–256 https://doi.org/10.4081/jae.2013.

European Commission. (2010). Making Our Cities Attractive and Sustainable. How the EU Contributes to Improving the Urban Environment (Publications Office of the European Union), pp.32.

European Commission. (2013). Building a Green Infrastructure for Europe (Publications Office of the European Union).

Kumar, R., and Kaushik, S.C. (2005). Performance evaluation of green roof and shading for thermal protection of buildings. Build. Environ. 40 (11), 1505–1511 https://doi.org/10.1016/j.buildenv.2004.11.015.

Perini, K. (2013). Retrofitting with vegetation recent building heritage applying a design tool—the case study of a school building. Front. Architec. Res. 2 (3), 267–277 https://doi.org/10.1016/j.foar.2013.06.002.

Santamouris, M. (2014). Cooling the cities – a review of reflective and green roof mitigation technologies to fight heat island and improve comfort in urban environments. Sol. Energy 103, 682–703 https://doi.org/10.1016/j.solener.2012.07.003.

Schettini, E., Blanco, I., Campiotti, C.A., Bibbiani, C., Fantozzi, F., and Vox, G. (2016). Green control of microclimate in buildings. Agric. Agric. Sci. Procedia 8, 576–582 https://doi.org/10.1016/j.aaspro.2016.02.078.

Trepanier, M., Boivin, M.A., Lamy, M.B., and Dansereau, B. (2009). Green roof and living walls. Chron. Hortic. 49 (2), 5–7.

Vox, G., Blanco, I., Fuina, S., Campiotti, C.A., Scarascia Mugnozza, G., and Schettini, E. (2017). Evaluation of wall surface temperatures in green façades. Eng. Sustain. 170 (6), 334–344 https://doi.org/10.1680/jensu.16.00019.

Supporting producers in designing more efficient and low-impact green roofs through the Life Cycle Analysis: environmental and energy performance

C. Bibbiani[1,a], F. Fantozzi[2], C. Gargari[2], C.A. Campiotti[3], L. Incrocci[4] and A. Pardossi[4]

[1]Dept. of Veterinary Science, Pisa, Italy; [2]Dept. of Energy, Systems, Territory and Construction Engineering (DESTEC), Pisa, Italy; [3]ENEA - Italian National Agency for New Technologies, Energy and Sustainable Economic Development, Rome, Italy; [4]Dept. of Agriculture Food and Environment, Pisa, Italy.

Abstract

The environmental performance of six green roof solutions currently available on the Italian market has been compared and a lack of information comes out, both on environmental and thermal issues that are necessary to run a consistent and specific assessment. Life Cycle Analysis (LCA) could support producers in designing more efficient and low-impact green roofs, selecting materials based on their environmental profile over their life cycle and taking into account potential reuse of recycle at the end of life. This paper presents an environmental assessment 'cradle to gate', based on a 1-m² functional unit (FU), according to European Standard EN 15804:2012+A1:2013. Five different scenarios, based on different "U-value" limits according to D.M. 26/06/2016, have been defined to run the comparison. Outcomes are expressed in parameters describing environmental impact and resources use. The results show that, despite a large interest in green roofs, currently considered to be a sustainable and energy saving solution for both cold and warm climate, no specific information and data are in fact available for designers and LCA practitioners to assess the environmental and energy performance accurately. Moreover, the insulation layer is the primary responsible for both the energy and environmental performance of the green roof and therefore, taking into account the LCA profile of the insulation material during the design stage is a crucial step to guarantee a low-impact building. Moreover, the new vegetative substrates available on the market are generally presented as more sustainable when, in fact, LCA quarrels with that. Therefore, a comparison between 7 different media currently available on the market has been carried out; results have been significantly affected by a large lack of specific LCI data.

Keywords: green roof, soil medium LCA, energy saving, thermal insulation, impact indicator

INTRODUCTION

Green roofs and walls are considered to be a valuable design solution in the urban context to mitigate the heat island effect, to reduce noise and pollution and to improve the rainwater management and increase air, water quality and biodiversity (Wong et al., 2003). But considering the net zero energy building – Net ZEB concept, introduced by the EPBD recast Directive 2010/31/UE, energy saving, renewable energy sources and other strategies usually adopted to lower the building energy consumption and limit greenhouse emissions are not sufficient from now on. The energy used by the building during its life is combined by energy in production, energy in transportation to the building site, energy in use (for heating, cooling, lighting), energy for building maintenance, and, at the end, energy for demolition. Energy in use in buildings in the Mediterranean area, dating back to the 1950s and 1960s, represents 70-90% of total energy, while 10-30% refers to building material extraction, process and production and 1% only to end of life processing (Sartori and Hestnes, 2007; Campiotti et al., 2013).

---

[a]E-mail: carlo.bibbiani@unipi.it

Net ZEB buildings, in fact, will have a near zero energy consumption in use but an increasing embodied energy in materials and technologies (Beccali et al., 2013). Therefore, assessing the energy and environmental performance of the building, throughout its full life cycle, including production, construction and end of life, and not just the use phase, becomes more and more relevant to assure a consistent evaluation. Thus, the sustainability certification and labeling for building materials becomes an urgent market request to that any conformity label includes quantified, replicable, comparable and harmonized environmental indicators (Gargari et al., 2016).

Standard EN15804:2013+A1 'Sustainability of construction works, Environmental product declarations, Core rules for the product category of construction products', defines the Product Category Rules (PCR) to draw up a Type III Environmental Product Declaration (EPD), according to ISO 14020 and ISO 14025. Such an EPD provides to the user quantified environmental information about a building product or service, that has been assessed in conformity to a harmonized and scientific method. A Product EPD is the primary source of data to perform an environmental assessment of a building. EPD also provides information about emissions to indoor air, soil and water during the use of the building, that can be potentially dangerous for human health.

MATERIALS AND METHODS

The aim of this research is to improve the quality and consistency of environmental information about green roofs, currently available for designers. The LCA assessment result allows a clear comparisons of the environmental impacts and use of resource of 6 different green roof types on a standard clay block slab, as a function of the growing medium.

Six different intensive or extensive roof types have been designed based on 4 performing layers:
- a vegetative layer or medium where the specific sedum is planted;
- a separating root inhibitor layer;
- a drain and insulating EPS layer;
- a waterproofing layer.

The root inhibitor membrane has a 1126 kg m^{-3} density, the EPS has 25 kg m^{-3} density, the waterproofing layer is a 5 kg m^{-2} bituminous membrane.

The medium used in the different scenarios has been selected from the ones currently available on the European market:
- TYPE a: made of 75% pumice, 15% lapillus, 10% compost;
- TYPE b: made of 20% pumice, 63% lapillus, 2% compost, 1% zeolite, 14% peat;
- TYPE c: made of 10% pumice, 80% recycled bricks, 8% peat, 2% grass;
- TYPE d: made of 25% pumice, 60% lapillus, 15% compost;
- TYPE e: made of 20% pumice, 80% compost;
- TYPE f: made of 25% pumice, 60% lapillus, 15% peat;
- TYPE g: made of 45% coconut fibre, 25% expanded perlite, 15% pumice, 15% gravel.

Moreover, considering that green roofs contribute to the environmental and energy performance of a building both in warm and cold climates, 5 different insulation scenarios have been designed for each of the 6 green roof types, when EPS layer thickness varies in order to relate the thermal performance to the environmental one.

Scenarios have been designed in order to satisfy the minimum thermal requirements for roofs as defined by the Italian Energy Regulation DM 26/06/15. The Life Cycle Assessment has been carried out in compliance with the modular approach as defined by the European standard EN 15804:2012+A1:2013. The LCA analysis covered the production stage A only, therefore is a so called cradle to gate assessment.

The assessment has been carried out using the software GaBi® and secondary data have been selected from the GaBi® database.

System boundary

Impacts over the life cycle of the green roof have been calculated taking into account flows entering and exiting the system during the manufacturing process as detailed below:

- A1, raw material extraction and processing, processing of secondary material input (e.g., recycling processes),
- A2, transport to the manufacturer,
- A3, manufacturing,

including provision of all materials, products and energy, as well as waste processing up to the end-of waste state or disposal of final residues during the product stage.

Modules A1, A2 and A3 are declared as one aggregated module A1-3.

The reference service life or durability of a the green roof, when properly maintained, is the same as the service life of the roof layer it is installed on.

LCA scenario and additional technical information

In order to refer the environmental performance of the green roof to the minimum energy performance required for roofs by DM 26/06/15, five different usage scenarios have been defined varying the thermal transmittance property of the roof layer, referring to values as in Table 2 Appendix A DM 26/06/15.

Thickness of the EPS insulation layer has been calculated assuming the green roof is installed over a 16+4 cm clay block slab: increasing thickness from 8 (default) -9-12-14 to 16 cm, the U-value decreases respectively from 0.33-0.31-0.24-0.21 to 0,18 W m^{-2} $°K^{-1}$, considering a ±5% tolerance. The functional unit has been defined as 1 m^2, including medium, the separating root inhibitor layer, the drain and insulating EPS layer and the waterproofing layer. Sedum is excluded as non-relevant and the slab as other indoor layers (additional insulation or plaster) as invariant.

Green roof assessment

The environmental core impacts have been calculated according to EN15804:2012+A1:2013 and are detailed in Table 1.

Table 1. Comparison between LCA core impact categories of the 6 different green roofs solutions (default scenario) 1 m^2 FU.

Impact category	Extensive HD type 1 medium a	Extensive LD type 2 medium b	Intensive recycled type 3 medium c	Intensive HD type 4 medium d+e	Extensive HD type 5 medium f	Extensive renewable type 6 medium g
Density	76 kg m^{-2}	46 kg m^{-2}	118 kg m^{-2}	81 kg m^{-2}	82 kg m^{-2}	114 kg m^{-2}
Abiotic depletion (ADP elements) (kg Sb-Equiv.)	1.97E-005	2.20E-005	2.99E-005	1.96E-005	1.96E-005	1.96E-005
Abiotic depletion (ADP fossil) (MJ)	1.51E+003	1.56E+003	1.64E+003	1.51E+003	1.61E+003	1.51E+003
Acidification potential (AP) (kg SO_2-Equiv.)	1.16E-001	1.03E-001	1.19E-001	1.74E-001	1.02E-001	1.01E-001
Eutrophication potential (EP) (kg Phosphate-Equiv.)	1.33E-002	9.83E-003	1.70E-002	2.89E-002	9.76E-003	9.39E-003
Global warming potential (GWP 100 y) (kg CO_2-Equiv.)	5.45E+001	4.88E+001	4.37E+001	8.33E+001	4.83E+001	4.81E+001
Ozone layer depletion potential (ODP, steady state) (kg R11-Equiv.)	3.21E-009	3.18E-009	3.77E-009	3.18E-009	3.18E-009	3.18E-009
Photochem. Ozone creation potential (POCP) (kg Ethene-Equiv.)	2,63E-001	2,63E-001	2,64E-001	2,66E-001	2,63E-001	2,62E-001

RESULTS AND DISCUSSION

For almost all roof types, impact categories as well as resource use and emission to air are caused by the production of EPS. Therefore, increasing the thickness of the insulation layer form the default scenario of 8 to 16 cm, leads to an evident and obvious aggravation of impacts. But values of impact categories in other U-value scenarios increase not proportionally to the decrease of thermal transmittance. Relationship between U-value and impact categories values when the reference U-value changes are the same for all green roof types and are generically represented by Type 1 medium values, as in Table 2.

Table 2. Impact categories for the 5 different U-value scenarios 1 m² FU – green roof Type 1.

Green roof Type 1	8 cm	9 cm	12 cm	14 cm	16 cm
U value W °K^{-1} m^{-2}	0.33	0.31	0.24	0.21	0.18
Abiotic depletion (ADP elements) (kg Sb-Equiv.)	1.97E-05	2.16E-05	2.60E-05	2.92E-05	3.24E-05
Abiotic depletion (ADP fossil) (MJ)	1.51E+03	1.72E+03	2.20E+03	2.54E+03	2.89E+03
Acidification potential (AP) (kg SO$_2$-Equiv.)	1.16E-01	1.29E-01	1.61E-01	1.84E-01	2.07E-01
Eutrophication potential (EP) (kg phosphate-Equiv.)	1.33E-02	1.45E-02	1.75E-02	1.96E-02	2.17E-02
Global warming potential (GWP 100 y) (kg CO$_2$-Equiv.)	5.45E+01	6.14E+01	7.75E+01	8.89E+01	1.00E+02
Ozone layer depletion potential (ODP, steady state) (kg R11-Equiv.)	3.21E-09	3.63E-09	4.63E-09	5.34E-09	6.05E-09
Photochem. ozone creation potential (POCP) (kg Ethene-Equiv.)	2.63E-01	3.02E-01	3.94E-01	4.59E-01	5.24E-01

The LCA comparison of the 7 medium layers has been carried out based on the declared unit 1 m², thickness 1 cm (Figure 1). In general terms, damage categories that mostly contribute to the medium environmental impacts are abiotic depletion (ADP fossil), global warming potential (GWP 100 y) and acidification potential (AP).

Then, it becomes relevant for designers to analyse elements that, in any of the different medium, causes high values of these impact categories in order to combine a proper mix that satisfies technical performance requirements for green roof, minimizing, at the same time, its environmental impact.

Primary energy consumption (Figure 2) are extremely high in media "c", "f", "g". Supposing that the high energy use from non-renewable sources in medium "c" is due to the crushing of recycled bricks, in medium "f" it is caused by peat extraction and in medium "g" by perlite production. It has to be noted that the % of primary energy from renewable resources used in medium "c" represents the local scenario of the energetic mix used in the assessment.
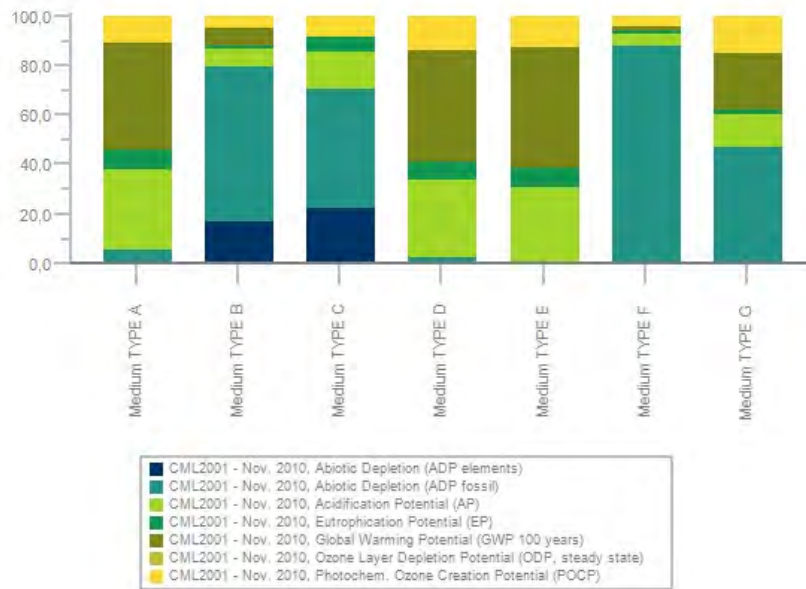
Figure 1. LCA comparison of 7 media.
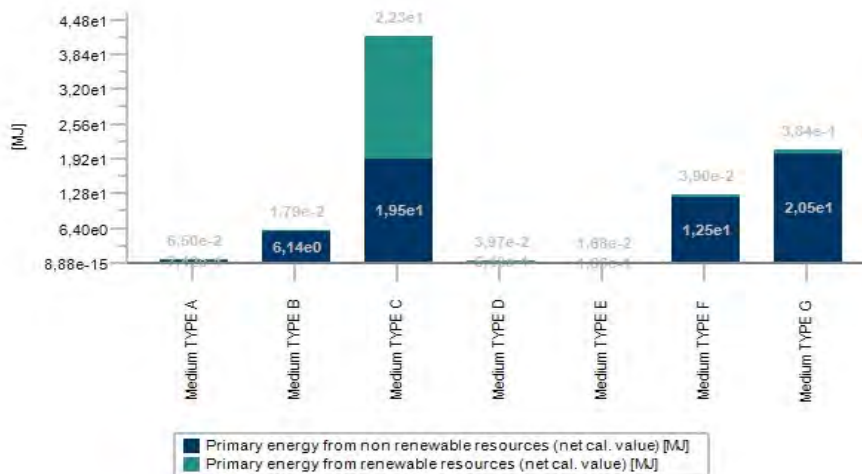
Figure 2. Primary energy use for the 7 different media.

CONCLUSIONS

A preliminary investigation on availability of both generic and specific environmental information about materials and components for green roofing has confirmed a severe lack of data, pointed out by previous researches again and again (Gargari et al., 2016).

Despite several new studies on environmental impacts of green roofs having been published recently and the first EPD of an extensive green roof has been verified and certified in May 2016 (KANUF, 2016), specific characteristics of vegetative substrate layers and its environmental and energy performances are still barely available.

Many of the national end European companies producing green roofs promote original mixes based on pumice, peat, lapillus together with new and innovative materials as vegetal fibres, recycled elements, water absorbing particulates.

Such components are promoted and recommended because of their sustainability, water absorption and retention and release of nutrients to plants, but any detailed information about their specific chemical composition (mixes are almost secret company

recipes) as well as any data referring to thermal performance under different humidity conditions are totally missing.

Therefore, from one hand the scientific research moves forward to demonstrate how much green roofs contribute to improve indoor comfort in buildings (and, more generally, environmental quality in urban spaces) and reduce energy consumption, from the other hand it has not yet performed a consistent evaluation of technical parameters needed to calculate U-value and thermal capacity values of these substrates in use.

Density, thermal conductibility, and specific heat values of the medium mixes are hard to be found in literature or in technical and commercial documentation, especially when related to different humidity values or as a function of the RSL.

Then, it is pretty much complicated for designers to calculate thermo-hygrometric performances of a building with a green roof with a good level of accuracy. A tight cooperation between research and industry is then needed to calculate, using accurate tools, performances of green roofs in use and, at the same time, monitoring and comparing results with data from a real 1:1 scale model.

Environmental specific data of substrates come to light because of the cooperation, can be collected and organized in a life cycle inventory database, supporting LCA studies on green roofs.

Furthermore, it is important to point out that a complete LCA, according to more recent PEF indication, must include other life cycle stages as end of life and recycle at least but, talking about green roof, the use stage should have a certain importance due to the large use of irrigation water, especially in warm/hot climate. Moreover, the use of fertilizers to feed plants has to be considered, together with a potential reuse or recycle of any of the different layers at the end of life.

Literature cited

Beccali, M., Cellura, M., Fontana, M., Longo, S., and Mistretta, M. (2013). Energy retrofit of a single-family house: life cycle net energy saving and environmental benefits. Renew. Sustain. Energy Rev. *27*, 283–293 https://doi.org/10.1016/j.rser.2013.05.040.

Campiotti, C.A., Alonzo, G., and Ardeleanu, M.P. (2013). Energy challenge and agriculture in Italy. Quality - Access to Success *14 (1)*, 18–22.

Gargari, C., Bibbiani, C., Fantozzi, F., and Campiotti, C.A. (2016). Environmental impact of green roofing: the contribute of a green roof to the sustainable use of natural resources in a life cycle approach. Agric. Agric. Sci. Procedia *8*, 646–656 https://doi.org/10.1016/j.aaspro.2016.02.087.

Sartori, I., and Hestnes, A.G. (2007). Energy use in the life cycle of conventional and low energy buildings: A review article. Energy Build. *39* (*3*), 249–257 https://doi.org/10.1016/j.enbuild.2006.07.001.

Wong, N.H., Tay, S.F., Wong, R., Ong, C.L., and Sia, A. (2003). Life cycle cost analysis of rooftop gardens in Singapore. Build. Environ. *38* (*3*), 499–509 https://doi.org/10.1016/S0360-1323(02)00131-2.

Sustainable and energy saving urban horticulture on rooftop gardens in Mediterranean climatic conditions

R. Di Bonito[1,a], D. Biagiotti[1,3], G. Giagnacovo[2], C. Viola[2] and C.A. Campiotti[2]

[1]BIOAG-PROBIO, ENEA, 00123 Rome, Italy; [2]UTEE, ENEA, 00123 Rome, Italy; [3]DAFNE, University of Tuscia, 01100 Viterbo, Italy.

Abstract

The aim of this work is the development of sustainable methods for the cultivation of vegetables in a seasonal succession on rooftop gardens, using containers and soilless substrates with addition of organic matter obtained from the recycling of food waste. The experiment was conducted on a terrace in central Italy in substrates of 17 cm depth, with controlled release fertilizer 15N-9P-15K and the following amendments: 5% compost, 5% biochar and 5% compost + 5% biochar. After the harvest the same substrates were used for the fall cultivation of *Cichorium endivia*, followed by *Lactuca sativa* in the spring. The amendment with compost + biochar produced an increase of the size of tomatoes, and biomass of the leafy vegetables. A second experiment evaluated the growth of aromatic species (*Rosmarinus prostratus*, *Salvia officinalis*, *Thymus citriodorus*) in soilless substrate and improvement of the plant growth was detected after amendment with 10% of compost. The evaluation of thermal parameters of installations with aromatic plants presented a decrease of the temperature of the substrates and the space under the structure, in relation to the plant development. The results suggest the feasibility of perennial aromatic plants for green roof installations aimed at mitigation of the indoor temperature in the summer periods.

Keywords: tomato, lettuce, *Lamiaceae*, green roof, soilless substrates, compost, biochar

INTRODUCTION

In 2030 about 60% of the world population is expected to live in the cities (FAO, 2009) and the development of urban and peri-urban agriculture could reduce the food chain and the energy cost for food transportation, improving the diet and increasing the food security. However, the densely populated urban settlements often lack available soils or they are polluted with chemicals from the anthropic activities and not suitable for food production (Manta et al., 2002). The installation of urban gardens on roof tops or paved surfaces could be exploited for vegetable production and several examples are reported (Orsini et al., 2015). Green roofs have gained popularity in the last decades for their environmental benefits as the abatement of pollutants and noise, the management of rainfall, the improvement of biodiversity (ISPRA, 2012). One valuable trait of the green roofs is their ability to reduce the absorption of the radiative heat by the evapotranspiration and shade of plants, with mitigation of the ambient temperature and the heat island effect in the surrounding environment (Wong et al., 2003; Bevilacqua et al., 2016). The aim of this work is the development of sustainable methods for horticultural production on roof tops in Mediterranean climatic conditions. We have evaluated the performance of low weight, low depth soilless substrates, the use of amendment from the re-cycling of food waste locally produced and the re-use of substrates for a seasonal succession of tomato and leafy vegetables. A second aspect of the work was the evaluation of growth parameters of Mediterranean aromatic shrubs (*Lamiaceae* family) in a long term installation. The thermal parameters of an installation with perennial aromatic plants were also evaluated in order to propose their possible use in green roof installations aimed at the mitigation of the temperature.

---

[a]E-mail: rita.dibonito@enea.it

MATERIAL AND METHODS

Substrates and structures

Commercial soilless substrates suitable for horticulture or green roof installations were provided by Perlite Italiana srl, Corsico, MI, Italy. The Agripan C™ was a mix of perlite and coconut fiber, Agrilit 3™ was expanded perlite with particle size of 2-5 mm, pH 6-7 and Agriterram TVS™ was a mix of lapilli, pumice, zeolite, 10% of peat, with particle size of 1-10 mm and pH 6-7. Agriterram TVS™ contained a slow-release fertilizer 16N-24P-12K at the dose of about 1.0 kg m^{-3}. Compost was obtained from food waste of a local cafeteria, at the Laboratory SSPT USER ENEA Casaccia, using a pilot community composter as previously described (Di Bonito et al., 2016). The biochar was obtained at the plant of DTE-SEN ENEA Trisaia, by pyrolysis of almond shells locally produced. The containers and platforms used for the experiments simulated the structure of green roofs and consisted of a wooden frame, containing a rigid support made of modules Drainroof™ (Geoplast, Grantorto, PD, Italy). The modules contained the substrates and had holes for drainage and hills forming an inter-space of 6 cm between the roof concrete and the structure. All the experiments were conducted on a terrace at the 3rd floor of a building in Rome, central Italy (42°04'N; 12°30'E).

Vegetable production

The experiment was conducted in containers of 0.25 m^2 and the substrate Agripan C (15 cm depth) was on the top of a layer of lapilli (2 cm depth). The amendments tested were: compost 5%, biochar 5% and compost 5% + biochar 5%. The substrates were used for a succession of typical horticultural crops: tomato (*Lycopersicon esculentum* 'Pantano'), endivia (*Chycorium endivia*) and lettuce (*Lactuca sativa* 'Romaine' and 'Canasta'). The plants of tomato were transplanted on June 27, 2014 (3 plants container^{-1}) with four replicates for treatment. Controlled release fertilizer (40 g m^{-2} 15N-9P-15K Osmocote) was added and irrigation was provided every other day. The fruits were periodically harvested at the stage of complete ripeness and their size and weight evaluated. After the harvest the plants were removed and endive was transplanted on October 27, 2014 with 4 replicates per treatment without any fertilization or watering. The third crop was lettuce 'Romaine' on May 19, 2015 or 'Canasta' on June 15, 2015 (5 plants treatment^{-1}). Fertilization was applied as described and irrigation provided 3 times week^{-1}. The weight of the leafy part of the plants was evaluated and the results were statistically analyzed by ANOVA using the IBM-SPSS software package.

Growth of aromatic species

The experiment was carried out on platforms of 1.5×3.5 m divided in two symmetric sections by a wooden sect. The substrate was a mix 1/1 (vol/vol) of Agrilit 3 and TVS™ deposed on a filter fabric on the top of the rigid support, with a depth of 17 cm. In one section 10% compost was added, subtracting some volume from the Agrilit 3. On July 11, 2014 six plants of *Rosmarinus officinalis*, four of *Salvia officinalis*, four of *Thymus citriodorus* were transplanted on each section with the same order. Irrigation was provided 3 times week^{-1} from May to September. Since the platform was installed as a long-term experiment, the growth of plants was evaluated by non-destructive methods. For the plants of *Thymus* and *Salvia* with a cylindrical shape, we used the measure of the diameter and circumference while in *Rosmarinus* plants, growing with a shape of a diamond or a polygonal shape, we have evaluated the size of diagonals and sides. The data were used for evaluation of the surface of the substrate covered by the canopy of each plant. The results were statistically analyzed.

Evaluation of thermal parameters

The evaluations were carried out on the platform previously described equipped with thermo-couple sensors connected to a datalogger (Campbell Scientific Inc., USA) recording the temperature of the substrates, the inter-space between the platforms and the roof concrete other than the air temperature. The evaluations were conducted in the summer

period.

RESULTS

Production of vegetables

The results of the harvest of the vegetables are reported in Figures 1 and 2. The amendment with compost and compost + biochar produced an increase in the average size of the tomato fruits, but did not affect the total fresh weight. An increase in fresh weight was reported for all the leafy vegetables planted in the 2nd and 3rd cycle of production in containers with compost and compost + biochar. The increase was statistically significant in the substrates amended with compost + biochar for endive, growing after tomato without additional fertilizer, and for lettuce 'Canasta' growing as the 3rd crop of the cycle. Compost amendment improved the plant growth in soilless substrates used for green roof (Olszewski et al., 2010; Di Bonito et al., 2016) and in this study has shown the best results on leafy vegetables when used in combination with biochar, that did not have a positive effect alone.
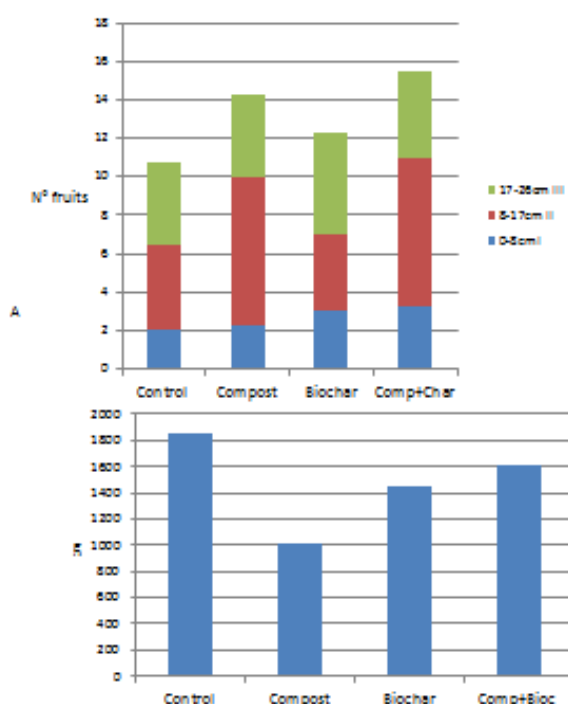
Figure 1. Average size of fruits (A) and fresh weight/plant (B) in tomato.
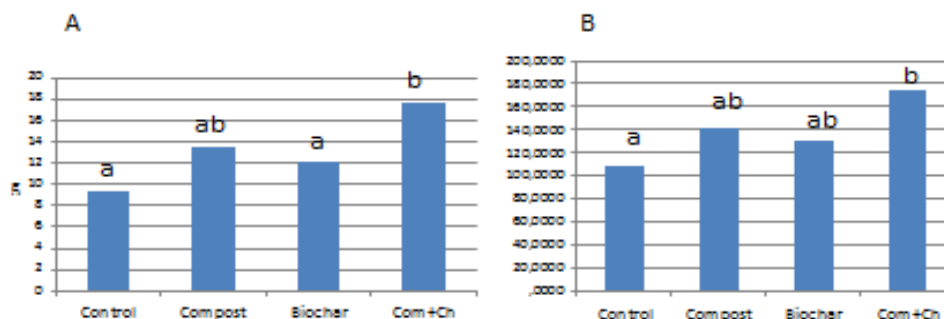
Figure 2. Fresh weight per plant of endive (A) and lettuce 'Canasta' (B). Different letters indicated significantly different means (Duncan's test).

385

Evaluation of aromatic species

The average surface coverage of plants of *Rosmarinus*, *Salvia* and *Thymus* after 18 weeks from the transplant are reported in Figure 3 and show an increase of the surface coverage for all the species with compost amendment, with significant differences for *Salvia*. The average height for the three species were, respectively, 24.5, 21.25 and 17.75 cm and the compost amendment produced an increase not statistically significant (26.33, 22.5 and 18.75 cm, respectively). The total surface covered by the plants with compost amendment represented 97.95% of the available surface, while for the control it was 67.80%. The prostrate growth habit and the ability of the canopy to cover the substrate are valuable traits for the selection of plants adapted to green roofs and several methods are used as the evaluation of leaf area index (LAI), the analysis of images or the empirical evaluation of the areas (Wong et al., 2003; Olszewski et al., 2010; Emilsson, 2008; Di Bonito et al., 2016). In this work we have used an empirical method and the results show a good performance of the three species under the conditions of the study, in accord with the Italian regulation for green roofs installations (UNI 11235, 2015) that requires a coverage of 80% of the substrate from the canopy after one year from the installation.

Evaluation of thermal parameters

After 2 years from the installation, some of the initial plants were dead because of adverse environmental conditions and replaced with similar aromatic plants and *Sedum reflexum* was used to cover the empty spaces. Figures 3 and 4 report the average hourly temperatures for the week July 7-13, 2016 for the platform, after two years from the installation. The visual estimation of the surface coverage from the plant biomass was 90% of the total available surface and the average height was 20 cm. In the hours of higher insulation, the temperatures of the inter-space and the substrate were lower with respect to the air temperature with a difference of the highest values respectively of -4.45 and -6°C. In the installations of green roof the effect of the canopy on the thermal parameters of the green roof and indoor temperature are reported (Wong et al., 2003) and the selection of plants adapted to the local climatic condition is needed (Nagase and Dunnett, 2010). In Mediterranean regions, some studies have been conducted to test the feasibility of cultivated or indigenous species in green roof installations (Caneva et al., 2015; Giagnacovo et al., 2014).
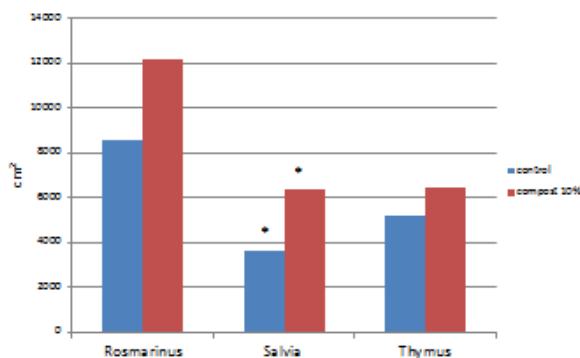
Figure 3. Average surface coverage of aromatic plants after 18 weeks from transplant. * means statistically different according to the Independent T-test (P=0.05).
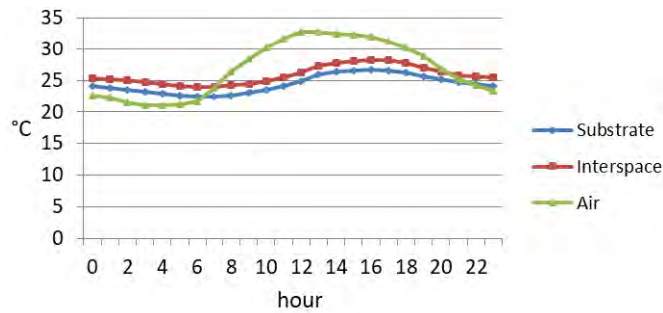
Figure 4. Average hourly temperatures detected in the platform with aromatic species in the week July 7-13, 2016.

CONCLUSIONS

The rooftops are useful surfaces for growing edible plants in urban settlements. In a Mediterranean climatic area three cycles year^{-1} of vegetables were grown in a shallow soilless substrate and perennial installations with aromatic shrubs of *Lamiaceae* were obtained. The amendment with compost or compost + biochar obtained from local food waste has improved the plant growth and represents a sustainable way to reduce the use of fertilizers and close the loop of the food chain in the urban agriculture. The aromatic perennial species used presented a prostrate growth and reduced height under the conditions of the study and resulted in good candidates for installation aimed at the mitigation of the temperature other than for the exploitation of their officinal properties.

Literature cited

Bevilacqua, P., Mazzeo, D., Bruno, R., and Arcuri, N. (2016). Experimental investigation of thermal performances of an extensive green roof in the Mediterranean area. Energy Build. *122*, 63–79 https://doi.org/10.1016/j.enbuild.2016.03.062.

Caneva, G., Kumbaric, A., Savo, V., and Casalini, R. (2015). Ecological approach in selecting extensive green roof plants: A data set of Mediterranean plants. Plant Biosyst. *149* (*2*), 374–383 https://doi.org/10.1080/11263504.2013.819819.

Di Bonito, R., Biagiotti, D., Giagnacovo, G., Canditelli, M., and Campiotti, C.A. (2016). Use of compost as amendment for soilless substrates of plants in green roof installations. Acta Hortic. *1146*, 143–148 https://doi.org/10.17660/ActaHortic.2016.1146.19.

Emilsson, T. (2008). Vegetation development on extensive vegetated green roofs: influence of substrate composition, establishment method and species mix. Ecol. Eng. *33* (*3-4*), 265–277 https://doi.org/10.1016/j.ecoleng.2008.05.005.

FAO. (2009). Foods for cities. www.fao.org/fcit

Giagnacovo, G., Biagiotti, D., Di Bonito, R., and Campiotti, C.A. (2014). Selezione di ecotipi spontanei di *Crassulaceae* per la realizzazione tetti verdi in ambiente Mediterraneo. Paper presented at: X Convegno Nazionale sulla Biodiversità (Rome, Italy).

ISPRA. (2012). Verde pensile: prestazioni di sistema e valore ecologico. http://www.isprambiente.gov.it/files/pubblicazioni/manuali-lineeguida/mlg-78.3-2012-verde-pensile.pdf.

Manta, D.S., Angelone, M., Bellanca, A., Neri, R., and Sprovieri, M. (2002). Heavy metals in urban soils: a case study from the city of Palermo (Sicily), Italy. Sci. Total Environ. *300* (*1-3*), 229–243 https://doi.org/10.1016/S0048-9697(02)00273-5. PubMed

Nagase, A., and Dunnett, N. (2010). Drought tolerance in different vegetation types for extensive green roofs: effect of watering and diversity. Landsc. Urban Plan. *97* (*4*), 318–327 https://doi.org/10.1016/j.landurbplan.2010.07.005.

Olszewski, M.W., Holmes, M.H., and Young, C.A. (2010). Assessment of physical properties and stonecrop growth in green roof substrates amended with compost and hydrogel. Horttechnology *20* (*2*), 438–444.

Orsini, F., Dubbeling, M., and Gianquinto, G. (2015). Multifunctional rooftop horticulture: a promising strategy for intensifying horticulture production in cities. Chron. Hortic. *55* (*4*), 12–17.

Wong, N.H., Chen, Y., Ong, C.L., and Sia, A. (2003). Investigation of thermal benefits of rooftop garden in the tropical environment. Build. Environ. *38* (*2*), 261–270 https://doi.org/10.1016/S0360-1323(02)00066-5.

Green walls for building microclimate control

E. Schettini[1,a], C.A. Campiotti[2], G. Scarascia Mugnozza[1], I. Blanco[1] and G. Vox[1]

[1]Department of Agricultural and Environmental Science DISAAT, University of Bari, Bari, Italy; [2]ENEA, Italian National Agency for New Technologies, Energy and Sustainable Economic Development, Technical Unit Energy Efficiency, Rome, Italy.

Abstract

   Green technology can represent a sustainable solution for construction of new buildings and for retrofitting of existing buildings, in order to reduce the energy demands of the cooling systems of buildings, to mitigate the urban heat island and to improve the thermal energy performance of buildings. Green walls can allow the physical shading of the building and promote evapotranspiration in summer and increase the thermal insulation in winter. Three vertical walls, made with perforated bricks, were tested at the University of Bari (Italy): two were covered with evergreen plants (*Pandorea jasminoides variegated* and *Rhyncospermum jasminoides*) while the third wall was kept uncovered and used as control. Several climatic parameters concerning the walls and the ambient conditions were collected during the experimental test. The daylight temperatures observed on the shielded walls during warm days were lower than the respective temperatures of the uncovered wall up to 8.4°C. The night-time temperatures during the cold days for the vegetated walls were higher than the respective temperatures of the control wall up to 3.6°C.

Keywords: urban agriculture, green façades, air-conditioning, energy savings, microclimate, urban heat island

INTRODUCTION

An environmental and sustainable technology to improve the energy efficiency of urban buildings is the implementation of green infrastructures in order to reduce the energy consumption for air conditioning in summertime and to increase the thermal insulation in wintertime. Greening systems have additional benefits such as mitigation of greenhouse gas emission, improving air quality and water management, and reducing noise.

Although there are significant published articles on green infrastructures, most of them generally focus on experimental data at real scale concerning short periods (Pérez et al., 2014, 2011; Vox et al., 2016b; Manso and Castro-Gomes, 2015; Raji et al., 2015; Wong et al., 2010). In summer the efficacy of greenery systems is achieved for all the climatic areas of the world while the performance of the greenery systems is strongly influenced by the climatic conditions in winter (Pérez et al., 2014; Vox et al., 2016a; Schettini et al., 2016).

The aim of this paper is to analyse experimental data for a long period in the Mediterranean region. Summer and winter results are analysed. Two different evergreen climbing plants were tested as green walls at the University of Bari, South Italy. Several climatic parameters concerning the walls equipped with the greenery systems and the ambient conditions were collected for estimating the variations of the walls surface temperature.

MATERIALS AND METHODS

From June 2014 to December 2016, an experimental research was conducted on prototype of walls built at the University of Bari in Valenzano (Bari, Italy), having latitude 41°05'N, longitude 16°53'E, altitude 85 m a.s.l. This area has a Mediterranean climate, characterized by warm and wet winters and calm, hot and dry summers.

Three walls facing south, each characterized by a width of 1.00 m, a height of 1.55 m,

[a]E-mail: evelia.schettini@uniba.it

and a thickness of 0.22 m, were built with perforated bricks joined with mortar. The bricks used (0.20×0.25×0.25 m) have a thermal conductivity λ (UNI EN 1745,2012) equal to 0.282 W m^{-1} K^{-1}, a specific heat capacity C equal to 840 J kg^{-1} K^{-1}, and an average density of the masonry work (including plaster) equal to 695 kg m^{-3}. An iron net was placed as plant supporting structure at a distance of 15 cm from the wall. On the backside of the walls a sealed structure was made to insulate and evaluate the influence of the vegetation layer on the wall. The backside structure was built with sheets of expanded polystyrene, having a thickness of 30 mm and a thermal conductivity of 0.037 W m^{-2} K^{-1}. A shading net was positioned onto the structures to reduce the effect of the incident solar radiation on the sealed structure.

Two different climbing plants, *Pandorea jasminoides variegated* and *Rhyncospermum jasminoides*, were transplanted on June 18, 2014 (Figure 1); a third wall was kept uncovered for control. The plants were irrigated with the drip method.

Figure 1. The three walls at the experimental field of the University of Bari; the right wall is covered with *Rhyncospermum jasminoides*, the central wall with *Pandorea jasminoides variegated* and the left wall is the uncovered control.

Different climatic parameters, such as the solar radiation incident on the vertical surface and the external air temperature, the surface temperature of the wall on the external plaster exposed to the solar radiation, were measured during the test. The external air temperature was measured by a Hygroclip-S3 sensor (Rotronic, Zurich, Switzerland); it was adequately shielded from solar radiation. The temperature of the external plaster surfaces exposed to the solar radiation was measured using thermistors (Tecno.el s.r.l. Formello, Rome, Italy). The solar radiation normal to the walls was measured using a pyranometer (model 8-48, Eppley Laboratory, Newport, RI, USA) in the wavelength range 0.3-3 mm. Data were measured with a frequency of 60 s, averaged every 15 min and stored in a data logger (CR10X, Campbell, Logan, USA).

RESULTS AND DISCUSSION

During 2016, the experimental field was characterized by values of the external air temperature ranging from 0.7 to 39.2°C and by the average yearly value of the cumulative solar radiation of 5129 MJ m^{-2}. The average monthly cumulative solar radiation was equal to 427 MJ m^{-2} and the average monthly value ranged from 177 MJ m^{-2} of January 2016 to 760 MJ m^{-2} of July 2016.

Surface temperature of the external plaster of the three walls exposed to solar radiation fluctuated over the course of the day and over the varying of the seasons. Figures 2 and 3 show the monthly average values of the maximum and minimum daily external air temperature and surface temperature of the external plaster of the three walls during 2016.

74
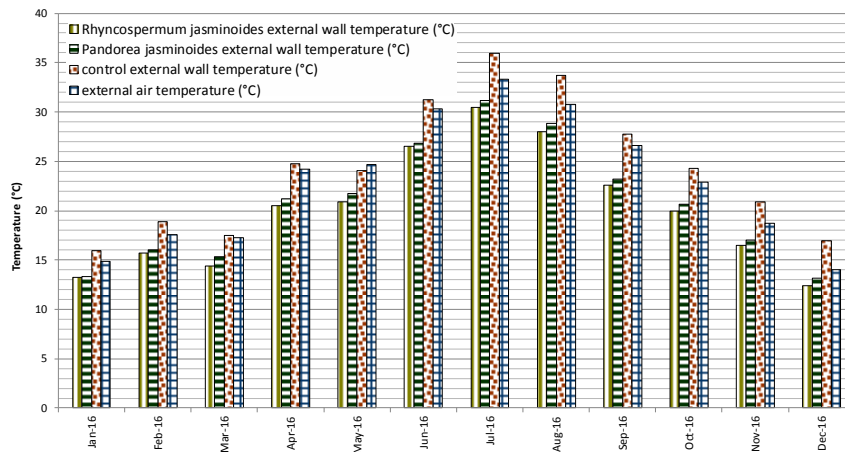
Figure 2. Monthly average values of the maximum daily external air temperature and surface temperature of the external plaster of the three walls exposed to solar radiation.
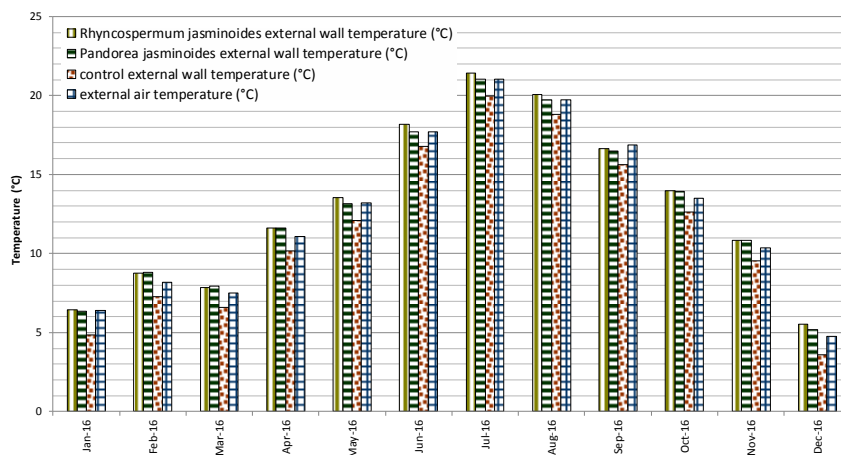
Figure 3. Monthly average values of the minimum daily external air temperature and surface temperature of the external plaster of the three walls exposed to solar radiation.

As shown in Figure 2, the monthly average values of the daily maximum surface temperatures recorded on the control wall were mainly higher than the values recorded on the green walls during all the seasons. This green technology showed its cooling effect during daytime. The higher differences were recorded from July to September. The cooling behaviour is desirable in the warm period. The differences between the average values of the maximum daily temperatures recorded for the control and for the green walls ranged between 2.7 and 5.7°C for the wall covered with *Rhyncospermum jasminoides*, and between 2.1 and 4.8°C for the wall covered with *Pandorea jasminoides variegated*. The daylight temperatures observed on the shielded walls during warm days were lower than the respective temperatures of the uncovered wall up to 8.4°C.

The monthly average values of the daily minimum surface temperatures recorded on the control wall were often lower than the values recorded on the green walls during all the seasons (Figure 3). This green technology showed its heating effect during nighttime, that is desirable in cold period. The differences between the lowest mean temperatures recorded for the wall shielded with plants and the control ranged from 1.0 to 1.9°C for *Rhyncospermum jasminoides*, and from 0.9 to 1.6°C for *Pandorea jasminoides variegated*. The minimum surface temperature of the external plaster protected with the two green walls

closely followed the daily minimum external air temperature. The night time temperatures during the cold days for the vegetated walls were higher than the respective temperatures of the control wall up to 3.6°C.

Future research should be addressed to evaluate throughout the year if and to what extent the resulting decrease in the summer cooling load counterbalances the increase in the winter heating load, if present. Anyway, the presence of the green layer provides the benefit of decreasing the exposure of building envelope to direct solar radiation and to large temperature fluctuations that can cause its early deterioration.

ACKNOWLEDGEMENTS

Literature cited

Manso, M., and Castro-Gomes, J. (2015). Green wall systems: a review of their characteristics. Renew. Sustain. Energy Rev. *41*, 863–871 https://doi.org/10.1016/j.rser.2014.07.203.

Pérez, G., Rincón, L., Vila, A., González, J.M., and Cabeza, L.F. (2011). Green vertical systems for buildings as passive systems for energy savings. Appl. Energy *88* (*12*), 4854–4859 https://doi.org/10.1016/j.apenergy.2011.06.032.

Pérez, G., Coma, J., Martorell, I., and Cabeza, L.F. (2014). Vertical greenery systems (VGS) for energy saving in buildings: a review. Renew. Sustain. Energy Rev. *39*, 139–165 https://doi.org/10.1016/j.rser.2014.07.055.

Raji, B., Tenpierik, M.J., and Van Den Dobbelsteen, A. (2015). The impact of greening systems on building energy performance: a literature review. Renew. Sustain. Energy Rev. *45*, 610–623 https://doi.org/10.1016/j.rser.2015.02.011.

Schettini, E., Blanco, I., Campiotti, C.A., Bibbiani, C., Fantozzi, F., and Vox, G. (2016). Green control of microclimate in buildings. Agric. Agric. Sci. Procedia *8*, 576–582 https://doi.org/10.1016/j.aaspro.2016.02.078.

UNI EN 1745. (2012). Masonry and Masonry Products - Methods for Determining Thermal Properties (UNI - Ente Nazionale Italiano di Unificazione - Italian Organization for Standardization; IT).

Vox, G., Maneta, A., and Schettini, E. (2016a). Evaluation of the radiometric properties of roofing materials for livestock buildings and their effect on the surface temperature. Biosyst. Eng. *144*, 26–37 https://doi.org/10.1016/j.biosystemseng.2016.01.016.

Vox, G., Blanco, I., Fuina, S., Campiotti, C.A., Scarascia Mugnozza, G., and Schettini, E. (2016b). Evaluation of wall surface temperatures in green façades. Proc. Inst. Civil Eng. – Eng. Sust. *170* (*6*), 334–344 https://doi.org/10.1680/jensu.16.00019.

Wong, N.H., Kwang Tan, A.Y., Chen, Y., Sekar, K., Tan, P.Y., Chan, D., Chiang, K., and Wong, N.C. (2010). Thermal evaluation of vertical greenery systems for building walls. Build. Environ. *45* (*3*), 663–672 https://doi.org/10.1016/j.buildenv.2009.08.005.

Le coltri vegetali nel settore residenziale

Il verde è da tempo un elemento di progetto nell'architettura degli edifici e nel decoro urbano delle città, ma il suo utilizzo è stato prevalentemente decorativo. Oggi, le realizzazioni di coltri vegetali sugli edifici vengono considerate veri e propri componenti edilizi che mitigano il microclima delle aree urbane e il comfort interno degli edifici e risultano particolarmente efficaci durante i periodi di caldo intenso poiché le coperture verdi agiscono da strato isolante per le superfici dell'edificio. Per valutare gli effetti delle coltri vegetali, l'ENEA ha avviato la realizzazione di un edificio dimostrativo presso il Centro Ricerche Casaccia. L'attività progettuale intende definire, in termini non soltanto energetici, ma anche biologici, gli effetti microclimatici dell'uso delle coltri vegetali in verticale

di **Carlo Alberto Campiotti, Germina Giagnacovo, Luca Nencini** e **Matteo Scoccianti,** *ENEA;*
Luciano Consorti, *CIRPS - Sapienza Università di Roma;* **Carlo Bibbiani,** *CIRAA - Università di Pisa*

Nelle aree geografiche mediterranee, i consumi di energia elettrica per la climatizzazione estiva di edifici (pubblici, residenziali e commerciali) costituiscono circa il 30% dei consumi complessivi e le previsioni mostrano una tendenza in crescita. In particolare, i consumi energetici medi di un edificio sono stimati in circa 200.000 kJ/m³ per il riscaldamento nel periodo invernale (periodo sotto riscaldato) e in circa 1"0.000 kJ/m³ per la climatizzazione nei periodi estivi (periodo eccessivamente riscaldato).

Gli obiettivi dell'Unione Europea, espressi già con il "Libro verde sull'Efficienza Energetica" nel 2005 e con la Direttiva 2002/91/CE sulle prestazioni energetiche degli edifici *(Energy Performance of Building Directive),* che ha previsto l'estensione della valutazione delle prestazioni energetiche di un edificio anche al regime estivo (come sottolineato dalla sostituzione del concetto di "prestazione termica invernale" con quello più ampio di "prestazione energetica globale"), sono quelli di contenere i consumi energetici sia per il riscaldamento invernale che per la climatizzazione estiva.

Un ulteriore avanzamento nella direzione dell'efficienza energetica sulla climatizzazione degli edifici si è avuto con la Direttiva 2010/31/UE, che prevede che gli edifici costruiti dopo il 31 dicembre 2020 dovranno essere ad energia "quasi zero" (le pubbliche amministrazioni già dal 2018 dovranno attenersi alla costruzione

di edifici ad energia "quasi zero"). Infine, con la Direttiva 2012/27/UE sull'efficienza energetica, recepita dall'Italia con il Decreto legislativo 4 luglio 2014, la Commissione Europea ha stabilito un quadro comune di misure per una strategia a lungo termine per la ristrutturazione degli edifici residenziali e commerciali, sia pubblici che privati.

In questo contesto, l'Unione Europea, ai fini della riduzione dei consumi di riscaldamento e di raffreddamento, con la COM(2013) 249 *final*

"Infrastrutture verdi – Rafforzare il capitale naturale in Europa", ha sottolineato l'importanza per il settore dell'edilizia di soluzioni basate sulle infrastrutture verdi, i.e.: coltri vegetali sugli edifici nelle aree urbane, giardini pensili, corridoi verdi, piantumazioni nelle città di siepi ed alberi, in quanto possono contribuire a migliorare l'efficienza energetica degli edifici oltre che a diminuire le emissioni di gas a effetto serra e la percentuale di particolato nelle città (il settore delle costruzioni è respon-

sabile nell'UE del 36% di emissioni di CO_2).

Su questi obiettivi si collocano il Patto dei Sindaci del 2008 *(The Covenant of Mayors)* e il *Global Covenant of Mayors for Climate* and Energy del 2017, per il Clima e l'Energia, mirati entrambi a sostenere tutte le azioni per accelerare la decarbonizzazione dei territori dell'Unione Europea. Tra gli obiettivi, il sostegno allo sviluppo di piani di azione *(Action plan)* per migliorare la sostenibilità energetica e ambientale dei territori e delle città

e il sostegno alle misure per sensibilizzare gli enti locali, le associazioni e i cittadini sulla necessità di fronteggiare gli effetti del cambiamento climatico quali fenomeni meteorologici estremi i.e.: precipitazioni violente e ondate di calore eccessivo. A supporto di queste misure, l'Italia con la Strategia Energetica Nazionale 2017 (SEN), ha previsto il raggiungimento di obiettivi che integrino ambiente, clima, energia, coerentemente con la COP 21 di Parigi. Tutti i settori sono interessati: trasporti, agricoltura, industria e costruzioni, ma l'apporto maggiore è previsto per il settore degli edifici residenziali.

Le coltri vegetali per migliorare l'efficienza energetica degli edifici

Il verde è da sempre un elemento di progetto nell'architettura degli edifici e nel decoro urbano delle città, ma fino a poco tempo fa il suo utilizzo era soltanto a scopo decorativo. Oggi, invece, le realizzazioni di coltri vegetali sugli edifici, definite tecnicamente *"Green Walls* (GW)" o "Pareti Verdi", vengono considerate nel mondo delle costruzioni un vero e proprio componente edilizio. Gli effetti delle coltri vegetali in termini di mitigazione del microclima che caratterizza le aree urbane e il comfort interno degli edifici risultano particolarmente efficaci durante i periodi di caldo intenso poiché le coperture verdi agiscono da strato isolante per

Tipologia vegetali	CO_2 sequestrata per anno	Bibliografia
Piante erbacee	4,38 kg/m²	Taiz & Zeiger. 2006
Piante arbustive	8,76 kg/m²	Schaefer, Rudd Vala. 2004
Piante rampicanti	6,57 kg/m²	Daniel Roeher, Jon. Laurenz. 2008

Tab. 1 Valori della quantità di CO_2 sequestrata dalle coltri vegetali

le superfici dell'edificio: esse aumentano l'efficacia di isolamento poiché ostacolano l'eccesso di radiazione solare incidente sulla superficie delle costruzioni.

Parte della radiazione solare, inoltre, viene utilizzata dalla pianta come calore latente per sostenere il fenomeno della traspirazione fogliare (la traspirazione di 1000 litri di acqua consente un assorbimento di energia fino a 700 kWh sotto forma di calore latente) e per il processo della fotosintesi clorofilliana. Da sottolineare, inoltre, il contributo delle piante nel sequestrare l'anidride carbonica (CO_2), attraverso il fenomeno della fotosintesi clorofilliana. In Tabella 1, ai fini delle politiche ambientali di riduzione della CO_2, è riportata la quantità di CO_2 mediamente sequestrata per anno dalle diverse tipologie di essenze vegetali utilizzabili per le coltri vegetali sugli edifici [5], [6].

Per valutare gli effetti delle coltri vegetali sugli edifici ai fini del miglioramento dell'efficienza energetica degli edifici, l'ENEA, attraverso il Programma RDS (Ricerca di Siste-

ma Elettrico) del Ministero Sviluppo Economico ha avviato un programma di ricerca e sperimentazione che ha previsto la realizzazione di un edificio dimostrativo presso il Centro Ricerche Casaccia. L'attività progettuale ha l'obiettivo di definire, in termini non soltanto energetici, ma anche biologici, gli effetti microclimatici dell'uso delle coltri vegetali applicate sugli edifici (Figura 1).

I vantaggi in termini di miglioramento dell'efficienza energetica dovuti all'impiego di sistemi vegetali sono valutati in un risparmio dei costi annuali del 3-10% per la riduzione di energia utilizzata per il riscaldamento e dell'8-15% per la riduzione di energia elettrica utilizzata per il raffrescamento degli spazi interni degli edifici. Per valutare l'effetto di schermatura della radiazione solare incidente sulle pareti di un edificio dotato di coltre vegetale, è stato definito l'indice *costante verde* (Kv) [1], [7], calcolato secondo la formula:

Costante verde = $\mathbf{K_v} = \dfrac{(T_{pn} - T_{pp})}{(T_{pn} - T_{ae})}$

da cui $T_{pn} - T_{pp} = K_v (T_{pn} - T_{ae})$;
con:

T_{pp} = Temperatura parete schermata dalla coltre vegetale

T_{pn} = Temperatura parete non schermata dalla coltre vegetale

Fig. 1 Prototipo della parete-verde sull'edificio dimostrativo del Centro Ricerche ENEA Casaccia

**Calcoli sulla valutazione del flusso termico che penetra
all'interno dell'edificio**

Il flusso termico totale (Q_{tot}) trasmesso attraverso una parete a facce piane e parallele, in condizioni di regime stazionario e per unità di superficie, può essere espresso come somma del *contributo convettivo* (Q_1) e del *contributo raggiante* (Q_2). In particolare:

$Q_{tot} = Q_1 + Q_2 = $ *flusso termico totale W/m²;*

avendo esplicitato:

$Q_{\#} = U \, (T_{ae} - T_{ai}); \quad Q_2 = U \left(\dfrac{a \cdot I}{h_e} \right);$ da cui: $Q_{tot} = U \, (T_{ae} - T_{ai}) + U \cdot \left(\dfrac{a \cdot I}{h_e} \right)$

ove:

U = trasmittanza $\left[\dfrac{W}{m^2 K} \right]$; a = assorbimento (UNI TS 11300-1/2014);

a= 0,3 pareti chiare;

a= 0,6 pareti medie;

a= 0,9 pareti scure;

I = irraggiamento [W]; h_e=fattore di adduzione $\left[\dfrac{W}{m^2 K} \right]$.

In presenza di coltre vegetale, si riduce, proporzionalmente al fattore K_v, il flusso termico totale (Q_{tot}), ovvero il contributo raggiante (Q_2) del flusso. Indicando con ΔQ, la variazione di flusso termico che attraversa la coltre vegetale, rispetto alla parete nuda, si può scrivere:

da cui se: $\Delta Q = U \cdot K_v \cdot \left(\dfrac{a \cdot I}{h_e} \right)$

$K_v = 0$ abbiamo $\Delta Q = 0$ *Non vi è effetto di riduzione del flusso termico entrante.*

$K_v = 1$ abbiamo $\Delta Q = U \left(\dfrac{a \cdot I}{h_e} \right)$ *La riduzione del flusso termico entrante è massima.*

In prima approssimazione, come valore massimo ottenibile in fase stazionaria, la riduzione del flusso termico dovuta a una coltre vegetale è pari a circa il 44% del flusso termico entrante nell'edificio.

T_{ae} = Temperatura aria esterna
La costante verde Kv varia tra 0 ed 1 e, in prima approssimazione, se:

- **Kv** vale zero (0), la coltre non esercita alcuna schermatura, pertanto, in condizioni estive, la temperatura della faccia esterna (Tpe), che assorbe completamente la radiazione solare, risulta essere uguale alla (Tpn), ovvero maggiore sia della temperatura dell'aria esterna (Tae) che della temperatura dell'aria interna (Tai);

- **Kv** vale uno (1), la coltre esercita completa schermatura, pertanto, in condizioni estive, la temperatura della faccia esterna (Tpe), risulta essere uguale alla temperatura dell'aria esterna (Tae).

Attraverso le azioni progettuali svolte in collaborazione con le Università di Pisa e Bari sono stati rilevati i seguenti valori nei confronti delle essenze vegetali sotto elencate:

*Pandorea jasminoides "variegata"
(Kv = 0,95)*

*Partenocissus quinquefolia
(Kv = 0,85)*

*Hedera helix
(Kv = 0,83)*

*Lonicera hall prolific
(Kv = 0,81)*

*Rhyncospermum jasminoides
(Kv = 0,81)*

I calcoli sulla valutazione del flusso termico che penetra all'interno dell'edificio sono illustrati nel riquadro a fianco
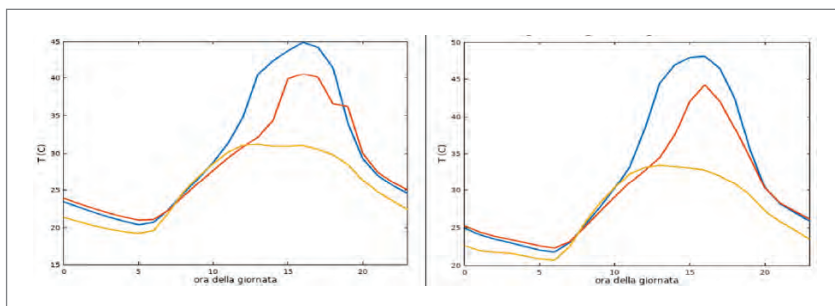
Fig. 2 Dati raccolti sull'edificio dimostrativo del Centro ENEA Casaccia.
Temperatura media della parete Sud Ovest nei mesi di luglio (a sinistra) e agosto (a destra).
Blu: temperatura della zona esposta al sole; Rosso: temperatura della zona protetta dalla coltre verde. **Giallo: temperatura dell'aria**

In accordo con quanto riportato nel riquadro, si è visto che la coltre vegetale riduce, proporzionalmente al fattore Kv, il differenziale del flusso termico entrante nelle pareti dell'edificio, come si evince dalla Figura 2. Sulla base delle valutazioni finora effettuate, il flusso termico puntuale che penetra all'interno dell'edificio, durante le ore di massima insolazione, si riduce, proporzionalmente al fattore Kv, fino al 44%. In particolare, la differenza di temperatura media superficiale nei mesi di luglio e agosto della parete schermata rispetto a quella priva di coltre vegetale negli stessi mesi risulta di circa 7 °C.

Coltri vegetali per migliorare l'efficienza energetica dei sistemi di climatizzazione

Le coltri vegetali risultano di particolare interesse per migliorare l'efficienza energetica dei sistemi di condizionamento soprattutto nei periodi di caldo intenso. In particolare, nei sistemi di condizionamento a compressione diretta, la temperatura di condensazione del gas refrigerante (tcond) è vincolata alla temperatura dell'aria esterna (t1) che li attraversa, pertanto, un aumento della temperatura dell'aria

esterna determina un aumento della temperatura e della pressione di condensazione del gas refrigerante. Viene altresì aumentato il rapporto di compressione (pressione di mandata gas refrigerante/pressione di aspirazione gas refrigerante), e dunque l'assorbimento di potenza elettrica (W). In definitiva, una temperatura dell'aria più elevata provoca una diminuzione della resa frigorifera e quindi un consumo maggiore di elettricità. Le coltri vegetali quando utilizzate a copertura dei sistemi di condizionamento localizzati sui solai esterni, soprattutto quelli impiegati dai supermercati e dagli uffici, contribuiscono a mantenere condizioni inferiori di temperatura dell'aria che circonda le macchine di condiziona-

mento (Figura 4) che, in ultima analisi, migliorano l'efficienza energetica dei sistemi di condizionamento con vantaggi energetici, ambientali ed economici [2], [3].

Conclusioni

L'integrazione diffusa di vegetazione nelle città sostiene lo sviluppo di processi di riqualificazione energetica degli edifici e contribuisce al raggiungimento degli obiettivi previsti dalle diverse Direttive europee sulla efficienza energetica, il risparmio di energia e la protezione dell'ambiente. La presenza di vegetazione sugli edifici scherma la radiazione solare, riduce la temperatura media radiante delle costruzioni e aumenta l'umidità delle aree urbane attraverso il processo dell'evapotraspirazione delle piante. Inoltre, le coltri vegetali filtrano la quota delle polveri inquinanti, incrementano la biodiversità e contribuiscono al riequilibrio del ciclo dell'acqua meteorica e della regimazione dell'afflusso delle acque piovane verso le reti di drenaggio urbano. Vengono riconosciuti anche benefici estetici per gli edifici e psicologici per i cittadini. La costruzione di pareti verdi, in linea generale, si può applicare in aree industriali, centri-semi-periferie delle città,
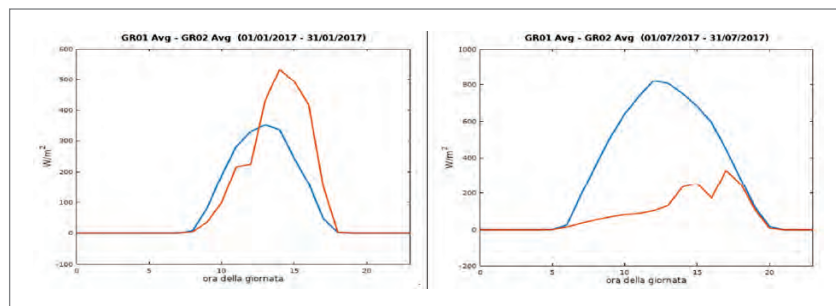
Fig. 3 A sinistra: mese di gennaio; a destra: mese di luglio. Confronto fra le intensità medie della radiazione incidente nel corso della giornata, rilevata dai sensori posti sul tetto dell'edificio *(linea blu)* e sulla parete Sud Ovest *(linea rossa)*
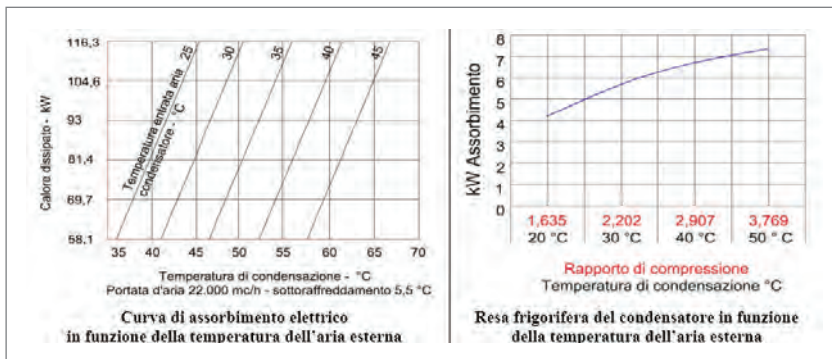
Fig. 4 Influenza della temperatura dell'aria esterna sull'efficienza energetica dei condizionatori

edifici residenziali (quartieri nuovi) e comunali (soprattutto scuole). Lo sviluppo di linee guida per migliorare l'efficienza energetica degli edifici mediante la realizzazione di coltri vegetali disposte in orizzontale e in verticale rappresenta uno degli obiettivi prioritari del progetto in corso presso il Centro Ricerche Casaccia, anche nella prospettiva di sviluppare la progettazione di edifici *future proof* – a prova di futuro – per contrastare il cambiamento climatico. Le azioni di ricerca e sperimentazione sviluppate dal Dipartimento Unità Efficienza Energetica dell'ENEA risultano funzionali anche alla definizione di Piani di sviluppo nazionali, in linea con il position paper dell'Alliance to Save Energy "Energy Efficiency: A Tool for Climate Change Adaptation, in particolare per valorizzare i sistemi vegetali non soltanto in funzione di decoro urbano ma soprattutto come tecnologia naturale capace di migliorare la sostenibilità energetica ed ambientale dei territori, di contrastare i mutamenti climatici e di favorire la maggiore resilienza per le città.

Per saperne di più:
carloalberto.campiotti@enea.it

BIBLIOGRAFIA

1. C.A. Campiotti, E. Schettini, G. Alonzo, C. Viola, C. Bibbiani, G. Scarascia Mugnozza, I. Blanco,2 G. Vox2. Building green covering for a sustainable use of energy. *Journal of Agricultural Engineering* 2013; volume XLIV(s2):e50

2. G. Parolini, Del Monaco A., Fontana D.M., *Fondamenti di Fisica Tecnica.* Ed. Utet, 1983

3. C. Pizzetti, *Condizionamento dell'aria e refrigerazione* voll. 1 e 2. Ed. Ambrosiana, 2012

4. Roeher D., Jon. Laurenz . *Greening the Urban Fabric: Contribution of green surfaces in reducing CO_2 emissions.* LA '08, Algarve, Portugal, June 11-13, 2008

5. Schaefer, V., Rudd, H., Vala, J. 2004. *Urban Biodiversity.* Captus Press, Ontario, 2004

6. Taiz L., Zeiger, E., *Plant Physiology,* Sinauer Associates, Inc, Sunderland, MA, 2006

7. Vox G., I. Blanco, S. Fuina, C.A. Campiotti, G. S. Mugnozza, E. Schettini. Evaluation of wall surface temperatures in green facades. *Proceedings of the Institution of Civil Engineers-Engineering Sustainability.* Volume 170 Issue 6, December 2017, pp. 334-344

GREEN COVERINGS FOR IMPROVING ENERGY EFFICIENCY OF BUILDINGS

Carlo Alberto CAMPIOTTI

PhD.,*"Italian National Agency for New Technology and Sustainable Economic Development"*, Rome, Italy,
carloalberto.campiotti@enea.it

Germina GIAGNACOVO

researcher,*"Italian National Agency for New Technology and Sustainable Economic Development"*, Rome, Italy,
germina.giagnacovo@enea.it

Luca NENCINI

researcher, *"Italian National Agency for New Technology and Sustainable Economic Development"*, Rome, Italy,
luca.nencini@enea.it

Alessandro CAMPIOTTI

student with thesis,*"Italian National Agency for New Technology and Sustainable Economic Development"*, Rome, Italy,
alessandro.campiotti1@gmail.com

ABSTRACT

Nowadays, buildings in Europe account for a consume of 40% of total energy use and about 65% of total electricity consumption. Green Roofs and Walls (GRWs) are in tune with the Directive on the energy performance of buildings which outlines that GI (Green Infrastructures) solutions such as GRWscan help reduce GHG emissions on urban areas, and improve the appearance of the cities. In addition, plant systems covering the building surfaces allow to reach an improvement of the building's energy efficiency. This paper shows the first results achieved at the test building-platform of ENEA Casaccia Centre, in the frame of Programme Research of Electrical System. The general objective of this research is to provide a basis for the development of standards and design of the GRW application for civil and public buildings. Preliminary data showed a strong reduction of the solar radiation values on the wall shaded with the plants which led to a lower temperature of surface wall in comparison with the wall not shaded with the plants layer.

INTRODUCTION

Today, establishing vegetation on rooftops and walls of buildings attracts more and more attention in many cities of the world. Green Roof and Wall (GRW) systems offers a number of benefits e.g.: improve the building's energy efficiency, minimize contaminants from rainwater, reduce potential damages from stormwater, and contribute to improve environmental quality of urban areas, and thus contributing significantly to both the sustainability and aesthetical environment of cities (Santamouris, 2012; Schettini et al., 2016). The use of vegetation contribute to ameliorate the negative thermal effects of conventional building since plants of GRW absorb most solar radiation (evapotranspiration, photosynthesis, etc.) releasing water vapor which increase the air humidity and decreasing the air temperature. The selection of native species with suitable characteristics as low water demand, ogrowing rate, disease and pest resistance, transmissivity and reflectivity power, represents another important area of research (Trepanier et al., 2009). Furthermore, GRWs are also regarded as an important solution for improving energy efficiency of buildings by reducing energy demand of Heating, Ventilation, and Air Conditioning systems especially in summer periods (Wang F. and Yoshida, 2012; Gargari et al., 2016; Campiotti et. al., 2017). Since buildings are responsible for 40% of energy consumption and 36% of CO_2 emissions in the EU Directive about Energy Performance of Buildings (European Union, 2011), GRWs are also in tune with the same Directive which outlines that GI (Green Infrastructures) solutions such as GRWs can help reducing GHG emissions on urban areas, and improve the appearance of the cities (European Commission, 2013). In addition, the Covenant of Mayors of European Commission outlined to develop innovative technologies combating the Urban Heat Island Effect (UHI, an elevation of temperature due to the high concentration of heat absorbed and re-irradiated by rooftops and pavements) through GRWs or networks of green spaces as ventilation areas (Petralli et al., 2006). GRW solutions represent an entirely new market opportunity for a number of companies, with benefits for the entire economic of metropolitan areas. On the other hand, this natural solution can identify and encourage synergies between adapting buildings to climate change and mitigating their GHG emissions, recognising potential for multiple benefits. Governments should encourage people to GRWs construction in order to reduce the building energy use for acclimatization especially in summer since 30% of total electricity consumption in most of the countries of southern areas of Europe are ascribed to building acclimatization.

1. GREEN ROOF AND WALLS (GRW)

Green Roofs and Walls provide a range of energetical and environmental benefits for buildings (Pérez et al., 2014; Gargari et al., 2016) in terms of energy consumption reduction for air conditioning in summer, and thermal insulation increment in winter. They improve aesthetically the liveing and working spaces, remove airborne pollutants and improve air quality, promove and increase biodiversity and contribute to the mitigation of the frequency and magnitude of the heat events due to UHI. Urban heat island is the name given to the worldwide phenomenon of higher air temperature in urban area. Green roofs and vertical systems are passive energy saving systems because they intercept solar radiation by the vegetation layer, provide thermal insulation by means of the vegetation and substrate, induce evaporative cooling by evapotranspiration from the plants and the substrate, and influence the effect of the wind on the building (Perez et al., 2011). The green wall and facades reduce the temperature of the air surrounding the building envelope (i.e., ambient air), by transferring radiant heat to latent vapor via transpiration and by reflecting radiant energy away from the building. Evaporation of 1000 kg of water needs about 700 kWh, and this represents a high value. The amount of

temperature reduction provided by the green facades is directly related both to the amount of leaf area (LAI) present in the canopy and its spatial extent (i.e., percent cover) (Figure 1). Moreover, GRF improve air-conditioners' energy efficiency utilizing the cooling effect and solar shading. If outdoor air temperature decreases, the air-conditioner with variable speed drive compressor decreases the compressor's rotational speed in order to meet the requirement of low compression rate and maintain high efficiency as well (Figure 2). Low compressor rotational speed directly relates to a lower energy consumption because the energy consumption of conditioners are oughly linear to the compressor's rotational speed, and this low the energy demand (Parolini et al. 1983; Pizzetti, 2012; Wang and Yoshida, 2012).
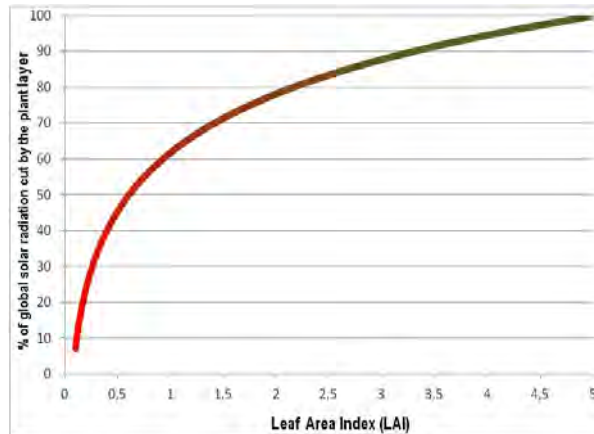
Figure 1. Relation between Leaf Area Index (LAI) and shadowing effect.
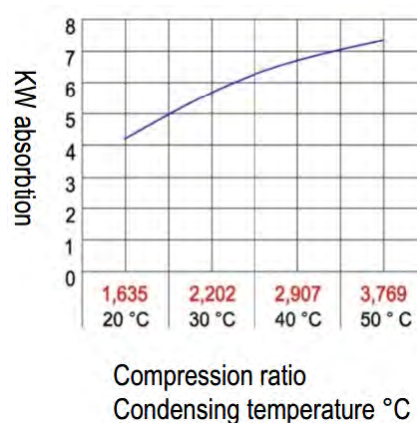
Figure 2. Electricity demand in relation to the outside air temperature

In order to evaluate the capacity of plant species on the variation of cooling load demand in buildings, ENEA has set up a demonstrative platform to study both thermal fluxes and microclimatic effects of plant systems applied to buildings to collect quantifiable data to definitely account the benefits that plant systems can really provide to the energy efficiency and the environment of buildings. A parameter to define the density of the plant leaves or "green factor" was developed (Ariaudo et al., 2009; Campiotti et al., 2011; Campiotti et al., 2013; Bibbiani et al., 2017; Vox et al., 2017) as reported by the equation 1:

$K_g = T_s - T_{gw}/T_s - T_{air} = 1 - \tau_g \cdot h_e/h_e^*$
where:
K_g = "green factor",
τ_g = solar transmission coefficient of the green layer,
h_e , h_e^* = surface heat transfer coefficient without, and with the green layer,
T_{gw} = external surface temperature of the green wall,
T_s = external surface temperature of the bare wall,
T_{air} = external air temperature.
The K_g factor varies between 0 and 1, the former when no temperature decrease is obtained by the green wall, the latter when T_{gw} is equal to T_{air}. The coefficients T_g and h_e^* come from test values and therefore the K_g factor can be easily calculated by the reported equation. Many possibilities exist for constructing of GRW, depending on the characteristics of plant species, buildings and climate.

2. MATERIALS AND METHODS
The experimental activity was carried out at the experimental platform of ENEA Casaccia Centre of Rome, located north of Rome (latitude: 42°02'36", longitude: 12°18'28"). The walls of the building prototype are made with perforated bricks having 20 cm thick, 25 cm height and 25 cm length as commonly used for residential and rural construction in the Mediterranean regions. Two vertical walls of the building prototype were equipped with a metallic structure on the front side as two vertical walls. They were respectively south-

west and east oriented (Figure 3 and Figure 4). A set of different plant species, i.e.: *Hedera helix, Lonicera japonica Hall's prolific Partenocissus quinquefolia, Trachelospermum jasminoides,* were grown in plastic plot of 46 cm height, 40 cm width and 100 cm lenght, with drip-one irrigation. An iron gable was placed at a distance of 0.6 m from the building wall for plant cultivation.

Figure 3. Technical evolution of the green wall at the ENEA Casaccia Centre.

The irrigation method for all the plants was the drip system, with the nutrient solution re-circulated from a manifold, and then collected in a gutter to be filtered and recicurlated. Data were collected from February 2017 to September 2017 on the south-west wall that was provided with a set of sensors for measuring relative humidity, surface wall temperature, and both the PAR and the global radiation. The sensors were placed respectively on the front and at the back side of the plant layer (Figure 5). Data were collected by a data logger (CR10X, Campbell, Logan, UT, USA) and measured with a frequency of 60s, averaged every 15 min and stored in the data logger. A Campell-pyranometer for the solar radiation, and a Rotronic-Hygroclip-S3 sensor for the air temperature were used. In this paper, we present the data collected on the south-west wall of the building, mainly covered with the *Hedera helix* and the *Lonicera japonica*.
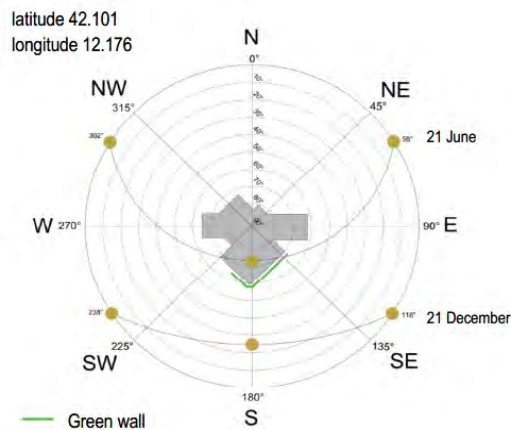
Figure 4. Paper sun of the building prototype
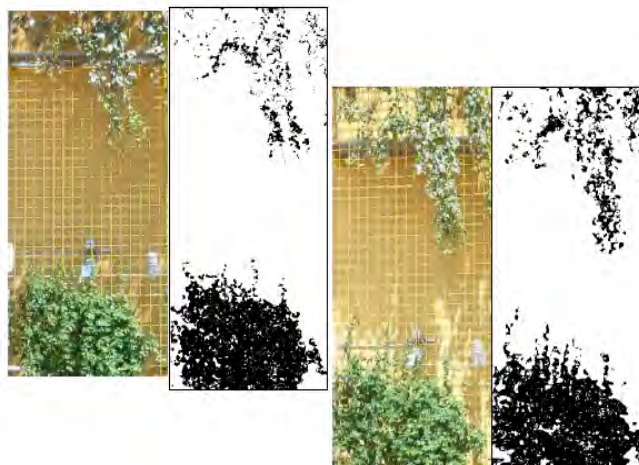
Figure 5. Monitoring system.

3. RESULTS AND DISCUSSION

The observations showed that the walls were covered sufficiently by the mix of plants species , from mid June 2017 to mid September, even if *Hedera helix* and *Lonicera japonica* showed a better growth than the other plant species. The data were interpolated by a simple logistic curve, in order to achieve the growth parameters of each plant species by the following logistics function:

were:

$C(t)$ is the plant covered area, C_{max} is the maximum asinthotic covered area, t is the plant development period and $t_{0.5}$ is the inflection point of the curve at the maximum velocity of plant development. Table 1 shows the growth analysis of the *Lonicera japonica*, made by imaging technique analysis calculating the shaded area during the different months.

Table 1. Covered area (m²) during plant growth of Lonicera japonica

Dates, year 2017	Lonicera japonica 'Hall's Prolific'
23 March	0.18
10 April	0.64
19 April	0.95
10 May	1.29
31 May	1.80
07 June	2.07
20 June	1.86
06 July	1.88
20 July	2.28
31 July	-
31 August	2.24

Parameters of logistic curve	Lonicera Japonica 'Hall's Prolific'
C_{max} (m²)	2.54
τ (days)	30.7
$t_{0.5}$ (days)	100
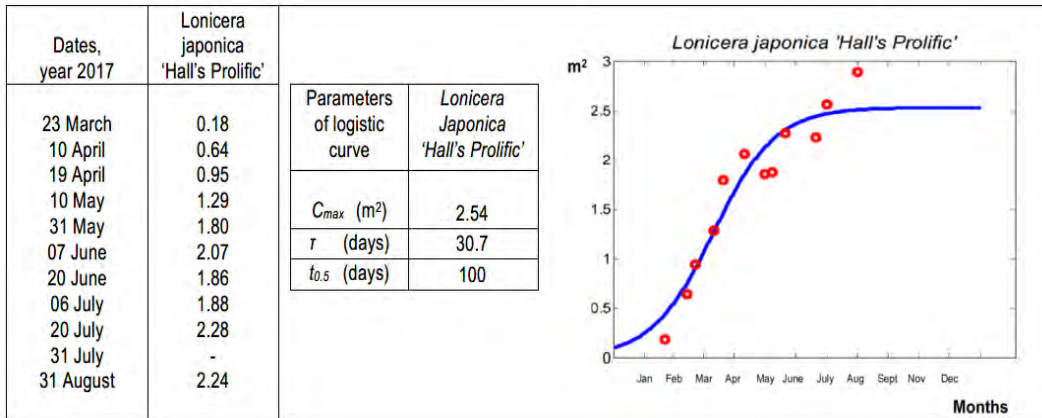
During summertime, the presence of vegetation decreased the quantity of solar radiation absorbed by the walls leading to a strong reduction of the surface temperature of the wall covered by the climbing plants in respect to the uncovered wall (Figure 6).
A difference up to 10 °C was recorded between the highest temperatures measured for the uncovered wall and for the walls covered with the plants.
The differences of the surface temperatures show a correlation (R=0.468) with the global solar incidence on the building wall (Figure 7). However, this investigation needs a deeper analysis since it was not considered the temperature dynamics of the building wall.
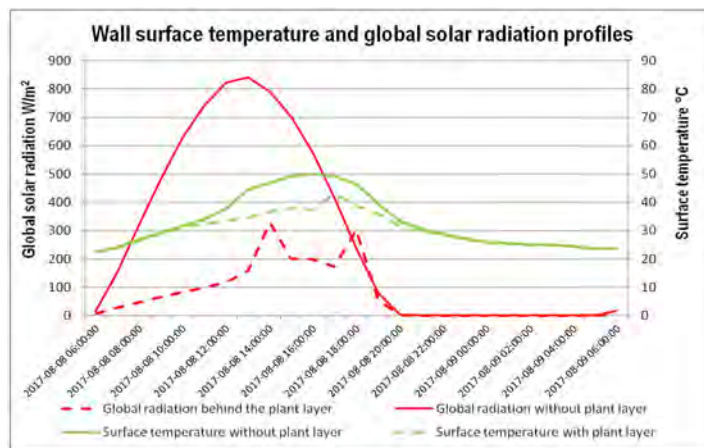
Figure 6. Surface temperature and global radiation profiles.
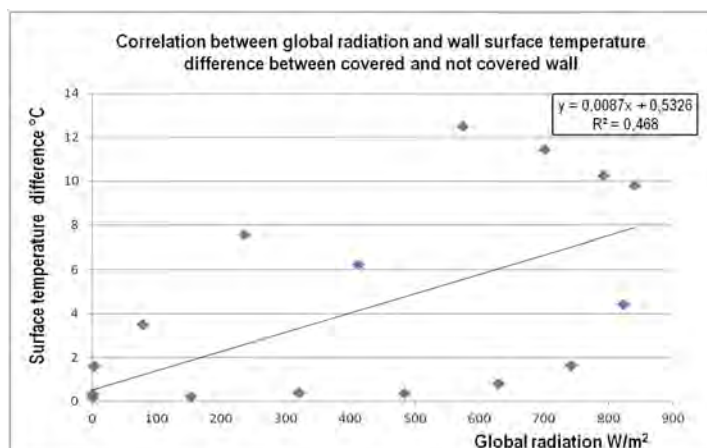
Figure 7. Global solar radiation and surface temperature correlation.

CONCLUSIONS

The experimental activity was carried on the vegetated vertical systems from February 2017 to September 2017 taking into consideration both warm and cold periods. The application of the green walls during warm months allowed cutting the heat gain due to solar radiation by reducing the external surface temperature in daytime hours up to about 10°C. Green roofs and vertical greenery popularity is growing because of their high potential to be used as sustainable solution for reducing the thermal performance of building envelopes and for reducing energy consumption of buildings in the Mediterranean area. A widespread use of the different typologies of GRW can become a part of the response actions to the objectives of both the Kyoto Protocol and the European Energy Efficiecy Directive. The vegetated buildings allows reducing the electricity demand for air conditioning in summer and increasing the thermal insulation in winter, mostly in Mediterranean countries. In addition, GRW technology contributes to mitigate the urban heat island effect and improve the quality of the environment. It is becoming a key design in the modern building sector, where GRW technology is emerging as an element of architectural design as well as of retrofitting of existing buildings. Further work of ENEA will focus on the study of energy efficiency performances of both roof and walls of buildings provided with vegetated surfaces, in order to allow collection of data to fully explore the mechanisms underlying the energy efficiency potential of plant systems, and to develop a technical guide with the *blue lines* for the sustainable application of the GRW in cities.

REFERENCES

1. Ariaudo, F., Fracastoro, G.V., & Corgnati, S. (2009). Cooling Load reduction by green walls. Proceedings IBPC, Istanbul, 2009.
2. Bibbiani, C., Campiotti, A., Giagnacovo, G., Incrocci, L., Pardossi, A., Latini, A., Schettini, E., & Vox. G. (2017). Green roofs and green wall for improving energy efficiency of buildings. Proc. IS on Greener Cities for more Efficient Ecosystem Services in a Climate Changing World. Acta Hort. *in print*.
3. Campiotti C.A., Bibbiani, C., Alonzo, G., Giagnacovo, G., Ragona, R., & Viola C. (2011). Green roofs and façades agriculture (grf) for supporting building energy efficiency. Journal of Sustainable Energy, vol. II, 3:24-29.
4. Campiotti, C.A., Schettini E., Bibbiani C., Alonzo G., & Viola C. (2013). Scarascia Mugnozza G., Blanco I., Vox G. Building green coverings for a sustainable use of energy. Journal of Agricultural Engineering 2013; volume XLIV(s2):e50.
5. Campiotti, C.A., Consorti, L., Giagnacovo G., Latini, A., Puglisi, G., Scoccianti, M., & ,Viola, C. (2017). Caratterizzazione di tipologie di sistemi vegetali per migliorare l'efficienza energetica degli edifici nella città metropolitana. Report RdS/2015/141. (in Italian).
6. EU Directive Energy Performance of Buildings (European Union, 2011).
7. European Commission (2013). Building a Green Infrastructure for Europe. ISBN 978-92-79-33428-3.
8. Gargari, C., Bibbiani, C., Fantozzi, F., & Campiotti, C.A. (2016). Simulation of the thermal behaviour of a building retrofitted with a green roof: optimization of energy efficiency with reference to Italian climatic zones. Agriculture and Agricultural Science Procedia, 8:628–636.
9. Parolini, G., Del Monaco, A., & Fontana, D.M., Fondamenti di Fisica Tecnica. Ed. Utet, 1983.
10. Petralli, M., Prokopp, A., & Morabito, M. (2006). Ruolo delle aree verdi nella mitigazione dell'isola di calore urbana: uno studio nella città di Firenze. Rivista Italiana di Agrometeorologia 1: 51–58 (in Italian).
11. Pérez, G., Rincón, L., Vila, A., González, J.M., & Cabeza, L.F. (2011). Green vertical systems for buildings as passive systems for energy savings. Applied Energy 88(12): 4854–4859, http://dx.doi.org/10.1016/j.apenergy.2011.06.032.
12. Pérez, G., Coma, J., Martorell, I., & Cabeza, L.F. (2014). Vertical Greenery Systems (VGS) for energy saving in buildings: a review. Renewable and Sustainable Energy Reviews 39:139–165, http://dx.doi.org/10.1016/j.rser.2014.07.055.
13. Pizzetti, C. (2012). Condizionamento dell'aria e refrigerazione voll. 1 e 2. Ed. Ambrosiana.
14. Santamouris, M. (2012). Cooling the cities – a review of reflective and green roof mitigation technologies to fight heat island and improve comfort in urban environments. Solar Energy 103: 682–703, http://dx.doi.org/10.1016/j.solener.2012.07.003.
15. Schettini, E., Blanco, I., & Campiotti, C.A. (2016). Green control of microclimate in buildings. Agriculture and Agricultural Science Procedia 8: 576–582, http://dx.doi.org/10.1016/j. aaspro.2016.02.078.
16. Trepanier, M., Boivin, M.A., Lamy, M.B., & Dansereau, B. (2009). Green Roof and living walls, Chronica Horticulture, l49 (2), 2009.
17. Vox, G., Blanco, I., Fuina, S., Campiotti, C.A., Scarascia Mugnozza, G., & Schettini, E. (2017). Evaluation of wall surface temperatures in green facades. Proceedings of the Institution of Civil Engineers. Engineering Sustainability http://dx.doi.org/10.1680/jensu.16.00019.
18. Wang, F., & Yoshida, H. (2012). Improving air-conditioners'energy efficiency using green roof plants. www.interchopen.com.

Day-ahead multi-objective energy optimization of a smart building in a dynamic pricing scenario

M.Botticelli[1], G.Comodi[1], A.Monteriù[1], A. Pallante[2], S.Pizzuti[3]

[1] Marche Polytechnic University

[2] Roma Tre University

[3] ENEA – Energy, New technologies and sustainable Economic development Agency

Abstract

The identification of techniques aimed at a rational use of electric power has nowadays become more important than the production of energy itself. This is caused by different factors, and by the progressive saturation of the Italian electricity grid, which is increasingly subject to connection requests, mainly due to the development of plants which make use of renewable energy sources.

In order to reduce the building's energy costs during the summer season taking into account the user comfort, in this work we propose a new approach based on Pareto multi-objective optimization combined with a simulator developed in the MATLAB/Simulink environment. The electrical consumption of the entire building is taken into consideration with the aim of air-conditioning it. The goal is to find, the day before, the optimal hourly scheduling of the set points which have to be applied the next day, taking into consideration all external conditions, namely the weather conditions and the hourly energy price. To achieve this objective, the control variables we change are the room temperature set points and the flow water temperature set point. As required by the UNI EN ISO 7730:2006 standard, comfort measurement has been calculated with the PPD (Predicted Percentage of Dissatisfied) index.

Different scenarios have been investigated. The results show that there is an average of 15% potential cost saving, while maintaining a high level of comfort. Experimentation has been carried out by simulating a real office building in Italy, and the comparisons are shown regarding the actual settings applied to it.

I. Introduction

Buildings represent an energetic complex system, made up by a main structure and by its envelope, by air conditioning system and energy vectors which supply it. Only a precise knowledge of subsystems performances and relations among them, allows finding proper strategies for energy saving, maintaining at the same time appropriate comfort levels for residents.

Finding proper techniques for a rational use of electrical energy has become, nowadays, more and more important than the production of energy itself, because the Italian power grid is gradually becoming saturated and being affected by many connection requests coming mostly from plants which use renewable energies.

The present energy consumption which is necessary to the thermal comfort achievement of rooms and of clean water represents almost 30% of the national energetic consumption and it responsible for almost 25% of the national CO_2 emission, which is one of the principal cause of greenhouse effect and temperature heating [1]

An intervention is crucial to reach a new equilibrium, in harmony with environment and respectful of future generation's rights. A change in terms of energetic consumption is necessary [2]:

- for an ethical and social issue: 28% of the world's population currently consumes 77% of the world's energy production, while the other 72% live with only the remaining 23%.

- For a strategic reason: Europe (and Italy in particular) depends on non-EU countries (some highly unstable) for fossil fuel needs and consequently security of supply is not always guaranted.

- For an economic reasons: the annual cost of energy bills is now one of the most important items in the family budget (exceeding the income of a month for an average household).

According to the latest Italian Energy Strategy Plan, Rationale Use-of-Energy is considered the cornerstone in order to pursue sustainable economic growth.

The building sector is the largest user of energy and CO2 emitter in the European Union (EU) and is responsible for about 40% of the EU's total final energy consumption and CO2 emissions. As a consequence, the cornerstone of the European energy policy has an explicit orientation to the conservation and rational use of energy in buildings as the energy performance of building directive (EPBD) 2002/91/EC and its recast (EPBD) 2010/31/EU indicate [11,12]. The EPBD's main objective is to promote the cost-effective improvement of the overall energy performance of buildings. In Europe, member states have set an energy savings target of 20% by 2020 and 27% by 2030, mainly through energy efficiency measures. A number of methodologies for optimizing real-time performance, automated fault detection and isolation were developed in IEA-Annex 25 [13].

So it is clear that in order to reduce the consumption of electricity, it is necessary to act on the consumption of buildings. The solutions can therefore be two:

- Envelope and plants retrofitting, which leads to a scenario of high savings at the cost of high investments and therefore to a long payback period.
- Automation and intelligence through smart buildings, which leads to medium savings with low investment with a consequent short payback period.

In fact, with more 10 buildings the payback period is around 3 years, which is much lower than the payback period of retrofitting solutions which is around 15-20 years.

Therefore, monitoring of energy consumption in buildings, especially public buildings, is critical in order to reduce consumption. In a smart building we can control heating, ventilation, air conditioning, lighting, presence, security and other. With sensors, actuators and microchips, we can collect data and manage it according to a business' functions and services. Thanks to appropriate optimization, control and diagnostics algorithms, we can minimizes the environmental impact of buildings.

This article describes a possible strategy of optimization, suitable for smart buildings, focused both on the energy consumption reduction and minimization of unhappy residents percentage caused by thermal "discomfort". This percentage was determined by PMV index (Predicted Mean Vote) and PPD index (Predicted Percentage of Dissatisfied) [14] in the current regulation UNI EN ISO 7730:2006.

According with our studio, we can introduce the most advanced concept of Smart Building, conceived as a component of an integrated system that also includes other actors. The energy demand of a building, in fact, is integrated with the dynamic daily price of energy (NUP - National Unique Price) the production of energy through photovoltaic systems and electrical storage. The management of this scenario with several players is managed by an Energy Management System.

This article is an evolution of a previous work [5], that had analyzed, with a previous version of the Simulator, the optimization of methane consumption for an entire winter season. the difference of this experimentation is about a different objective function and a single day. In fact, the FO examined in this report takes into account the dynamic price of energy and not the consumption of methane. On the other hand, with a period reduction of simulation, it is possible to set the different set-points from hour to hour making the whole system more dynamic and efficient in view of a hypothetical functioning in real life.

2. Description (Use "Heading 2" style or Arial 10 bold justified here)

A real office building located at ENEA (Casaccia Research Centre, Rome, Italy) was considered as a case study (Fig. 1). The building has an L-shaped structure, it is oriented 15° north-east and it was built between 1970 and 1972 and it is composed of three floors and a heating plant in the basement. There are 41 offices of different size with a floor area ranging from 14 to 36 m^2, 2 EDP rooms each of about 20 m2, 4 Laboratories, 1 Control Room and 2 Meeting Rooms, for a total of 1277,3 m^2. Each office room has from 1 up to 2 occupants. Each room and laboratory is equipped with fan-coils with on-off fan speed controlled by a room thermostat with hysteresis. The heating plant consists of a traditional natural gas boiler.

Figure 1: Case study: Smart Building at ENEA F40

The building is equipped with an advanced monitoring system aimed at collecting data about both external and internal ambient conditions, electrical and thermal energy consumption. In order to simulate the variables of interest, a MATLAB Simulink simulator based on HAMBASE model [14,15] was developed.

The control variables are:

- Zone set point which can be set using thermostats in each room
- Flow setpoint which can be set by means of special instrumentation in the building's thermal power plant.

In fact, the variables that can be set in the simulator are actually modifiable in the modeled building.

Simulink was used to model the described building and all its thermal and electrical components and to simulate the behavior of the F40 building was used the HAMbase software, which exploited the internal temperature model, the relative humidity of the indoor air and the energy consumption required for the heating and cooling of a multi-zone building.

The purpose of the software developed is to simulate the energy saving strategies and control logics in order to maximize energy savings, and therefore to minimize the cost. The outputs are:

- environmental comfort;
- euros.

The thermo-hygrometric comfort index returned by the simulator is a subjective condition that depends on a series of factors. The PMV-index (Predicted Mean Vote) predicts the subjective ratings of the environment in a group of people and it is experimentally related to the PPD, an index that represents the percentage of dissatisfied people. The standard UNI EN ISO 7730: 2006 establishes the acceptable range of PMV between -0.5 and +0.5, and therefore states that to be in a situation of well-being, the PPD must not exceed 10%. The PPD can be computed using PMV model. Among those taken from the building model, there are four variables, that were set to their typical values - metabolism (70 [Wm^{-2}]), external work (0 [Wm^{-2}]), clothing (1 [−]), and air velocity (0.1 [ms^{-1}]).

2.1 Description of optimization problem

The analysis of the objective function was carried out going to change a decisional variable at a time (zone set-point and delivery set-point), setting it progressively to each single value assumable, respecting the constraints of the problem.

We have a formulation of problem as follow:

Figure 2: formulation of problem.

$$\textbf{Min} \quad f_1(X1, X2) , \quad f_2(X1, X2)$$

Subject to :

$$\begin{cases} LB_1 \leq X1 \leq UB_1 \\ LB_2 \leq X2 \leq UB_2 \end{cases}$$

Where:

- f_1 (X1, X2) is the objective function of euro consumption;
- f_2 (X1, X2) is the objective function of the PPD;
- X1 is the zone set-point and variation step is 0,5;
- X2 is the flow set-point and variation step is 0,5;
- LB1 is the lower limit of the variable X1 and is equal to 22 ° C;
- UB1 is the upper limit of the variable X1 and is equal to 25 ° C;
- LB2 is the lower limit of the variable X2 and is equal to 8 ° C;
- UB2 is the lower limit of the variable X2 and is equal to 12 ° C;

So we have a minimization problem with two objective functions as the consumption in euro [€] and PPD index with two vectors of 24 elements, X1 (the zone set-point that change from 22 to 25 celsius degree) and X2 (the flow setpoint that change from 8 to 12 celsius degree). X1 and X2 are the two control variables.

3. Experimentation (Use "Heading 2" style or Arial 10 bold justified here)

Each simulation is about a single day in which it is possible to set the different set-points from hour to hour. This made the system dynamic and efficient in the vision of a hypothetical functioning in reality.

The first step was to integrate the simulator with the optimizer that is a genetic optimizer (NSGA-2) [15].

The simulator takes in input both the values of the decision variables that we have just set up and the final states of the simulator returned by the optimization system.

The goal of the problem is to minimize a multi objective function with cost and comfort (euro [€] and PPD [%]).

For this type of algorithm the fundamental parameters have been chosen and set, such as:

- Population = 8
- Generation = 4
- Crossover rate =0,8
- Mutation rate =0,5

These parameters have been chosen in order to obtain a Pareto front that can be easily reconstructed for each hour. The simulations, however, were also carried out by reversing the number of population and generation.

Crossover and mutation in useful to obtain new solutions that previously did not exist by combining or changing the bits of two solutions.

The total number of fitness evaluations for the exhaustive search is 63 while with the proposed approach is 40.

Therefore in the proposed approach the number of performance evaluations is fewer.

In the problem's solution for minimizing cost consumption, expressed in terms of euro, and PPD, is dynamically calculating the values of the set-points in the totality of their combinations, using the genetic evolutionary algorithm NSGA-2. Solutions are ordered according to the concept of non-dominance.

The population of individuals is random initialized and the optimization process begins. When the population is initialized, the chromosome phenotype associated with each individual is calculated and, subsequently, the fitness of each individual is calculated. If the stop condition of the algorithm is verified the algorithm ends, otherwise the genetic selection operators are applied, crossover and mutation. The count of the number of generations carried out is increased and the new population, which replaces the previous one, is evaluated again.

Figure 3: Problem's solution
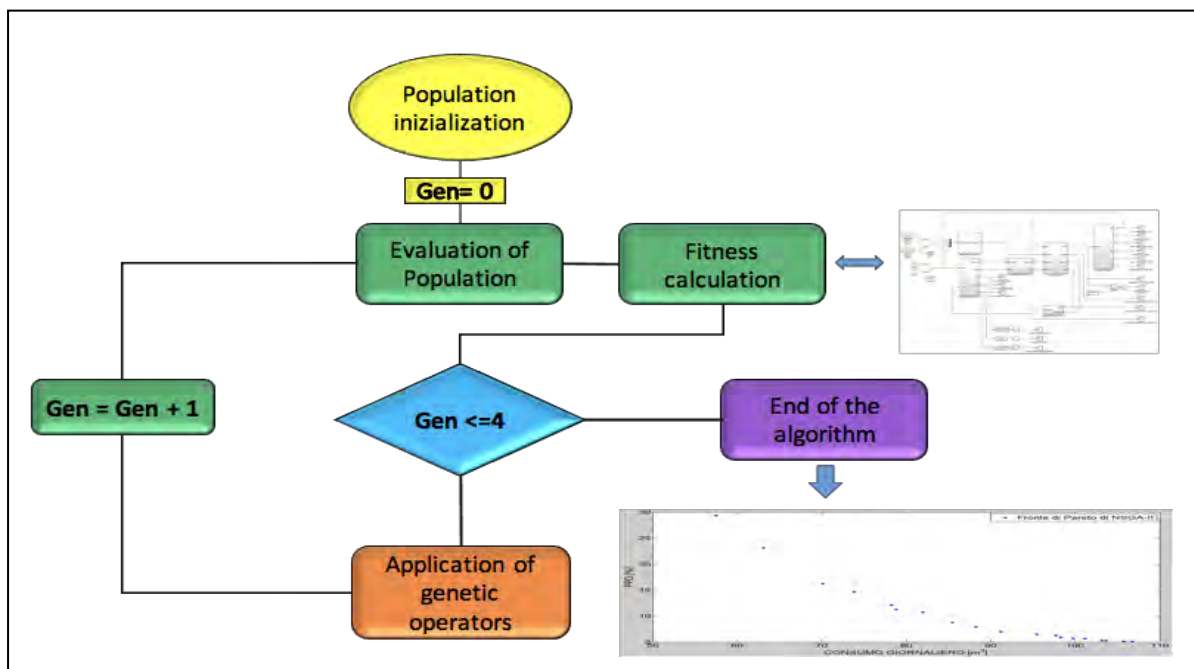
As we have already said for the next hours the optimal solution of the previous hour is used as an initialization

For the choice of best solution, the logic used is therefore to order the Pareto front based on increasing euro consumption and scroll through this list checking the PPD. The first value just below 10%, is the chosen one. If all solutions have a PPD higher than 10, then the best solution is the chosen one with the smallest possible PPD value.

The daily simulations were carried out on a one average day in summer.

To evaluate the efficiency of the algorithm, the combination of set-points with which the F40 building is currently air-conditioned during the summer season has been taken into consideration:

• Zone set-point = 22 ° C;

• Delivery set-point = 10 ° C;

which have been kept constant throughout the simulation period.
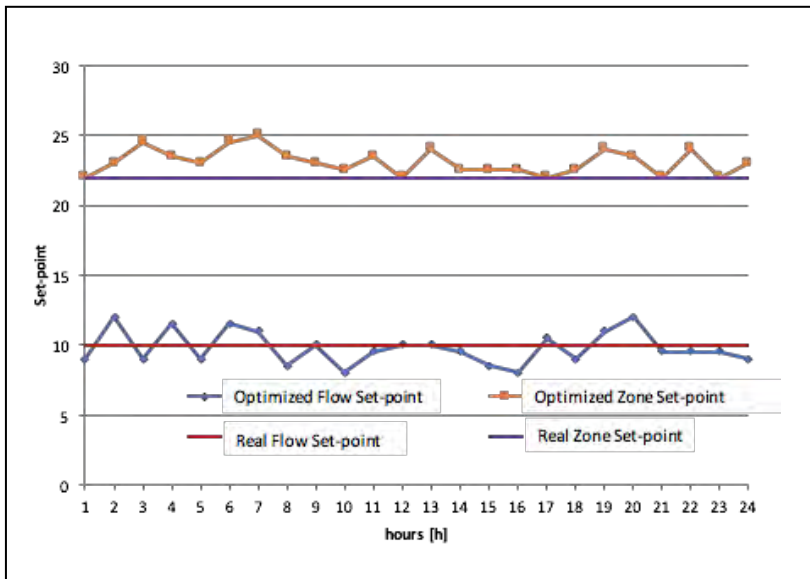
Fi**gure 4: real functioning of the building in comparison with the optimized one**

The simulations took place by taking three different initial internal temperatures:

T0 = 21; 23; 25 [°C]

We can observe the results obtained by simulating the real functioning of the building (table 1), without any kind of optimization, with static set-point, in comparison with the optimized one, in which each simulation involved changing the flow set-point and the zone set-point in specific ranges.

Initial Temperature	21°C	23°C	25°C
Euro consumption[€]	22,74	29,84	36,84
PPD [%]	6,17	6,74	10,82

Table 1: Reference case (Summer, one average day)

For the identification of the optimal set-point combination with NSGA-2, the same initial internal temperatures were considered and the different solutions obtained were compared.

It can be seen from the results in table 2, on average we found a "theoretical" saving of 14.09% compared to the reference case, with an average PPD value of 8.78.

We talk about "theoretical savings" because the strategy has not been applied to the real building.

Initial Temperature	21°C	23°C	25°C	Average
Saving [%] NSGA-2	-9,76	-21,15	-11,36	-14,09
PPD (average) NSGA-2	7,13	8,25	10,89	8,76

Table 2: Result optained

In the first graphs below we can see how the punctual consumption expressed in euros varies in the 24 hours, comparing the one of the reference case (in blue) with the consumption obtained using the NSGA-II optimizer (in red).

We can therefore note that savings were obtained at all hours of the day, obtaining an overall saving equal to the difference between the integrals related to the two curves

Figure 5: Punctual Euro Consumption in 24h
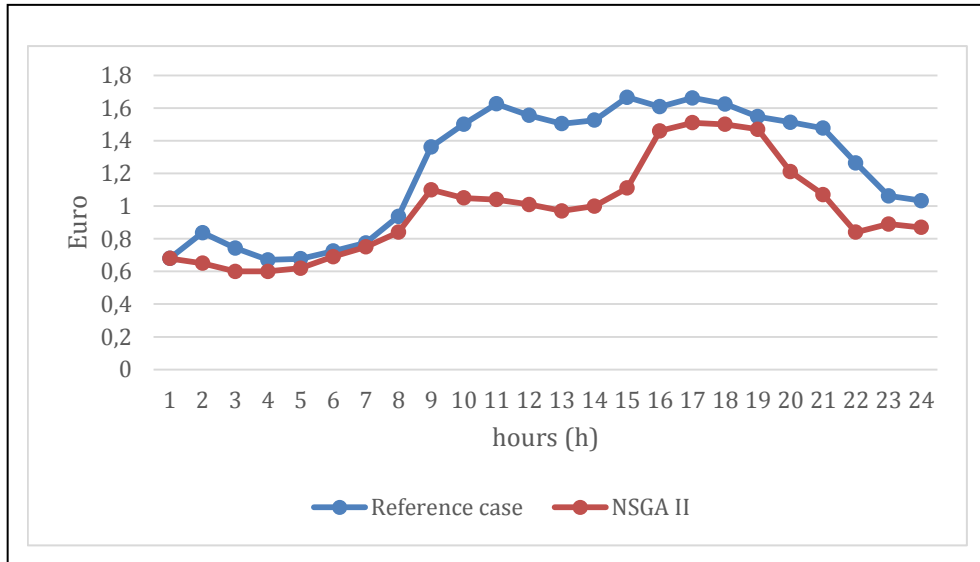
In the second graphs below we can see how the punctual PPD value varies in the 24 hours, comparing the one of the reference case (in blue) with the consumption obtained using the NSGA-II optimizer (in red).

It is clear that in the face of savings, we are going to lose the value of PPD, but it is always below 10% as defined by the UNI standard.

So with a small increase of PPD value, but always respecting the legislation, we have however a great cost saving.
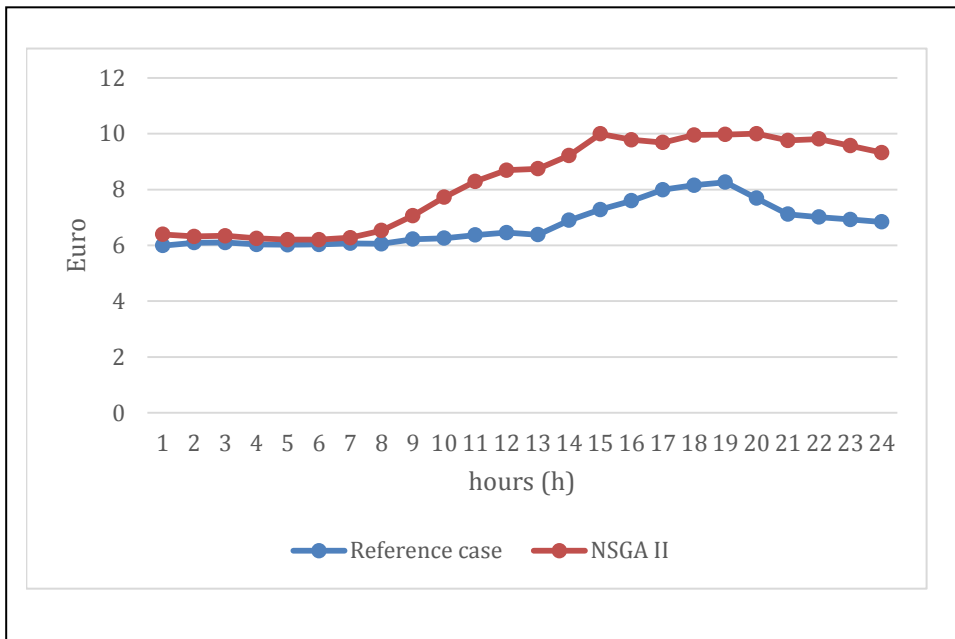
Figure 6: Punctual PPD value in 24h

4. Conclusion (Use "Heading 2" style or Arial 10 bold justified here)

In this work we proposed an approach based on multi-objective optimization combined with simulation tools in order to improve the building thermal energy performance during summer by keeping into account euro consumption and occupant comfort. Results were carried out by simulating the behavior of a real building on a one average day in summer. In particular different scenarios were investigated and results showed that there is a nearly 15% average potential of energy saving with little increase of user discomfort through an hour-by-hour multi-objective optimization.

Future developments include firstly the comparison of this results by using other optimization methods. Then it will be introduced a new version of the simulator that integrates PV (PhotoVoltaic) and storage for even more efficient management of energy consumption. To obtain a more complete scenario, simulations will have to be carried out covering the winter season. Finally, to validate the solutions proposed in a real case, the application of this strategy to the smart building F40 is envisaged. Further future development could consist in adapting the work done to residential buildings.

References

[1] "Risparmi energetico nelle case",
http://efficienzaenergetica.acs.enea.it/doc/risparmio_casa_agg.pdf

[2] "L'uso razionale dell'energia negli edifici pubblici", 2008,
https://www.google.it/url?sa=t&rct=j&q=&esrc=s&source=web&cd=1&ved=0ahUKEwi1y_L0rvD
XAhWEbRQKHV4CCqMQFggrMAA&url=http%3A%2F%2Fwww.ri.camcom.it%2Fdownload%2
F775.html&usg=AOvVaw0LNQCreHWzF9Lb0RoqZJbA

[3] "Doe microgrid workshop report," Report 06-03, The U.S. Department of Energy (DOE) Office
of Electricity Delivery and Energy Reliability, August 30-31,2011.

[4] F. Katiraei, R. Iravani, N. Hatziargyriou, and A. Dimeas, "Microgrids management," Power and
Energy Magazine, IEEE, vol. 6, no. 3, pp. 54–65, 2008.

[5] M. Camponeschi, A. Fonti, F. Leccese, G. Comodi, M. Grossoni, S. Pizzuti, "Winter Thermal
Multi-Objective Optimization: a Simulation Case Study", http://hdl.handle.net/11590/283981

[6] G. Bovesecchi, "Comfort termo-igrometrico: equazione del comfort, PPD e PVM", Università di r
Roma Tor Vergata, http://didattica.uniroma2.it/assets/uploads/corsi/144485/04_-_TT1_-
_Comfort_Termoigrometrico_-_Fanger_PPD_e_PMV1.pdf

[7] Normativa UNI EN ISO 7730:2006, Ergonomics of the thermal environment-Analytical
determination and interpretation of thermal comfort using calculation of the PMV and PPD
indices and local thermal comfort criteria, 2006

[8] G. Comodi, A. Fonti, A. Giantomassi, F. Polonara, S. Longhi, "Sviluppo di un simulatore di
edifici orientato alla gestione attiva della domanda", ENEA, 2013

[9] Ottimizzazione multi obiettivo,
http://www.uniroma2.it/didattica/PSSPS/deposito/multiobiettivo_metodi_esempi_1.pdf

[10] "A fast and elitist multiobjective genetic algorithm: NSGA-II", IEEE Transactions on Evolutionary
Computation (Volume: 6, Issue: 2, Apr 2002)

[11] Official Journal of the European Communities, Directive 2002/91/EC of the European
Parliament and of the Council of 16 December 2002 on the energy performance of buildings,
L1/65, 2003.

[12] Directive 2010/31/EU of the European Parliament and of the Council of 19 May 2010 on the
energy performance of buildings (recast).

[13] J. Hyvarinen, S. Karki, "Building optimization and fault diagnosis source book," IEA Annex
(1996).

[14] P. O. Fanger, „Thermal Comfort: Analysis and applications in environmental engineering,"
McGraw-Hill, 1970.

[15] K. Deb, A. Pratap, S. Agarwal, T. Meyarivan, "A fast and elitist multiobjective genetic algorithm:
NSGA-II," IEEE Transactions on Evolutionary Computation 6 (2): 182.
doi:10.1109/4235.996017
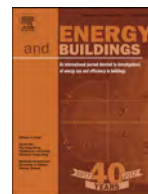
Optical, thermal, and energy performance of advanced polycarbonate systems with granular aerogel

Elisa Moretti [a,*], Michele Zinzi [b], Francesca Merli [c], Cinzia Buratti [a]

[a] Department of Engineering, University of Perugia, Via G. Duranti 93, Perugia 06125, Italy
[b] ENEA Casaccia Research Centre, Via Anguillarese 301, Rome 00123, Italy
[c] CIRIAF (Interuniversity Research Center on Pollution and Environment "Mauro Felli"), University of Perugia, Via G. Duranti 63, Perugia 06125, Italy

ARTICLE INFO

ABSTRACT

Polycarbonate panels could be considered as a suitable and cheap solution for walls, roofs, and sheds in non-residential buildings and, at the same time, granular silica aerogel is one of the most promising nano-materials for energy saving in buildings. In the paper, three types of advanced multiwall PC panels (thickness 16, 25, and 40 mm) with translucent granular aerogel were investigated by experimental (thermal and optical) and numerical characterization. By comparing thermal performance of air and aerogel-filled PC systems, it can be noticed that the impact of the aerogel is remarkable: the reduction in U-value is 46%-68%, depending on the aerogel layer thickness. U-value is 1.4 W/m²K for the 16 mm thickness sample and it is 0.6 W/m²K when the thickness increases up to 40 mm. The systems keep their performance in horizontal position, when they are used as roofs. Light transmittance is 0.61 and 0.42 for 16 mm and 40 mm respectively and the reduction with respect to air-filled panels is acceptable (15%) for 16 mm and significant (40%) for 40 mm thickness. The aerogel has also a remarkable impact on the reflectance spectrum, especially between 400 and 1400 nm. The solar factor is 0.58 for 25 mm thickness, quite similar to the low-e glazing one. Finally, energy simulations for a case study showed that aerogel-filled PC systems outperform conventional double glazing systems both for heating and cooling energy demands. However, when compared to low-e glazings, the benefits of the translucent material (also considering the highest thickness) in the interspace are lower for heating and negligible for cooling energy demands. The aerogel-filled polycarbonate systems could be a valid solution for non-residential buildings, enhancing the thermal performance and the light control of the building envelope, especially when they are used as roofs.

1. Introduction

Transparent building envelopes play a significant role in energy performance, especially when considering highly glazed non-residential buildings. In order to reduce energy consumptions, a plethora of advanced materials for building envelopes have been investigating and they have been proposed in the market. Recently, a lot of attention has been devoted to nanomaterials, such silica aerogels [1–5].

Meanwhile, polycarbonate (PC) multiwall panels for building applications have been spreading in the market, because of the low weight, durability, fire, weather, and UV resistance. A lot of applications are allowed in fenestration systems, continuous windows, shed, roofs, and walls by employing products with different cell geometric characteristics, colors, and thicknesses. Moreover, PC pan-

els are cheaper than conventional glazings and, once appropriately designed, they improve thermal performance reducing significantly energy costs, especially in commercial and industrial buildings.

In a previous study [6] multiwall air-filled polycarbonate panels were investigated as a solution for commercial and industrial buildings. The thermal and optical performance was assessed also considering the influence of male-female interlock junctions (which are used for in-situ installation) on their performance. The optical property measurements highlighted that a large integrating sphere is needed, due to the geometry and structural complexities, as well as for scattering phenomena in non-regular materials [7]. Moreover, the geometry of the samples showed that the PC panels optical properties have an angular dependence, much more than in conventional glass units [6]. Furthermore, the panel joints can influence thermal and optical performance: the variation could be positive or negative, depending on the number of layers and on the sample characteristics. All the polycarbonate multi-sheets panels showed good thermal performance: the U-values are com-

* Corresponding author.
E-mail address: elisa.moretti@unipg.it (E. Moretti).

prised in the 1.2−1.9 W/m²K range, depending on the sample features, quite similar to the values of double glazing units. At the same time, the complexity of the geometry allowed a reduction in light transmittance (about - 30% with respect to a conventional DGU (DGU = Double glass unit)) and an increasing in solar transmittance. However, these systems are light diffusing, preventing from glare problems and improving visual comfort [6].

When higher thermal insulation levels are required, granular silica aerogels can be used in order to fill the air gaps in the panels. Aerogels are nanostructured solid materials with high porosity (> 90%) and low density (80−200 kg/m³), which can be defined as superinsulation materials, due to their low thermal conductivity, comprised in the 0.012−0.023 W/mK range, depending also on the granule size [8,9]. Due to these interesting properties, the granules have been successfully incorporated in different innovative aerogel-based solutions for energy saving in buildings, both opaque, such as concrete, plasters [10], flexible blankets [11], and translucent, such as highly energy-efficient windows [12–15]. Granular aerogel in glazing systems does not allow the view through it: a completely diffuse light transmittance could be achieved, also contributing to reduce glare problems. Thermal, optical, and acoustic performance of glazing systems with silica aerogels is widely discussed in the literature [16–23], whereas detailed studies on advanced aerogel-filled PC systems are lacking.

Buratti et al. [23] recently investigated thermal and optical properties of a double glazing (4 mm float clear glasses) with only 15 mm of silica granular aerogel in the interspace. The experimental results highlighted the aerogel impact on heat transfer in the glazing: the thermal transmittance was 1.0−1.1 W/(m²K), allowing a 63% reduction when compared to conventional DGU with air, together with a good optical behavior: the light transmittance is 0.57, corresponding to a 30% reduction with respect to air-filled DGU. However, when the aerogel thickness increases up to 60 mm, a U-value of 0.3 W/(m²K) could be achieved [20,23]. The light transmittance of granular aerogels is about 80% considering 10 mm thickness and it decreases by 20% each 10 mm thickness increasing [13]. However, optical and thermal performance is significantly affected by the particle size of the aerogel granules [8,11,18].

Huang and Niu [24] studied the energy performance of aerogel glazing systems in humid subtropical cooling-dominant climates: in a commercial building in Hong Kong, aerogel glazing systems can reduce the total annual space cooling load by about 4% with respect to conventional windows, while the annual cooling load reduction is comparable to the one achieved by application of a shading-type low-e glazing. The results highlighted that glazing systems with granular aerogel in interspace could be a suitable solution for energy saving in buildings, also considering cooling-dominated climates. These findings were confirmed by Ihara et al. [22], who investigated the energy performance of granular aerogel glazings used as spandrels. The results showed that the considered systems allowed a lower energy demand than a double glazing facade in cooling dominated climates, namely Tokyo and Singapore. In heating dominated climates (Oslo), the aerogel granulate glazing facade does not achieve the same performance of triple glazings. However, a combination of aerogel and triple glazing systems could be a suitable solution for cold climates. Buratti et al. [25] studied the energy performance of glazing systems filled with granular and monolithic silica aerogel as a solution for the refurbishment of an Evolutive House built in Perugia (Italy) in 1978. The results showed that an important energy saving was obtained for all the proposed glazing solutions (about 60−70%).

An experimental investigation on two prototypes of polycarbonate panels filled with granular aerogel (6 mm and 10 mm aerogel thickness) was carried out by Dowson et al. [26]. Considering the retrofit of an office building in London (UK), the prototypes were installed on an existing single glass window, with a 15 mm air gap between the PC panels and the glazing. In-situ measurements highlighted excellent performance of the proposed solutions: the heat flux reduction was about 73% for 6 mm aerogel PC panel and it increased up to 80% considering 10 mm of aerogel; at the same time, the light transmission decrease in was acceptable: light transmission values through the 6-mm aerogel PC panel, 10 mm aerogel PC panel, and the control single glass were 58%, 51% and 73% respectively.

Starting from the previous findings, in the present paper, advanced polycarbonate panels with aerogel are studied in terms of thermal, optical, and energy performance. An extended experimental campaign starting from the preliminary results obtained in [27] is presented for three types of aerogel-filled polycarbonate panels, considering different thicknesses and geometry (total thickness of 16, 25, and 40 mm).

A large sphere apparatus [28] was used to accurately investigate optical properties of these complex transparent systems, characterized by a scattering nature [6,7]. The equipment available in ENEA (Rome, Italy) allowed a careful optical characterization of the panels, due to also depending on the light incidence angle (0°; 30°; 45°; 60°). The broad band properties (Light transmittance τ_v, Solar transmittance τ_e, and Light ρ_v and Solar reflectance ρ_e) were then calculated in compliance with EN 410 [29], by using the spectral transmittance and reflectance data.

Thermal performance was investigated by means of the guarded hot plate apparatus and the U-value was calculated [30]. The proposed solutions are often used roof solutions in buildings, due to their lightness: in the experimental campaign the U-value was measured also considering the sample in horizontal position.

In order to evaluate the impact of aerogel on optical and thermal performance, the measurements were performed also considering the empty panels, without aerogel in interspace.

The solar factor was estimated following the procedure suggested by the EN 410 and ISO 9050 standards [29,31], considering the PC panels as multiple glazing systems: the calculation of the properties of the assembled product was carried out [31] starting from single PC layer data measured using a conventional spectrophotometer, available at the University of Perugia Labs.

As final output of the study, the accurate experimental analysis and the estimation of the solar factor provided reliable data which were used as inputs for building energy simulations in a case study in different climate conditions (hot, moderate, and cold) and their energy performance was finally compared to the one of conventional double glass units.

2. Materials and methods

2.1. Samples

Advanced aerogel-filled polycarbonate panels were introduced in the market quite recently and they have been widely used in the USA and Northern Europe as skylights, roofs and walls in non-residential buildings (Fig. 1).

In the paper, three aerogel-filled multiwall polycarbonate panels were investigated. Each sample is formed by three walls, two external (with a thickness of 1 mm) and an internal one (0.4 mm thickness), and the granules of aerogel are sandwiched in between (Fig. 2a). They differ in geometry (the orthogonal layers have a different distance) and thickness (Table 1 and Fig. 2b): PC 16-AER (16 mm total thickness), PC 25-AER (25 mm total thickness), and PC 40-AER (40 mm total thickness). Granular aerogel are characterized by diameter of the particles in the 0.7−4.0 mm range [32]. The maximum size of polycarbonate panels is 2100 mm (width) × 7000 mm (length) and they are installed by means of male-female joints.
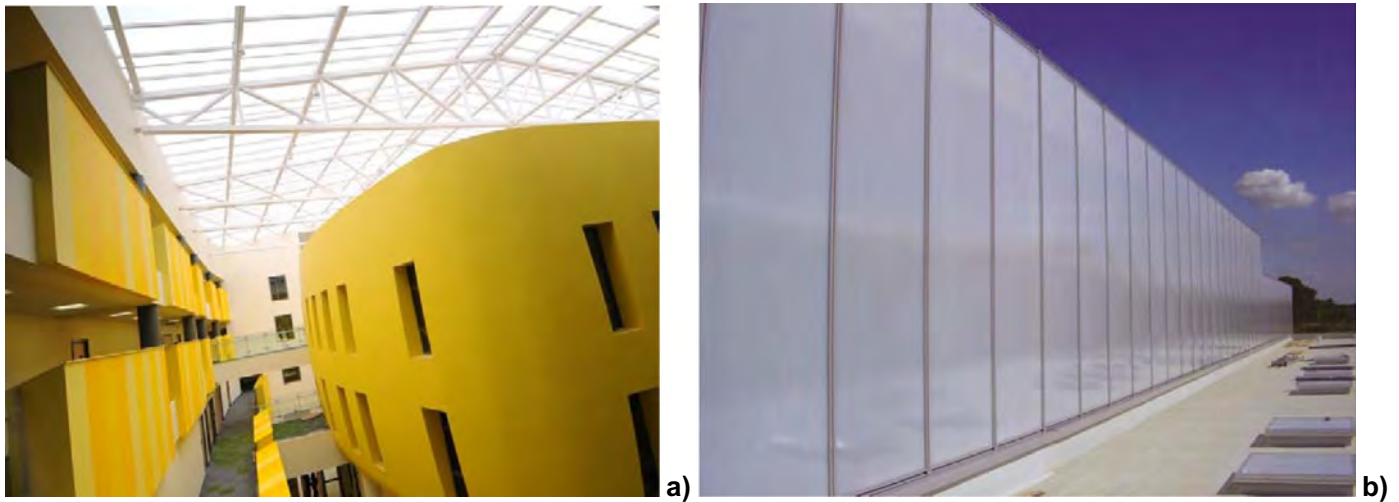
Fig. 1. Granular aerogel filled PC panels' application in non-residential buildings as roofs (a) and walls (b).
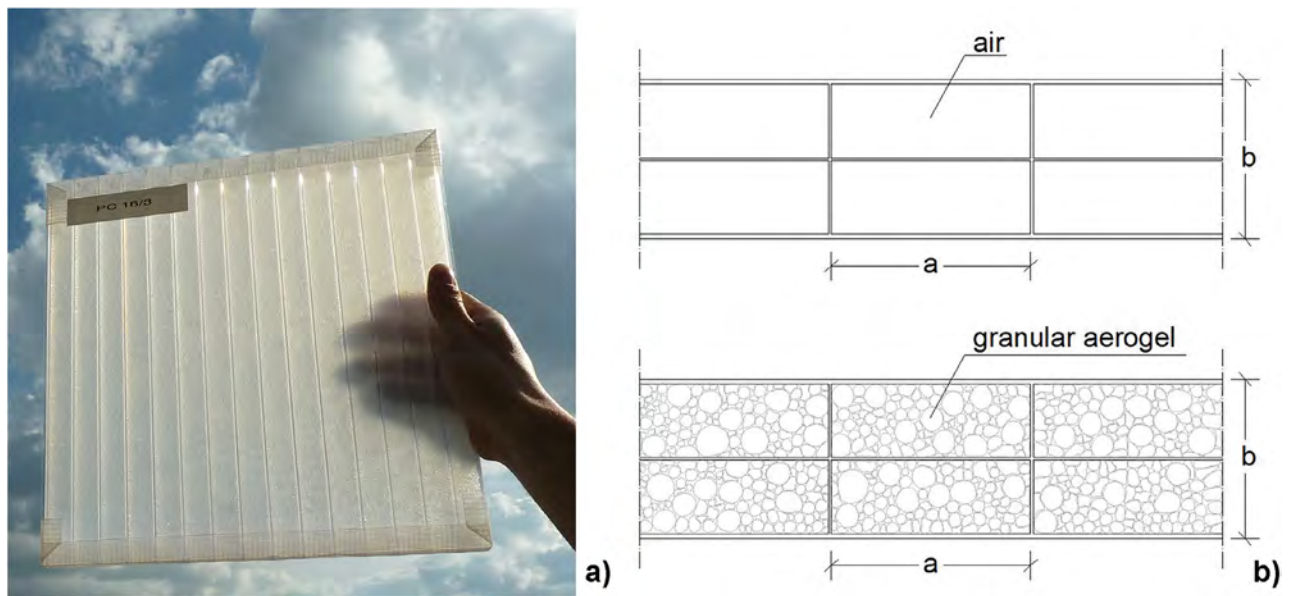
Fig. 2. View of PC systems with aerogel (a) and scheme of the panels (b).

Table 1
Characteristics of the samples.

Sample	Filling	a (mm)	b (mm)	Sample size (mm)
PC 16	Air	20	16	Both 300 × 300 and 800 × 800
PC 16-AER	Granular aerogel (0.7–4.0 mm)			
PC 25	Air	20	25	300 × 300
PC 25-AER	Granular aerogel (0.7–4.0 mm)			
PC 40	Air	35	40	500 × 500
PC 40-AER	Granular aerogel (0.7–4.0 mm)			

The experimental campaign was carried out on the samples with (PC 16-AER, PC 25-AER, and PC 40-AER) and without (PC 16, PC 25, and PC 40) aerogel. Thermal measurements were carried out on the samples with 16 and 40 mm thickness, because PC 25 is only available in the 300 mm x 300 mm size, too small for hot plate apparatus (minimum dimensions 500 × 500 mm).

2.2. Experimental facility

A built-in spectrophotometer with large diameter integrating sphere allowed an accurate optical characterization of the samples, which have high scattering optical behavior. The sphere, with an internal surface made of Spectralon, has a 750 mm diameter.

The spectrophotometer is a single beam type: the samples are mounted outside the sphere and during the procedure the measurements are corrected with the auxiliary port method [6,28]. Full description can be found in [6,27–28]. The estimated measurement uncertainty is 0.02, both for transmittance and reflectance measured spectral data.

Transmittance measurements were performed considering the following incidence angles: 0°; 30°; 45°; 60°, while only the near-normal incidence reflectance (8° angle of incidence) was measured.
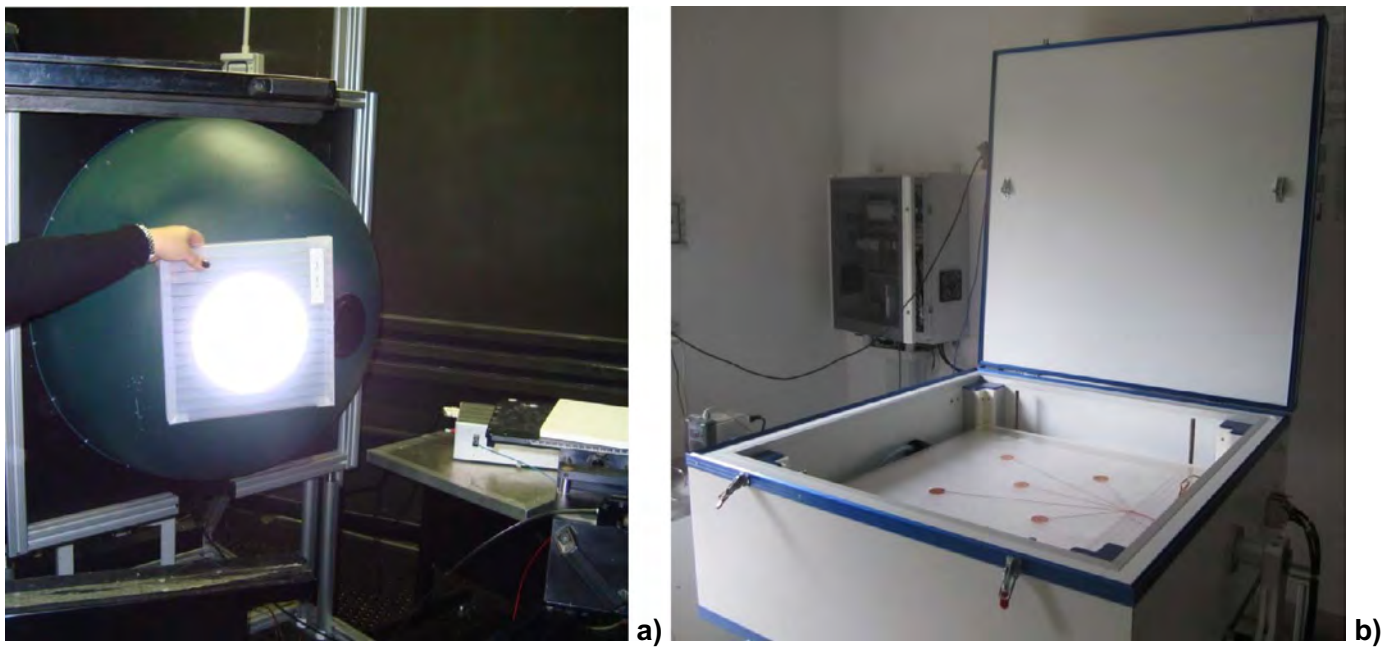
Fig. 3. Optical (a) and thermal (b) measurements.

All the measurements were carried out in the 400 - 2300 nm range, by assuring a characterization of the samples in 96% of the solar spectrum. Fig. 3.a shows the experimental facility during a test.

Transmission and reflection coefficients vs. wavelength of the single PC layers were measured with a conventional double beam type spectrophotometer, Shimadzu SolidSpec 3700, provided with a 60 mm Barium Sulphate coated sphere [19,20].

The U-value was measured with a Guarded Hot Plate facility, according to EN 674:2011 [30]. The test specimens are installed between heating and cooling plates and a constant heat flow occurs through the specimen in steady-state (this condition is satisfied when the variation of the measured thermal resistance is lower than 0.3% for three consecutive measurements). During the experimental campaign, the measuring tool worked in the single sample mode, by using a thermal compensator which replaced one of the two samples.

Thermal resistance is determined by the heat flow and the mean temperature difference between the sample surfaces, measured in five different points [33]. The measurement uncertainty, calculated according to GUM method (Type B standard evaluation [34,35]), was lower than 0.03 W/m^{2}K for all the measurements carried out on the investigated samples. According to EN 674 [30], the U-value should be rounded up to the first decimal place; therefore the U-values were not reported together with the uncertainty in the paper.

Full description of the apparatus can be found in a previous work [27].

A view of the facility with an aerogel filled PC sample mounted on can be observed in Fig. 3b.

2.3. Numerical analysis

The data from experimental campaign were used in a lot of simulations performed by means of Energy Plus software [23,25]. The energy performance of a typical office building (Fig. 4) was investigated, considering several solutions for the transparent envelope: PC systems with and without aerogel in the interspace and conventional systems for a comparison (DGU and LOW-E DGU,

the construction is described in Table 2). The external dimensions are 48 m × 24 m × 8.5 m and large strip windows (window-to-wall ratio about 28%) are in all the walls: thermal transmittance of opaque surfaces is reported in Table 2.

Different climatic conditions were taken into account, by performing the simulations in Rome (Italy), chosen for its hot climate, London (UK), for its moderate climate, and Helsinki (Finland) for the cold climate: the wheatear data (IWEC, International Weather for Energy Calculations) were taken from the Library of Energy Plus [36]. The simulation hypotheses are summarized in Table 2: the heating and cooling system operating periods vary with the climatic zone (the temperature set-points being 20 °C in winter and 26 °C in summer). Moreover, in the model were defined infiltration rate values and internal loads for people, lighting, and any equipment: artificial light is automatically reduced and switched off when the illuminance level is equal to the designed value of 500 lx (the lights were fully dimmable).

3. Results and discussion

3.1. Thermal performance

Detailed measured data about thermal experimental campaign are reported in [27]. U-values were calculated from the measured thermal resistance between the two sample faces, by applying the surface thermal resistance values reported in the standard [30] and considering the sample position. The external surface thermal resistance depends on the wind speed near the glazing, on its emissivity, and on other climatic factors. It is assumed equal to 0.04 m^{2}K/W for ordinary vertical and horizontal glasses. The internal surface thermal resistance depends on the sample position: it can be assumed equal to 0.13 m^{2}K/W for vertical ordinary glasses, whereas it is lower when considering horizontal samples under winter conditions (0.10 m^{2}K/W) [30]. The calculated U-values of all the samples are presented in Fig. 5.

The impact of the aerogel on the thermal performance of transparent polycarbonate systems is remarkable: U-value is 1.4 W/m^{2}K for the 16 mm thickness sample (PC 16-AER), whereas it could reach 0.6 W/m^{2}K when the thickness increases up to 40 mm (PC
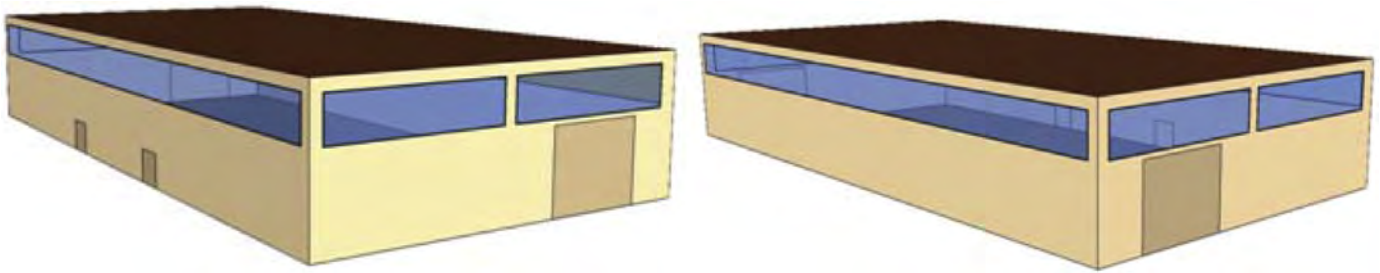
Fig. 4. Model of the building: view south-east (left), view north-west (right).

Table 2
Envelope features and model simulation hypotheses.

Envelope			
Opaque wall	$U = 0.34\,W/m^2K$		
Roof	$U = 0.50\,W/m^2K$		
Floor	$U = 0.31\,W/m^2K$		
DGU	float clear glass (6 mm) - argon 90% (16 mm) - float clear glass (4 mm)		
LOW-E DGU	low-e float glass (4 mm) - argon 90% (16 mm) - float clear glass (6 mm)		
Internal loads			
Lighting (500 lx, fully dimmable)	7 W/m^2		Working days from 7:00 a.m. to 6:00 p.m.
People	30 people (108 W/person)		
Equipment	10 W/m^2		
Heating and cooling system: operating periods			
	Heating (18 °C)	**Cooling (26 °C)**	
Rome	11/01 – 04/15	04/16 – 10/14	Working days from 7:00 a.m. to 6:00 p.m.
London and Helsinki	10/15 – 04/15		
Infiltration rate			
Rome, London, and Helsinki	0.6 vol/h		Working days from 07:00 a.m. – 6:00 p.m.
	0.4 vol/h		Weekends and working days from 6 p.m. to 7 a.m
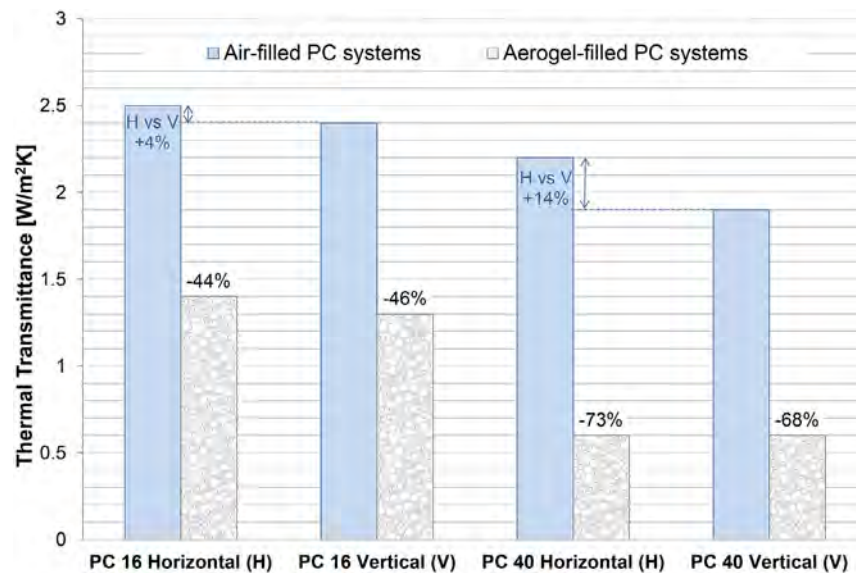
Fig. 5. Thermal transmittance: comparison of samples with and without aerogel.

40-AER). Multiwall PC systems, as far as double or triple glazing systems, are characterized by air gap between PC layers, where the convection has a large influence on thermal performance and, in general, it depends on the tilt angle of the glazing system and on temperature difference. When aerogel granules are packed into gap, a reduction of the convection heat transfer is caused: firstly, aerogels have a thermal conductivity lower than air; secondly, the

small granules reduce the airflow within the air gap, depending on the gas permeability in the granules due to the voids between them [37,38]. Despite a higher thermal conductivity for bulk silica, the one of aerogel granules is indeed very low: nevertheless the contribution of conduction in the solid skeleton is limited because the fraction of the solid (1–10%) is very small. The gas thermal conductivity in the pores is low (lower than that of the air) at
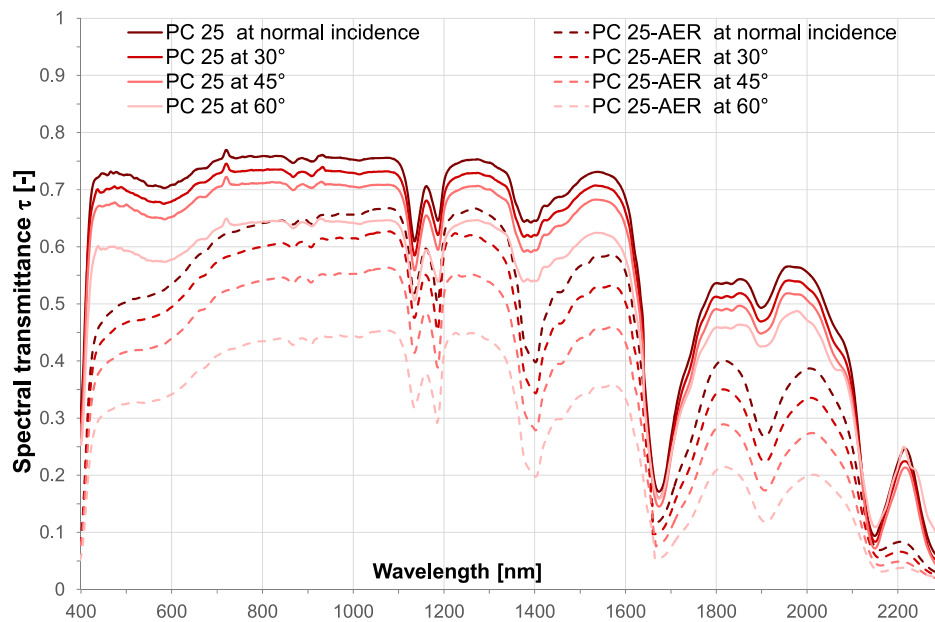
Fig. 6. Spectral transmittance of PC 25 and PC 25 -AER: Impact of the aerogel and of incidence angle.

ambient pressure, due to the Knudsen effect within the nanopores of aerogels (pore diameter of about 20 nm): the air has a free mean path similar to the size of the nanopores which drastically reduces gaseous molecular collision, allowing a reduction in heat transfer [4,38]. Aerogel granules can also reduce the radiative heat transfer because they have relatively large extinction coefficient with respect to air [37]. Therefore, when compared to air-filled PC systems, the reduction in U-value due to aerogel (vertical position of the sample) is about 46% and 68% for 16 and 40 mm thickness, respectively. When the sample is tilted from the vertical to the horizontal position, the reduction is higher (73%) considering the 40 mm thickness sample.

In general, the aerogel in the gap is a packed bed of granules with macropores, which can influence the convection depending on the tilt angle, but the permeability of the aerogel granules in a cavity has not been yet investigated [38]. The results of the experimental campaign (Fig. 5) showed that thermal resistance values measured for aerogel filled systems are irrespective of the sample position (horizontal and vertical) and the difference in U-values is only due to surface thermal resistance values; therefore, the convection in the cavity does not appear to affect the overall thermal performance of the PC systems, as previously showed by Ihara et al. [38] for granular aerogel glazing systems

When compared to conventional double glazings or PC panels with air in interspace, granular aerogel systems have also significant benefits when they are used as roof solutions: U-values are not dependent on the tilted angle to vertical plane, such as in the gas-filled glazings (air, argon, or krypton) which have a worse behaviour when used as roofs instead if vertical panels, due to an increasing in convective heat transfer in the air-gaps under winter conditions [13,38].

3.2. Optical and solar performance

The measured spectral transmittance and reflectance of the sample PC 25 and PC 25-AER are reported in Figs. 6 and 7, also considering the variation of the incidence angle. Then the broadband values were calculated for transmittance, reflectance, and absorptance in the visible and solar range, in compliance with ISO 9050 [31,39]. The detailed results for all the samples at normal incidence were showed in a previous work [27].

As expected, when comparing granular silica aerogel in PC panels with air-filled PCs, transmittance values decrease and a change in the spectral response shape in the 400–700 nm range can be observed (Fig. 6). The optical properties can be described by the Rayleigh scattering theory and by the exterior surface scattering. Rayleigh scattering is caused by the interaction of the light with inhomogeneities in solids, liquids, or gases. The efficiency of scattering depends on the size of the scattering centres and becomes more effective when the size of the particles is similar to the wavelength of the incident light. The presence of a certain number of pores within this range in aerogels can act as scattering centres. However, the aerogel microstructure has predominantly a smaller scale than visible light wavelength, therefore scattering amount in the visible range is small and the light transmittance is still high [4]. Moreover, some selective absorption in the spectral transmission values are shown, especially at 1400 nm, as shown in previous studies [15,19].

As expected, the spectral transmittance of air-filled PC and the one of aerogel filled panels decreases with increasing the incidence angle: the reduction is modest when the angle increases from normal incidence to 30° and from 30° to 45, whereas it is higher when the angle increases from 45° to 60°.

The aerogel has a remarkable impact on the reflectance spectrum (Fig. 7), especially between 400 and 1400 nm, where the reflectance is higher than the one of the air filed PC panels and increases with the aerogel thickness [27]. Due to the high increase of reflectance spectrum in the 420–510 nm range (peak value at 430 nm), the light reflected from the PC systems with aerogel appears bluish.

Among the several parameters associated with glass performance, the most important for building energy calculation are: U-value, light transmittance (τ_v), and solar factor (g-value), also called solar heat gain coefficient (SHGC), which is the total solar transmittance of the glazing. Measurements of g-value are complex, therefore it was calculated as the sum of τ_e and the secondary heat transfer factor of the glazing towards the inside (q_i), resulting from heat transfer which has been absorbed by the glazing [29,31,39]. The calculation method is applied for components made of parallel surfaces: the PC panels have transversal support layers, but this configuration is not considered in the calculation
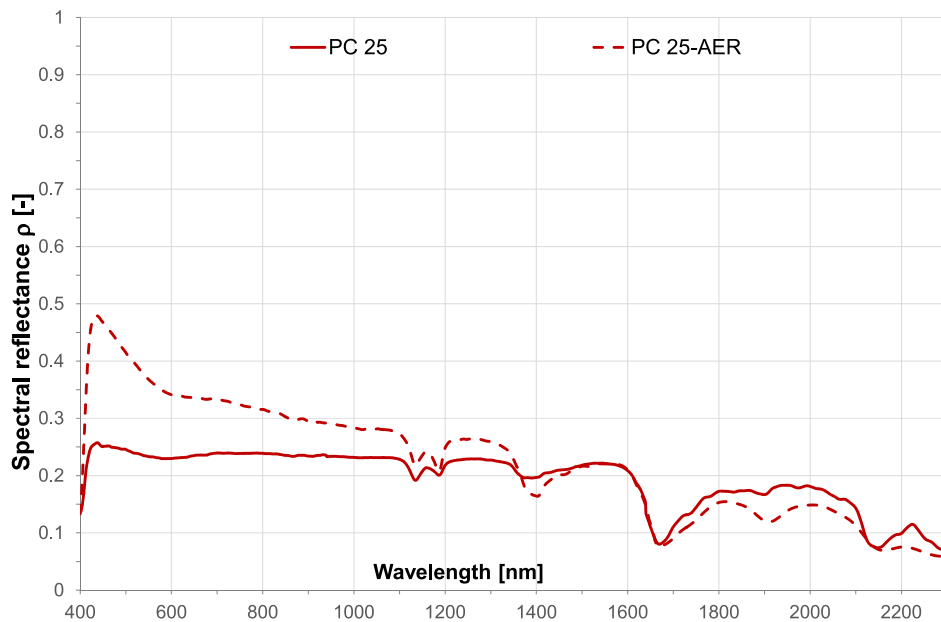
Fig. 7. Impact of aerogel on spectral reflectance for PC 25-AER.

Table 3
Solar factor calculation.

Sample	Solar transmittance τ_e [-]	Solar absorptance α_e [-]	q_i [-]	g-value [-]
PC 16	0.70	0.07	0.02	0.72
PC 16-AER	0.61	0.10	0.03	0.64
PC 25	0.68	0.11	0.02	0.70
PC 25-AER	0.53	0.16	0.05	0.58
PC 40	0.68	0.11	0.02	0.70
PC 40-AER	0.44	0.21	0.07	0.51

method as well. The method was applied in a previous work for similar samples and the results showed a good agreement with the measured data [6]. Following the same procedure, the systems with aerogel in interspace could be approached as multiple glazings with 5 components. The calculations are subjected to an uncertainty, due to the diffusive nature and the inhomogeneity of the aerogel layers, which calculation procedures are not strictly described by the standards.

By means of spectral transmittance and reflectance of the single polycarbonate layers measured with the spectrophotometer SOLID-SPEC 3700, the secondary heat transfer factor of the glazing towards the inside (q_i) and the solar factor for all the samples were calculated (Table 3). The presence of granular aerogel in the panel's air gaps produced a modest increasing of the q_i, which is a fraction of the solar absorptance (+ 0.05 for 40 mm thickness).

In order to assess the potential of the investigated solutions, the performance of the different PC systems was analyzed and then compared to those of commercial windows (conventional DGU and LOW-E DGU) in terms of τ_v, g, and U values (Fig. 8). The PC systems data come from the experimental campaigns, except the U value of sample PC 25, provided by the manufacturer [32]. Data related to glazing system solutions result from the Literature [40,41].

The light transmittance of the aerogel-filled PC panels is lower than the air-filled ones; the reduction in the 15%–40% range, increasing with aerogel thickness. When compared to glazing units, the air-filled PC panels highlights comparable values of τ_v, while the aerogel-filled ones show a reduction in the 20–45% range. However, they can diffuse the light, allowing comfortable visual comfort conditions in buildings and reducing glare areas, especially the zones near the windows [42].

The solar factors of air-filled PC panels are high (0.7) and comparable with the ones of a conventional DGU, whereas the presence of aerogel reduces it significantly (11–27%, depending on the thickness): for PC 25-AER it is 0.58, quite similar to the low-e glazing one and it diminishes to 0.51 for 40 mm thickness.

The U-value of the PC 25, which has the same thickness (25 mm) of the glazing units, is about 1.5 W/m^{2}K, lower than the one of a DGU but higher than the one of a low-e DGU. When considering aerogel-filled solutions, the panels have best performance than both glazing units: the U-value is lower than 1 W/m^{2}K for 25 mm thickness. When considering 40 mm thickness, aerogel-filled PC systems amount to the same performance of a triple glazing window with two low-e layers and argon in the interspaces (U-value equal to 0.6 W/m^{2}K). However, PC panels could be installed easier, especially when considering roofs, because of the lower weight (equal or lower than 5 kg/m^2 instead of 30–40 kg/m^2 for triple glazings). Obviously, at same time, the aerogel allowed a penalization in terms of light transmission (about 30%), but the value is still satisfying.

3.3. Angular dependence of optical properties

The angular optical properties of windows are important during energy modelling in building simulations, because the solar incidence angles are usually high. In general, the programs, as for instance EnergyPlus, use correlations to estimate the glazing system's angular performance at 10° increments and interpolate between them during simulations. The correlations are based on model validated for conventional windows, therefore they might over/underestimate the performance of aerogel-filled advanced solutions.
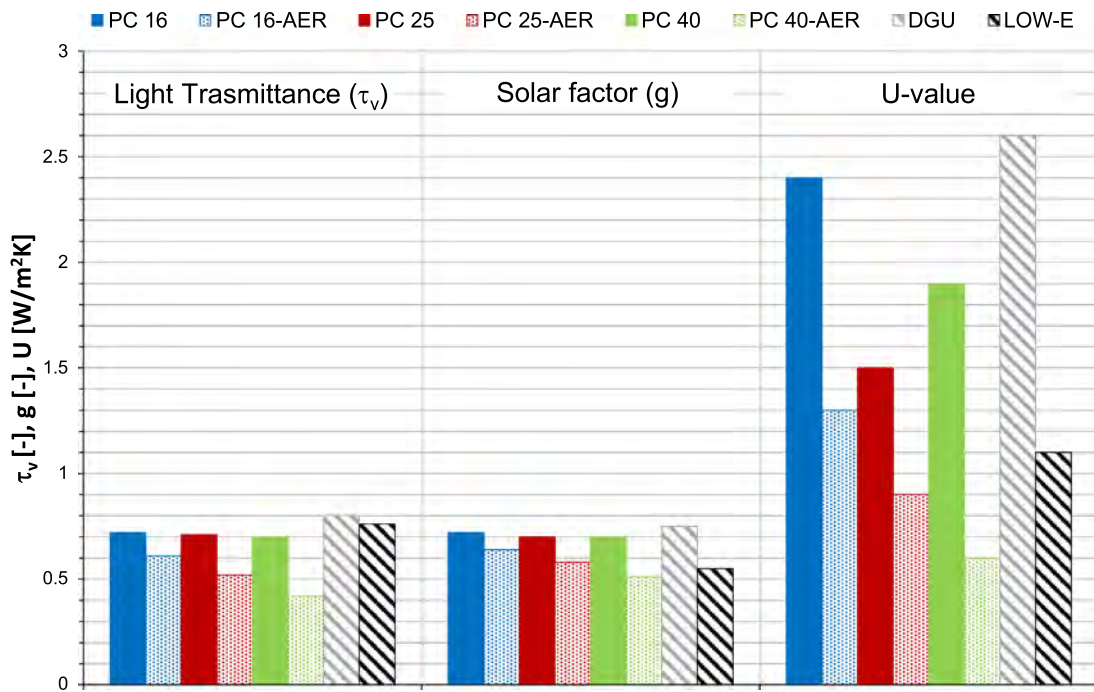
Fig. 8. Comparison of light, solar, and thermal performance.
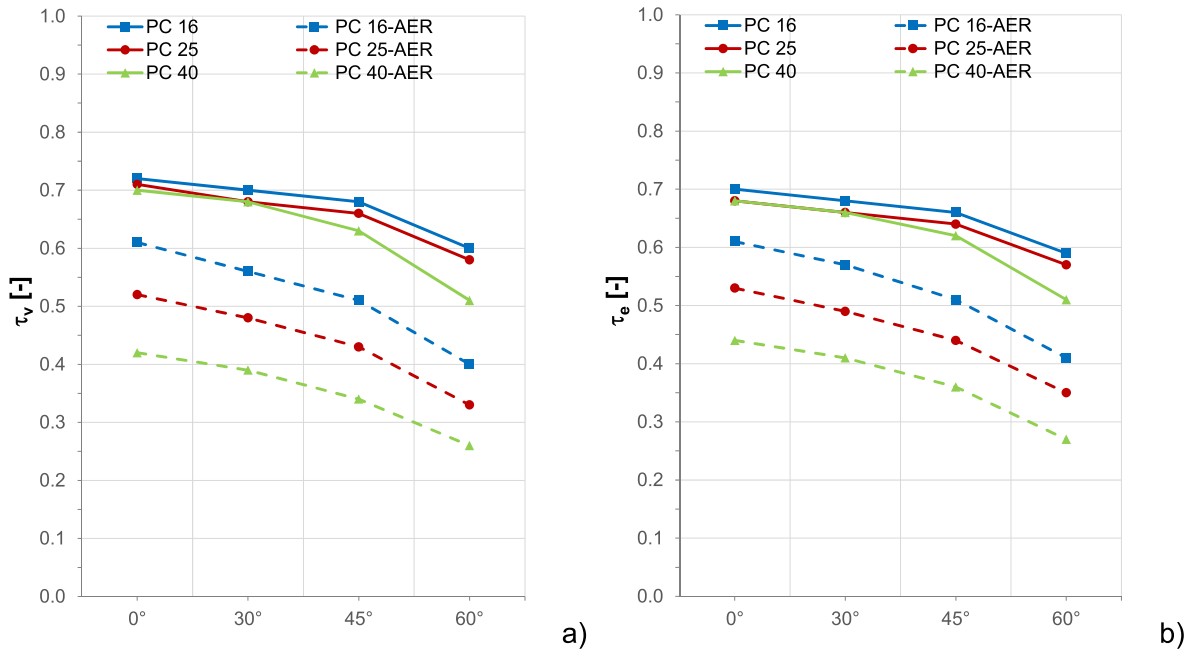
Fig. 9. Angular dependence of light transmittance (a) and solar transmittance (b).

Fig. 9 shows the angular values and decay of the light (a) and solar transmittance (b) of PC samples with and without aerogel in the gap, calculated from measured spectral data in compliance with [29]. In general, the results change in absolute values for the visible and the solar spectra, but their angular dependence has the same behaviour.

When considering PC samples without aerogel (continuous lines in Fig. 9), the τ_v and τ_e values diminish of about 3% when the incidence angle increases from 0° to 30° and from 30° to 45° for the samples with 16 mm and 25 mm thickness; when the angle increases from 45° to 60°, the values decrease of about 12%. The

sample with 40 mm thickness has a different behaviour, decreasing both τ_v and τ_e of about 3%, 7%, and 19% when the incidence angle increases from 0° to 30°, from 30° to 45°, and from 45° to 60°, respectively. In particular, when compared to the other samples, the PC 40 showed the highest reduction when the incidence angle increases from 30° to 45° and from 45° to 60°: at high incidence angles, the contribution of orthogonal layers reflectance is lower, due to the higher distance between the orthogonal layers in the panel, therefore the sample showed a higher reduction in τ_v and τ_e values.
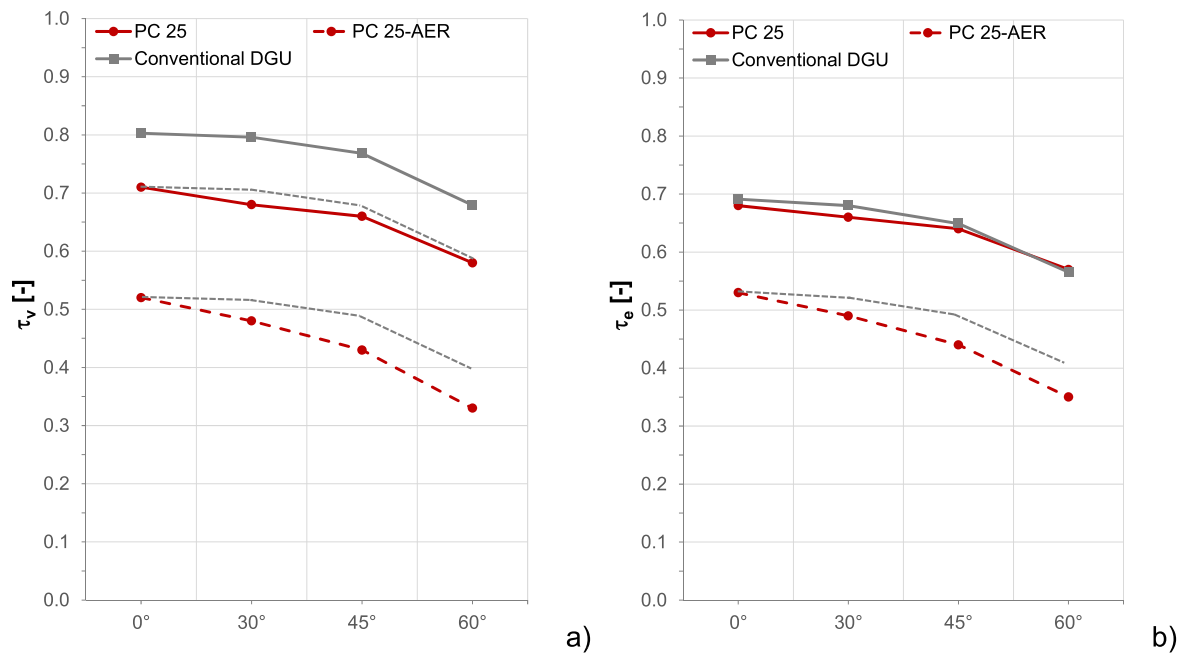
Fig. 10. Angular dependence of light transmittance (a) and solar transmittance (b) of 25 mm sample and comparison with conventional double glazing at the same thickness.
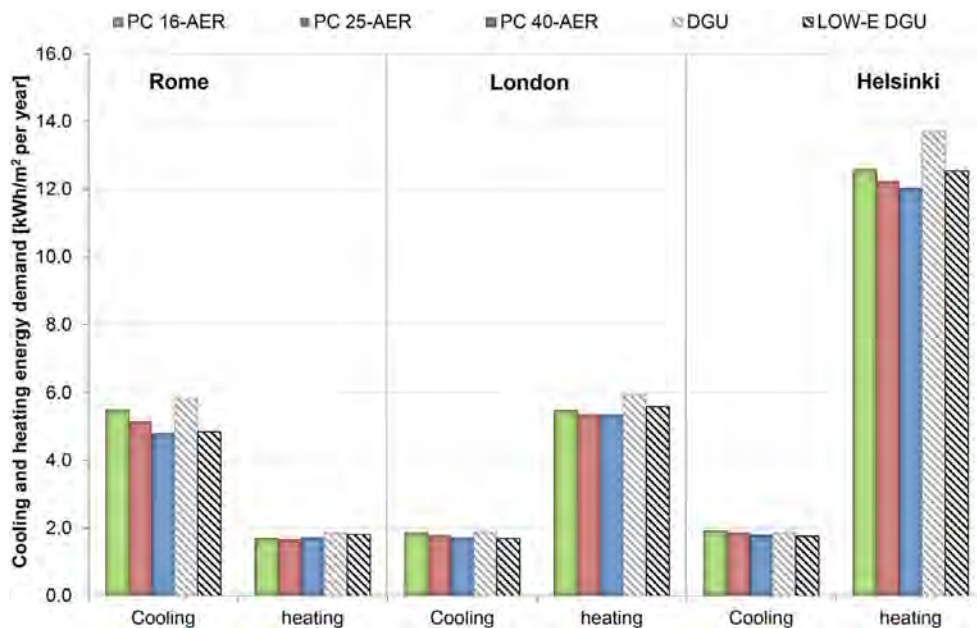
Fig. 11. Annual energy demand for heating and cooling: comparison of PC-aerogel with traditional glazing systems.

The angular decay of PC samples filled with aerogel (dashed lines in Fig. 9) has a higher slope: τ_v and τ_e values decrease of about 7–8%, 9–13%, and 20–24%, when the incidence angle increases from 0° to 30°, from 30° to 45°, and from 45° to 60°, respectively. The range of variation depends on the considered parameter (τ_v or τ_e) and on the sample thickness.

The air-filled PC systems have an angular decay that is slightly different from conventional glass units with a similar thickness [43] (Fig. 10): PC elements perpendicular to the main structure are used to improve the mechanical resistance and, at the same time, they change the incident radiation optical path. The difference is more evident when considering aerogel-filled solutions: conventional glazings have a curve practically flat from normal incidence

to 30°, whereas the reduction about 8% when considering aerogel-filled solutions.

3.4. Energy performance simulations

The impact of the new solutions on building energy performance were evaluated in terms of heating and cooling energy demands, expressed in kWh/m²: ideal energy loads were calculated as the heating and cooling heat transfer rates that needed to be removed or added to the zone to maintain the indoor temperature conditions, without considering any equipment for heating, cooling, and ventilation.

PC systems with granular aerogel in interspace result as the most efficient systems for heating in all climate conditions: the re-

duction in energy demand is in the 7–12%, depending on the building site, and on the aerogel thickness, when compared to the conventional double glazing, as inferred in Fig. 11. The percentage of reduction (2–7%) decreases when they are compared to low-e glazing. In general, the winter performance increases with the aerogel thickness, except for Rome, which has the highest solar daily radiation especially in the winter time. The reduction is consistent with U and g values of the windows: an increasing in aerogel thickness allows lower heat losses from windows (due to the lower U-values), but at the same time the solar factor reduction due to the aerogel thickness increasing diminishes the heat gain from the sun, penalizing the overall result.

By comparing annual cooling energy demand for aerogel- filled PC systems and DGUs, a reduction of about 6%−18% (PC 16-AER and PC 40-AER respectively) can be observed in Rome, consistent with the decrease in solar factor. The reduction is lower or negligible for London and Helsinki. However, when considering low-e glazings in the comparison, the translucent solutions (also considering the highest thickness) have comparable the energy demands for cooling.

4. Conclusions

In the paper, three types of advanced multiwall PC panels (thickness 16, 25, and 40 mm) with translucent granular aerogel were investigated by experimental characterization (thermal and optical performance with large sphere apparatus) and the results were used as input data in energy simulations.

The comparison between thermal performance of air and aerogel-filled PC systems highlighted that the impact of the aerogel is remarkable: the reduction in U-value is 40%–46%, depending on the aerogel layers thickness. U-value is 1.4 W/m^{2}K for the 16 mm thickness sample and it is 0.6 W/m^{2}K when the thickness increases up to 40 mm. Moreover, thermal performance does not depend on the position, showing that the convection heat transfer in the aerogel layer is negligible. Therefore, roof applications are suitable, because the U-values are not influenced by the inclination, such as in the gas-filled glazing systems which have a worse behavior when used as roofs instead of vertical panels [13,37].

At the same time, the reduction in light transmittance due to granular aerogel in the panel is acceptable (15%) for 16 mm and significant (40%) for 40 mm thickness.

The accurate optical experimental campaign highlighted that the geometry of the samples and the aerogel granules in air-gaps allowed an angular dependence very different with respect to conventional multiple glazing systems. Therefore, the numerical software that is widely used to estimate energy and lighting performance of buildings may lead to wrong estimates of the angular performance of advanced PC panels. The method introduced here gives more accurate data, which can be used to accurately predict energy performance in terms of the real solar radiation conditions.

Following the method reported in ISO 9050, the solar factor was estimated by using the optical properties of the layers. The aerogel in air-gaps can reduce g-value significantly: it is quite similar to the low-e glazing one for 25 mm aerogel thickness ($g = 0.58$).

Finally, energy simulations for a case study showed a reduction in energy demand for silica aerogel PC systems both for heating and cooling, when compared to the conventional glazings. However, when compared to low-e glazings, the benefits of the translucent material (also considering the highest thickness) in the interspace are lower for heating and negligible for cooling energy demands.

An added value of the investigated solutions are the significant benefits in terms of visual comfort: they are light diffusing and can prevent from glare, especially when used in roofs, and further studies will focus on daylighting performance analyses.

References

[1] H. Ye, X. Meng, L. Long, B. Xu, The route to a perfect window, Renew. Energy 55 (2013) 448–455.

[2] B.P. Jelle, A. Hynd, A. Gustavsen, D. Arasteh, H. Goudey, R. Hart, Fenestration of today and tomorrow: A state-of-the-art review and future research opportunities, Solar Energy Mater. Solar Cells 96 (2012) 1–28.

[3] M. Koebel, A. Rigacci, P. Achard, Aerogel-based thermal superinsulation: an overview, J. Sol. Gel Sci. Technol. 63 (2012) 315–339.

[4] R. Baetens, B.P. Jelle, A. Gustavsen, Aerogel insulation for building applications: a state-of-the-art review, Energy Build. 43 (2011) 761–769.

[5] S.B. Riffat, G. Qiu, A review of state-of-the-art aerogel applications in buildings, Int. J. Low Carbon Technol. 8 (1) (2012) 1–6.

[6] E. Moretti, M. Zinzi, E. Belloni, Polycarbonate panels for buildings: experimental investigation of thermal and optical performance, Energy Build. 70 (2014) 23–35.

[7] B. Chevalier, M.G. Hutchins, A. Maccari, F. Olive, H. Oversloot, W. Platzer, P. Polato, A. Roos, J.L.J. Rosenfeld, T. Squire, K. Yoshimura, Solar energy transmittance of translucent samples: a comparison between large and small integrating sphere measurements, Sol. Energy Mater. Sol. Cells 54 (1998) 197–202.

[8] C. Buratti, F. Merli, E. Moretti, Aerogel-based materials for building applications: influence of granule size on thermal and acoustic performance, Energy Build. 152 (2017) 472–482.

[9] E. Moretti, F. Merli, E. Cuce, C. Buratti, Thermal and acoustic properties of aerogels: preliminary investigation of the influence of granule size, Energy Procedia 111 (2017) 472–480.

[10] C. Buratti, E. Moretti, E. Belloni, Aerogel plasters for energy building efficiency, in: F. Pacheco Torgal, C. Buratti, S. Kalaiselvam, C.G. Granqvist, V. Ivanov (Eds.), Nano and Biotech Based Materials For Energy Building Efficiency, Springer International Publishing, Switzerland, 2016, pp. 17–40.

[11] E. Cuce, P.M. Cuce, C.J. Wood, S.B. Riffat, Toward aerogel based thermal superinsulation in buildings: a comprehensive review, Renew. Sustain. Energy Rev. 34 (2014) 273–299.

[12] C. Buratti, E. Moretti, Silica nanogel for energy-efficient windows, in: F. Pacheco Torgal, M.V. Diamanti, A. Nazari, C.G. Granqvist (Eds.), Nanotechnology in Eco-Efficient Construction, Woodhead Publishing Limited, Cambridge, 2013, pp. 207–235.

[13] C. Buratti, E. Moretti, Chapter 20 - Nanogel windows, in: F. Pacheco Torgal, M. Mistretta, A. Kaklauskas, C.G. Granqvist, L.F. Cabeza (Eds.), Nearly Zero Energy Building Refurbishment, Springer-Verlag, Londra, 2013, pp. 555–582.

[14] U. Berardi, The development of a monolithic aerogel glazed window for an energy retrofitting project, Appl. Energy 154 (2015) 603–615.

[15] C. Buratti, E. Moretti, E. Belloni, Nanogel windows for energy building efficiency, in: F. Pacheco Torgal, C. Buratti, S. Kalaiselvam, C.G. Granqvist, V. Ivanov (Eds.), Nano and Biotech Based Materials For Energy Building Efficiency, Springer International Publishing, Switzerland, 2016, pp. 41–69.

[16] M. Reim, A. Beck, W. Körner, R. Petricevic, M. Glora, M. Weth, T. Shliermann, J. Fricke, C.H. Schmidt, F. Pötter, Highly insulating aerogel glazing for solar energy usage, Sol. Energy 72 (1) (2002) 21–29.

[17] C. Buratti, E. Moretti, Lighting and energetic characteristics of transparent insulating materials: experimental data and calculation, Indoor Built Environ. 20 (4) (2011) 400–401.

[18] T. Gao, B.P. Jelle, T. Ihara, A Gustavsen, Insulating glazing units with silica aerogel granules: the impact of particle size, Appl. Energy 128 (2014) 27–34.

[19] C. Buratti, E. Moretti, Experimental performance evaluation of aerogel glazing systems, Appl. Energy 97 (2012) 430–437.

[20] C. Buratti, E. Moretti, Glazing systems with silica aerogel for energy savings in buildings, Appl. Energy 98 (2012) 396–403.

[21] F. Cotana, A.L. Pisello, E. Moretti, C. Buratti, Multipurpose characterization of glazing systems with silica aerogel: in-field experimental analysis of thermal-energy, lighting and acoustic performance, Build. Environ. 81 (2014) 92–102.

[22] T. Ihara, T. Gao, S. Grynning, B.P. Jelle, A. Gustavsen, Aerogel granulate glazing facades and their application potential from an energy saving perspective, Appl. Energy 142 (2015) 179–191.

[23] C. Buratti, E. Moretti, M. Zinzi, High energy-efficient windows with silica aerogel for building refurbishment: experimental characterization and preliminary simulations in different climate conditions, Buildings 7 (2017) 8.

[24] Y. Huang, J. Niu, Application of super-insulating translucent silica aerogel glazing system on commercial building envelope of humid subtropical climates: Impact on space cooling load, Energy 83 (2015) 316–325.

[25] C. Buratti, E. Belloni, D. Palladino, Evolutive housing system: refurbishment with new technologies and unsteady simulation of energy performance, Energy Build. 74 (2014) 173–181.

[26] M. Dowson, D. Harrison, S. Craig, Z. Gill, Improving the thermal performance of single- glazed windows using translucent granular aerogel, Int. J. Sustainable Eng. 4 (2011) 266–280.

[27] E. Moretti, M. Zinzi, E. Carnielo, F. Merli, Advanced polycarbonate transparent systems with aerogel: preliminary characterization of optical and thermal properties, Energy Procedia 113 (2017) 9–16.

[28] A. Maccari, M. Montecchi, F. Treppo, M. Zinzi, CATRAM: an apparatus for the optical characterization of advanced transparent materials, Appl. Opt. 37 (1998) 5156–5161.

[29] EN 410, Glass in building - Determination of luminous and solar characteristics of glazing, CEN (European Committee for Standardization), Brussels: Belgium 2011.

[30] EN 674, Glass in building - Determination of thermal transmittance (U value) - guarded hot plate method, CEN (Europeen Committee for Standardization), Brussels: Belgium 2011.

[31] ISO 9050, Glass in building - Determination of light transmittance, solar direct transmittance, total solar energy transmittance, ultraviolet transmittance and related glazing factors, ISO: Geneva, Switzerland 2013.

[32] RODA – E.M.B. Products AG, available at https://www.roda.de/products/daylight-technology/lumira-aerogel/info. (Last access on May 30th 2017).

[33] E. Moretti, E. Belloni, F. Agosti, Innovative mineral fiber insulation panels for buildings: thermal and acoustic characterization, Appl. Energy 169 (2016) 421–432.

[34] ISO/IEC Guide 98-3, Uncertainty of measurement – part 3: guide to the expression of uncertainty in measurement, ISO: Geneva, Switzerland 2008.

[35] JCGM 100, GUM 1995 with minor corrections Evaluation of measurement data — guide to the expression of uncertainty in measurement, ISO: Geneva, Switzerland 2008.

[36] EnergyPlus Wheater Data, available at https://energyplus.net/weather (Last access on May 30th 2017).

[37] T. Gao, T. Ihara, S. Grynning, B.P. Jelle, A. Gunnarshaug Lien, Perspective of aerogel glazings in energy efficient buildings, Build. Environ. 95 (2016) 405–413.

[38] T. Ihara, S. Grynning, T. Gao, A. Gustavsen, B.P. Jelle, Impact of convection on thermal performance of aerogel granulate glazing systems, Energy Build. 88 (2015) 165–173.

[39] B.P. Jelle, Solar radiation glazing factors for window panes, glass structures and electrochromic windows in buildings - measurement and calculation, Sol. Energy Mater. Sol. Cells 116 (2013) 291–323.

[40] H. Manz, U. Menti, Energy performance of glazings in European climates, Renewable Energy 37 (2012) 226–232.

[41] AGC Glass Europe, available at: http://www.yourglass.com/configurator/tp/it/toolbox/configurator/main.html (Last access on May 30th 2017).

[42] Y. Huang, J. Niu, Energy and visual performance of the silica aerogel glazing system in commercial buildings of Hong Kong, Constr. Build. Mater. 94 (2015) 57–72.

[43] M.G. Hutchins, A.J. Topping, C. Anderson, F. Olive, P. van Nijnatten, P. Polato, A. Roos, M. Rubin, Measurement and prediction of angle-dependent optical properties of coated glass products: results of an inter-laboratory comparison of spectral transmittance and reflectance, Thin Solid Films 392 (2001) 269–275.

10th International Conference on Applied Energy (ICAE2018), 22-25 August 2018, Hong Kong, China

Thermo-chromic glazing in buildings: a novel methodological framework for a multi-objective performance evaluation

Luigi Giovannini[a]*, Fabio Favoino[a], Valentina Serra[a], Michele Zinzi[b]

[a]Politecnico di Torino, Department of Energy, C.so Duca degli Abruzzi, 24, 10129 Turin,, Italy
[b]ENEA, Via Anguillarese 301, 00123 Rome, Italy

Abstract

Transparent adaptive façade components can improve the energy performance and the indoor environmental quality of buildings. Nevertheless, their utilization is not widespread, due also to the lack of a robust methodology to comprehensively evaluate their potentialities and find out their most suitable applications. The present paper introduces a novel methodology to characterize the behavior of a transparent adaptive façade component, a thermo-chromic glazing, and predict its effects, through numerical simulations, on energy performance and visual comfort aspects. An experimental characterization on the thermo-chromic glazing was performed to determine its optical properties at the variation of its surface temperature. The component was found to be able to switch its visible transmittance between 0.71 and 0.13, and its solar transmittance between 0.65 and 0.28. The experimental results were used to feed the numerical model created on purpose to describe the adaptive behavior of the component. Finally, a numerical simulation campaign was performed to assess the effects of the thermo-chromic glazing on energy and visual comfort aspects of an enclosed office located in Turin. It was found that the thermo-chromic glazing reduced the overall energy performance compared to a static selective glazing, but it allows improving the visual comfort conditions within the space considered.

1. Introduction

In the last few years, particular emphasis was given to researches related to advanced glazing for smart building envelopes, which can significantly contribute to the achievement of decarbonization targets. The development of

transparent façades able to change their thermal/solar/luminous properties according to boundary conditions and user needs, in order to optimize indoor environmental quality and maximize the energy efficiency, is one of the current research direction mainly pursued by designers, manufacturers and scientists [1].

Among the so called adaptive façades (confining the analysis to the material/component scale only), the switchable glazing represents a very promising solution. In more detail, strong research efforts in this field are currently devoted to improve the spectrally selective properties of the glazing, to better manage heat, solar and visual transmission. Within the different dynamic glazing, i.e electro-chromics, gaso-chromics, liquid crystals, suspended particle devices, photo-chromics and thermo-chromics, the last one, based on a color and properties change due to temperature variations, is enjoying ever-increasing popularity. The most relevant drawbacks due to the poor switching efficiency of the conventional VO_2 coatings, onto which thermochromism is based, are being solved by working on different aspects, i.e. film thickness, dopant and microstructure [2, 3, 4, 5, 13]. A widespread implementation in real buildings is therefore approaching [6].

Alongside the innovation at material/component level, parallel researches have to be carried out, aimed on one hand at fully characterizing its performance and on the other hand at providing tools able to manage contemporarily energy and comfort aspects. During actual building operation, an adaptive glazing should meet several requirements, pertaining to different physical domains [7]. Thus, when adopting these dynamic glazing, the capability to provide a clear picture of the overall behavior and performance, through the adoption of the right metrics, indicators and tools, becomes of paramount importance to make the expected energy savings, together with the high comfort level expectations, really achievable.

2. Methodology

The present study proposes i) to determine the optical properties of the thermo-chromic glazing at the variation of its surface temperature and ii) to evaluate the effects of its application on a case study office, in respect to those relative to a traditional selective glazing. The methodology followed to perform this study can be subdivided into two distinct parts: an experimental characterization of the thermo-chromic sample and, starting from the results obtained in the first phase, a numerical analysis of a case study office equipped with the thermo-chromic glazing. The first phase, carried out by means of an integrating sphere at ENEA Casaccia Research Center, allowed an accurate determination of the optical behavior of the thermo-chromic glazing at the variation of its driving factor, i.e. its surface temperature. A numerical model to describe the thermo-chromic behavior was created starting from the outcomes of the first phase. The numerical model was then implemented into a novel simulation tool, under development at Politecnico di Torino, to numerically evaluate the effects of the application of the thermo-chromic glazing to an office case study. The tool used allowed performing a simultaneous evaluation of the effects of the adaptiveness of the thermo-chromic glazing on energy and visual comfort aspects. This was done by managing different simulation software, for different purposes, together in a unique integrated simulation process. The outcomes of this phase were then compared to a reference case, represented by a traditional selective glazing.

In the combination of an experimental campaign and a simulative analysis lies one of the strength of the present work, as it allows creating a numerical model for the behavior of the thermo-chromic glazing starting from accurate data (more accurate than those commonly provided by manufacturers). This aspect becomes even more important when considering that the numerical analysis here performed, being very accurate, requires a heavy computation; feeding thus the numerical model with high resolution input data assures a higher precision in the analytical results.

2.1. Material and sample

The Vanadium Oxide VO_2 thermochromic material is embedded in the interlayer of a laminated glass unit composed of: double layer of 3 mm of float glass; approximately 1 mm of polymeric interlayer integrating the nanostructured functional material. The characterized thermochromic laminate sample has a size of 400 mm by 400 mm. For the numerical analysis the LGU was combined has the outermost laminate of an IGU as discussed in Section 3.1.

Fig. 1. Different states of TC glass, 400 x 400 mm sample under direct solar radiation.

2.2. Experimental characterization

The optical characterization of the thermo-chromic sample was carried out with an in-built spectrophotometer, able to perform measurements on complex samples, which conventional instruments are not suitable for. The experimental set-up consists of the following components:

- The light source is a 300 Watt xenon arc-lamp with adjustable power, which covers the whole visible spectrum and 94% of the solar spectrum, as defined in the relevant standard [8]. The size of the collimated beam can be modulated through a system of lenses and diaphragms according to the measurement requirements and sample geometric complexity. The light beam diameter was set to 60 mm for this measurement campaign.
- The spectrophotometer is equipped to an integrating sphere with a 75 cm diameter. The sphere external shell is made of aluminum, while the internal surface is made of Spectralon, a white material with reflectivity greater than 95% in the whole solar range. The sphere is equipped with several ports to perform transmittance and reflectance measurements with the auxiliary port method, needed for single beam-type spectrophotometers. The sample port diameter can be varied according to sample characteristics, a 200 cm port was used for this test.
- The detection system consists of three array spectrometers and three detectors to analyze different spectral bands: NMOS for the 250–1000 nm range (dispersion 1.4 nm/pixel) and InGaAs for the 900–1700 nm range (dispersion 3.125 nm/pixel). In the post elaboration, spectral data are re-built with 1 nm as spectral resolution. The signal (radiant power) in the sphere is transmitted to the detection system via optic fibers.

The measurement procedures used in the present study are the following:

- the transmission coefficient is measured as the ratio between the radiation transmitted by the specimen mounted on the sample port and the energy directly entering the sphere by the same port without specimen;
- in the reflection mode, the light beam entering the sphere hits the sample with an 8 deg. angle of incidence. The reflection coefficient is measured as the ratio between the radiation reflected by the specimen and that of a calibrated white target, both mounted in turn on the sample port. Full measurement procedure is explained in [9].

The instrument error is estimated to be 0.02 for the different measurement modes.

Measurements were carried out at (near) normal incidence for different surface temperature values. The sample was heated-up by direct exposure to solar radiation and the surface temperature was monitored during each measurement through thermo-graphic analyses. Since the optical transition of such systems may vary in cooling and heating, it is stated that the test was carried out in heating mode.
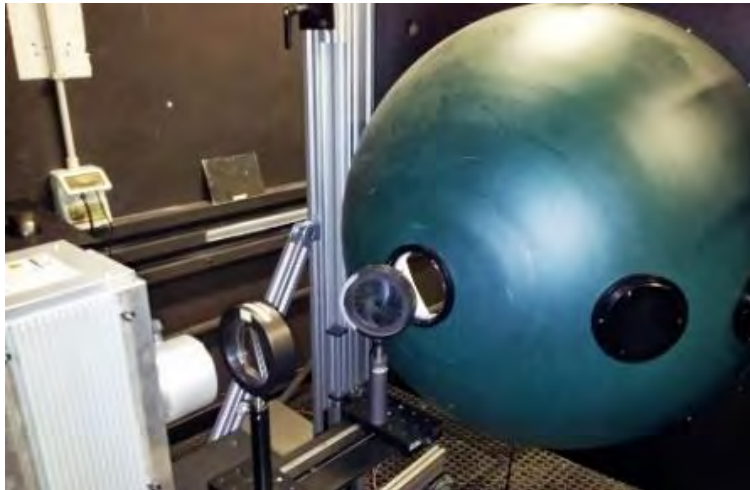
Fig. 2. Spectrophotometer with large integrating sphere and light source used to characterise the thermochromic sample.

2.3. Numerical analysis

The measured optical properties were used to create a numerical model describing the behavior of the component at the variation of its surface temperature. The numerical model was then implemented in a Building Performance Simulation Tool to perform a simultaneous evaluation of the effects of the adaptiveness of the thermo-chromic glazing on energy and visual comfort aspects. This was done by managing together a daylight simulation software (DAYSIM, which in turn uses Radiance computation engine) [10] and an energy simulation software (EnergyPlus) [11]. The case study chosen was an enclosed office, located in Turin, 3.6 large, 4.5 m deep and 2.7 m high. One of the short walls, South-oriented, was equipped with a window 3.3 m large and 1.5 m high, for a Window-to-Wall Ratio (WWR) of 50%. The wall equipped with the window had an average thermal transmittance of 0.77 W/m^{2}K, while all the other surfaces were considered as adiabatic. The window was alternatively equipped with the thermo-chromic glazing and with a selective glazing, as reference case, with the same visible transmittance as that of the thermo-chromic glazing in its clearer state. Glazing performance indicators for the thermochromic and selective glazing are summarized in the Section 3.2.

The energy aspects were evaluated by means of the Energy Performance Index (EP), representing the annual primary energy demand per unit of floor area. The global average efficiency of the heating system is 0.9, while for the cooling system the SEER is 3.1. For cooling and lighting energy uses 2.17 is considered as the conversion factor for electric energy to primary energy, while 1 is adopted for heating energy uses as per local national context of the numerical study). The global EP was calculated as sum of the energy performances relative to heating (EP$_h$), cooling (EP$_c$) and lighting (EP$_l$).

Visual Comfort aspects were evaluated by means of the Useful Daylight Illuminance (UDI) [12], a Climate-Based Dynamic Metric that quantifies the percentage of occupied time of the year in which daylight is above, below and between an upper and a lower threshold value. These thresholds, respectively of 2500 lx and 100 lx, represent the limits of the range in which daylight is considered useful, i.e. neither too strong, which would cause a glare sensation to the user, nor too poor to perform a visual task. UDI was evaluated for a grid of sensors located at 0.75 m above the floor and at 0.50 m from each wall. For the sake of brevity the present paper focuses on the outcomes of the analyses presented rather than describing in detail the methodology followed.

3. Results

3.1. Experimental results

Preliminary measurements were carried out on the two faces of the sample, to check if the different layers of sample may affect the optic response; as no differences were found the measurement campaign was carried out with side 1 of the sample on the outdoor, as indicated by the manufacturer. The transmittance results are presented in figure 3 for the following temperature values: 15, 30, 45 and 60°C. It can be observed that the material has a higher switching behavior in the visible range (380-780 nm) than in the near-infrared region (780-1700 nm).

This different response is better highlighted in figure 4, where the evolution of broad-band parameters is calculated for measurements carried out every 5°C between extreme surface temperatures (15-70°). The visible transmittance ranges between 0.71 and 0.13, with a switching factor of 5.5; the switching factor decreases to 2.3 for the solar transmittance in the same temperature range, due to the fact that the switching factor in the near-infrared range is 1.3. In absolute figures, the solar transmittance ranges between 0.65 in the cold state and 0.28 in the hot state. Reflectance measurements were also carried out for the different temperature levels, and this quantity showed not to be significantly affected by the thermal conditions. Visible and solar reflectance are both 0.07 in the cold state, while the values decrease to respectively 0.06 and 0.05 in the hot state. According to these results, the absorptance values can be calculated, which account for: 0.22 and 0.28 respectively in the visible and solar ranges in the cold state, raising to 0.81 and 0.67 in the hot state.

The laminate overall optical properties obtained are summarized in Table 1 in the following section.
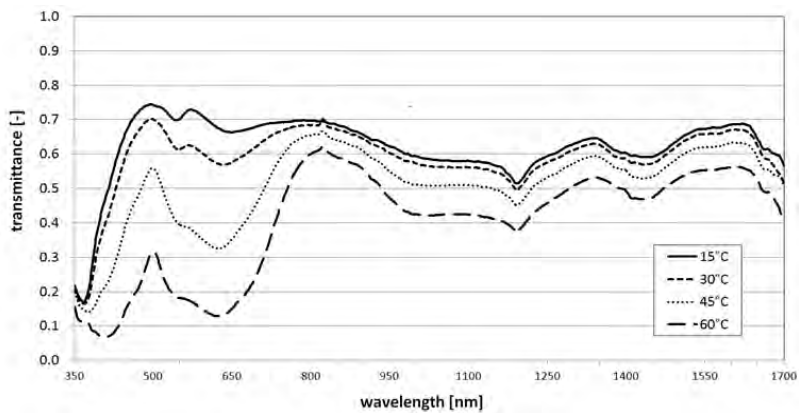
Fig. 3. Spectral transmittance for different surface temperatures of the sample.
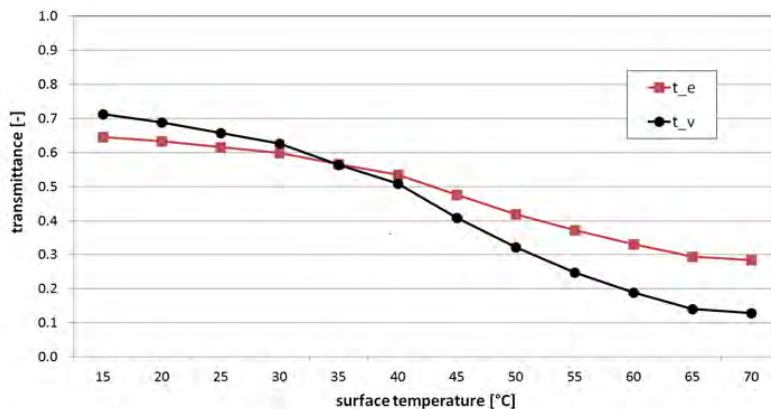
Fig. 4. Visible and solar transmittance for different surface temperatures.

3.2. Numerical results

3.2.1. Glazing Performance

In order to understand what could be the performance achievable by the thermochromic glazing in comparison to traditional glazing, in the numerical analysis a TC glazing unit (TCG) is compared to a standard reference double glazing unit with Selective Coating (SG), both composed by: an external laminate, 16 mm Argon cavity and a 6 mm clear inner pane of glass. For the sake of comparison the only difference between the two glazing unit (TCG and SG) lies in the external laminate, in one case (TCG) composed by the TC laminate, and in the other (SG) composed by a clear glass laminate with a selective coating on the outer surface of the cavity. The model of the compared glazing units is created by means of WINDOW software [14] and imported within Energyplus [11], which uses the validated model *Window calculation module* [15].

In table 1 the integral optical characteristics (visible and solar) of the thermochromic laminate are summarized, as measured according to Section 3.1, moreover the characteristic of the external laminate of the DGU are included for comparison. In table 2 the overall characteristic of the compared glazings are summarized, where it is shown that the dynamic range of the thermochromic glazing is relatively limited, 0.11 range for the g-value and 0.25 range for the visible transmission between the clearest and darkest state.

Table 1. Optical properties of the thermo-chromic glazing (in its cold and hot state) and selective glazing considered.

External laminate properties	τ_{vis}	τ_{sol}	ρ_{vis}	ρ_{sol}	α_{vis}	α_{sol}
	(-)	(-)	(-)	(-)	(-)	(-)
Thermo-chromic laminate (cold state)	0.65	0.39	0.05	0.03	0.3	0.58
Thermo-chromic laminate (hot state)	0.37	0.25	0.04	0.03	0.59	0.72
Glass with selective coating	0.65	0.38	0.16	0.41	0.19	0.21

Table 2. Optical properties of the thermo-chromic glazing (in its cold and hot state) and selective glazing considered.

IGU properties	T_{vis}	g-value	U-value (W/m^{2}K)
TCG (cold state)	0.58	0.45	2.5
TCG (hot state)	0.33	0.34	2.5
DGU	0.59	0.39	2.5

3.2.2. Energy Performance

Figure 5.a shows the results relative to the annual energy performance of the office case study equipped with the thermo-chromic glazing (TCG) and with the selective glazing (SG). It is possible to observe how, for the latitude and climate of Turin, the office equipped with the thermo-chromic glazing shows a slightly worse energy performance than that equipped with the selective glazing, with an increase of 3.14 kWh/m^2·year. Table 3 summarizes the energy performances relative to heating, cooling and lighting obtained for the two glazing technologies analyzed. It is possible to observe how the application of the thermo-chromic glazing is able to significantly reduce the EP_h (-20.6%) and its effects on the EP_l are negligible (+0.6%), but it significantly increases the EP_c (+23.2%).

Table 3. Energy performance relative to heating, cooling and lighting for the two glazing technologies analyzed.

	SG	TCG	Percent variation
	[kWh/m^{2}y]	[kWh/m^{2}y]	[%]
EP Heating	7.36	5.85	-20.6%
EP Cooling	19.56	24.09	+23.2%
EP Lighting	27.38	27.54	+0.6%

3.2.3. Visual Comfort

Figure 5.b shows the outcomes relative to the annual visual comfort conditions of the office case study equipped with the thermo-chromic glazing (TCG) and with the selective glazing (SG). The results show that the application of the thermo-chromic glazing is able to improve the visual comfort conditions, in respect to those obtained for the selective glazing. In more detail, it is possible to observe that the case study equipped with the thermo-chromic glazing, in respect to the one equipped with the selective glazing, shows:

- nearly an equal value of the $UDI_{\leq 100\,lx}$, (+0.1%), which accounts for the moments of the year in which daylight is too poor;
- a higher value of $UDI_{100-2500\,lx}$, (+7.9%), which accounts for the moments of the year in which daylight is suitable to perform a visual task;
- a lower value of $UDI_{>2500\,lx}$, (-8.0%), which accounts for the moments of the year in which daylight is too strong, potentially creating hence a glare sensation to the users.
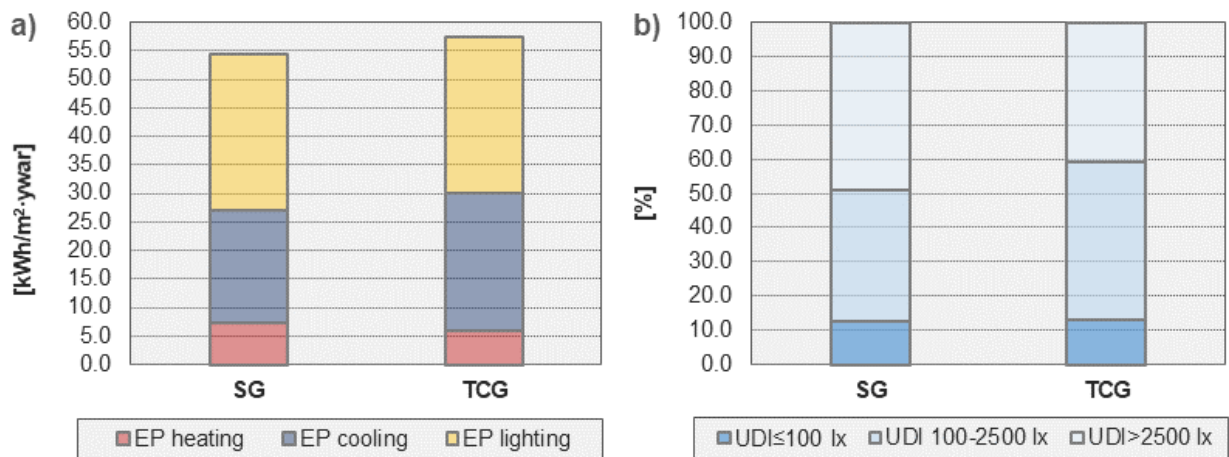
Fig. 5. Numerical outcomes relative to: a) Energy performance and b) Useful Daylight Illuminance.

4. Discussion

From the outcomes of the present study, a different behavior of the thermo-chromic glazing in terms of energy performance and visual comfort can be observed. On the energy performance side, the application of a thermo-chromic glazing shows to be inconvenient for the latitude and case study selected. In fact, the energy use relative to the thermo-chromic glazing is lower than the one relative to the selective glazing, due to higher cooling energy use. This is due to the fact that, when the glazing switches to its darker states, the glass surface temperatures are higher compared to the selective glazing. This is caused by an increased absorption of solar radiation by the thermo-chromic functional layer (from 0.28 to 0.67, as visible in Section 3.1), increasing the secondary heat flow transferred to the indoor environment. This results in a higher cooling need and potentially higher overheating risk. Nevertheless, during winter this has a positive impact, slightly reducing the heating energy demand and increasing radiant temperatures.

On the visual comfort side instead, the thermo-chromic glazing is able to improve the visual comfort conditions in respect to those obtained for the selective glazing, as far as daylight availability ($UDI_{100-2500\,lx}$) and glare risk ($UDI_{>2500\,lx}$) are concerned. This happens mainly because, as in summer the thermo-chromic glazing is able to reach a darker state (due to a higher outdoor air temperature), it reduces the incoming solar radiation, resulting in an illuminance on the horizontal plane which could increase the glare risk [12]. In winter instead the thermo-chromic glazing, not being able to reach its darker state (due to a lower outdoor air temperature and/or high switching temperature of its thermo-chromic functional layer), allows the same daylight penetration as the selective glazing. This is beneficial as in winter there are generally poorer daylight conditions (in terms of duration and intensity).

Globally the lighting energy use does not vary according to the glazing adopted, as the UDI fell-short (UDI$_{\leqslant 100\,\text{lx}}$) is practically unchanged, in fact the lighting system control is designed to ensure a target of 500 lux on the work-plane.

5. Conclusions

An optical characterization of a thermo-chromic glazing was carried out for different surface temperatures and it was found to present a different switching range, for the same temperature variation, for visible and solar transmittance. For the former the switching factor was found to be 5.5, while for the latter it was 2.3. The reason for this difference lies in the fact that the switching factor for the near-infrared range is extremely low (1.3), which in turn influences the overall solar transmittance, but not the visible transmittance.

The outcomes of the optical characterization were used to feed a numerical model created ad hoc to describe the behavior of the thermo-chromic glazing. This one was used, within a novel building performance simulation tool, to simultaneously evaluate the effects of the thermo-chromic glazing on energy and visual comfort aspects for an enclosed office located in Turin. It was found that the application of this component, for such a case study, is not a suitable choice for the energy performance, as this one is slightly worse than the one relative to a selective glazing. In fact the thermo-chromic glazing, in such a temperate climates, could have advantages to reduce space heating, while reducing potential glare at the same time, although might introduce higher cooling energy needs and potential overheating. On the other hand, the use of the thermo-chromic glazing improves visual comfort conditions, compared to the selective glazing, as it is able to reduce the amount of hours in which daylight is too strong to perform office visual task during summer.

This methodological framework and multi-objective analysis can allow a further investigation on the integration of thermo-chromic glazing in buildings, and in particular the implications of material characteristics not only on the building energy use, but also on visual and thermal comfort. The effects on all these aspects of the application of thermo-chromic glazing in buildings will be extensively investigated considering also different climates, different orientations and spaces with different geometric features.

References

[1] Perino M., Serra,V., Switching from static to adaptable and dynamic building envelopes: A paradigm shift for the energy efficiency in buildings, Journal of Façade Design and Engineering, 2015, 3:2, 143-163

[2] Kamalisarvestani, M. Saidur R., Mekhilef S., Javadi F.S., Performance, materials and coating technologies of thermochromic thin films on smart windows, Renewable and Sustainable Energy Reviews, Volume 26, 2013, 353-364

[3] Gagaoudakis E., Aperathitis E., Michail G., Panagopoulou M., Katerinopoulou D., Binas V., Raptis Y.S., Kiriakidis G., Low-temperature rf sputtered VO$_2$ thin films as thermochromic coatings for smart glazing system, Solar Energy, 2018, 165, 115-121.

[4] Top, I., Binions, R., Warwick, M.E.A., Dunnill, C.W., Holdynski, M., Abrahams, I., VO2/TiO2 bilayer films for energy efficient windows with multifunctional properties, Journal of Materials Chemistry 2018, 6 (16), 4485-4493.

[5] Warwick, M.E.A., Ridley, I., Binions, R., Variation of thermochromic glazing systems transition temperature, hysteresis gradient and width effect on energy efficiency, Buildings, 201 (2), art. no. 22,

[6] Granqvist, C.G., Recent progress in thermochromics and electrochromics: A brief survey, Thin Solid Films, 2016, 614, 90-96

[7] Favoino, F., Fiorito, F., Cannavale, A., Ranzi, G., Overend, M., Optimal control and performance of photovoltachromic switchable glazing for building integration in temperate climates, Applied Energy, 2016, 178, pp. 943-961

[8] ISO 9050. Glass in building-determination of light transmittance, solar direct transmittance, total solar energy transmittance, ultraviolet transmittance and related glazing factors; 2003.

[9] Maccari A, Montecchi M, Treppo F, Zinzi M. CATRAM: an apparatus for the optical characterization of advanced transparent materials. Applied Optics, 1998;37:5156-5161.

[10] http://daysim.ning.com/, accessed Sept 2018.

[11] https://energyplus.net/, accessed Sept 2018.

[12] Nabil A, Mardaljevic J. Useful daylight illuminance: a new paradigm for assessing daylight in buildings. Lighting Research & Technology, 2005;37(1):51-59.

[13] Granqvist CG. Electrochromics and thermochromics: towards a new paradigm for energy efficient buildings. In5th International Conference on Functional Materials and Devices (ICFMD), AUG 04-06, 2015, Johor Bahru, MALAYSIA 2016 (Vol. 3, pp. S2-S11).

[14] LBL, WINDOW software, https://windows.lbl.gov/tools/window/software-download, accessed Sept 2018.

[15] Winkelmann FC. Modeling windows in EnergyPlus. Proceedings IBPSA Building Simulation. 2001 Aug 13.

[16] https://www.berlin-innovation.de/uploads/tx_innodb/product_information_gesimat.pdf, accessed Sept 2018.

IIETA International Information and Engineering Technology Association
Advancing the World of Information and Engineering

Numerical modelling of the thermal energy demand in Italian households through statistical data

Matteo Caldera[1*], Giovanni Puglisi[1], Fabio Zanghirella[1], Paola Ungaro[2], Giuliano Cammarata[3]

[1] ENEA (Italian National Agency for New Technologies, Energy and Sustainable Economic Development), via Anguillarese 301, 00123 Roma, Italy
[2] ISTAT (Italian National Institute of Statistics), viale Oceano Pacifico 171, 00144 Roma, Italy
[3] Università degli Studi di Catania, piazza Università 2, 95125 Catania, Italy

Corresponding Author Email: matteo.caldera@enea.it

ABSTRACT

The availability of reliable and up-to-date data on energy uses and consumption is a key aspect in order to achieve the goals set out by European Directives on energy efficiency, and to monitor the effectiveness of energy policies supporting buildings' retrofit actions. In such a context, a numerical model, implemented in Excel® and Matlab®, was developed in order to determine the energy consumption for space heating, domestic hot water and cooking in households, based on a statistical dataset of 20,000 records collected in a survey on the energy consumption of Italian families carried out by the National Institute of Statistics (ISTAT). The space heating model is based on the definition of classes of dwelling-types, while the energy use for DHW and cooking are calculated on a record-by-record basis according to a Standard-based approach. The present paper presents the results of a refined version of the model, in particular the calibration of relevant parameters accounted for the secondary equipment for space heating, resulting in improvements in the reliability for the allocation of the fuel consumption among the end-uses. The refinement and validation of the model are still in progress, since they are functional for the assessment of the energy consumption of households in the period between two subsequent surveys.

1. INTRODUCTION

European policies encourage solutions for the reduction of the energy demand and the improvement of energy efficiency in the residential sector, which covers by itself around 30% of the total primary energy demand. In Italy, current Laws [1-2] provide financial incentives for energy retrofit measures addressed both to the envelope and to the energy system. They are mainly in the form of tax deduction covering part of the investment costs (from 65% up to 75% for common parts of block of flats) and accorded in ten years, or of capital grant covering variable quotas of the investment costs and given in two to five years. Just a few numbers, taken from ENEA's Annual report on energy efficiency [3], which demonstrate the performance of these incentives: the mechanism "*Ecobonus*" (i.e. tax deductions) financed around one million of retrofit interventions during the period 2014-2016, and in the last year, it activated 3.3 Billion Euro of investments mainly for the replacement of windows (50%) and of heating systems (20%), and for the installation of solar shadings (12%). Moreover, the incentive "*Conto Termico*" (i.e. capital grant), which addresses to the improvement of the energy efficiency and the use of renewables for thermal energy production, registered in 2016 an increase +80% of requests with respect of 2015.

In such a context, the availability of reliable and up-to-date data on energy uses and consumption is a key aspect in order to achieve the goals set out by Directives and to monitor the effectiveness of energy policies supporting buildings' retrofit actions. In response to these needs, the Regulation EC/1099/2008 of the European Parliament and of the Council of 22 October 2008 on energy statistics, and the amending Commission Regulation EU/431/2014 of 24 April 2014 on energy statistics require Member States to provide data on the annual energy consumption of households for final destination and energy source.

In Italy, the National Institute of statistics (ISTAT), in collaboration with the National Agency for energy and sustainable economic development (ENEA) and the Ministry for the economic development (MiSE), carried out a survey on households' energy consumption to comply the obligation. The survey was conducted in 2013 on a representative sample of 20,000 households and provided information on the consumption habits, the characteristics and types of plant, and on the energy expenditures of Italian households specified by energy carrier. These data provide a comprehensive overview of the residential sector in the National energy context and represent an official background for the development of future energy strategies addressed to domestic users.

The assessments of the energy savings potential and of the impact of public energy policies aimed at retrofitting existing buildings are complex tasks. Energy consumption and potential energy savings depend not only on the objective characteristics of the building and of the thermal equipment, but also on the occupants' behaviour [4-5], and on urban and socio-economic variables [6].

Many models and software are currently available for the evaluation of the energy performance and the cost-optimal analysis of existing dwellings, also intended for energy audits, but they generally perform detailed simulations of single buildings on an hourly basis [7] and therefore they are time-

consuming and not suitable for large-scale scenarios. Approaches based on statistical data are more effective in evaluating the energy consumption on an urban, regional or national scale. They can consider building typologies, the so-called building types that is a reference building for an entire building category [8]. Alternatively, representative building samples employ a group of buildings instead of a single reference dwelling, in order to represent the whole category by accounting for the heterogeneous characteristics of the various cases. On the other hand, statistical analyses of a robust reference dataset or hybrid deterministic-statistical models can be considered to find simplified correlations for the assessment of the energy demand [9].

The availability of accurate data and their level of detail and aggregation play a fundamental role in the implementation and calibration of energy models, which can be used not only to evaluate the observed energy consumption on different spatial and temporal scales but also to make predictions, e.g. based on a historical dataset and on forecasting data [10-11].

The present paper describes the results of a refined model, implemented in Excel® and Matlab®, aimed at determining the energy consumption for space heating, domestic hot water (DHW) and cooking in the Italian residential sector, based on the dataset from ISTAT survey. The results were obtained from the updated version of a numerical tool, which was presented at the AIGE-IIETA Conference 2017. The space heating model relied on the definition of classes of dwelling-types, by accounting for the geometrical and thermo-physical properties of the dwellings. The energy consumption for DHW and cooking were calculated on a record-by-record basis according to a Standard-based approach. In the current version of the tool, the calibration of relevant parameters specifically used for DHW and cooking accounted for secondary equipment for space heating, resulting in improvements for the allocation of the fuel consumption among the end-uses. The refinement and validation of the model are still in progress, since they are functional for the assessment of the energy consumption of households in the period between two subsequent surveys.

2. METHODOLOGY

The numerical tool consisted of two sets of models for the estimation of the energy demand in the residential sector: one set for the space heating and the other for DHW and cooking uses. The input data were obtained from the ISTAT survey.

The models, which were described in [12], were revised and updated. In particular, the secondary equipment for space heating has been accounted for the selection of the records required by the calibration of relevant parameters. For each end use, a three-dimensional matrix was created in order to allocate the fuel and the type of system (centralised, independent, local appliances for space heating and DHW, ovens and hobs for cooking) for the complete dataset on a record-by-record basis, regardless of the primary or auxiliary function.

Moreover, the revision of the model included the automated algorithm for the congruity check of the dataset, the algorithm for the calculation of the actual occupation of the apartment by the family members during the reference year, the algorithm for DHW production, and new reference prices for natural gas and LPG based on regional data instead of national averages. The most important features of the updated models are

summarised below.

2.1 Space heating

Keeping in mind the objectives of the activity, the methodology selected for the space heating model was a compromise between the type and level of detail of the information provided by the survey, and the level of complexity required by the simulations. These constraints led to the definition of classes of dwelling-types; the national residential building stock was subdivided into twenty classes of dwellings, summarized in Table. The classification of the dwelling-types accounted for the:

- Year of construction: before 1950, 1950-1969, 1970-1989, after 1990;
- Type of dwelling: single-family house, multi-family house, ground floor apartment, middle floor apartment and top floor apartment.

The core of the space heating model relied on the equivalent resistance-capacitance model R5C1 described in [13] and based on the European standard EN ISO 13790 [14], and it was implemented in Excel®.

Table 1. Dwelling type classes for the space heating model

Type of Dwelling *	Construction period			
	Before 1950	1950-'69	1970-'89	After 1990
SFH	DTC1	DTC6	DTC11	DTC16
MFH	DTC2	DTC7	DTC12	DTC17
GFA	DTC3	DTC8	DTC13	DTC18
MFA	DTC4	DTC9	DTC14	DTC19
TFA	DTC5	DTC10	DTC15	DTC20

* Note. SFH: single-family house; MFH: multi-family house; GFA: ground floor apartment; MFA: middle floor apartment; TFA: top floor apartment.

The main information obtained by the survey were:
- Characteristics of the envelope of the building, for the definition of the classes of dwelling-types;
- Characteristics of the primary heating systems, for the estimation of the global seasonal efficiencies;
- Hours of operation of the heating systems, for the reduction factor for intermittent heating;
- Energy expenditure for the fuel, for the model validation.

The model estimated the energy consumption for space heating through the following steps:
1. Calculation of the thermal energy demand under continuous operation of each dwelling-type in five climatic zones;
2. Calculation, for each dwelling-type class in each climatic zone, of the reduction factor for intermittent operation, based on the average number of hours per day when the heating system was turned on;
3. Assumption of reference values for the global efficiency of the different types of heating plant, for each dwelling-type class in each climatic zone;
4. Calculation of the primary energy demand under intermittent operation, for each dwelling-type class in each climatic zone;
5. Estimation of the total annual energy consumption for space heating for each dwelling-type class on a national basis.

In order to perform the calculations for each climatic zone, the weather data (temperature, radiation and humidity) referred to the main town whose heating degree-days (HDD) was "barycentric" with respect to the HDD in each climatic

zone.

2.2 Domestic hot water

The model was implemented in Matlab®, and analysed the energy consumption for DHW production for each single household of the survey by means of a Standard-based approach. Moreover, the relevant parameters were obtained from the analysis of the state of the art, BATs and a market survey of domestic equipment.

Two options were available for the calculation of the energy demand for DHW: either according to the number of occupants or to the floor area of the apartment. The average daily hot water demand was estimated according to the Italian Standard UNI 9182 [15] in the former case, and according to Standard UNI/TS 11300:2 [16] in the latter case. In the present context, the approach based on the number of occupants was followed, and the annual DHW net energy demand was calculated with the following relation:

$$Q_{DHW} = K_r \cdot c_w \cdot V_{w,occ} \cdot \Delta T_w \cdot \sum_{occ} d_{occ} \qquad (1)$$

where:

- K_r is a correction factor provided by [15], which accounted for the number of rooms in the apartment;
- c_w is the thermal capacity of water, i.e. $1.162 \cdot 10^{-3}$ kWh/kg/K;
- $V_{w,occ}$ is the average daily hot water demand per capita (in litres);
- $\Delta T_w = 25°C$ is the temperature difference of water, i.e. the supply temperature was set to 40°C while mains were set to 15°C;
- d_{occ} is the number of days in a year of occupation of the apartment by each component of the family.

If solar collectors for DHW production were available, the annual contribution of solar thermal was estimated by considering the number of solar collectors and the typical design solar fractions for DHW, and it was deducted from the net energy demand.

The model accounted only for the main/primary DHW heating system, as secondary DHW system were sporadic (present in just 3.3% of the records of the survey). The equipment efficiencies were determined according to the reference values reported in [16-17], as a function of the fuel, of the age and type of the system (local boiler, independent or centralised system).

As anticipated, new features were added in the current version of the model, in order to refine its accuracy. In particular, heat loss coefficients were associated to the presence of thermal energy storages and of recirculation piping. DHW recirculation was accounted in centralised systems installed after 1990 and in independent systems installed after 2000. The absence of water recirculation in the older systems was accounted by an extra hot water demand.

2.3 Cooking

Similarly, the model for cooking was implemented in Matlab® and calculated the energy consumption for each single record by means of a Standard-based approach. Moreover, the relevant parameters were obtained from the analysis of the state of the art, BATs and a market survey of domestic appliances. In agreement with Eurostat guidelines

[18] only ovens and hobs were considered, since small appliances (e.g. microwave ovens, kettles, coffee makers and toasters) generally have a sporadic or limited use. Energy consumption was correlated to the number of occupants, corrected in order to account for periods spent away.

The theoretical basis of the model was obtained from the European Commission Regulations on Ecodesign requirements [19-20], and Standard EN 60350 [21] on methods for measuring the performance of household electric cooking appliances. ISTAT survey provided the type of fuel, the usage frequency of ovens and hobs, and the classes of age and size for the ovens.

The energy consumption of a single cycle (EC_{oven}) for electrical and gas-fired ovens was calculated with the following formula [19]:

$$EC_{oven} = SEC \cdot \frac{EEI}{100} \qquad (3)$$

where EEI is the energy efficiency index of the ovens in a single cycle, while SEC is the standard energy consumption required to heat up a normalized load during a cycle, which depended on the energy source and was calculated according to one of the following relations:

- Electrical ovens (in kWh):

$$SEC = 0.0042 \times V + 0.55 \qquad (4)$$

- Gas fired ovens (in MJ):

$$SEC = 0.0440 \times V + 3.53 \qquad (5)$$

where V is the volume of the cavity, extrapolated from the classes provided by the ISTAT survey: small (assumed equal to 40 L), medium (54 L), and large (65 L). As for the other fuels, no data were available from the survey, hence ovens fueled with gas or LPG were assumed with $V = 65$ L based on a market analysis. The SEC for LPG ovens was calculated with the formula (5) as well.
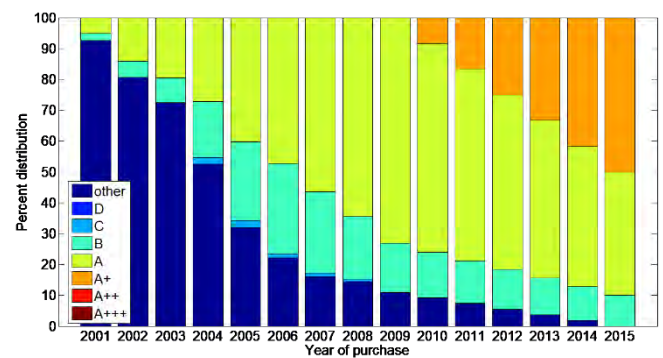
Source: ENEA elaborations of Gfk data from [22]

Figure 1. Energy efficiency index of ovens

The index EEI, which defined the energy efficiency class of the ovens according to the European classification [19], was estimated according to the age; as shown in Figure 1, an EEI value was calculated for each year, according to the weighted average of the energy efficiency classes of ovens sold in that year. Data related to the sales of ovens according to the energy labelling in the Italian market up to 2009 were taken from Gfk database, as reported in [22], while the extrapolation for the

following years was based on a market survey [23].

Eq. (3) to (5) refer to a normalized cooking cycle, which was considered equivalent to the energy demand of two occupants. The annual energy consumption was then calculated by multiplying the energy demand times the average weekly usage frequency of the oven provided by the survey.

A slightly different model was used for the hobs, because no historical sales data were available. The energy consumption of a single cooking cycle EC_{hob} was calculated as the ratio between the energy demand ED_{hob}, i.e. the theoretic minimum energy in a single cooking cycle, and the average hob efficiency ε_{hob}:

$$EC_{hob} = \frac{ED_{hob}}{\varepsilon_{hob}} \qquad (6)$$

Normalised tests, which include heating up and keeping the temperature for a defined period, were considered representative of a typical household cooking process [21]. As described in the results, the average mass load per cooking cycle was determined in order to minimise the median deviation between the data from the survey and the results of the model. While ED_{hob} was assumed independent of the fuel (it refers to a normalised load), the efficiency depended on the hob type. Missing the data on the specific technology (e.g. electrical resistance, radiant, induction), electrical hobs were assumed inductive; a market analysis showed that induction hobs represented the majority of electrical units and the most efficient category. Reference efficiency depended on the type of fuel, and these values were selected [24-25]:

- Electrical: 74%;
- Natural gas: 40%;
- LPG: 45%;
- Biomass: 14%.

According to Annex I of [20] and to a market analysis [23], the normalised energy consumption (EC_{hob}) for induction hobs was assumed equal to 230 Wh/kg. Therefore, according to Eq. (6), it was possible to calculate the energy demand (ED_{hob}) and, finally, the energy consumption for the other fuels. Hence, the annual energy consumption of the hobs was obtained by multiplying the energy demand per cycle times the number of occupants' times the average weekly usage frequency and the actual occupation period of each person.

2.4 Calibration of the model

As described in the previous sections, the results of the model for DHW and cooking depended on some parameters, which provided average information on the energy uses of Italian families. The calibration of such parameters was done by comparing the results of the model with the energy consumption calculated for each household from the expenditures of the last 12 months obtained from the ISTAT survey. In the selected records, the fuel was used only for a specific end-use (e.g. only for cooking), in order to avoid approximations associated with the extrapolation of the energy consumption of the other end-uses. Therefore, it was not possible to consider electricity, because electrical appliances, lighting and space cooling strongly affect the electrical bill. The ongoing activity on the model is addressing to this issue, and the next versions will include electrical appliances and space cooling in order to extend the validation related to all domestic end-uses.

The calibration consisted in a single-parameter tuning for each end-use. The selected parameters were the average load per cycle of the hobs for cooking (i.e. the mass of water heated up according to a Standard test procedure [21]), and the average daily hot water demand per capita for DHW production. These parameters depended mainly on the occupants' behavior; therefore, the values obtained with the selected fuel were applied also to the other fuels with an acceptable approximation.

The preliminary step consisted in converting into energy values the expenditures collected by the survey. As mentioned above, the survey provided the annual costs from the bill of the main fuels in the last 12 months between the second semester of 2012 and the second semester of 2013, without distinction of the type of end-use. Therefore, it was necessary to select proper average end prices of the fuels for that period and for the domestic market. The current version of the numerical code calculated the average prices per kilowatt-hour of natural gas and LPG on a regional scale, which was an improvement of the average national prices used in.

As regards natural gas, the final price with tax was determined with reference to the economic conditions of the protected market set by the Italian National Authority (AEEGSI) [26], by considering the variable network component, the regional surtax and the excise duty for each Region. The calculation of the energy consumption of gas in terms of kilowatt-hour accounted for the ranges of gas consumption defined by AEEGSI, and for a lower heating value LHV = 9.59 kWh/Sm^3 (since the system efficiencies referred to the LHV).
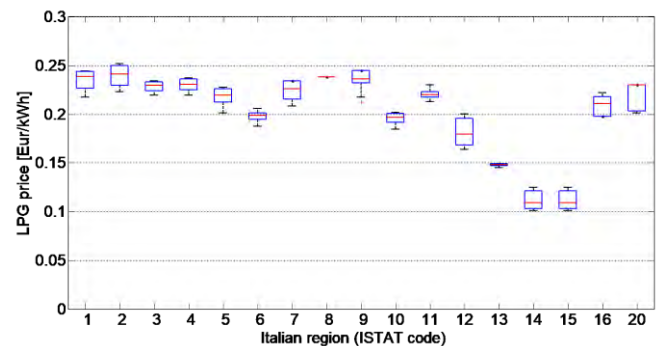
Source: ENEA elaborations of data obtained from the database of list prices of oil products of selected provincial Chambers of commerce in Italy

Figure 2. Regional list prices of LPG delivered in tanks up to 15 kg in the residential market

As regards LPG, there is not a National Authority that regulates the prices, similarly to natural gas; instead, the provincial Chambers of commerce collect the list prices communicated by local distributors twice per month. In the context of the present study, the price of LPG was obtained for each Region from a province that was selected based on the population (very few data were found on the local sales of LPG, therefore population was used as the reference criteria). Two delivery methods were considered: LPG sold in tanks up to 15 kg, which is a common solution for cooking, and LPG sold in bulk for tanks up to 5,000 L, which is a more common option for space heating and DHW. The average domestic list prices for tanks up to 15 kg are depicted in Figure 2, which shows both the variability (boxplots) and the medians (red line inside the boxes) during years 2012 – 2013. The average price for LPG sold in bulk was about 18% higher, mainly because

tax (i.e. VAT) was higher (even if there were remarkable differences from province to province). According to personal communications with operators in the market of the LPG distribution, discounts of 10% and 25% to the list prices were applied to LPG in tanks up to 15 kg and to LPG sold in bulk, respectively.

As regards the other fuels, the following average prices with tax were used: 14.5 cent€/kWh for diesel oil (elaboration of data taken from MiSE), 4.46 cent€/kWh for wood logs and 6.38 cent€/kWh for wood pellets (from a market survey)

3. RESULTS AND DISCUSSION

3.1 Main outcomes from the survey

ISTAT survey on energy consumption of households represented the basic source of input data for the model. The statistical analysis revealed that in 2013 Italian families spent over 42 billion Euros for the energy bill, with an average expense per family of 1,635 Euros. Figure 3 summarises the average actual expenditures of Italian families for energy-related products, calculated as the ratio between the gross costs in the last 12 months and the number of families that purchased the fuel. Diesel oil registered the highest average gross expense per family, while LPG the lowest. On a territorial level, the expenses were 30% higher in Northern than in Southern Italy (with a difference of about 400 Euros per family). The average cost increased with the number of occupants and the age, even if there was no direct proportionality with these quantities.

The main fuel for space heating and DHW was natural gas, used by more than 70% of the families. As summarised in Table 2 (that refers only to the main heating systems), biomass, LPG and electricity were more common with portable or fixed appliances, while diesel oil was still used in more than 11% of centralised space heating systems. The independent heating system was the most common type, both for space heating (in 66% of the families) and for DHW (74% of the families).

Local heating appliances were more common in Southern Italy (31% for space heating and 29% for DHW), while centralised heating systems were used above all in North-western Italy (31% for space heating and 10% for DHW), mainly because of the colder winter season in these regions. The majority of families (65%) used the same heat generator both for space heating and for DHW. Secondary DHW systems were sporadic; hence, they were not considered in the model.

Biomass was used by a significant part of the population; more than 20% families used wood logs, with an average annual consumption of 3.2 ton, while pellets were limited to 4.1%. As expected, the wood consumption was higher in the mountain municipalities (above 40% of the families).

The space heating systems were turned on every day during the heating season in 87% of the families, but with significant local differences (98% in Bolzano, 62% in Sicily).

As regards cooking appliances, in the statistical dataset ovens and hobs were available in 93% and 99% of the households, respectively. According to the fuel, 14% of the ovens used natural gas, 81% electrical energy, 4% LPG and 1 % biomass (wood log or pellets), while 73% of the hobs used natural gas, 4% electricity, 22% LPG and less than 1%

biomass. More details of the results of the ISTAT survey can be found in [28].
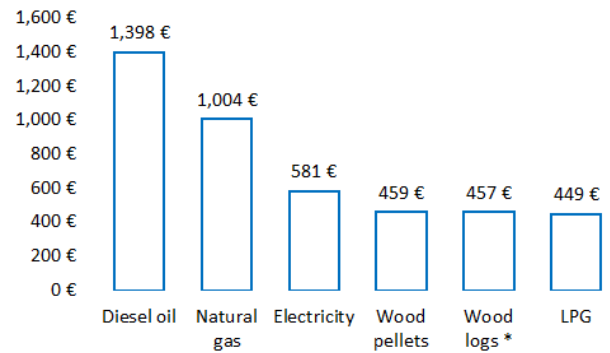
Source: Istat Survey on energy consumption of households – 2013
* Note. Data for wood logs refer only to the purchased quota; they do not consider the self-produced quantities.

Figure 3. Average actual expenditures in a year of Italian families for energy products

Table 2. Families (percent) by type of fuel and typology of the main heating system, both for space heating and DHW

	Space heating				
	Centralised	Independent	"Fixed" appliances	"Portable" apppliances	Total
Natural gas	83.8	86.5	6.1		70.9
Electricity	1.4	0.4	17.7	54.2	5.1
Biomass	0.7	4.8	73.9		14.5
LPG	2.5	5.3	2.3	45.8 *	5.8
Diesel oil	11.6	3.0			3.7
	Domestic hot water			
	Centralised	Independent	Local boilers	Total
Natural gas	80.8	83.9	26.0	71.9
Electricity	2.3	0.9	66.8	14.4
Biomass	1.5	2.7	1.6	2.4
LPG	4.4	8.6	5.0	7.6
Diesel oil	10.7	2.9	0.6	2.9
Solar Thermal	0.1	1.0		0.7

* Note. Kerosene included
Source: Istat Survey on energy consumption of households - 2013

3.2 Model calibration and results

As detailed in the Methodology, the calibration of the model was aimed at finding the proper average values of the relevant parameters for DHW and cooking. In fact, the models should be able to estimate the energy consumption of households between two subsequent surveys. In order to achieve this objective, the survey data was used to calibrate the following parameters, which strongly affected the users' consumption and were directly related to their daily needs: the average daily hot water demand for DHW, and the average load per cycle of the hobs for cooking.

The percent deviation between the model and the survey was calculated on a record-by-record basis according to the following formula (subscript m and s refer to the model and to the survey, respectively):

$$\Delta EC = \frac{EC_s - EC_m}{EC_m} \times 100 \qquad (7)$$

The calibration was divided into three steps. In the first step, only cooking was considered: the calculated energy consumption was compared with the records of the ISTAT survey in which each fuel was used only for cooking, in order

to avoid approximations related to space heating and DHW, which would involve uncertainties comparable to the target variable (i.e. the energy consumption for cooking). From a statistical point of view, the robustness of the estimates depended on the sample size associated with the specific end-uses. The sample size associated to each fuel led to select LPG as the reference fuel for this analysis, because the number of records where LPG was used exclusively for cooking (considering also secondary equipment for space heating) was the most representative. In fact, as summarised in Table 3, LPG was used exclusively for cooking in 2,165 records (that is 49% of the records using LPG for cooking), much larger than natural gas (657 over 14,450 that is 4.6%). As regards biomass, the number of records that could be used was too small for reliable results, i.e. only six records corresponding to 3.6% of the 168 records were biomass was used for cooking. Therefore, the average load per cycle of the hobs – expressed in terms of kg of water heated up according to the standard test procedure – was determined for LPG by minimising the median deviation between the selected data from the survey and the model. The result was 1.86 kg of water per capita, and it was applied to the other fuels as well, because it depended mainly on the user behavior and much less significantly to the fuel. Figure summarises the relative deviation of the model from the statistical "actual" data related to the annual energy consumption for cooking.

The boxplots represent the interquartile ranges while the (red) intermediate lines represent the median for each distribution. Moreover, the notches below and above the median display the variability of the median between samples. The width of a notch is computed so that box plots whose notches do not overlap have different medians at the 5% significance level. The significance level is based on a normal distribution assumption, but comparisons of medians are reasonably robust for other distributions. Whiskers extend from each end of the box to the adjacent values in the data; by default, the most extreme values are within 1.5 times the interquartile range from the ends of the box. Outliers (displayed with a red + sign) are data with values beyond the ends of the whiskers [25].

As shown by the width of the box in Figure 4, the model for cooking consumption fitted quite well with records associated with LPG. Instead, higher deviations were found for natural gas, since both the median and the width of the box were sensibly higher: the model underestimated to half the natural gas consumption obtained from the survey. This result may be largely due to the lower robustness of the data sample related to this fuel (the comparison was made on 4.6% of the records, which used natural gas only for cooking), which may increase the probability to consider record with incomplete information. In particular, some records were characterised by energy consumptions unusually high for cooking only, i.e. above 5,000 kWh/y per capita. As regards biomass, the median deviation of 0% (i.e. model in line with the survey data) was a good result; nevertheless, the minimal data sample (only six records) did not allow guaranteeing adequate reliability for this fuel. It is important to emphasise that no standard test procedure and benchmark were found for domestic biomass appliances, consequently the assumptions done could be very approximate. Moreover, biomass appliances are used also for space heating, hence the relative contribution is difficult to extrapolate and quantify.

In the next step, the daily hot water demand per capita was tuned on the records where each fuel was used only for DHW

production. As reported in Table, LPG had the highest data sample, with 172 records, while biomass had the lowest representativeness, with only 13 records. Therefore, LPG was used also for the calibration of the DHW model, which resulted in an average daily hot water demand of 60 L per capita, which was between the demand prescribed by UNI 9182 for social housing (40 - 50 L) and for middle class housing (70 - 80 L). The deviations obtained for each fuel are depicted in Figure 5, which shows that similar considerations outlined for cooking were also valid for DHW. In this case, the median deviation for natural gas and biomass increased to 63% and 86%, respectively. The high relative deviation between the survey and the model for these fuels was largely due to the lower robustness of the estimates determined by the small data sample associated to DHW uses.

Table 3. Available number of records where each fuel was associated exclusively to a specific end-use

Fuel*	Cooking	DHW	Cooking + DHW
Natural gas	657 (4.6%)	43 (0.3%)	1151 (7.6%)
LPG	2165 (49.0%)	172 (9.5%)	2745 (58.3%)
Diesel oil	n/a	93 (10.1%)	93 (10.1%)

* Note. The small data sample associated with biomass for dedicated end-uses was not adequate for a reliable calibration as regards this fuel.
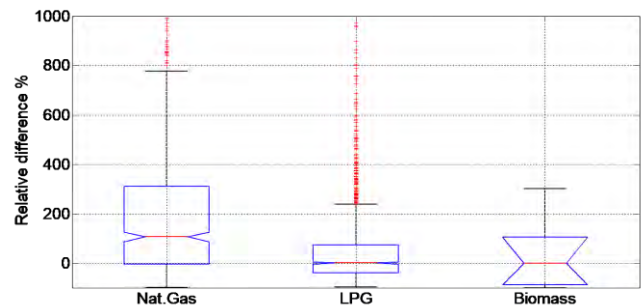
Figure 4. Relative difference survey vs. model for cooking
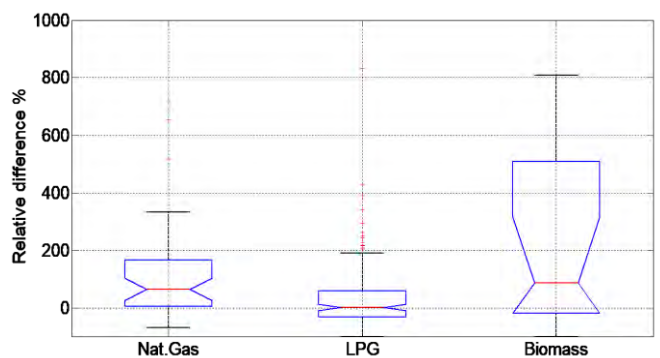
Figure 5. Relative difference survey vs. model for DHW

The effectiveness of the tuned values of the selected parameters was checked in the last step of the calibration, by considering all the records in which a fuel was used either for DHW or for cooking, or for both uses. A shown in Figure 6, the selected values confirmed good results for LPG (median deviation was limited to -7.8%, i.e. the model slightly overestimated the energy consumption), while they improved

the median deviation with natural gas and biomass, i.e. 47% and 31% respectively. Unfortunately, the calibration was unsuccessful for diesel oil, because the selected daily hot water demand underestimated, on an average, by a factor of four the selected data sample (diesel is not used for cooking). The reasons of such large discrepancies must be found in the small data sample (only 93 records), but also in some inconsistencies of the statistical data for diesel oil, e.g. costs of the bill approximate or provided in a (large) range of values. Moreover, some data suggested that this fuel was indicated in the dataset only for DHW but actually it could be used also for space heating.
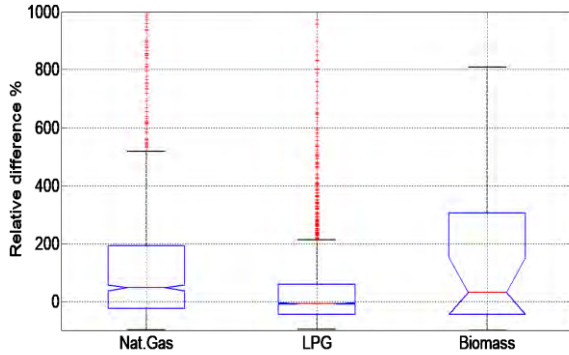
Figure 6. Relative difference survey vs. model for records using a fuel exclusively for DHW or cooking

Table 4. Average (median) annual consumption (kWh/y) for DHW and cooking calculated by the model

Fuel	Family		Per capita	
	Cooking	DHW	Cooking	DHW
Nat. gas	1086	2399	543	1120
LPG	1049	2515	483	936
Diesel	n/a	3054	n/a	1258
Biomass	4267	4638	1585	1633
Average	1229	2399	578	1080

The average annual consumptions for DHW and cooking calculated by the model for each family and per capita level are summarised in Table. The results related to DHW were obtained with the global seasonal efficiencies calculated on the basis of reference values taken from [16-17], leading to the values summarised in Figure 7. As described in the Methodology, generation efficiencies depended on the age, the type and the fuel of the system. Similarly, distribution losses depended on the age and the type of the system. In the last version of the model, the absence of recirculation in centralised and independent DHW systems was associated with an increase of 20% of hot water supply, while on the other side the presence of recirculation was associated with a 20% increase in the distribution loss. Moreover, the presence of thermal energy storages was accounted by a thermal loss of 10%. If solar collectors were available for DHW production, the model assumed an average annual solar fraction of 50% (or up to 75% according to the total collector area) of the net energy demand for hot water.

Regardless of the fuel, the average (median) annual energy consumption for cooking calculated by the model was:
- 1,229 kWh (i.e. 3.37 kWh/day) for the average family unit;
- 578 kWh (i.e. 1.58 kWh/day) per person;
- 1,086 kWh for the hobs;

Therefore, the energy demand calculated for the hobs was

almost one order of magnitude higher than ovens, thus explaining why the average mass load per cycle of the hobs was selected for the calibration of the model for cooking uses. 156 kWh for the ovens.
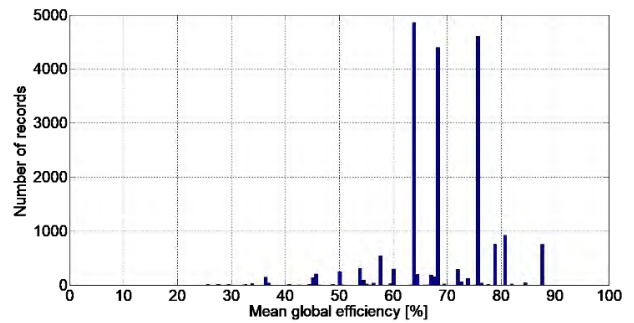
Figure 7. Average calculated DHW seasonal global efficiency

These results were compared with the benchmarks found in the literature. According to edition 2008 of part 2 of the Italian technical specification UNI/TS 11300, the daily energy consumption for domestic cooking would be:
- 4 kWh, for dwellings up to 50 m^2 of floor area;
- 5 kWh, between 50 m^2 and 120 m^2;
- 6 kWh, above 120 m^2 of floor area.

Moreover, in the district of Turin in North-Western Italy, the annual energy consumption for cooking uses was estimated around 350 kWh per capita by the authors of [29]. As regards the annual energy consumption of single appliances, some benchmarks were found in [30]: electrical hobs (with a total burner heating rate of 3 kW and an average daily use of 45 minutes) consume around 1,100 kWh/year, while electrical ovens consume from 65 kWh to 100 kWh per year. It is worth to highlight that the energy demand is greatly influenced by the user behaviour, which affects the usage frequency and length of the cooking cycles.

The average annual energy consumption per floor area for space heating and for each dwelling-type class on a national basis is summarised from Table 5 to Table 8. Regardless of the fuel, the energy consumption per area increased with the age and decreased for the dwellings with smaller external surfaces (apartments and middle floor apartment in particular). In addition to the thermo-physical and geometrical properties, the space heating demand was significantly influenced by the geographical distribution, the climatic zones and by the number of hours of operation of the heating system.

Table 5. Average annual consumption per floor area (kWh/m^2/y) for space heating with natural gas

Type of dwelling	Construction period			
	Before 1950	1950-'69	1970-'89	After 1990
SFH	263	229	151	145
MFH	246	215	144	136
GFA	163	114	91	97
MFA	73	58	35	34
TFA	136	92	79	80

Regarding the space heating consumption, the comparison between the survey and the results of the model, summarized in Table 9, showed that the model underestimated the energy consumption for natural gas of about 20% and slightly overestimated the consumption of diesel oil (about 10%),

whereas larger differences were found for the other fuels. These values were obtained by comparing the results of the model with the records of the survey were each fuel was used only in the primary space heating system.

Table 6. Average annual consumption per floor area (kWh/m²/y) for space heating with LPG

Type of dwelling	Construction period			
	Before 1950	1950-'69	1970-'89	After 1990
SFH	247	178	110	118
MFH	241	222	101	106
GFA	119	67	53	69
MFA	47	33	23	19
TFA	82	49	39	45

Table 7. Average annual consumption per floor area (kWh/m²/y) for space heating with diesel oil

Type of dwelling	Construction period			
	Before 1950	1950-'69	1970-'89	After 1990
SFH	328	274	184	198
MFH	307	277	198	199
GFA	212	127	122	153
MFA	108	70	40	45
TFA	158	132	99	175

Table 8. Average annual consumption per floor area (kWh/m²/y) for space heating with biomass

Type of dwelling	Construction period			
	Before 1950	1950-'69	1970-'89	After 1990
SFH	331	255	162	166
MFH	296	237	157	173
GFA	252	161	112	141
MFA	125	80	49	54
TFA	189	137	112	126

Table 9. Average (median) space heating consumption (kWh/y), and cumulative difference of the survey vs. Model

Fuel	Survey	Model	Difference
Nat. gas	9552	7934	20.4%
LPG	1197	3710	-67.7%
Diesel oil	7586	8456	-10.3%
Biomass	11100	17933	-38.1%

Further analysis is required in order to evaluate the reasons of such differences, which can be mainly attributed to the following factors:

- The space heating model allocated all the consumption to the fuel used in the main/primary heating system, since the data collected in the survey for secondary heating systems were not as detailed as required to directly assess their energy consumption;
- The uncertainty associated with the estimation of the energy consumption from the expenditures obtained from the survey;
- The approximations made in the estimation of the thermo-physical characteristics of the dwelling-type classes (i.e. opaque envelope type, transparent envelope type, thermal capacitance) were obtained on a national basis, whereas there can be significant differences at regional and local levels;
- The assumptions made for the HDD; in particular, each climatic zone was represented by a reference location.

On an aggregate level at national level, the calculated energy consumption for space heating, DHW and cooking slightly overestimated the energy consumption for natural gas (of about 6%), which was the most representative fuel in the residential sector since it was used by approximately 70% of the Italian families according to the survey. The overestimations for the other fuels varied between approx. 22% (LPG) and 35% (biomass), as reported in Table 10. Contrary to the comparisons related to the single end-uses described before, the aggregate results were compared on the whole dataset of the survey, regardless of the end-use and without distinctions on the type of system and between primary or secondary heating systems.

Figure 8 shows the quota of each end-use calculated by the models on a national level; biomass and diesel oil were mostly used for space heating, with quota exceeding 91% and 87%, respectively, while LPG registered larger quotas for DHW (19%) and cooking (22%). As regards natural gas, space heating covered 74% of the total consumption, followed by DHW (16%) and cooking (10%).

Table 10. Median of the aggregate energy consumption (kWh/y) without distinction of the end-use, and difference survey vs. Model

Fuel	Survey	Model	Difference [%]
Natural gas	9553	10161	-6.1
LPG	1340	1718	-22.0
Diesel oil	8965	10851	-17.4
Biomass	12950	19962	-35.1
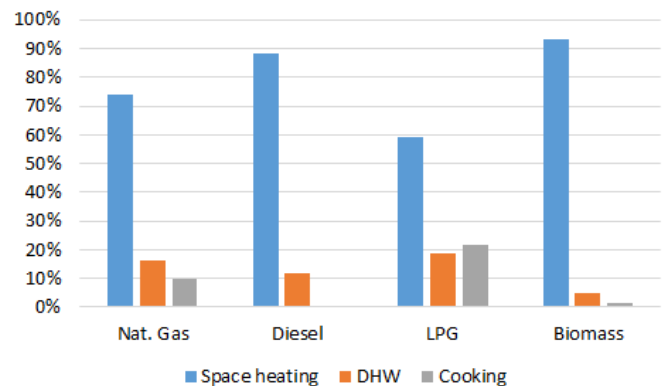
Figure 8. Calculated allocation of the energy consumption according to the fuel and the end-use

4. CONCLUSIONS

The numerical tool described in the present paper was aimed at determining the energy consumption for space heating, domestic hot water and cooking in households, based on a statistical dataset of 20,000 records collected in a survey on the energy consumption of Italian families carried out by the National Institute of Statistics. The energy consumption for space heating was based on the definition of dwelling-type classes and calculated with the equivalent resistance-capacitance model of the European standard EN ISO 13790. The energy consumption for DHW and cooking was modeled using a Standard-based approach, and results were compared on a record-by-record basis on the ISTAT survey.

The current version of the numerical code was refined with new features, starting from an updated automated algorithm for the congruity check of the statistical dataset. Moreover, the presence of hot water recirculation and of storage tanks were included in the model for DHW and new reference prices for natural gas and LPG were based on regional data instead of national averages. The selection of the records for the calibration of the relevant parameters in order to estimate the energy consumption for DHW and cooking was refined by accounting for the presence of secondary space heating equipment.

From a statistical point of view, the robustness of the model calibration depended on the sample size associated with the specific end-uses. For this reason, LPG was selected as the reference fuel, because the number of records where LPG was used exclusively for cooking or DHW was the most representative. The deviation between the model and the survey provided acceptable results for LPG and, to a minor degree, for natural gas and biomass, mainly because of the small data sample associated to the specific end-uses.

As regards space heating, the model showed promising results as far as natural gas and diesel oil were concerned. The main reasons of the deviations depended on the fact that the space heating model allocated all the consumption to the fuel used in the primary heating system, and also to the approximations underlying the dwelling-type classes, and the assumptions made on the heating degree-days.

The energy consumptions were calculated for each fuel and end-use. As regards the aggregate energy consumption on a national basis, the model slightly overestimated (about 6%) the natural gas consumption, which was used by approx. 70% of the Italian families according to the ISTAT survey. The overestimations for the other fuels varied between approx. 22% for LPG and 35% for biomass.

Biomass and diesel oil were mostly used for space heating, while LPG registered larger consumption fractions for DHW and cooking. As regards natural gas, space heating covered 74% of the total consumption, then DHW (16%) and cooking (10%).

The refinement and validation of the model are still in progress, since they are functional for the assessment of the energy consumption of households in the period between two subsequent surveys. Future works will focus on extending the validation of the model on the electrical equipment, and on addressing to the issues related to the space heating model.

ACKNOWLEDGMENTS

REFERENCES

[1] Italian Parliament, Law (2016). 232.

[2] Italian inter-ministerial Decree (2016). Aggiornamento della disciplina per l'incentivazione di interventi di piccole dimensioni per l'incremento dell'efficienza energetica e per la produzione di energia termica da fonti rinnovabili. (in Italian).

[3] Agenzia nazionale efficienza energetica. (2017). Rapporto annuale efficienza energetica – Analisi e risultati delle policy di efficienza energetica del nostro Paese, ENEA, Rome, Italy, Report RAEE-2017.

[4] Yan D, O'Brien W, Hong T, Feng X, Gunay HB, Tahmasebi F, Mahdavi A. (2015). Occupant behavior modeling for building performance simulation: Current state and future challenges. Energy and Buildings 107: 264–278. https://doi.org/10.1016/j.enbuild.2015.08.032

[5] Chen S, Yang W, Yoshino H, Levine MD, Newhouse K, Hinge A. (2015). Definition of occupant behavior in residential buildings and its application to behavior analysis in case studies. Energy and Buildings 104: 1-13. https://doi.org/10.1016/j.enbuild.2015.06.075

[6] Delmastro C, Mutani G, Schranz L, Vicentini G. (2015). The role of urban form and socio-economic variables for extimating the building energy savings potential at the urban scale. International Journal of Heat and Technology 33(4): 91-100. https://doi.org/10.18280/ijht.330412

[7] Poel B, Van Cruchten G, Balaras CA. (2007). Energy performance assessment of existing dwellings. Energy and Buildings 39: 393-403. https://doi.org/10.1016/j.enbuild.2006.08.008

[8] Ballarini I, Corgnati SP, Corrado V. (2014). Use or reference buildings to assess the energy savings potentials of the residential building stock: The experience of TABULA project. Energy Policy 68: 273-284. https://doi.org/10.1016/j.enpol.2014.01.027

[9] Caldera M, Corgnati SP, Filippi M. (2008). Energy demand for space heating through a statistical approach: application to residential buildings. Energy and Buildings 40: 1972-1983. https://doi.org/10.1016/j.enbuild.2008.05.005

[10] Spoladore A, Borelli D, Devia F, Mora F, Schenone C. (2016). Model for forecasting residential heat demand based on natural gas consumption and energy performance indicators. Applied Energy 182: 488–499. https://doi.org/10.1016/j.apenergy.2016.08.122

[11] Soldo B. (2012). Forecasting natural gas consumption. Applied Energy 92: 26-37. https://doi.org/10.1016/j.apenergy.2011.11.003

[12] Puglisi G, Zanghirella F, Ungaro P, Cammarata G. (2016). A methodology for the generation of energy consumption profiles in the residential sector. International Journal of Heat and Technology 34(3): 491-497. https://doi.org/10.18280/ijht.340320

[13] Capizzi G, Lo Sciuto G, Cammarata G, Cammarata M. (2017). Thermal transients simulations of a building by a dynamic model based on thermal-electrical analogy: Evaluation and implementation issue. Applied Energy 199: 323-334. https://doi.org/10.1016/j.apenergy.2017.05.052

[14] Energy performance of buildings - Calculation of energy use for space heating and cooling (2008). EN ISO 13790.

[15] Impianti di alimentazione e distribuzione d'acqua fredda e calda - Progettazione, installazione e collaudo (2010). UNI Standard 9182, Italy.

[16] Prestazioni energetiche degli edifici - Parte 2: Determinazione del fabbisogno di energia primaria e dei rendimenti per la climatizzazione invernale, per la produzione di acqua calda sanitaria, per la ventilazione e per l'illuminazione in edifici non residenziali (2014). UNI/TS Standard 11300 Part 2, Italy.

[17] Italian inter-ministerial Decree 26/06/2015. Description of the reference building and test parameters, Chapter 3, Annex 1, Appendix A (in Italian)

[18] Eurostat. (2013). Manual for statistics on energy consumption in households, from http://ec.europa.eu/eurostat/documents/3859598/593582 5/KS-GQ-13-003-EN.PDF/baa96509-3f4b-4c7a-94dd-feb1a31c7291

[19] Commission Delegated Regulation (EU) No 65/2014 of 1 October 2013 supplementing Directive 2010/30/EU of the European Parliament and of the Council with regard to the energy labelling of domestic ovens and range hoods (2014). Official Journal of the European Union.

[20] Commission Regulation (EU) No 66/2014 of 14 January 2014 implementing Directive 2009/125/EC of the European Parliament and of the Council with regard to ecodesign requirements for domestic ovens, hobs and range hoods (2014). Official Journal of the European Union.

[21] Household electric cooking appliances - Part 2: Hobs - Methods for measuring performance (2013). CEI EN Standard 20350 Part No. 2.

[22] Presutto M, Villani MG, Scarano D, Fumagalli S. (2010). Il mercato degli elettrodomestici e la sua evoluzione temporale, ENEA, Italy, Report RdS/2010/255, from http://www.enea.it/it/Ricerca_sviluppo/documenti/ricerc a-di-sistema-elettrico/tecnologie-riduzione-consumi/5-rapporto-indagine-mercato.pdf

[23] Cooperativa Sociale Eliante Onlus. Forni Elettrici a Incasso, from www.eurotopten.it, accessed on July 2017.

[24] Hager TJ, Morawicki R. (2013). Energy consumption during cooking in the residential sector of developed nations: a review. Food Policy 40: 54-63. https://doi.org/10.1016/j.foodpol.2013.02.003

[25] DOE (2012). Energy Conservation Program: Test Procedures for Conventional Cooking Products, DOE, USA, from https://energy.gov/sites/prod/files/2015/06/f23/conventi onal_ovens_tp_finalrule.pdf

[26] AEEG. Condizioni economiche di fornitura del gas naturale per il servizio di tutela, from http://www.autorita.energia.it/it/dati/condec_gas.htm.

[27] The Mathworks. MATLAB® Statistics Toolbox™ User Guide.

[28] ISTAT, I consumi energetici delle famiglie, from http://www.istat.it/it/archivio/142173, accessed on Sep. 2017 (in Italian).

[29] Fracastoro GV, Serraino M. (2009). Valutazione delle prestazioni energetiche degli edifici alla scala provinciale, Politecnico di Torino, Torino, Italy, from http://www.provincia.torino.gov.it/ambiente/file-storage/download/energia/pdf/relazione_polito_eff_fina le.pdf

[30] Conti P, et al. (2011). Definizione di una metodologia per l'audit energetico negli edifici ad uso residenziale e terziario, ENEA, Italy, Report RdS/2011/143, from http://www.enea.it/it/Ricerca_sviluppo/documenti/ricerc a-di-sistema-elettrico/risparmio-energia-settore-civile/rds-143.pdf

NOMENCLATURE

c	thermal capacity, $kJ/kg^{-1}/K^{-1}$
EC	energy consumption, kWh
ED	energy demand, kWh
EEI	energy efficiency index, %
HDD	heating degree days
n	number of persons
Q	thermal energy, kWh
S	floor surface, m^2
SEC	standard energy consumption, kWh or MJ
T	temperature, K
V	volume, m^3

Greek symbols

ε	efficiency

Subscripts

apt	apartment
m	model
occ	occupants/persons
s	survey
w	water

Abbreviations and acronyms

DTC	dwelling-type class
GFA	ground floor apartment
MFA	middle floor apartment
MFH	multi-family house
SFH	single-family house
TFA	top floor apartment

Paper 25

Survey-based Analysis of the Electrical Energy Demand in Italian Households

M. Caldera [1], P. Ungaro [2], G. Cammarata [3], G. Puglisi [1]

1. ENEA, Roma, Italy

2. ISTAT, Roma, Italy

3. Università degli Studi di Catania, Catania, Italy

Objective

- Determination of the electrical energy demand based on the ISTAT survey on the energy consumption of households:
  - ✓ Lighting
  - ✓ Electrical appliances
  - ✓ Cooking appliances
  - ✓ DHW production
  - ✓ Space heating and cooling

- The implemented numerical model is useful for:
  - ➤ analysing the evolution of the electrical consumption of Italian households;
  - ➤ evaluating the potential energy savings of specific retrofit measures;
  - ➤ providing recommendations for policy actions supporting the improvement of the energy efficiency in the residential sector.

ISTAT survey

Eurostat: Electrical energy covered 17.5% of the final energy consumption in Italian households in 2015 (+3% compared to 2014)

2013 ISTAT survey on energy consumption of households

- 20,000 households

- General info on the occupants;

- Consumption habits;

- Characteristics of the building;

- Characteristics of the equipment for all the various end-uses;

- Expenditures for the main energy sources;

→Comprehensive overview of the Italian residential sector

ELECTRICAL EQUIPMENT
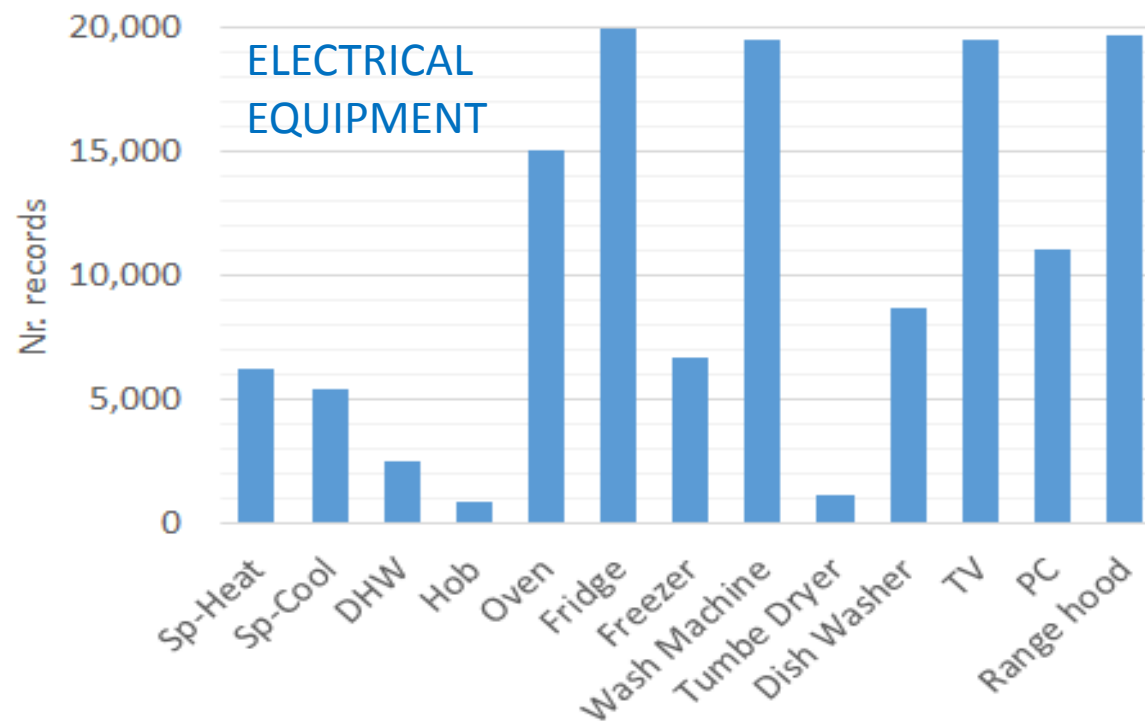
Source: ENEA elaborations on ISTAT data

Methodology

- Implementation a numerical code in Matlab®
  - Specific models/functions for each electrical end-use

- Allocation of the consumption of electrical energy:
  - ✓ for each end-use
  - ✓ on a record-by-record basis [1]

- ISTAT survey:
  - ✓ Input data, provided by 210 questions of the survey
  - ✓ Calibration of the models
  - ✓ Validation of the models

[1] With the exception of space heating

Methodology – Calibration of the model

- The models implemented for different end-uses are calibrated on a specific subset (cluster) of the ISTAT dataset:
  - A. Cluster A (10,249 records): electricity used only for lighting and for electrical appliances (ovens included) → model for lighting
  - B. Cluster B (1,267 records)→ model for DHW production
  - C. Cluster C (522 records) → model for hobs
  - D. Cluster D (1,089 records)→ model for space cooling

- Clusters → definition of the main parameters for specific end-uses.

Results - Electrical appliances

- White goods and appliances with larger consumption (fridges, freezer, washing machines, tumble dryers, dishwashers, range hoods, TVs, PCs)

  Detailed models:

  - ✓ Based on <u>Ecodesign and Energy labelling normative</u> valid at time of purchase of the appliance

  $$AE_C = SAE_C \cdot \frac{EEI}{100}$$

  - ✓ Energy consumption in stand-by mode included.

- Small appliances (cleaning, cooking, electronic accessories, auxiliaries for space heating and DHW)

  Simplified model:

  - ✓ average consumption (obtained from <u>BATs and market survey</u>)

  - ✓ actual period of occupation of the dwelling (from the survey)
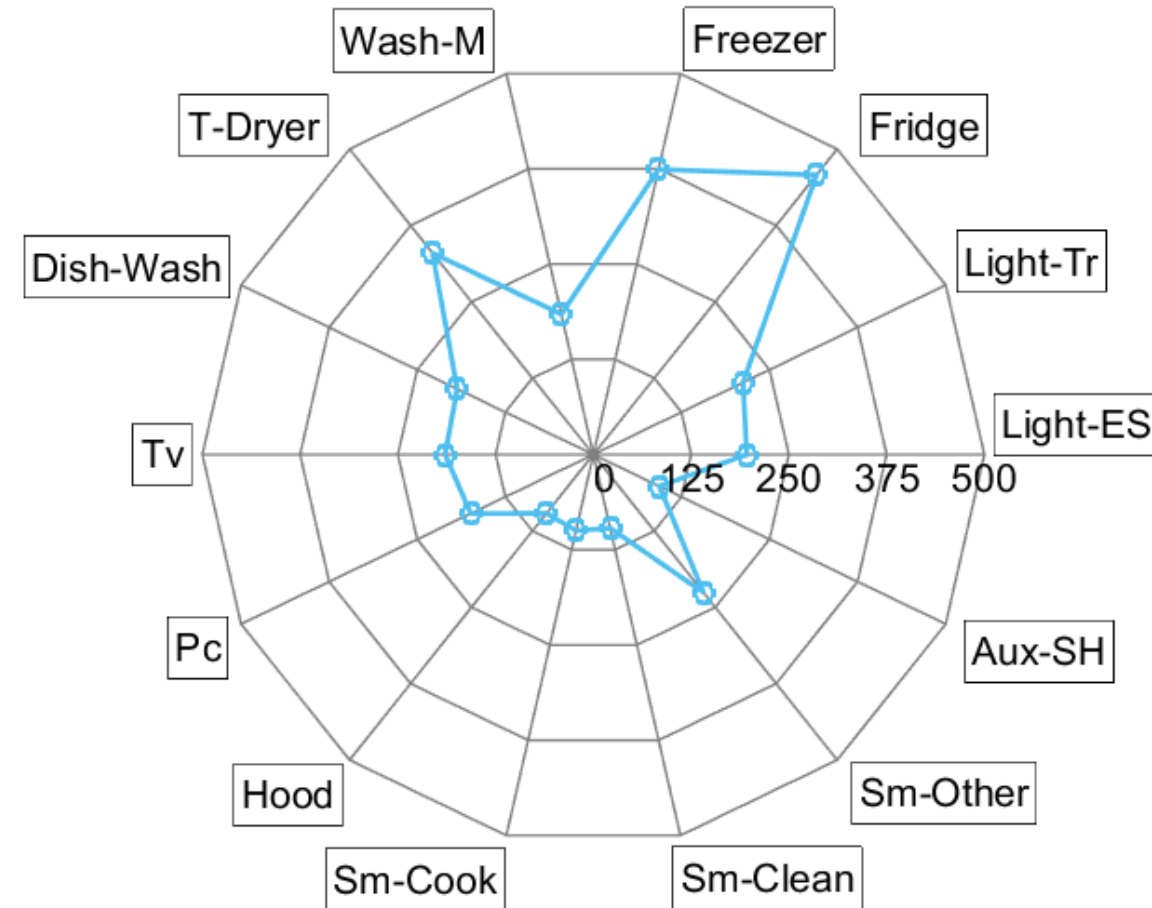
Median annual consumption of the electrical appliances, kWh/y

Results - Lighting

- Traditional light bulbs (avg. 60 W)

- Energy-saving light bulbs (avg. 20 W)

- Average number of hours of use, for each type of light bulbs:
  - Records of Cluster A: record-by-record calibration, i.e. minimisation of the difference of E_c between the survey and the model
  - Records outside Cluster A: mean value calculated on a regional basis for Cluster A
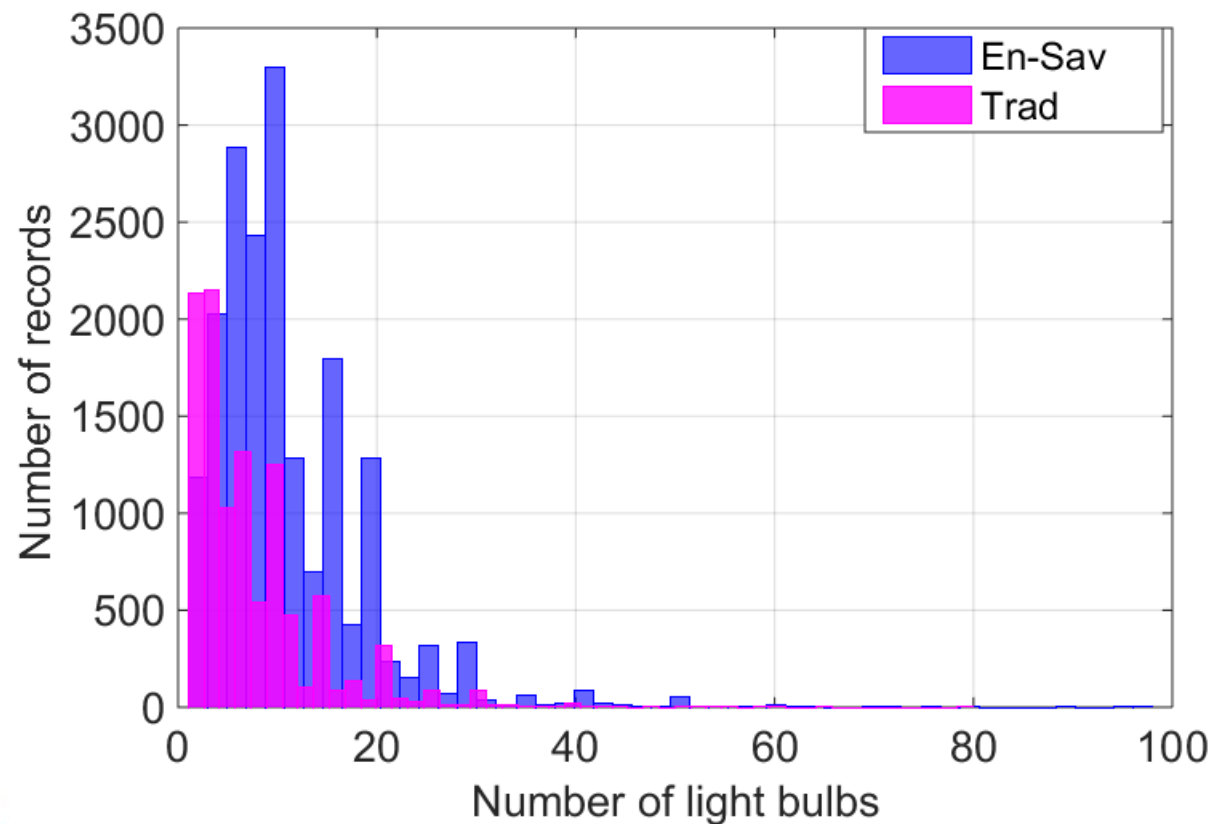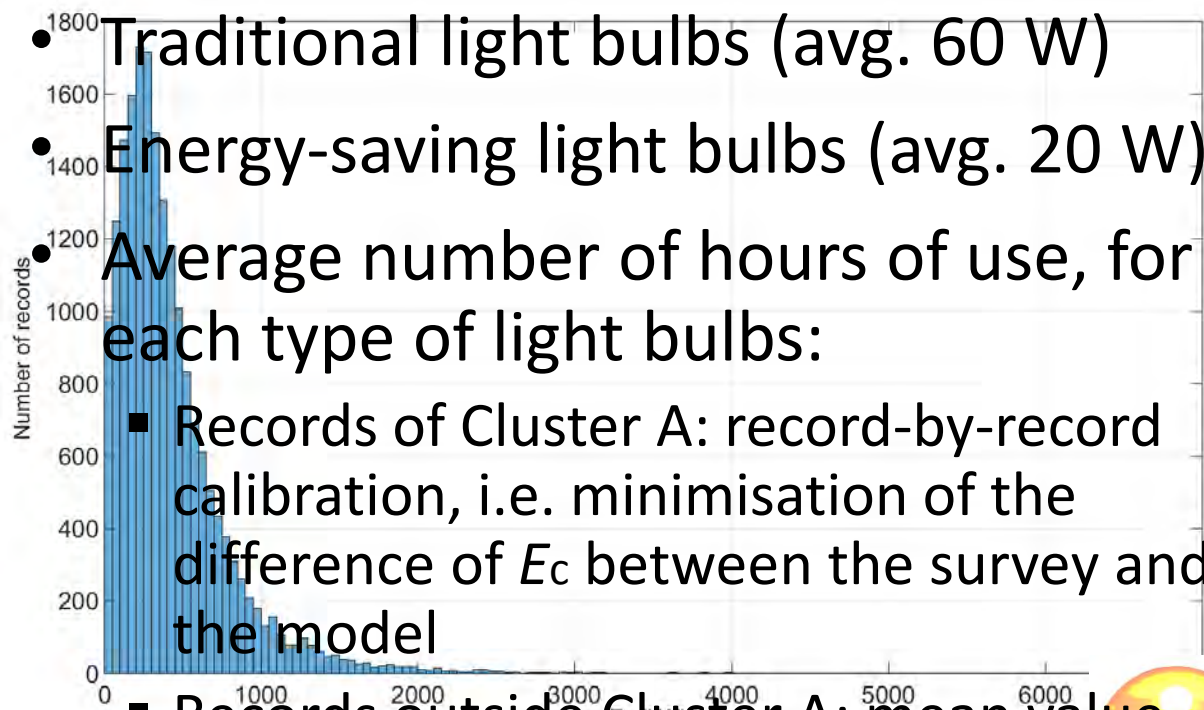
Lighting: median E_c = 332.6 kWh/y
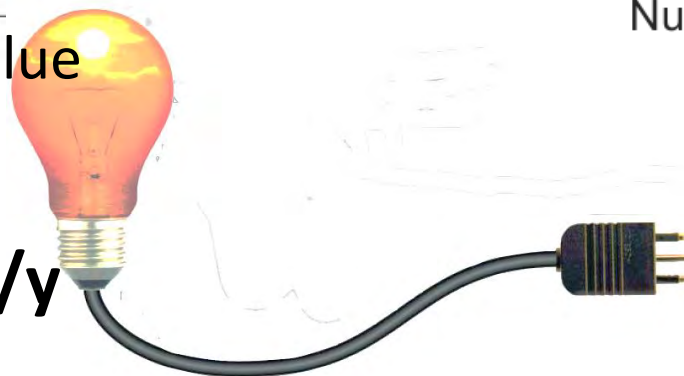
Results - DHW production

Annual net energy demand:

$$Q_{DHW} = c_w \cdot V_{w,occ} \cdot \Delta T_w \cdot \sum_{occ} d_{occ}$$

- Average Daily hot water demand per capita ($V_{w,occ}$):
  - ✓ Records of Cluster B: $V_{w,occ}$ calibrated record-by-record in the range 30 L to 120 L
  - ✓ Records outside Cluster B: mean value of $V_{w,occ}$ obtained for Cluster B (49 L/d)
- Contribution of solar collectors for DHW based on the number of collectors (from the survey)
- Only primary DHW systems considered (secondary systems are negligible)
- Equipment efficiencies set according to:
  - ✓ type of equipment (centralised, independent, boilers, heat pumps)
  - ✓ Age of the system
- → Annual energy consumption
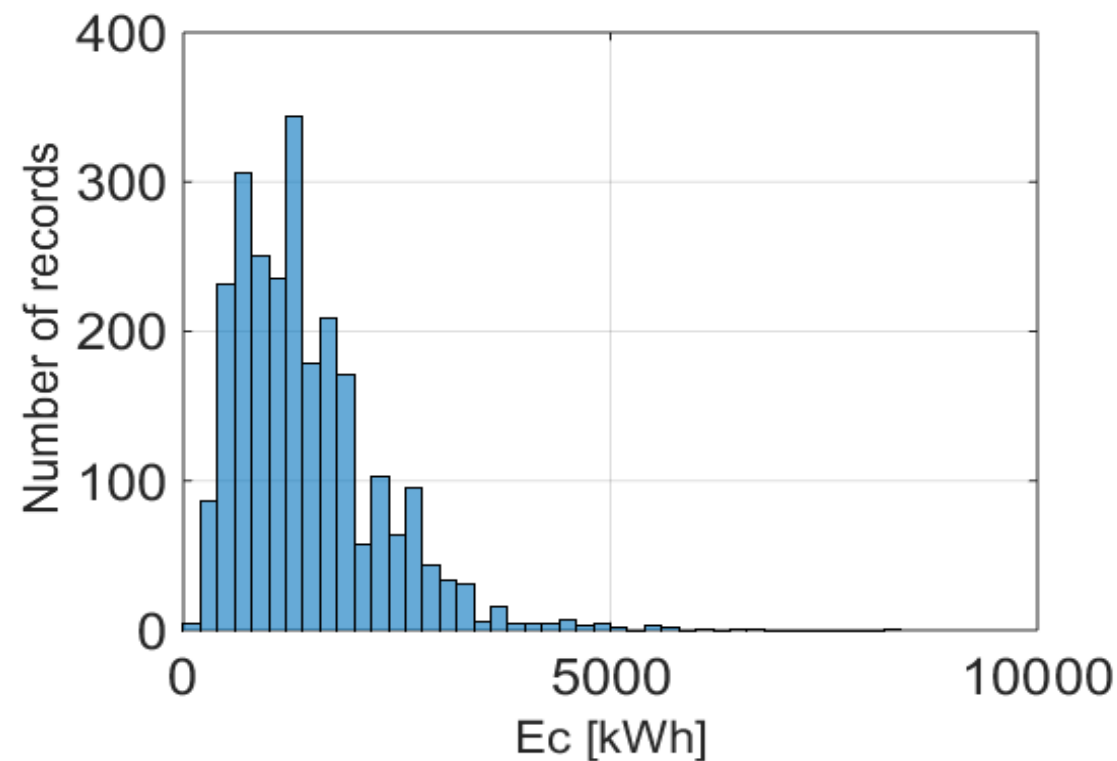
DHW: median E_c = 1,303 kWh/y

Results - Cooking

- <u>Ovens</u>: model based on EU normative on Ecodesign and Energy labelling

- <u>Hobs</u>:

$$EC_{hob} = \frac{ED_{hob}}{\varepsilon_{hob}}$$

  - Efficiency ε_{hob} set according to a market survey:
    - ✓ Resistance/halogen: ε_{hob} = 60 % (before 2005)
    - ✓ Induction: ε_{hob} = 74 % (after 2005)

  - Average mass load per cooking cycle M_L:
    - ✓ Records of Cluster C: M_L calibrated record-by-record in the range 0.5 ÷ 2.0 kg
    - ✓ Records outside Cluster C: mean value of M_L obtained for Cluster C (1.2 kg)

- <u>Small cooking appliances</u> (e.g. microwave ovens, coffee makers, toasters, etc.) included among the small electrical appliances.

Ovens: magenta
Hobs: blue
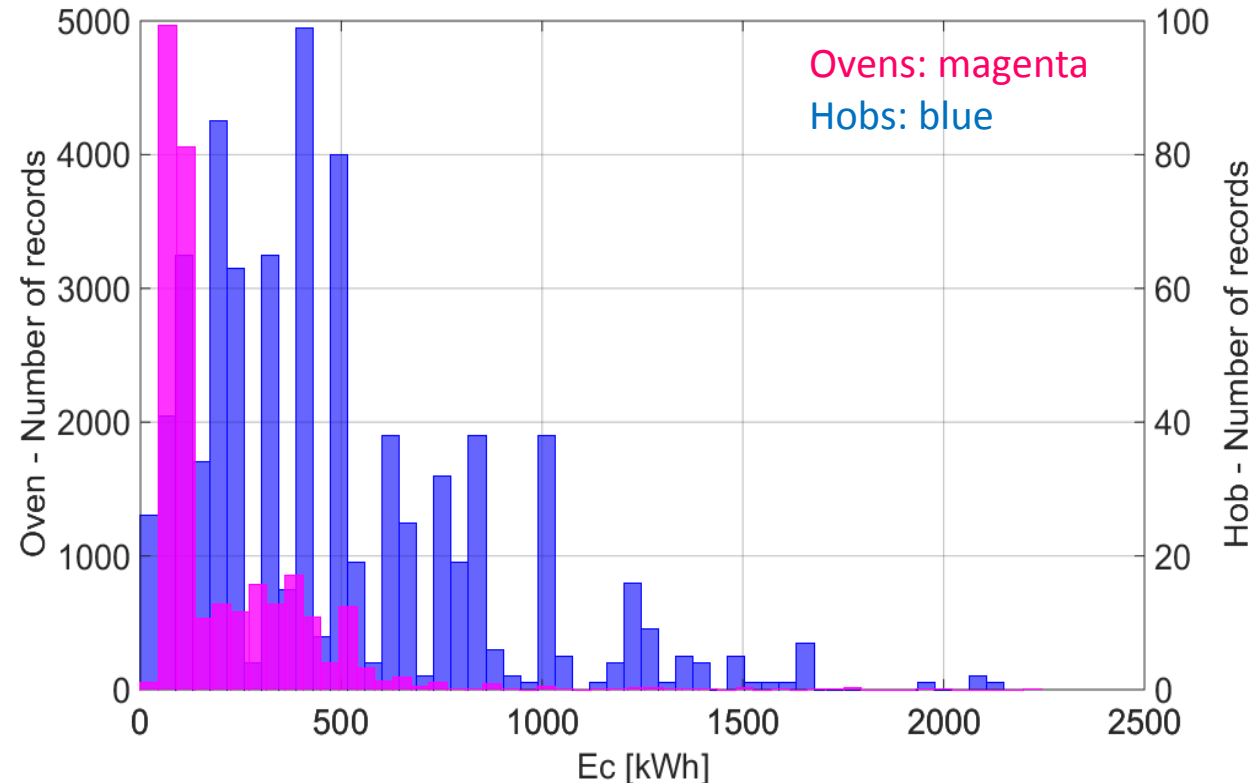
Ovens: median E_c = 107 kWh/y
Hobs: median E_c = 404 kWh/y

Results – Space cooling and heating

Space cooling   Regression model $E_{cooling} = f(CDD, EER, h, A_{f,cool})$

- ✓ *CDD*: estimation based on the region and municipal typology
- ✓ *EER*: set according to the type of conditioner/heat pump and to the technology (air, water or ground-source)
- ✓ *h*: estimated based on the usage frequency provided by the survey (cooling season of 3 months)
- ✓ $A_{f,cool}$: calculated from the survey

Space heating

- • Most of the electrical SH systems in the survey are secondary (only 13 % unique SH system);
- • Very little information available from the survey;
- → Global fraction of E_C for SH determined on the whole dataset by difference between:
  - ✓ the electrical bill
  - ✓ the sum of E_C calculated for the other end-uses.

Space cooling:
median E_c = 376 kWh/y
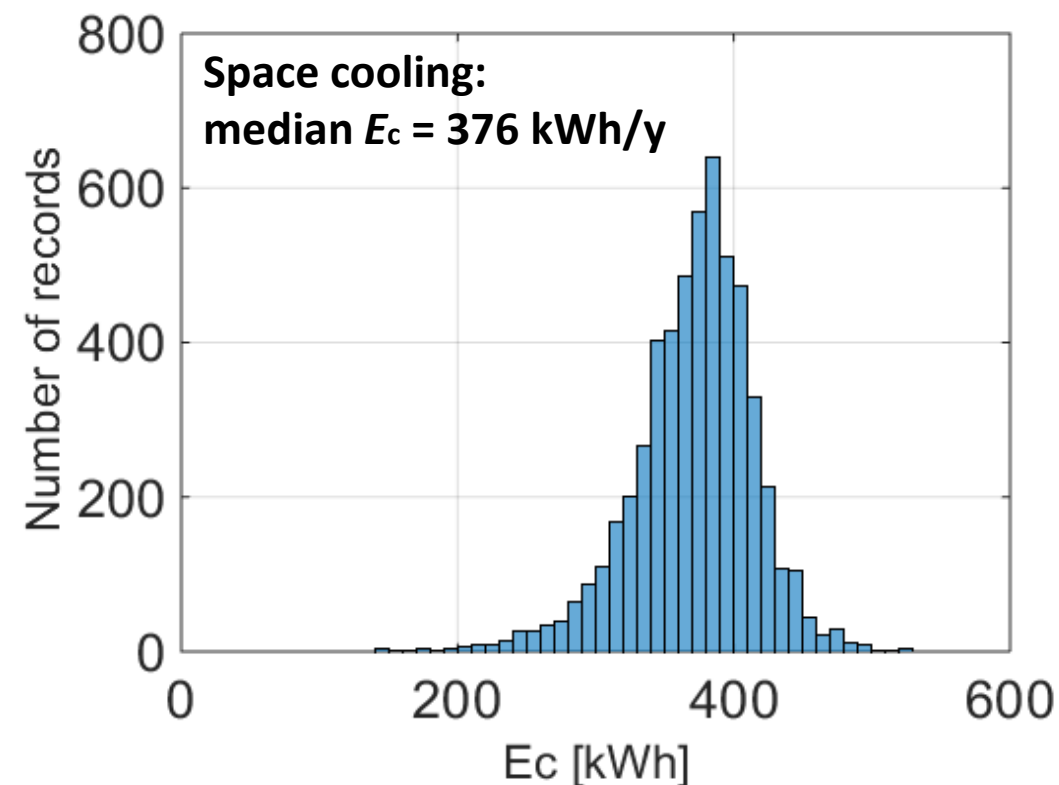
Model validation

Validation no.	V1	V2	V3	V4	V5	V6	V7	V8	V9
Electrical appliances	X	X	X	X	X	X	X	X	X
Lighting	X	X	X	X	X	X	X	X	X
Oven	X	X	X	X	X	X	X	X	X
Hob		X				X	X	X	X
DHW				X	X		X	X	X
Space cooling			X		X	X		X	X
Space heating									X

$$\Delta EC \% = \frac{EC_s - EC_m}{EC_m} \cdot 100\%$$
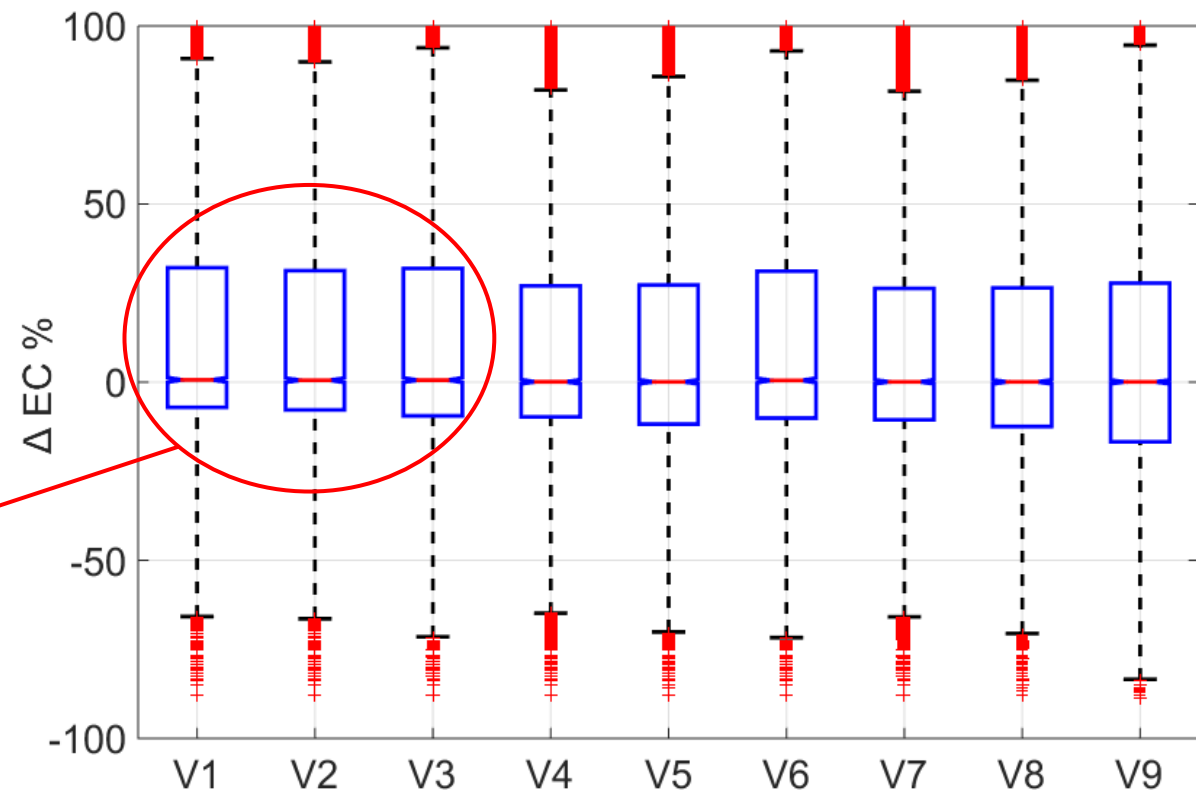
In all the groups of records:
- Median value close to 0 %
- Interquartile range around 40%

Results – Average national quotas

Allocation of electrical consumption among various end-uses
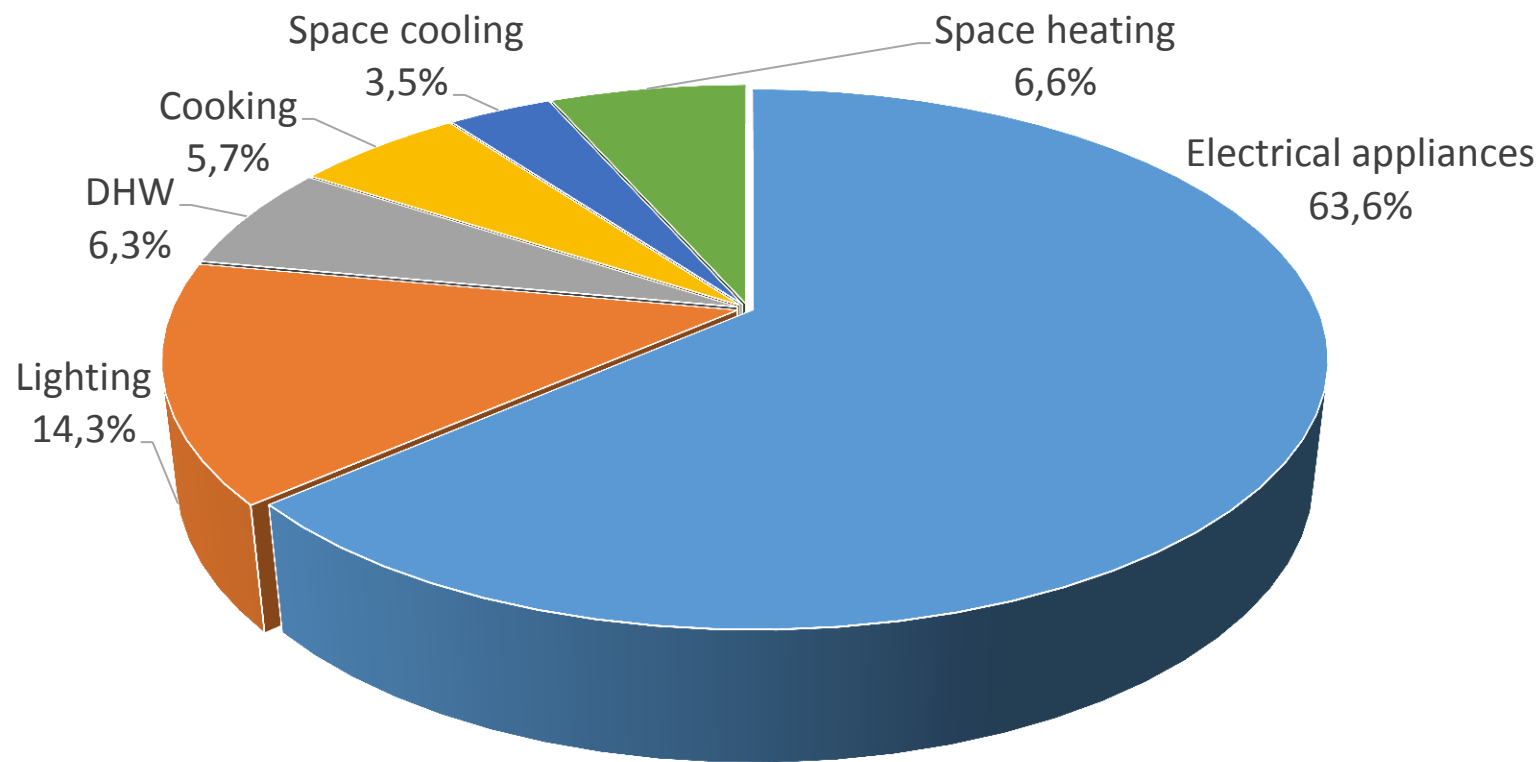
Conclusions

- The numerical model allows allocating the electrical energy consumption for each end-use on a record-by-record basis

- Goal: reliable estimation of the households' electrical consumption, based on:
  - ✓ Characteristics of the building & equipment
  - ✓ Habits of the occupants

- Different approaches, in order to maximise the quantity and quality of information available from the ISTAT survey:
  - ✓ Electrical appliances: EU Ecodesign and energy labelling normative
  - ✓ Lighting, DHW, hobs: model calibration of specific parameters on the survey
  - ✓ Space cooling: robust regression algorithm

- Model validation shows good results

- The numerical code can be applied to the next surveys, in order to evaluate the evolution of the energy consumption of Italian households.

Matteo Caldera
matteo.caldera@enea.it
www.agenziaefficienzaenergetica.it
www.enea.it

Thanks for your attention

Fiscal deduction in Italy for energy efficiency in residential buildings: Some insights

Domenico Prisinzano[*], *Alessandro Federici*[**], *Amalia Martelli*[***], *Chiara Martini*[****] and *Roberto Moneta*[*****]

Abstract

After more than 10 years since its introduction, the fiscal deduction scheme of 55-65% for energy renovation of existing buildings has represented a veritable break in the Italian energy efficiency world. Such incentives have allowed to limit the serious economic crisis faced by the Italian building sector, at the same time implying the valorisation of buildings and improving life quality of Italian people.

In this article, the EU and national regulatory context where the 55-65% tax deduction scheme operates will be briefly summarised, as well as their role relative to the Italian objectives within the implementation of the Energy Efficiency Directive. The savings achieved by different types of interventions will be described, together with the associated investments. The trends on the market of incentivised technologies will be finally identified, also estimating employment impacts on the construction sector and developing other economic considerations and policy implications in order to untap a huge energy saving potential.

Keywords: energy efficiency, energy efficiency directive (Directive 2012/27/EU), energy efficiency targets, energy saving, tax deduction scheme, incentives for existing buildings, building renovation.

JEL classification: K32, N74, O13, Q42, Q43

First submission: 22 December 2017, accepted: 29 January 2018

[*] ENEA – Italian National Energy Efficiency Agency. E-mail: domenico.prisinzano@enea.it.

[**] ENEA – Italian National Energy Efficiency Agency.

[***] ENEA – Italian National Energy Efficiency Agency.

[****] ENEA – Italian National Energy Efficiency Agency.

[*****] ENEA – Italian National Energy Efficiency Agency.

1. The tax deduction scheme

Directive 2012/27/UE set indicative national energy efficiency targets: such targets, as defined in the National Energy Strategy (NES) (Ministry of Economic Development, 2013), are monitored yearly in the Annual Report prepared for the European Commission, as envisaged by article 3 of the Directive. In particular, from 2011 to 2020, the 2017 National Energy Efficiency Action Plan (NEEAP) indicated that Italy should save 15.5 Mtoe of final energy consumption (20 Mtoe of primary energy), reducing her consumption by around 24% relative to the value projected for 2020 by the European reference scenario, based on an inertial evolution of the system (Ministry of Economic Development, 2014a and 2017a). More specifically, Italy complies with article 7 of the Energy Efficiency Directive with the White Certificates obligation scheme, from which a saving of around 5.5 Mtoe/year of final energy is expected, combined with two alternative measures, Fiscal Deductions (1.38 Mtoe/year) and Thermal Account (1.47 Mtoe/year starting from 2014) (Ministry of Economic Development, 2014b).

Tax deductions for the energy upgrading of buildings were introduced in Italy by the Budget Law for 2007, and then renewed every year through the related Budget or Stability Law, resulting in a key driver of energy efficiency improvements in the housing sector, with more than 3 million of actions implemented as at 31 December 2017. Since the Nineties tax deductions for "common refurbishment" of buildings are in force: implemented measures are not specifically addressed to the energy performance of buildings or dwellings, but energy related technologies also may be embodied within the implemented actions (i.e. replacement of windows, boilers, etc.). For this reason, every year an assessment of energy savings from this incentive scheme is carried out (see Tables 2 and 3, and chapter 4 for further information).

The 65% tax deductions (55% till 2013) can be claimed by all taxpayers: individuals, including persons pursuing trades or professions; taxpayers with income from business activities (individuals, partnerships, limited liability companies); professional associations; public and private entities not pursuing business activities. For individuals, the incentive may also be claimed by: the holders of a right in rem on the property; co-owners, for actions on common parts of the buildings; tenants; those holding the property in loan for use. The tax deductions for energy efficiency improvement actions are granted to existing buildings of both residential and services sector, parts thereof or any real estate units of any cadastral category, including rural buildings, owned or otherwise held. The incentive consists of a ten-year reduction of IRPEF (personal income tax) or IRES (corporate income tax) granted for expenses incurred to[1]:
- reduce heating demand by means of overall upgrading of the building's energy performance (Paragraph 344);

---

[1] The common name in brackets refers to the paragraphs of 2007 Budget Law (Italian Parliament, 2006).

- improve the building's thermal insulation (replacement of windows, including blinds or shutters, and insulation of roofs, walls and floors) (Paragraph 345);
- install solar thermal panels (Paragraph 346);
- replace heating systems with condensing boilers or heat pumps, replace electrical water heaters with heat pump water heaters (Paragraph 347);
- installation of building automation system (BA).

More recently, the 2017 Italian Stability Law extended fiscal deductions for all the interventions already incentivised with previous regulations. Relative to the energy renovation of common parts of apartment blocks, the mechanism has been extended for five years, for interventions involving the envelope with an incidence higher than 25% on the gross dispersing surface, with a deduction equal to 70%; if such interventions achieve at least the average quality for winter and summer energy performance, the deduction increases to 75%. The main innovation is that, in both cases, the beneficiaries could choose the transfer of receivables to the suppliers realising the interventions or to other private actors, with the aim to attract new capitals in this segment of the market, boosting this way the number of such more incentivized actions (Italian Parliament, 2016).

Table 1 provides a picture of the characterisation of the fiscal deduction mechanism and the main technologies associated to incentivised interventions.

Table 1 – Characterisation of the tax deductions for energy renovation

Measure	Description	Associated technologies
Paragraph 344	Reduction of energy demand for heating the whole building	Biomass boilers; overall renovation
Paragraph 345a	Improvement of thermal performance of buildings opaque structures	Thermal insulation of vertical walls, roofs, slabs
Paragraph 345b		Replacement of windows and shutters
Paragraph 345c		Solar shading
Co Paragraph mma 346	Installation of solar panels	Solar panel for sanitary hot water
Paragraph 347	Replacement of winter air conditioning systems	Condensation boilers; heat pumps; biomass boilers; heat pump boilers for sanitary hot water
B.A.	Installation of building automation system	
Condominium 70%	Intervention on common parts of apartment blocks involving the envelope for more than 25% of the dispersing surface and, for interventions called *Condominium 75%*, achieving the average quality for winter and summer performances.	
Condominium 75%		

Source: Stability Law 2017

2. Achieved energy savings

Relative to the 2011-2020 target as set in 2014 NEEAP (Ministry of Economic Development, 2014b) and consistent with 2013 NES, energy savings achieved in 2016 amounted to slightly more than 6.4 Mtoe/year of final energy, equivalent to more than 40% of the target (Table 2). Around one quarter of such savings derives from fiscal deductions for energy renovation of existing buildings (ENEA, 2017a).

Table 2 – Achieved energy saving by sector, years 2011-2016, and expected saving for 2020 (final energy, Mtoe/year), according to 2014 NEEAP

| Sector | White Certificates | Fiscal Deductions for existing buildings* | Thermal Account | Other measures** | Energy saving | | Achieved Vs target (%) |
					Achieved 2016***	Expected for 2020	
Residential	0.59	1.56	-	0.94	3.09	3.67	84.2%
Services	0.13	0.02	0.003	0.05	0.19	1.23	15.4%
Industry	1.84	0.03	-	0.09	1.95	5.10	38.3%
Trasport	–	–	-	1.17	1.18	5.50	21.4%
Total	2.56	1.60	0.003	2.35	6.41	15.50	41.4%

* 65% tax deduction for energy renovation; 50% tax deduction for refurbishment; Bonus Mobili
** Legislative Decree 192/05 for new buildings; Ecoincentives for new vehicles, EU Regulations and High-Speed railways in the transport sector; replacement of big appliances in the residential sector
*** Net of duplications
Source: ENEA elaboration based on data from Ministry of Economic Development, Gestore dei Servizi Energetici S.p.A., ENEA, ISTAT, FIAIP, GFK

According to the transposition of the art.7 of the Directive, a cumulative energy saving target of 25.8 Mtoe of final energy is also set over the 2014-2020 period. Table 3 shows the results achieved in 2014, 2015 and 2016 (estimated with regards to fiscal deductions) for each of the measures notified to the European Commission. Figures are on track of expected trend towards the 2020 target: of the over 4.5 Mtoe of cumulated energy saving obtained in the period 2014-2016, around one third derives from the fiscal deductions (Ministry of Economic Development, 2017b).

Table 3 – Achieved energy saving by notified measure, according to EED Article 7 (final energy, Mtoe), years 2014, 2015 and 2016

Notified policy measures	New achieved savings 2014	New achieved savings 2015	New achieved savings 2016	Cumulated savings 2014-2016	Cumulated savings expected for 2020
Obligation scheme – White Certificates	1.050	0.896	1.135	3.081	16.00
Alternative measure 1 – Thermal Account	0.000004	0.001	0.002	0.003	5.88
Alternative measure 2 – Fiscal Deductions	0.248	0.502	0.731	1.481	3.92
Total savings	1.298	1.399	1.868	4.564	25.80

Source: Ministry of Economic Development

Concerning the 65% tax deduction scheme, in the 2014-2016 period approximately a million of interventions were realised (Table 4), of which more than 360,000 in 2016, when more than half involved the replacement of windows and shutters (paragraph 345b), and around 20% the replacement of winter air conditioning systems (paragraph 347) and the installation of solar shading (paragraph 345c).

The investments activated in the three-year period equalled around 9.5 billion euros: more than 40% of resources were allocated to para 345b; 25% to the thermal insulation of slabs and roofs (paragraph 345a); slightly more than 9% to the reduction of energy demand for heating the whole building (paragraph 344). The total investments activated in 2016 were equal to more than 3.3 billion euros (7% more

than in 2015): the maximum potential of fiscal deduction which could be claimed by beneficiaries in the next ten years is equal to 2.1 billion euros (ENEA, 2017b).

Table 4 – Number of realised interventions and activated investments (M€) by measure, year 2016 and total of years 2014-2016

Measure	Interventions 2016		Investments 2016		Interventions 2014-2016		Investments 2014-2016	
	n.	%	M€	%	%	n.	M€	%
Paragraph 344	3,517	1.0%	303.9	1.1%	9.2%	10,578	862.9	9.1%
Paragraph 345a	21,661	6.0%	764.2	7.4%	23.1%	72,755	2,401.6	25.4%
Paragraph 345b	185,909	51.6%	1,355.5	56.1%	41.0%	552,629	3,997.0	42.2%
Paragraph 345c	69,874	19.4%	148.4	11.9%	4.5%	117,548	248.8	2.6%
Paragraph 346	8,883	2.5%	56.4	3.5%	1.7%	34,842	222.6	2.4%
Paragraph 347	69,762	19.4%	671.0	20.0%	20.3%	196,663	1,721.3	18.2%
B.A.	661	0.2%	9.2	0.1%	0.3%	661	9.2	0.1%
Total	360,267	100%	3.308,7	100%	100%	985,676	9.463,3	100%

Source: ENEA

An analysis of the ratio between activated investments and net disposable income at regional level shows an average value equal to 0.3%, with peaks equal to around 0.7% in Aosta Valley and Trentino South Tyrol and lower values in Southern Italy. This is only partially due to the fact that 65% tax deduction scheme is addressed to the heating of existing buildings. Indeed, the distribution of per capita investments at municipal level for energy renovation measures mirrors the typical North-South differences for the regional distribution of per capita net disposable income, with the result of a two-speed country for incentivized energy saving investments (also) (Figure 3). Such overview provides useful information for the monitoring of Sustainable Energy (and Climate) Action Plans submitted under the Covenant of Mayor initiative.

The achieved energy savings corresponding to these investments are equal, over the period 2014-2016, to around 3,300 GWh/year, equivalent to slightly more than 0.28 Mtoe/year (Table 5). Also in terms of energy saving achieved in the 2014-2016 period, the main contribution derives from the replacement of windows and shutters (46.6% of the total), followed by the interventions on horizontal and sloping walls (18.4%), and vertical walls (10.7%), as well as on the installation of condensation boilers (13%).

The interventions realised in 2016 allowed to reach a saving higher than 1,100 GWh/year, more than 41% of which is associated to the replacement of windows and shutters. Almost one third of the saving was achieved thanks to intervention on walls, vertical and horizontal (346 GWh/year), with a main contribution of slabs and roofs.

Figure 1 – Investments per capita (€ per capita) at municipal level, year 2016
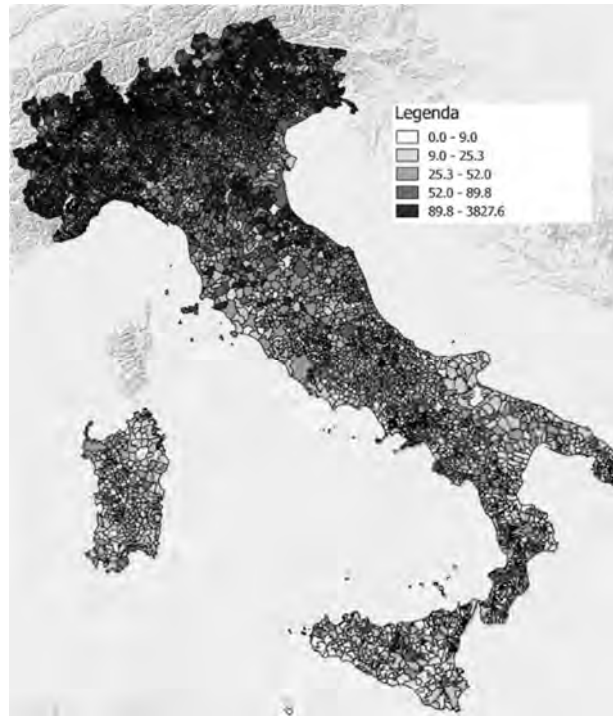
Source: ENEA

Table 5 – Savings (GWh/year) by technology, year 2016 and total of years 2014-2016

Year	2016		2014-2016		SAVINGS 2014-2016 (GWh/YEAR)			
Technology/intervention	GWh/year	%	GWh/year	%	0	500	1.000	1.500
Vertical walls	106.9	9.6%	351	10.7%				
Horizontal walls	239.1	21.5%	603	18.4%				
Windows and shutters	482.3	43.4%	1,531	46.6%				
Solar thermal	40.3	3.6%	160	4.9%				
Solar shading	19.8	1.8%	33	1.0%				
Condensation boilers	167.8	15.1%	428	13.0%				
Geothermal plants	0.9	0.1%	3	0.1%				
Heat pumps	37.5	3.4%	138	4.2%				
Hot water heat pumps	5.6	0.5%	16	0.5%				
Building automation	5.4	0.5%	5	0.2%				
Other	6.9	0.6%	13	0.4%				
Total	1,112.5	100%	3,282	100%				

Source: ENEA

The thermal insulation of slabs and roofs, together with the reduction of energy demand for heating the whole building, are characterised by the best cost-effectiveness, with an associated cost in the 9-12 eurocent range for each kWh of energy saved during the whole useful life of intervention (Table 6).

20

Table 6 – Cost-effectiveness by paragraph (€/kWh), average of years 2014-2016

Measure	Useful life	€/kWh	0,00	0,05	0,10	0,15	0,20	0,25
Paragraph 344	30	0.12 €						
Paragraph 345a	30	0.09 €						
Paragraph 345b	30	0.10 €						
Paragraph 345c	30	0.15 €						
Paragraph 346	15	0.09 €						
Paragraph 347	15	0.21 €						
B.A.	10	0.17 €						

Source: ENEA

Table 7 shows the investments, both for 2016 and the 2014-2016 period, broken down by technology or by type of intervention: in the three-year period, the main share of resources - around 4.36 billion euros - was allocated to the replacement of 1.9 million windows and shutters (which could be incentivised not only by para 345b, but also by paras 344 and 345a in the case of multiple interventions); more than 1.7 billion euros were instead allocated to more than 52,000 interventions on horizontal walls.

The distribution of investments in 2016 mirrors the one observed in the three-year period, with around 1.5 billion euros for 647,000 replaced windows and shutters, more than 650 million euros for around 16,000 interventions on horizontal walls, and more than 300 million for around 16,000 interventions on vertical walls.

Table 7 – Investments (M€) by technology, year 2016 and total of years 2014-2016

Year	2016		2014-2016		INVESTMENTS 2014-2016 (M€)			
Technology/Intervention	M€	%	M€	%	0 1.000 2.000 3.000 4.000			
Vertical walls	301.1	9.1%	1,074	11.4%				
Horizontal walls	651.2	19.7%	1,734	18.3%				
Windows and shutters	1,447.9	43.8%	4,357	46.0%				
Solar thermal	56.4	1.7%	223	2.4%				
Solar shading	148.4	4.5%	249	2.6%				
Condensation boilers	543.3	16.4%	1,412	14.9%				
Geothermal plants	4.1	0.1%	11	0.1%				
Heat pumps	110.3	3.3%	297	3.1%				
Hot water heat pumps	20.7	0.6%	59	0.6%				
Building automation	9.2	0.3%	9	0.1%				
Other	16.1	0.5%	39	0.4%				
Total	3,308.7	100%	9,463	100%				

Source: ENEA

Around 80% of investments activated in 2016 (2.6 billion euros out of 3.3) were devoted to buildings built before the '80s; in particular, around one fourth of total resources (more than 810 million euros) was spent on buildings built in the '60s. The main market segments of energy renovation identifiable in 2016 are the buildings with more than three floors of the '60s (45,000 interventions for more than 330 million euros invested) and the detached houses of the post-war period (around 19,000 interventions, around 250 million euros of investments), in '60s (around 25,000 interventions, around 320 million euros of investments) and in '70s (more than 23,000 interventions, around 280 million euros of investments). The allocation of resources observed for years 2014 and 2015 is very similar to the one observed in 2016, shown in Table 8.

Table 8 – Investments (M€) by building period and typology, year 2016

	Detached house	Block of flats with less than three floors	Block of flats with more than three floors	Other	Total	Total (M€)
< 1919	3,4%	1,8%	2,2%	0,4%	7.8%	258.3
1919-1945	3,2%	1,5%	2,2%	0,3%	7.2%	239.6
1946-1960	7,5%	3,2%	6,4%	1,0%	18.0%	596.6
1961-1970	9,6%	3,5%	10,0%	1,5%	24.5%	811.5
1971-1980	8,4%	4,3%	6,1%	2,5%	21.3%	706.1
1981-1990	3,6%	2,9%	2,3%	1,7%	10.4%	344.9
1991-2000	1,8%	1,6%	0,8%	1,0%	5.3%	175.0
2001-2005	0,5%	0,5%	0,2%	0,2%	1.5%	50.3
> 2006	1,9%	1,0%	0,6%	0,2%	3.8%	125.8
Total (%)	39.8%	20.3%	31.1%	8.8%	100%	
Total (M€)	1,317	672	1,028	291		3,308

Source: ENEA

The saving distribution (Table 9) mirrors the allocation of resources: 36% of total savings (400 GWh/year) is achieved in the four segments previously mentioned.

Table 9 – Savings (GWh/year) by building period and typology, year 2016

	Detached house	Block of flats with less than three floors	Block of flats with more than three floors	Other	Total	Total (GWh/y)
< 1919	3,3%	1,8%	2,0%	0,4%	7.4%	82.8
1919-1945	3,1%	1,5%	2,0%	0,3%	6.9%	77.2
1946-1960	7,4%	3,2%	6,3%	1,2%	18.2%	201.9
1961-1970	9,7%	3,6%	10,2%	2,0%	25.6%	284.3
1971-1980	8,5%	4,3%	6,2%	3,1%	22.0%	244.7
1981-1990	3,4%	2,5%	2,1%	2,5%	10.5%	117.0
1991-2000	1,7%	1,3%	0,7%	1,4%	5.1%	57.0
2001-2005	0,5%	0,4%	0,2%	0,2%	1.3%	14.5
> 2006	1,6%	0,7%	0,4%	0,2%	3.0%	33.0
Total (%)	39.3%	19.2%	30.1%	11.5%	100%	
Total (GWh/y)	436.9	213.6	334.4	127.6		1,112

Source: ENEA

Interventions to reduce energy demand for heating the whole building (para 344) and to thermal insulation of slabs and roofs (para 345a) covered around one third of total investment (1.07 billion euros) and achieved more than one third of total saving observed in 2016 (378 GWh/year, equivalent to 0.032 Mtoe). In particular, around 80% of such resources were devoted to interventions on buildings built before the '80s and, more in detail, more than 40% concentrated on an envelope dating '60s and '70s (Table 10).

Table 10 – Investments (M€) and savings (GWh/year) for interventions on the building enve-lope, year 2016

	Investiments		Savings		
	M€	%	GWh/y	%	
< 1919	108.6	10.2%	34.8	9.2%	
1919-1945	89.6	8.4%	29.2	7.7%	
1946-1960	194.8	18.2%	66.9	17.7%	
1961-1970	237.5	22.2%	84.8	22.4%	
1971-1980	216.4	20.3%	78.5	20.8%	
1981-1990	104.7	9.8%	42.5	11.2%	
1991-2000	56.1	5.3%	21.9	5.8%	
2001-2005	13.2	1.2%	4.7	1.2%	
> 2006	47.2	4.4%	14.7	3.9%	
Total (%)	1,068.1	100%	378.2	100%	

Source: ENEA

Table 11 shows the distribution of investments in windows and shutters that have been replaced. In 2016 more than half of frames of the new windows have been in PVC (53%); while glazing was more than 70% of low emission type.

Table 11 – Distribution of investments in windows by frame and glazing typology (%), year 2016

Glazing type	Wood		Metal, thermal cut		PVC		Mixed		Total
Double		3,8%		3,8%		11,2%		1,9%	20.7%
Triple		1,2%		0,9%		2,8%		1,3%	6.1%
Low emission		11,3%		13,2%		38,3%		7,8%	70.6%
Other		0,3%		0,4%		0,7%		1,3%	2.7%
Total		16.5%		18.2%		53.0%		12.3%	100.0%

Source: ENEA

In particular, PVC windows with low-emission glazing cover more than 38% of the market (more than 550 million euros of investments), to which corresponds around 45% of achieved savings (214 GWh/year) by this intervention typology.

3. The market of incentivised technologies

In recent years the market for technologies incentivised by fiscal deductions has changed considerably: the products and services offered combine innovation and limited costs, as joint result of incentives and regulation. For example, with the entrance into force of the Ecodesign Directive in September 2015 all heating devices can be sold only if they satisfy minimum energy efficiency requirements and pursue environmental protection. For instance, this implies that at least condensing boilers can now be sold.

In 2016, more than 540,000 condensing boilers fuelled by gas were sold, an 86% share of the total number of boilers sold and an increase by around 70% relative to 2015 even if in a smaller market than a few years ago (Table 12).

Table 12 – Boilers sold on the national market, years 2010-2016

	Traditional boilers	Condensing boilers	Total				
				0	200.000	400.000	600.000
2010	668,000	325,500	993,500				
2011	650,000	302,000	952,000				
2012	601,500	269,000	870,500				
2013	513,000	301,000	814,000				
2014	466,500	277,800	744,300				
2015	446,000	340,000	786,000				
2016	85,600	540,600	626,200				
Total	3,430,600	2,355,900	5,786,500				

Source: Assotermica

The introduction, in 2014, of a new electricity experimental tariff for the heat pumps used as primary heating device in the residential sector (named "D1"), the possibility to obtain different incentives at national level, and the climatic conditions in the last few years, all together have contributed remarkably and in a synergic way to the growth of the heat pump market. The new tariff seems to have reached the objective: in December 2016, the heat pumps benefitting of D1 tariff were 16,000, three fourths of which installed between 2014 and 2016, during the experimental phase of the tariff. Moreover, around 60% of users having installed heat pumps and applied for D1 tariff have, at the same time, combined the plant with a photovoltaic net-metering system (the so-called "scambio sul posto"). D1 tariff has then contributed to the increase in heat pumps sales, or better, given its characteristics, to the increase in the sales of plants usable in the residential sector (Autorità di Regolazione per Energia Reti e Ambiente, 2014).

The national market in 2016 of the heat pumps used as primary heating device in the residential sector can be estimated in around 220,000 units, of which 176,000 with split and multi-split, given the ease of application. Also air cooled chillers, conceived for use in the service sector and now commonly used also in the residential one, in 2016 had a good increase in their sales: for those with capacity up to 17 kW, the increase was 25% relative to previous year, and the increase in turnover equalled 27% (Table 13).

Table 13 – Heat pumps used as primary heating device sold on the national market (million units), years 2016

	N.	%	
Heat pumps with split and multisplit	176,000	80.1%	
Air cooled chillers (capacity lower than 17 kW)	19,000	8.6%	
Air cooled chillers (capacity between 18 and 50 kW)	4,000	1.8%	
Air cooled chillers (capacity higher than 50 kW)	2,700	1.2%	
VRF systems	18,000	8.2%	
Total	219,700	100.0%	

Source: Assoclima

As regards prices of heating and cooling appliances, in the last five years the price of split and multi-split heat pumps decreased, whereas in 2016 a yearly increase equal to 2% for reversible chillers and a decrease equal to 3% for variable refrigerant flow systems (VRF) were observed (Assoclima, 2017).

In 2016 the overall demand for windows, shutters and continuous facades in the Italian market reached a value equal to about 4.27 billion euros, 2.75 of which in the residential sector and 1.52 in the non-residential, including 485 million euros of continuous facades (UNICMI, 2017). In particular, in the last three years the sales of windows in the residential sector for renovation remained stable, around 4.5 million units per year, with a slight increase in the sales in 2016 (4.53 million units), which allows to foresee a sale of 4.59 million units in 2017. On the contrary, the sales of windows in new buildings have undergone a severe reduction, showing a first weak reversal in this trend (1.24 million units) only in 2016, with a further increase in the sales (1.25 million units) foreseen for 2017 (Table 14). Between 2008 and 2016 a gradual change was observed in the market shares of the three main materials used to produce windows: the most significant increase concerned those in PVC, moving from a market share equal to 16% in 2008 to one equal to 26% in 2016, to the detriment of wood windows; aluminium windows did not undergo significant changes in time. In 2016 the market value equalled 990 million euros for PVC windows, 1,420 million euros for wood windows and 1,400 million euros for metallic ones.

Table 14 – Windows sold in the residential sector for new buildings and renovation of existing ones (million units), years 2004-2017

	New	Renovation	Total						
				0	1	2	3	4	5
2004	4.02	4.24	8.26						
2005	4.42	4.31	8.73						
2006	4.71	4.49	9.20						
2007	4.66	4.62	9.28						
2008	4.27	4.52	8.79						
2009	3.34	4.50	7.84						
2010	2.82	4.66	7.48						
2011	2.63	5.36	7.99						
2012	2.27	5.09	7.36						
2013	1.97	5.04	7.01						
2014	1.35	4.48	5.83						
2015	1.23	4.49	5.72						
2016	1.24	4.53	5.77						
2017*	1.25	4.59	5.84						
Total	22.37	47.26	69.63						

* Estimated

Source: UNICMI

The increase in market shares of PVC windows is clearly attributable to their good quality-price ratio which, for the same thermal performance required to access fiscal incentives, has a lower sale price relative to other technologies. Such advantage is attributable to the increasing imports of these products, since 2012, from countries as Poland and Romania, at lower prices relative to the traditional trade partners, Germany and Austria, from which Italy still imports PVC windows. In 2016 total imports of PVC windows (considering all partners, not only the main four mentioned above),

reached a total volume of sales equal to 200 million euros, almost 7% of the total market of windows and shutters. Although the impact is numerically negligible when examining the overall market value, it still contributes to influence the trend of minimum prices for final users. Faced with the competition of PVC windows, in the last years the producers of aluminium windows focused on average and high-quality products, meeting the demand from medium-high income users: a decrease of units sold was observed, combined with a stability of the market turnover.

4. Employment impacts and other economic implications

Fiscal incentives for "common refurbishment" (50% deduction) and for "energy renovation" (65% deduction) caused between 1998 and 2016 more than 14.2 million interventions, carried out by 55% of total Italian households. The investments corresponding to these interventions are equal to 237 billion euros, 205 billion of which concerned building refurbishment and slightly less than 32 billion energy renovation.

In terms of estimation of employment impacts, in the last four years (2013-2016) the incentivised investments generated slightly less than 270,000 full-time equivalent (FTE) direct jobs every year, whilst considering also indirect jobs the total is greater than 400,000 FTE employees per year: only in 2016, 419,000 jobs have been created. Fiscal incentives have been an important tool against the crisis and fundamental to the recovery, as shown by the fact that overall, between 2008 and 2016, 600,000 jobs have been lost in the sector (Chamber of Deputies, 2017).

The Stability Law 2017 favours global efficiency interventions of the whole building-plant system and of envelope insulation, in particular for medium-large buildings, showing the highest energy efficiency potential. More than 60% of buildings were built before 1976, the year of Law no. 373 that introduced technical performances to regulate energy performances. Moreover, when Law no 10 of 1991 entered into force, aimed at limiting energy consumption for thermal uses in buildings, 82% of buildings in Italy had already been built. Also for this reason, from a qualitative point of view, 30% of building blocks is currently in mediocre or very bad conservation conditions (Italian National Institute of Statistics, 2011). Moreover, in more than 400,000 of analysed buildings (around one third of the total) having central heating systems, around two thirds were installed more than 15 years ago and would need renovation interventions, aimed at improving energy efficiency and living comfort (ENEA, 2017b).

Such types of interventions ensure the greatest energy savings, but at the same time require the highest financial contribution from the owners. This constitutes a relevant barrier to the realisation of interventions, since the incentive is conceived as ex-post reimbursement, split on 10 years: then, the burden of financial contribution to realise the interventions is borne entirely by the owners, who should pay for the works before getting the incentive. Another obstacle to the use of the incentive as a deduction on income tax is the uncertainty on future recovery capacity, since the fiscal coverage of tax payer could change consistently due to reasons not depending on the intervention itself (job loss, retirement, etc.) and/or due to the access to

other fiscal deductions (for example, deductions for dependents, for salaries or retirement incomes). Especially in the case of global renovation interventions that are the most expensive and imply a potentially higher incentive amount, the actual fiscal deduction could turn out to be lower than 65% of incurred cost. Indeed, during the ten years in which the incentive is provided, the tax owed by the beneficiary could prove to be lower than the deductions he is entitled to, nullifying in this way, completely or partly, the possibility to enjoy the fiscal benefit.

When a building consists of many apartments with different owners such economic and fiscal issues could make it difficult to reach the majority in the condominium assembly to approve the renovation works. Indeed, the approval phase has always represented the weakest link to implement whatever activity at building block level. Moreover, reaching the ordinary quorum in the assembly is not enough to get the works started in the case of global renovation.

For these reasons also, the Stability Law 2017 introduced the possibility, in the case of energy renovation of common parts of buildings, to transfer the corresponding credit to the suppliers who realised the interventions, or to other private actors having an adequate fiscal coverage. This allows to make the amount of the incentive certain, and in the case of transfer to the suppliers, to consistently reduce the initial payment for the co-owners, condition which could turn out to be crucial to the approval of works in the condominium assembly. The lack of any possibility to transfer the credit to financial institutions and intermediaries does not impede virtuous mechanisms to arise, which could make it possible to take out a condominium loan for the expenditure share not transferred as tax credit, relying on the lower amount required and, more in general, on the higher solvency of single co-owners.

5. Conclusions and policy implications

Tax deductions for the energy renovation of buildings are an effective policy for the improvement of the energy efficiency of the Italian building stock, adopted by Italy as an alternative measure to fully comply with article 7 of the Energy Efficiency Directive, and recognized as a best practice at international level also (International Energy Agency, 2014).

More in general, energy efficiency renovation of buildings is a priority in the Italian political agenda, as witnessed by the 2013 and 2017 Italian National Energy Strategy. Indeed, more than two thirds of the stock was built before 1976, the year of the first Italian law on energy performance of buildings. More specifically, the Italian Strategy for the energy renovation of the national building stock assesses an energy saving potential of almost 5.7 Mtoe/year in the 2014-2020 period. The corresponding level of investments in the residential sector is about 13.6 billion euros per year for interventions aimed at the overall renovation of buildings, and 10.5 billion euros per year for partial interventions (roof, facade, windows, heating system). Concerning the services sector, the amount of necessary investments is about 17.5 billion euros per year (Ministry of Economic Development, 2017c).

Energy saving potential is wide yet, and often achievable through interventions characterised by a short payback period. Implemented actions are mainly at single-dwelling level yet: in order to exploit the huge and untapped energy saving potential, end-user demand must by shifted to the more cost-effective overall renovation of (big) buildings. Most recent dispositions foreseen by the 2017 Budget Law pave the way towards this direction, thanks to higher deduction rates for condominiums and the possibility of credit transfer. This should imply higher investments from private stakeholders, allowing bigger volumes of energy savings as well, resulting in a big business opportunity.

Indeed, the Italian construction sector is taking a new and evolutionary phase, reshaping strategic visions, processes and products, thus supporting the implementation of the aforementioned strategies. Some mature technologies are already available, though not so common in the market yet. This is mainly due to a lack of expertise of practitioners and/or higher costs compared to the market average. But innovation is only one of the different factors guiding the process, together with the adoption of new products and evolution of systems and components (for instance 3D printing, development of robotics, so-called Internet of things), and new processes resulting from the integration of different operative levels, able to (re)activate and radically improve the productivity of the construction sector, opening it to the future (ENEA, 2016).

References

Assoclima (2017). Indagine statistica sul mercato dei componenti per impianti di condizionamento dell'aria, file:///C:/Users/alessandro/Downloads/Rilevazione_Assoclima-2016-v2.pdf.

Autorità di Regolazione per Energia Reti e Ambiente (2014). Delibera 205/2014/R/eel, https://www.arera.it/allegati/docs/14/205-14ti.pdf.

Chamber of Deputies (2017). Il recupero e la riqualificazione energetica del patrimonio edilizio: una stima dell'impatto delle misure di incentivazione – Quinta edizione, http://documenti.camera.it/leg17/dossier/pdf/Am0051d.pdf.

ENEA (2016). Energy Efficiency Annual Report, http://www.enea.it/it/seguici/pubblicazioni/pdf-volumi/raee-2016-versione-integrale.pdf (full report in Italian) and http://www.enea.it/it/seguici/pubblicazioni/pdf-volumi/executive-summary-2016-eng.pdf (executive summary in English).

ENEA (2017a). Energy Efficiency Annual Report, http://www.enea.it/it/seguici/pubblicazioni/pdf-volumi/raee-2017.pdf (full report in Italian) and http://www.enea.it/it/seguici/pubblicazioni/pdf-volumi/raee-executive-summary-en.pdf (executive summary in English).

ENEA (2017b). 65% Tax Deduction Scheme Annual Report, http://www.enea.it/it/seguici/pubblicazioni/pdf-volumi/detrazioni-65-2017.pdf (full report in Italian) and http://www.enea.it/it/seguici/pubblicazioni/pdf-volumi/detrazioni-65-executive-summary-2017-en.pdf (executive summary in English).

International Energy Agency (2014). Energy Efficiency Market Report 2014, https://www.iea.org/publications/freepublications/publication/EEMR2014.pdf.

Italian National Institute of Statistics (2011). 2011 general census, http://dati-censimento
  popolazione.istat.it/Index.aspx?lang=it.

Italian Parliament (2006). 2007 Budget Law, http://www.parlamento.it/parlam/
  leggi/06296l.htm.

Italian Parliament (2016). 2017 Budget Law, http://www.gazzettaufficiale.it/
  eli/id/2016/12/21/16G00242/sg.

Ministry of Economic Development (2013). Italy's National Energy Strategy: for a more com-
  petitive and sustainable energy, http://www.sviluppoeconomico.gov.it/images/stories/
  documenti/SEN_EN_marzo2013.pdf.

Ministry of Economic Development (2014a). Italian Energy Efficiency Action Plan,
  https://ec.europa.eu/energy/sites/ener/files/documents/ItalyNEEAP2014en.pdf.

Ministry of Economic Development (2014b). Application of Article 7 of Directive
  2012/27/EU on energy efficiency obligation schemes Notification of methodology,
  https://ec.europa.eu/energy/sites/ener/files/documents/article7_en_italy.pdf.

Ministry of Economic Development (2017a). Piano d'Azione Italiano per l'Efficienza Ener-
  getica, https://ec.europa.eu/energy/sites/ener/files/documents/it_neeap_2017_it_1.pdf.

Ministry of Economic Development (2017b). Relazione annuale sull'efficienza energetica:
  risultati conseguiti e obiettivi al 2020, http://www.sviluppoeconomico.gov.it/images/
  stories/documenti/Relazione-Annuale-Efficienza-Energetica-2017.pdf.

Ministry of Economic Development (2017c). Strategia Energetica Nazionale,
  http://www.sviluppoeconomico.gov.it/images/stories/documenti/testo_della_Strategia
  EnergeticaNazionale_2017.pdf (in Italian) and http://www.sviluppoeconomico.gov.it/
  images/stories/documenti/BROCHURE_ENG_SEN.PDF (brochure in English).

UNICMI (2017). Rapporto sul mercato italian dell'Involucro Edilizio,
  http://www.unicmi.it/in_evidenza/in_evidenza/rapporto_unicmi_2017.html.

Efficienza energetica: combustibile nascosto dell'economia e fonte di risparmio per le famiglie italiane

L'efficienza energetica ha assunto un ruolo sempre più importante nel panorama delle politiche energetiche nazionali e internazionali, diventando il primo "combustibile" nel mix di produzione e consumo a livello mondiale. Un simile trend implica conseguenze pervasive su aspetti chiave del sistema economico, come ad esempio la povertà energetica

di **Alessandro Federici** e **Chiara Martini**, *ENEA*, e **Paola Ungaro**, *ISTAT*

I dati dell'Agenzia Internazionale per l'Energia evidenziano, per il triennio 2014-2016, una riduzione delle emissioni di CO_2 affiancata a un rafforzamento dell'attività economica mondiale, fenomeno che potrebbe rappresentare l'inizio di un *decoupling* tra PIL e consumi energetici. Un simile *trend* sembra dovuto per due terzi all'efficienza energetica e per un terzo al cambiamento nella composizione dell'offerta di energia.

In Italia nel 2014 e 2015 non si è osservato un disallineamento tra andamento dell'economia e consumi energetici, ma occorre tener conto che l'intensità energetica italiana storicamente ha sempre mostrato valori ben al di sotto della media dei 28 paesi UE e, in particolare, inferiori rispetto ai principali *competitor*, ad eccezione del Regno Unito. Sicuramente il settore residenziale appare un settore chiave, in cui la risposta comportamentale all'adozione di politiche energetiche, così come la penetrazione di nuove tecnologie, possono produrre rilevanti risparmi.

Gli obiettivi nazionali di efficienza energetica

Il 2017 è stato un anno di particolare importanza per le politiche nazionali sull'efficienza energetica, in quanto è stato redatto il Piano d'Azione per l'Efficienza Energetica (PAEE) ed è stata elaborata la Strategia Energetica Nazionale (SEN), le cui principali scelte strategiche sono coerenti con il *Clean Energy Package*, pubblicato dalla Commissione Europea a fine 2016.

Rispetto all'obiettivo previsto per il periodo 2011-2020 incluso nel PAEE 2014 e confermato nel PAEE 2017, i risparmi energetici conseguiti al 2016 sono stati pari a poco più di 6,4 Mtep/anno di energia finale, equivalenti a oltre il 40% dell'obiettivo finale. A livello settoriale, il residenziale ha già raggiunto l'84% dell'obiettivo atteso al 2020 (Tabella 1).

I risparmi energetici riportati in Tabella 1 implicano al 2016 un risparmio annuale cumulato nella fattura energetica del nostro Paese di quasi 3,5 miliardi di euro, dovuto a minori importazioni di gas naturale e greggio (Figura 1).

Tale risultato si concretizza anche in un risparmio significativo per gli utenti finali: considerando soltanto le detrazioni fiscali per il settore residenziale, nel 2016 le famiglie italiane hanno evitato il consumo di oltre 3,3 miliardi di m³ di gas naturale per il riscaldamento delle proprie abitazioni, per un risparmio di oltre 2 miliardi e mezzo di euro.

In particolare, tra il 2007 e il 2016 sono stati incentivati, tramite le detrazioni fiscali del 65% per la riqualificazione energetica degli edifici esistenti, circa 3 milioni di interventi, con quasi 32 miliardi di euro investiti da parte delle famiglie. Il risparmio complessivo di energia primaria e finale nel periodo 2007-2016 è di circa 1,08 Mtep/anno (Tabella 2).

A tale risparmio energetico, per gli anni 2014, 2015 e 2016 è possibile associare un risparmio medio sulla bolletta annuale dei consumatori che varia da 238 euro nel 2014, a 175 euro nel 2015, a 168 euro nel 2016.

I consumi e la spesa energetica delle famiglie

Tra il 2001 e il 2015 i consumi energetici delle famiglie per uso domestico (al netto dei consumi per i trasporti) sono cresciuti da 29,5 a 31,4 milioni di tonnellate equivalenti di petrolio, +6,4% su tutto il periodo (Figura 2). Gli impieghi del settore residenziale hanno mostrato un andamento caratterizzato da una prima complessiva fase di crescita, culminata nel 2010 con un picco di oltre 35 Mtep, ed una seconda fase di decrescita, sia pur discontinua, con una variazione del -10,5% rispetto al 2010. Benché le spese devolute all'acquisto di beni energetici siano solo parzialmente contraibili, la riduzione dei consumi osservata negli ultimi anni risulta correlata ad una più generale esigenza di risparmio economico nel periodo post-crisi.

Il periodo in cui le spese energetiche pesano maggiormente sul bud-

Settore	Certificati Bianchi	Detrazioni fiscali*	Conto Termico	Decreto Legislativo 192/05*	Ecoincentivi e Regolamenti Comunitari*	Altre misure**	Risparmio energetico		Obiettivo raggiunto (%)
							Conseguito 2016***	Atteso al 2020	
Residenziale	0,59	1,56		0,91		0,02	3,09	3,67	84,2%
Terziario	0,13	0,02	0,003	0,05			0,19	1,23	15,4%
Industria	1,84	0,03		0,09			1,95	5,10	38,3%
Trasporti					1,13	0,04	1,18	5,50	21,4%
Totale	2,56	1,60	0,003	1,05	1,13	0,07	6,41	15,50	41,4%

* Detrazioni fiscali del 65% per la riqualificazione energetica degli edifici esistenti e detrazioni fiscali del 50% per il recupero del patrimonio edilizio; stima per il 2016; ** Il settore residenziale conteggia i risparmi derivanti dalla sostituzione di grandi elettrodomestici; il settore trasporti conteggia i risparmi derivanti dall'Alta Velocità; *** Al netto di duplicazioni

Tab. 1 Risparmi energetici annuali conseguiti per settore, periodo 2011–2016 e attesi al 2020 (energia finale, Mtep/anno) ai sensi del PAEE 2014
Fonte: ENEA (2017a)

get familiare è infatti quello tra il 2009 ed il 2013[1] (con quote di spesa che variano da un minimo del 4,8% ad un massimo del 5,4%), anche per effetto di una tendenza alla contrazione della spesa media complessiva familiare (diminuita, tra il 2008 e il 2013, di oltre il 5%).

Nel 2016[2], la quota di spesa destinata dalle famiglie italiane all'acquisto di prodotti energetici per uso domesti-co è pari al 4,4% delle spese media annuale, in leggero calo rispetto a quella registrata nei due anni prece-denti (4,6% per entrambi).

In termini monetari, dal 2014 al 2016 la spesa per consumi energeti-ci a carico delle famiglie italiane di-minuisce[3] da 35,6 a 34,3 miliardi di euro, con un decremento comples-sivo del 3,6%, superiore per il Nord ed il Centro (-7,0% e -7,5%), laddove

nel Mezzogiorno si registra un incre-mento del 6,2%.

Nel 2016, alla determinazione del-la complessiva spesa energetica nazionale per usi domestici han-no contribuito soprattutto il gas e l'energia elettrica, al cui acquisto sono stati devoluti, rispettivamen-te, 16,5 e 15,3 miliardi di euro, pari al 93% delle spese energetiche complessive (48% per il gas e 45% per l'energia elettrica).

La contrazione di spesa energetica del settore residenziale registrata nel corso dell'ultimo triennio si deve in particolar modo al decremento della spesa per il gas, diminuita del 12% rispetto al 2014. In calo anche la spesa per gli impieghi domestici di gasolio (-14,3%) e combustibili soli-di (-4,5%). L'energia elettrica, vice-versa, registra dal 2014 un'espansio-ne di spesa pari, a livello nazionale, all'8,3%, con un picco di crescita nel Mezzogiorno (+21%).

In termini medi, la spesa per prodot-ti energetici del settore residenzia-
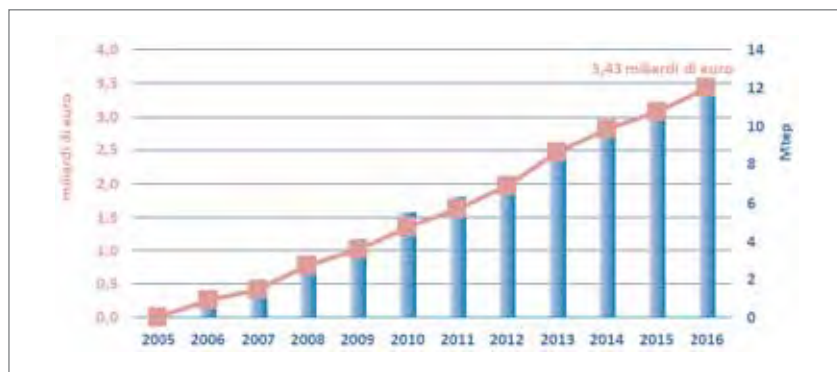
Fig. 1 Risparmio cumulato in fattura energetica (miliardi di euro) e di energia (Mtep), anni 2005–2016
Fonte: ENEA (2017a)

Intervento	2007-2013	2014	2015	2016*	Totale
Riqualificazione globale	0,04	0,01	0,01	0,01	**0,07**
Coibentazioni pareti, sostituzione serramenti, schermature solari	0,33	0,07	0,06	0,07	**0,53**
Impianti di riscaldamento efficienti	0,37	0,02	0,02	0,02	**0,43**
Selezione multipla	0,05	-	-		**0,05**
Totale	**0,79**	**0,09**	**0,09**	**0,10**	**1,08**

* Stima

Tab. 2 Risparmi da detrazioni fiscali per riqualificazione energetica degli edifici esistenti (energia primaria, Mtep/anno), anni 2007–2016
Fonte: ENEA (2017b)

le ammonta, nel 2016, a 1.329 euro annui a famiglia. Di fatto, gli interventi di riqualificazione energetica possono arrivare a far risparmiare mediamente il 15% del totale della spesa per prodotti energetici delle famiglie. Nell'ipotesi che tale risparmio sia attribuibile interamente al gas, grazie all'efficienza energetica la relativa spesa si ridurrebbe in media di circa il 30%.

Nonostante l'incremento registrato nell'ultimo triennio, il Mezzogiorno è la ripartizione italiana in cui si spende meno per energia (spesa media annuale 1.219 euro); le famiglie meridionali spendono circa il 15% in meno delle famiglie del Nord (1.431 euro) e circa il 4% in meno di quelle del Centro (1.264 euro).

Nel 2016, le famiglie hanno speso in media 640 euro per il gas e 595 per l'energia elettrica. Le spese per il gas pesano in misura superiore alla media nel Centro (50,3% della spesa energetica complessiva, 636 euro) e ancor più nel Nord (53,4%, 764 euro). La spesa destinata in media all'acquisto di energia elettrica è maggiore nel Mezzogiorno, dove, grazie anche ad un più ampio ricorso alle funzioni di raffrescamento, rappresenta il 55% della spesa energetica complessiva (pari a quasi 670 euro).

La spesa media per consumi energetici è connessa alla dimensione familiare, aumentando progressivamente da 1.000 euro circa all'anno per una famiglia monocomponente fino ad arrivare a 1.635 euro nei nuclei con 5 o più componenti[4]. La presenza di economie di scala si manifesta in un incremento delle spese non proporzionale rispetto al numero di componenti. Una famiglia composta da 5 membri spende infatti in media annualmente solo il 62% in più rispetto a una famiglia monocomponente.

L'andamento dei consumi energetici risulta correlato anche alla situazione socio-economica e culturale della famiglia, mostrando una certa variabilità rispetto sia alla condizione socio-professionale della persona di riferimento sia al suo titolo di studio. A dimostrazione di come le spese energetiche lascino margini di risparmio inferiori ad altri tipi di spesa (elemento, quest'ultimo, che sottolinea la rilevanza dell'approfondimento del tema della povertà energetica), l'incidenza di questa voce sul totale delle spese familiari risulta più elevata nei nuclei che sperimentano un maggior disagio occupazionale ed economico. Nel 2016, il consumo di prodotti energetici incide sul totale della spesa familiare in misura superiore alla media nelle famiglie con persona di
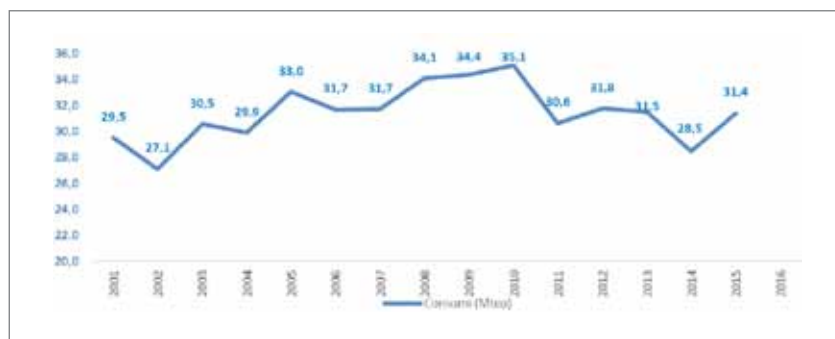
Fig. 2 Impieghi energetici delle famiglie per uso domestico (a) (Mtep) – Anni 2001–2016

(a) Fonte: Elaborazioni su dati Istat – Contabilità ambientale. Sono compresi i consumi per riscaldamento/raffrescamento, acqua calda, uso cucina, elettrodomestici

riferimento non occupata (4,9%, rispetto a un valore medio del 4,4%) e, ancor più, in cerca di occupazione (5,4), ma è elevato anche nelle famiglie di operai e assimilati (4,8). Sia pur correlata, alla dimensione economica e professionale si affianca quella socio-culturale: la quota di spesa familiare devoluta al consumo energetico cala infatti all'aumentare del livello di istruzione, passando dal 6,0% nelle famiglie con al più la licenza elementare, al 4,9% per la licenza media, al 4,0% per il diploma di scuola secondaria superiore, per arrivare, infine, al 3,3% per le famiglie con istruzione universitaria.

Conclusioni

La caratterizzazione socio-culturale dei consumi energetici sottolinea come, ai fini della realizzazione di obiettivi di efficienza energetica, sia importante incidere sui comportamenti della popolazione, sugli stili di vita e di consumo, attraverso una sempre maggiore diffusione di informazioni e conoscenze che contribuiscano alla costruzione di una nuova cultura della sostenibilità energetica ed ambientale.

La Strategia Energetica Nazionale va proprio in questa direzione. Nonostante l'Italia parta già da un livello di intensità energetica inferiore alla media UE, permane infatti un potenziale elevato di risparmio energetico, in particolare nei settori residenziale, terziario e trasporti. Per sfruttare al meglio questo potenziale, le iniziative in ambito residenziale rappresentano la priorità di intervento della SEN 2017. Il meccanismo delle detrazioni fiscali del 65% è stato confermato, prevedendo una sua revisione e potenziamento. È stata inoltre prevista l'operatività del Fondo per l'efficienza energetica, con introduzione di una riserva per la concessione di garanzie sull'eco-prestito e un'evoluzione degli standard minimi di prestazione.

Nel settore residenziale gli interventi di efficienza energetica sono ancora ostacolati da alcune importanti barriere all'adozione, in particolare la scarsa consapevolezza da parte dei consumatori sui potenziali benefici e l'elevato costo degli investimenti iniziali, anche a causa della mancanza di sistemi di credito agevolato. Il tentativo di quantificare i risparmi nella bolletta di gas naturale e la ricognizione delle spese energetiche proposti in questo lavoro vogliono essere un primo passo per aumentare la consapevolezza dei benefici dell'efficienza energetica e chiarire come i tempi di *pay back* degli investimenti siano resi profittevoli dalla presenza delle iniziative di *policy* sopra descritte.

Per saperne di più:
alessandro.federici@enea.it
ungaro@istat.it

[1] Fonte: Indagine Istat sui consumi delle famiglie

[2] Fonte: Indagine Istat sulle spese delle famiglie, che, a partire dal 2014, ha sostituito la precedente indagine Istat sui consumi

[3] Sono escluse le spese per riscaldamento/condizionamento centralizzato.

[4] La spesa media ammonta a 1.378 Euro nei nuclei con due componenti; 1.505 con tre componenti e 1.622 con quattro

BIBLIOGRAFIA

1. ENEA (2017a); Rapporto Annuale Efficienza Energetica 2017, http://www.enea.it/it/seguici/pubblicazioni/pdf-volumi/raee-2017.pdf

2. ENEA (2017b); Rapporto Annuale Detrazioni Fiscali 2017, http://www.enea.it/it/seguici/pubblicazioni/pdf-volumi/detrazioni-65-2017.pdf

3. ISTAT (2017); http://dati.istat.it/

4. ISTAT (2015); La spesa per consumi delle famiglie - Anno 2014, http://www.istat.it/it/archivio/164313

5. Ministero dello Sviluppo Economico (2017); Piano d'Azione per l'Efficienza Energetica 2017, https://ec.europa.eu/energy/sites/ener/files/documents/it_neeap_2017_it_1.pdf

6. Ministero dello Sviluppo Economico, Ministero dell'Ambiente e della Tutela del Territorio e del Mare (2017); Strategia Energetica Nazionale – SEN 2017, http://www.sviluppoeconomico.gov.it/images/stories/documenti/Testo-integrale-SEN-2017.pdf

Italy's National Energy Strategy 2017 - Targets

Targets to be achieved by 2030 are in line with both the plan of the European Energy Union and the EU Energy Roadmap 2050:

- **Enhancing Italy's <u>competitiveness</u>, by continuing to bridge the gap between Italian energy prices and costs and European ones, in a global context of rising energy prices.**

- **Attaining Europe's <u>environmental and decarbonisation targets</u> by 2030 in sustainable ways, in line with the future targets set by COP21.**

- **Continuing to improve the <u>security</u> of energy supply and the <u>flexibility</u> of energy systems and infrastructures.**

NATIONAL AGENCY
FOR ENERGY EFFICIENCY
ENEA

Italy's National Energy Strategy 2017 - Energy sector

The path towards a decarbonized energy sector by 2050.

CO_2 emissions in the energy sector $(MtCO_2)$
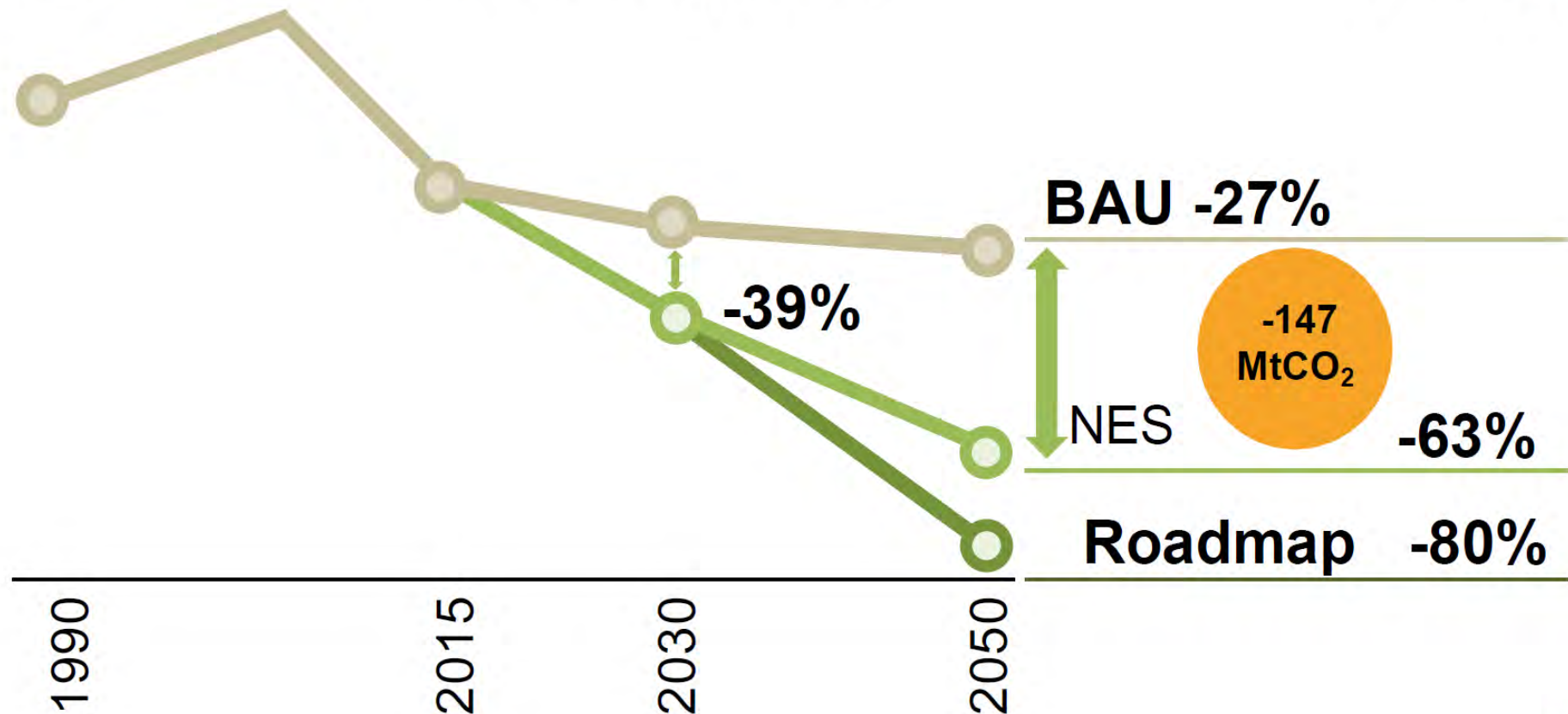
BAU -27%

-39%

-147 $MtCO_2$

NES -63%

Roadmap -80%

1990 · 2015 · 2030 · 2050

Source: Italy's Ministry of Economic Development

NATIONAL AGENCY FOR ENERGY EFFICIENCY

ENEA

Italy's National Energy Strategy 2017 - Energy efficiency

Final consumption reduction by sector at 2030 (Mtoe)

10.2

1.6

2.3

2.6

3.7

Residential | Transport | Services and Agriculture | Industry | Total
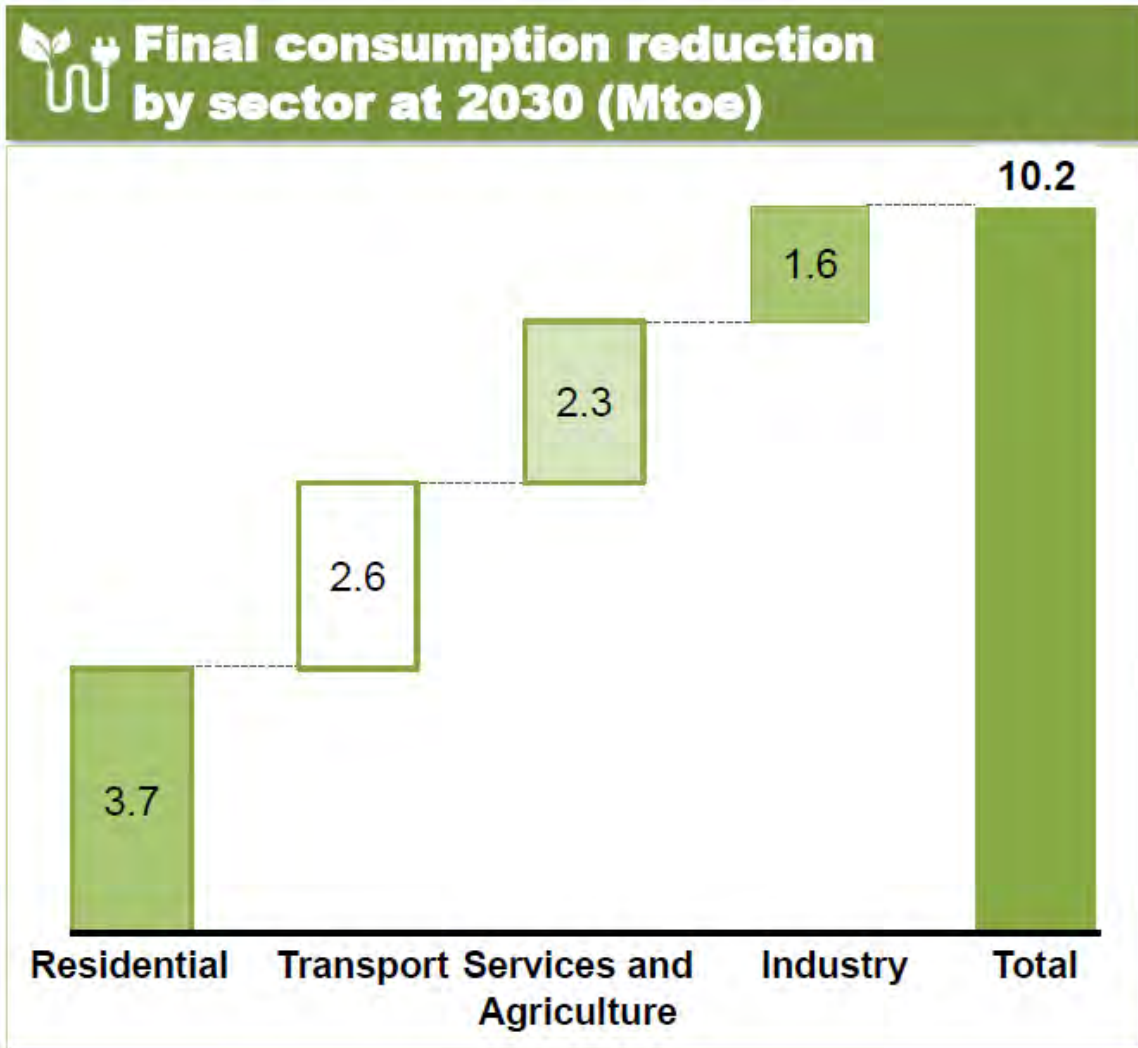
Source: Italy's Ministry of Economic Development

Residential: revising, strengthening and confirming the tax deduction scheme for energy-efficiency investments (so-called "Ecobonus"); putting the energy-efficiency fund into operation.

Services: adoption of Energy Performance Contracting (EPC) for the renovation of public buildings; energy renovation programme for public buildings.

EED art. 7 – Obligation Scheme - White Certificates

White Certificates are tradable securities certifying achieved energy saving in the final uses of energy through energy efficiency measures and projects.

The system rests on the obligation for electricity and gas distributors with more than 50 000 end users to generate each year a certain amount of savings or, alternatively, to purchase an equivalent amount of certificates from non-obliges parties.

Non obliged parties are electricity and gas distributors with less than 50 000 end users, ESCOs, companies with an energy manager or ISO 50001 certified.

Cumulative energy savings

Year	Mtoe
2017	25.7
2016	23.8
2015	21.8
2014	20.1
2013	17.4
2012	14.9
2011	11.8
2010	8.5
2009	5.2
2008	2.7
2007	1.3
2006	0.6

Mtoe

Source: GSE

NATIONAL AGENCY FOR ENERGY EFFICIENCY

ENEA

Since 2007, tax deductions scheme for the energy renovation of existing residential buildings resulted as a key driver of energy efficiency improvements in the housing sector, with more than 3.3 million of implemented actions, and almost 35.5 billion euros of leveraged private investments

The Budget Law 2018 has extended the possibility of tax credit transfer to all taxpayers and all eligible actions: tax credit can be transferred to suppliers who implemented works or to other private entities, with the possibility of an only one subsequent transfer to other entities than suppliers, as long as they are linked to the works that implied the tax deduction.

For taxpayers out of the no-tax area, credit cannot be transferred to credit institutions and financial intermediaries.

NATIONAL AGENCY
FOR ENERGY EFFICIENCY

ENEA

EED art. 7 – Alternative measures - Ecobonus / 2

Eligible actions at building level

Code	Action	Maximum eligible deduction (€) (^)	Maximum eligible expense (€)	Deduction (%)
344	Reduction of heating energy demand of the whole building	100,000.00		65%
345	a) insulation of vertical walls, roof, slabs (*)	60,000.00		65%
	b) windows and shutters replacement (*)	60,000.00		50%
	c) installing solar shades (*)	60,000.00		50%
	d) actions on common parts, involving over 25% of the building surface area		40,000.00 (#)	70%
	e) same actions as in d) to achieve at least the average quality as per tables 3 and 4 of Annex 1, of the Italy's Ministerial Decree 26/06/2015 "Guidelines for the Energy Certification Decree"		40,000.00 (#)	75%
	f) actions as in d) and e) implemented in seismic zones 1,2 and 3, aimed to reduce seismic risks also, resulting in one lower class of the seismic risk classification		136,000.00 (#)	80%
	g) actions as in d) and e) implemented in seismic zones 1,2 and 3, aimed to reduce seismic risks also, resulting in two or more lower classes of the seismic risk classifications		136,000.00 (#)	85%

Source: ENEA

NATIONAL AGENCY FOR ENERGY EFFICIENCY

EED art. 7 – Alternative measures - Thermal Account

The Ministerial Decree of 28 December 2012 introduced a new incentive system for actions to improve energy efficiency and generate thermal energy from renewable sources. It is the first scheme encouraging public administrations to implement energy efficiency improvement actions in buildings and technical installations.

In 2017 the Thermal Account showed a clear acceleration for the public administration (from 141 requests in 2016 to 333 in 2017, +136%), for almost 62 million euros of investments.

Source: GSE
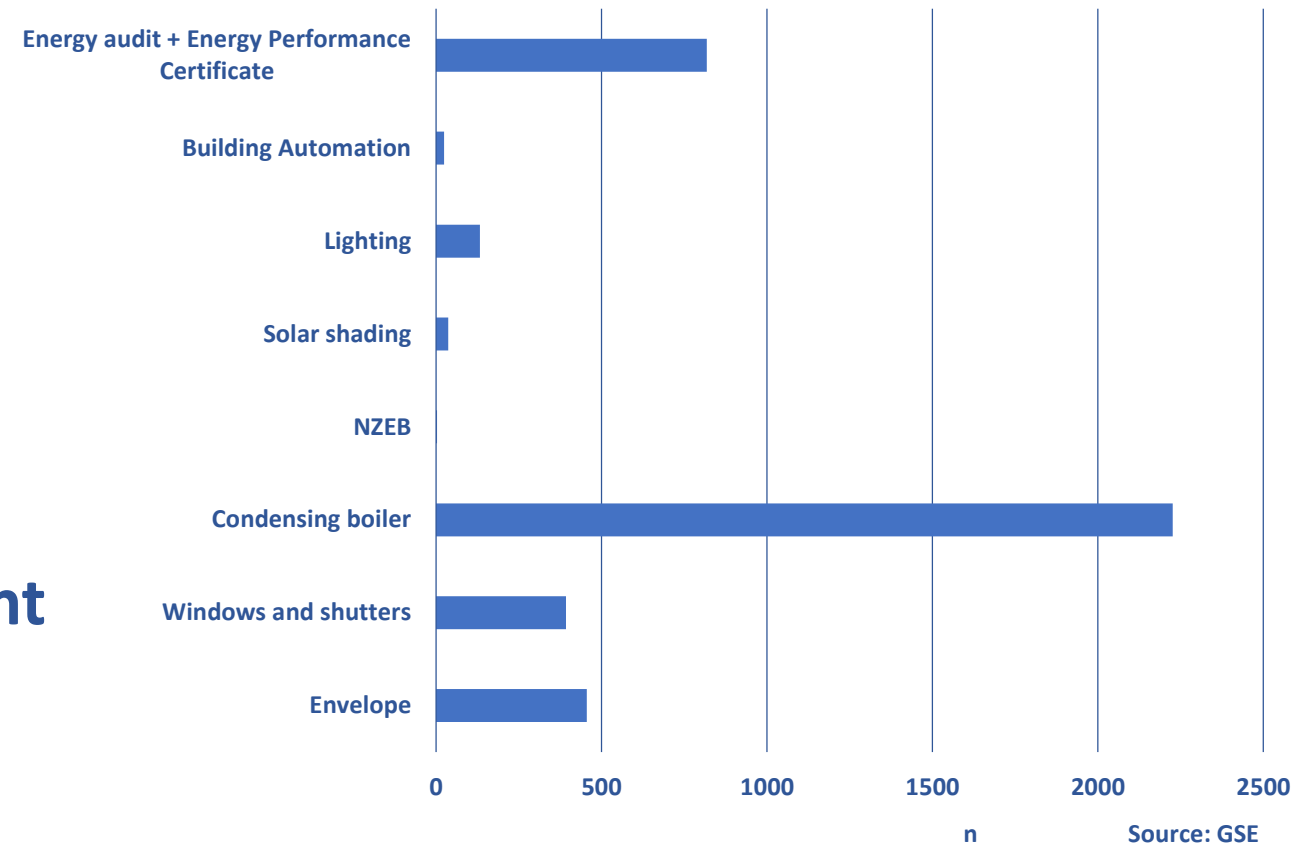
EED art. 7 – Alternative measures - Impresa 4.0

Hyper depreciation (250%) investments in new tangible assets, devices and technologies enabling companies' transformation to "Impresa 4.0" standards.

Gross fixed capital inv.[1]	Main categories	Δ Domestic orders '17 vs '16
≈€80bn (100%)		
35%	Machinery and other equipment	+ 13%
10%	Electric and electronic equipment[2]	+ 7%
18%	Upkeep and installation of machinery	n.a.
37%	Other categories	+ 10%
Total[3]		+ 11%

1. Automotive not included;
2. Includes codes 261 and 27 of Italy's Ateco classification of economic activities;
3. Weighted average, excluding repairs, upkeep and installation costs.
Source: MISE analysis of ISTAT data (January – November 2017 vs same period in 2016)

Nuova Sabatini: **contribution partially covering interest paid by business on bank loans of between 20,000 and 2,000,000 euros, with an annual interest rate of 2.75% and is increased by 30% in the case of investment in "Impresa 4.0" technologies.**

NATIONAL AGENCY FOR ENERGY EFFICIENCY

ENEA

Achieved savings (final energy, Mtoe/year), 2011-2017

Measure / Sector	White Certificates	Tax Relief *	Conto Termico	Impresa 4.0 National Plan *	European Regulations and High-Speed Rail *	Italian Legislative Decrees 192/05 and 26/6/15 **	Energy savings		Achieved target (%)
							Achieved in 2017 **	Expected by 2020	
Residential	0.71	2.08	-	-	-	0.85	**3.64**	**3.67**	**99.2%**
Services	0.15	0.02	0.005	-	-	0.04	**0.22**	**1.23**	**17.5%**
Industry	2.1	0.03	-	0.3	-	0.07	**2.5**	**5.1**	**49.0%**
Transport	0.01	-	-	-	1.68	-	**1.69**	**5.5**	**30.7%**
Total	**2.97**	**2.13**	**0.005**	**0.3**	**1.68**	**0.96**	**8.05**	**15.5**	**51.9%**

* Estimate for the year 2017.

** Estimate for the period January-September 2017. The residential sector includes the savings from the replacement of large household appliances also.

Source: ENEA elaboration of data from the Ministry of Economic Development, ISTAT, Gestore dei Servizi Energetici S.p.A., ENEA, FIAIP, GFK

NATIONAL AGENCY FOR ENERGY EFFICIENCY

ENEA

EED art. 7: achieved savings (final, Mtoe), 2014-2017

Notified measures	New Savings achieved				Cumulative savings	
	2014	**2015**	**2016**	**2017 ***	**2014-2017**	**Expected in 2020**
Mandatory scheme White Certificates	0.872	0.859	1.101	1.341	4.174	12.51
Alternative measure 1 Conto Termico	0.003	0.008	0.019	0.045	0.075	0.43
Alternative measure 2 Tax relief	0.306	0.597	0.873	1.164	2.940	8.39
Alternative measure 3 National Energy Efficiency Fund	0.000	0.000	0.000	0.000	0.000	0.18
Alternative measure 4 Impresa 4.0 National Plan	0.000	0.000	0.000	0.300	0.300	4.00
Total savings	**1.181**	**1.465**	**1.993**	**2.850**	**7.489**	**25.50**

* Preliminary estimate on data not yet consolidated

Source: Elaboration of the Ministry of Economic Development based on data from ENEA and Gestore dei Servizi Energetici S.p.A

NATIONAL AGENCY
FOR ENERGY EFFICIENCY
ENEA

Cost-effectiveness of incentive schemes

A preliminary assessment of the economic balance of the main incentive schemes takes into account the cumulative amount over time of: economic savings; excise duties; expenditure for investments in efficient components/plants business turnover; tax and contributory income (IRES, IRPEF, social security contributions, VAT, etc.).

Mechanism	Years (n)	I_0 (G€)	Savings Energy (Mtoe)	Savings Financial (G€)	Costs (G€)		Cost-effectiveness (c€/kWh)
White Certificates	13	12.0	57.3	38.0	7.0		2.9
Ecobonus	11	34.6	8.6	5.4	20.5		8.6
PV (Feed-in Tariff)	12		82.7		134	(20 y)	32.0
Other electric RES	<25				110	(20 y)	

Source: ENEA elaboration of data from ARERA, CSEA, Chamber of Deputies, ENEA, GME, Gestore dei Servizi Energetici S.p.A., Ministry of Economic Development

NATIONAL AGENCY FOR ENERGY EFFICIENCY

ENEA

3-year Information & Training Programme

The second year's operational programme was divided into four macro-projects for individual targets (schools, SMEs and banks, the public administration and households living in condominiums) and four horizontal multi-target actions
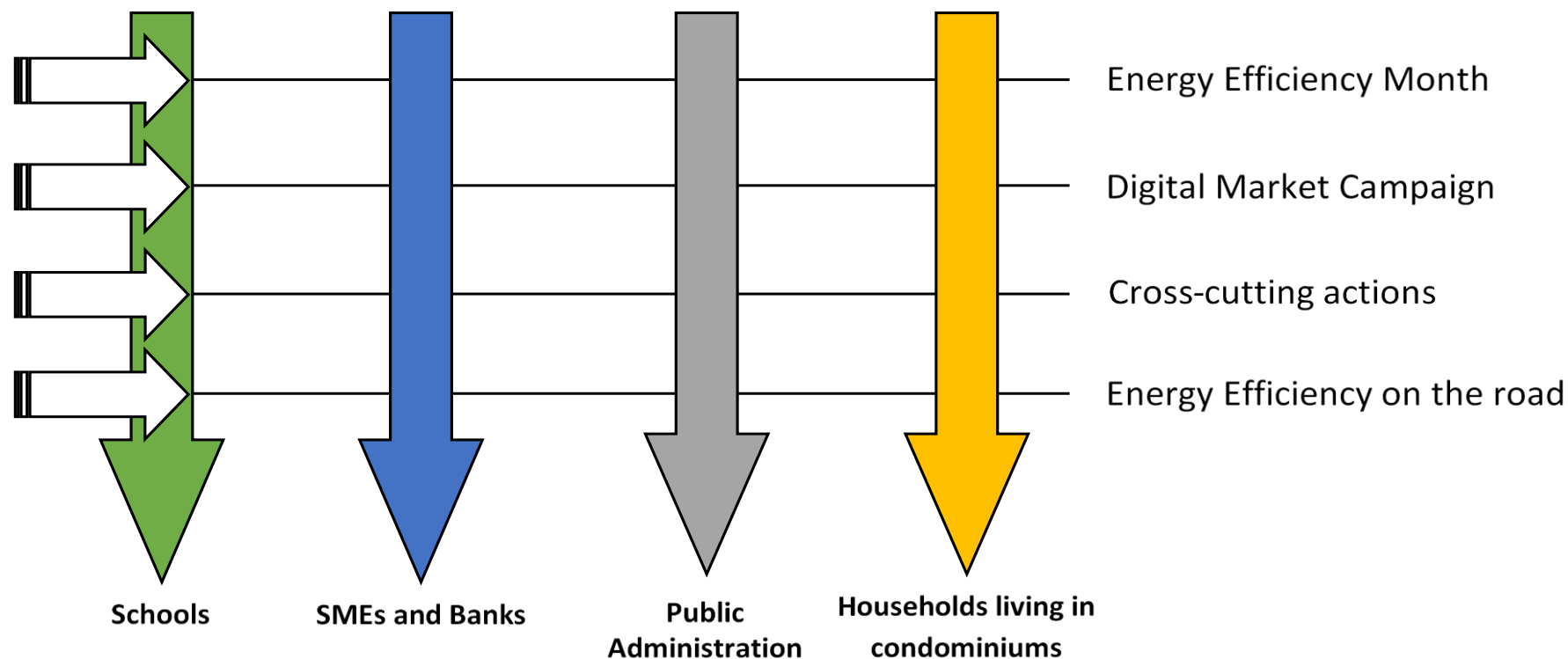
2018 Energy Efficiency Annual Report
Executive summary in English:
http://www.enea.it/it/seguici/pubblicazioni/pdf-volumi/2018/raee-2018-executivesummary-en.pdf

THANK YOU!

alessandro.federici@enea.it

2018 Ecobonus Annual Report
Executive summary in English:
http://www.enea.it/it/seguici/pubblicazioni/pdf-volumi/2018/detrazioni-2018-executivesummary-en.pdf

TRAVELLING FOR 3.750 KM

1:51

ITALIA IN CLASSE A
Campagna nazionale per l'efficienza energetica
http://www.italiainclassea.enea.it/

NATIONAL AGENCY FOR ENERGY EFFICIENCY

Energy Efficiency roadshow
#ItaliainClasseA: a 6-month journey, 3750 km long
https://www.youtube.com/watch?v=coljoWlxY4g